Durham E-Theses

Structural studies of novel molecular systems

Jacquelyn Marie Burke

How to cite:

Burke, Jacquelyn Marie (2002) *Structural studies of novel molecular systems.* Doctoral thesis, Durham University.

Use policy

Structural Studies of Novel

Molecular Systems

Jacquelyn Marie Burke

Thesis submitted in part fulfilment of the requirements for the degree of

Doctor of Philosophy
at the
University of Durham

Department of Chemistry
University of Durham
September 2002

Structural Studies of Novel Molecular Systems

Submitted for the degree of Doctor of Philosophy, September 2002

by Jacquelyn M. Burke, Chemistry Department, University of Durham.

ABSTRACT

This work investigates two main areas of interest. The first is the synthesis and study of a variety of Lewis acid-Lewis base adducts of general formula $X_3B \cdot PR_3$ (X = Cl, Br; R = alkyl or aryl). The ^{11}B-P and ^{10}B-P NMR coupling phenomena are investigated. The partial dissociation of some of these compounds in solution is probed by ^{31}P and ^{11}B NMR. The crystal structures of many of these compounds are presented and analysed for correlations between the properties of the phosphines and B-P bond length. It was found that only the Tolman cone angle gave a good correlation to B-P bond length. A compound containing a novel B_2O_2 ring was synthesised during these studies, and theoretical calculations performed to gain an insight into the planarity of this unusual 4-membered ring. The first crystallographically characterised example of the tri(o-tolyl)phosphonium cation is also presented.

The related compounds $X_3B \cdot pyridine$, $X_3B \cdot 2$-picoline and $X_3B \cdot 4$-picoline (X = Cl, Br) are investigated by various analytical methods. Crystal structures of these B-N adducts are presented. It is found that the structure of $Cl_3B \cdot 4$-picoline exhibits an interesting phase transition from orthorhombic *Pnma* at higher temperatures to monoclinic space group *P2₁/n* below *ca.* 170K.

The second area of work involves crystal structure analyses of a variety of co-crystals of bis(phenylethynyl)benzene compounds, of general type R-Ph-CC-Ph-CC-Ph-R, with R = H, F, MeO, MeS, CH_3 and CF_3 and a varying fluorination pattern on the phenyl rings. The effect of these *para* substituents on the arene-perfluoroarene interaction was investigated. The effect of each substituent was found to be subtle. In most cases, the co-crystallisation induced an arene-perfluoroarene interaction that was not present in the individual components.

Starting materials for the bis(phenylethynyl)benzene compounds often include halogenated tolans of the form Ph-CC-Ph-X (X = Cl, Br, I), with either the halogenated or the non-halogenated ring fluorinated. Crystal structures of PhF_5-CC-Ph-X (X = I, Br, Cl), Ph-CC-PhF_4-I and Ph-CC-PhF_4-CC-$SiMe_3$ are presented and the arene-perfluoroarene interaction investigated. It is found that the PhF_5-CC-Ph-X (X = I and Br) compounds show no evidence of the interaction. The dominating intermolecular force is a Type II halogen···halogen short contact. In contrast, the structure of the chloro analogue is dominated by the arene-perfluoroarene interaction, with no halogen···halogen short contacts. Neither intermolecular force is present in the Ph-CC-PhF_4-I or Ph-CC-PhF_4-CC-$SiMe_3$ structures.

TABLE OF CONTENTS

CHAPTER 5: HALOGEN-SUBSTITUTED TOLANS – A FURTHER LOOK AT ARENE-PERFLUOROARENE INTERACTIONS 228

CHAPTER 6: REFERENCES 262

LIST OF FIGURES

LIST OF TABLES

DECLARATION

The work described in this thesis was carried out in the Department of Chemistry at the University of Durham between September 1998 and September 2001, under the supervision of Prof. Judith A. K. Howard and Prof. T. B. Marder. All the work is my own, unless otherwise stated, and has not been submitted previously for a degree at this or any other university

Jacquelyn M. Burke

STANDARDS, ABBREVIATIONS AND POINTS OF NOTE:

All hydrogen atoms for structures from X-ray data are given at positions derived from X-ray data, i.e. the hydrogen atom positions have not been 'neutron normalised', unless directly stated. All atomic scale distances are measured in angstroms (Å), all laboratory scale distances such as crystal dimensions are measured in millimetres (mm) and all angles measured in degrees (°). In diagrams showing thermal ellipsoid plots, all thermal ellipsoids have been plotted at 50% probability levels.

Abbreviations:

BPEB	bis(phenylethynyl)benzene
cat	catecholato
COD	cyclooctadiene
CSD	Cambridge Structural Database
DSC	density scanning calorimetry
esd	estimated standard deviation
Et	ethyl
HFB	hexafluorobenzene
MOCVD	metal-organic chemical vapour deposition
NMR	nuclear magnetic resonance
PFB	pentafluorobenzene
Ph	phenyl

ACKNOWLEDGEMENTS

...something of the use and beauty of mathematics I think I am able to understand. I know that in the study of material things number, order and position are the threefold clue to exact knowledge; and that these three, in the mathematician's hands, furnish the first outlines for a sketch of the Universe.

D'Arcy Wentworth Thompson (1860-1948)

Chapter 1: Crystal Structure Determination using Single Crystal X-Ray Crystallography

1.1 Introduction

1.1.1 A Brief History of Crystallography

The word 'crystal' originated from the Greek word 'krustallas', which, literally translated, means 'solidified from cooling'. This was because the Greeks believed that quartz (rock crystal) was formed through transformation of ice from cooling.[1] The field of crystallography was originally a branch of geology and mineralogy until it was realised that the crystalline state of matter was common to many materials and not solely to rocks. Crystallography is now, quite rightly, a branch of science in its own right, sitting in the niche between physics and chemistry. The science of crystals encompasses the external state, internal structure, growth and physical properties of crystals.[2]

The modern day field of X-ray crystallography was born in 1895 with the discovery of X-rays by Röntgen.[3] In 1912, von Laue suggested that the spacing between atoms in a crystal should be about the right distance (1 Å) to act as a diffraction grating for X-rays, which are of a comparable wavelength. He managed to obtain a diffraction pattern of spots using an X-ray generator and a copper sulphate crystal. This proved that X-rays were indeed electromagnetic in nature. The work won him the Nobel prize for physics in 1914.

The father and son team William Henry Bragg and William Lawrence Bragg, in 1913, took this research one step further and showed that the diffraction pattern produced in such an experiment could be used to determine the arrangement of atoms in crystals. They solved the first ever crystal structures: those of sodium chloride, zinc sulphide and diamond.

As part of this study, they built on von Laue's work in suggesting that a crystal could be thought of as an infinite array of imaginary parallel planes, and that these lattice planes within the crystal can behave as mirrors. X-rays were found to 'reflect' off the lattice planes. The planes can be thought of as a diffraction grating, and X-rays are a comparable wavelength to the spacing between the planes. Each series of planes only shows diffraction when the reflections combine constructively. In other words, the path length difference must be an integral number of wavelengths, n. Diffraction is therefore also dependent on the wavelength of the beam, λ, the spacing between the lattice planes, d, and on the angle of incidence of the beam, θ. This is shown in Figure 1.1.[4]
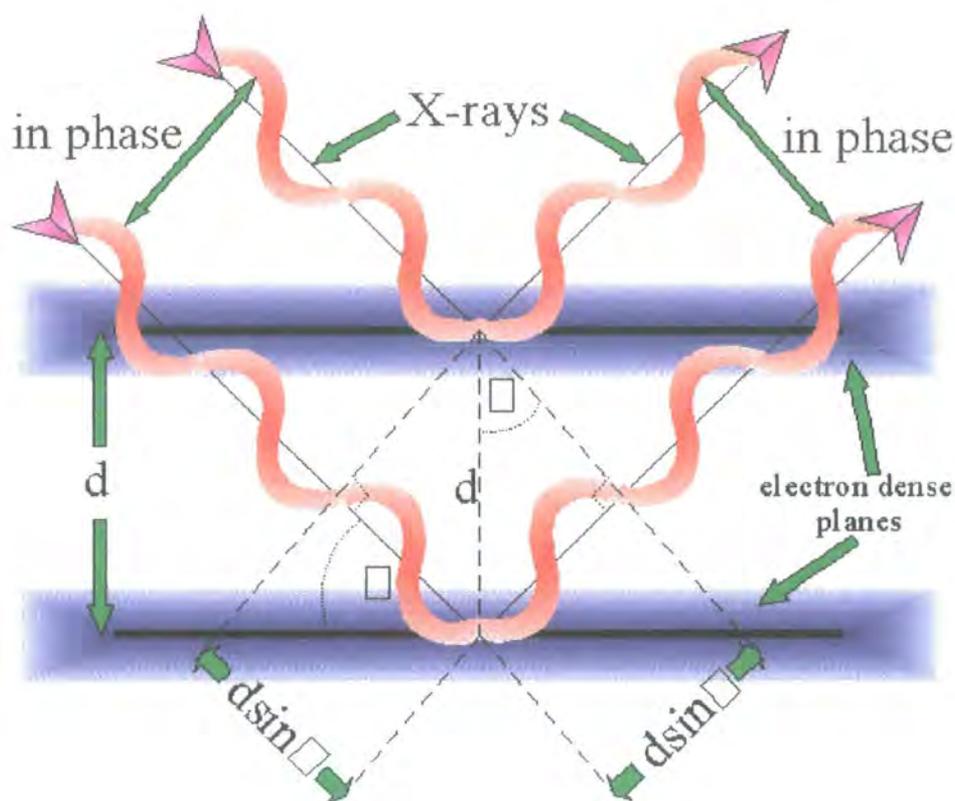
Figure 1.1: Diffraction from parallel lattice planes

The relationship between these terms is expressed by the Bragg equation:

$$n \lambda = 2 d \sin\theta$$

<div style="text-align: right">**Equation 1.1**</div>

This equation understandably underpins the whole of crystallography, and this important work was rewarded with the Nobel Prize for Physics in 1915, awarded jointly to both father and son.

The diffraction pattern obtained in an X-ray diffraction experiment, along with additional phase information, can be used to reconstruct the electron density pattern and thus the arrangement of the atoms in the crystal. Before the advent of computers this was a time consuming laborious process, but now can be done in a matter of hours or days.

1.1.2 The Equipment

X-ray generation

To produce X-rays, a metal target must be bombarded with fast moving electrons; the decrease in kinetic energy is released as X-rays. The radiation produced consists of a continuum of radiation (white radiation) which is due to the collision and also sharp emission lines corresponding to the type of metal target used. The sharp emissions are caused when outer shell electrons move towards the nucleus to replace inner shell electrons that have been ejected by fast collisions. The emission of excess energy as the outer electrons move causes the sharp characteristic peaks. It is these characteristic peaks that are used in X-ray diffraction. Usually there are several sharp emission lines for a particular type of metal. The two most commonly used target metals in X-ray diffraction experiments are copper and molybdenum. The emission lines which are used as the source of X-rays for these materials are the Kα emissions at 1.5418×10^{-10} m for

copper, and 0.71069×10^{-10} m for molybdenum. In this thesis, only Mo-Kα emissions

were used. In order to use only one specific emission, all others must be removed. This

is achieved by use of a monochromator. For molybdenum, graphite is used. Once the

radiation is monochromatic, a collimator is used on the desired emission to produce a

narrow beam of radiation of known diameter (usually approximately 0.5 mm), which is

chosen to optimise the exposure of the crystal to the beam and to minimise any

background radiation.

The Diffractometer

The diffractometer used in the experiments presented in this thesis was a SMART CCD-

area detector diffractometer (see Figure 1.2).

Figure 1.2: The Bruker SMART-CCD area detector diffractometer

The area detector allows many reflections to be collected at once and reduces

experimental time to hours rather than days as is necessary for a point detector. The

benefits of reducing experimental time are numerous, including reducing the time the crystal is on the machine, reducing problems caused by crystal degradation.
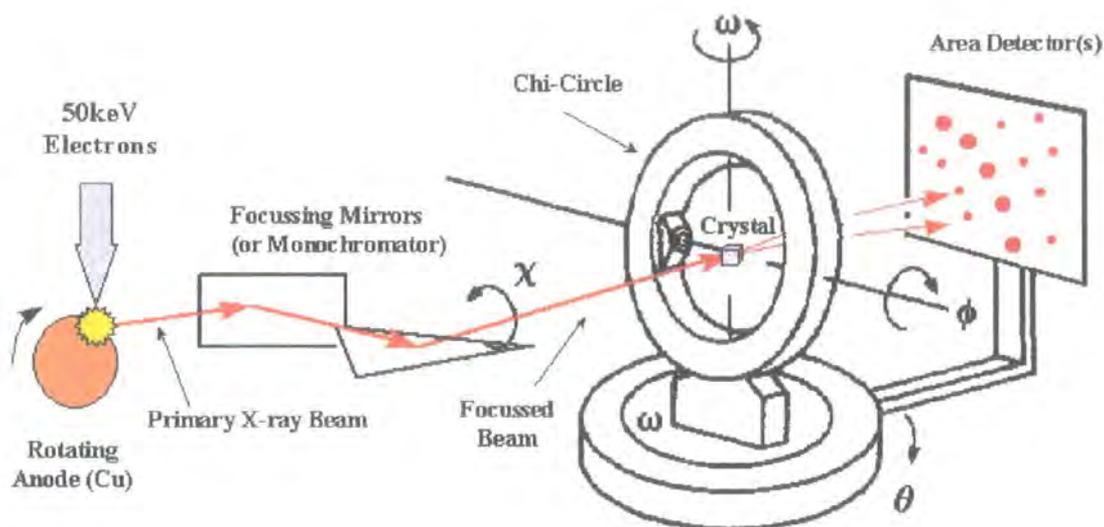
Figure 1.3: Simplified diagram of a diffraction experiment.[5]

During a diffraction experiment, the single crystal is bathed in the beam produced by the X-ray source. The area detector is oriented so that it collects the reflected X-rays, whilst the direct beam passing through the crystal hits a lead beam stop. The crystal is mounted on a goniometer head and can be rotated to enable the crystal to be put in almost any position within the X-ray beam. The orientation of the crystal is represented by three Eulerian angles which define three dimensional space: the rotation about the axis of the goniometer head, ϕ, the rotation of the whole goniometer head, χ, and the angle of rotation about the χ circle, ω. The fourth angle, 2θ, represents the motion of the detector. Older style point detectors have all four circles and are thus often known as 'four-circle' instruments. Use of an area detector enables the collection of diffraction data corresponding to the 2θ and χ circles simultaneously, and so can be thought of as three-circle instruments (see Figure 1.3). The Bruker SMART-CCD used in

experiments presented in this thesis has no χ circle: instead the value of χ is fixed at 54.74°.

The Cryostream

The diffractometer is fitted with a liquid nitrogen cryostream[6] to allow experiments to be performed routinely at low temperatures (90K – 300K).

1.1.3 General Experimental Procedures

Outlined below are the methods and basic principles used to solve the crystal structures reported in this thesis.

Choosing a good crystal

Choosing a good crystal can save hours or even days of work later on in the structure refinement, so it is important to take time selecting a 'good' crystal. Good in this case means a single crystal (not twinned), with few or no imperfections and ideally a block which has all three dimensions between 0.1 and 0.5 mm. This is to ensure the crystal diffracts well in all dimensions and that it is completely bathed by the X-ray beam. If the crystal is too small, either in general or in one dimension, like a plate rather than a block, the crystal will not diffract strongly enough for the diffractions to be detected. If the crystal is too large it will not all fit fully within the X-ray beam. Larger crystals can sometimes be cut carefully with a razor blade or scalpel, but this leads to the possibility of the crystal shattering under the pressure of cutting.

To help select a good crystal the sample is analysed under a microscope. The crystal morphology is examined to check for straight, sharp edges and flat faces. Any rounded,

curved or aggregate crystals can be rejected straight away. Crystals with good general morphology can be checked to see if they are truly single crystals by using a cross-polarising microscope. A single crystal will usually appear light then dark on rotation by 90°. Powders or amorphous samples do not. Care must be taken when using this technique since cubic crystals do not extinguish polarised light. Tetragonal or hexagonal crystals will also not extinguish polarised light when viewed along their c axis. This is still, however, a useful technique for identifying poor crystals. Imperfect crystals may change gradually from light to dark, or show different shades in different sections of the crystal. Such samples can be discarded. If no suitable crystal can be found using this method, then the sample is abandoned.

Mounting the crystal

To place the crystal in the X-ray beam, the selected crystal is mounted onto a glass fibre, or more often for the crystals presented in this thesis, on a hair. This is secured with plasticine or glue into a brass pip and then mounted onto a goniometer head. To reduce diffraction by the glass fibre or hair, it needs to be as thin as possible, but strong enough to hold the crystal and not oscillate in the nitrogen stream. Both glass fibres and human hair are largely amorphous and thus no diffraction occurs.

To fix the crystals onto the hair either epoxy glue or oil can be used. Glue works well for room temperature data collections since it can hold the crystal very firmly. At lower temperatures, however, poly-perfluorinated oil is often used. This has the advantage that at low temperatures it freezes, acting as a reasonably strong glue, and, as a greasy substance, it also protects the crystal from the air by completely surrounding it, which is very useful if the crystal is air sensitive. It also means that when the experiment is finished the crystal should be able to be retrieved intact. This was the chosen method of

mounting the crystals used in the course of this thesis since all the structures were

carried out at low temperatures. It is important that the crystal is mounted on the very

tip of the hair or fibre, not at the side, again to reduce any diffraction caused by the hair.

Once the crystal is mounted, the goniometer head is screwed onto the diffractometer.

The crystal is centred in the beam using the adjustable screws on the goniometer head.
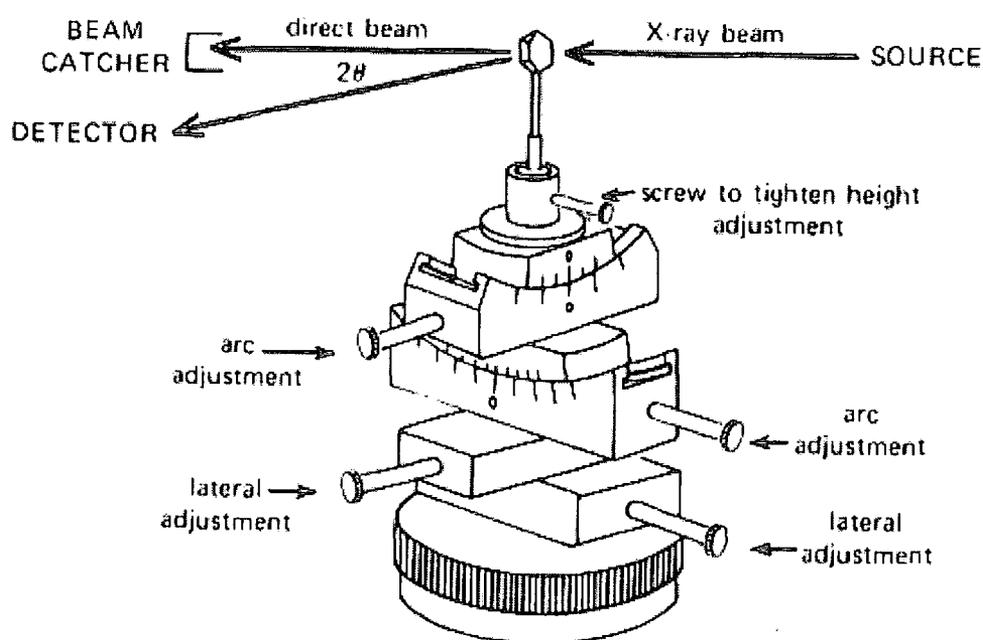
Figure 1.4: Diagram of a goniometer head, showing the adjustments which can be made to centre the crystal in the X-ray beam.

To check that the crystal is centred it is viewed through a telescope with a crosswire.

This can often take some time with odd-shaped crystals, since it is important to be sure

that, on rotation of any of the circles, the crystal remains centred (see Figure 1.5).

(1) height adjustment

cross hairs
of telescope

goniometer head

(2) lateral adjustment

glass fiber

views 180° degrees apart
around vertical axis
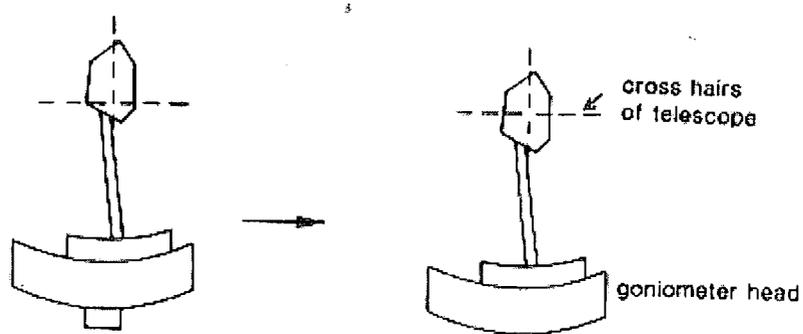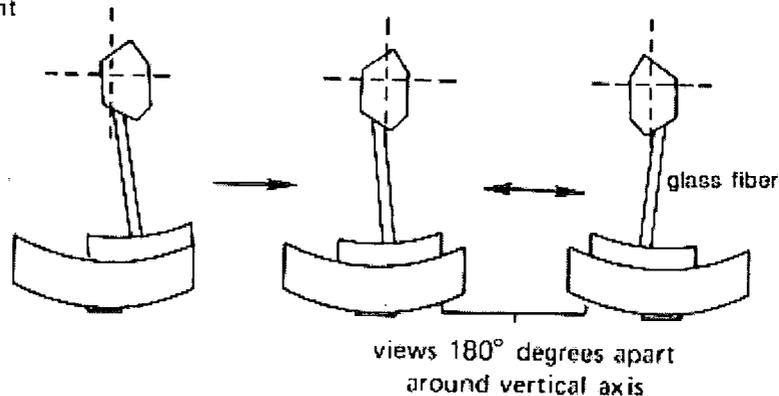
Figure 1.5: Diagram to show the adjustments which can be made to centre the crystal in the X-ray beam.

Once the crystal is satisfactorily centred, a rotation frame is recorded to give a visual check as to the quality of the crystal. A good quality crystal will give a nice array of spots. A sub-standard crystal could give smudges or smears, and should be discarded. A nice array of sharp spots, however, does not necessarily guarantee that the crystal is going to be good enough for a full data collection and more checks are made later.

Low temperature experiments

The data collections for the structures presented in this thesis were done at low temperatures. This is because reducing the temperature reduces the thermal motion of the atoms. This in principle allows a more accurate determination of the positions of the atoms in the crystal. X-ray crystallography essentially gives a time-averaged idea of

atom positions, thus if thermal motion is high and the atoms are vibrating quite vigorously, then the average picture will be a smear rather than a sharp sphere. Thus low temperature experiments, which reduce vibrations, give more intense reflections overall and so allow a better refinement to the complete structure.

There are some problems, however, associated with low temperature work. Phase transitions may occur on cooling, which means that the crystal structure at the experimental temperature is different from that at room temperature, which in turn can be a problem if it is the room temperature properties of the solid that are being investigated. Any atomic movements during the phase transition could also cause the crystal to shatter on cooling.

Data Collection – The Matrix

The first data collection performed is the collection of the orientation matrix. This is a usually the collection of four sets of fifteen frames collected from various orientations of the crystal. The data are refined by least squares methods. The spots are visually inspected on the computer screen. The matrix allows the crystallographer to check whether a crystal that looked reasonable under the microscope is in fact good enough for a diffraction experiment. The cell parameters and the basic cell symmetry can be found, and the orientation matrix calculated. The orientation matrix allows the transformation of real space into reciprocal lattice space. The collection of the matrix data also allows the crystallographer to decide the length of the experiment. Crystals that diffract well and are quite large need only 10 second frames, whereas smaller, poorer crystals may need longer time frames. The crystal system itself may also determine the length of the experiment. To solve a triclinic system, half a sphere of data need to be collected (a hemisphere), monoclinic cells need a quarter of a sphere of data

and orthorhombic cells only need an eighth of a sphere. This is due to the higher symmetry of the latter cells. It is always best to collect more data than are needed, however the demand on diffractometer time also plays a part in determining the experiment length.

When a good matrix has been collected, and the spots look good, the data collection can be started. If a good matrix can not be obtained, the sample is discarded and the experiment abandoned.

Absorption and extinction coefficients

Heavy atoms can absorb X-rays strongly. This can have a detrimental effect on the data collected and a correction needs to be applied. This is to ensure that the intensity of the peaks is consistent, regardless of the orientation of the crystal. An absorption correction can be applied by inputting the crystal dimensions into the computer once the matrix has been found and after the integration of the data (see later). This allows the computer to correct equivalent reflections that should obviously have equivalent intensities.

Another way of applying an absorption correction is after the integration (see later). This was the method used for the crystals presented in this thesis. This absorption correction is a program written for CCD area detector diffractometers called SADABS, which corrects for factors specific to area detectors. The program compares the intensities of equivalent reflections to gauge the scaling of the intensities needed to account for absorption. It is therefore advisable to have many more data than are needed in order to provide the best comparison.

There are two types of extinction: primary and secondary. Primary extinction is the reduction in strength of the incident X-ray beam caused by Bragg reflection (see Figure 1.6). This is where the incident X-ray beam is reflected twice by the same set of planes as is travels through a perfect crystal, resulting in attenuation of the beam due to destructive interference. The 'perfect' crystal is however is rarely found and in reality crystals are usually made up of small regions of perfect crystals known as 'mosaic blocks'. This causes secondary extinction, where individual blocks in the same crystal are perfectly aligned. The incident beam is reflected by both the first block and the second block, which is deeper into the crystal. The reflections from the second block are less intense due to the beam having to travel further into the crystal.
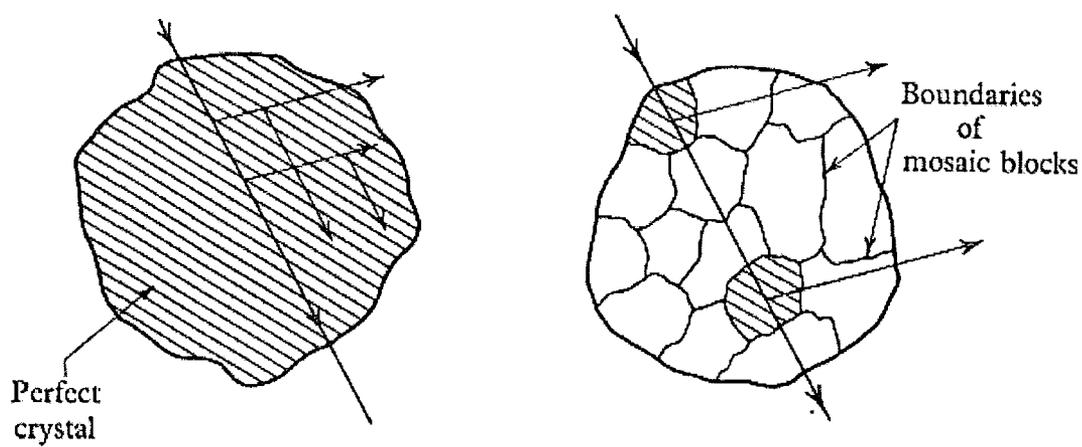
Figure 1.6: Primary extinction (left) and secondary extinction caused by a crystal made up of mosaic blocks (right).

Full data collection

Once the crystal has been chosen, a full data collection can be started. First, a 'dark' scan is carried out that enables background radiation to be subtracted from the collected frames. The experiment is run using the parameters calculated from the matrix data collection. Data is collected by ω scans typically with a data collection time of nine to twelve hours. Data collected at low temperature used the cryostream system detailed above.

Thresholding

Once the data are collected, more accurate unit cell parameters can be calculated using up to 999 strong reflections from all crystal orientations. The SMART software is used.[7] Only peaks above a certain intensity are considered, hence this process is termed "thresholding". The cell parameters found in this way are the ones that are finally reported. These 999 reflections then undergo least squares refinement to see if the individual reflections give h k and l integer values. If there are a significant number of non-integer values, then it is possible that the unit cell is incorrect, or that the crystal was twinned, or that the crystal contained areas of amorphous material. The data are then checked for higher symmetry and the peak profiles viewed to check that the data quality are good. The spots are analysed in terms of their widths in the x and y direction, and the full-width-half-maximum of the rocking curve, which gives the z direction.

Integration (data reduction)

Once the precise unit cell has been calculated, the data can be integrated using appropriate software.[8] This is the process where the intensities of the reflections are converted into structure factor magnitudes. Structure factors and intensities are related by the following expression:

$$|F_{hkl}| = K \sqrt{\frac{I_{hkl}}{(Lp)(Abs)}}$$

Equation 1.2

The Lorentz correction, L, corrects for the relative time each reflection spends in the diffracting position; the polarisation correction, p, accounts for the partial polarisation of the beam by the monochromator crystal, Abs is the absorption correction and K is a scale factor. The scale factor relates to the crystal and radiation used. Thanks to the

advances of computer technology, integration now takes approximately half an hour, as opposed to the many hours or even days it used to take in the past.

Space group determination

The space group of the crystal can be determined using XPREP, part of the SHELXTL application, which uses the cell parameters, Laue symmetry, Bravais lattice types and systematic absences to determine the correct space group. Systematic absences in a diffraction pattern are caused by the presence of a symmetry element which means that exact destructive interference occurs between diffracted reflections (e.g. a 2_1 screw axis generates reflections where l = odd are absent).

The data are tested for the presence of an inversion centre by using normalised structure factors. These are structure factors corrected for the decrease in intensity as $\sin\theta/\lambda$ increases due to atomic size. For a non-centrosymmetric structure, $|E^2-1|$ will tend towards 0.97 and for a centrosymmetric structure it will tend towards 0.74, thus the presence, or otherwise, of an inversion centre can be suggested at this stage.

Obtaining a trial structure

The structure factor amplitudes gained by integration of the data need to be converted into an electron density distribution to enable structure refinement. This is not a simple process due to the 'phase problem'. The measured intensities lead to only the amplitudes of the structure factors, $|F_{hkl}|$. The phase information, $\alpha(hkl)$ is not available from the experimental data. To convert the structure factor amplitudes into electron densities, the Fourier synthesis given below must be performed. This requires the phase angles, which are not yet available.

$$\rho(xyz) = \frac{1}{V} \sum_h \sum_k \sum_l |F(hkl)| \cos 2\pi(hx + ky + lz - \alpha(hkl))$$

Equation 1.3

V is the cell volume. Overcoming the phase problem can be done in two ways, usually depending on the type of structure. Either direct methods or Patterson methods (heavy atom methods) can be used. The calculations are performed by SHELXTL software.[9]

Direct Methods

Direct methods[10] assume that the electron density map is everywhere positive and that it consists of sharp isolated peaks in atomic positions. This restricts the number of possible solutions that can fit the data. Phases are assigned to the data. Any phases which produce negative electron density or which generate a peak too close to another are rejected due to the original assumptions. This procedure is carried out several times and a factor of 'fit' assigned to each possible solution. The best 'fit' solution is then used to generate an electron density map to which atomic positions can be assigned. It is very unlikely that all atomic positions will be found at the first attempt. The remaining atoms can be found by applying a difference Fourier synthesis, shown below:

$$\rho(obs) - \rho(calc) = \frac{1}{V} \sum_h \sum_k \sum_l \left\| F_{obs}(hkl) \right| - \left| F_{calc}(hkl) \right\| \cos 2\pi(hx + ky + lz - \alpha_{calc}(hkl))$$

Equation 1.4

The electron density of the first model is calculated and then subtracted from the observed electron density distribution. The difference density map is plotted, with the 'missing' atoms showing as additional peaks. The trial structure can then be refined. Direct methods were used for all the structure solutions presented in this thesis.

Patterson Methods (the heavy atom method)

If the crystal contains a heavy atom such as a transition metal then Patterson methods[11] can be used to overcome the phase problem. The Patterson function contains no terms for the phase angle. It uses the structure factor amplitudes to produce a vector map using the Fourier synthesis below.

$$P(uvw) = \frac{1}{V} \sum \sum \sum |F(hkl)|^2 cos2\pi(hu + kv + lw)$$

Equation 1.5

The peaks in the Patterson map correspond to vectors between the atoms. The height of each peak is proportional to the product of the atoms linked by the vector. Because of this, it is the heavy atoms which dominate the map. The peaks corresponding to the heavy atoms can be easily found using space group symmetry. The position of some of the light atoms can be found relative to the heavy atoms, and a set of trial phases generated. Because of the reliance on the difference between atomic weights, Patterson is best used when the compound consists of only a few heavy atoms combined with light atoms.

Refinement of the Trial Solution

Once a trial solution has been found, by (usually) direct methods or by Patterson methods, the approximate arrangement of the atoms in the unit cell is known. This approximate structure then needs to be refined, which is done using the XLS program, which is part of the SHELXTL application. First, the peaks corresponding to atoms (if direct methods are used) can be assigned to atoms on the basis of the size of the peak (since larger atoms have more electron density than smaller atoms). The assignment is

checked to make sure connectivity and bond distances are sensible. Once as many atoms

as possible have been assigned, a least squares refinement cycle is performed which can

yield 'missing' peaks ion the resultant difference map.

The principle[12] of least squares, the method that is used to refine the solution, is to

minimise D, the sum of the squares of the differences between the observed and the

calculated structure factors. This function is given below.

$$D = \sum_{hkl} w_{hkl} \left(\left(|F_{hkl}|_{obs} \right)^2 - \left(|F_{hkl}|_{calc} \right)^2 \right)^2$$

Equation 1.6

where w_{hkl} is the weight of the reflection hkl, which is an indication of the precision of

the measurement.

The least squares program also produces other parameters which describe the precision

of the refinement. The first of these is R, the residual index:

$$R = \frac{\sum_{hkl} \left| |F_{obs}| - |F_{calc}| \right|}{\sum_{hkl} |F_{obs}|}$$

Equation 1.7

The R factor gives a measure of how well the observed structure factor amplitudes fit

those calculated for the model. A good structure should have a value of R under 0.08

(generally, the lower the better).

The second parameter which gives an idea as to the quality of the refinement is the goodness of fit, S. For a perfect model, S will have a value of 1.

$$S = \sqrt{\frac{\sum_{hkl} w(Fobs^2 - Fcalc^2)^2}{(N - P)}}$$

<div align="right">**Equation 1.8**</div>

where N is the number of reflections used and P is the number of parameters refined.

A weighted residual index, wR$_2$ can also be used:

$$wR_2 = \sqrt{\frac{\sum w(F_{obs}^2 - F_{calc}^2)^2}{\sum w(F_{obs}^2)^2}}$$

<div align="right">**Equation 1.9**</div>

where w is the weighting of each reflection (an estimation of the precision of the measurement). Other weighting schemes can be used. The one used in SHELX is

$$w = \frac{1}{\left[\sigma^2(F_{obs}^2) + (aP)^2 + (bP)^2\right]}$$

<div align="right">**Equation 1.10**</div>

where P is $[2F_{calc}^2 + max(F_{obs}^2, 0)] / 3$. Once all the larger atoms have been found, the hydrogen atoms can be added. In a good structure these can often be found via the difference map. This is not, however, always possible since hydrogen atoms have only one electron and thus only have a small scattering factor. If this is the case, the

hydrogen atoms can be 'fixed' into a chemically sensible position using the XP program.

After this is completed, further least squares refinement is carried out until the successive least squares cycles see no change in the solution.

The non-hydrogen atoms are usually refined as thermal ellipsoids, which are ellipsoids showing the spread of electron density with anisotropic displacement parameters. An ellipsoid better describes the spread of electron density when the atom is undergoing thermal motion. Six parameters of an ellipsoid are used to describe the electron distribution, and refined using least squares as before. A problem that can be encountered when trying to refine anisotropic atoms is that the result may not be sensible, especially in a low quality refinement. It is important to check for non-sensible solutions. For example, it is possible for the program to define a surface which is not closed, which obviously makes no sense in the real world.

Post Refinement

The final structure and notes concerning the refinement are put into .cif file format, which can then be checked manually and via the IUCr website[13] for any obvious problems. Graphics to accompany the data, as well as intermolecular contact distances, dihedral angles and other parameters can then be calculated via the XP program, or using Platon.[14]

Chapter 2: Prototypical Lewis acid – Lewis base adducts of boron trihalides with tertiary phosphines; compounds of the type $X_3B \cdot PR_3$ (X = halogen; R = alkyl or aryl).

2.1 Introduction

Our group has recently reported[15] that compounds of the type $X_3B\cdot PR_3$ (X = Cl; R = alkyl or aryl) are among the products of the phosphine-promoted substituent redistribution of B-chlorocatecholborane (ClBcat). A search of the literature revealed that although compounds of the type $X_3B\cdot PR_3$ (X = any halogen; R = H, alkyl or aryl) are well reported, many are poorly characterised, with little crystallographic or NMR spectroscopic data, in part due to the fact that the simplest adducts were first synthesised more than 100 years ago,[16] with some characterisation data published in the 1940s.[17] Many of the simple $Br_3B\cdot PR_3$ adducts were patented in the 1960s by Wagner[18] for use as anti-knock agents in petrol; however, no characterisation data were published. Other boron halide-phosphine adducts have been studied by NMR spectroscopy to examine any possible relationship between chemical shift and adduct strength.[19]

The only crystal structures of these adducts to have been reported previously are of $X_3B\cdot PMe_3$ (X = Cl, Br, I),[20] $Br_3B\cdot P(^nPr)_3$[21] and $Br_3B\cdot PPh_3$.[22] The latter two structures will be discussed later. $Me_3P\cdot BCl_3$ and $Me_3P\cdot BBr_3$ were both found to crystallise in monoclinic space group $P2_1/m$, whereas the iodine-containing analogue, $Me_3P\cdot BI_3$, crystallised in orthorhombic space group $Pbca$. B-P bond lengths in the three structures were 1.957(5) Å, 1.92(1) Å and 1.92(2) Å for the chlorine, bromine and iodine structures respectively. The similarity in the chlorine and bromine-containing structures was noted. The difference in the structure of the iodine compound was rationalised by the larger size of the halogen compared to chlorine or bromine.

The crystal structure of an unusual cycloborataphosphoniane, 2,2,4,4-tetraiodo-1,1,3,3,-tetraphenylcyclodiborataphosphoniane, $[(Ph_2P)\cdot BI_2]_2$, was published at around the same

time as the structures of the $Me_3P \cdot BX_3$ (X = Cl, Br, I) compounds. This elegant molecule forms by elimination of hydrogen and iodine from the adduct $Ph_2PH \cdot BI_3$. It crystallises in space group $P2_1/c$. The B-P bond distances range from 1.94(2) Å to 2.02 (2) Å, B-I bond distances range from 2.17(2) Å to 2.22(2) Å and P-C bonds from 1.78(2) Å to 1.83(2) Å. Bond angles inside the four-membered B-P-B-P ring range from 86.8(7)° to 89.1(7)°.

There has recently been a resurgence of interest in compounds containing boron and phosphorus bonds. This mainly concerns adducts of BH_3, but also some aspects of transition metal chemistry and work involving oligomeric, cyclic and polymeric phosphinoboranes. Some of this work is briefly summarised below.

A recent review[23] has discussed the chemistry of amine and phosphine adducts of BH_3, H_2BR, HBRR' and BR_3. A vast number of B-N adducts were included, and the latest developments were discussed in detail. The review discusses the main routes of synthesis of the wide variety of $H_nR_{3-n}B \cdot NR_3$, and, more relevant to this chapter, the analogous $H_nR_{3-n}B \cdot PR_3$ compounds. The recent use in organic chemistry of these adducts as hydroborating or reducing agents is summarised, and mainly concerns complexes of BH_3. The B-P and B-N adducts, which are more stable than the well-studied $THF-BH_3$ and Me_2S-BH_3 adducts which are commonly used for hydroborations, can also be used as hydroborating agents. Hydroboration of this type has also been reported for the allyl-t-butylphosphine-BH_3 phosphine-borane adduct. BH_3 was found to react with bis(diphenylphosphino)alkane-type phosphines, usually forming the *bis*-adduct. The single exception to this is 1,2-bis((S,S)-2,4-dimethylphosphetano)benzene which forms the mono-BH_3 adduct. BH_3 was shown to act as a protecting group for amines and phosphines, and as an activating group. Some adducts were shown to

undergo radical reactions. Other uses of boron-amine and boron-phosphine adducts were as boron analogues of biological molecules for potential therapeutic use, and for use in molecular recognition techniques.

Manners *et al.* have researched into oligomeric, cyclic and polymeric phosphinoboranes. The group have succeeded in making the first high molecular weight poly(phenylphosphinoborane)[24] as part of their work investigating main group inorganic polymer systems. The reaction was facilitated by Rh^I catalysts, including [Rh(1,5-cod)$_2$][OTf], and proceeded via the dehydrocoupling of the phosphine-borane adduct $PhPH_2 \cdot BH_3$. In further studies, many catalytic routes[25] to linear, cyclic and other polymeric phosphinoboranes were detailed. These reactions are again catalysed by a variety of rhodium-based catalysts. In the course of investigating the mechanistic pathways involved in these reactions, a novel platinum complex was synthesised[26] with a ligand comprising of a phosphine-borane adduct. Two complexes, differing in the phosphine substituent of the adduct, were studied. They were $(PEt_3)_2PtP(H)(Ph) \cdot BH_3$ and $(PEt_3)_2PtP(Ph)_2 \cdot BH_3$. It was found that if the latter complex was treated with one equivalent of $P(H)(Ph) \cdot BH_3$, exchange occurred, resulting predominantly in the first platinum complex.

In related studies by the same group[27] it was found that the formation of the BH_3 or BCl_3 adducts of a ferrocene complex, $(\eta^5\text{-}C_5H_4)_2FeP(Ph) \cdot BX_3$ (X = H or Cl), aided the transition metal catalysed polymerisation of bridged ferrocenophanes. It was thought that the ligation of the phosphorus atom in the ligand to the metal centre was preventing polymerisation. The BX_3 moiety protects the phosphorus, preventing its ligation to the metal centre, thus facilitating polymerisation. Use of this method led to the synthesis of poly(ferrocenylphenylphosphine), $[(\eta^5\text{-}C_5H_4)_2FeP(Ph)BX_3]_n$ (X = H or Cl).

Starzewski *et al.* also utilised B-P chemistry in the course of organometallic research.[28]

They used the B-P dative bond to fine-tune zirconium metallocene catalysts. The work

focuses on donor/acceptor (D/A) metallocenes where one π-ligand of the sandwich

complex has a donor substituent and the other π-ligand has an acceptor substituent. A

coordinate bond forms between the donor and the acceptor, which has the effect of

influencing the π-ligand-M-π-ligand angle, altering the selectivity for substrates. The

coordinate bond also inhibits rotation of the ligands. The prototype complex involved a

$ZrCl_2$ fragment, with a Cp-PMe_2 π-ligand and a Cp-BCl_2 π-ligand.
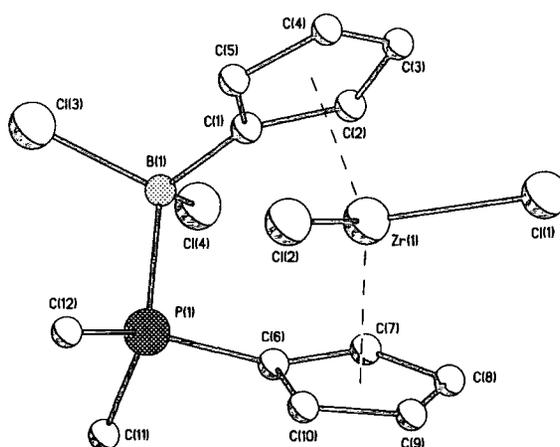
Figure 2.1: Diagram of $Cl_2Zr(Cp$-PMe_2-$BCl_2Cp)$. Hydrogen atoms have been omitted for clarity.

This complex proved to be an effective and thermally stable catalyst for ethene

polymerisation. Utilising the same methodology, it was found that a PEt_2 substituent on

a 2-methylindenyl π-ligand, and BCl_2 substituent on the second 2-methylindenyl ligand

formed a P-B dative bond which held the π-ligands in a *rac* arrangement on the $ZrCl_2$

fragment. This catalyst was successfully used to produce highly isotactic polypropylene.

A ferrocenophane system has been reported which utilised the B-P coordinate bond as a donor-acceptor self-assembling ligand.[29] The weak dative bond enables the rigidity of the ligand, and thus the catalytic activity of the molecule, to be altered by choice of solvent, addition of other Lewis acids or bases, or even changes in temperature. It was found that the $Cr(CO)_5$ fragment is sufficiently Lewis acidic to compete successfully with the boron for the phosphorus lone pair. This idea of reversible coordination has considerable potential for a tailored adaptable catalytic system. Later work by the same group has extended upon these early results, generating some elegant ferrocenophane molecules.[30]

An *ansa*-metallocene with a single boron atom as a bridge has been found to catalyse the polymerisation of ethane when activated by methylaluminoxane.[31] The boron atom was found to be susceptible to attack by nucleophiles, but is protected by coordination by triphenylphosphine.

An interesting area of research into compounds containing B-P bonds is by Haubold *et al.*. Their research into elegant phosphaboranes, analogous in many ways to carboranes, has produced numberous new B-P compounds in the last decade.[32] Other groups have presented structures of more complex phosphacarboranes.[33]

The interest of our group in B-P compounds stems from our work with rhodium boryl complexes.[34] It is known[35] that the labile phosphines in Wilkinsons-type rhodium compounds interact with ClBcat to give, amongst other things, the adducts $ClBcat \cdot PMe_3$ and $Cl_3B \cdot PMe_3$. Use of ClBcat as a source of boron in the presence of rhodium complexes with labile phosphine ligands can thus be complicated by disproportionation of the ClBcat.[36]

Our group has published[37] structures of the phosphine adducts of $B_2thiocat_2$, shown below.
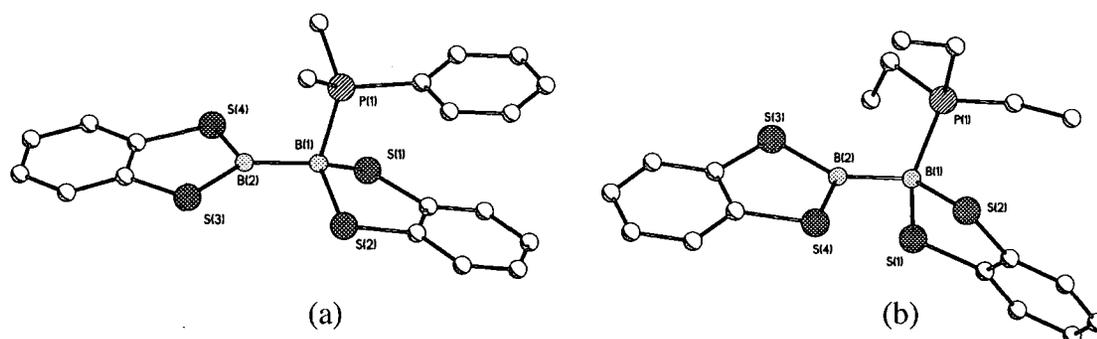
Figure 2.2: Diagram to show the structures of the PMe_2Ph adduct (a) and PEt_3 adduct (b) of $B_2thiocat_2$. Atoms are shown as spheres of arbitrary radius. Hydrogen atoms have been omitted for clarity.

The structure of the bis-dimethylphenylphosphine adduct, (a) above, was also reported at the same time. The P-B bond lengths were 1.979(4) Å and 1.967(2) Å for (a) and (b), above, respectively. The bis-adduct, which is not shown, had a comparable B-P bond distance of 1.974(2) Å.

Our investigations into ClBcat and $B_2thiocat_2$ adducts of tertiary phosphines highlighted the lack of organised data in the literature for the simple $X_3B \cdot PR_3$ compounds. This is somewhat surprising for such prototypical Lewis acid-base systems, especially in the light of recent interest in Group 13-15 adducts. Alkyl Al-Sb and Ga-Sb adducts[38] have been investigated for their potential use as MO-CVD precursors, as have the Group 13-15 metal halide adducts of the type $X_3M \cdot DH_3$ (X = F, Cl, Br, I; M = Al, Ga, In; D = P, N, As).[39]

A search of the Cambridge Structural Database revealed a dearth of structural information about BX_3 adducts of phosphines. The PMe_3 adducts of BX_3 (X = Cl, Br, I),

discussed above, have been known for more than 25 years. It is only much more recently, during the course of the studies presented here, that two other directly related crystal structures have been published.

The $Br_3B \cdot P(^nPr)_3$ adduct[20] was synthesised and the crystal structure solved by Klapötke et al. as part of their research into $X_3B \cdot PX_3$ adducts. The compound was found to crystallise in the trigonal space group $P\bar{3}c1$ at 200K. The P-B bond distance is 1.95(1) Å. The molecules possess C_3 symmetry.

The $Br_3B \cdot PPh_3$ adduct[21] crystallises in monoclinic space group $P2_1/n$ at room temperature. Selected bond lengths and angles are given later for comparison purposes.

Related structures of $X_3B \cdot P(SiMe_3)_3$ (X = Cl, Br) have also been reported.[40] B-P bond lengths were 2.022(9) Å and 2.00(2) Å for the chloro and bromo analogues respectively. Both compounds crystallised in orthorhombic space group $Pbca$, with the cell dimensions for the bromo analogue very similar but slightly larger than for the chloro analogue.

Herein are presented the results of a systematic study of $X_3B \cdot PR_3$ (X = F, Cl, Br; R = alkyl or aryl) compounds. The study was started by previous members of the group and my work has extended upon these results; data from the whole study have been included here and referenced accordingly. These findings have both aided our own identification of products in the complicated mixtures of compounds which result from the substituent redistribution reaction of ClBcat with tertiary phosphines, and contributed to a more thorough understanding of compounds containing B-P bonds.

2.2 Scope of this study

Presented in this chapter are synthetic data for the compounds $X_3B \cdot PR_3$ where X = Cl, Br and PR_3 = PMe_3, PEt_3, $P(^iPr)_3$, $P(^nBu)_3$, $P(^tBu)_3$, PCy_3, PMe_2Ph, $PMePh_2$, PPh_3 and $P(o\text{-tolyl})_3$. NMR studies revealed interesting ^{11}B-P and ^{10}B-P coupling phenomena, which is discussed, and the unexpected behaviour of $Cl_3B \cdot PPh_3$ and $Cl_3B \cdot PMePh_2$ in solution, which is probed at low temperature. Data are examined for the known structures of $Cl_3B \cdot PMe_3$, $Br_3B \cdot PMe_3$ $Br_3B \cdot P(^nPr)_3$ and $Br_3B \cdot PPh_3$ (295K). The molecular structures of $Cl_3B \cdot PCy_3$, $Cl_3B \cdot PMe_2Ph$ and $Cl_3B \cdot PPh_3$ have been obtained previously,[i] but are analysed briefly here, along with the new structures of $Cl_3B \cdot PEt_3$, $Cl_3B \cdot P(^iPr)_3$, $Cl_3B \cdot P(^nBu)_3$, $Cl_3B \cdot P(^tBu)_3$, $Br_3B \cdot PEt_3$, $Br_3B \cdot PPh_3$ (110K) and $Br_3B \cdot P(o\text{-tolyl})_3$.

Also discussed are the structures of two additional compounds, $\{[Ph_3PH]^+\}_2[B_4O_2F_{10}]^{2-}$ and $[HP(o\text{-tolyl})_3]^+[BCl_4]^-$ which were obtained during this study.

---

[i] Structures $Cl_3B \cdot PCy_3$ and $Cl_3B \cdot PMe_2Ph$ solved by Andrei Churakov and $Cl_3B \cdot PPh_3$ by Christian Lehman, University of Durham, England, 1997.

2.3 Results and Discussion

Treatment of PMe_3, PEt_3, $P(^iPr)_3$, $P(^nBu)_3$, $P(^tBu)_3$, PCy_3, PMe_2Ph, $PMePh_2$, PPh_3 and

$P(o\text{-tolyl})_3$ as hexane solutions with a slight excess of BCl_3 in heptane affords

respectively $Cl_3B \cdot PMe_3$ (**2a**), $Cl_3B \cdot PEt_3$ (**2b**), $Cl_3B \cdot P(^iPr)_3$ (**2c**), $Cl_3B \cdot P(^nBu)_3$ (**2d**),

$Cl_3B \cdot P(^tBu)_3$ (**2e**), $Cl_3B \cdot PCy_3$ (**2f**), $Cl_3B \cdot PMe_2Ph$ (**2g**), $Cl_3B \cdot PMePh_2$ (**2h**), $Cl_3B \cdot PPh_3$

(**2i**) and $Cl_3B \cdot P(o\text{-tolyl})_3$ (**2j**) as white solids in high yields. Similarly, reaction of the

phosphines with a slight excess of BBr_3 gave analogous adducts $Br_3B \cdot PMe_3$ (**2aa**),

$Br_3B \cdot PEt_3$ (**2bb**), $Br_3B \cdot P(^iPr)_3$ (**2cc**), $Br_3B \cdot P(^nBu)_3$ (**2dd**), $Br_3B \cdot P(^tBu)_3$ (**2ee**), $Br_3B \cdot PCy_3$

(**2ff**), $Br_3B \cdot PMe_2Ph$ (**2gg**), $Br_3B \cdot PMePh_2$ (**2hh**), $Br_3B \cdot PPh_3$ (**2ii**) and $Br_3B \cdot P(o\text{-tolyl})_3$

(**2jj**). Compounds (**2a**)-(**2j**) and (**2aa**)-(**2jj**) were fully characterised by ^1H, $^{11}B\{^1H\}$ and

$^{31}P\{^1H\}$ NMR spectroscopy.

Attempts to prepare the BCl_3 adduct of $P(C_6F_5)_3$ failed, consistent with the low Lewis

basicity and large steric bulk of this phosphine. An *in situ* NMR scale reaction with a

20:1 excess of BCl_3 to $P(C_6F_5)_3$ also failed to produce any indication of adduct

formation.

2.3.1 NMR Data

In the ambient temperature $^{31}P\{^1H\}$ NMR spectra of both (**2a**) – (**2i**) and (**2aa**) – (**2ii**) it

was possible to observe a 1:1:1:1 quartet due to coupling with quadrupolar ^{11}B (I = 3/2).

It was also possible to observe coupling to ^{10}B (^{10}B, I = 3, 20% abundance) when a large

number of scans on a concentrated sample provided a sufficient signal/noise ratio

(except for (**2dd**) and (**2ff**)). The observed coupling constants were, as expected, in

proportion to the magnetogryric ratios[41] of the boron isotopes ($\gamma(^{11}B)$ = 8.5794 x 10^7 rad

T^{-1} s^{-1}; $\gamma(^{10}B)$ = 2.8740 x 10^7 rad T^{-1} s^{-1}). This is a ratio of approximately 3:1.

Observation of resolved coupling to ^{10}B is less common than observation of resolved

coupling to ^{11}B because of the larger quadrupole moment of ^{10}B ($Q(^{10}B)$ = 7.4 x 10^{-30}

m^2; $Q(^{11}B)$ = 3.55 x 10^{-30} m^2), and strongly suggests that in these compounds the boron

nucleus must be in a highly symmetric electronic environment so that the interaction of

the quadrupole moment with the electric field gradient is vanishingly small. The

$^{31}P\{^1H\}$ NMR data is shown below, with the $^{11}B\{^1H\}$ NMR data and B-P bond lengths,

where applicable, in Table 2.1 for the BCl_3 adducts (2a)-(2j) and in Table 2.2 for the

BBr_3 adducts (2aa)-(2jj).

Table 2.1: $^{11}B\{^1H\}$ and $^{31}P\{^1H\}$ NMR data (in C_6D_6) and B-P bond lengths for adducts (2a)-(2j)

Compound	#	$^{31}P\{^1H\}$ NMR shift (ppm)[a]	$^{11}B\{^1H\}$ NMR shift (ppm)	J_{B-P} (Hz)[b]	B-P bond length (Å)
$Cl_3B \cdot PMe_3$	(2a)	-11.73, q (-11.74, sept)	3.0, d	164 (55)	1.957(5)[19]
$Cl_3B \cdot PEt_3$	(2b)	-0.05, q (-0.05, sept)	3.0, d	157 (52)	1.981(3)
$Cl_3B \cdot P(^iPr)_3$	(2c)	4.75, q (4.75, sept)	3.7, d	148 (50)	2.004(4)
$Cl_3B \cdot P(^nBu)_3$	(2d)	-3.56, q (-3.56, sept)	3.2, d	156 (51)	1.975(3)
$Cl_3B \cdot P(^tBu)_3$	(2e)	19.14, q (19.14, sept)	5.2, d	137 (46)	2.055 (3)[d]
$Cl_3B \cdot PCy_3$	(2f)	-3.16, q (-3.16, sept)	3.9, d	148 (48)	2.025(2)
$Cl_3B \cdot PPhMe_2$	(2g)	-11.19, q (-11.20, sept)	3.4, d	160 (53)	1.975(1)
$Cl_3B \cdot PPh_2Me$	(2h)	-8.38, q (-8.38, sept)	3.8, d	156 (52)	-
$Cl_3B \cdot PPh_3$	(2i)	-1.66, q (-1.66, sept)	4.6, d	152 (51)	2.014(3)
$Cl_3B \cdot P(o\text{-tol})_3$[c]	(2j)	12.08, s (br)	6.9, s (br)	-	-

[a] values in parentheses are for the ^{10}B-^{31}P isotopomer
[b] values in parentheses are $J_{^{10}B-^{31}P}$
[c] $CDCl_3$ solvent
[d] average of the values for 4 independent molecules in the unit cell.

Table 2.2: $^{11}B\{^1H\}$ and $^{31}P\{^1H\}$ NMR data (in C_6D_6) and B-P bond lengths for adducts (2aa)-(2jj)

Compound	#	$^{31}P\{^1H\}$ NMR shift (ppm)[a]	$^{11}B\{^1H\}$ NMR shift (ppm)	J_{B-P} (Hz)[b]	B-P bond length (Å)
$Br_3B\cdot PMe_3$	(2aa)	-11.80, q (-11.80, sept)	-13.9, d	157 (53)	1.924(12)[19]
$Br_3B\cdot PEt_3$	(2bb)	-3.39, q (-3.39, sept)	-15.0, d	149 (50)	1.970(3)
$Br_3B\cdot P(^iPr)_3$	(2cc)	-1.68, q (-1.68, sept)	-14.5, d	139 (47)	-
$Br_3B\cdot P(^nBu)_3$	(2dd)	-6.91, q	-14.6, d	146	-
$Br_3B\cdot P(^tBu)_3$	(2ee)	10.83, q (10.84, sept)	-15.6, d	126 (42)	-
$Br_3B\cdot PCy_3$	(2ff)	-9.79, q	-14.6, d	138	-
$Br_3B\cdot PPhMe_2$	(2gg)	-12.46, q (-12.47, sept)	-13.8, d	152 (50)	-
$Br_3B\cdot PPh_2Me$	(2hh)	-11.21, q (-11.21, sept)	-14.3, d	149 (49)	-
$Br_3B\cdot PPh_3$	(2ii)	-5.51, q (-5.51, sept)	-14.1, d	145 (48)	1.991(5)
$Br_3B\cdot P(o\text{-tol})_3$[c]	(2jj)	-23.06, s (br)	-12.2, d	130	2.044(6)

[a] values in parentheses are for the $^{10}B-^{31}P$ isotopomer
[b] values in parentheses are $J_{10B-31P}$
[c] $CDCl_3$ solvent

A further area of interest arising from the coupling of the quadrupolar boron nuclei to ^{31}P was noted for the spectrum of $Cl_3B\cdot PMe_2Ph$ (2g). Deconvolution of the spectrum allowed accurate determination of the linewidths and intensities of the individual lines in the multiplets. In the case of the septet for the ^{10}B isotopomer the lines showed a systematic variation in linewidth and intensity across the septet. The major effect observed was that the outermost lines are relatively narrow, becoming broader and more intense on moving inwards before narrowing again towards the centre of the pattern (see Figure 2.3, Table 2.3 and Table 2.4, below).

MULTICOMPONENT FIT

TOP: SPECTRUM

CENTRE: FIT

BOTTOM: COMPONENTS
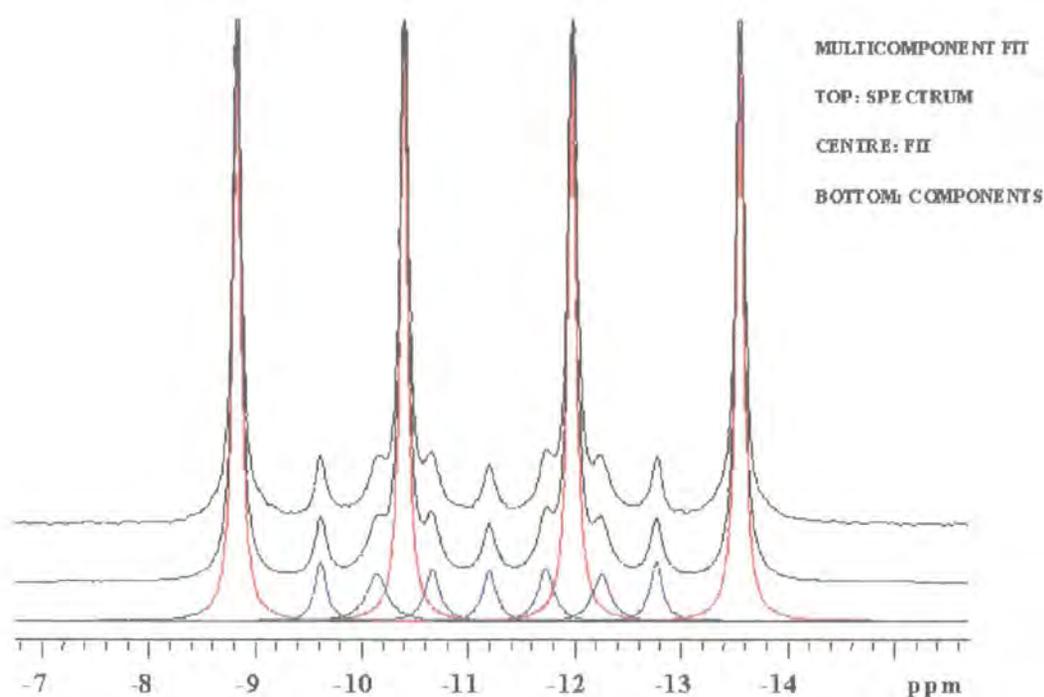
Figure 2.3: Deconvolution of the $^{31}P\{^1H\}$ NMR spectrum of $Cl_3B \cdot PMe_2Ph$ (2g). The top section (in black) shows the original spectrum, the bottom section shows the deconvoluted septet (blue) and quartet (red), and the centre section shows how well the deconvoluted spectrum fits the original one.

Table 2.3: Results of the deconvolution of the ^{11}B isotopomer of (2g)

Frequency (Hz)	Height (mm)	Width (Hz)	Integral (a.u.)
-1372.02	140.75	9.10	2012.15
-1212.62	141.68	8.96	1994.00
-1052.98	142.27	8.84	1975.62
-893.53	141.66	9.03	2009.87

Table 2.4: Results of the deconvolution of the ^{10}B isotopomer of (2g).

Frequency (Hz)	Height (mm)	Width (Hz)	Integral (a.u.)
-1292.64	15.10	14.07	333.71
-1240.54	12.29	19.26	371.91
-1187.33	13.73	17.90	385.87
-1133.19	13.18	14.88	308.04
-1079.90	13.26	15.88	330.94
-1026.80	12.35	22.73	441.05
-973.76	15.28	12.66	304.01

The pattern shows that the peaks have a symmetrical variation in the linewidths and the outer peaks of the septet are narrowest, forming "fangs". This is the sort of pattern expected for a spin-1/2 nucleus (A) coupled to a spin-3 nucleus (X) when $T_{1(X)} > 1/J_{AX}$, and where $T_{1(X)}$ is dominated by quadrupolar, rather than dipolar, interactions.[42] However, the slight asymmetry which is readily discernable in the pattern shows that pure quadrupolar interaction is not the only mechanism contributing to the relaxation of X, and indicates that a significant contribution from the interaction of the quadrupole moment with the shielding anisotropy is likely.

The interesting phenomenon of the variation in linewidths forming "fangs", was reported in 1963 for NbF_6^- where the decet produced in the ^{19}F spectrum (from coupling to the ^{93}Nb nucleus, I=9/2) has similar "fangs".[43] This is due to the difference in relaxation times for the different levels in the quadrupolar nucleus. Thus, in our system, the ^{10}B (I = 3) has seven possible states (3, 2, 1, 0, -1, -2, -3) with different relaxation times. All the different states are 'seen' by the ^{31}P nucleus, and thus any difference in relaxation times between these states of the ^{10}B nucleus influences the ^{31}P spectrum.

This results in the differing linewidths of the ^{31}P spectrum. Slower relaxation times result in a sharp peak on the ^{31}P spectrum, thus the "fangs" are caused by the slowest relaxation time for the 3 and –3 state of the ^{10}B. The peaks with the largest linewidths result from the fastest relaxation times between the states in the ^{10}B.

The relaxation times of the different states are a complex issue governed by the number of possible relaxation pathways (quantum transitions). A first quantum transition, which is the most likely, is one in which relaxation occurs to the next state i.e. +3 to +2 (or –3 to –2). There is also the lower probability of second quantum transitions i.e. from +3 to +1 (or –3 to –1) and progressively lower probabilities of third, fourth, fifth and sixth quantum transitions (ignored here due to the very low probabilities of them occurring, although some of these are likely to make contributions to the relaxation). It can be seen that nuclei in state +3 can only have one first quantum transition, to the +2 state, but nuclei in the +2 state can have 2 possible first quantum transitions (to the +3 or the +1 state). These differing relaxation mechanisms mean that the relaxation times for nuclei in the different states can vary and thus explains why the linewidths in the septet in the ^{31}P spectrum are different.

The integrated intensity of peaks due to the ^{10}B isotopomer is expected to be a quarter of that due to the ^{11}B isotopomer; due to the relative abundances of ^{11}B and ^{10}B (80.42% and 19.58% respectively). It was found, however, that in several of the ^{31}P{^{1}H} spectra acquired under "typical" conditions (20° pulse, 1 s acquisition, 2 s recycle, continuous decoupling) the relative intensity of the signals from the ^{10}B isotopomer compared with those from the ^{11}B isotopomer was significantly less than would be expected from the natural abundances of the nuclei. On re-running the spectrum of one sample (**2g**) with a much longer recycle time (20 s), the relative intensities of the two isotopomers gave the

expected ratio, indicating a difference in the ^{31}P T_1 of the two isotopomers. The same

sample was therefore used in a ^{31}P T_1 experiment, the results of which are given below.

Table 2.5: T_1 results for the ^{11}B isotopomer of (2g).

Frequency (Hz)	T_1 (s)	Error (s)
-1372.02	14.76	0.17
-1212.62	14.83	0.16
-1052.98	14.82	0.16
-893.53	14.76	0.17

Table 2.6: T_1 results for the ^{10}B isotopomer of (2g).

Frequency (Hz)	T_1 (s)	Error (s)
-1292.64	16.56	0.21
-1240.54	15.72	0.36
-1187.33	15.75	0.63
-1133.19	16.33	0.41
-1079.90	15.41	0.24
-1026.80	15.84	0.35
-973.76	16.40	0.41

Two things are apparent. First, the ^{31}P T_1 of the ^{11}B isotopomer is significantly less than

that of the ^{10}B isotopomer, which explains the observation above. Second, there is a

systematic variation in the ^{31}P T_1 across the septet of the ^{10}B isotopomer, mirroring the

T_2 (linewidth) variations discussed previously. These effects in the NMR spectra of

spin-1/2 nuclei coupled to boron have been observed before in the ^{19}F T_1 times of BF_4

anions.[44]

In the $^{31}P\{^{1}H\}$ NMR spectrum of both $Cl_3B \cdot PPh_2Me$ (**2h**) and $Cl_3B \cdot PPh_3$ (**2i**), two peaks are observed. One is the expected adduct quartet, however, the other is somewhat broad, and does not coincide with that expected for free phosphine (-20.9 ppm for (**2h**) vs. –27.5 ppm for $PMePh_2$ and –5.5 for (**2i**) vs. –4.3 ppm for PPh_3). Analysis indicated a pure compound, thus, the cause was suspected to be slow exchange of phosphine in the solution. The $^{31}P\{^{1}H\}$ NMR spectrum for (**2j**) and (**2jj**) showed only a broad singlet, with no quartet, shifted from the value expected for the free phosphines (12.1 ppm and –23.1 ppm, free phosphine at –28.6 ppm), which again suggests phosphine exchange but at a more rapid rate.

Low temperature $^{31}P\{^{1}H\}$ NMR studies on (**2g**), (**2h**), and (**2i**) were performed to establish whether exchange was occurring. For compound (**2g**), where there was no evidence for exchange at ambient temperature, no change was observed in the spectrum at $-31°C$ as expected. In the spectrum of (**2h**), however, the peak at –20.85 ppm in the ambient temperature spectrum was no longer observed at $-31°C$, suggesting that either the equilibrium constant for adduct formation had increased, or exchange had been slowed enough to broaden the peak to the point where it was not detected, or both. In the spectrum of (**2i**) at $-31°C$, the peak at –5.53 ppm was still visible, although it was much smaller and broader, again suggesting that exchange was occurring.

To further support this conclusion, $^{31}P\{^{1}H\}$ MAS (Magic Angle Spinning) solid-state NMR experiments were performed on (**2a**), (**2g**), (**2h**), (**2i**), (**2j**).

Table 2.7: Solid-State $^{31}P\{^1H\}$ MAS NMR results

#	Solid State Shift of adduct (ppm)	Solid State Shift of Free Phosphine, δ_{iso} (ppm)[45]	Difference	Solution ^{31}P shift (in C_6D_6) of adduct (ppm)
(2a)	-7.71	liquid	-	-11.73
(2g)	-6.84	liquid	-	-11.19
(2h)	-7.79	liquid	-	-8.38
(2i)	5.03	-10.3	15.3	-1.66
(2j)	23.10	-31.5	54.6	12.08

[a] $CDCl_3$ solvent.

It can be seen that the solid state chemical shifts are shifted significantly to the left (upfield) of the solution state spectra. The presence of only a single peak in the spectra again support the evidence that the compounds are pure, but that exchange occurs in solution.

The $^{11}B\{^1H\}$ NMR spectra of the adducts (2a) – (2i) and (2aa) – (2ii) all display a doublet caused by coupling of ^{11}B to the phosphorus atom ^{31}P (I = 1/2). The spectrum of compound (2jj) also shows B-P coupling, which was not observed in the $^{31}P\{^1H\}$ NMR spectrum. The spectrum of (2j) shows only a broad singlet, with no B-P coupling at ambient temperature. The fact that the coupling for (2jj) can be seen, but the coupling for (2j) cannot, suggests that there is a stronger interaction between $P(o\text{-tolyl})_3$ and BBr_3 than with BCl_3 which means the barrier to dissociation is higher and therefore exchange is comparably much slower. This is consistent with BBr_3 being a stronger Lewis acid[46] than BCl_3. Slow exchange in (2h), (2i), (2j) and (2j) which is implied by the $^{31}P\{^1H\}$ NMR spectra should lead to broadening in the $^{11}B\{^1H\}$ NMR spectra. This is not

evident, however, due to the fact that quadrupolar nuclei give peaks that are inherently

broad.[47] It is conceivable that if exchange occurs in (**2j**) and (**2jj**), presumably due to the

steric bulk (Tolman cone angle = $194°$)[48] and low Lewis basicity (pK_a (HP(*o*-tolyl)$_3^+$) =

3.08) of the phosphine, it could occur to a lesser extent in (**2i**) and (**2h**), which have less

bulky phosphines (cone angle (PPh$_3$) = $145°$, (PMePh$_2$) = $136°$). Exchange is not

observed in the other adducts, as these have generally less bulky, more basic phosphines

(e.g. PCy$_3$, although being very bulky (cone angle = $170°$), has a much higher Lewis

basicity (pK_a (HPCy$_3^+$) = 9.7).

2.3.2 Crystallographic Data

The crystal structure of (**2a**) has been reported previously.[19] Structural analyses of (**2b**),

(**2c**), (**2d**), (**2e**), (**2f**) and (**2g**) were performed, and the molecular structures are shown

below. Selected crystal data for all compounds are shown in Table 2.8. Selected bond

length and angles are presented in Table 2.9. The boron and phosphorus atoms in each

structure are approximately tetrahedral. Varying the phosphine seems to have very little

effect on the B-Cl bond length, with all B-Cl distances falling in the range 1.843(3) Å

(in (**2b**)) to 1.866(5) Å (in (**2a**)). The P-C(alkyl) distance shows a greater dependence

on phosphine, as is to be expected, with bond lengths ranging from 1.807(1) Å, 1.807

(6) Å and 1.807(3) Å in (**2g**), (**2a**) and (**2b**), which have the least bulky methyl and ethyl

phosphine groups, to 1.913(2) Å in (**2e**), with the bulkiest *tert*-butyl substituent. These

are all comparable with published data.[49]

Table 2.8: Crystal data for compounds (2a) - (2g) and (2i)[a]

Compound	$Cl_3B \cdot PMe_3$ (Literature)[19]	$Cl_3B \cdot PEt_3$ (2b)	$Cl_3B \cdot P(^iPr)_3$ (2c)	$Cl_3B \cdot P(^nBu)_3$ (2d)	$Cl_3B \cdot P(^tBu)_3$ (2e)	$Cl_3B \cdot PCy_3$ (2f)	$Cl_3B \cdot PMe_2Ph$ (2g)	$Cl_3B \cdot PPh_3$ (2i)
Formula	$C_3H_9BCl_3P$	$C_6H_{15}BCl_3P$	$C_9H_{21}BCl_3P$	$C_{12}H_{27}BCl_3P$	$C_{12}H_{27}BCl_3P$	$C_{18}H_{33}BCl_3P$	$C_8H_{11}BCl_3P$	$C_{18}H_{15}BCl_3P$
Formula weight	193.25	235.31	277.39	319.47	319.47	397.57	255.30	379.43
Crystal System	monoclinic	orthorhombic	monoclinic	trigonal	monoclinic	trigonal	orthorhombic	monoclinic
Space Group	$P2_1/m$	$P2_12_12_1$	$P2_1/c$	$R3c$	Pc	$R3c$	$P2_12_12_1$	$P2_1/n$
a / Å	6.9570(10)	7.0992(5)	14.897(1)	14.990(1)	14.7580(11)	14.7121(1)	6.2432(1)	11.8911(1)
b / Å	10.6300(10)	11.8304(8)	14.008(1)	14.990(1)	14.0241(12)	14.7121(1)	10.7745(1)	9.7556(1)
c / Å	6.4760(5)	13.4392(8)	15.076(1)	13.579(1)	16.0336(14)	16.3817(3)	17.6431(2)	15.8195(1)
α / °	90	90	90	90	90	90	90	90
β / °	112.76(1)	90	116.01(1)	90	90.093(5)	90	90	92.4650(10)
γ / °	90	90	90	120	90	120	90	90
U / Å^3	441.6	1128.71(13)	2827.5(4)	2642.4(3)	3318.4(5)	3070.71(6)	1186.80(3)	1833.44(3)
Z	2	4	8	6	8	6	4	4
D_c / g cm^{-3}	1.45	1.385	1.303	1.205	1.279	1.290	1.429	1.375
μ / mm^{-1}	1.1	0.896	0.726	0.592	0.628	0.523	0.859	0.582
Temperature	ambient	150(2)	110(2)	120(2)	110(2)	110(2)	110(2)	110(2)
F(000)	-	488	1168	1020	1360	1272	520	776
Crystal Size / mm	0.5 x 0.30 x 0.15	0.36 x 0.09 x 0.08	0.36 x 0.24 x 0.06	0.68 x 0.05 x 0.04	0.40 x 0.55 x 0.85	0.60 x 0.30 x 0.30	0.60 x 0.30 x 0.20	0.40 x 0.40 x 0.10

[a] This work unless otherwise indicated.

Table 2.9: Selected bond lengths (Å) and angles (°) for compounds (2a) – (2g) and (2i)[a]

	(2a)[19] Cl$_3$B· PMe$_3$	(2b) Cl$_3$B· PEt$_3$	(2c)[b] Cl$_3$B· P(^{i}Pr)$_3$	(2c)[b]	(2d) Cl$_3$B· P(^{n}Bu)$_3$	(2e)[c] Cl$_3$B· P(^{t}Bu)$_3$	(2e)[c]	(2e)[c]	(2e)[c]	(2f)[50] Cl$_3$B· PCy$_3$	(2g)[48] Cl$_3$B· PMe$_2$Ph	(2i)[49] Cl$_3$B· PPh$_3$
B-P	1.957(5)	1.981(3)	1.996(3)	2.011(3)	1.975(3)	2.0537(17)	2.0552(18)	2.0554(17)	2.0571(19)	2.025(2)	1.9749(14)	2.014(3)
B-Cl	1.850(3)	1.857(3)	1.859(3)	1.848(3)	1.853(1)	1.8531(17)	1.852(2)	1.8576(19)	1.845(2)	1.8543(8)	1.8531(14)	1.852(3)
	1.866(5)	1.844(3)	1.855(3)	1.855(3)	1.853(1)	1.8610(19)	1.8564(19)	1.8523(18)	1.854(2)	1.8543(8)	1.8518(14)	1.856(3)
	1.866(5)	1.843(3)	1.845(3)	1.848(3)	1.853(1)	1.8486(18)	1.8501(19)	1.8539(18)	1.8562(19)	1.8543(8)	1.8472(14)	1.845(3)
P-C	1.822(4)	1.807(3)	1.838(3)	1.842(3)	1.817(2)	1.9062(16)	1.9032(16)	1.9063(16)	1.9074(16)	1.8413(11)	1.8109(12)	1.822(2)
	1.807(6)	1.814(3)	1.840(3)	1.844(3)	1.817(2)	1.9112(16)	1.9093(16)	1.9113(15)	1.9105(16)	1.8413(11)	1.8065(13)	1.817(2)
	1.807(6)	1.814(3)	1.849(2)	1.849(3)	1.817(2)	1.9130(16)	1.9012(16)	1.9114(16)	1.9105(16)	1.8413(11)	1.8076(13)	1.821(2)
P-B-X (X=Cl)	108.0(2)	107.02(14)	111.14(17)	111.17(15)	108.29(9)	111.76(9)	110.79(9)	111.21(9)	110.54(10)	109.17(7)	107.84(7)	107.78(13)
	107.0(2)	108.70(15)	107.91(15)	108.85(15)	108.29(9)	110.66(8)	110.13(9)	110.62(8)	110.11(9)	109.17(7)	105.59(7)	107.99(13)
	107.0(2)	109.00(15)	108.20(14)	107.89(15)	108.29(9)	109.61(9)	111.32(9)	110.28(9)	111.27(9)	109.17(7)	108.36(7)	107.79(13)
X-B-X (X=Cl)	110.9(2)	110.52(16)	109.71(15)	109.07(16)	110.63(8)	108.47(9)	108.12(9)	108.37(9)	108.24(9)	109.77(7)	111.63(7)	110.69(14)
	111.8(2)	110.63(16)	109.98(16)	110.01(16)	110.63(8)	108.16(9)	107.90(10)	108.11(9)	108.14(10)	109.77(7)	111.54(7)	111.12(14)
	111.8(2)	110.85(15)	109.86(18)	109.84(15)	110.63(8)	108.07(9)	108.47(10)	108.16(9)	108.45(10)	109.77(7)	111.58(7)	111.31(13)
C-P-C	108.0(2)	106.43(14)	110.90(13)	109.46(12)	107.36(6)	109.84(7)	109.42(7)	109.49(7)	109.62(8)	111.56(4)	108.73(6)	107.76(11)
	107.8(3)	107.33(15)	105.27(12)	105.14(12)	107.36(6)	109.66(7)	109.78(8)	109.97(7)	109.43(7)	111.56(4)	107.82(6)	108.13(11)
	107.8(3)	107.25(14)	108.25(12)	109.59(13)	107.36(6)	109.64(7)	110.05(7)	109.82(7)	109.94(7)	111.56(4)	108.50(6)	108.35(11)
C-P-B	113.3(2)	111.60(14)	113.85(13)	115.13(13)	111.50(5)	109.02(8)	109.44(8)	109.48(7)	109.49(8)	107.30(4)	111.92(6)	111.03(11)
	110.3(2)	112.18(14)	110.87(12)	109.97(12)	111.50(5)	108.79(7)	109.14(7)	109.19(7)	109.22(8)	107.30(4)	109.65(6)	111.16(11)
	110.3(2)	111.74(14)	107.33(13)	107.33(12)	111.50(5)	109.88(7)	109.00(8)	108.87(7)	109.12(7)	107.30(4)	110.15(6)	110.30(11)

[a] This work unless otherwise indicated.
[b] 2 independent molecules in the unit cell.
[c] 4 independent molecules in the unit cell.

The molecular structure of (2b) at 150K is shown in Figure 2.4. It crystallises in the orthorhombic space group $P2_12_12_1$, which is chiral and non-centrosymmetric.
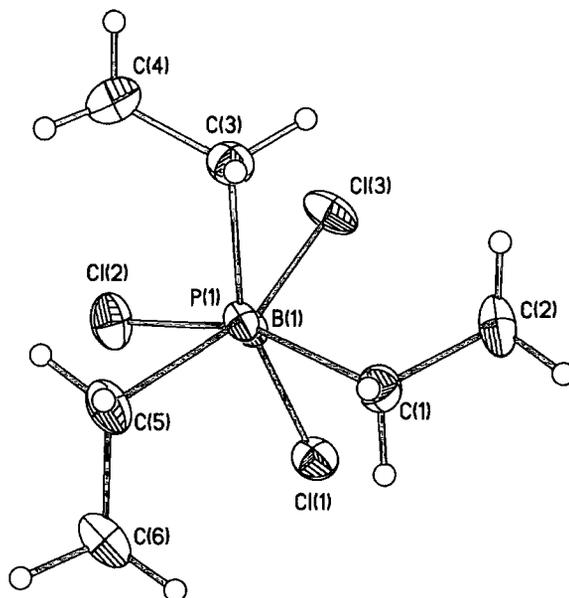
Figure 2.4: Molecular structure of (2b), showing the atom labelling scheme. The thermal ellipsoids are plotted to 50% probability level.

The molecular structure of compound (2c) at 110K is in the common centrosymmetric space group $P2_1/c$. There are two independent molecules in the asymmetric unit, one of which is shown for illustration in Figure 2.5.
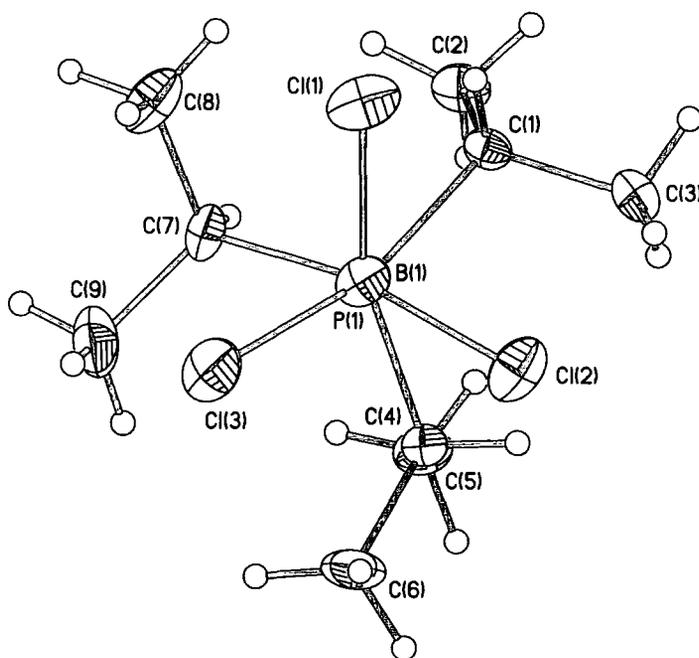
Figure 2.5: Molecular structure of one of the independent molecules of (2c), showing the atom labelling scheme. The thermal ellipsoids are plotted to 50% probability level.

The two independent molecules differ in the conformation of the *iso*-propyl arms of the

phosphine as shown in Figure 2.6.
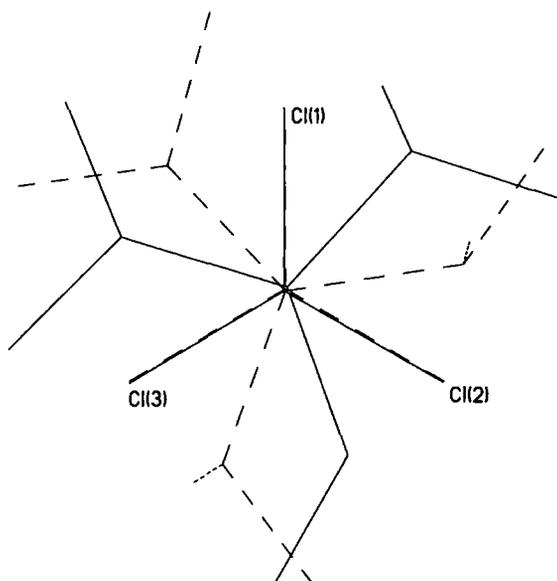
Figure 2.6: 'OFIT' overlap diagram of the two independent molecules of (2c).

One is *almost* an inversion of the other, and the B-P distances (1.996(3) and 2.011(3) Å) are within 3 e.s.d.s of each other, with an average distance of 2.004(3) Å. There is one very small P-C-P bond angle in both molecules (105.27(12) and 105.14(12)°), which occurs where the *iso*-propyl arm is aligned directly between chlorine atoms Cl(2) and Cl(3), presumably to reduce steric crowding of the carbon atoms.

There is pseudo-C_3 symmetry along B-P, as seen in Figure 2.5. The 'OFIT' diagram in Figure 2.6, where the three chlorine atoms of each molecule have been superimposed, interestingly shows almost mirror symmetry between the superimposed *iso*-propyl groups. There is, however, no crystallographic symmetry in either of the independent molecules in the structure.

Compound (**2d**) (Figure 2.7) has exact C_3 symmetry, crystallising in the trigonal space group R3c. It has the same B-P bond length as (**2b**) (1.981(3) Å), which is to be expected since the two phosphines have the same cone angle[33] (132°) and very similar pK_a values ($[HPEt_3]^+$ = 8.69, $[HP(^nBu)_3]^+$ = 8.43).
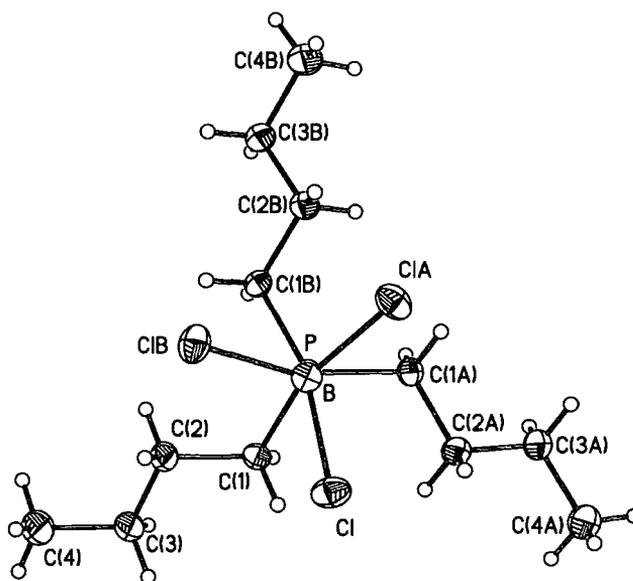
Figure 2.7: Molecular structure of (2d), showing the atom labelling scheme. The thermal ellipsoids are plotted to 50% probability level.

Compound (2e) crystallises in the monoclinic space group Pc. There are four molecules in the asymmetric unit, one of which is shown for illustration in Figure 2.8, all of which are very similar. Indeed, Figure 2.9 shows all four molecules plotted superimposed on each other (over atoms P(1), B(1), Cl(1), Cl(2) and Cl(3)) demonstrating how similar they all are.
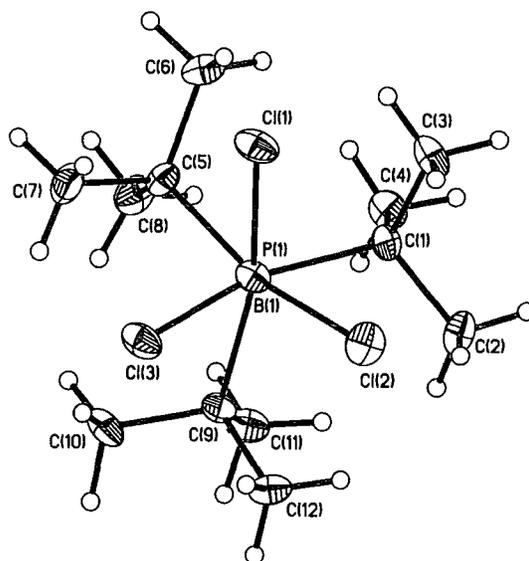
Figure 2.8: Molecular structure of one of the four independent molecules in the unit cell of (2e), showing the atom labelling scheme. The thermal ellipsoids are plotted to 50% probability level.
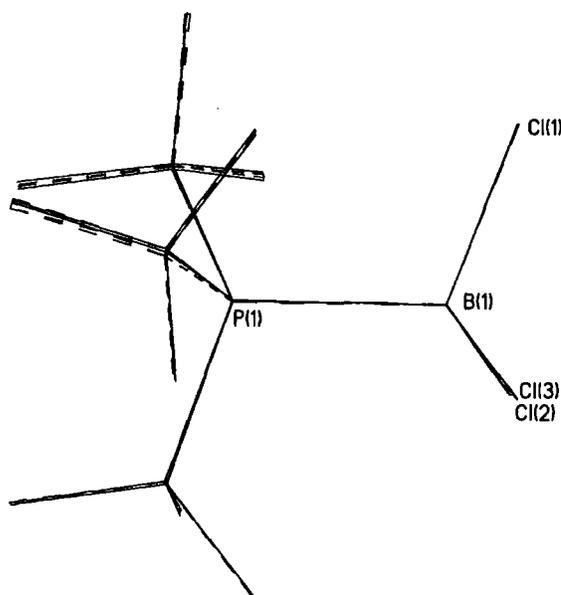
Figure 2.9: 'OFIT' plot of the four independent molecules in $Cl_3B \cdot P(^tBu)_3$, (2e), demonstrating the similarity of all molecules.

The B-P bond lengths in this structure are longer than in any of the other BCl_3 adducts presented herein (2.057(2) Å, 2.055(2) Å, 2.055(2) Å and 2.054(2) Å). The P-C bond lengths are also the longest of these adducts (ranging from 1.913(2) Å to 1.903(2) Å). These two characteristics are most probably due to the sheer bulk of the phosphine (cone angle = 182°). Indeed, it is so bulky that the very fact that the adduct forms at all is a demonstration of the very high Lewis basicity of the phosphine (pK_a of $[HP(^tBu)_3]^+$ = 11.4).

The molecular structure of (2f) at 100K is shown in Figure 2.10. It crystallises in the trigonal space group R3c, the same as compound (2d). It has a large B-P bond distance (2.025(2) Å), since it again has a bulky phosphine (cone angle = 170°) with a relatively high Lewis basicity (pK_a ($HPCy_3^+$) = 9.7).
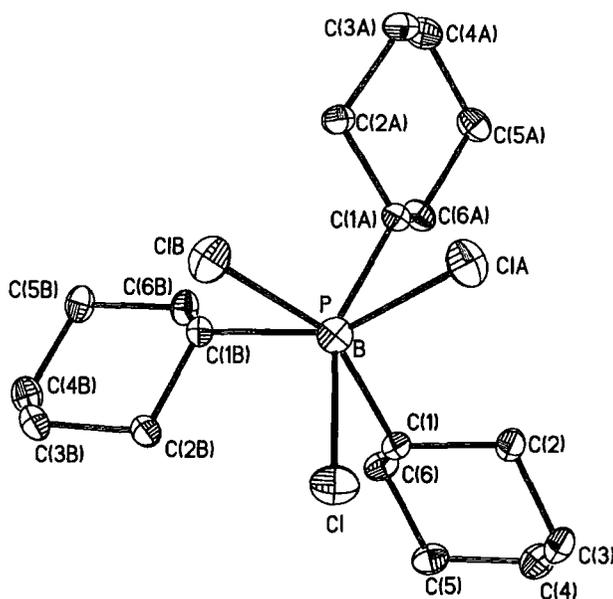
Figure 2.10: Molecular structure of (2f), showing the atom labelling scheme. The thermal ellipsoids are plotted to 50% probability level. Hydrogen atoms have been omitted for clarity.

Compound (2g) (Figure 2.11) crystallises in orthorhombic space group $P2_12_12_1$. This is the same space group as (2b).
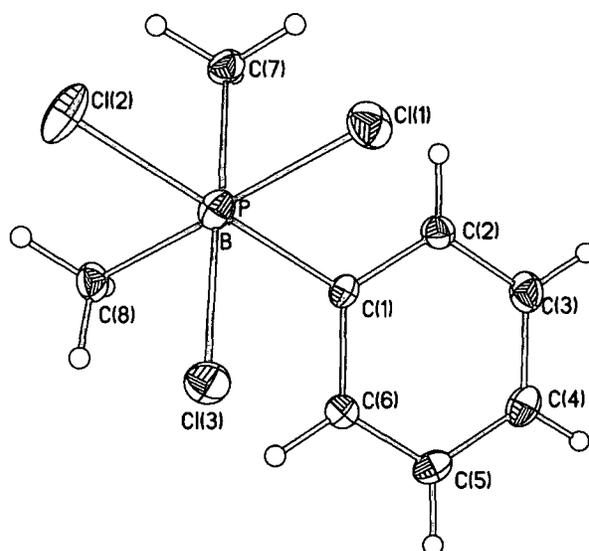
Figure 2.11: Molecular structure of (2g), showing the atom labelling scheme. The thermal ellipsoids are plotted to 50% probability level.

Compound (2i) crystallises in the monoclinic, centrosymmetric space group $P2_1/n$. This is the same space group as the BBr_3 analogue, which was reported previously,[51] and the lower temperature version (2ii) presented herein. The molecular structure is shown in Figure 2.12. The cone angle of PPh_3 is 145°, which is larger than that for the linear alkyl phosphines (PMe_3 = 118°, PEt_3 = 132°, $P(^nBu)_3$ = 132°) but significantly smaller than the branched alkyl phosphines, would suggest that a reasonably short B-P bond length should be found in (2i). The Lewis basicity, however, is much lower (pK_a ($HPPh_3^+$) = 3.84) thus the bond is almost as long as that in (2e) and (2f) at 2.014(3) Å.
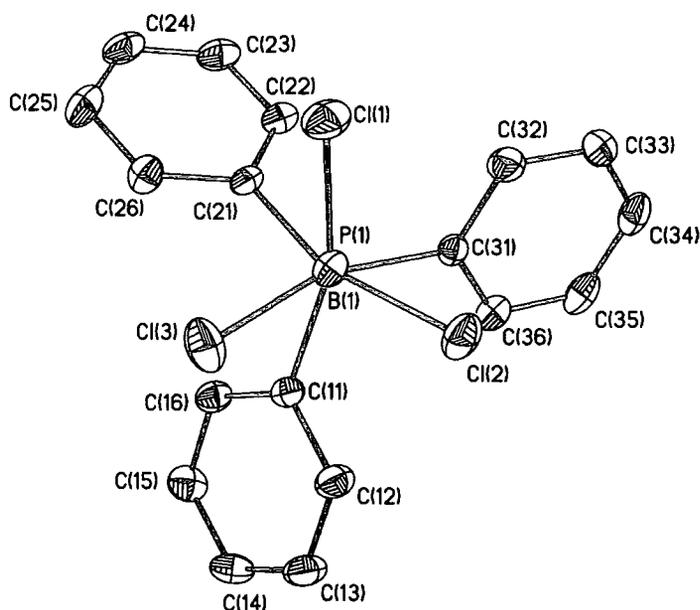
Figure 2.12: Molecular structure of (2i), showing the atom labelling scheme. The thermal ellipsoids are plotted to 50% probability level. Hydrogen atoms have been omitted for clarity.

The crystal structures of (**2aa**) and (**2ii**) (both at 295K) have been reported elsewhere,[19,21] as has the structure of $Br_3B\cdot P(^nPr)_3$ (at 200K).[20] The low temperature structure of (**2ii**) has been determined by our group.[ii] Below are presented crystal data for all five known adducts and selected bond lengths and angles and the low temperature structures of (**2bb**) and (**2jj**).

[ii] Crystals grown by F. S. Souza, structure solved by W. Clegg, University of Newcastle-upon-Tyne.

Table 2.10: Crystal data for the five known $Br_3B \cdot PR_3$ adducts (2aa), (2bb), $Br_3B \cdot P(^nPr)_3$, (2ii) and (2jj).

Compound	$Br_3B \cdot PMe_3$ (Literature)[19]	$Br_3B \cdot PEt_3$ (2bb)	$Br_3B \cdot P(^nPr)_3$ (Literature)[20]	$Br_3B \cdot PPh_3$ (2ii) (ours)	$Br_3B \cdot PPh_3$ (Literature)[21]	$Br_3B \cdot P(o\text{-tolyl})_3$ (2jj)
Formula	$C_3H_9BBr_3P$	$C_6H_{15}BCl_3P$	$C_9H_{21}BBr_3P$	$C_{18}H_{15}BBr_3P$	$C_{18}H_{15}BBr_3P$	$C_{21}H_{21}BBr_3P$
Formula weight	326.60	277.39	410.343	512.81	512.81	554.89
Crystal System	monoclinic	orthorhombic	trigonal	monoclinic	monoclinic	orthorhombic
Space Group	$P2_1/m$	$P2_12_12_1$	$P\text{-}3c1$	$P2_1/n$	$P2_1/n$	$Pna2_1$
a / Å	7.091(2)	7.2464(2)	11.5423(6)	12.0247(16)	12.093(1)	20.4261(12)
b / Å	10.996(2)	12.2020(3)	11.5423(6)	9.9857(13)	10.038(1)	10.1260(6)
c / Å	6.672(1)	13.7193(4)	13.8066(7)	15.833(2)	16.009(2)	10.2236(6)
α / °	90	90	90	90	90	90
β / °	112.38(1)	90	90	93.128(3)	93.10(1)	90
γ / °	90	90	90	90	90	90
U / Å^3	481.1	1213.1(1)	1593.0(1)	1898.3(4)	1940.5	2114.6(2)
Z	2	4	4	4	4	4
D_c / g cm^{-3}	2.25	2.019	1.711	1.794	1.755	1.743
μ / mm^{-1}	13.8	10.055	7.667	6.455	8.441	5.802
Temperature (K)	ambient	110.0(2)	200(3)	160(2)	293	110(2)
F(000)	-	704	799	992	-	1088
Crystal Size / mm	0.50 x 0.34 x 0.10	0.61 x 0.06 x 0.04	0.39 x 0.29 x 0.16	0.50 x 0.44 x 0.26	0.28 x 0.35 x 0.54	0.10 x 0.10 x 0.05

Table 2.11: Selected bond lengths (Å) and angles (°) for compounds (2aa), (2bb), (2ii) and (2jj).

	$Br_3B \cdot PMe_3$ (Literature)[19]	(2bb) $Br_3B \cdot PEt_3$	$Br_3B \cdot P(^nPr)_3$ (Literature)[20]	(2ii) $Br_3B \cdot PPh_3$	$Br_3B \cdot PPh_3$ (Literature)[21]	(2jj) $Br_3B \cdot P(o\text{-}tolyl)_3$
B-P	1.924(12)	1.970(3)	1.95(1)	1.991(5)	1.988(10)	2.044(6)
B-Br	2.025(6)	2.020(3)	2.009(3)	2.000(5)	2.005(8)	2.021(6)
	2.016(10)	2.005(3)	2.009(3)	2.003(4)	2.013(9)	2.018(6)
	2.016(10)	2.026(3)	2.009(3)	1.998(4)	1.978(9)	2.014(6)
P-C	1.806(8)	1.812(3)	1.816(6)	1.811(4)	1.808(4)	1.820(5)
	1.825(12)	1.813(3)	1.816(6)	1.800(4)	1.802(4)	1.825(4)
	1.825(12)	1.815(3)	1.816(6)	1.802(4)	1.803(4)	1.831(4)
P-B-Br	108.9(4)	110.08(17)	109.2(3)	108.2(2)	108.6(4)	110.1(2)
	107.8(5)	109.13(16)	109.2(3)	108.8(2)	107.6(4)	109.8(3)
	107.8(5)	107.21(15)	109.2(3)	107.9(2)	108.8(4)	109.6(3)
Br-B-Br	110.6(4)	110.25(15)	109.7(3)	110.3(2)	109.7[a]	109.4(3)
	110.0(5)	110.32(16)	109.7(3	110.7(2)	111.5[a]	109.0(3)
	110.0(5)	109.80(16)	109.7(3	110.9(2)	110.6[a]	109.0(2)
C-P-C	107.2(4)	105.70(17)	105.7(2)	107.75(18)	108.0[a]	106.0(2)
	107.3(7)	106.89(16)	105.7(2)	108.44(18)	107.5[a]	107.7(2)
	107.3(7)	107.05(17)	105.7(2)	107.23(18)	107.5[a]	106.3(2)
C-P-B	111.8(3)	112.10(16)	113.0(2)	110.76(19)	111.9(3)	112.1(2)
	111.3(5)	112.72(15)	113.0(2)	110.83(18)	110.4(3)	113.1(2)
	111.3(5)	111.94(16)	113.0(2)	108.44(18)	111.3(3)	111.3(2)

[a] e.s.d.s not given

A structural analysis of **(2bb)** showed that it crystallised in the same space group $(P2_12_12_1)$ as the BCl_3 analogue, **(2b)**, both having similar B-P bond lengths (**(2bb)** = 1.970(3) Å and **(2b)** = 1.981(3) Å).
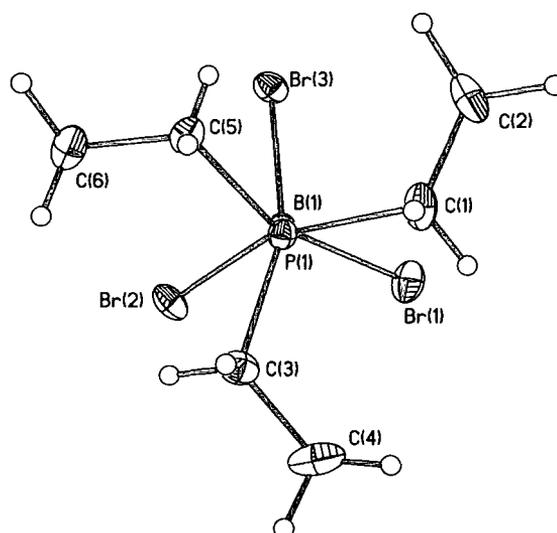
Figure 2.13: Molecular structure of (2bb), showing the atom labelling scheme. The thermal ellipsoids are plotted to 50% probability level.

In the molecular structure of (**2jj**) (Figure 2.14), the bromine atoms are almost eclipsed by the *ipso* carbons of the phenyl rings of the *o*-tolyl moieties, which shows a rotation of the phosphine about the B-P bond in comparison to the triphenylphosphine analogue. This is presumably to accommodate the extra bulk of methyl groups *ortho* to the P-C bonds.
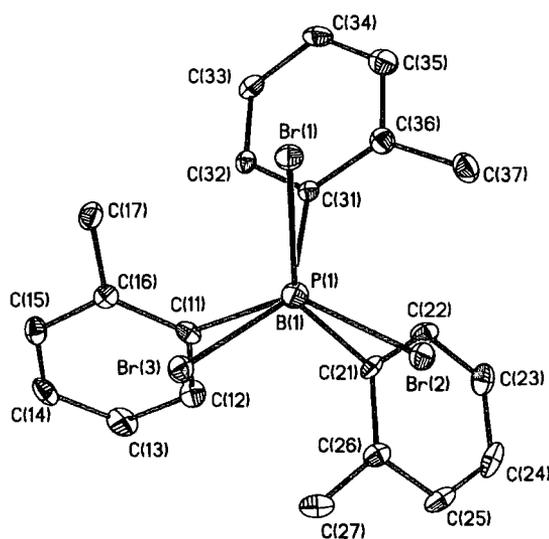
Figure 2.14: Molecular structure of (2jj), showing the atom labelling scheme. The thermal ellipsoids are plotted to 50% probability level. Hydrogen atoms are omitted for clarity.

Comparing the BBr_3-containing structures with the BCl_3 analogues reveals that changing from chlorine to bromine has little effect on the crystal or molecular structure. Although BBr_3 is a stronger Lewis acid, the B-P bond lengths are not significantly longer. B-Br distances are not affected by changing the phosphine moiety, in the same way as observed for the BCl_3 analogues.

2.3.3 Data correlations

Many authors have attempted to correlate the apparent strength of the B-P bond with various physical data. As the majority of crystal structures have only been reported here, it seems prudent to attempt correlations with the B-P bond length. There are several properties of phosphines that could provide a possible correlation with bond length. The data used in these correlations are shown below.

Table 2.12: Phosphine data used in the correlation study of the B-P adducts.

Compound	#	$^{31}P\{^1H\}$ NMR shift (ppm)	$^{31}P\{^1H\}$ NMR shift of oxide (ppm)	Tolman cone angle[46] (°)	Tolman 'electronic parameter' ν (cm^{-1})[46]	pK_a[52] of R_3PH^+
PMe_3	a	-61.5	36.2	118	2064.1	8.65
PEt_3	b	-21	48.3	132	2061.7	8.69
$P(^iPr)_3$	c	19.16	-	160	2059.2	-
$P(^nBu)_3$	d	-31.1	43.2	132	2060.3	8.43
$P(^tBu)_3$	e	61.5	-41	182	2056.1	11.40
PCy_3	f	10.9	50	170	2056.4	9.65[53]
PMe_2Ph	g	-45.4	34.3	122	2065.3	6.49[54]
$PMePh_2$	h	-27.5	-	136	2067.0	4.57
PPh_3	i	-4.3	29.3	145	2068.9	2.73
$P(o\text{-tolyl})_3$	j	-28.6	-	194	2066.6	3.08[46]
$P(C_6F_5)_3$	-	-73.8	-8.2	184	2090.9	-

The first property to be considered is the pK_a of HPR_3^+. A correlation would be predicted if the B-P bond is purely a σ-bond. If this is the case, it would be predicted that the B-P bond length will increase with decreasing pK_a values.[55] To test this hypothesis, a plot of pK_a of HPR_3^+ vs. B-P bond length was generated.
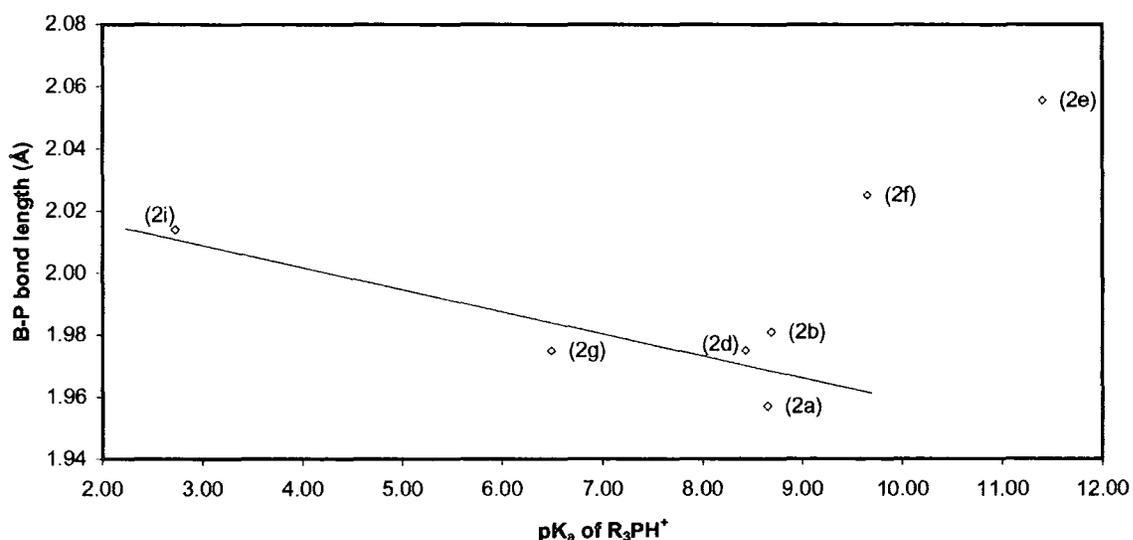
Graph 2.1: B-P bond lengths plotted against R_3PH^+ for adducts (2a) to (2g) and (2i).

We observe a general trend in the expected direction, but (2e) and (2f) are far from the expected locations. Whilst the two PR_3 ligands involved are certainly very basic, they are also the largest of the ligands so it seemed possible that steric factors could become much more important as the ligand bulk increases.

A plot of the same property, pK_a of HPR_3^+, against B-P bond lengths for the BBr_3 adducts is shown below. Although the correlation is not a very good one, the general trend towards decreasing B-P separation with increasing phosphine basicity is apparent even for the very large $P(o\text{-tolyl})_3$ in (2jj).
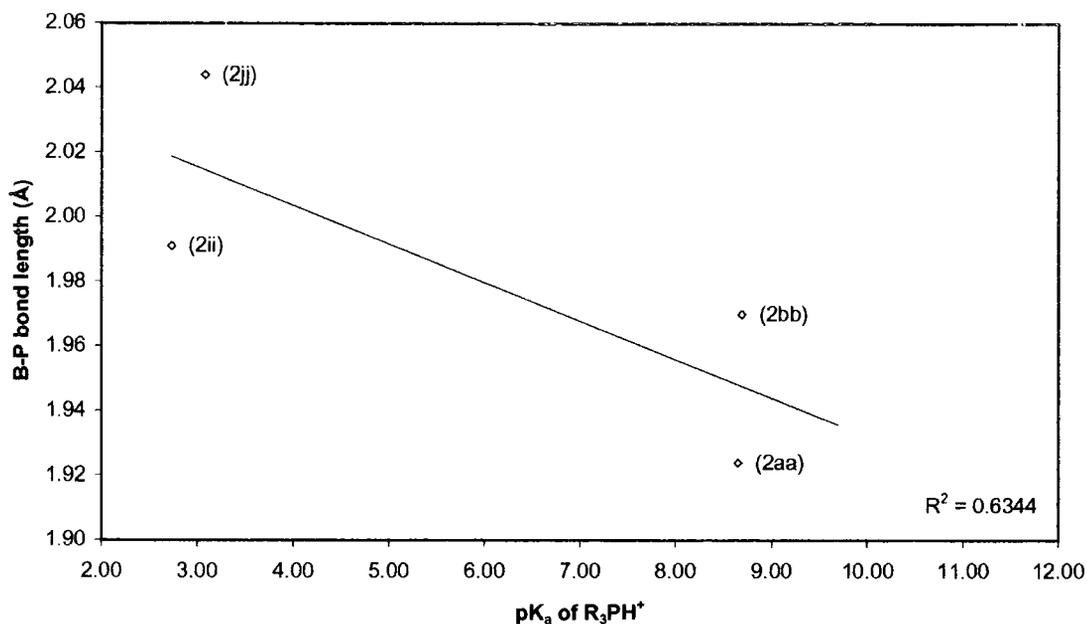
Graph 2.2: B-P bond lengths plotted against R_3PH^+ for adducts (2aa), (2bb), (2ii) and (2jj).

It is highly probable that steric factors affect the length of the B-P bond, thus for the next attempt at correlation we used a measure of the bulk of the phosphines, namely the Tolman cone angles.[46] A plot of PR_3 cone angles against B-P bond length is shown below for the BCl_3 adducts.
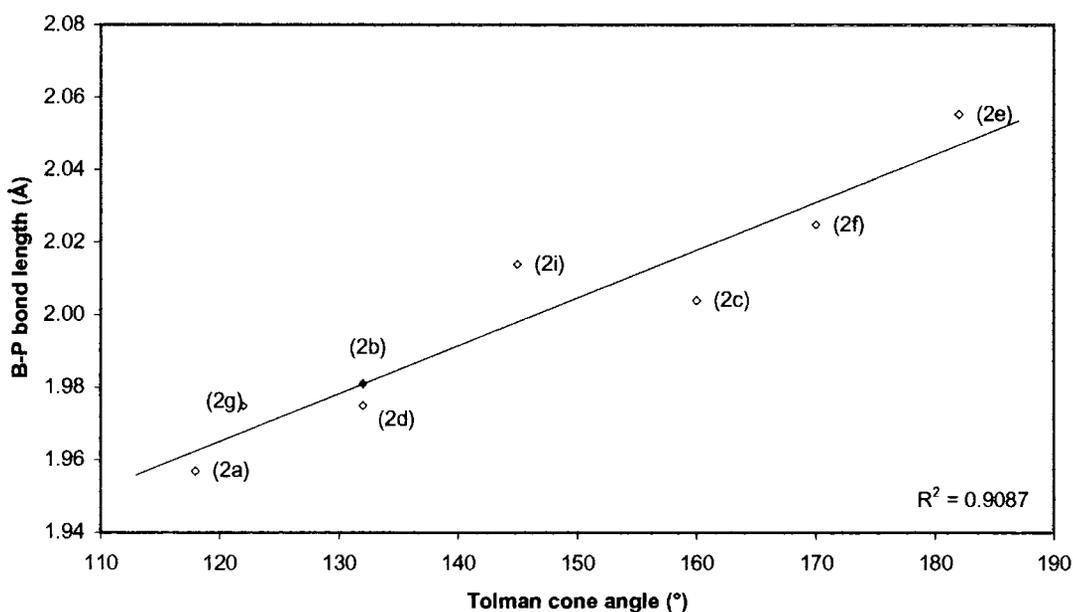
Graph 2.3: B-P bond lengths plotted against the Tolman cone angle for adducts (2a) to (2g) and (2i)

It can be seen that, to an extent, the larger the cone angle, the greater the B-P bond length (goodness-of-fit of the trendline, R^2, = 0.91). This is not unexpected, but again, the deviation of values away from a trendline implies that more than just sterics affect the B-P bond length. A similar plot for the BBr_3 adducts (shown below) shows that they fit slightly better to a trendline, however it must be remembered that there are fewer structures to consider for the BBr_3 adducts, thus care must be taken when drawing conclusions about the quality of the trend fits.
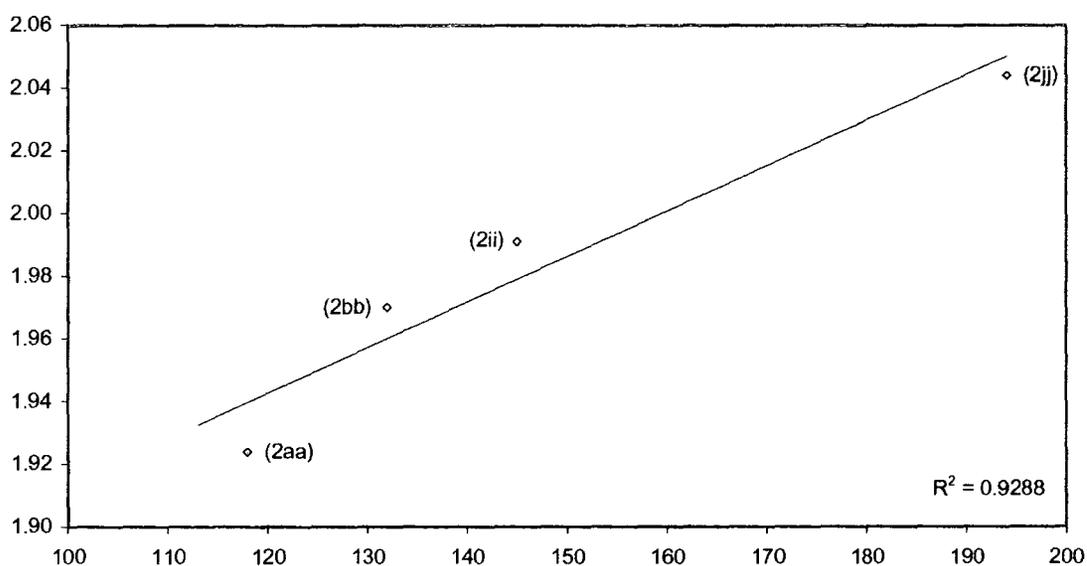
Graph 2.4: B-P bond lengths plotted against the Tolman cone angle for adducts (2aa), (2bb), (2ii) and (2jj).

Evidently, some kind of compromise between electronic (both σ- and π-interactions) and steric factors must be used if we are to obtain a reasonable correlation. We should be able to develop such a 2 parameter fit i.e. d_{B-P} = a(cone angle) + b(pK$_a$) where a and b will differ for BCl_3 vs. BBr_3.

Another characteristic of the adduct which reflects all these features of the phosphine is the ^{31}P chemical shift. On adduct formation, the ^{31}P resonance shifts from that of the

free phosphine, some moving to a higher and some to lower field. The extent of this change should reflect the degree of interaction between R_3P and BX_3. The plots for the BCl_3 and BBr_3 adducts are shown below.
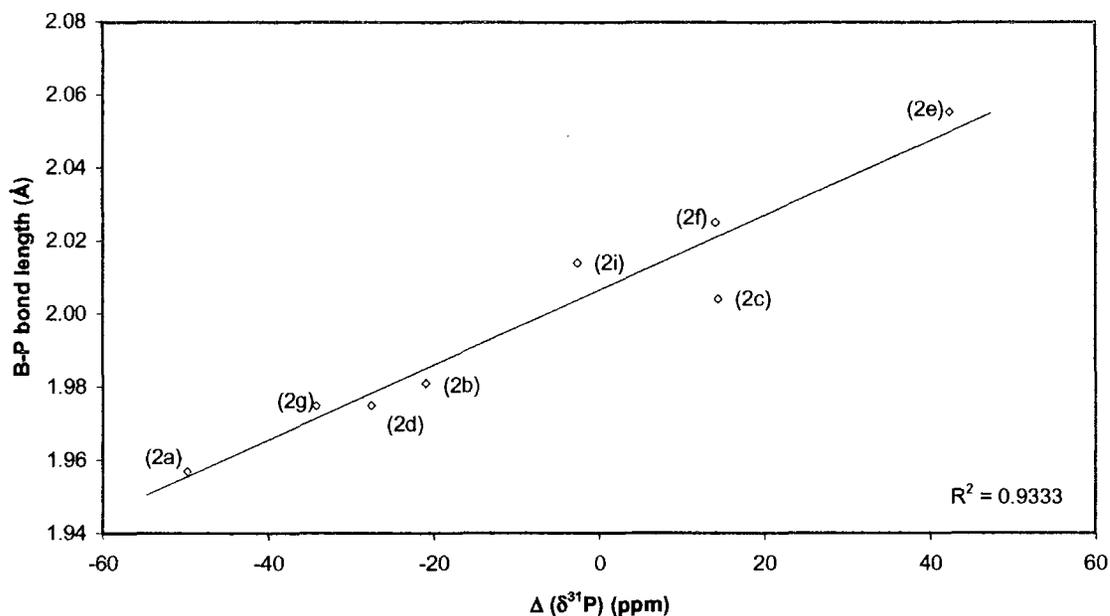
Graph 2.5: B-P bond lengths plotted against the difference in ^{31}P NMR shift between the adduct and the free phosphine for adducts (2a) to (2g) and (2i)
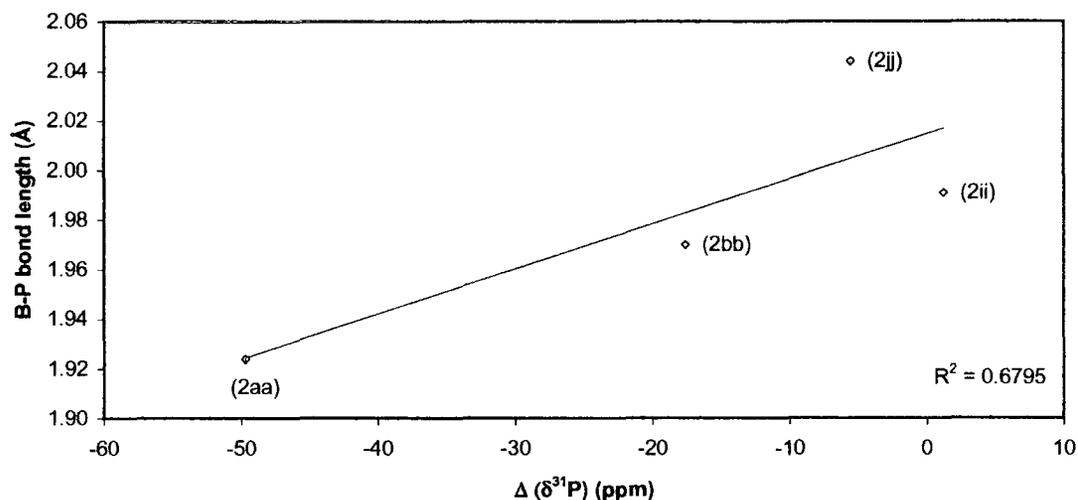
Graph 2.6: B-P bond lengths plotted against the difference in ^{31}P NMR shift between the adduct and the free phosphine for adducts (2aa), (2bb), (2ii) and (2jj).

There is indeed a good correlation for the BCl_3 adducts (goodness-of-fit, $R^2 = 0.93$). Again, the general trend is also observed for the BBr_3 adducts. On similar grounds, it might be expected that B-P bond length would correlate with ^{11}B-^{31}P coupling constant, as shown below (goodness of fit, $R^2 = 0.93$ for BCl_3 adducts and 0.98).
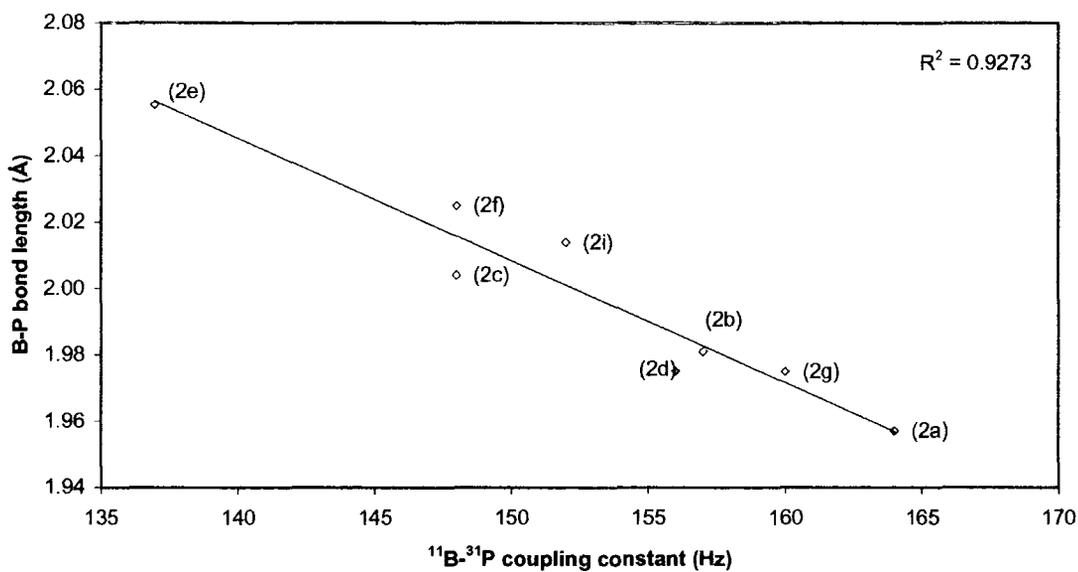
Graph 2.7: B-P bond lengths plotted against ^{11}B-^{31}P coupling constant for adducts (2a) to (2g) and (2i).
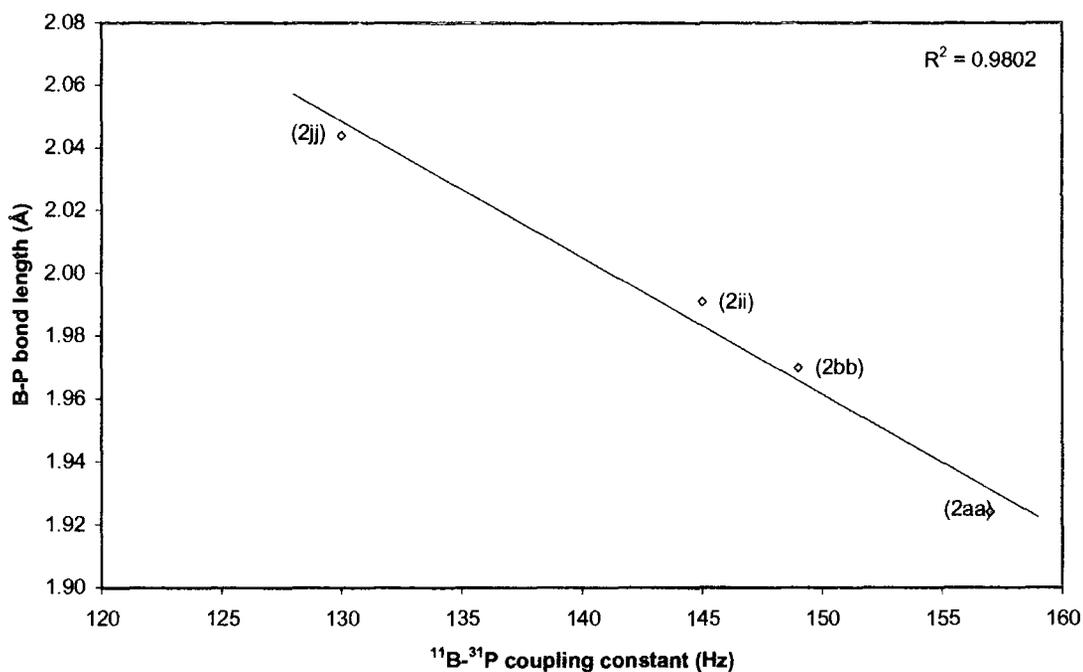
Graph 2.8: B-P bond lengths plotted against ^{11}B-^{31}P coupling constant for adducts (2aa), (2bb), (2ii) and (2jj).

Another interesting correlation can be seen when the smallest X-B-P-C torsion angle is plotted against the cone angle of the phosphine. Generally, the cone angle has little effect on the torsion angle, with most adducts having a Cl-B-P-C torsion angle between 35° and 45°. Exceptions to this are the adducts of the very small small cone angle phosphines PMe_3 and PMe_2Ph (adducts (2a) and (2g)), which have larger Cl-B-P-C torsion angles near 60°, and the very large cone angle phosphine PCy_3, which has a smaller Cl-B-P-C torsion angle of just 30°.
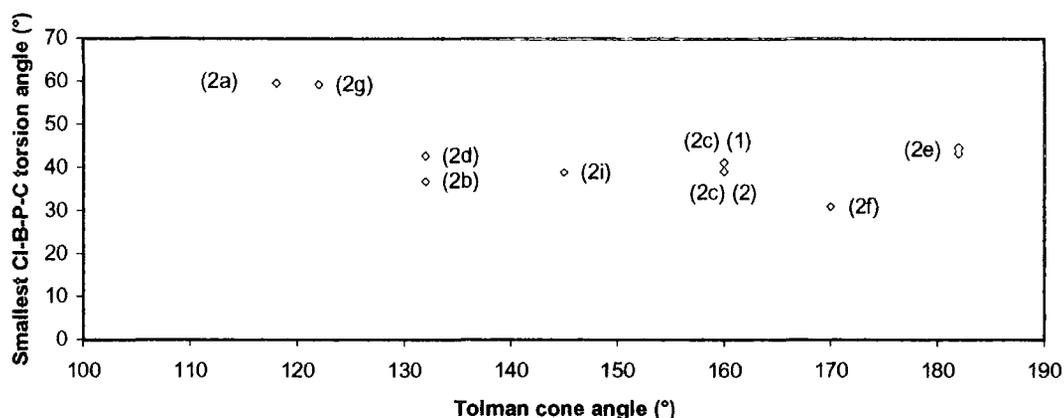
Graph 2.9: Tolman cone angle plotted against the smallest Cl-B-P-C torsion angle for adducts (2a) to (2g) and (2i)

Despite the small amount of data available for the analogous BBr_3 adducts, a similar trend can be seen. Adducts (2bb), (2ii) and $Br_3B \cdot P(^nPr)_3$ have very similar Br-B-P-C torsion angles, despite differences in cone angle. The adduct of PMe_3, however, which has a very small cone angle, has a much larger Br-B-P-C torsion angle of near 60°, as in the case of the BCl_3 analogue. Adduct (2jj), which contains $P(o\text{-tolyl})_3$, a phosphine with a very large cone angle, displays the smallest Br-B-P-C torsion angle of close to 10°.

It seems that for phosphine adducts with small cone angles, the molecule adopts a staggered formation, with a large X-B-P-C torsion angle, to minimise repulsions between phosphine alkyl groups and halogen atoms. When cone angle increases, the X-B-P-C torsion angle decreases to better accommodate the phosphine P-C bond whilst remaining in a partially staggered conformation.
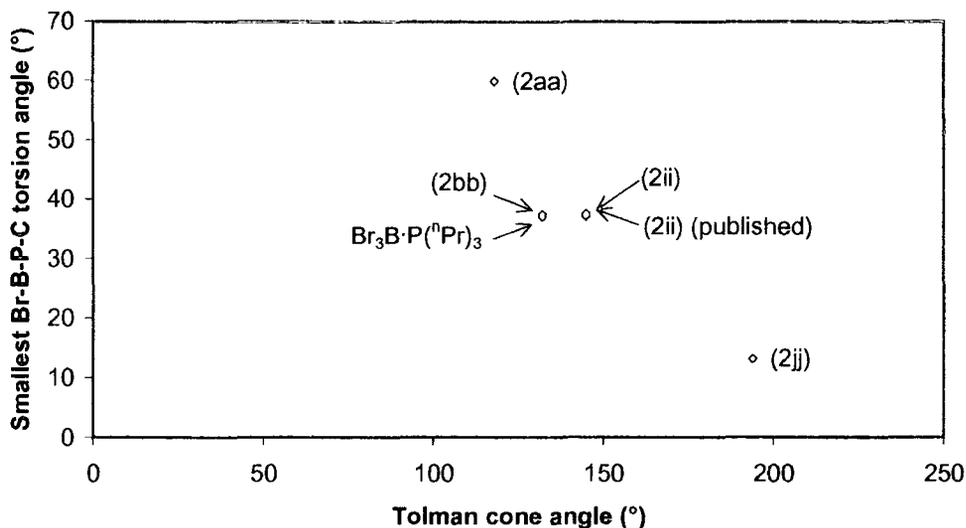
Graph 2.10: Tolman cone angle plotted against the smallest Cl-B-P-C torsion angle for adducts (2aa), (2bb), (2ii), $Br_3B \cdot P(^nPr)_3$ and (2jj)

When the phosphine cone angle is very large, for example in PCy_3 or $P(o\text{-tolyl})_3$, the X-B-P-C cone angle decreases dramatically, since any repulsions caused by adopting a non-staggered conformation of the P-C bond are presumably compensated for by creating more room for the bulky alkyl or aryl substituents, which occupy the staggered positions in preferences to the P-C bond.

2.4 Conclusion

We have presented for the first time an extensive study of a simple group of prototypical Lewis acid-Lewis base adducts, $X_3B \cdot PR_3$. Coupling phenomena between ^{11}B and ^{10}B nuclei with the ^{31}P nucleus have been investigated and dissociation of some species in solution that is visible by NMR has been noted. The chemical structures of new $X_3B \cdot PR_3$ compounds have been presented, along with a brief comparison to previously solved and published structures of a similar type. Data correlations have been attempted to achieve an *a priori* method for B-P bond length and bond strength prediction. Correlations of B-P bond length with phosphine cone angle look promising, as do correlations with pK_a. However, the correlations are not simple and many factors seem to influence the B-P bond distance and strength. It seems that a correlation with cone angle, with some kind of 'correction' for pK_a would probably give an excellent correlation, showing that the bond length is dependent upon base strength until a certain steric 'threshold', where cone angle begins to dictate over pK_a.

2.5 Related Work

During the studies on these adducts, two related compounds have been fortuitously isolated. The presence of adventitious water in solvent in an attempt to isolate $F_3B \cdot PPh_3$ led to the formation of a novel B_2O_2 ring system $\{[HPPh_3]^+\}_2[B_4F_{10}O_2]^{2-}$ (**2k**). Similarly, an attempt to prepare $Cl_3B \cdot P(o\text{-tolyl})_3$ led to the isolation of $[HP(o\text{-tolyl})_3]^+[BCl_4]^-$ (**2l**), the first crystallographically characterised example of the $[HP(o\text{-tolyl})_3]^+$ cation. The structures of these two compounds are discussed below.

2.5.1 $\{[HPPh_3]^+\}_2[B_4F_{10}O_2]^{2-}$: a discussion of B_2O_2 rings.

Attempts to grow single crystals of $F_3B \cdot PPh_3$ from slow diffusion of a dichloromethane solution into toluene led to the formation of colourless crystals of two different morphologies: needles and cubes. X-ray diffraction studies on the cubic-shaped crystals showed these to be $\{[Ph_3PH]^+\}_2[B_4O_2F_{10}]^{2-}$ (**2k**), whose anion contains an unusual B_2O_2 ring.

The novel dianion in the crystal of $\{[Ph_3PH]^+\}_2[B_4O_2F_{10}]^{2-}$ (**2k**), (shown in Figure 2.15) lies on a centre of inversion and thus the B_2O_2 ring is rigorously planar.
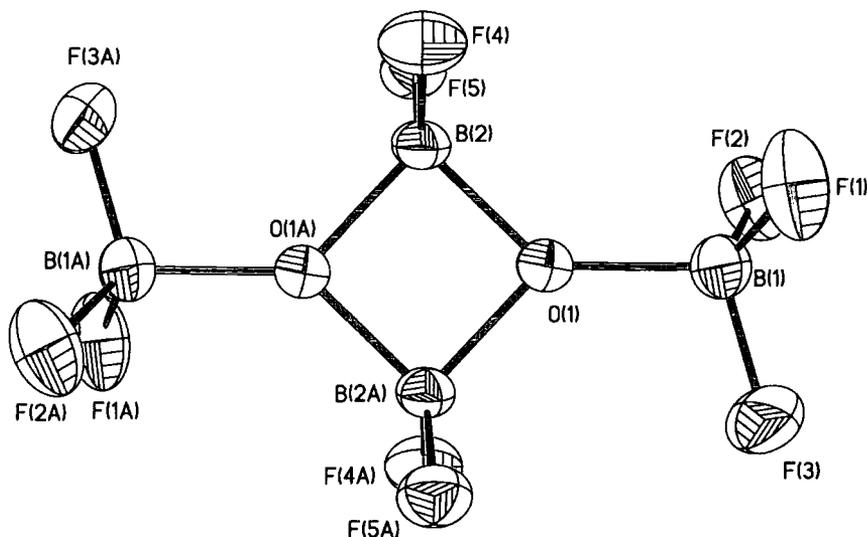
Figure 2.15: Structure of the $B_4O_2F_{10}^{2-}$ dianion in $\{[Ph_3PH]^+\}_2[B_4O_2F_{10}]^{2-}$ (2k) showing the atom numbering, plotted with 50% probability ellipsoids

The B-O bond distances in the ring are 1.498(2) Å and 1.505(2) Å. The ring is nearly square, with O-B-O and B-O-B internal angles of 88.8(1) and 91.2(1)° respectively. A BF_3 group is coordinated to each oxygen atom, with the B-O bond distance of 1.512(2) Å, and two fluorine atoms are bonded to each ring boron atom. The B-F bond distances in the BF_2 and BF_3 groups are very similar, averaging 1.362(3) and 1.374(5) Å respectively. Interestingly, the coordination about oxygen is trigonal planar with the sum of the angles being 359.9(2)°. A search of the CSD revealed that, of the nine known occurrences of three coordinate oxygen in a B_3O fragments, only the B_2O_2 rings have angles which sum very close to 360°. Crystallographic data is shown in Table 2.13, and selected bond lengths and angles are available in appendix A2k.

Table 2.13: Selected crystal data for $\{[Ph_3PH]^+\}_2[B_4O_2F_{10}]^{2-}$ (2k)

Compound	$\{[Ph_3PH]^+\}_2[B_4O_2F_{10}]^{2-}$
Formula	$C_{18}H_{16}B_2F_5OP$
Formula weight	395.90
Crystal System	monoclinic
Space Group	$P2_1/n$
a / Å	11.638(3)
b / Å	12.174(3)
c / Å	13.542(3)
α / °	90
β / °	93.688(3)
γ / °	90
U / Å^3	1914.6(8)
Z	4
D_c / g cm^{-3}	1.373
μ / mm^{-1}	0.194
Temperature (K)	150(2)
F(000)	808
Crystal Size / mm	0.34 x 0.22 x 0.18

X-ray diffraction data were collected for the needle shaped crystals, but would not solve satisfactorily. The uncertainties in the symmetry and the inherent weakness of the data is reflected in a large R_1 value of 20%, but this model (see Figure 2.16) is still substantial evidence for the formation of $[HPPh_3]^+[BF_4]^-$. The $\{[Ph_3PH]^+\}_2[B_4O_2F_{10}]^{2-}$ (2k) salt apparently results from hydrolysis of $F_3B\cdot PPh_3$ due to traces of adventitious water. Attempts to prepare $\{[Ph_3PH]^+\}_2[B_4O_2F_{10}]^{2-}$ (2k) and $[HPPh_3]^+[BF_4]^-$ by stoichiometric addition of water in C_6D_6 solution led to a complex mixture of products when analysed by in situ ^{11}B NMR spectroscopy.
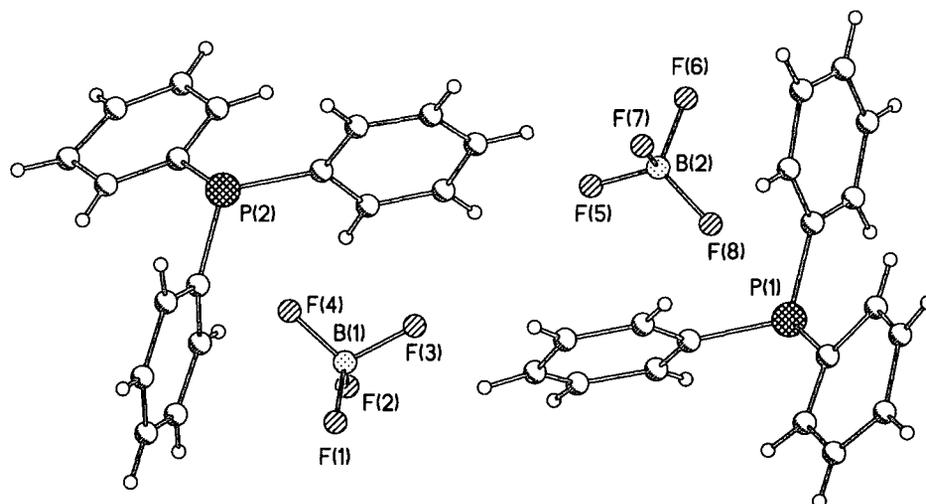
Figure 2.16: Isotropic possible solution for the needle shaped crystals which formed with those of {[Ph₃PH]⁺}₂[B₄O₂F₁₀]²⁻. It is plausible that they are [HPPh₃]⁺[BF₄]⁻ as shown, but the refinement was far from satisfactory.

If [HPPh₃]⁺[BF₄]⁻ does form, however, it is possible that the hydrolysis reaction in the presence of minute traces of water proceeds as shown below.

$$6\ Ph_3P{\cdot}BF_3 + 2H_2O \rightarrow 2[Ph_3PH]^+[BF_4]^- + [Ph_3PH]_2^+[B_4O_2F_{10}]^{2-} + 2PPh_3$$

Equation 2.1

Although fluoroborates with rings containing five or more atoms are known,[56,57] the dianion in {[Ph₃PH]⁺}₂[B₄O₂F₁₀]²⁻ (**2k**) represents the only structurally well-characterised discrete ring consisting solely of boron, fluorine and oxygen atoms. Unlike the common six-membered rings containing alternating boron and oxygen,[58] and four-membered rings containing alternating aluminium and oxygen,[59] only four crystal structures containing four-membered B₂O₂ rings have been reported.[60] Three of the structurally characterised compounds contain three coordinate oxygen atoms. The first two, the porphyrin complex, [B₂O₂(BCl₃)₂(T*p*Cl*pp*)] (T*p*Cl*pp* = dianion of 5,10,15,20-

tetra-*p*-chlorophenyl-porphyrin)[61] and [Me$_2$B-O-BMe$_2$]$_2$ (shown in Figure 2.18), [62] contain trigonal planar oxygens in the B$_2$O$_2$ ring.
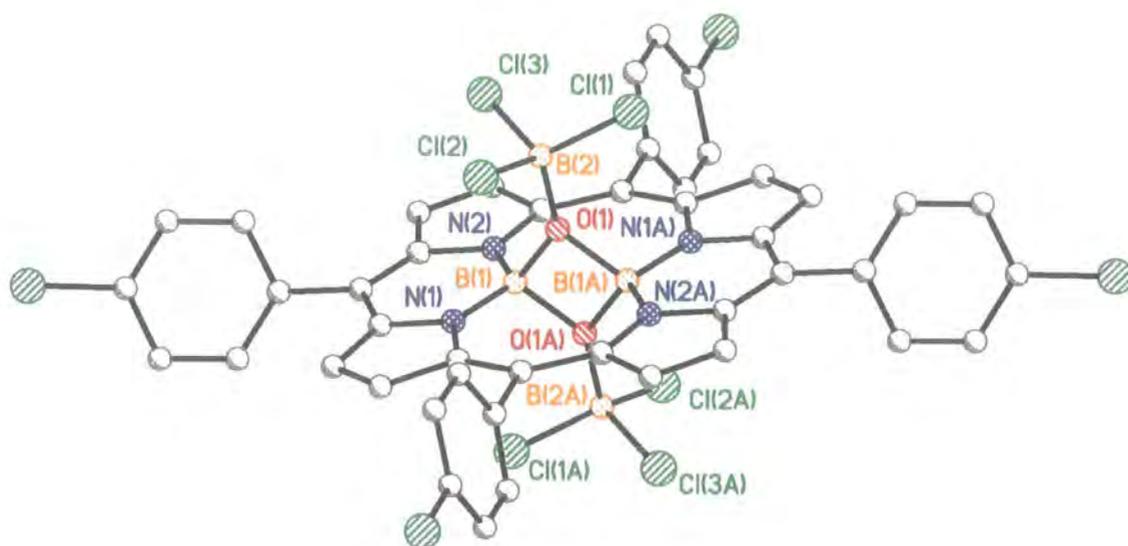
Figure 2.17: Diagram of [B$_2$O$_2$(BCl$_3$)$_2$(T*p*Cl*pp*)] (T*p*Cl*pp* = dianion of 5,10,15,20-tetra-*p*-chlorophenyl-porphyrin). Atoms are shown as spheres of arbitrary radius. Hydrogen atoms have been omitted for clarity.
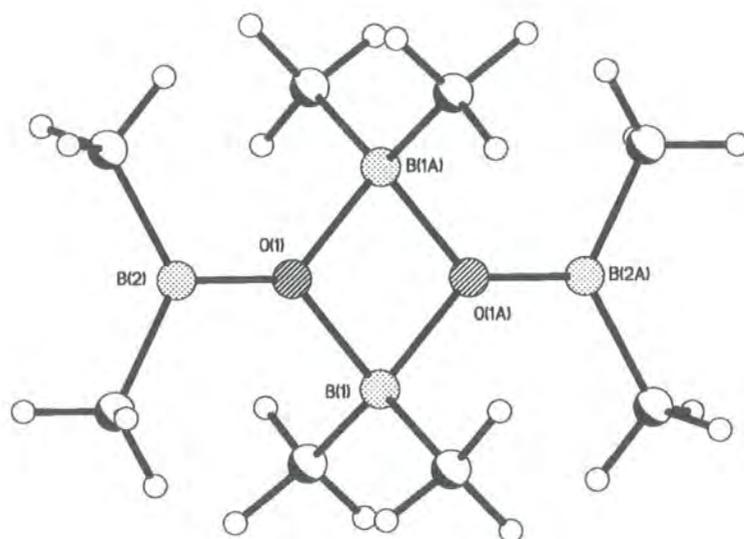
Figure 2.18: Diagram of bis(tetramethyl)diboroxane. Atoms are shown as spheres of arbitrary radius.

The third structure does not have a trigonal planar oxygen atom, although it is three coordinate. [63] A diagram of the molecule, 4-oxa-3-borahomoadamantane dimer, is shown below.
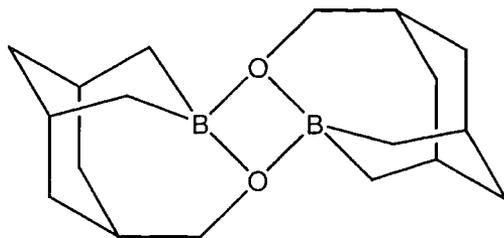
Figure 2.19: Diagram of 4-oxa-3-borahomoadamantane dimer.

The internal B-O bond lengths in the porphyrin-trapped structure from Brothers *et al.* are very similar to those in $\{[Ph_3PH]^+\}_2[B_4O_2F_{10}]^{2-}$ (**2k**). The authors noted that the B-O bond lengths were the shortest reported and that this could be a result of the constraints of complexation within the bulky porphyrin. The similarity of the B-O bond distances with $\{[Ph_3PH]^+\}_2[B_4O_2F_{10}]^{2-}$ would, however, imply that the porphyrin ring is not responsible for the phenomenon. It may, however, affect the internal angles of the B_2O_2 ring since the O-B-O angle (91.154°) is less acute than the angle in $\{[Ph_3PH]^+\}_2[B_4O_2F_{10}]^{2-}$ (88.82(12)°), and the ring is therefore "squashed" in the other direction. The explanation for the trigonal planar oxygen in this compound was also attributed to the bulk of the porphyrin, but since our non-bulky $\{[Ph_3PH]^+\}_2[B_4O_2F_{10}]^{2-}$ is similarly planar, this is not a true explanation for the effect. The neutral B_2O_2 ring system $[Me_2B-O-BMe_2]_2$ from Vahrenkamp *et al.* also displays a trigonal planar oxygen but is not excessively bulky.

Another example of a B_2O_2 ring has been reported by Nöth *et al.*[64] The structure of 2,4-bis(2,2,6,6-tetramethylpiperidino)-1,2,3,4-dioxadiboretane, an elegant molecule, is dissimilar to the structures shown above in that the oxygen is 2-coordinate.
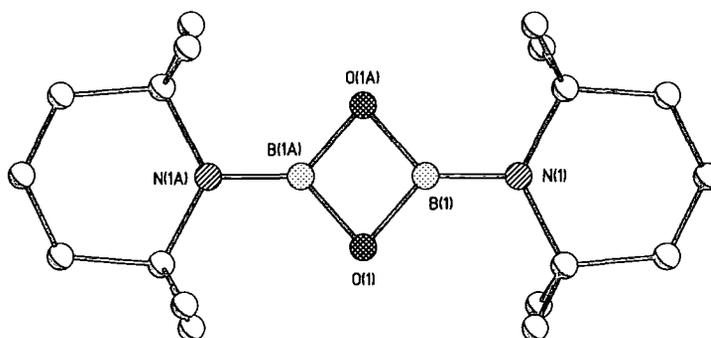
Figure 2.20: Diagram of 2,4-bis(2,2,6,6-tetramethylpiperidino)-1,2,3,4-dioxadiboretane. Atoms are shown as spheres of arbitrary radius. Hydrogen atoms have been omitted for clarity.

A further example of trigonal planar oxygen was recently described by the group of Schröder[65] in a complex with alkoxide bridging between BF_3 and a copper atom. In $\{C_6F_4\text{-}1,2\text{-}[B(C_6F_5)_2]_2(\mu\text{-OR})\}^-$ (R = CH_3, C_6F_5), it was suggested[66] that the planar geometry about the oxygen could be due either to the bulky groups about O, or to the bite angle of the bidentate moiety coordinated to it.

The dianion $B_4O_2F_{10}^{2-}$ in $\{[Ph_3PH]^+\}_2[B_4O_2F_{10}]^{2-}$ (**2k**) is simple and elegant with only 16 atoms, making it ideal for theoretical studies. Extended Hückel and *ab initio* MO calculations were carried out[67] on the dianion (disregarding the two phosphine counter cations) to gain insight into the bonding within the ring and the geometrical preference at oxygen in $[B_4O_2F_{10}]^{2-}$. EHMO calculations[68] were performed on both the dianion $B_4O_2F_{10}^{2-}$ and the $B_2O_2F_4^{2-}$ fragment, and the resulting energy level diagram is shown in Figure 2.21, along with plots of the frontier orbitals of the $B_2O_2F_4^{2-}$ fragment; lower lying orbitals include the B-F bonds, fluorine p-electrons and the oxygen and boron s-orbitals. The bonding in the $B_2O_2F_4^{2-}$ square can be seen to arise from the B-O σ bonds in HOMO-3 and HOMO-4. The in- and out-of-plane combinations of the other oxygen p-orbitals produce the four remaining orbitals shown for the $B_2O_2F_4$ fragment in Figure 2.21; from the HOMO downwards these are O-O σ*, π*, π, σ. The Lewis basicity of the

$B_2O_2F_4^{2-}$ square arises from the in-plane HOMO and HOMO-5 which overlap with the out-of-phase and in-phase combinations of BF_3 acceptor orbitals in the $B_4O_2F_{10}^{2-}$ dianion. The O-O π^* and π orbitals are not involved in bonding to the BF_3 groups. The fact that O-O σ^* is the $B_2O_2F_4^{2-}$ HOMO is thus likely responsible for the observed trigonal planar coordination at oxygen.
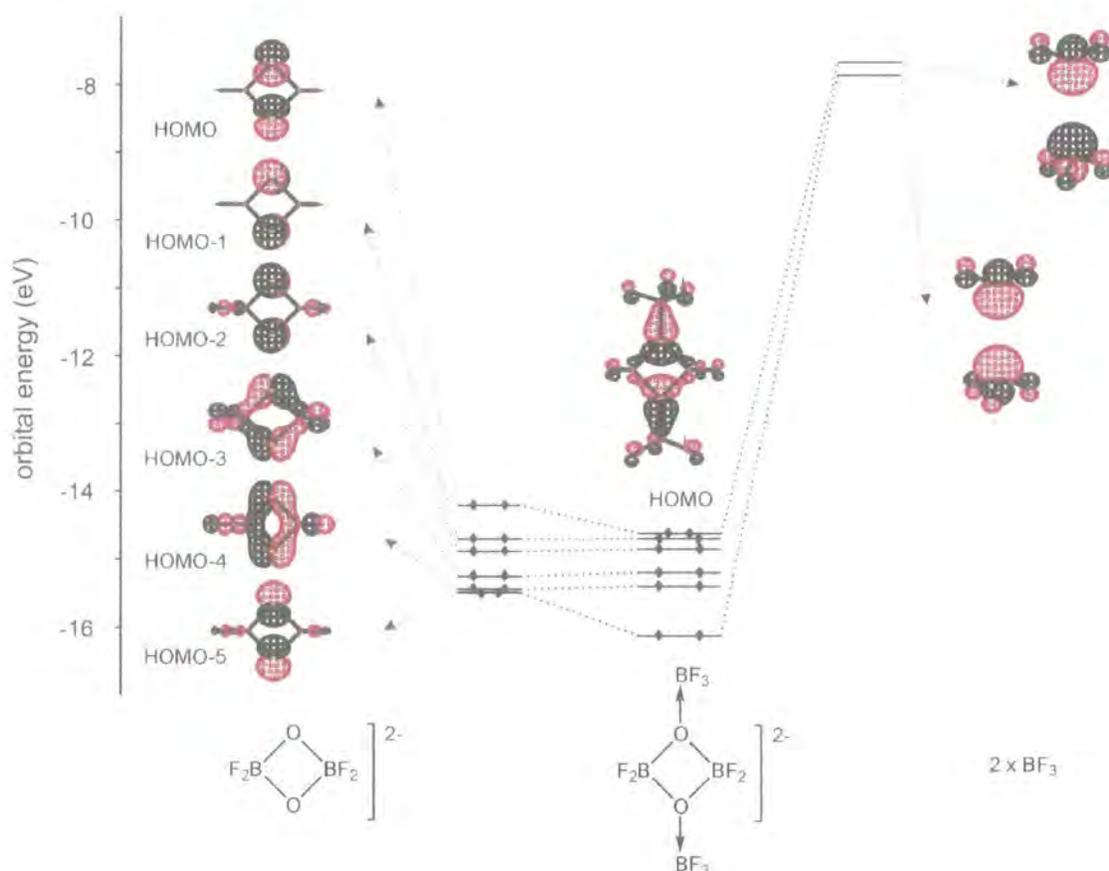
Figure 2.21: Extended Hückel molecular orbital interaction diagram[69] for the $B_4O_2F_{10}^{2-}$ anion in $\{[Ph_3PH]^+\}_2[B_4O_2F_{10}]^{2-}$ (2k).

Ab initio MO calculations (GAUSSIAN94)[70] on the $B_2O_2F_4^{2-}$ fragment at the MP2/6-31G* level of theory revealed the energies of the frontier orbitals to be in the same order as in Figure 2.21 with the O-O σ^* and σ orbitals (HOMO and HOMO-5) significantly lower in relative energies. On coordinating two BF_3 groups to $B_2O_2F_4^{2-}$ to generate $[B_4O_2F_{10}]^{2-}$, the O-O σ and σ^* orbitals provide the electrons used in O-BF_3 bonding and are significantly lowered in energy; as a result the unperturbed O-O π^* and π orbitals

become HOMO and HOMO-1 respectively. Geometry optimisation of the dianion $B_4O_2F_{10}^{2-}$ in (2k) at MP2/6-31G* revealed a minimum virtually identical to that found experimentally with O-B-O and B-O-B internal angles of 89.1° and 90.9° respectively. However, geometry optimisation of the discrete fragment $B_2O_2F_4^{2-}$, resulted in a minimum with O-B-O and B-O-B internal angles of 97.5° and 82.5° respectively, and the O-O π* orbital as the HOMO. Thus, coordination of the two BF$_3$ Lewis acids to the in-plane oxygen orbitals stabilises the strongly antibonding O-O σ* level without the need for significant lengthening of the O-O separation via distortion of the B_2O_2 square.

Alternative structures involving pyramidalisation at each oxygen atom can be accounted for by a mixing of the oxygen in- and out-of-plane orbitals (HOMO/HOMO-1 and HOMO-2/HOMO-5) to generate donor orbitals in either *cisoid* or *transoid* arrangements. These have been examined through qualitative Walsh diagrams (Figure 2.22) with the observed structure at the energy minimum.
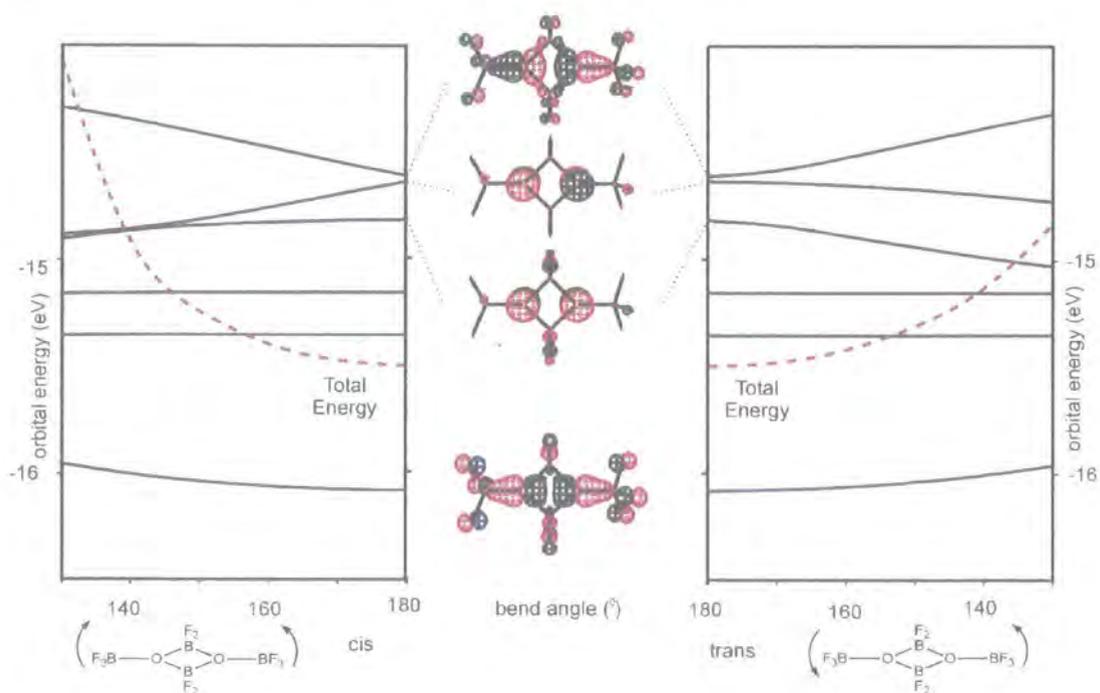
Figure 2.22: Walsh diagrams[54] for pyramidalisation at oxygen in the $B_4O_2F_{10}^{2-}$ dianion, calculated at the extended Hückel level. Total energies (in eV): planar, -2229.245; 130° trans, -2228.578; 130° cis, -2227.807.

Clearly, B_2O_2 rings are inherently destabilised by 4 electron interactions of both σ- and

π-symmetry between the oxygen atoms. Stable systems can be formed by complexation

of Lewis acids such as BX_3, or, in the case of Al_2O_2 systems, by increasing the

separation between the oxygen centres.

2.5.2 [HP(o-tolyl)₃]⁺[BCl₄]⁻: the first crystallographically characterised example of the [HP(o-tolyl)₃]⁺ cation.

Attempts[71] to grow high-quality single crystals of $Cl_3B \cdot P(o\text{-tolyl})_3$ by slow diffusion of

dichloromethane solution into hexane led to characterization by X-ray diffraction of the

hydrolysis product $[HP(o\text{-tolyl})_3]^+[BCl_4]^-$ (**2I**). The formation of this hydrolysis product

is assumed to be due to the presence of adventitious water in the dichloromethane

solvent, leading to the formation of HCl on reaction with BCl_3, with the acid going on

to form the title compound.

The structure contains the first crystallographically characterised example of the tri-(o-

tolyl)-phosphonium ion, which is shown below.

The average P-C bond length in this molecule of 1.7985(18) Å is *ca.* 2% shorter than

that in $P(o\text{-tolyl})_3$ (P-C (average) = 1.836 Å)[72] and the C-P-C bond angle of 110.69(14)°

is greater than in the parent phosphine (C-P-C (average)= 102.8(2)°).
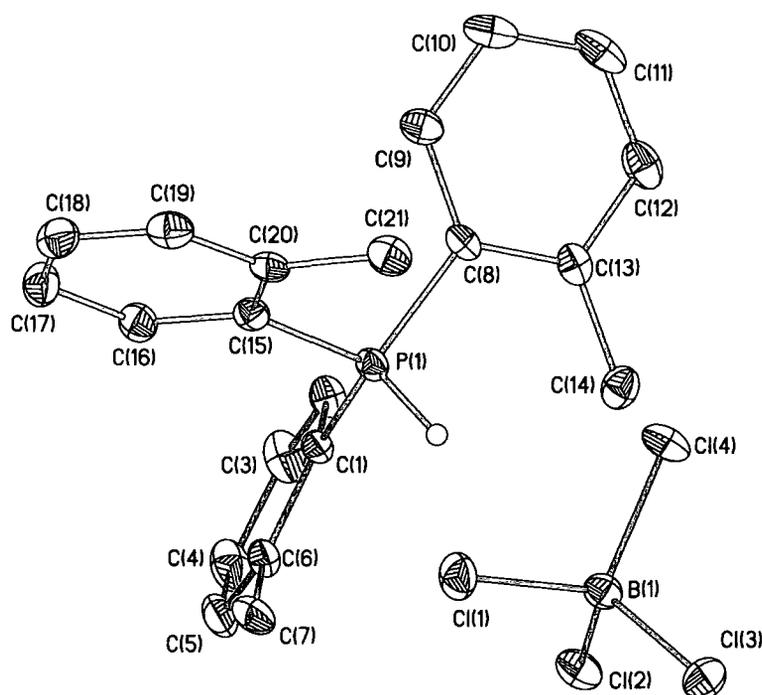
Figure 2.23: Molecular structure of [HP(o-tolyl)₃]⁺[BCl₄]⁻ (2l) with ellipsoids at 50% probability. Hydrogen atoms on the o-tolyl substituents have been omitted for clarity.

The cation has a near-tetrahedral phosphorus atom (C-P-C angles $111.09(9)°$, $109.90(8)°$ and $111.07(8)°$) and the BCl_4^- anion is near-tetrahedral at boron (Cl-B-Cl angles range from $108.78(11)°$ to $110.40(11)°$). There are no unusually short cation-anion contacts. The librational corrections to the title structure at 100K were small and the comparisons of its molecular parameters with published structures remain valid.

A search of the Cambridge Structural Database[73] for related $HPPh_3$ cations reveals that there are 11 such structures known. The average P-C bond length is 1.788 Å, less than 1% shorter than for the HP(o-tolyl)₃ cation. This value would be expected to be shorter because the latter has greater steric hindrance about this bond due to the extra methyl groups on the phenyl rings, but the difference is minimal. The overall range of this P-C bond length in the triphenylphosphonium cation is 1.753 Å to 1.849 Å, presumably displaying a dependence on the counter ion present. The example with the shortest

average P-C bond length[74] (1.769 Å) contained the $PrCl_6^-$ anion, and the structure displaying the largest average P-C bond length[75] (1.809 Å) contained the $CdBr_4^{2-}$ dianion. The bond angle data display few differences, with the average triphenylphosphonium ion C-P-C bond angle of $110.62°$ being identical within experimental error to the value of $110.69(14)°$ for the tri(o-tolyl)phosphonium ion. The tetrachloroborate anion shows weak interactions from three of the chlorine atoms to three different methyl group hydrogen atoms of the cation, with donor···acceptor distances ranging from 3.59 to 3.76 Å and D-H···A angles from 136 to 171°. There is no evidence for the hydrogen atom H(1) of the phosphonium cation to be involved in H-bonding.

2.6 Experimental

2.6.1 General Procedures

Air sensitive compounds were manipulated in a nitrogen atmosphere using Schlenk techniques or an Innovative Technology, Inc. System 1 glove box. Glassware was dried in an oven before transfer into the glove box. NMR spectra were recorded on Varian Mercury 200 (^{1}H, ^{13}C, ^{19}F, ^{31}P), Bruker AM-250 (^{1}H, ^{13}C, ^{31}P), Varian Unity 300 (^{1}H, ^{13}C, ^{11}B), and Varian Unity Innova 500 (^{1}H, ^{11}B) instruments. Proton NMR spectra were referenced to external SiMe$_4$ via residual protons in the deuterated solvents, ^{11}B, ^{19}F, and ^{31}P shifts were referenced to external BF$_3$·OEt$_2$, CCl$_3$F and 85% H$_3$PO$_4$ respectively. Variable temperature ^{31}P NMR experiments were conducted on a Varian VXR-400 instrument. Chemical shifts are reported in ppm and coupling constants in Hz. Multiplicities are reported as (s) singlet, (d) doublet, (t) triplet, (q) quartet and (m) multiplet. Elemental analyses were conducted in the Department of Chemistry at the University of Durham using an Exeter Analytical Inc. CE-440 Elemental Analyzer. Mass spectra were run in the Department of Chemistry at the University of Durham on a Micromass Autospec machine with EI ionisation. Toluene was dried and deoxygenated by passage through columns of activated alumina and BASF-R311 catalyst under argon pressure using a modified version of the Innovative Technology, Inc. SPS-400 solvent purification system.[76] Chloroform and CDCl$_3$ were dried over calcium hydride, C$_6$D$_6$ was dried over potassium metal, and hexane was dried over sodium. All were distilled under nitrogen before use. Phosphines were purchased from Aldrich and Strem and were checked for purity by ^{31}P{^{1}H} NMR before use.

2.6.2 Synthesis

Synthesis of $Cl_3B \cdot PMe_3$ (2a). A solution of PMe_3 (0.078 g, 1.03 mmol) in hexane (5 cm^3) was added dropwise to 1.0M BCl_3 in heptane (1.5 cm^3, 1.5 mmol). A white solid formed immediately. After standing overnight, the solid was isolated by filtration, washed with hexane (3 x 2 cm^3) and dried *in vacuo* yielding 0.159 g of (2a) as a white powder (80%). NMR (C_6D_6): ^1H δ 0.58 (d, $^2J_{H-P}$ = 12 Hz), $^{11}B\{^1H\}$ δ 3.0 (d, J_{B-P} = 164 Hz), $^{13}C\{^1H\}$ δ 4.8 (d, J_{C-P} = 44 Hz), $^{31}P\{^1H\}$ δ -11.73 (q, J^{11}_{B-P} = 164 Hz, $^{11}B \cdot P$), -11.74 (septet, J^{10}_{B-P} = 55 Hz, $^{10}B \cdot P$). (Found: C, 18.49; H 4.70%. Calculated for $C_3H_9BCl_3P$: C, 18.65; H, 4.69%).

Synthesis of $Cl_3B \cdot PEt_3$ (2b). A solution of PEt_3 (0.035 g, 0.296 mmol) in hexane (8 cm^3) was added dropwise to 1.0M BCl_3 in heptane (0.45 cm^3, 0.45 mmol). A white solid formed immediately. After standing overnight, ~75% of the solvent was removed *in vacuo*. The product was isolated by filtration, washed with cold hexane (2 x 2 cm^3) and dried *in vacuo* yielding 0.045 g of (2b) as fine white needles (64%). NMR (C_6D_6): ^1H δ 0.66 (m, CH_2CH_3), 1.26 (m, CH_2CH_3), $^{11}B\{^1H\}$ δ 3.0 (d, J_{B-P} = 155 Hz), $^{31}P\{^1H\}$ δ -0.05 (q, J^{11}_{B-P} = 157 Hz, $^{11}B \cdot P$), -0.05 (septet, J^{10}_{B-P} = 52 Hz, $^{10}B \cdot P$). (Found: C, H %. Calculated for $C_6H_{15}BBr_3P$: C, 30.62; H, 6.42%).

Synthesis of $Cl_3B \cdot P(^iPr)_3$ (2c). A solution of $P(^iPr)_3$ (0.47 g, 0.293 mmol) in hexane (5 cm^3) was added dropwise to 1.0M BCl_3 in heptane (0.45 cm^3, 0.45 mmol) in hexane (3 cm^3). The reaction mixture turned cloudy instantly, and a fine white precipitate formed. After stirring overnight 75% of the solvent was removed *in vacuo* and the reaction mixture was cooled to –30 °C. The product was isolated by filtration, washed with cold hexane (2 x 2 cm^3) and dried *in vacuo* yielding 0.057 g of (2c) as a white powder

(70%). NMR (C$_6$D$_6$): ^{1}H δ 0.97 (m, C(CH$_3$)$_3$), 2.21 (septet, CH(Me)$_3$), ^{11}B{^{1}H} δ 3.7 (d,

J$_{B-P}$ = 147 Hz)) ^{31}P{^{1}H} δ 4.75 (q, J^{11}$_{B-P}$ = 148 Hz, ^{11}B·P), 4.75 (septet, J^{10}$_{B-P}$ = 50 Hz,

^{10}B·P). (Found: C, 38.82; H, 7.71%. Calculated for C$_9$H$_{21}$BCl$_3$P: C, 38.97; H, 7.63%).

Synthesis of Cl$_3$B·P(^{n}Bu)$_3$ (2d). A solution of P(^{n}Bu)$_3$ (0.099 g, 0.49 mmol) in hexane

(4 cm^3) was added dropwise to 1.0M BCl$_3$ in heptane (0.75 cm^3, 0.75 mmol). A white

solid formed immediately. After standing overnight, the solid was isolated by filtration,

washed with hexane (3 x 2 cm^3) and dried *in vacuo*, yielding 0.130 g of (2d) as a white

powder (83%). NMR (C$_6$D$_6$) ^{1}H δ 0.74 (t, 3H, J$_{H-H}$ = 7 Hz, CH$_2$CH$_2$CH$_2$CH$_3$), 1.08 (q of

t, 2H, J$_{H-H}$ = 7 Hz, 6 Hz, CH$_2$CH$_2$CH$_2$CH$_3$), 1.34 (m, 2H, CH$_2$CH$_2$CH$_2$CH$_3$), 1.58 (m,

2H, CH$_2$CH$_2$CH$_2$CH$_3$), ^{11}B{^{1}H} δ 3.2 (d, J$_{B-P}$ = 155 Hz), ^{13}C{^{1}H} δ 24.4 (d, J$_{C-P}$ = 3

Hz), 24.3 (d, J$_{C-P}$ = 5.5 Hz), 18.2 (d, J$_{C-P}$ = 22 Hz), 13.3 (s), ^{31}P{^{1}H} δ -3.56 (q, J^{11}$_{B-P}$ =

156 Hz, ^{11}B·P), -3.56 (septet, J^{10}$_{B-P}$ = 51 Hz, ^{10}B·P). (Found: C, 45.13; H, 8.66%.

Calculated for C$_{12}$H$_{27}$BCl$_3$P: C, 45.11; H, 8.52%).

Synthesis of Cl$_3$B·P(^{t}Bu)$_3$ (2e). A solution of P(^{t}Bu)$_3$ (0.061 g, 0.302 mmol) in hexane

(5 cm^3) was added dropwise to 1.0M BCl$_3$ in heptane (0.45 cm^3, 0.45 mmol). The

solution turned cloudy, and a white precipitate formed. After stirring overnight, and

then cooling to −30 °C, the product was isolated by filtration, washed with hexane (2 x 2

cm^3) and dried *in vacuo* yielding 0.072 g of (2e) as a white powder (75%). NMR (C$_6$D$_6$)

^{11}B{^{1}H} δ 5.2 (d, J$_{B-P}$ = 138 Hz), ^{31}P{^{1}H} δ 19.14 (q, J^{11}$_{B-P}$ = 137 Hz, Cl$_3$B·P(^{t}Bu)$_3$),

19.14 (septet, J^{10}$_{B-P}$ = 46 Hz, Cl$_3$B·P(^{t}Bu)$_3$) . (Found: C 43.39, H 8.38%. Calculated for

C$_{12}$H$_{27}$BCl$_3$P: C, 45.11%; H, 8.52%).

Synthesis of Cl₃B·PCy₃ (2f). A solution of PCy₃ (0.140 g, 0.50 mmol) in hexane (10 cm³) was added dropwise to a 1.0M BCl₃ in heptane (0.75 cm³, 0.75 mmol). A fine white solid precipitated immediately. After standing for 2 h, the solid was isolated by filtration and dried *in vacuo*, yielding 0.188 g of (**2f**) as a white powder (95%). NMR (C₆D₆) ^{1}H δ 1.00 (m, 3H), 1.49 (m, 5H), 2.08 (m, 2H), 2.38 (m, 1H), ^{11}B{^{1}H} δ 3.90 (d, J_{B-P} = 150 Hz), ^{31}P{^{1}H} δ -3.16 (q, J^{11}_{B-P} = 148 Hz ^{11}B·P), -3.16 (septet, J^{10}_{B-P} = 48 Hz, ^{10}B·P). (Found: C, 54.02; H, 8.53%. Calculated for C₁₈H₃₃BCl₃P: C, 54.37; H, 8.37%).

Synthesis of Cl₃B·PMe₂Ph (2g). A solution of PMe₂Ph (0.138 g, 1.00 mmol) in hexane (4 cm³) was added dropwise to 1.0M BCl₃ in heptane (1.5 cm³, 1.5 mmol). A white solid formed immediately. After shaking and standing overnight, the product was isolated by filtration and dried *in vacuo*, yielding 0.188 g of (**2g**) as a white powder (74%). NMR (C₆D₆) ^{1}H δ 7.29 (m, 2H, Ph), 6.94 (m, 3H Ph), 1.02 (d, 6H J_{H-P} = 12 Hz, Me), ^{11}B{^{1}H} δ 3.40 (d, J_{B-P} = 161 Hz), ^{13}C{^{1}H} δ 132.1 (d, J_{C-P} = 3 Hz, Ph), 131.8 (d, J_{C-P} = 8 Hz, Ph), 128.8 (d, J_{C-P} = 11 Hz, Ph), 126.7 (d, J_{C-P} = 20 Hz, Ph), 5.2 (d, J_{C-P} = 44 Hz, Me), ^{31}P{^{1}H} δ -11.19 (q, J^{11}_{B-P} = 160 Hz, ^{11}B·P), -11.20 (septet, J^{10}_{B-P} = 53 Hz, ^{10}B·P). (Found: C, 37.58; H, 4.35%. Calculated for C₈H₁₁BCl₃P: C, 37.63; H, 4.34%). MS (EI)

Synthesis of Cl₃B·PPh₂Me (2h). A solution of PPh₂Me (0.101 g, 0.50 mmol) in hexane (4 cm³) was added dropwise to 1.0M BCl₃ in heptane (0.75 cm³, 0.75 mmol). A white solid formed immediately. After standing overnight, the solid was isolated by filtration and dried *in vacuo*, yielding 0.142 g of (**2h**) as a white powder (89%). NMR (C₆D₆) ^{1}H δ 7.49 (m, 4H, Ph); 6.946 (m, 6H, Ph), 1.50 (d, 3H, J_{H-H} = 12 Hz, Me), ^{11}B{^{1}H} δ 3.75 (d, J_{B-P} = 155 Hz), ^{31}P{^{1}H} δ -20.85 (s, br,), -8.38 (q, J^{11}_{B-P} = 156 Hz, ^{11}B·P), -8.38

(septet, J^{10}_{B-P} = 52 Hz, $^{10}B\cdot P$). (Found: C, 48.96; H, 4.10 %. Calculated for $C_{13}H_{13}BCl_3P$: C, 49.20; H, 4.13%).

Synthesis of $Cl_3B\cdot PPh_3$ (2i). A solution of PPh_3 (0.210 g, 0.80 mmol) in hexane (10 cm^3) was added dropwise to 1.0M BCl_3 in heptane (1.20 cm^3, 1.20 mmol) in hexane (5 cm^3). A white solid formed immediately. After standing overnight, the solid was isolated by filtration, washed with cold hexane (3 x 2 cm^3), and dried *in vacuo*, yielding 0.293 g of (2i) as a white powder (96%). NMR (C_6D_6) ^1H δ 6.91 (m, 2H, Ph), 7.01 (m, 1H, Ph), 7.96 (m, 2H, Ph), $^{11}B\{^1H\}$ δ 4.59 (d, J_{B-P} = 152 Hz), $^{13}C\{^1H\}$ δ 134.3 (d, J_{C-P} = 39 Hz, Ph), 132.4 (s, Ph), 129.0 (d, J_{C-P} = 11 Hz, Ph), 128.7 (d, J_{C-P} = 7 Hz, Ph), $^{31}P\{^1H\}$ δ -5.53 (s (br)), -1.66 (q, J^{11}_{B-P} = 152 Hz, $^{11}B\cdot P$), -1.66 (septet, J^{10}_{B-P} = 51 Hz, $^{10}B\cdot P$). (Found: C, 57.02; H, 3.98%. Calculated for $C_{18}H_{15}BCl_3P$: C, 56.98, H, 3.98%). MS (EI) m/z = 262 (PPh_3), 185 (PPh_2), 108 (PPh). No adduct ions are observed.

Synthesis of $Cl_3B\cdot P(o\text{-tolyl})_3$ (2j). A solution of $P(o\text{-tolyl})_3$ (0.152 g, 0.50 mmol) in hexane (12 cm^3) was added dropwise to 1.0M BCl_3 in heptane (0.75 cm^3, 0.75 mmol). A fine white precipitate formed immediately. After standing overnight, the solid was isolated by filtration, washed with hexane (3 x 2 cm^3) and dried *in vacuo*, yielding 0.190 g of (2j) as a white powder (90%). NMR (C_6D_6) ^1H δ 7.00 (m, 3H, free $P(o\text{-tolyl})_3$); 6.73 (m, H, free $P(o\text{-tolyl})_3$); 2.61 (s; free phosphine CH_3); $^{11}B\{^1H\}$ δ 6.9 (s (br)), $^{13}C\{^1H\}$ δ , $^{31}P\{^1H\}$ δ: -29.75 (s; P(o-tolyl)$_3$). (Found C 59.92, H 5.20 %. $C_{12}H_{27}BCl_3P$ requires C 59.84, H 5.02%). MS (m/z) 304 ($P(o\text{-tolyl})_3$), 289 ($P(o\text{-tolyl})_2(C_6H_4)$). No adduct peaks observed.

In situ reaction of BCl₃ with P(C₆F₅)₃. A solution of P(C₆F₅)₃ (0.006 g; 0.011 mmol) in a small amount of C_6D_6 was placed in a 5 mm NMR tube and 1.0M BCl₃ in heptane (0.02 cm³; 0.02 mmol) was added. No new signals were observed by $^{31}P\{^1H\}$ NMR (C_6D_6).

In situ reaction of BCl₃ (20:1 excess) with P(C₆F₅)₃. A solution of P(C₆F₅)₃ (0.004 g; 0.0075 mmol) in a small amount of C_6D_6 was placed in a 5 mm NMR tube, and 1.0M BCl₃ in heptane (0.15 cm³; 0.15 mmol) was added. No new signals were observed by $^{11}B\{^1H\}$, $^{19}F\{^1H\}$ or $^{31}P\{^1H\}$ NMR (C_6D_6).

Synthesis of Br₃B·PMe₃ (2aa). A solution of PMe₃ (0.076 g, 0.999 mmol) in hexane (4 cm³) was added dropwise to a solution of BBr₃ (0.224 g, 0.894 mmol) in hexane (4 cm³). A white solid formed instantly. After stirring overnight, the solid was isolated by filtration, washed with cold hexane (2 x 2 cm³) and dried *in vacuo*, yielding 0.260 g of (2aa) as a white powder (89%). NMR (C_6D_6) ^1H δ 0.65 (d, J_{H-P} = 12 Hz), $^{11}B\{^1H\}$ δ -14.0 (d, J_{B-P} = 158 Hz), $^{31}P\{^1H\}$ δ -11.80 (q, J^{11}_{B-P} = 157 Hz, $^{11}B·P$), -11.80 (septet, J^{10}_{B-P} = 53 Hz, $^{10}B·P$). (Found: C, 11.43; H, 2.90%. Calculated for C₃H₆BBr₃P: C, 11.03; H, 2.78%).

Synthesis of Br₃B·PEt₃ (2bb). A solution of PEt₃ (0.118 g, 0.999 mmol) in hexane (4 cm³) was added dropwise to a solution of BBr₃ (0.255 g, 1.018 mmol) in hexane (4 cm³). A white solid formed immediately. After stirring overnight, 75% of the solvent was removed *in vacuo*). The product was isolated by filtration, washed quickly with cold hexane (1 x 2 cm³) and dried *in vacuo*, yielding 0.304 g of (2bb) as a white powder (83%). NMR (C_6D_6) ^1H δ 0.69 (m, 3H, CH₂C*H₃*), 1.40 (m, 2H, C*H₂*CH₃), $^{11}B\{^1H\}$ δ -

15.0 (d, J_{B-P} = 150 Hz), $^{31}P\{^1H\}$ δ -3.39 (q, $J^{11}{}_{B-P}$ = 149 Hz, $^{11}B \cdot P$), -3.39 (septet, $J^{10}{}_{B-P}$ = 50 Hz, $^{10}B \cdot P$). (Found: C, 19.58; H, 4.15%. Calculated for $C_6H_{15}BBr_3P$: C, 19.55; H, 4.10%).

Synthesis of $Br_3B \cdot P(^iPr)_3$ (2cc). A solution of $P(^iPr)_3$ (0.160 g, 0.999 mmol) in hexane (4 cm^3) was added dropwise to a solution of BBr_3 (0.251 g, 1.002 mmol) in hexane (4 cm^3). A white solid formed immediately. After stirring overnight, 75% of the solvent was removed *in vacuo*. The product was then isolated by filtration, washed quickly with cold hexane (2 x 2 cm^3) and dried *in vacuo*, yielding 0.319 g of (2cc) as a white powder (78%). NMR (C_6D_6) ^1H δ 1.02 (m, 6H, CH_3), 2.43 (m, 1H, CH), $^{11}B\{^1H\}$ δ -15.0 (d, J_{B-P} = 138 Hz), $^{31}P\{^1H\}$ δ -1.68 (q, $J^{11}{}_{B-P}$ = 139 Hz, $^{11}B \cdot P$), -1.68 (septet, $J^{10}{}_{B-P}$ = 47 Hz, $^{10}B \cdot P$). (Found: C, 26.40; H, 5.40%. Calculated for $C_9H_{21}BBr_3P$: C, 26.32; H, 5.15%).

Synthesis of $Br_3B \cdot P(^nBu)_3$ (2dd). A solution of $P(^nBu)_3$ (0.061 g, 0.302 mmol) in hexane (4 cm^3) was added dropwise to a solution of BBr_3 (0.077 g, 0.307 mmol) in hexane (4 cm^3). A white solid formed immediately. After stirring overnight, 50% of the solvent was removed *in vacuo*. The product was then isolated by filtration, washed with cold hexane (2 x 2 cm^3) and dried *in vacuo*, yielding 0.087 g of (2dd) as a white powder (64%). NMR (C_6D_6) ^1H δ 0.51 (t, 9H, J_{H-H} = 7 Hz, $(CH_2)_3CH_3$), 1.04 (q of t, 6H, J_{H-H} = 7 Hz, $CH_2CH_2CH_2CH_3$), 1.35 (m, 6H, $CH_2CH_2CH_2CH_3$), 1.68 (m, 6H, $CH_2CH_2CH_2CH_3$). $^{11}B\{^1H\}$ δ -14.6 (d, J_{B-P} = 150), $^{31}P\{^1H\}$ δ -6.91 (q, $J^{11}{}_{B-P}$ = 146 Hz, $^{11}B \cdot P$). (Found: C, 32.13; H, 6.25%. Calculated for $C_{12}H_{27}BBr_3P$: C, 31.83; H, 6.01%).

Synthesis of $Br_3B \cdot P(^tBu)_3$ (2ee). A solution of $P(^tBu)_3$ (0.061 g, 0.302 mmol) in hexane (5 cm^3) was added dropwise to a solution of BBr_3 (0.077 g, 0.307 mmol) in hexane (3

cm^3). A white solid formed immediately. After stirring overnight, the solid was isolated by filtration, washed with cold hexane (2 x 2 cm^3) and dried *in vacuo*, yielding 0.082 g of (**2ee**) as a white powder (60%). NMR (C_6D_6) $^{11}B\{^1H\}$ δ -15.6 (d, J_{B-P} = 127), $^{31}P\{^1H\}$ δ 10.83 (q, J^{11}_{B-P} = 126 Hz, ^{11}B·P), 10.84 (septet, J^{10}_{B-P} = 42 Hz, ^{10}B·P). (Found: C, 31.39; H, 6.05%. Calculated for $C_{12}H_{27}BBr_3P$: C, 31.83; H, 6.05%).

Synthesis of Br_3B·PCy_3 (2ff). A solution of PCy_3 (0.084 g, 0.300 mmol) in hexane (10 cm^3) was added dropwise to a solution of BBr_3 (0.077 g, 0.307 mmol) in hexane (3 cm^3). A white solid formed immediately. After stirring overnight, the solid was isolated by filtration, washed with cold hexane (2 x 2 cm^3) and dried *in vacuo*, yielding 0.106 g of (**2ff**) as a white powder (67%). NMR (C_6D_6) ^1H δ 1.01 (m, 3H, Cy), 1.51 (m, 5H, Cy), 2.17 (d, 2H, J_{H-H} = 13 Hz, Cy), 2.60 (d of t, 1H, J_{H-H} = 12 Hz, Cy), $^{11}B\{^1H\}$ δ -14.6 (d, J_{B-P} = 141 Hz) $^{31}P\{^1H\}$ δ -9.79 (q, J^{11}_{B-P} = 139 Hz, ^{11}B·P). (Found: C, 40.74; H, 6.34%. Calculated for $C_{18}H_{33}BBr_3P$: C, 40.72; H, 6.26%).

Synthesis of Br_3B·PMe_2Ph (2gg). A solution of PMe_2Ph (0.041 g, 0.297 mmol) in hexane (5 cm^3) was added dropwise to a solution of BBr_3 (0.076 g, 0.303 mmol) in hexane (3 cm^3). A white solid formed immediately. After stirring, then cooling to -30 °C, the product was isolated by filtration, washed with cold hexane (2 x 2 cm^3) and dried *in vacuo*, yielding 0.072 g of (**2gg**) as a white powder (62%). NMR (C_6D_6) ^1H δ 1.12 (d, 6H, J_{H-H} = 12Hz, Me), 6.93 (m, 2H, *meta*-Ph), 7.01 (m, 1H, *para*-Ph), 7.32 (m, 2H, *ortho*-Ph), $^{11}B\{^1H\}$ δ -13.8 (d, J_{B-P} = 152 Hz), $^{31}P\{^1H\}$ δ -12.46 (q, J^{11}_{B-P} = 152 Hz, ^{11}B·P), -12.47 (septet, J^{10}_{B-P} = 50 Hz, ^{10}B·P). (Found: C, 24.67; H, 2.87%. Calculated for $C_8H_{11}BBr_3P$: C, 24.72; H, 2.85%).

Synthesis of Br$_3$B·PMePh$_2$ (2hh). A solution of PMePh$_2$ (0.060 g, 0.300 mmol) in hexane (4 cm^3) was added dropwise to a solution of BBr$_3$ (0.077 g, 0.307 mmol) in hexane (4 cm^3). A white solid formed immediately. After stirring overnight, 25% of the solvent was removed *in vacuo*. The product was isolated by filtration, washed with cold hexane (2 x 2 cm^3) and dried *in vacuo*, yielding 0.088 g of (2hh) as a white powder (65%). NMR (C$_6$D$_6$) ^{1}H δ 1.61 (d, 3H, J_{H-H} = 12 Hz, Me), 6.90 (m, 4H, *meta*-Ph), 6.98 (m, 2H, *para*-Ph), 7.57 (m, 4H, *ortho*-Ph), ^{11}B{^{1}H} δ -14.3 (d, J_{B-P} = 150 Hz), ^{31}P{^{1}H} δ -11.21 (q, $J^{11}{}_{B-P}$ = 149 Hz, ^{11}B·P), -11.21 (septet, $J^{10}{}_{B-P}$ = 49 Hz, ^{10}B·P). (Found: C, 34.88; H, 2.96%. Calculated for C$_{13}$H$_{13}$BBr$_3$P: C, 34.64; H, 2.91%).

Synthesis of Br$_3$B·PPh$_3$ (2ii). A solution of PPh$_3$ (0.130 g, 0.519 mmol) in hexane (4 cm^3) was added dropwise to a solution of BBr$_3$ (0.131 g, 0.499 mmol) in hexane (8 cm^3). A white solid formed immediately. After stirring overnight, the solid was isolated by filtration, washed with cold hexane (2 x 2 cm^3) and dried *in vacuo*, yielding 0.195 g of (2ii) as a white powder (76%). NMR (C$_6$D$_6$) ^{1}H δ 6.92 (m, 2H, Ph), 7.01 (m, 1H, *para*-Ph), 7.88 (m, 2H, Ph), ^{11}B{^{1}H} δ -14.1 (d, J_{B-P} = 144 Hz), ^{31}P{^{1}H} δ -5.51 (q, $J^{11}{}_{B-P}$ = 145 Hz, ^{11}B·P), -5.51 (septet, $J^{10}{}_{B-P}$ = 48 Hz, ^{10}B·P). (Found: C, 42.17; H, 2.95%. Calculated for C$_{18}$H$_{15}$BBr$_3$P: C, 42.16; H, 2.95%).

Synthesis of Br$_3$B·P(o-tolyl)$_3$ (2jj). A solution of P(*o*-tolyl)$_3$ (0.091 g, 0.299 mmol) in hexane (10 cm^3) was added dropwise to a solution of BBr$_3$ (0.077 g, 0.307 mmol) in hexane (3 cm^3). A white solid formed immediately. After stirring overnight, the product was isolated by filtration, washed with cold hexane (2 x 2 cm^3) and dried *in vacuo*, yielding 0.110 g of (2jj) as a white powder (66%). NMR (C$_6$D$_6$) ^{1}H δ 2.70 (s (br), Me), 6.68 (m, Ph), 7.00 (m, Ph), 7.41 (m, Ph), ^{11}B{^{1}H} δ -12.2 (d, J_{B-P} = 130 Hz), ^{31}P{^{1}H} δ -

23.06 (s (br)). (Found: C, 45.28; H: 3.78%. Calculated for $C_{21}H_{21}BBr_3P$: C, 45.45; H, 3.81%).

Synthesis of $F_3B \cdot PPh_3$. A solution of $BF_3 \cdot Et_2O$ (0.5 ml; 4.08 mmol) was added dropwise to a solution of triphenylphosphine (0.525 g; 2.00 mmol) in hexane. A white solid formed instantly. After stirring for 1 h, the solution was left to recrystallise at -30 °C. The solid was isolated by filtration, washed with toluene, and dried *in vacuo*, yielding 0.555 g of $F_3B \cdot PPh_3$ (84%). $C_{18}H_{15}BF_3P$ requires: C, 65.50; H, 4.58; Found: C, 65.03; H, 4.52%. Solid-state $^{31}P\{^1H\}$ NMR: δ -8.8 ppm. Partial characterisation of $F_3B \cdot PPh_3$ has been reported previously.

Experiment to determine concentration effect on ^{31}P NMR of (2g), (2h) and (2i)

Five NMR samples were made from the five following solutions: Solution A: Cl_3BPPh_3 **(2i)** (0.010 g; 0.026 mmol) in 90% toluene/10% C_6D_6 (6.7 cm^3) [0.0039 M]; $^{31}P\{^1H\}$ NMR (400 MHz): δ: -0.656 (q; 151 Hz); -4.260 (s). Solution B: 1 cm^3 of solution A diluted with 1 cm^3 of 90% toluene/10% C_6D_6 [0.0020M]; $^{31}P\{^1H\}$ NMR (400 MHz): δ: -0.66 (q; 151 Hz); -4.254 (s). Solution C: $Cl_3BP \cdot Ph_2Me$ **(2h)** (0.015 g; 0.047 mmol) in 90% toluene/10% C_6D_6 (12.1 cm^3) [0.0039 M]; $^{31}P\{^1H\}$ NMR (400 MHz): δ: -7.33 (q; J = 155 Hz); -26.07 (s). Solution D: 1 cm^3 of solution C diluted with 1 cm^3 of 90% toluene/10% C_6D_6 [0.0020M]; $^{31}P\{^1H\}$ NMR (400 MHz): δ: -7.33 (q; J = 155 Hz); -26.08 (s). Solution E: $Cl_3B \cdot PPhMe_2$ **(2g)** (0.008 g; 0.031 mmol) in 90% toluene/10% C_6D_6 (8 cm^3) [0.0039 M]; $^{31}P\{^1H\}$ NMR (400 MHz): δ: -10.25 (q; J = 159 Hz).

VT NMR experiments on (2h) and (2i) Concentrated solutions of **(2h)** and **(2i)** were made up using 90% toluene/10% C_6D_6 solvent in two NMR tubes. **(2h)**: $^{31}P\{^1H\}$ NMR

(400 MHz): 30°C: δ -7.38 (q; J = 154.7 Hz); -26.01 (s); 20°C: δ -7.31 (q; J = 155.0 Hz);

-26.26 (s); 0°C: δ -7.16 (q; J = 155.5 Hz); -26.20 (s); -20°C: δ -6.97 (q; J = 155.6 Hz).

(2i): ^{31}P{^{1}H} NMR (400 MHz): 30°C: δ -0.63 (q; 150.8 Hz); -4.06 (s); 20°C: δ -0.66 (q;

J = 150.8 Hz); -4.28 (s); 0°C: δ -0.70 (q; J = 151.8 Hz); -4.74 (s); -20°C: δ: -0.74 (q; J =

151.8 Hz); -5.26 (s); -60°C: δ -0.78 (q; coupling constant was indiscernible); -6.16 (s).

2.6.3 Crystallography

Crystals of (2b), (2c), (2d), (2e), (2f), (2g), (2bb), (2ii), (2jj), (2k) and (2l) were

examined on a Bruker AXS SMART CCD diffractometer with Mo-Kα radiation (λ=

0.71073Å) and a Cryostream (Oxford Cryosystems) open-flow N_2 gas cryostat. Semi-

empirical absorption corrections, by comparison of Laue equivalents, were applied. The

structures were solved by direct methods, and refined on F^2 values for all unique

reflections. The largest electron density features were close to heavy atoms. Programs

were standard manufacturers' control and data processing software, together with

SHELXTL[77] and local programs.

Chapter 3: Lewis acid – Lewis base adducts of boron trihalides with pyridine, 2-picoline and 4-picoline.

3.1 Introduction

Pyridine adducts of boron trihalides were primarily studied more than 40 years ago[78] to probe the relative Lewis acidity of the boron trihalides. Until studies of this type were carried out, it was generally believed that the relative acceptor abilities of the boron trihalides were $BF_3 > BCl_3 > BBr_3 > BI_3$ on the basis of the relative electronegativities of the halogen atoms involved. The results of the pyridine adduct study, among others, showed that the stabilities of the adducts of the boron trihalides reversed this trend, suggesting a reversal in Lewis acidity. Indeed, this was the basis of many papers around that time, as researchers attempted to rationalise this phenomenon. Of course, the accepted explanation for this, that the electronegativities of the halides do not compensate for the loss of planarity and thus π-overlap on changing geometry from trigonal planar to tetrahedral at the boron atom, evolved from this early work.

The facile synthesis of the boron trihalide adducts of pyridine prompted publication of characterisation data for these compounds, including crystal structures of $F_3B \cdot pyridine$[79], $Cl_3B \cdot pyridine$[80] and $Br_3B \cdot pyridine$.[81] Photoelectron spectroscopic and theoretical studies including *ab initio* MO calculations have been carried out on $F_3B \cdot pyridine$ to examine the structure and, among other things, to calculate binding energies and ionisation energies.[82]

The $F_3B \cdot pyridine$ adduct was studied theoretically by a group who were using ^{15}N-pyridine to probe the acidity of sites on sulphated zirconia catalysts.[83] Modelling the entire catalyst would have been a large and complicated system for calculation, so BF_3 was used as a model of a Lewis acid site, where calculated data could be compared to

experimental data to check consistency. This system, however, did not prove to be the best approximation and many other prototypical Lewis acids were also studied.

The pyridine adduct of BBr_3 was reported[84] to be formed on addition of pyridine to the compound $(Ph_3P)_2Rh(CO)Br \cdot BBr_3$. This was said to be further proof of the existence of the rhodium-boryl compound, a supposition which has been questioned, particularly since the data presented are not consistent with more recent characterisation of Rh-B containing compounds.[85] It is more likely that the pyridine actually displaced PPh_3 from a $Ph_3P \cdot BBr_3$ adduct which formed alongside the rhodium complex (which was probably boron-free). Evidence for this is in the ^{11}B NMR data. The authors suggested that the rhodium-boron coupling could be resolved, giving rise to a doublet with a ^{103}Rh-^{11}B coupling constant of the order of 145-149 Hz. The ^{11}B NMR for rhodium-boryl complexes reported since display broad peaks for which Rh-B coupling is not resolved. Indeed, the coupling constants of 145-149 Hz are consistent with those of the $Ph_3P \cdot BX_3$ adducts reported here in Chapter 2, and these adducts are probably responsible for the ^{11}B NMR signal. It is completely plausible that the phosphine in a BX_3 adduct was displaced by pyridine resulting in the observed $X_3B \cdot$pyridine adduct since the B-N dative bond is stronger than the B-P dative bond.

In contrast, picoline adducts of boron trihalides have not been studied. A search of the Beilstein database[86] for adducts of BX_3 (X = halogen) with 2-, 3- or 4-picoline revealed that the only published[87] compounds of this type are $F_3B \cdot 2$-picoline and $F_3B \cdot 4$-picoline. In this study, formation of the BF_3 adduct was found to activate the methyl group of the picoline moiety. Subsequent reaction of the adduct with an aromatic aldehyde (4-(dimethylamino)benzaldehyde)) gave a facile route to 2- and 4-styrylpyridines.

Our group has previously examined BF_3 adducts of pyridine derivatives[88] during research into the effect of BR_3 coordination on the non-linear optical (NLO) properties of DMAP ($4\text{-Me}_2\text{N-C}_5\text{H}_4\text{N}$) and related compounds. Binding of Lewis acids, including BF_3, to the nitrogen donor alters the electron distribution in the donor molecule, consequently enhancing the second-order NLO properties.
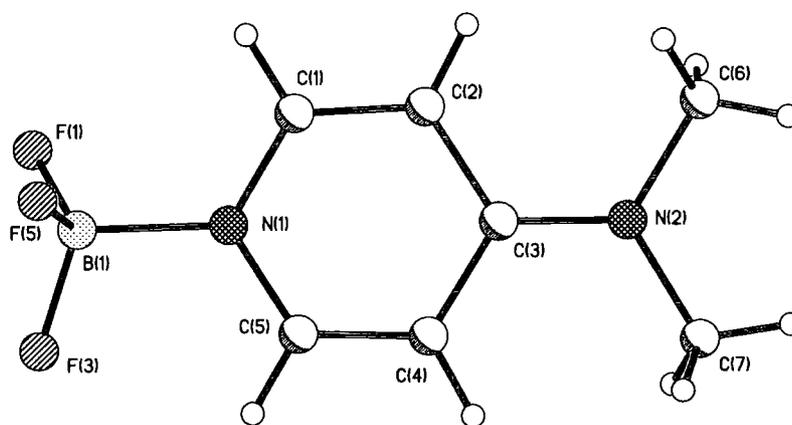
Figure 3.1: Diagram of the DMAP adduct of BF_3. Atoms are shown as spheres of arbitrary radius.

We have previously studied[89] the formation of B-N adducts between the diborane(4) compound B_2cat_2 (cat = catecholato; $1,2\text{-O}_2\text{C}_6\text{H}_4$) and 4-picoline. Addition of 1 equivalent of 4-picoline to B_2cat_2 yields the mono-adduct B_2cat_2(4-picoline), where a B-N bond has formed between one boron atom and the nitrogen on the picoline. ^{11}B NMR studies on the adduct displayed two different boron signals: one from the tetrahedral boron atom at $\delta = 13$ ppm and one from the 3-coordinate boron at $\delta = 32$ ppm consistent with the 3-coordinate boron shift in the parent B_2cat_2 compound. Structural studies confirmed these results, with a B-N bond distance of 1.644(2) Å. The B-B bond distance lengthens on complexation from 1.678(3) Å in B_2cat_2 to 1.706(3) Å in the adduct, due to the change from a trigonal planar sp^2 3-coordinate boron atom to a

tetrahedral sp^3 4-coordinate boron atom. Addition of 2 equivalents of 4-picoline gives the bis-adduct B_2cat_2(4-picoline)$_2$.
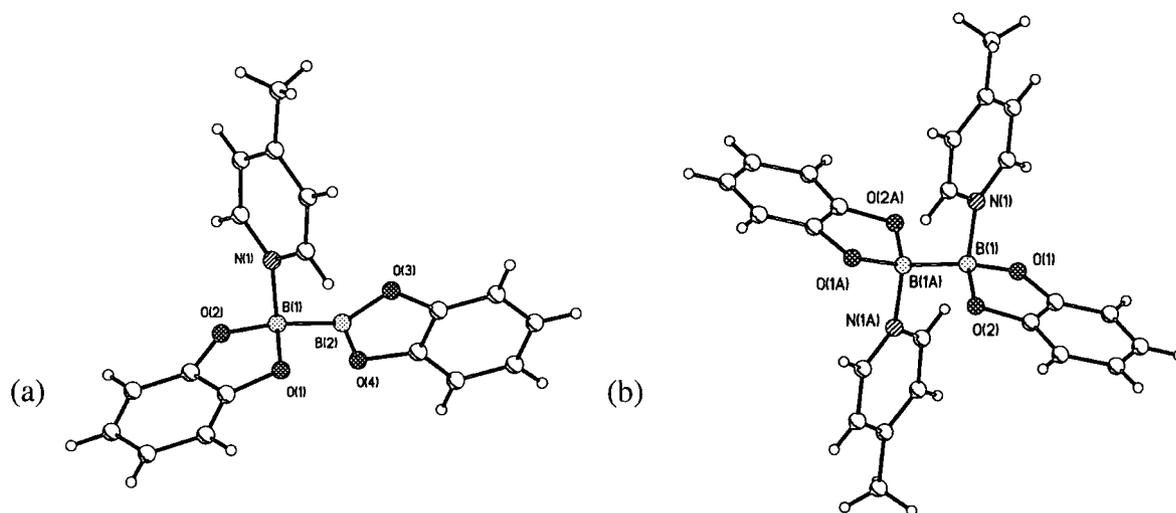
Figure 3.2: Diagram of the (a) *mono*-adduct and (b) *bis*-adduct of 4-picoline with B_2cat_2. Atoms are shown as spheres of arbitrary size.

There was only one signal on the ^{11}B NMR spectrum from the tetrahedral boron atoms at $\delta = 13$ ppm, wholly consistent with the formation of a bis-adduct. Structural studies revealed a similar B-N bond distance (1.659(2) Å) and B-B bond distance (1.713(4) Å) to the mono-adduct. It was found that 4-picoline would not react with the more sterically hindered B_2pin_2 (pin = pinacolato; $OCMe_2CMe_2O$) or $B_2(NMe_2)_4$

The thiocatecholate analogue of B_2cat_2 ($B_2(1,2-S_2C_6H_4)_2$) also forms adducts with 4-picoline.[90] Both the mono- and bis-adducts have been structurally characterised, and the B-N bond distances are found to be similar to those of the B_2cat_2 adducts, being 1.648(5) Å for the mono-adduct and 1.645(6) Å for the bis-adduct. The B-B distances are also similar, showing the same lengthening from that of B_2cat_2 (1.701(7) Å for the mono-adduct and 1.715(10) Å for the bis-adduct.

(a)

(b)
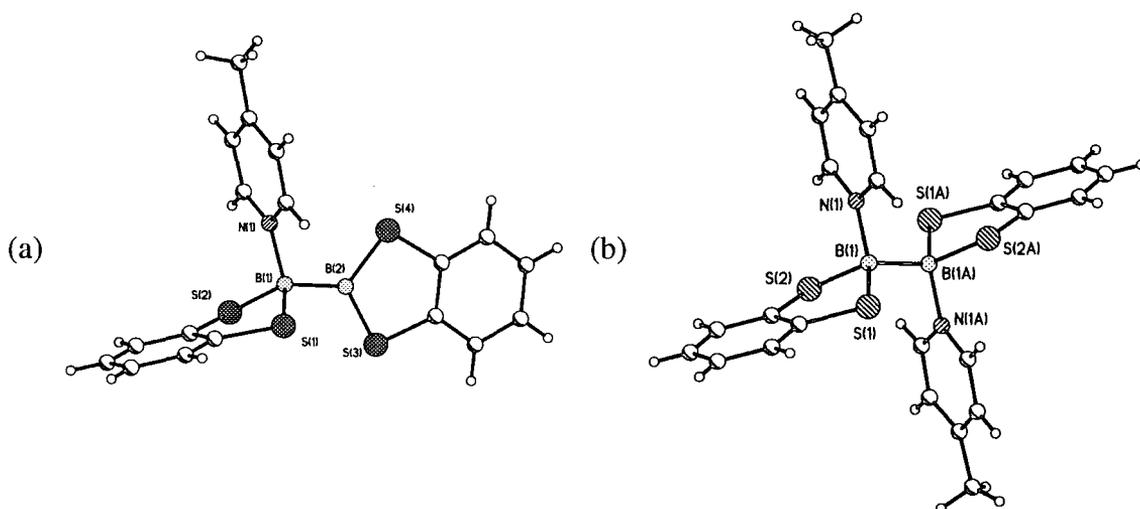
Figure 3.3: Diagram of the (a) *mono*-adduct and (b) *bis*-adduct of 4-picoline with $B_2thiocat_2$. Atoms are shown as spheres of arbitrary size.

In a related study, the 4-picoline adducts of MeBcat (2-methyl-2-(4-methylpyridine)-1,3,2-benzodioxaborole) and PhBcat (2-(4-methylpyridine)-2-phenyl-1,3,2-benzodioxaborole) were structurally characterised.[91] MeBcat·4-picoline crystallises in the orthorhombic space group *Pbca*, and PhBcat·4-picoline in the triclinic space group $P\bar{1}$. Each structure had two independent molecules in the unit cell with 2 similar B-N bond distances (1.660(2) and 1.6444(19) for MeBcat·4-picoline and 1.651(3) and 1.654(4) for PhBcat·4-picoline).

A search of the Cambridge Structural Database[73] revealed that there are 397 structures containing 4-picoline. The majority of these, (266) involve 4-picoline as a metal ligand and 113 involve 4-picoline bound to a non-metal. The N-A (A = atom bound to N) bond distances vary, as expected, as A changes. There are discrete ranges for different types of atom A, which are detailed below, where the N-A bond distance is available on the CSD.

Table 3.1: Discrete bond distance ranges for 4-picoline adducts (from a search of the CSD).

Bond Type	Occurrence	Range (Å)
N-M	207	3.081 – 1.954
N-B	10	1.680 – 1.641
N-C	16	1.530 – 1.421
N-N	2	1.409 – 1.385
N-O	5	1.349 – 1.305
N-H	21	1.197 – 0.789

As can be seen from the above table, there are ten instances of N-B bonds in 4-picoline compounds. Eight of these have been published by our group and have been discussed above. The other two contain the longest and shortest examples of known B-N (where N is in 4-picoline) bond distances. The longest B-N bond distance of 1.681(3) Å occurs in the 4-picoline *bis*-adduct[92] of the unusual 1,4-diethyl-2,5-bis(trimethylsilyl)-1,4-diborinane. The long B-N distance can be attributed to the presence of bulky trimethylsilyl groups adjacent to each coordinating boron atom.
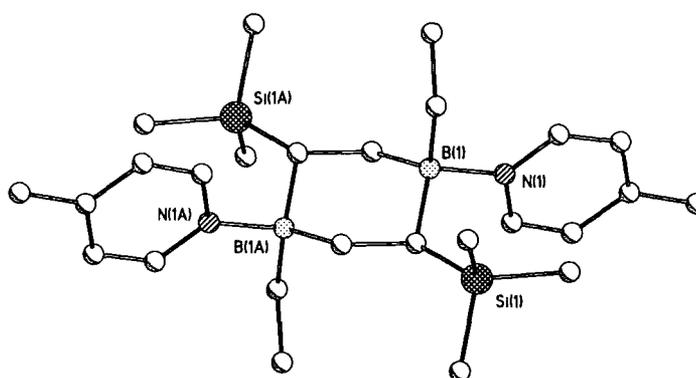
Figure 3.4: Diagram of the *bis*-4-picoline adduct of 1,4-diethyl-2,5-bis(trimethylsilyl)-1,4-diborinane, CSD refcode PIVHOR. Atoms are shown as spheres of arbitrary radius. Hydrogen atoms have been omitted for clarity.

The shortest B-N bond distance of 1.641(3) Å is for the 4-picoline mono-adduct[93] of 2,3,4,5-tetraethyl-1,2,3-oxadiborole. The short B-N distance in this case could be due to the presence of the adjacent oxygen atom which withdraws electron density from the boron atom, thus increasing the Lewis acidity of the boron.
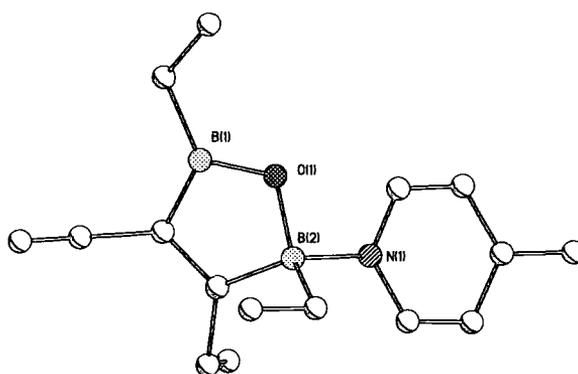
Figure 3.5: Diagram of the 4-picoline adduct of 2,3,4,5-tetraethyl-1,2,3-oxadiborole, CSD refcode YENXEU. Atoms are shown as spheres of arbitrary radius. Hydrogen atoms have been omitted for clarity.

The CSD search also revealed that there were several examples of structures with 4-picoline as a solvent of crystallisation or as part of a co-crystal. Examples of the latter were studied to probe hydrogen-bonding in 4-picoline systems with alcohols. Some examples of this are outlined below.

Malarski *et al.* have investigated how changes in temperature and the isotopic substitution of hydrogen by deuterium affects the hydrogen bonding in the co-crystal of 4-picoline with pentachlorophenol. The room temperature X-ray structure of these two systems,[94] both the OH and OD analogues, showed that the hydrogen-containing system had a short, strong hydrogen bond, with an O-H···N distance of 2.552(4) Å. This distance was significantly greater in the deuterium containing system with O-D···N = 2.638(3) Å. The effect of cooling[95] the hydrogen-containing system to 80K was a significant contraction in the O-H···N distance to 2.515(4) Å. There is very little effect on the deuterium analogue where only a slight reduction in O-D···N to 2.628(6) Å was observed.
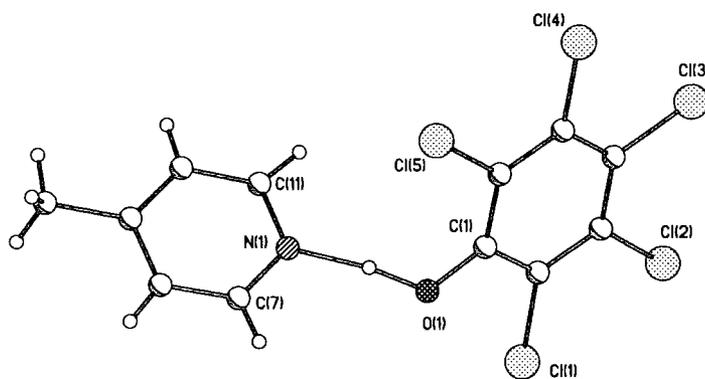
Figure 3.6: Diagram of 4-picoline with pentachlorophenol, CSD Refcode GADGUN, showing the very short hydrogen bond (centre). Atoms are shown as spheres of arbitrary radius.

The strong O-H···N hydrogen bonding between 4-picoline and phenols understandably led to the investigation of the use of this interaction in crystal engineering. Zaworotko and Biradha reported[96] the self-assembly of 4-picoline groups into a novel cluster when co-crystallised with 1,3,5-trihydroxybenzene in the ratio 3:1. The O-H···N interaction links the cluster to the 1,3,5-trihydroxybenzene.
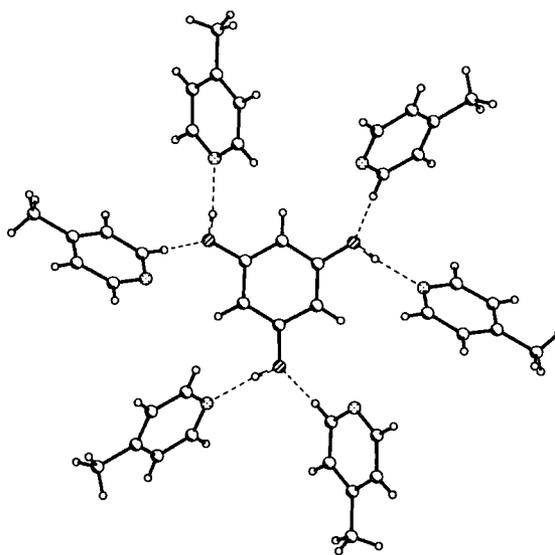
Figure 3.7: Diagram of the 4-picoline hexamer (CSD Refcode HIMGAL) surrounding a molecule of 1,3,5-trihydroxybenzene. Atoms are shown as spheres of arbitrary size.

The cluster itself has the appearance of a supramolecular analogue of cyclohexane. C-H···π interactions join the hexamer together, with the C-H···π interactions replacing

what would be C-C bonds in cyclohexane. The 4-picoline molecules are arranged in a chair conformation, with the methyl group of each unit of the hexamer accommodated in the central void of the clusters of 'cyclohexane' analogues. This is an interesting structure since the strong O-H⋯N interaction, although integral in forming the 3(4-picoline)·1,3,5-trihydroxybenzene unit, is not the controlling influence in the hexamer formation. The O-H⋯N interaction is relegated in importance, despite its strength, by the C-H⋯π interaction which governs the structure of the supramolecular cyclohexane analogue.

The compound 1,1,6,6-tetraphenylhexa-2,4-diyne-1,6-diol ((Ph₂)(OH)C-C≡C-C≡C-C(OH)(Ph)₂) forms elegant inclusion compounds[97] on crystallisation with either pyridine, 3-picoline or 4-picoline, in a 1:2 ratio. The host molecule forms cages, with two pyridine or picoline molecules located in each cage (see Figure 3.8).
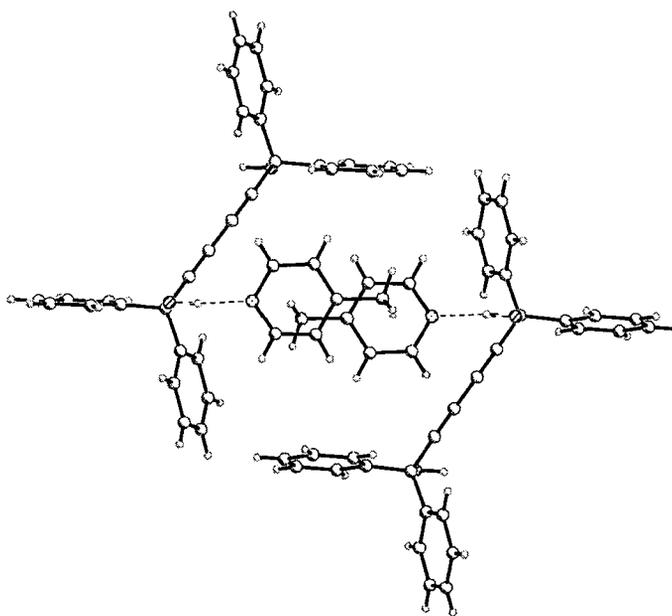
Figure 3.8: Diagram of the inclusion compound of 1,1,6,6-tetraphenylhexa-2,4-diyne-1,6-diol with 4-picoline, CSD Refcode XELKUU. Atoms are shown as spheres of arbitrary radius.

The guest molecules are all held in the host cage by O-H$\cdots$N hydrogen bonds with the hydroxyl groups. The D$\cdots$A hydrogen bond distances range from 2.747(2) Å at 165(2)° for the pyridine guest, to 2.768(2) Å at 169(1)° for the 4-picoline guest. Competition studies showed that 4-picoline is always favoured for inclusion by this host, but competition between 3-picoline and 4-picoline depends upon the guest concentrations in the mother liquor. The different affinity of the pyridine and 4-picoline guests for the host compound means the inclusion crystallisation process could be utilised to separate mixtures of the two guest molecules.

The 1:1 complex of 4-picoline with 4-nitrophenol[98] is also held by an O-H$\cdots$N hydrogen bond which, at 2.668(2) Å, is shorter than in the inclusion compound discussed above. The O-H$\cdots$N angle is slightly larger at 174(2)°. The mean planes of the phenyl rings in the complex are at an angle of 57.8° to each other. The dimers adopt a herringbone packing motif in the crystal.

The crystal structure of 4-picoline was originally published over 40 years ago.[99] The compound crystallises in the space group $P2_1/n$. It has since been redetermined a number of times. The most recent of these[100] was in the space group $I4_1/a$. Selected bond distances and angles are shown in Table 3.2 to allow comparisons later in this chapter.

Table 3.2: Selected bond distances and angles for 4-picoline, taken from the CSD.

Bond Distances (Å)		Bond Angles (°)	
N(1)-C(1)	1.337(2)	C(1)-N(1)-C(1')	116.2(2)
C(1)-C(2)	1.396(3)	N(1)-C(1)-C(2)	123.7(2)
C(2)-C(3)	1.397(3)	C(1)-C(2)-C(3)	119.3(2)
C(3)-C(4)	1.506(3)	C(2)-C(3)-C(4)	121.4(1)
		C(2)-C(3)-C(2')	117.3(2)

There are significantly fewer published structures of crystals containing 2-picoline. A search of the Cambridge Structural Database revealed 118 structures, none of which contain a B-N bond. The N-A bond distances again fall into discrete ranges (see Table 3.3) depending on A (A = atom bound to N), as seen for the 4-picoline structures.

Table 3.3: Discrete bond distance ranges for 2-picoline adducts (from a search of the CSD).

Bond Type	Occurrence	Range (Å)
N-M	75	2.697 – 1.942
N-C	4	1.494 – 1.468
N-O	3	1.358 – 1.321
N-H	13	1.504 – 0.82

Many of the structures containing 2-picoline have been published by White et al., who investigated[101] structures of the type
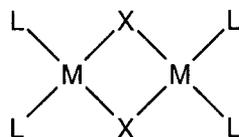
where M = a metal, X = a halogen and L = a unidentate nitrogen ligand. As the specific metals, ligands and halogens are varied, so is the macromolecular motif. The version with L = 2-picoline, M = copper and X = iodine forms a dimer of the type shown above. Other combinations of ligand, metal and halogen lead to different types of structure,

from small molecules like the dimer shown, to elegant cubane-type structures and ladder-type polymers. An interesting polymer was formed from the M = copper and X = iodine compound shown above by changing the ligand from 2-picoline to acridine (anthracene with a nitrogen atom substituted at the 2 position of the central ring). The result is a long $-(Cu-I)_n-$ polymer backbone with pendant acridine ligands.

A more recent study[102] by White *et al.* explored the effect of stoichiometry on complexes formed between Al_2Cl_6 and unidentate nitrogen base adducts including 2-picoline. The dimer disproportionates with $Me-C\equiv N$ to give ionic species of different types e.g. $[AlCl(NCMe)_5][AlCl_4]_2 \cdot MeCN$. It was found that reaction of the dimer with bases such as NMe_3 gave a 1:2 complex of $AlCl_3 \cdot 2NMe_3$ with a *trans* trigonal bipyramidal geometry. Reaction with 2-picoline, however, gave the 1:1 complex $Cl_3Al \cdot 2$-picoline. The X-ray crystal structure of this compound will be discussed in detail in comparison with $Cl_3B \cdot 2$-picoline later in this chapter.

Other studies involving 2-picoline have investigated hydrogen bonding. A recent example is the neutron diffraction study of 2-picoline co-crystallised with pentachlorophenol.[103] This revealed a particularly short $O-H \cdots N$ hydrogen bond (1.535(7) Å). This was the shortest one from neutron data at the time of publication. Other very short $O-H \cdots N$ hydrogen bonds have been presented[104] involving 4,4'-bipyridines.

3.2 Scope of this study

During our study of the phosphine-promoted redistribution of B-chlorocatecholborane ClBcat,[105] we also examined pyridine, 2-picoline, 4-picoline and triethylamine adducts of ClBcat, to investigate the effect of nitrogen σ-donors on the stability of the adduct with respect to the redistribution. It was this work which led to the study presented herein. It seemed prudent to investigate also the adducts which these compounds formed with BCl_3 and BBr_3, in addition to the $X_3B \cdot PR_3$ adducts discussed at length in Chapter 2, for a complete comparison.

The study presented here contains the first details and characterisation of boron trihalide adducts with 2-picoline and 4-picoline, including the first structural characterisation of $X_3B \cdot$picoline adducts. A comparative study of the known boron trihalide adducts with pyridine is also presented.

3.3 Results and Discussion

Treatment of pyridine, 2-methyl-pyridine (2-picoline) and 4-methyl-pyridine (4-picoline) with BCl_3 afforded $Cl_3B \cdot$pyridine (3a) as a cream solid, $Cl_3B \cdot 2$-picoline (3b) as an off-white solid and $Cl_3B \cdot 4$-picoline (3c) as a white solid. Similarly, reaction with BBr_3 generates comparable adducts $Br_3B \cdot$pyridine (3d) as a white solid, and $Br_3B \cdot 2$-picoline (3e) and $Br_3B \cdot 4$-picoline (3f) as off-white solids. Compounds 3a and 3d have been reported and structurally characterised elsewhere[106] and have been synthesised and included here for comparison of characterisation data. Compounds (3a-c) and (3d-f) were fully characterised by ^1H, $^{13}C\{^1H\}$ and $^{11}B\{^1H\}$ NMR spectroscopy, and (3b), (3c) and (3e) by single crystal X-ray diffraction techniques.

The NMR data for compounds (3a-f) are presented in Table 3.4. The ^1H NMR chemical shift of the *ortho* proton in all cases was higher than 8.5 ppm, due to the influence of the nitrogen, and though this peak in the BCl_3 adducts was only a broad singlet, in the BBr_3 adducts splitting due to coupling to the boron could be seen. This suggests a stronger interaction between the N-BBr_3 than with N-BCl_3. As mentioned above, this is to be expected since the Lewis acidity of BBr_3 is greater than[107] for BCl_3, although the B-N bond length in (3c) is not *significantly* longer than that in (3f).

Table 3.4: NMR data in C_6D_6 for adducts 3a-f

Compound	#	$^{11}B\{^1H\}$ NMR shift (ppm)	^1H NMR shifts (ppm)	$^{13}C\{^1H\}$ NMR shifts (ppm)
$Cl_3B \cdot$pyridine	(3a)	8.9	8.75 (s, br, 2H, Py)	144.1 (s, Py)
			6.47 (t, J = 7 Hz, 1H, Py)	142.1 (s, Py)
			6.12 (t, J = 7 Hz, 2H, Py)	125.0 (s, Py)
$Cl_3B \cdot$2-picoline	(3b)	8.9	9.28 (s, br, 1H, Py)	145.1 (s, Py)
			6.38 (m, 1H, Py)	141.6 (s, Py)
			5.99 (m, 2H, Py)	129.7 (s, Py)
			2.82 (s, 3H, CH$_3$)	122.1 (s, Py)
				24.5 (s, CH$_3$)
$Cl_3B \cdot$4-picoline	(3c)	8.8	8.68 (m, 2H, Py)	143.4 (s, Py)
			6.03 (d, 2H, Py)	125.9 (s, Py)
			1.38 (s, 3H, CH$_3$)	20.7 (s, CH$_3$)
$Br_3B \cdot$pyridine	(3d)	-6.8	9.00 (s, br, 2H, Py)	124.8 (s, Py)
			6.34 (m, 1H, Py)	142.1 (s, Py)
			5.99 (m, 2H, Py)	145.3 (s, Py)
$Br_3B \cdot$2-picoline	(3e)	-7.9	9.58, (s, br, 1H, Py)	147.1 (s, Py)
			6.35 (m, 1H, Py)	142.1 (s, Py)
			5.96 (m, 2H, Py)	130.3 (s, Py)
			2.91 (s, 3H, CH$_3$)	122.3 (s, Py)
				25.8 (s, CH$_3$)
$Br_3B \cdot$4-picoline	(3f)	-6.9	8.90 (s, br, 2H, Py),	144.6 (s, Py)
			5.86 (m, 2H, Py),	125.6 (s, Py)
			1.25 (s, 3H, CH$_3$)	20.6 (s, CH$_3$)

The published data[108] for the 2- and 4-picoline adducts with BF$_3$ contain only the ^1H NMR shifts of the picoline methyl groups: δ = 2.87 ppm (F$_3$B·2-picoline) and δ = 2.68 ppm (F$_3$B·4-picoline). The value for the 2-picoline adduct is very similar to that of the BCl$_3$ and BBr$_3$ adducts presented here (δ = 2.82 ppm and δ = 2.91 ppm respectively). The values for the 4-picoline adducts, however, differ significantly from values in this

study for the BCl_3 adducts and BBr_3 adducts which are $\delta = 1.38$ ppm and $\delta = 1.25$ ppm respectively. The prior study used $CDCl_3$ as a solvent whereas the BCl_3 and BBr_3 NMR experiments were run in C_6D_6 which may account for the differences.

The $^{11}B\{^1H\}$ NMR spectra display the singlet which would be expected, since ^{11}B does not couple to ^{14}N (I = 1). The stronger Lewis acidity of BBr_3 compared to BCl_3 is reflected in adduct shifts which differ by approximately 16 ppm on changing the halide.

The crystallographic data for compounds (3b), (3c) and (3f) are shown in Table 3.5 alongside the literature data for (3a) and (3d), with selected bond lengths and angles in Table 3.6.

Table 3.5: Crystallographic data for compounds (3b), (3c) and (3f)

Compound	$Cl_3B\cdot2$-picoline (3b)	$Cl_3B\cdot4$-picoline (3c1) 100K	$Cl_3B\cdot4$-picoline (3c2) 180K	$Br_3B\cdot4$-picoline (3f)
Formula	$C_6H_7BCl_3N$	$C_6H_7BCl_3N$	$C_6H_7BCl_3N$	$C_6H_7BBr_3N$
Formula weight	210.29	210.29	210.29	343.67
Crystal System	orthorhombic	monoclinic	orthorhombic	monoclinic
Space Group	Pnma	$P2_1/n$	Pnma	$P2_1/m$
a / Å	10.0304(9)	7.214(1)	8.990(1)	6.4829(4)
b / Å	6.8481(5)	8.954(1)	7.256(1)	9.8812(6)
c / Å	12.8675(10)	13.963(2)	14.076(2)	7.7791(4)
α / °	90	90	90	90
β / °	90	94.65(2)	90	91.145(4)
γ / °	90	90	90	90
U / Å^3	883.86(12)	899.0(2)	918.2(2)	498.22(5)
Z	4	4	4	2
D_c / g cm^{-3}	1.580	1.554	1.521	2.291
μ / mm^{-1}	0.966	0.949	0.929	12.083
Temperature	110(2)	100(2)	180(2)	110(2)
F(000)	424	424	424	320
Crystal size (mm^3)	0.40 x 0.42 x 0.60	0.43 x 0.36 x 0.21	0.21 x 0.36 x 0.43	0.30 x 0.30 x 0.18
θ_{max} / °	28.98	29.09	29.0	29.0
Maximum indices h,k,l	13, 9, 17	9, 12, 19	12, 9, 19	8, 13, 10
Reflections Measured	10143	6716	11250	4232
Unique reflections	1259	2367	1312	1379
R_{int}	0.0254	0.0653	0.0355	0.0360
Transmission factors	0.7323-0.6171	0.8404-0.7064	0.8497-0.6913	0.2103-0.1087
Number of refined parameters	83	102	73	74
Extinction parameter	-	-	0.005(2)	0.0151(15)
R' (all data, on F^2)	0.0688	0.3380	0.0893	0.0686
R [data with $F^2 > 2\sigma(F^2)$]	0.0258	0.1160	0.0297	0.0262
Goodness of fit on F^2	1.098	1.166	1.051	1.064
Largest difference-map features / e Å^{-3}	+0.329, -0.386	+2.035. -2.008	+0.283, -0.222	+0.631, -0.680

Table 3.6: Selected bond lengths (Å) and angles (°) for compounds 3a-d and 3f[*]

Bond or angle (X = Cl or Br)	(3a)[109] $Cl_3B\cdot$pyridine	(3b) $Cl_3B\cdot$2-picoline	(3c1) (100K) $Cl_3B\cdot$4-picoline	(3c2) (180K) $Cl_3B\cdot$4-picoline	(3d)[110] $Br_3B\cdot$pyridine	(3f) $Br_3B\cdot$4-picoline
B-N	1.592(3)	1.609(2)	1.592(7)	1.585(2)	1.59(2)	1.582(5)
B-X	1.835(2)	1.8466(10)	1.841(7)	1.843(1)	1.99(2)	2.027(4)
	1.839(3)	1.8437(17)	1.850(7)	1.838(2)	2.01(2)	2.003(2)
	1.836(3)		1.838(7)	1.908(7)	1.96(2)	2.003(2)
				1.763(13)		
N-C	1.346(3)	1.3667(17)	1.358(7)	1.348(2)	1.32(2)	1.360(3)
	1.348(3)	1.3719(18)	1.371(7)	1.357(2)	1.33(2)	1.360(3)
C-CH$_3$		1.500(2)	1.497(7)	1.499(2)		1.498(5)
N-B-X	110.5(1)	108.29(6)	110.0(4)	110.82(13)	106.8	110.86(16)
	107.3(2)	111.00(10)	108.9(4)	107.62(8)	109.8	110.86(16)
	108.7(2)		106.1(4)	105.2(2)	109.5	106.2(2)
X-B-X	110.2(1)	108.22(6)	110.2(3)	109.32(7)	109.6	109.15(19)
	109.8(2)	112.84(9)	110.1(3)	112.12(12)	111.5	109.85(14)
	110.3(1)		111.4(3)		109.6	109.85(14)
C-N-C	118.8(2)	118.83(12)	118.7(5)	118.65(15)	121.5	118.4(3)
C-N-B	121.6(2)	119.24(12)	124.3(5)	123.61(15)	117.9	120.58(17)
	119.6(2)	121.93(12)	117.0(4)	117.74(15)	120.6	120.58(17)

[*] This work unless otherwise indicated.

Compound (3b) crystallises in the orthorhombic space group *Pnma* (Figure 3.9).
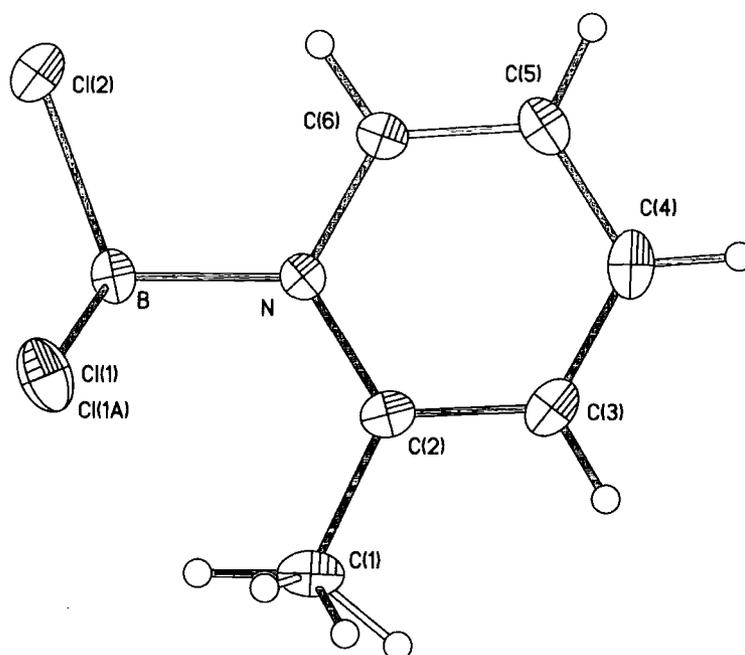
Figure 3.9: Cl₃B·2-picoline (3b) showing atom labelling. Thermal ellipsoids are plotted at the 50% probability level.

The atoms in the pyridine ring and atoms Cl(2), B and C(1) lie on a crystallographic mirror plane. The compound contains the longest B-N bond length recorded for these pyridine-based adducts, 1.609(2) Å, which is probably due to the methyl group in the 2-position affecting coordination to BCl_3. This B-N bond length is significantly shorter than any of the B-P lengths in the phosphine adducts. This could be because the nitrogen in a pyridine ring has little steric crowding compared to that in a tertiary phosphine, but mainly because nitrogen is much smaller than phosphorus. The van der Waals radius[111] of nitrogen is 1.54 Å compared to 1.90 Å for phosphorus. Similarly the B-P bond length[112] in $Cl_3B·PMe_3$ is much longer at 1.957(5) Å than the corresponding B-N bond length in $Cl_3B·NMe_3$ which is recorded twice in the Cambridge Structural Database[73] as 1.574 Å[113] and 1.611 Å.[114] In (3b), there are no significantly short

contacts between the Cl atoms and the H atoms on the methyl group, with the shortest Cl(1)⋯H(14) separation being 3.096 Å.

To compare the B-N bond length with other links to 2-picoline, a search of the Cambridge Structural Database was performed. There are 118 crystal structures containing 2-picoline recorded in the Cambridge Structural Database. None of these contain a B-N bond as seen in (**3b**). There are, however, a wide variety of compounds, with the N atom of the picoline most commonly found bound to a copper atom. The bond distance from the nitrogen atom of the picoline to the bound atom varies considerably but with some general trends.

Graph 3.1: Graph to show bond distances for N-A (A = any atom) containing compounds of 2-picoline in order of size.

The longest bond distance is for a lead adduct (CSD Refcode KIFHEM), shown by ◊, with a N-Pb bond distance of 2.697 Å. This is considerably longer than any of the other

species listed in the CSD. This large bond distance is most likely attributable to the large size of the lead atom. The next longest, shown by ◊, is a calcium adduct (CSD Refcode TAPJID), with a N-Ca bond distance of 2.580 Å. This large bond distance could be partly attributable to the fact that the calcium is 6 coordinate. Other structures containing a Ca-N bond where the calcium is 6 coordinate have Ca-N distances ranging from 2.633 Å to 2.206 Å, so this example is still quite large. The rest of the 2-picoline-metal adducts, shown by ◊, have B-M (M = metal) bond distances within a relatively small range, from 2.354 Å for silver-containing system (CSD Refcode DEDNOP) down to the AlCl$_3$ adduct (CSD Refcode TOGSAJ) with a bond distance of 1.942 Å. This latter compound will be discussed in more detail later on. There is a significant reduction in bond distance for species which contain a N-CH$_3$ bond, shown by ◊, the longest bond distance for this type of compound being 1.504 Å. The B-N bond distance in adduct (3b), shown by ◊, is intermediate of these distances, being shorter than the N-Al compound but longer than any of the N-CH$_3$ species at 1.609 Å. The N-CH$_3$ ones range from 1.504 Å to 1.468 Å. The picoline N-oxides, shown by ◊, have N-O distances ranging from 1.358 to 1.321 Å. The shortest bond distances are all attributable to 2-picolinium ion, shown by ◊. Due to the inherent difficulties in locating H atoms accurately using X-ray diffraction these data are not always reliable, however it is reasonable to expect that the N-H distance will be much smaller than any other N-A distances, due to the small size of the H atom.

There are no other 2-picoline-boron adducts in the database, but there is a 2-picoline-AlCl$_3$ adduct recorded (refcode TOGSAJ). As another Group 3-Group 5 adduct it is worth considering for comparison purposes. The compound was synthesised by White *et al.* as part of their studies into the effect of stoichiometry on formation of unidentate N-donor compounds with AlCl$_3$ dimer.[115] Thus, 2-picoline formed a 1:1 adduct, which

looks very similar to (**3b**). The symmetry-related chlorine atoms also 'straddle' the

methyl group to minimise repulsions. The larger Al-N bond distance of 1.942 Å

compared to the B-N bond distance in (**3b**) (1.609 Å) is attributable to the greater size

of the Al atom. This is supported by the larger Al-N-C_{Me} bond angle (126.6°) compared

to the B-N-C_{Me} angle (121.93°).

The structure of (**3c2**) at 180K is shown in Figure 3.10. It crystallises in the

orthorhombic space group *Pnma*.
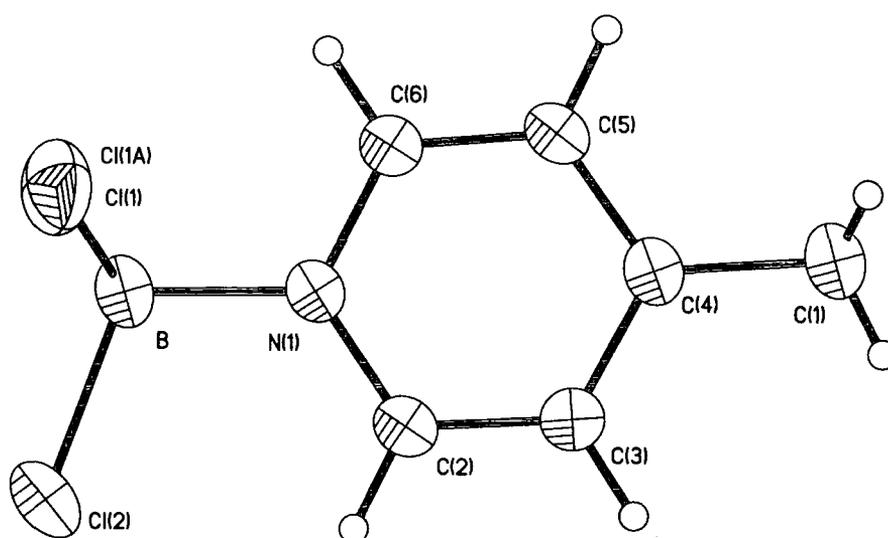
Figure 3.10: Cl_3B·**4-picoline** (**3c2**) at 180K, showing atom labelling. Thermal ellipsoids are plotted to 50% probability level. Disordered Cl atoms have been omitted for clarity.

There is minor rotational disorder of the BCl_3 group. Cl(1) and Cl(2) have occupancies

of 0.95 and 0.475 whereas Cl(3) and Cl(4) have occupancies of 0.05 and 0.025

respectively. The molecule sits on a mirror plane including B, Cl(2) [Cl(4)], C(1) and all

of the atoms in the pyridine ring (see Figure 3.11).
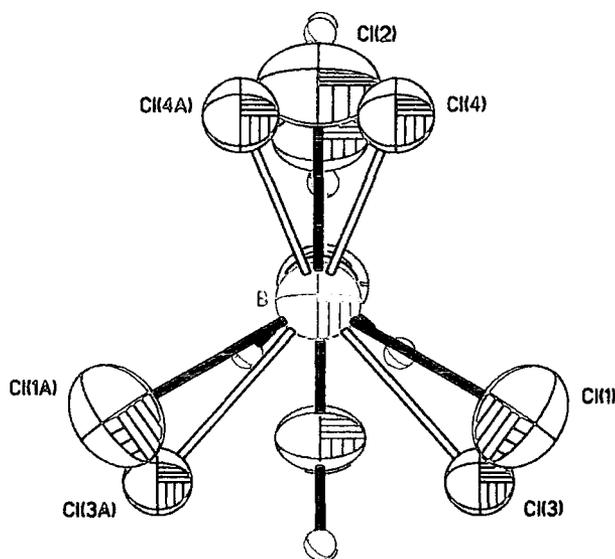
Figure 3.11: Ortep diagram of (3c2), viewed down the axis of the molecule, showing the rotational disorder in the chlorine atoms.

On cooling to 100K, a phase transition was found to occur at *ca.* 170K. The overall change in the structure is relatively small, however twinning occurs, and the crystal system becomes monoclinic (space group $P2_1/n$). (Figure 3.12):
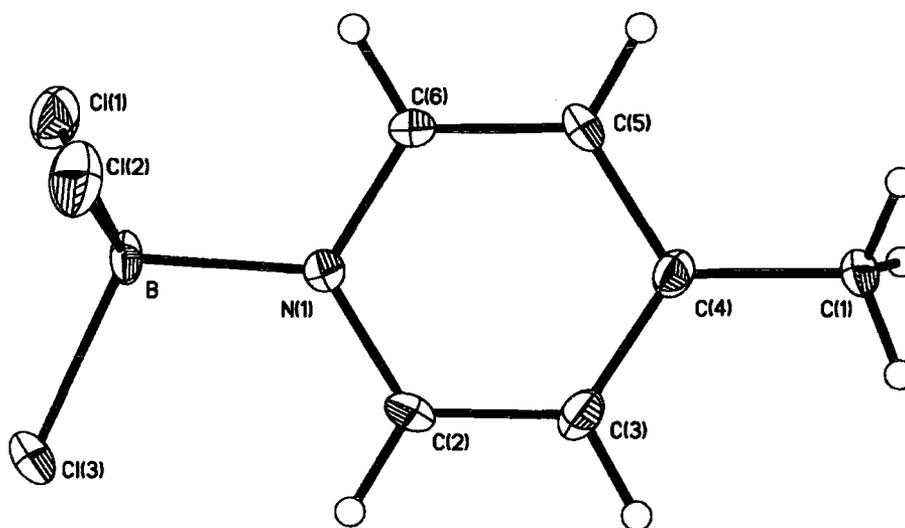
Figure 3.12: Cl₃B·4-picoline (3c1) at 100K, showing atom labelling. Thermal ellipsoids are plotted at the 50% probability level.

The B-N bond lengths in the low- and high-temperature structures are not significantly

different (1.592(7) and 1.585(2) Å respectively), and none of the other bond lengths or

angles change significantly. In the low temperature structure, the molecule does not sit

on a mirror plane. This can be seen more clearly when examining packing diagrams for

the two different structures.
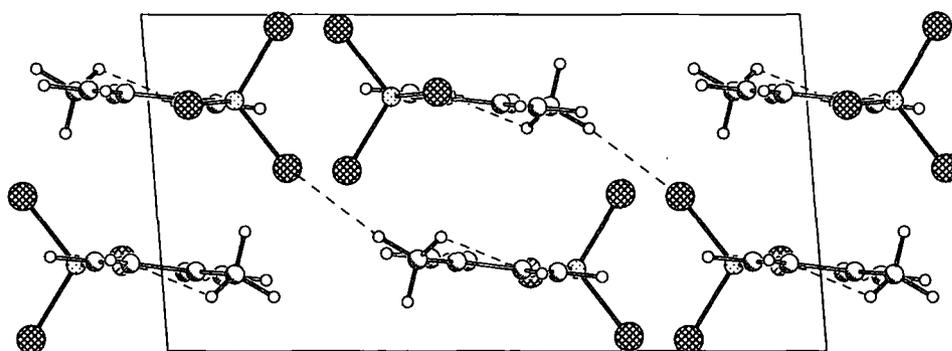
Figure 3.13: Packing diagram for (3c1) (100K), projected down the b cell axis. Short contacts
between the chlorine and methyl group are shown by dotted lines.
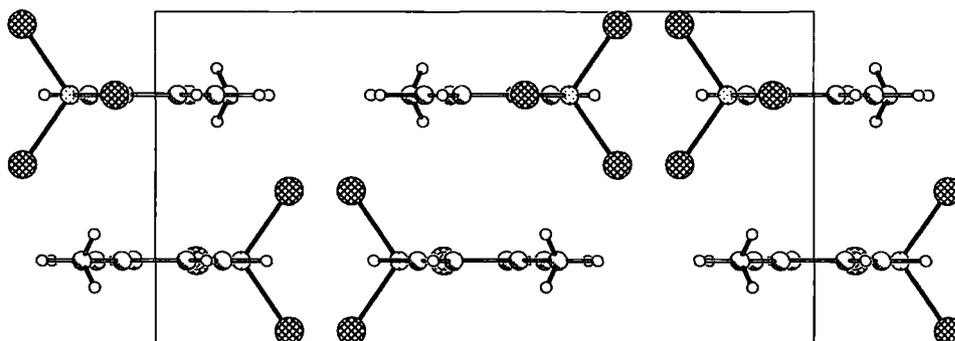
Figure 3.14: Packing diagram for (3c2) (180K), projected down the a cell axis. The greater
symmetry can be seen, with more atoms in the molecule co-planar. (Two low occupancy chlorine
atoms Cl(3) and Cl(4) have been omitted for clarity).

In the 100K structure 3c1 (data shown in Table 3.4), the molecules are closer together

than in the higher temperature structure; the shortest distance being from the methyl

group to a chlorine atom (for C(1)-H(1A)···Cl(1), the C···Cl distance is 3.722(6) Å. This

is 0.27 Å greater than the sum of the covalent radii). The atoms of the pyridine ring are almost co-planar, but the BCl_3 group and the methyl group sit just out of the plane. This distance between the molecules increases after the phase transition (Table 3.6) because the molecules move away from each other and the methyl groups and BCl_3 groups move and rotate slightly so that the boron atom, Cl(3) and the methyl carbon, C(1) become co-planar with the atoms of the ring. The greater symmetry can be clearly seen in Figure 3.14.

The stacking diagrams shown in Figure 3.15 illustrate this more clearly. In the lower temperature structure (3c1), the two molecules "overlap" a little bit, with the methyl group of one molecule being positioned over the area of the phenyl ring of the next molecule in the stack. In the higher temperature structure, the molecules move away from each other somewhat, so there is no overlap of methyl groups and phenyl rings.

(3c1)   100K   (3c2)   180K
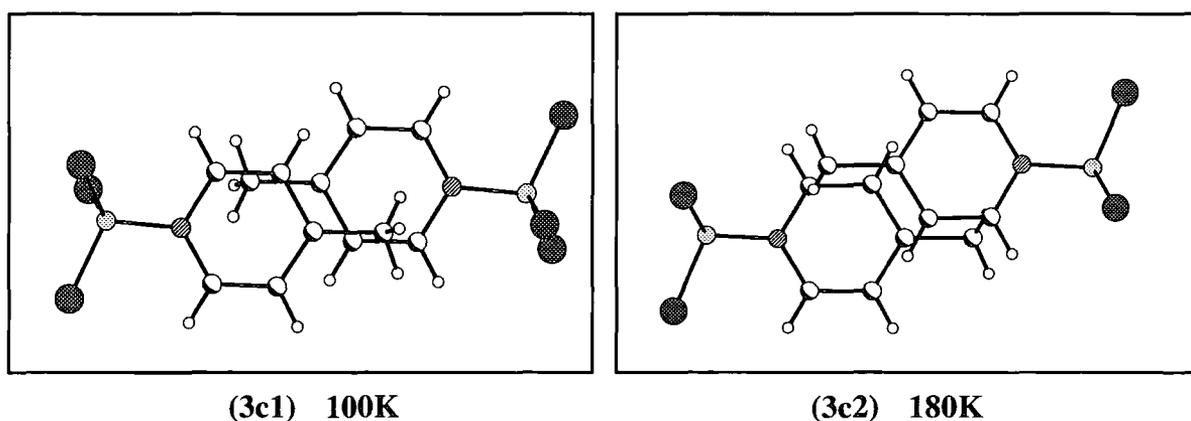
Figure 3.15: Stacking diagrams for structures (3c1) and (3c2). The projection if perpendicular to the plane of the N(1)-C(2)-C(3)-(C4)-C(5)-C(6) ring.

The only structural characterisation of a $Br_3B \cdot picoline$ adduct obtained in this study is for (3f), and is shown in Figure 3.16. The compound crystallises in the monoclinic space group $P2_1/m$. The B-N distance of 1.582(5) Å is not significantly different from

those in the BCl_3 analogues, which is also the case for the $Br_3B \cdot$pyridine adduct.[116]. This suggests that changing the halogen atom on the boron has little effect on the B-N distance. Indeed, the B-N bond length in the BF_3 analogue[117] is 1.603(6) Å (the average of the two similar independent molecules). This is very similar to the BCl_3 and BBr_3 analogues, despite the fact that BF_3 is a weaker Lewis base than BBr_3 and BCl_3. Other than the obvious difference in the B-X bond length due to the different halogens, there are no significant differences in any of the bond lengths or angles.
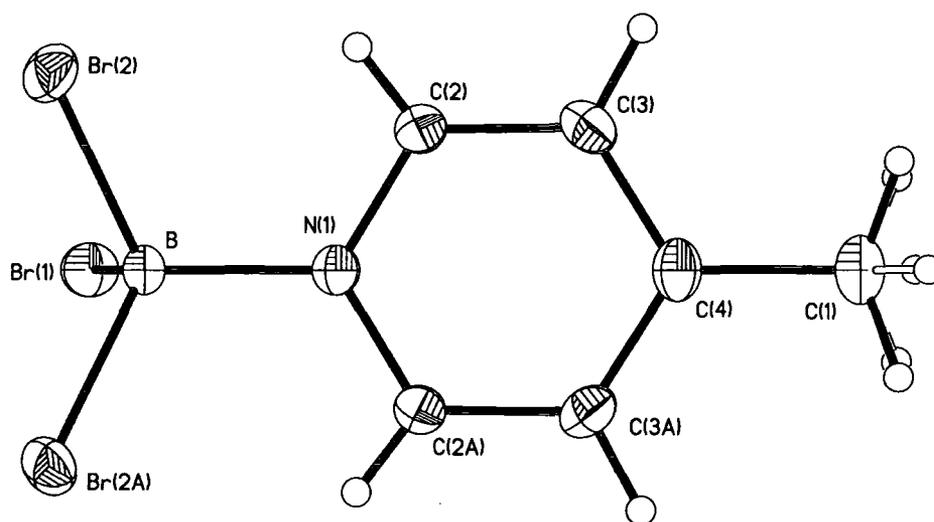
Figure 3.16: $Br_3B \cdot$4-picoline (3f) showing atom labelling. Thermal ellipsoids are plotted at the 50% probability level.

One point of interest is that although $Br_3B \cdot$4-picoline lies on a crystallographic mirror plane; the orientation of the pyridine ring is different from (3c2). The ring in (3f) lies perpendicular to the crystallographic mirror plane, not parallel to it as is seen for the chlorine-containing analogues.

A comparison of the structures presented above and the crystal structures of the picoline base alone is not possible for the 2-picoline adduct, since this structure has not been published. Structural data for 2-picoline species is only available where it has crystallised as a solvent hydrogen-bonded to another compound.[118] The structural

characterisation of 4-picoline, however, has been published.[119] Selected bond lengths

and angles for this structure are shown in Table 3.7 for comparison with analogous bond

lengths and angles in the BX_3 adducts (given in Table 3.6).

Table 3.7: Selected bond lengths and angles in 4-picoline from published data (CSD Refcodes ZZZIVG11 [A] and ZZZIVG02 [B], a neutron diffraction study, respectively).

#	$N-C_2$ (Å)	C_2-C_3 (Å)	C_3-C_4 (Å)	C_4-Me (Å)	C_2NC_3 (°)
A	1.337	1.397	1.392	1.506	116.77
B	1.344	1.390	1.397	1.499	116.10

No esds are provided as data was taken from the CSD.

It can be seen (from Table 3.6 and Table 3.7) that the N-C bond distances in the

uncoordinated 4-picoline are a little bit shorter (by 0.1 - 0.2 Å) than in the coordinated

4-picolines, and the C-N-C angles are 2° smaller when the base is uncoordinated. This

is presumably because of redistribution of the electron density on complex formation

with BX_3. The $C_{ring}-C_{methyl}$ bond distances are very similar in all structures (average

1.503 Å in uncoordinated 4-picoline and average 1.498 Å in coordinated 4-picoline),

suggesting that the electron density movement on complex formation does not affect

this bond greatly.

The bases used in these experiments all have very similar pKa values, thus changing the

base would not be expected to yield structural differences unless steric factors are

involved.

Table 3.8: pKa values[120] of the pyridine and picoline Lewis bases used in this study

Lewis Base	pKa value
pyridine	5.25
2-picoline	5.97
4-picoline	6.02

The nitrogen atom is expected to be a better donor atom to BX_3 than the phosphorus donors used in Chapter 2 due to the better size compatibility of nitrogen with boron, allowing better orbital overlap, forming a stronger dative bond. This meant that there was no real expectation of any exchange in solution as seen with the phosphine adducts of Chapter 2, and indeed no evidence for this was seen in the NMR data (Table 3.4).

The B-N bond lengths would be expected to shorten as Lewis acidity increased i.e. N-BF_3 > N-BCl_3 > N-BBr_3 with a possible difference due to increased steric hindrance caused by the adjacent methyl group when forming the 2-picoline adduct, but the variation in bond lengths are all within experimental error (Table 3.6) so no further conclusions can be drawn. The published F_3B·pyridine B-N bond length[121] of 1.603(5) Å is also within experimental error of the other pyridine adducts, so this was no surprise.

The structural data for (3b), (3c1), (3c2) and (3f) were analysed using Platon[122] and no unexpected short contacts or other packing phenomena were detected.

3.4 Conclusion

The characterisation data for these compounds hold few surprises. The proton NMR data shows very similar chemical shifts for all the adducts, with only a slight change noticeable on changing the Lewis acid from BCl_3 to BBr_3, this being accounted for by the increase in Lewis acidity. The $^{11}B\{^1H\}$ NMR data also reflects this change in acidity a little more significantly with a change in chemical shift of approximately 16 ppm on changing the acceptor molecule (the BCl_3 adducts have a shift close to 9 ppm, the BBr_3 adducts have a shift close to –8 ppm). Changing the Lewis base from pyridine to 2- and 4-picoline has little effect on the data which again is not surprising due to the similarity in pK_a values of the bases. The 2-picoline adduct NMR data, especially in the case of BBr_3, show a slightly anomalous shift if only pK_a values are considered since 2-picoline has a lower pK_a value than 4-picoline, but this discrepancy can be accounted for by the steric hindrance of forming the dative bond adjacent to the methyl group. This is only a small influence on the bond formation though since it is not reflected in the bond lengths (within experimental error).

3.5 Experimental

3.5.1 General Procedures

Air sensitive compounds were manipulated in a nitrogen atmosphere using Schlenk techniques or an Innovative Technology, Inc. System 1 glove box. Glassware was dried in an oven before transfer into the glove box. NMR spectra were recorded on Varian Mercury 200 (^{1}H, ^{13}C), Bruker AM-250 (^{1}H, ^{13}C), Varian Unity 300 (^{1}H, ^{13}C, ^{11}B), and Varian Unity Innova 500 (^{1}H, ^{11}B) instruments. Proton NMR spectra were referenced to external SiMe$_4$ via residual protons in the deuterated solvents, and ^{11}B chemical shifts were referenced to external BF$_3$·OEt$_2$. Chemical shifts are reported in ppm, coupling constants are reported in Hz and multiplicities are reported as (s) singlet and (m) multiplet. Elemental analyses were conducted in the Department of Chemistry at the University of Durham using an Exeter Analytical Inc. CE-440 Elemental Analyzer. Toluene was dried and deoxygenated by passage through columns of activated alumina and BASF-R311 catalyst under argon pressure using a modified version of the Innovative Technology, Inc. SPS-400 solvent purification system.[123] Chloroform and CDCl$_3$ were dried over calcium hydride, C$_6$D$_6$ was dried over potassium metal, and hexane was dried over sodium. All were distilled under nitrogen before use. Pyridine and picolines were purchased from Aldrich and Strem and were checked for purity by ^{1}H NMR before use.

3.5.2 Experimental Procedures

Synthesis of Cl$_3$B·pyridine (3a). A solution of pyridine (0.040 g, 0.506 mmol) in hexane (4 cm^3) was added dropwise to 1.0M BCl$_3$ in heptane (0.75 cm^3, 0.75 mmol) which had been diluted in hexane (4 cm^3). An off-white precipitate formed immediately.

After stirring for 6 h and cooling to –30 °C, 25% of the solvent was removed *in vacuo*. The product was isolated by filtration, washed with cold hexane (2 x 2 cm^3) and dried *in vacuo*, yielding 0.063 g of (**3a**) as a cream-coloured powder (65%). NMR (C$_6$D$_6$) ^{1}H δ 6.03 (m, 2H, *meta*-Py), 6.38 (m, H, *para*-Py), 8.72 (s (br), 2H, *ortho*-Py), ^{11}B{^{1}H} δ 8.9 (s), ^{13}C{^{1}H} δ 124.9 (s, Py) 141.9 (s, Py) 144.1 (s, Py). Found: C, 30.51; H, 2.67; N, 6.95%. Calculated for C$_5$H$_5$BCl$_3$N: C, 31.40; H, 2.63; N, 7.32%.

Synthesis of Cl$_3$B·2-picoline (3b). A solution of 2-picoline (0.047 g, 0.505 mmol) in hexane (4 cm^3) was added dropwise to 1.0M BCl$_3$ in heptane (0.75 cm^3, 0.75 mmol) which had been diluted in hexane (4 cm^3). An off-white precipitate formed immediately. After stirring for 6 h and cooling to –30 °C, 25% of the solvent was removed *in vacuo*. The product was isolated by filtration, washed with cold hexane (2 x 2 cm^3) and dried *in vacuo*, yielding 0.059 g of (**3b**) as an off-white powder (56%). NMR (C$_6$D$_6$) ^{1}H δ 2.82 (s, 3H, Me), 5.98 (m, 2H, *meta*-Py), 6.37 (m, 1H, *para*-Py), 9.72, (s (br), 1H, *ortho*-Py) ^{11}B{^{1}H} δ 8.9 (s, *B*-N), ^{13}C{^{1}H} δ 24.5 (s, CH$_3$), 122.1 (s, Py), 129.7 (s, Py), 141.6 (s, Py), 145.1 (s, Py). Found: C, 34.02; H, 3.44; N, 6.38%. Calculated for C$_6$H$_7$BCl$_3$N: C, 34.27; H, 3.35; N, 6.66%.

Synthesis of Cl$_3$B·4-picoline (3c). A solution of 4-picoline (0.047 g, 0.505 mmol) in hexane (4 cm^3) was added dropwise to 1.0M BCl$_3$ in heptane (0.75 cm^3, 0.75 mmol) which had been diluted in hexane (4 cm^3). A white precipitate formed immediately. After stirring for 6 h and cooling to –30 °C, 25% of the solvent was removed *in vacuo*. The product was isolated by filtration, washed with cold hexane (2 x 2 cm^3) and dried *in vacuo*, yielding 0.081 g of (**3c**) as a white powder (76%). NMR (C$_6$D$_6$) ^{1}H δ 1.30 (s, 3H, Me), 5.94 (m, 2H, *meta*-Py), 7.74 (m, 2H, *para*-Py), ^{11}B{^{1}H} δ 8.8 (s), ^{13}C{^{1}H} δ 20.7

(s, CH_3) 125.9 (s, Py) 143.4 (s, Py). Found: C, 34.48; H, 3.49; N, 6.46%. Calculated for $C_6H_7BCl_3N$: C, 34.27; H, 3.35; N, 6.66%.

Synthesis of $Br_3B \cdot$pyridine (3d). A solution of pyridine (0.040 g, 0.506 mmol) in hexane (4 cm^3) was added dropwise to BBr_3 (0.129 g, 0.515 mmol) in hexane (3 cm^3). A white precipitate formed immediately. After stirring overnight, and cooling to -30 °C, the product was isolated by filtration, washed with cold hexane (2 x 2 cm^3) and dried *in vacuo*, yielding 0.104 g of (**3d**) as a white powder (62%). NMR (C_6D_6) ^1H δ 5.99 (m, 2H, *meta*-Py), 6.34 (m, 1H, *para*-Py)), 9.00 (s (br), 2H, *ortho*-Py), $^{11}B\{^1H\}$ δ -6.8 (s), $^{13}C\{^1H\}$ δ 124.8 (s, Py), 142.1 (s,Py), 145.3 (s, Py). Found: C, 18.22; H, 1.53; N, 4.25%. Calculated for $C_5H_5BBr_3N$: C, 18.43; H, 1.57; N 4.15%.

Synthesis of $Br_3B \cdot$2-picoline (3e). A solution of 2-picoline (0.047 g, 0.505 mmol) in hexane (4 cm^3) was added dropwise to a solution of BBr_3 (0.129 g, 0.515 mmol) in hexane (3 cm^3). An off-white precipitate formed immediately. After stirring overnight and cooling to -30 °C, 25% of the solvent was removed *in vacuo*. The product was isolated by filtration, washed with cold hexane (2 x 2 cm^3) and dried *in vacuo*, yielding 0.128 g of (**3e**) as an off-white powder (74%). NMR (C_6D_6) ^1H δ 2.91 (s, 3H, Me), 5.96 (m, 2H, *meta*-Py), 6.35 (m, 1H, *para*-Py), 9.58, (s (br), 2H, *ortho*-Py). $^{11}B\{^1H\}$ δ -7.9 (s), $^{13}C\{^1H\}$ δ 25.8 (s, CH_3) 122.3 (s, Py), 130.3 (s, Py), 142.1 (s, Py), 147.1 (s, Py). Found: C, 21.04; H, 2.07; N, 3.97%. Calculated for $C_6H_7BBr_3N$: C, 20.97; H, 2.05; N, 4.08%.

Synthesis of $Br_3B \cdot$4-picoline (3f). A solution of 4-picoline (0.047 g, 0.505 mmol) in hexane (4 cm^3) was added dropwise to a solution of BBr_3 (0.132 g, 0.527 mmol) in

hexane (3 cm^3). An off-white precipitate formed immediately. After stirring overnight and cooling to -30 °C, 25% of the solvent was removed *in vacuo*. The product was isolated by filtration, washed with cold hexane (2 x 2 cm^3) and dried *in vacuo*, yielding 0.117 g of (**3f**) as an off-white powder (67%). NMR (C$_6$D$_6$) ^{1}H δ 1.25 (s, 3H, Me), 5.86 (m, 2H, *meta*-Py), 8.90 (s (br), 2H, *ortho*-Py), ^{11}B{^{1}H} δ -6.9 (s), ^{13}C{^{1}H} δ 20.6 (s, CH$_3$) 125.6 (s, Py) 144.6 (s, Py). (Found: C, 21.21; H, 2.09; N, 4.00%. Calculated for C$_6$H$_7$BBr$_3$N: C, 20.97; H, 2.05; N, 4.08%).

3.5.3 Crystallography

Crystals of (**3b**), (**3c**), and (**3f**), were examined on a Bruker AXS SMART CCD diffractometer with Mo-Kα radiation (λ= 0.71073Å) and a Cryostream (Oxford Cryosystems) open-flow N$_2$ gas cryostat. Semi-empirical absorption corrections, were applied using SADABS.[124] The structures were solved by direct methods, and refined on F^2 values for all unique reflections. The largest electron density features were close to heavy atoms. Programs were standard manufacturers' control and data processing software, together with SHELXTL[125] and local programs.[126]

Chapter 4: Substituted and selectively fluorinated 1,4-bis(phenylethynyl)benzenes: arene-perfluoro-arene interactions and crystal packing motifs.

4.1 Introduction

Non-covalent interactions play a very important role in determining the structure of crystals, and a detailed knowledge of the many different types is the aim of those looking to prepare the 'designer crystal'.[127] The vast variety of these interactions, however, mean there is much work still to be done before crystal engineering approaches an 'exact science' and not educated guess work! The strongest non-covalent interaction is the hydrogen bond. It has been studied in much detail,[128] and has been used widely to enable crystal engineering. Other weaker, more subtle interactions, however, are often implicated in molecular self-assembly and are being investigated widely in further attempts to engineer crystals to a specific motif and control crystalline, including liquid crystalline, behaviour.[129]

One such subtle effect, the arene-arene interaction, which occurs between two phenyl rings of aromatic compounds, is thought to be the origin of certain, often biological, phenomena. The interaction of aromatic bases in DNA is, for example, thought to play a role in the double helix motif by contributing some of the attractive forces which holds the elegant structure together. Indeed, the carcinogenic properties of certain aromatic compounds is thought to be due to their ability to intercalate themselves between other bases in the double helix, thus altering the conformation of the DNA. Aromatic interactions have also been implicated[130] in the catalytic activity of metallocene complexes where the interaction helps to align the substrate prior to binding in the organisation of peptides and proteins, and in the molecular recognition[131] of ammonium and imminium ions by a cyclophane host (a cation-π-interaction).[132]

A special case of the arene-arene interaction, the arene-perfluoroarene interaction, was first reported in 1960.[133] It was found that a 1:1 mixture of benzene and hexafluorobenzene (HFB), which have melting points of 5.4°C and 5.0°C respectively, formed a solid with a melting point of 23.7°C. A phase diagram was later constructed for varying compositions of the two components. The maximum melting point was found to occur for the equimolar mixture, and thus it was postulated that a 1:1 complex formed, held together by arene-perfluoroarene interactions. The nature of the interaction, however, was to remain a puzzle for some time. A similar white solid was also observed in the 1:1 mixture of aniline and HFB, which showed that this phenomenon was not solely observed for the benzene·HFB system.

Further work was carried out on these and other such systems to determine the nature of these complexes and their interactions. Phase diagrams for the mixtures of HFB with a variety of methyl-substituted benzene derivatives[134] showed that, for the majority, the complexes seemed to form when the composition was 1:1. A complex did not occur in the mixture of HFB and pentafluorobenzene (PFB), but complexes were shown to be present in mixtures of PFB with methyl-substituted benzenes.[135]

Differential scanning calorimetry (DSC) studies[136] alluded to the possibility of four different solid-state phases in the complex. The highest temperature phase was probed by single crystal X-ray diffraction[137] and although the structure was quite disordered it did demonstrate the presence of infinite stacks of alternating benzene·HFB units. This is significantly different to the herringbone packing displayed in the crystals of the individual components.[138] X-ray crystal structures of the other phases could not be obtained due to the crystals breaking into powder when cooled, but information was obtained some years later by neutron powder diffraction.[139] Again, it was found that the

structures of the lower temperature phases also consisted of infinite columns of alternating benzene and HFB molecules (see Figure 4.1).
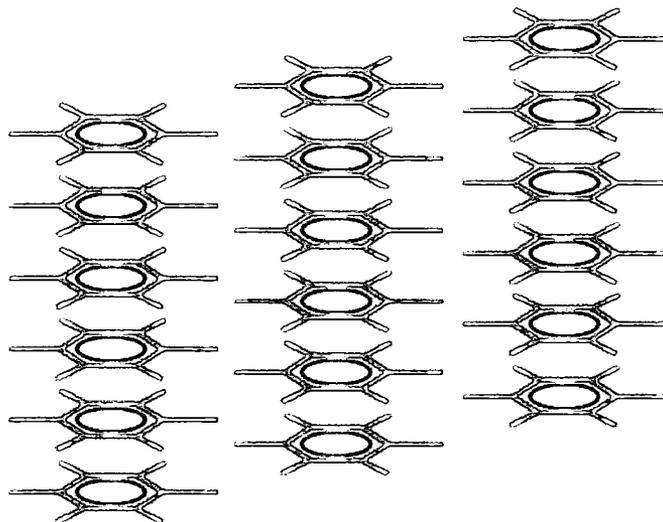
Figure 4.1: Infinite stacks of alternating phenyl (black and red) and perfluorophenyl (black and green) units in the 1:1 complex of benzene with hexafluorobenzene.

The attractive forces which held these structures together was originally believed to originate via charge transfer between a donor and an acceptor, but since there were no characteristic UV absorptions for the HFB and methylbenzene complex, this theory was abandoned in favour an explanation based on electrostatic interactions. The basis of this interaction is the quadrupole moment present in both benzene and hexafluorobenzene.

It is widely accepted that benzene is non-polar. It has no net dipole moment, which occurs if one end of the molecule has more electron density than the other. The distribution of electron density across the benzene ring, however, is not uniform. The slightly greater electronegativity of carbon compared to hydrogen leads to the electrons in the π-system being localised on the carbon atoms. This makes the area above and below the centre of the ring slightly negatively charged, but the area at the periphery, where the hydrogen atoms are located, slightly positively charged. It can be thought of

as an electron rich core surrounded by an electron-poor torus (doughnut-shape) of hydrogen atoms. This electrostatic inhomogeneity is known as a quadrupole. The quadrupole in benzene[140] is of magnitude -29×10^{-40} C m^{-2}.

The presence of this quadrupole can explain the common T-shaped arene-arene interaction seen in its most simple form in crystalline benzene. The phenyl rings align perpendicular to each other, so that the slightly positive area of one ring is pointing directly towards the negative centre section of an adjacent ring. This quadrupolar effect can also explain how benzene, a hydrocarbon which can be thought of as being hydrophobic, can interact with polar molecules such as water.[141] The δ+ hydrogen atoms in the water molecule align so they are pointing into the negative area of the benzene quadrupole.

Hexafluorobenzene also has a quadrupole. It again has no net dipole and consists of two atom types, carbon and fluorine, with differing electronegativities. In this case, however, fluorine is more electronegative than carbon, so the centre of the ring, nearest the carbon atoms, is the electron poor area, and the torus of fluorine atoms is electron rich. The magnitude[140] of this quadrupole is 31.7×10^{-40} C m^{-2}. This is of approximately the same magnitude, but opposite in sign, to benzene. Like benzene, in its pure form, hexafluorobenzene crystallises in a perpendicular fashion, end-to-face, so that the positive areas on one ring interact directly with the negative areas on the adjacent molecules. Hexafluorobenzene can also utilise the quadrupole to interact with water. This time, it is the oxygen atom which is oriented towards the centre of the ring, the opposite way to the benzene-water complex. The nature of the two quadrupoles in benzene and hexafluorobenzene – similar magnitudes but opposite signs – demonstrate

how it can be favourable for the two molecules to stack alternately on top of each other.[142]

Similar stacking motifs were seen[143] for complexes of hexafluorobenzene with methyl-substituted benzenes and aniline derivatives. The stacking is not restricted to benzene derivatives, with the 1:1 complex[144] of biphenyl and perfluorobiphenyl published in the late 70s demonstrating the same phenomenon. Other larger molecules have exhibited this stacking, and with their publication debate has raged as to the extent of electrostatic contribution to the system. Many calculations have been performed suggesting varying degrees of contribution from electrostatics, the remainder of the attractive force coming from van der Waals contributions.[145] A recent density functional calculation[146] suggested that the contribution to the overall potential from electrostatic component could be only 15% of the total, with dispersive (van der Waals) forces responsible for the remaining 85%. This is contrary to the common suggestion that the major influence in arene-perfluoroarene interactions is electrostatic. Recent unpublished results[147] from our collaborators, however, suggest that this result may have arisen from the over-simplification of the calculation by assigning partial charges to all the atoms and performing a time independent study. Since van der Waals forces are time dependent, the conclusions drawn from a time independent study seem doubtful. When a full electron distribution study[148] is undertaken, it is found that the electrostatic contribution is actually nearer to 90% of the total, with very little van der Waals contribution at all.

Potential applications of the arene-perfluoroarene interaction are plentiful, with some already being demonstrated in the literature. An elegant example was published by Grubbs *et al.*, who utilised it[149] to align monomers for solid state dimerisation and polymerisation initiated by UV radiation. The phenyl-substituted butadiynes

polymerised in this way are thought to give *cis*-polydiacetylenes, whereas normal polymerisation would give the *trans* isomers. The same group treated fluorinated stilbenes and distyrylbenzenes in the same way to give cyclobutanes and polycyclobutanes.[150]

The potential for use in molecular recognition was reported using a di-nuclear palladium macrocycle containing fluorinated phenyl rings which associates with benzene derivatives. The selectivity for the fluorinated macrocycle with *p*-dimethoxybenzene was 25 times that for *p*-dicyanobenzene. This specificity was not seen with the non-fluorinated macrocycle.[151]

Although the arene-perfluoroarene interaction is weak in the solution state, with attractive forces decreasing at a rate of r^{-5} (where r is the distance between two quadrupoles), it has been shown that it can influence solution state synthesis of macrocycles.[152] Arene-perfluoroarene attractive forces stabilised a transition state for partially fluorinated macrocycles, leading to a greater yield than for the non-fluorinated or completely fluorinated analogues where the transition state was not stabilised in this way.

A very recent example of the interaction occurring in the solution state was demonstrated by Grubbs.[153] When octafluoronaphthalene (OFN) is dissolved in high molecular weight (n $\approx$ 180) poly(ethylene glycol) (PEG) end capped with 1-pyrene butyroyl chloride followed by the addition of water, the PEG shows a large increase in viscosity. This is due to the the arene-perfluoroarene interaction between the pyrene groups and the OFN causing aggregation in solution, forming a hydrogel.

The interaction can influence the crystal structure in substituted ferrocenes[154] of the type $Fe(PhCp)_2$, with three different structural motifs observed for the $Fe(PhCp)_2$, $Fe(PhF_5Cp)_2$ and $(PhCp)Fe(PhF_5Cp)$. In the first compound, the two phenyl rings are in the anti conformation, avoiding each other. The unsymmetrical ferrocene shows an eclipsed conformation due to arene-perfluoroarene interaction between the two phenyl rings. Interestingly, the perfluoro derivative also shows an eclipsed formation, this time controlled by stacking of the fluorinated ring of one molecule interacting with the cyclopentadienyl ligand on the next molecule; again an example of arene-perfluoroarene interaction.

Other conjugated organic materials have been investigated and have shown interesting arene-perfluoroarene packing motifs. For example 4,4'-bis(2,3,4,5,6-pentafluorostyryl)stilbene, which it is hoped will have interesting electronic and optical properties, self-assembles into a 'brick-wall' structure held together by the arene-perfluoroarene interaction; each molecule overlaps with two halves of neighbouring molecules in the rows above and below it.[155] Many distyrylbenzene derivatives were investigated by Bazan[156] and co-workers, and many selectively fluorinated 1:1 co-crystals exhibited the influence of the arene-perfluoroarene interaction.

Our group's contribution to work in this area arose as part of continuing studies into bis-phenylethynylbenzene (BPEB) 'rigid rod' molecules. The structure, linear and non-linear optical properties and liquid crystal phase behaviour of these conjugated rigid rod systems is being investigated. Work on a huge variety of rigid rods has been widespread, in our group and others, over the last decade and is an area of continuing interest.[157]

The BPEBs in which our group is interested are prepared by palladium (or copper) catalysed cross-coupling reactions of the appropriate terminal alkenes with iodoarenes. This method allows synthesis of different variations and combinations of arene and perfluoroarene moieties in the rod.

Our emerging interest in arene-perfluoroarene interactions led to attempts to crystallise and co-crystallise (where two components are crystallised together to form a crystal made of both componenents) the BPEBs to investigate any interactions of this type, and also to investigate how the presence or absence of the interaction affects the liquid crystal (LC) phase behaviour.

To compare and contrast these crystals with each other and with their individual components, there are many parameters which can be used. First, there are the key bond lengths and angles within the molecule, and the dihedral angles between the phenyl rings. To describe the intermolecular arrangement, two main parameters are used:

1. **Inter-centroid distance:** (or **inter-ring** distance): The distance between the ring centroids of aromatic rings on adjacent molecules in the stack. The larger this is, the greater the 'ring slip'. If the molecules were aligned directly on top of each other, the inter-centroid distance and the inter-planar would be almost identical.

2. **Inter-planar distance:** The perpendicular separation between the mean planes of the molecules in the stacks. This is calculated by finding the perpendicular distances between the mean plane of one phenyl ring (usually the central ring) and the centroid of the ring directly above, and vice versa, then averaging the two values.

The possibility of intermolecular interactions can also be assessed by considering the van der Waals radii of the atoms in question. The radii used here[158] are 1.20 Å (H), 1.47 Å (F), 1.55 Å (N) and 1.70 Å (C).

The packing coefficient, K, is calculated[159] to give an idea of the efficiency of packing in the crystal. It is defined as

$$K = \frac{ZVo}{V}$$

where Z = number of molecules in the unit cell

V_o = molecular volume

V = volume of the unit cell

It has been calculated here using the crystallographic analysis package PLATON.[160] This application applies a grid to the unit cell with a grid step of 0.20 Å. The grid points are probed for electron density using a knowledge of the atomic coordinates of the molecules within the unit cell. The percentage of space filled by the molecules is then calculated. A value of K = 0.74 is that of a close packed arrangement of spheres, and structures typically have a packing coefficient of K ≈ 0.65. The larger the value of K, the more efficient the packing.

Halogen⋯halogen contacts[161] also feature in certain structures. There are two major types of these. Type I contacts generally have two very similar bond angles around the contact, and are thought to arise as a consequence of other close packing forces. Type II contacts, where the two angles are different, can potentially be stabilising forces in the structure. These halogen⋯halogen contacts are discussed further in Chapter 5.

The first investigation used the unsubstituted 'parent' BPEBs shown in Figure 4.2.
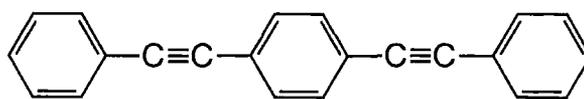
Ph-CC-Ph-CC-Ph

1,4-bis(phenylethynyl)benzene
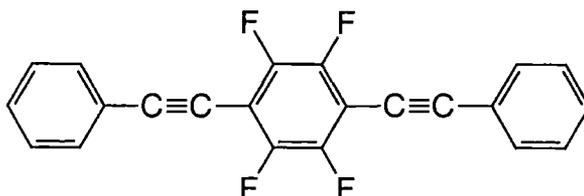
Ph-CC-PhF$_5$-CC-Ph

1,4-bis(pentafluorophenylethynyl)tetrafluorobenzene
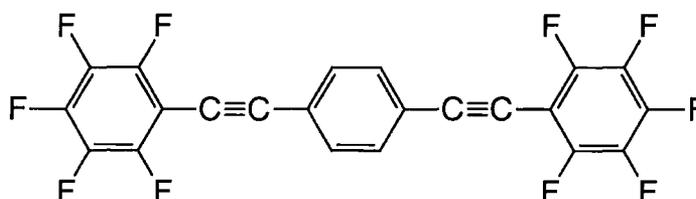
PhF$_5$-CC-Ph-CC-PhF$_5$

1,4-bis(phenylethynyl)tetrafluorobenzene)
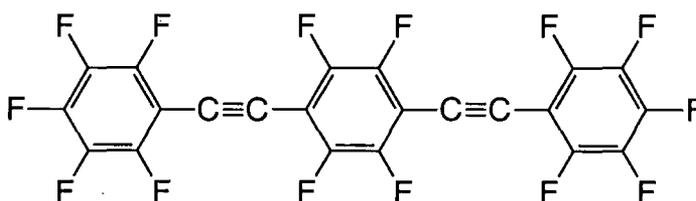
PhF$_5$-CC-PhF$_5$-CC-PhF$_5$

1,4-bis(pentafluorophenylethynyl)benzene

Figure 4.2: Structures of the 'parent' BPEB compounds, shown with their shorthand structures and full names.

Their individual crystal structures were determined and the LC phase behaviour investigated.[162] The structure of Ph-CC-Ph-CC-Ph (Figure 4.3) shows that the molecules pack perpendicularly to each other to avoid any face-to-face interactions, and the unit cell packing shows a herringbone motif.
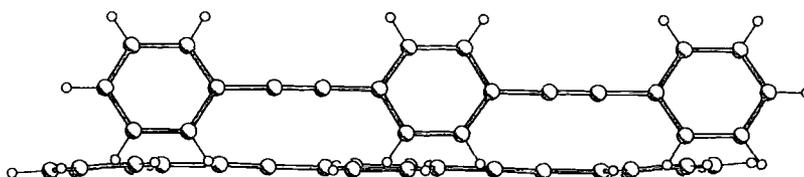
Figure 4.3: Structure of Ph-CC-Ph-CC-Ph showing how the perpendicular packing avoids face-to-face interaction of the phenyl rings.

The herringbone packing can clearly be seen in Figure 4.4.
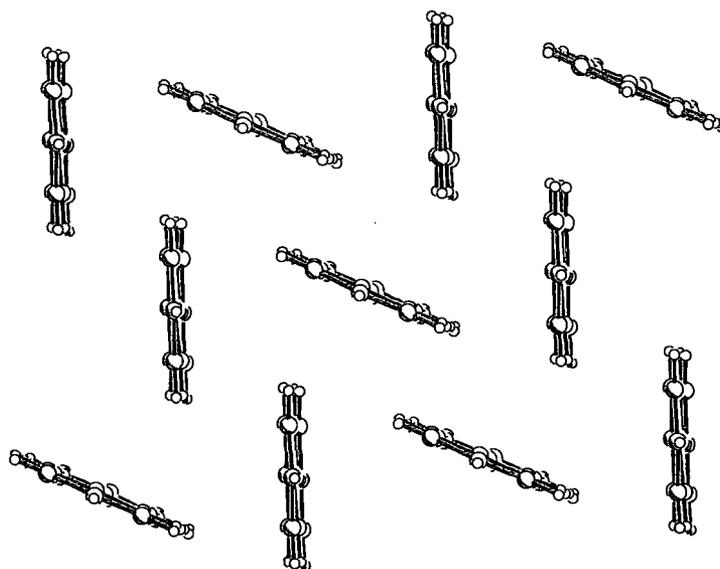
Figure 4.4: Packing diagram for Ph-CC-Ph-CC-Ph, viewed down the molecular axis, showing the herringbone packing motif.

The other three parent molecules stack in infinite columns but the rods are arranged to minimise any unfavourable interactions by positioning the phenyl rings above and below (and offset from) the triple bond of the adjacent molecule, as shown in Figure 4.5 to Figure 4.7 below.
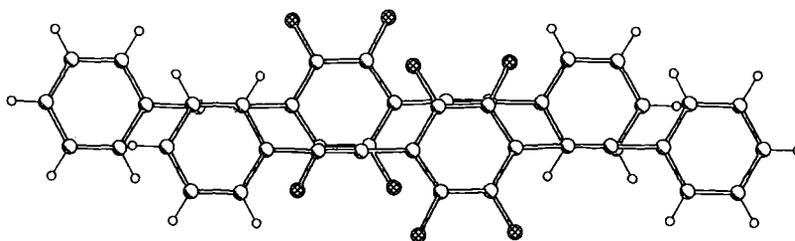
Figure 4.5: Structure of Ph-CC-PhF$_5$-CC-Ph showing how the stacking avoids face-to-face interaction of the phenyl rings.
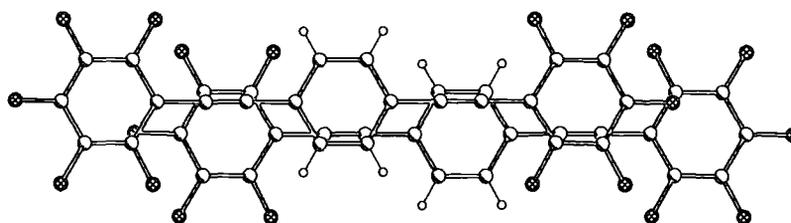
Figure 4.6: Structure of PhF$_5$-CC-Ph-CC-PhF$_5$ showing how the stacking avoids face-to-face interaction of the phenyl rings.
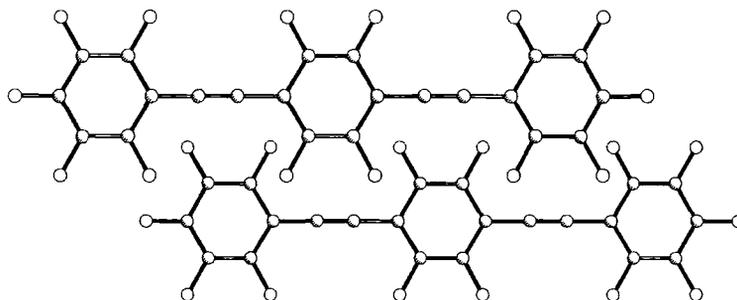
Figure 4.7: Structure of PhF$_5$-CC-PhF$_5$-CC-PhF$_5$ showing how the stacking avoids face-to-face interaction of the phenyl rings.

In an attempt to activate the arene-perfluoroarene interaction for these systems, PhF$_5$-CC-Ph-CC-PhF$_5$ and Ph-CC-PhF$_5$-CC-Ph were co-crystallised by dissolving solid samples of the two components into hot CHCl$_3$; the crystals were collected on cooling. The single crystal structure showed clear π-stacking of alternating phenyl and perfluorophenyl moieties along the b axis of the unit cell (see Figure 4.8, below). The spacing between all molecules along the b axis is equal since all molecules are sitting on

inversion centres. The interplanar distance is 3.337 Å, and the inter-ring distance is 3.770 Å.
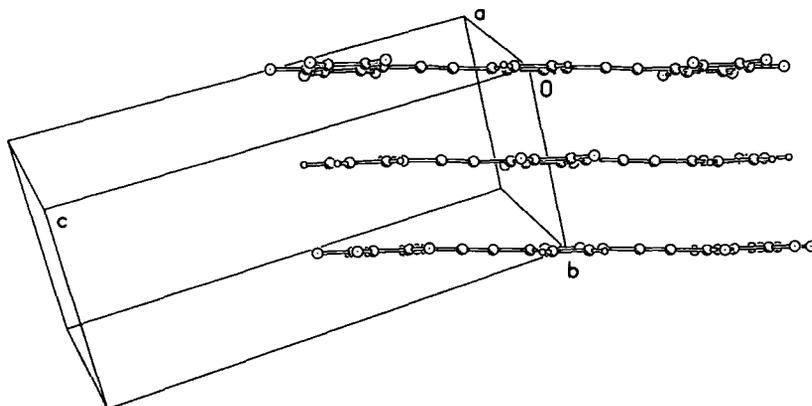
Figure 4.8: Packing diagram showing the stacking along the *b* axis.

When viewed perpendicular to the C_6H_6 central ring of PhF$_5$-CC-Ph-CC-PhF$_5$, it can be seen that there is a lateral ring slippage of about one C-C bond length (see Figure 4.9 below). The dihedral angle between the inner and outer rings is 3.9° in Ph-CC-PhF$_4$-CC-Ph and 3.0° for PhF$_5$-CC-Ph-CC-PhF$_5$. This is small compared to the corresponding angles in the crystal structures of the individual molecules (16.7° and 9.7° respectively). Near-planarity is presumably necessary for optimum arene-perfluoroarene interaction.
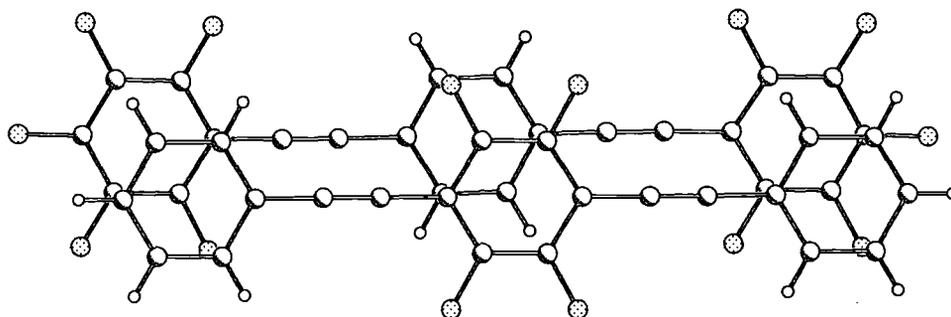
Figure 4.9: Plot of two molecules viewed perpendicular to the central C_6H_6 ring, showing the 'slippage' of about one C-C bond distance.

The intermolecular distances between the stacks are quite small, with C-H···F-C distances of 2.500 – 2.574 Å. This is just smaller than the sum of the van der Waals

radii (2.67 Å). C-F···H and C-H···F angles are 120° - 160°, thus the molecules almost form planar sheets. The distances between the ring centroids in adjacent molecules are 3.770 Å for the central rings, and 3.750 Å for the outer rings. These inter-centroid vectors are inclined on average 25.7° to the plane normals.

Liquid crystal phase transitions on heating, and the axial ratio for all of the parent compounds, were also presented in the co-crystal paper[32] by Marder *et al.*. The four individual compounds showed little liquid crystal behaviour. The rod with the largest axial ratio, which is the length of the molecule divided by its width, is Ph-CC-Ph-CC-Ph, which shows no liquid crystal behaviour on heating, but does show a small nematic phase on cooling. PhF_5-CC-Ph-CC-PhF_5 is transiently nematic. The co-crystal detailed above, however, does show liquid crystal behaviour, with evidence of a nematic phase present between 189.3 and 199.0°. This is evidence to suggest that the arene-perfluoroarene interaction could be responsible for this behaviour. First, nematic liquid crystals tend to form where there are rod-like molecules present, so it seems unlikely that the C-H···F interactions persist and hold any sheets together at higher temperatures. Second, one of the single component systems with both fluorophenyl and phenyl moieties showed liquid crystal behaviour. Third, the axial ratio of even the longest rod here is 4.45. This is very small and unlikely to stabilise a liquid crystal without extra interactions providing added stability. Thus it seems likely that the arene-perfluoroarene stacking interactions are the cause of the liquid crystal behaviour.

The other two component system, Ph-CC-Ph-CC-Ph with PhF_5-CC-PhF_4-CC-PhF_5, was tested for liquid crystalline behaviour in this study. It was found again that the two component system had a greater range of liquid crystallinity, and the temperature at

which an isotropic phase was reached was higher, than for the individual components. This was the same for both of the two component systems.

Crystals of the two component system with the AAA⋯BBB motif has been solved[iii] but it is as yet unpublished. It is, however, quite an unusual structure and will be included here for reference purposes later. The crystal structure determinations of the two individual components show no arene-arene interactions (Figure 4.3 and Figure 4.7). When they are mixed together a 2:1 co-crystal of Ph-CC-Ph-CC-Ph with PhF$_5$-CC-PhF$_4$-CC-PhF$_5$ forms exhibiting the influence of the arene-perfluoroarene interaction. The fluorinated molecule is sandwiched by two molecules of the hydrogen analogue (see Figure 4.10 and Figure 4.11), although the top and bottom molecules are offset from the fluorinated rod.
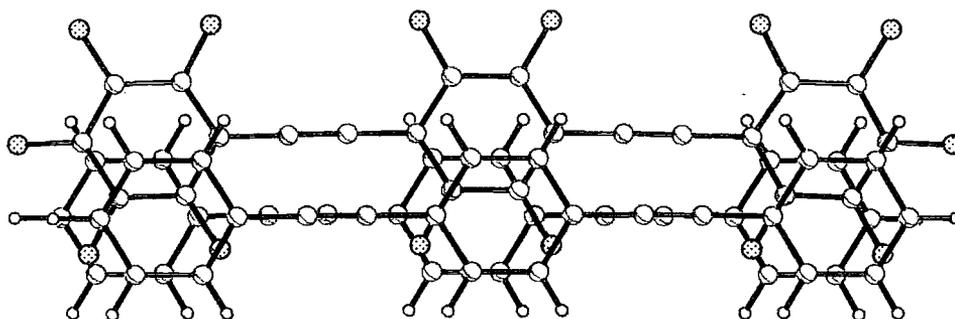
Figure 4.10: Overlap diagram showing the offset sandwich, viewed perpendicular to the central fluorinated ring.
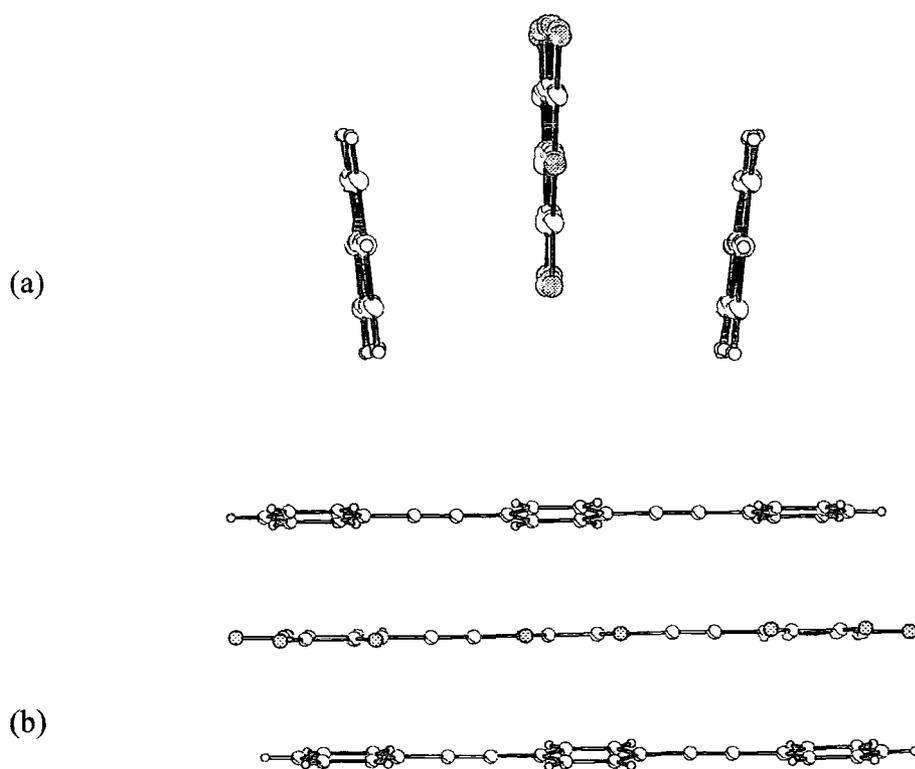
Figure 4.11: The 2:1 co-crystal sandwich, shown (a) down the rod and (b) parallel to the fluorinated rod.

The system crystallises in the orthorhombic space group *Fddd*. The fluorinated molecule lies on a crystallographic two-fold rotation axis which passes through opposite C-C bonds of its central ring and it is symmetrically sandwiched by the 2 hydrogen analogue molecules. The molecules are approximately parallel to each other. Adjacent stacked rings have dihedral angles of less than 10°, as can be seen in Figure 4.11(b), above. The fluorinated rod is not exactly parallel to the two sandwiching rods, which makes determining an interplanar distance problematic since it is difficult to know where to measure. The mean stacking separation is 3.571 Å, determined by assessing the distance between the two outer molecules of the sandwich.

These three molecule units pack within the crystal in two diagonal stacking directions at an angle of 82.7°. This almost orthogonal stacking makes for an attractive packing motif

(see Figure 4.12 and Figure 4.13). For adjacent 'sandwiches', the adjacent Ph-CC-Ph-CC-Ph molecules on each sandwich are related by inversion symmetry and separated by 3.553 Å.
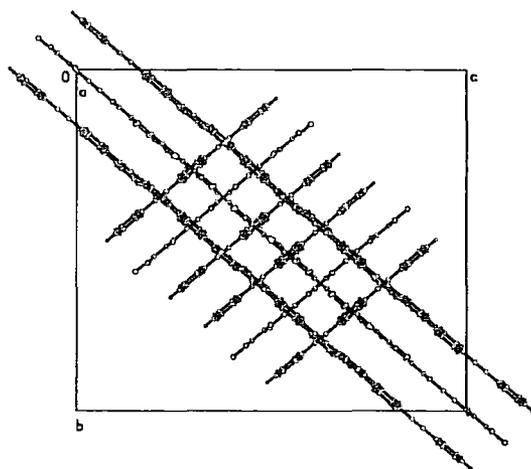
Figure 4.12: Stacking diagram down the a axis showing the almost perpendicular stacks.
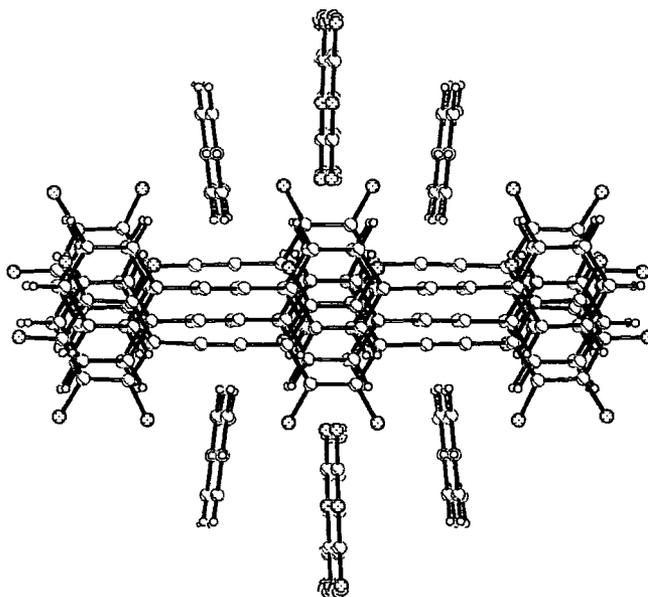
Figure 4.13: Stacking diagram shown perpendicular to the plane of the centre fluorinated ring of one of the stacks, again illustrating the almost perpendicular stacking arrangement.

The shortest intermolecular contact between side-by-side stacks is the F···F contact in the 4 position on the fluorinated rod; this is 2.528 Å, which compares to the sum of the van der Waals radii of 2.94 Å. The shortest H···F contacts (after the C-H bonds were

extended[iv] to 1.08 Å) were 2.52 to 2.66 Å (sum of van der Waals radii 2.67 Å). A computer modelling study was undertaken to establish whether the crystal structure was dominated by face-to-face or edge-to-edge contacts.[163] The face-to-face interactions were found to be the major source of π-stacking stability.

Liquid crystal behaviour of this unusual system was investigated by differential scanning calorimetry (DSC) and transmitted polarised light microscopy, and suitably surprising results were encountered. On cooling from an isotropic phase, the melted crystal exhibits two different sequences of phase changes over several samples and runs, and with no obvious preference for either. The melt either cools via a smectic (S1) LC phase to a solid (X1) which, when re-heated, behaves in the same way as the original co-crystal, or a different smectic (S2) phase is seen followed by a solid of a different visual appearance (X2). The transition temperatures from smectic to solid are also different.

[iv] C-H bond distances determined by single crystal X-ray diffraction are usually of the order 0.95 Å. This distance is often 'neutron corrected' to 1.08 Å since this is the usual distance as determined by neutron diffraction. X-ray diffraction locates electron distribution and the nuclei involved in a C-H bond are placed at the points of maximum density in the experimentally determined electron density. These do not always coincide with nuclei positions.

A neutron beam is scattered by the nucleus itself, thus giving a more accurate determination of the nuclear position for structures where the positions of the hydrogen atoms are important. When discussing hydrogen bonded arrays, colinearity, coplanarity etc. of various moieties, it has become general practice to 'extend' the C-H to be equal to the neutron determined values. It is not strictly 'accurate', but it does enable better understanding and interpretation of the supramolecular structure, the packing and in some cases properties of the structures than the the fore-shortened X-ray derived distances.

4.2 Scope of this Study

The co-crystal data of the parent BPEB systems, cited above, will be analysed further since these structures are the background to my work in this chapter. The majority of this early work was carried out by the authors of the original paper, with most of the crystallography performed by Andrew Scott at the University of Newcastle-upon-Tyne. The structure of some substituted BPEBs, again solved by Andrew Scott, will be incorporated into the discussion since my own structures, which are BPEB co-crystals, where one or both of the components have substituents in the 4 position on the terminal phenyl groups, are directly related to these above. The effect of the substituents on the packing, with a view to determining the limitations of the arene-perfluoroarene interaction with respect to other functionalities, is considered. Liquid crystal data, determined by Stephen Watt at Heriot-Watt University under supervision of Prof. Christopher Viney, is presented in brief for comment.

4.3 Results and Discussion

Crystal structures of two distinct types have been investigated. The first set consist of BPEBs of formula:
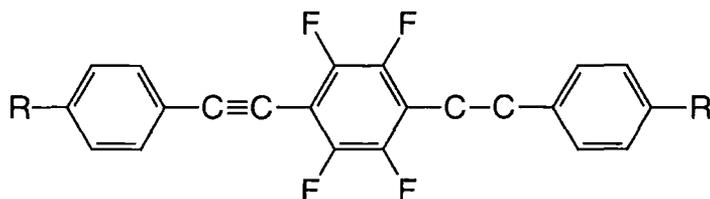
where R = CH$_3$ (**4b**), SMe (**4c**) and CF$_3$ (**4d**) which have been co-crystallised with parent BPEB PhF$_5$-CC-Ph-CC-PhF$_5$ (**4a**). The co-crystals can be said to have an ABA⋯BAB motif; that is they consist of two molecules, one with a fluorinated inner ring (an ABA ring) and one with two fluorinated outer rings (a BAB molecule).

The second set consist of two BPEB co-crystals with AAA⋯BBB motif, both containing:
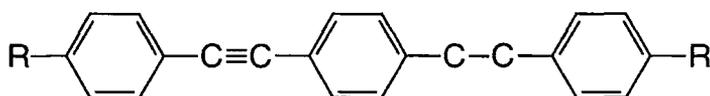
where R = CF$_3$ (**4f**) and OMe (**4g**), but with the second component of the co-crystal being PhF$_5$-CC-PhF$_4$-CC-PhF$_5$ (**4e**) and MeO-PhF$_4$-CC-PhF$_4$-CC-PhF$_4$-OMe (**4h**) respectively.

It can be seen that in each of the two different co-crystal motifs, the two components can pair up in a variety of ways, including directly on top of each other, slipped by a small amount or slipped by one or two rings, leading to many possible crystal packing patterns.

4.3.1 ABA···BAB packing motif

The structures of the separate components

The single crystal X-ray structures of PhF_5-CC-Ph-CC-PhF_5 (**4a**), CH_3-Ph-CC-PhF_4-CC-Ph-CH_3 (**4b**), MeS-Ph-CC-PhF_4-CC-Ph-SMe (**4c**) and F_3C-Ph-CC-PhF_4-CC-Ph-CF_3 (**4d**) were determined previously.[164] Single crystals of CH_3-Ph-CC-PhF_4-CC-Ph-CH_3 (**4b**) were grown from the melt[v] and colourless single crystals of F_3C-Ph-CC-PhF_4-CC-Ph-CF_3 (**4d**) were grown by evaporation from toluene. The structures of these two compounds were determined again, at 110(2)K and 100(2)K respectively. These four components were combined to make the co-crystals presented in this section, thus some discussion of the structures of the individual components is necessary for comparison purposes. The new structures of (**4b**) and (**4d**) will be presented in detail.

PhF_5-CC-Ph-CC-PhF_5 (**4a**) crystallises in space group $P2_1/c$. The molecule lies on a centre of symmetry. The mean planes of the inner and outer rings are at 9.7° to each other, indicating some slight deviation from planarity. The C≡C triple bond length is typical (1.198(3) Å). The C-C single bond length adjacent to the fluorinated ring (1.424(3) Å) is comparable to the equivalent bond adjacent to the non-fluorinated ring (1.438(3) Å). The crystallographic unit cell dimensions show that the b-axis length is short compared to a and c (a = 15.100(1), b = 4.9040(5), c = 11.709(1), β = 99.580(2)). This short axis defines the packing, as described by Desiraju and Gavezzotti,[165] which can be described in this case as a flattened herringbone, or γ-type packing, as shown in Figure 4.14.
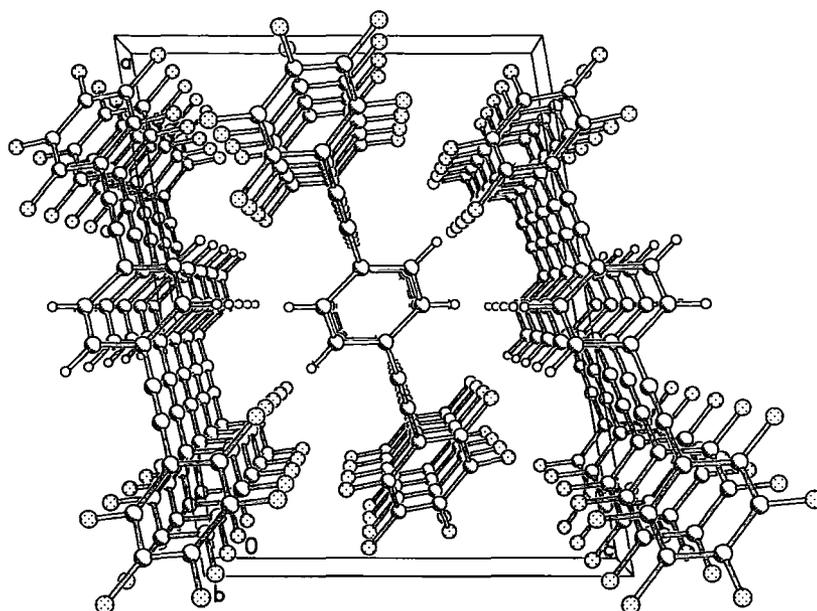
Figure 4.14: Packing plot for PhF$_5$-CC-Ph-CC-PhF$_5$ (4a), viewed down the *b*-axis, showing the γ-type flattened herringbone packing.

The molecules themselves, when viewed perpendicularly to the plane of the central ring, can be seen to line up with the phenyl rings over the C≡C of the adjacent ring (see Figure 4.15). The inter-centroid distance is 4.866 Å. This appears to be large because the phenyl rings are not stacked directly on top of each other but are displaced and so align above and below the triple bond. The inter-planar distance is 3.392 Å , and the packing coefficient is 0.737, both indicating a relatively closely packed.
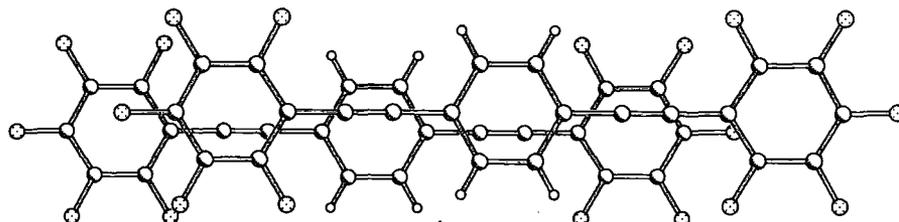
Figure 4.15: Plot of two adjacent molecules of PhF$_5$-CC-Ph-CC-PhF$_5$ (4a) plotted perpendicular to the central ring, showing how the phenyl rings line up with the C≡C triple bonds.

The structure of CH$_3$-Ph-CC-PhF$_4$-CC-Ph-CH$_3$ (4b) was first obtained at 180K by Nick Taylor at the University of Waterloo. This structure was found to be monoclinic,

crystallising in space group $P2_1/c$, with cell parameters a = 14.704(1), b = 4.9542(5), c = 11.819(1), β = 94.292(7). These parameters are very similar to those for PhF_5-CC-Ph-CC-PhF_5, which packed with the phenyl rings above and below a triple bond. The short *b* axis distance again suggests a γ-type pack, but the full coordinate set are not available to compare the structure fully.

Further crystals of **(4b)** became available during studies into LC behaviour. Data were collected from one of these to obtain a complete analysis of the structure; the crystal and refinement data are available in Appendix A4b. Structural data, however, at 110(2)K indicated a different polymorph which, unlike the Waterloo structure, showed arene-perfluoroarene interactions. The compound crystallised in space group $P\bar{1}$ with cell parameters (a = 6.1102(6), b = 8.0296(7), c = 9.3699(9), α = 81.971(2), β = 82.178(2), γ = 75.552(2)). It is this polymorph to which reference will be made for the rest of this work. (See Figure 4.16).
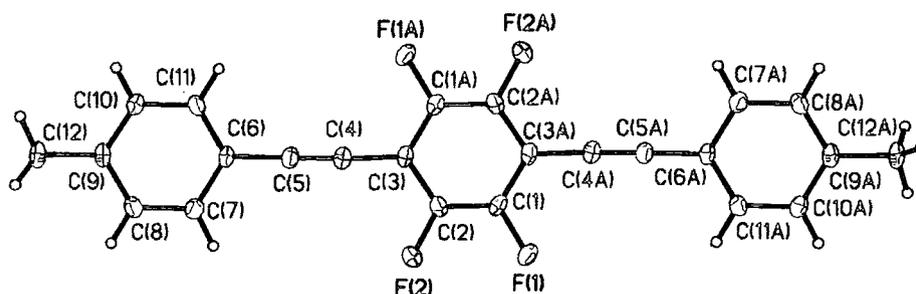
Figure 4.16: Ortep diagram for (4b). Thermal ellipsoids are plotted at 50% probability level.

The molecule of **(4b)** lies on an inversion centre. The C-C single bond distance adjacent to the fluorinated ring (1.434(2) Å) is similar to the distance of the equivalent bond adjacent to the non-fluorinated ring (1.429(2) Å), and both are significantly shorter than the C-CH_3 bond distance (1.509(2) Å). The C≡C triple bond length of 1.201(2) Å is typical. The bond angles between the phenyl ring and the triple bond section of the rod

are very close to 120°, indicating the linear nature of the rod. The dihedral angle (the

angle between the mean planes of the inner and outer rings) is 8.9°, indicating a slight

deviation from planarity. The methyl groups at each end of the rod are eclipsed,

presumably to minimise steric repulsion with the adjacent rod. The packing coefficient,

K, is 0.721.
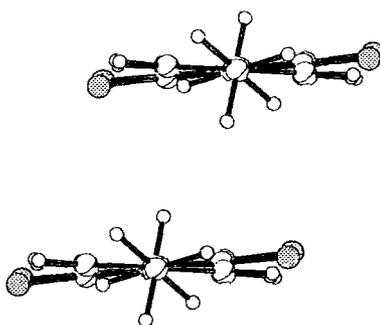
Figure 4.17: Diagram of two stacked molecules of **4b**, viewing down the rod axis. The fluorinated ring (with fluorine atoms shown in green), can be seen to be at an angle (9.0°) to the non-fluorinated phenyl ring (five atoms in a row, shown as unfilled circles).

As can be seen in Figure 4.17, above, the molecules stack on top of each other with a

slight lateral offset (approximately one C-C bond distance). The molecules arrange

themselves so the rods are slipped by one ring to maximise the number of times a

phenyl ring can sit directly above a perfluorophenyl ring, suggesting an arene-

perfluoroarene interaction is influencing the stacking. (see Figure 4.18, below). The

inter-centroid distance between a phenyl and a perfluorophenyl ring is 3.929 Å, and

between a phenyl and a phenyl ring is 4.066 Å. The inter-planar distance, calculated

using the rings involved in arene-perfluoroarene interaction, is found to be 3.478 Å.

(a)
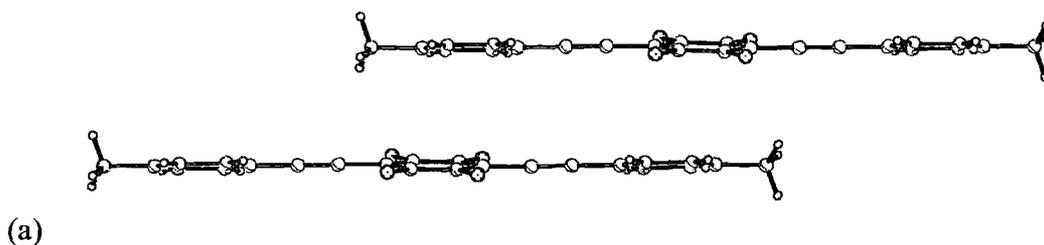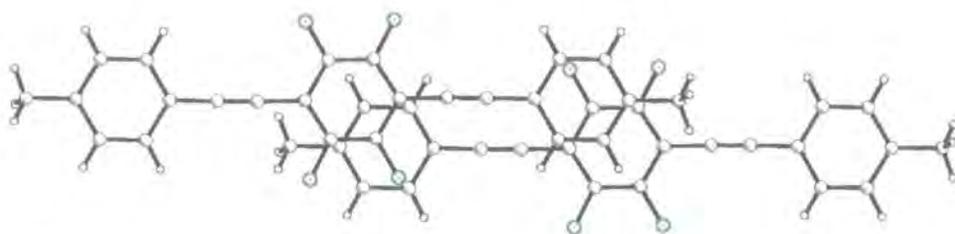
(b)

Figure 4.18: Diagram of (4b) viewed (a) parallel to plane of outer C_6H_6 rings and (b) perpendicular to the mean plane of the central C_6F_4 ring , showing how the molecules stack slipped by one ring to allow two arene-perfluoroarene interactions.

These stacks of slightly offset molecules, each with two rings influenced by phenyl-perfluorophenyl interactions, are aligned in columns stacking in the [0 1 1] direction. This can be seen by viewing parallel to the a axis (see Figure 4.19).
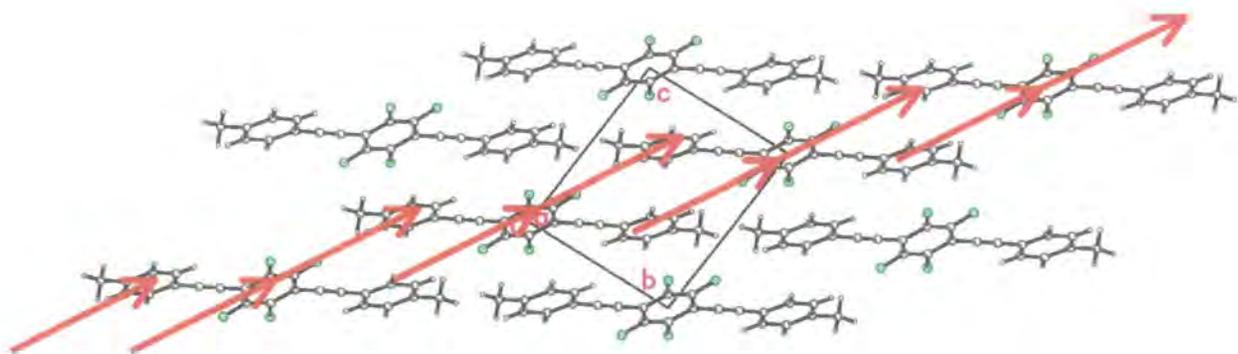
Figure 4.19: Plot of (4b) viewed down the a axis (with no perspective so no stacks visible), showing the arene-perfluoroarene stacking in the [0 1 1] direction (marked by red arrows), and how having more such interactions is prevented by having to incorporate double the amount of phenyl rings than perfluorophenyl rings into the structure.

For every column where there are phenyl-perfluorophenyl ring stacks, there is also some necessity for phenyl rings to stack on top of each other to complete the structure (since there are two phenyl rings for each perfluorophenyl ring). This can also be seen in Figure 4.19, above. From b to c, a pattern of fluoroarene···arene···arene···fluoroarene can clearly be seen down the centre of the diagram. This packing leads to a 'brick-wall' motif of columns. This is not quite the same as that seen in the structure published

recently[166] since there is disruption to the arene-perfluoroarene packing caused by having two phenyl groups for each perfluorophenyl group in this case.

The structure of MeS-Ph-CC-PhF$_4$-CC-Ph-SMe (**4c**) was solved at 160(2)K by Andrew Scott, but is as yet unpublished. The compound was found to crystallise in the triclinic space group $P\bar{1}$ with cell parameters a = 7.221(2), b = 8.675(2), c = 8.865(2), α = 63.192(5), β = 86.723(5), γ = 86.521(5). The C≡C bond length is 1.199(4) Å, with the C-C single bond adjacent to the fluorinated phenyl ring (1.422(3) Å) again a similar length to the C-C single bond adjacent to the non-fluorinated ring (1.428(3) Å). The angles where the phenyl ring joins the triple bond section of the rod slightly deviates from 120° (119.4(2)° and 121.6(2)°). The thiomethyl substituent is almost in the plane of the ring (torsion angle 3.4(3)°). The stacking is very similar to that found in (**4b**), with the rings stacked slipped by one ring to ensure two arene-perfluoroarene interactions per pair of molecules. The inter-centroid distance is 3.814 Å, the inter-planar distance, again calculated using the rings involved in arene-perfluoroarene interaction, is 3.407 Å. This is shorter than for (**4b**), suggesting closer packing, but the packing coefficient is also smaller (K = 0.710). This slight difference is probably due to the fact that the thiomethyl-substituted rods cannot get as close together, due to the larger substituent on each end, compared to the methyl substituted analogue.

The crystal structure of F$_3$C-Ph-CC-PhF$_4$-CC-Ph-CF$_3$ (**4d**) has been determined before[vi] (but remains unpublished) at 160(2)K. It was determined as part of this study at 100(2)K; crystal data and refinement details are available in Appendix A4d. The

---

[vi] By Andrew Scott, University of Newcastle-upon-Tyne.

structures are essentially the same, so the lower temperature one will be used for discussion herein.
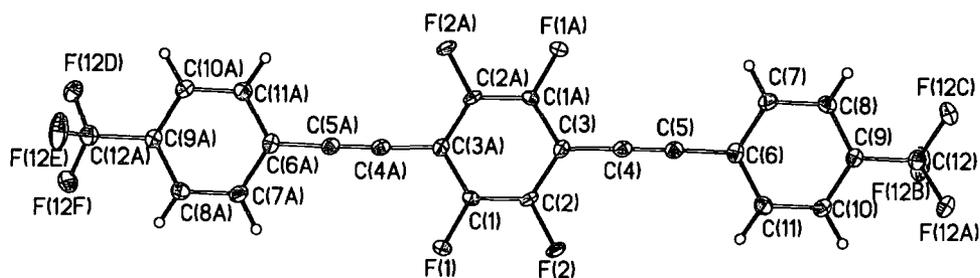
Figure 4.20: Ortep plot of (4d), with ellipsoids plotted at 50% probability level.

The compound crystallises in space group $P2_1/c$ with cell parameters a = 16.924(5) Å, b = 4.936(1) Å, c = 11.498(3) Å, β = 103.328(4)°. The packing of the molecules shows no evidence of arene-perfluoroarene interactions, with the molecules lining up with the phenyl rings eclipsed into the triple bond (see Figure 4.21), albeit in a different mode from that seen in (4b).
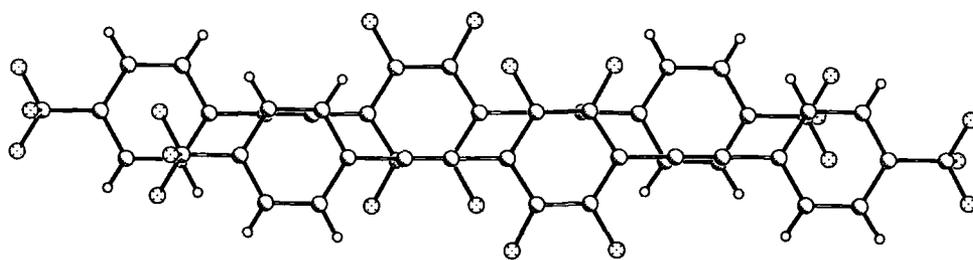
Figure 4.21: Stack of two molecules of (4d), viewed perpendicular to the mean plane of the central ring, showing how the phenyl rings are eclipsed, but slightly offset from, the C≡C triple bond.

The packing is a flattened herringbone γ-type stack, like (4a). Indeed, the cell parameters are similar to (4a), with both compounds having a very short *b* axis. The similarity can be seen when comparing Figure 4.22, below, with Figure 4.14.
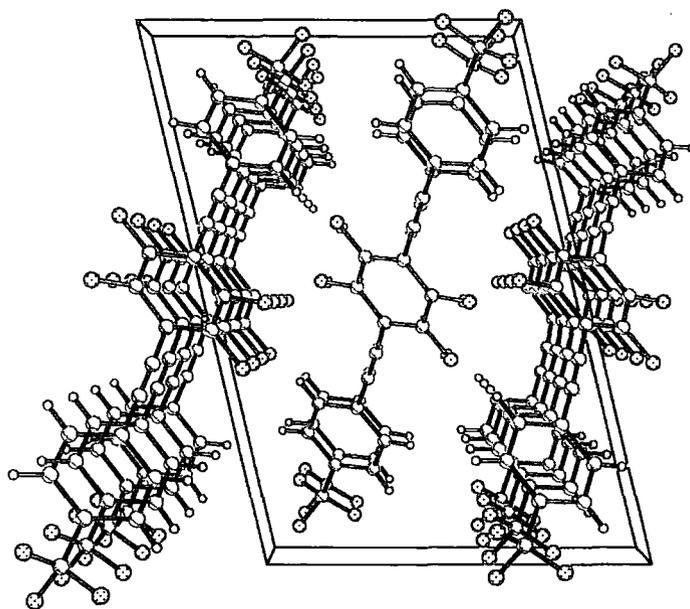
Figure 4.22: Stacking diagram for (4d), viewed down the *b* axis.

The inter-centroid distance between two central rings is large due to the large slip distance of the molecules in the stack (4.900 Å). The inter-planar distance (3.340 Å) is much smaller than for (4a), presumably because there are fewer of the larger perfluorophenyl rings to fit into the lattice thus the molecules can get closer together. The packing coefficient, K, is 0.737, indicating that the packing, despite the difference in the number of perfluorophenyl rings, is still very efficient.

It would appear that the presence of the fluoromethyl substituent is enough to disrupt the arene-perfluoroarene interaction, since other rods of this type have demonstrated the interaction despite having substituents (CH$_3$ and S-CH$_3$). The necessity to separate the fluorine atoms in the fluoromethyl group from each other would seem to overrule the ability to utilise the arene-perfluoroarene interaction.

The packing parameters discussed for the above compounds are presented in Table 4.1.

Table 4.1: Selected packing parameters for compounds (4a), (4b), (4c) and (4d).

Compound	Inter-centroid distance (Å)	Inter-planar distance (Å)	Dihedral angle	Packing coefficient
(4a) PhF_5-CC-Ph-CC-PhF_5	4.866	3.392	9.7°	0.737
(4b) H_3C-Ph-CC-PhF_4-CC-Ph-CH_3	3.929 (H··F) 4.066 (H··H)	3.478	8.9°	0.721
(4c) MeS-Ph-CC-PhF_4-CC-Ph-SMe	3.814	3.407	3.7°	0.710
(4d) F_3C-Ph-CC-PhF_4-CC-Ph-CF_3	4.900	3.340	6.6°	0.737

The structures of the co-crystals

The structures of the 1:1 co-crystals of **4a:4b**, **4a:4c** and **4a:4d** have been solved and are presented below. Crystal data and refinement details can be found in Appendices A4ab, A4ac and A4ad respectively.

The co-crystal[vii] of **4a:4b** is in space group $P\bar{1}$ with cell parameters a = 6.0725(11) Å, b = 7.4054(13) Å, c = 20.031(4) Å, α = 94.440(4)°, β = 96.620(4)°, γ = 96.242(4)°. Only half of each molecule is unique, with each independent molecule lying on an inversion centre.
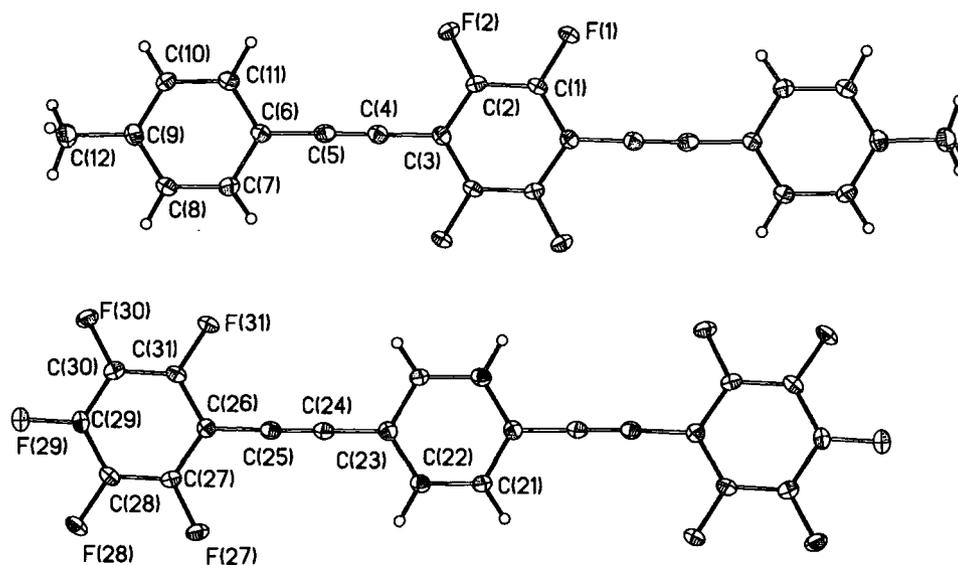
Figure 4.23: Plot of 4a:4b co-crystal, with thermal ellipsoids plotted at 50% probability.

The molecules do not sit side-by-side on exactly the same plane, as the above may suggest, but are separated by an inter-planar distance of 0.937 Å. Thus, adjacent columns are offset by this distance. This separation can be seen in Figure 4.24.

[vii] Crystals grown from an approximately 1:1 ratio of the two components dissolved in toluene followed by slow evaporation (by Stephen Watt, Heriot-Watt University)
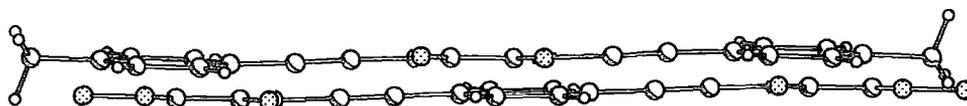
Figure 4.24: Side on view of the molecules in co-crystal 4a:4b, demonstrating that they are not co-planar, but separated by a distance of 0.937 Å

The two triple bond distances in the two independent half molecules are identical (1.196(3) Å), and there is no significant difference between the C-C single bond distances, which range from 1.425(3) Å to 1.433(3) Å. The bond angles around C(3) to C(6) and C(23) to C(26) are all close to $120°$ ($\pm 2°$). There is no significant difference in the single or triple bond distances, or the bond angles, of (4a) or (4b) on forming the co-crystal. The dihedral angles, however, have changed: (4a) from $9.7°$ to $3.2°$ in the co-crystal, and (4b) from $8.9°$ to $4.6°$. This is to maximise π-π interactions between rings.

The arene-perfluoroarene interaction present in the structure is instantly obvious from Figure 4.25, below. The rods line up directly over each other, with just a small slip distance with a third of the rings eclipsing each other.
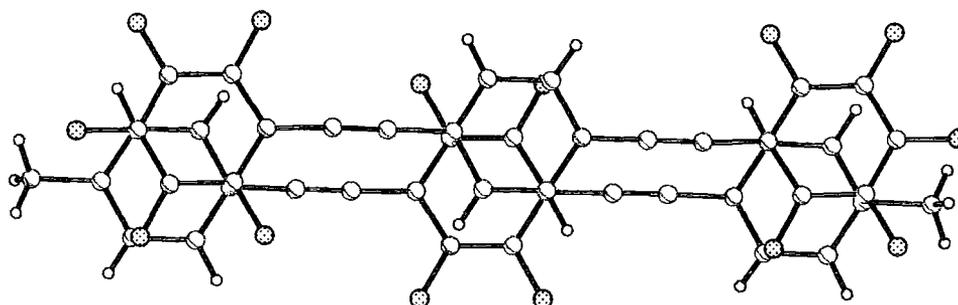
Figure 4.25: Diagram of 4a:4b viewed perpendicular to the central C_6F_4 ring (with no perspective), showing how the rods stack on top of each other.

The stacking is parallel to the b-axis (see Figure 4.26), and the molecules are separated by a distance of 3.339 Å (the inter-planar distance), with an inter-centroid distance (centre ring to centre ring) of 3.703 Å. The packing coefficient is 0.712, which is

slightly lower than for the two individual components, indicating a less tightly packed structure, although the packing is still efficient.
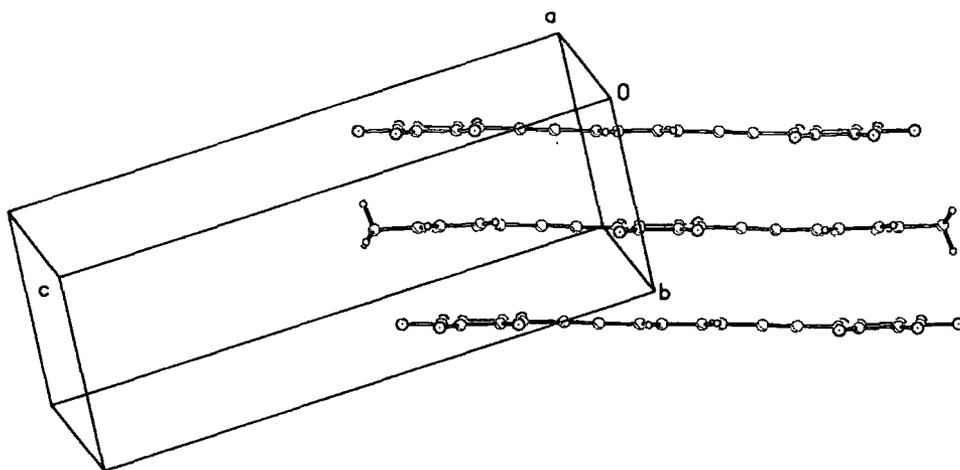
Figure 4.26: Diagram of 4a:4b viewed parallel to the plane of the molecule, showing the regular spacing of the molecules parallel to the *b* axis.

The C-CH$_3$ distance remains the same (1.509(2) Å in the single component structure; 1.510(3) Å in the co-crystal), as does the 4-position C-F bond distance (1.335(2) Å in the single component structure; 1.341(2) Å in the co-crystal). These are the bonds which are closest to the adjacent molecules in that row, and the larger length of the C-CH$_3$ bond almost acts as a 'spacer' to keep the fluoro molecules apart, preventing any disruptive influence on the delicate phenyl-perfluorophenyl interaction (see Figure 4.27(a)). The parallel columns of molecules pack very closely together (Figure 4.27(b)).
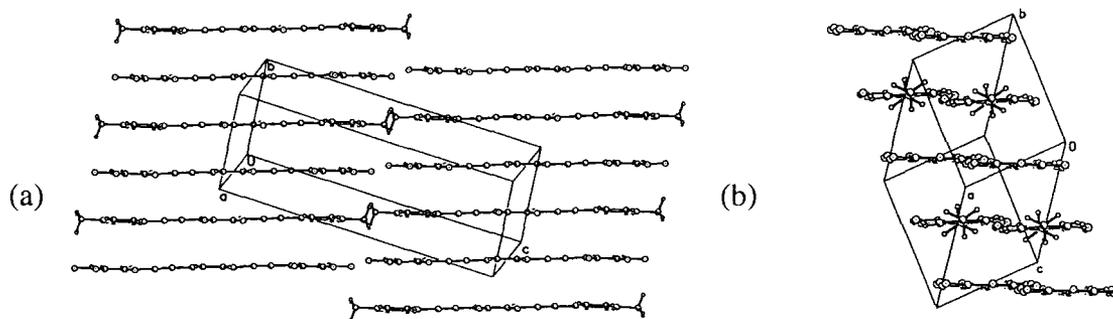
Figure 4.27: Side-on (a) and end-on (b) views of the columnar stacking in the 4a:4b co-crystal.

It is interesting to note that the co-crystallisation induces (**4a**) to utilise the phenyl-perfluorophenyl interaction which was not present in the single component structure. It also increases the efficiency of the interaction for the methyl-substituted molecule (**4b**). In the individual component structure there were more phenyl rings than perfluorophenyl rings, which led to some phenyl-phenyl face-to-face stacking. This is not normally favourable due to the same quadrupole being present on each ring. For this reason, phenyl rings usually prefer a herringbone arrangement. The co-crystallisation affords a 1:1 ratio of phenyl to perfluorophenyl rings, which means each ring can form a favourable π-π stacking interaction.

The co-crystal[viii] **4a:4c** is in space group $P\bar{1}$, with unit cell parameters a = 5.8227(15) Å, b = 7.4882(19) Å, c = 22.108(6) Å, α = 90.499(4)°, β = 95.599(5)°, γ = 92.675(5)°. This is a similar unit cell to the **4a:4b** co-crystal, and again half of each molecule is unique. Each molecule lies on an inversion centre.

[viii] Crystals grown from an approximately 1:1 ratio of the two components dissolved in chloroform followed by slow evaporation (by Stephen Watt, Heriot-Watt University)
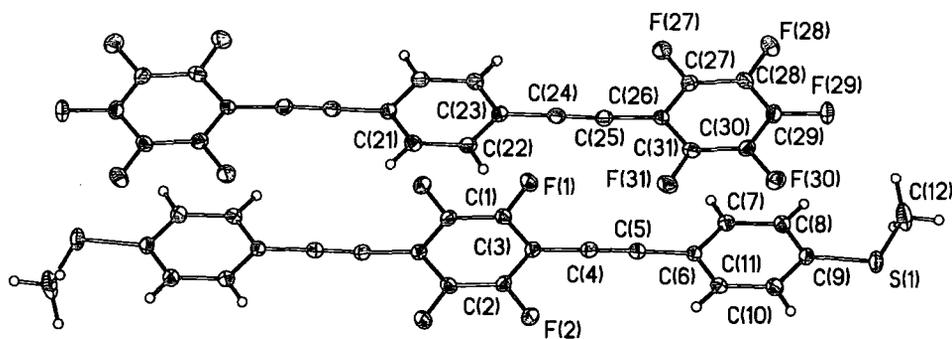
Figure 4.28: Ortep diagram for the co-crystal of 4a:4c. Ellipsoids are plotted to 50% probability level.

The triple bond and single bond distances are all of comparable magnitude, as seen in the individual structures. The bond angles at the phenyl rings are all within 1° of 120°. The thiomethyl group is closer to being in the plane of the outer ring than it was in the individual structure, but only slightly. The torsion angle containing the thiomethyl group is now 2.0(2)° compared to 3.4(3)°. The dihedral angle of the (4a) component has again changed quite significantly (from 9.7° to 4.5° in the co-crystal), but the dihedral angle of the (4c) component, which was small to start with, has hardly changed at all (3.7° to 3.9°). It seems sensible that the (4a) component has become more planar to maximise the favourable π-π stacking interactions.

The two molecules which make up the **4a:4c** co-crystal stack on top of each other in a similar way to **4a:4b**. There is a slight 'slip', again of approximately one C-C bond length (see Figure 4.29).
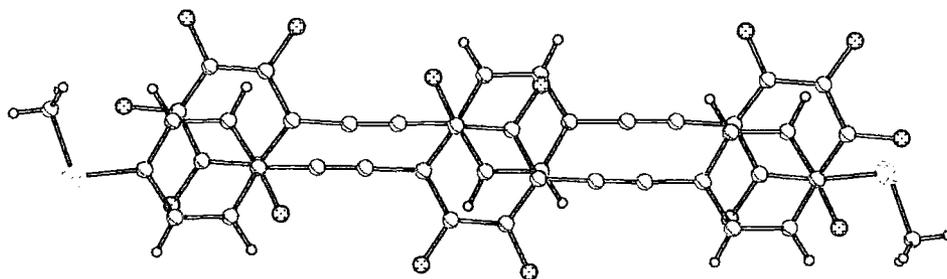
Figure 4.29: Diagram of 4a:4c viewed perpendicular to the central C_6F_4 ring (with no perspective), showing how the rods stack almost directly on top of each other.

The stacking is again parallel to the b axis (see Figure 4.30). The molecules are separated by a distance of 3.372 Å, with an inter-centroid distance of 3.744 Å. These are both slightly longer than for **4a:4b**.
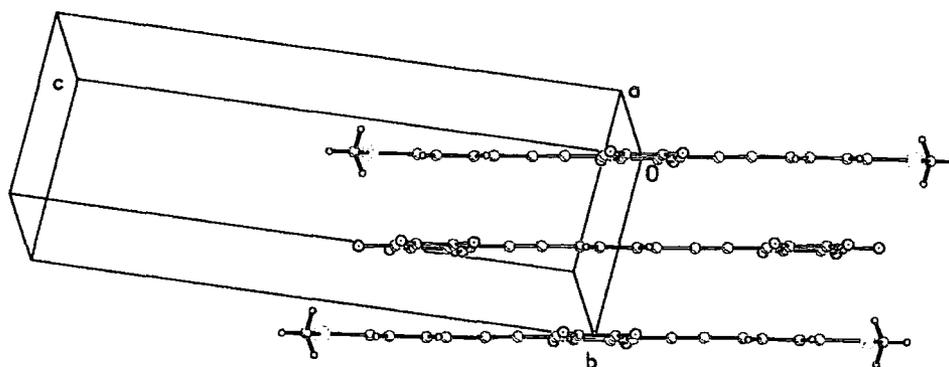
Figure 4.30: Diagram of 4a:4c viewed parallel to the plane of the molecule, showing the regular spacing of the molecules stacked in columns parallel to the b axis.

The packing coefficient for this structure (K = 0.698) is the smallest of any of the structures discussed in this section, although this still indicates efficient packing. This difference is possibly attributable to the fact that the thiomethyl group is the largest substituent involved in any of these structures. Indeed, the packing coefficient of **(4c)** alone, at 0.710, was the smallest of any of the individual components.

Again, co-crystallising **(4a)** with a substituted rod has forced it to adopt a crystal structure which favours phenyl-perfluorophenyl interactions, despite it not showing any

predilection to do so when crystallised alone. The arrangement of the molecules in the crystal does keep the fluorine atoms spaced out, and it seems a possibility that it is unfavourable fluorine-fluorine interactions which stop the phenyl-perfluorophenyl favouring π-π stacking motif in the structure of (4a).

The co-crystal[ix] 4a:4d is in space group $P\bar{1}$, with unit cell parameters a = 6.1246(8)) Å, b = 7.6693(11) Å, c = 20.125(3) Å, α = 84.283(4)°, β = 81.508(2)°, γ = 82.373(3)°. This is a similar unit cell to both the 4a:4b and 4a:4c co-crystals, and again half of each molecule is unique. Each molecule lies on an inversion centre.
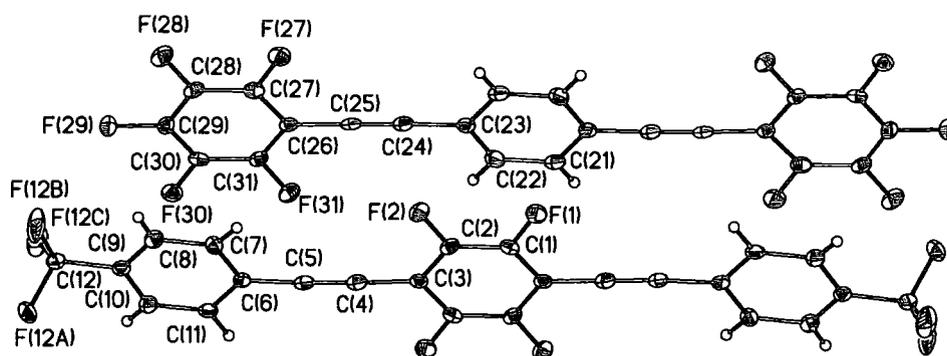
Figure 4.31: Ortep plot for 4a:4d co-crystal. Thermal ellipsoids are plotted at 50% probability level.

There is a very similer ring slip distance (of approximately one C-C bond length). The arene-perfluoroarene motif is unmistakable.
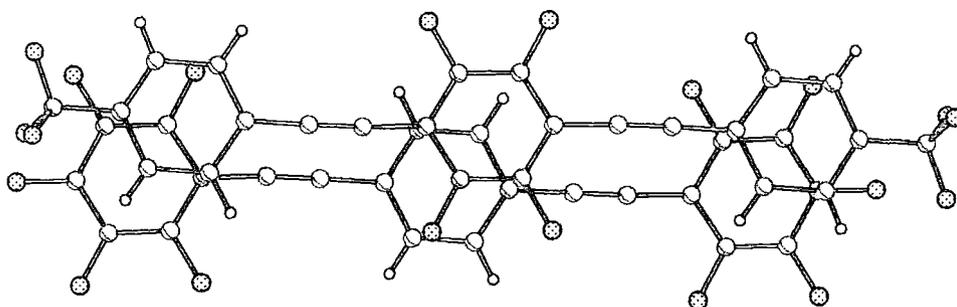
Figure 4.32: Diagram of 4a:4d viewed perpendicular to the central C_6F_4 ring (with no perspective), showing how the rods stack on top of each other.

The molecules are not exactly planar, with a slight bend in the (4d) rod not seen in the native structure. This is presumably to maximise favourable interactions between the molecules or to reduce unfavourable interactions of the CF_3 group (see Figure 4.33).
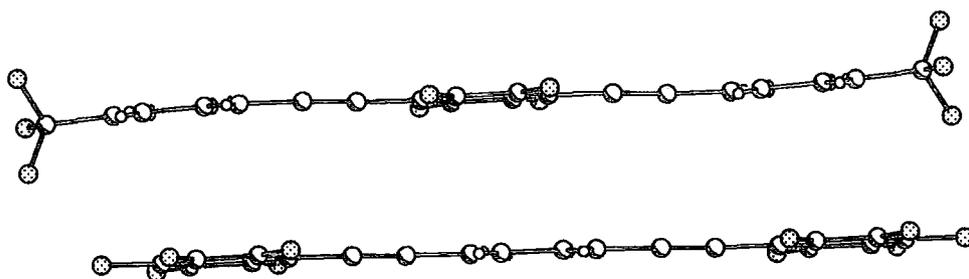
Figure 4.33: Diagram of the two molecules in the 4a:4d co-crystal, viewed side-on to demonstrate the non-planar nature of the 4d component.

The molecules stack in columns parallel to the b axis. The spacing between them (the inter-planar distance) is 3.425 Å , with an inter-centroid distance of 3.835 Å. The inter-planar spacing is not much greater than in the individual structures ((4a) 3.392 Å and (4d) 3.340 Å), but the inter-centroid distance is much reduced (in the individual structures, inter-centroid distances are (4a) 4.866 Å, (4d) 4.900 Å). This is due to the fact that the molecules are now stacking directly on top of each other, and are not slipped by a whole ring (see Figure 4.34).
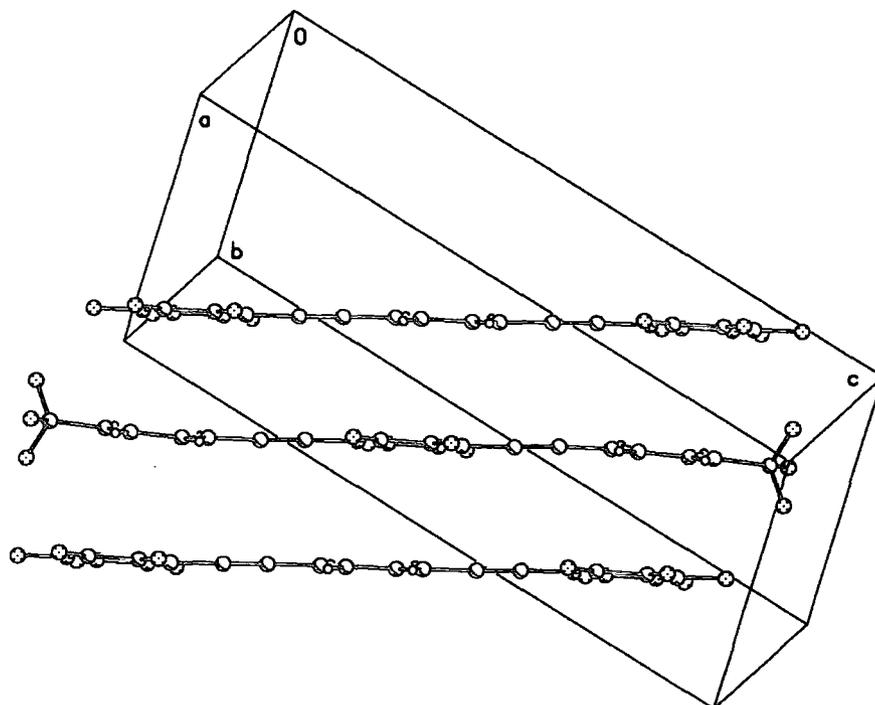
Figure 4.34: Diagram of 4a:4d, viewed parallel to the plane of the molecule, showing the regular spacing of the molecules.

The columns of molecules running parallel to the b axis line up side by side in the structure parallel to the a axis (see Figure 4.35).
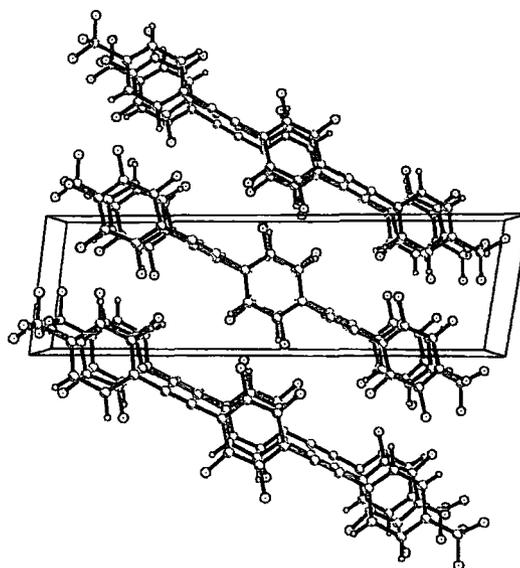
Figure 4.35: Diagram of 4a:4d, viewed down the b axis, showing how the columns stack parallel to the b axis and line up parallel to the a axis.

Co-crystal **4a:4d** shows how the arene-perfluoroarene interaction has influenced the structure in quite a dramatic way. The individual structures of *both* of the components in this case showed no evidence of face-to-face interactions at all, with the molecules slipping by a full ring distance to avoid it. In the individual structure of (**4a**), there are double the number of fluorinated rings to non-fluorinated rings, and vice versa in (**4d**), and it could be that the stabilisation gained by π-stacking two of the rings in each molecule does not compensate for the unfavourable phenyl-phenyl face-to-face interaction which needs to occur to ensure there are no 'holes' in the structure. Perhaps the face-to-face interaction of the perfluorophenyl rings (in (**4a**)) or interactions between CF_3 groups (in (**4d**)) is enough to eliminate any stabilising influence from two weak arene-perfluoroarene interactions per molecule. Co-crystallising the two, however, means there are the same number of phenyl and perfluorophenyl rings, and the stabilising influence of the interaction overcomes the destabilising face-to-face effects in the individual component structures.

For comparison purposes, the packing parameters for all ABA⋯BAB co-crystals in this section are presented in Table 4.2

Table 4.2: Packing parameters for co-crystals 4a:4b, 4a:4b and 4a:4c. Also included for comparison purposes is data for the parent co-crystal Ph-CC-PhF$_4$-CC-Ph with PhF$_5$-CC-Ph-CC-PhF$_5$.

Co-crystal	Inter-centroid distance (Å)	Inter-planar distance (Å)	Dihedral angles	Packing coefficient
4a:4b	3.703	3.369	**4a** 3.2° **4b** 4.6°	0.712
4a:4c	3.744	3.372	**4a** 4.5° **4c** 3.9°	0.698
4a:4d	3.835	3.425	**4a** 2.9° **4d** 4.0°	0.717
ABA···BAB parent co-crystal	3.770	3.337	**ABA** 3.9° **BAB** 3.0	0.700

This data can be compared with Table 4.1 for an insight into the changes in packing which occur on co-crystallisation. Generally, the inter-centroid distances of the co-crystals are much smaller than for the individual components. This is because the co-crystal components stack directly on top on each other. A large inter-centroid distance is indicative of a large ring 'slip'. Indeed, the largest inter-centroid distances presented in this section were (**4a**) and (**4d**), which are the two structures that packed with the phenyl rings above and below the triple bonds.

The dihedral angles of the molecules in the co-crystals are generally much smaller than in the single component structures. This move towards planarity would seem to be a necessity if the attractive face-to-face interactions in the co-crystal are to be maximised.

The packing coefficients generally decrease on co-crystallisation. This is possibly due to the fact that the substituent involved in most of the co-crystals needs space to be accommodated into the structure, and indeed the smallest packing coefficient (and so

the most loosely packed structure) is for **4a:4c**, which has the large thiomethyl group to

contain. This is also the structure with the largest inter-planar distance (i.e. with greater

separation between the molecules in the columns). A packing coefficient of 0.698 is

still, however, an efficiently packed structure, with most crystals having a packing

coefficient of around 0.65.

Liquid crystal data

Preliminary results[x] for the liquid crystal behaviour of single BPEB components are

given in Table 4.3. In the liquid crystal data tables presented herein, the abbreviations

used are: K = solely crystalline phase, N = nematic liquid crystal phase, S = smectic

liquid crystal phase and I = isotropic liquid phase.

Table 4.3: Preliminary liquid crystal data for selected BPEBs

Sample	Transitions on heating / °C	Transitions on cooling / °C
PhF$_5$-CC-Ph-CC-PhF$_5$ (**4a**)	K 196.5 N/I	
Ph-CC-PhF$_4$-CC-Ph	K 182.5 I	
Me-Ph-CC-PhF$_4$-CC-Ph-Me (**4b**)	K 238.3 N ? I	No change in the data from heating.
MeS-Ph-CC-PhF$_4$-CC-Ph-SMe (**4c**)	K 200.0 N 250.6 I	
F$_3$C-Ph-CC-PhF$_4$-CC-Ph-CF$_3$ (**4d**)	K 182.6 Rot 189.7 I	
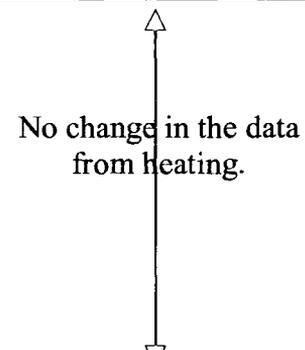
The liquid crystal behaviour of the co-crystals was then investigated to ascertain

whether any change in liquid crystal phase behaviour occurs on co-crystallisation. The

preliminary results are given in Table 4.4.

Table 4.4: Preliminary liquid crystal data for selected BPEB co-crystals

Co-crystal	Transitions on heating / °C	Transitions on cooling / °C
PhF$_5$-CC-Ph-CC-PhF$_5$ with Ph-CC-PhF$_4$-CC-Ph	K 189.3 N 199.0 I	
4a:4b	K 206.5 N 223.1* I Stabilises nematic	I 221.4 N 201.4 [S$_A$ + N] 192.5 [K$_1$ + N] 161.7 [K$_1$ + K$_2$]
4a:4c	K 186.8 N/I Destabilises nematic	I 184.3* N 182.6 S 167.8 K
4a:4d	K 178.0 I Only nematic on cooling	I 175.0 [K + N] 131.0 K

* Temperatures have not been detected by DSC, and are estimated by polarising light optical microscopy.

The overall effect of co-crystallisation of these systems on the liquid crystal phase behaviour is not yet fully understood, especially for the co-crystals with *para* substituents. It can be seen in the tables above that co-crystallisation has different effects on the liquid crystal behaviour depending on the *para* substituent present. More studies need to be carried out to establish a general trend for these systems. It is interesting that, in the parent co-crystal, the liquid crystal clearing point (the temperature when the system stops displaying liquid crystal behaviour) is increased when compared to the individual components. In effect, the addition of an "impurity" has increased the melting point of the system. There is evidently some co-operation between the two components, affecting the liquid crystal behaviour, even at high temperatures.

4.3.2 AAA···BBB packing motif

The second motif studied consists of co-crystals of systems where one rod is fully fluorinated, and one is non-fluorinated: the AAA···BBB type. The only example of this seen so far is for the parent co-crystal Ph-CC-Ph-CC-Ph with PhF_5-CC-PhF_4-CC-PhF_5, which co-crystallised in a 2:1 ratio with peculiar three layer 'sandwich' units making up the structure (see Figure 4.11). No co-crystals of this type have been seen which incorporate a substituent on the outer rings.

Presented in this section are two slightly different variations on the AAA···BBB system. The first is a co-crystal of PhF_5-CC-PhF_4-CC-PhF_5 (4e) with F_3C-Ph-CC-Ph-CC-Ph-CF_3 (4f), as shown in Figure 4.36.
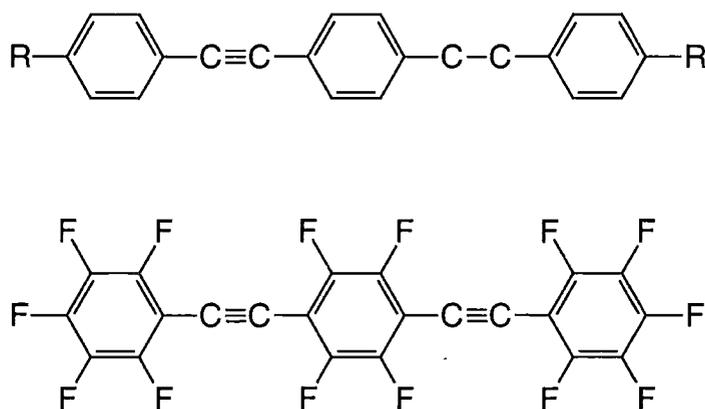
Figure 4.36: Diagram to show the constituents of co-crystal 4e:4f (R = CF_3).

The second system, with substituents on both molecules, is a co-crystal of MeO-Ph-CC-Ph-CC-Ph-OMe (4g) with MeO-PhF_4-CC-PhF_4-CC-PhF_4-OMe (4h).

Co-crystal 4e:4f

The structure of component (4e) has been solved before[167] at 160K, but was solved during this study at 100(2)K. The unit cells are essentially the same, so for comparison purposes the lower temperature structure will be used here. The structure of (4f) has also been solved[xi] before.

Table 4.5: Unit cell data for (4e), (4f) and the co-crystal of 4e:4f.

Compound	4e	4f	4e:4f
Crystal System	monoclinic	monoclinic	triclinic
Space Group	$C2/m$	$P2_1/c$	$P\bar{1}$
Temperature (K)	100(2)	160(2)	100(2)K
a (Å)	8.9294(7)	19.8314(19)	5.984(3)
b (Å)	7.6605(7)	7.8650(7)	8.867(4)
c (Å)	13.2005(11)	6.0953(6)	17.592(8)
α (°)	-	-	92.072(8)
β (°)	99.437(2)	91.502(2)	90.617(7)
γ (°)	-	-	98.555(8)

Compound (4e) crystallises at 100(2)K in monoclinic space group $C2/m$. A quarter of the molecule is unique, lying on a mirror plane and a two-fold rotation axis (which gives rise to an inversion centre). The triple bond distance (1.190(2) Å) is typical, and the C-C single bond distances (1.426(2) Å and 1.427(2) Å) are very similar. The molecules are close to planar (dihedral angle 1.3°).

[xi] By Andrew Scott, University of Newcastle-upon-Tyne.
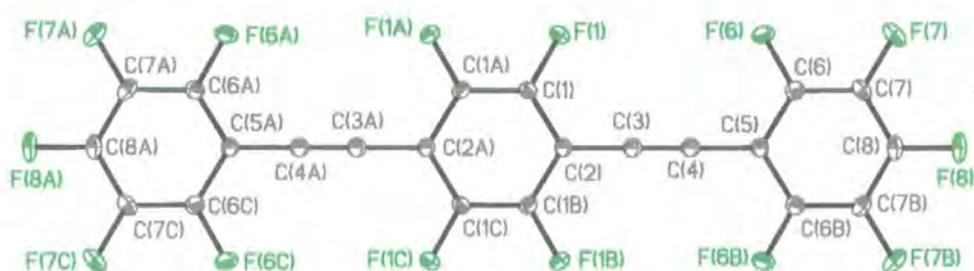
Figure 4.37: Ortep diagram for (4e) with thermal ellipsoids plotted at 50% probability level.

There is no face-to-face stacking of the perfluorophenyl rings, but the positioning of the molecules leads to an extremely closely packed structure (see Figure 4.38). The packing coefficient (K = 0.752) is the highest seen for the structures in this chapter. There is a short intermolecular F···F contact of 2.894(1) Å between F(7) and F(8) (the sum of the van der Waals radii is 2.94 Å).
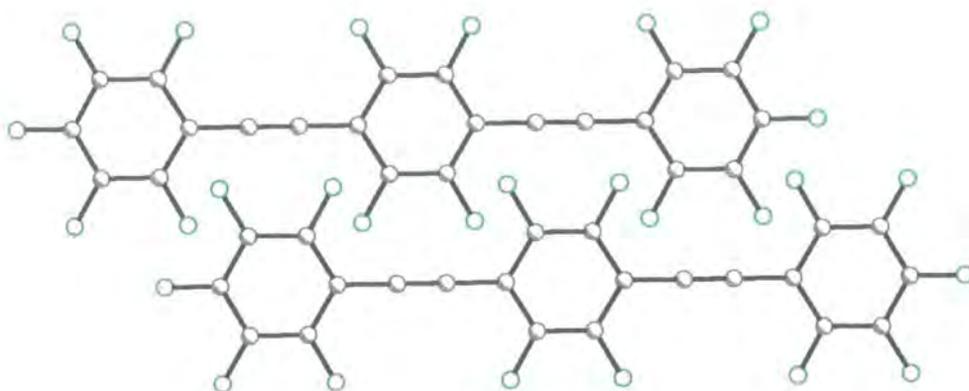
Figure 4.38: Diagram of two molecules of (4e) viewed orthogonal to the central ring showing the stacking pattern.

The other component of the co-crystal, (4f), crystallises in a monoclinic space group $P2_1/c$. There is rotational disorder in the fluoromethyl groups, as illustrated in Figure 4.39.
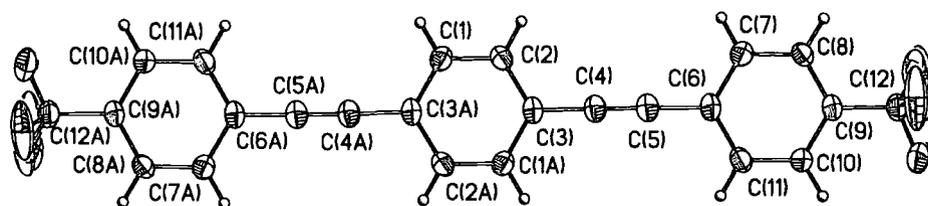
Figure 4.39: Ortep plot for (4f), showing the disordered CF_3 groups. Ellisoids to 50% probability.

The $C\equiv C$ triple bond distance (1.199(2) Å) and the two C-C single bond distances (both

1.437(2) Å) are comparable to distances seen in other BPEB molecules. The C-CF_3

bond distance is 1.505(2) Å. The bond angles at the phenyl rings are all within 1° of

120° (119.06(16)° to 120.64(15)°). There is a slight deviation from planarity along the

axis of the molecule, with the outer rings tilted away from the inner rings at an angle of

4.2° (see Figure 4.40). There are no face-to-face interactions in the stacking.
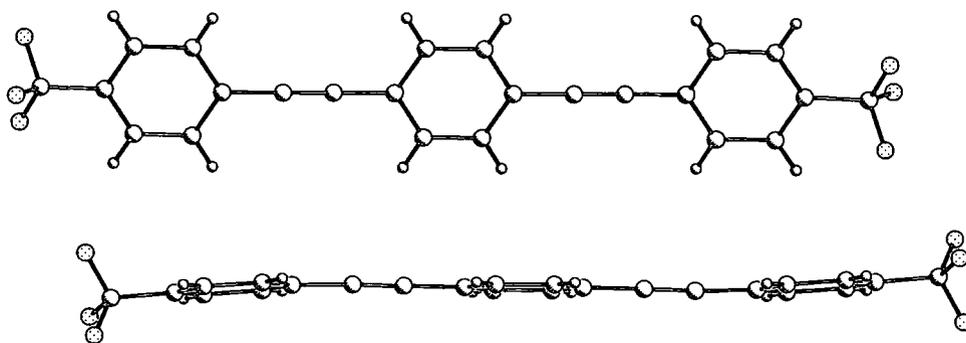
Figure 4.40: Diagram of two molecules of (4f), viewed side on to one molecule, showing how they are almost perpendicularly stacked in a flattened herringbone style. Disordered F atoms have been omitted for clarity.

The molecules are not perpendicular, but at an angle of 57.7° to each other (Figure

4.41). The closest carbon atom to the centroid of a phenyl ring on an adjacent molecule

is 3.618(2) Å (for C(8)).
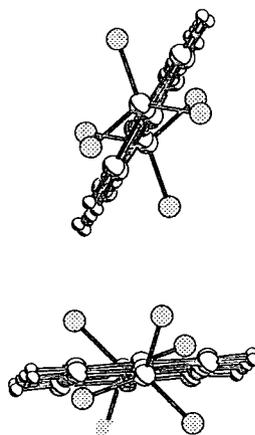
Figure 4.41: Diagram of two molecules of (4f) viewed along the axis of the molecule, to show the angle between the two. Disordered F atoms have been omitted for clarity.

This orientation leads to the flattened herringbone packing pattern (γ-type packing) demonstrated in Figure 4.42.
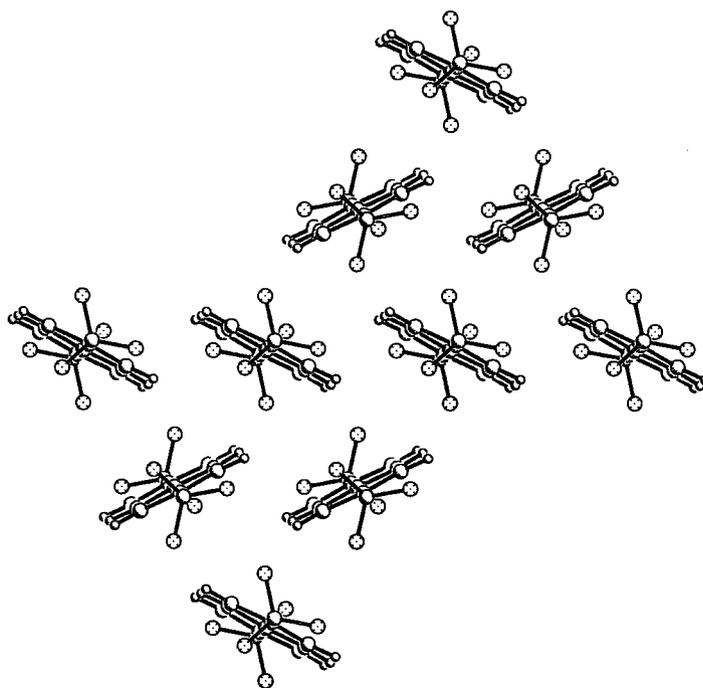
Figure 4.42: Packing diagram for (4f), demonstrating the flattened herringbone γ-type packing of the molecules in the crystal. Disordered F atoms have been omitted for clarity.

This is similar to the packing in PhF$_5$-CC-Ph-CC-PhF$_5$, which was considered in section 4.3.1. The packing coefficient could not be reliably calculated for this structure due to the disorder of the fluoromethyl moiety.

Neither (4e) or (4f) display any type of arene-perfluoroarene interaction in their individual structures. In an attempt to activate the interaction, the two were co-crystallised[xii] and the structure solved. Crystal data and refinement details can be found in Appendix A4ef. It was found to crystallise in space group $P\bar{1}$, with each molecule sitting on an inversion centre. The C≡C triple bond and C-C single bond distances of (4e) and (4f) do not significantly change on co-crystallisation. All angles at the phenyl rings are within 1° of 120°, with the exception of the outer ring of (4e) where the angles are almost 2° away from 120°.
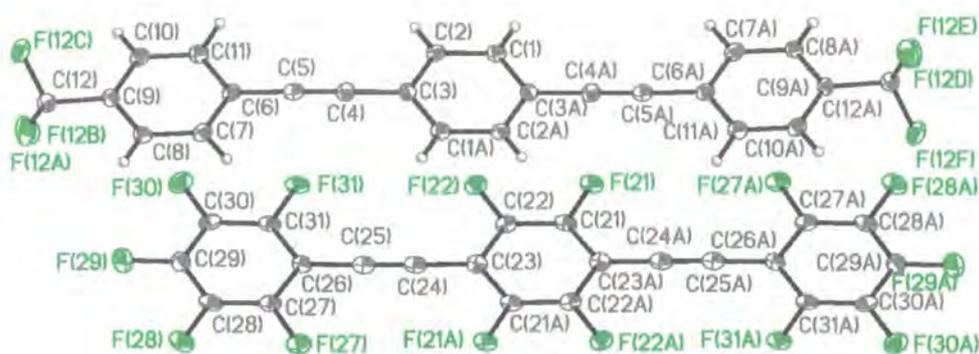
Figure 4.43: Ortep diagram of the co-crystal 4e:4f, with ellipsoids plotted to 50% probability level.

There is no face-to-face stacking in the structure. The molecules stack on top of each other but are slipped approximately one C-C bond distance along the axis of the molecules and one C-C bond length to the side, so that there is no overlap of the phenyl and perfluorophenyl rings (see Figure 4.44).

[xii] Crystals grown by Stephen Watt (Heriot-Watt University) by slow evaporation from THF.
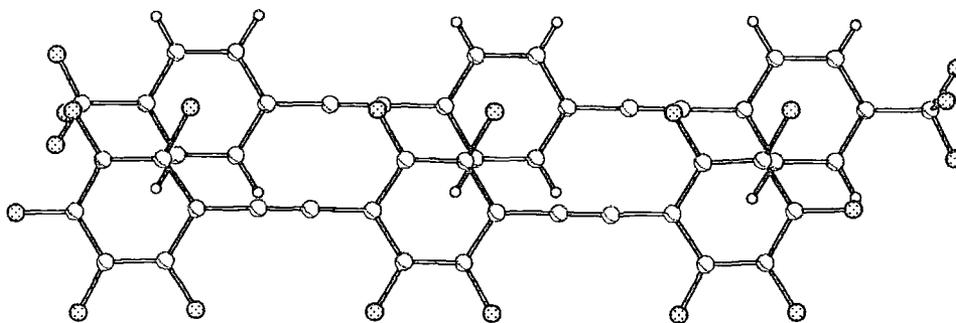
Figure 4.44: Diagram of the two molecules in the 4e:4f co-crystal, viewed orthogonal to the C_6F_4 central ring, showing the lap of overlap of the phenyl and perfluorophenyl rings.

Molecule (**4f**) is not completely linear. The outer rings and the CF_3 moieties bend away from the plane (4.6° away from the mean plane of the central ring), presumably to accommodate the fluoromethyl group at a reasonable distance from the *para* fluorine atom on (**4e**) (see Figure 4.45) and minimise steric repulsions.
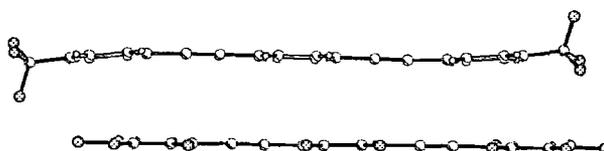
Figure 4.45: Diagram of the two molecules in the 4e:4f co-crystal, viewed side on, showing the bend in the outer rings and the fluoromethyl group.

This figure also shows that, despite the bend in (**4f**), the molecules are almost parallel to each other. The inter-planar separation of 3.324 Å, the smallest seen so far in this chapter, demonstrates how the molecules can get closer together when not stacked directly on top of each other. The large inter-centroid distance reflects just how much the molecules are slipped by. The packing coefficient, K, is 0.720, which is comparable to the other co-crystal structures presented in this chapter.

The fluorine atoms in the fluoromethyl group on (4f) rotate slightly so that the so that the axial atoms are not orthogonal to the plane of the outer ring, but at just less than 80°. Figure 4.46 shows how this could again be to minimise unfavourable interactions with the fluorine atoms on (4e).
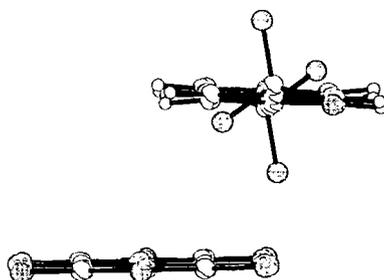
Figure 4.46: Diagram of the two molecules in the co-crystal of (4e) (bottom) and (4f) (top), viewed down the molecular axis, showing how the fluorine atoms in the fluoromethyl groups of (4f) rotate slightly to minimise any repulsive interactions with the fluorine atoms on (4f).

There are some intermolecular short contacts between fluorine atoms which are shorter than the sum of the van der Waals radii (2.94 Å). These are:

(1) C(21)-F(21)···F(21)-C(21)

(2.842(3) Å; angles 86.3(2)° and 86.3 (2)°respectively),

(2) C(28)-F(28)···F(31)-C(31)

(2.872(3) Å; angles 85.4(2)° and 86.2(1)° respectively)

(3) C(12)-F(12A)···F(29)-C(29)

(2.936(3) Å; angles 118.8(2)° and 128.3(2)° respectively).

All the contacts detailed above can be classified as **Type I** halogen···halogen contacts because the two angles between the fluorine atoms are approximately the same. They have arisen as a consequence of the close packing in the structure, and are probably not adding any stabilising influence.

There are also short C-H···F contacts, shown below as calculated by Platon.

Table 4.6: Short C-H⋯F contacts in co-crystal 4e:4f.

Donor-H⋯⋯F		D-H (Å)	H⋯A (Å)	D⋯A (Å)	D-H⋯A (°)
C(1)-H(1)	F(21)	0.91(4)	2.54(4)	3.178(4)	128(3)
C(8)-H(8)	F(31)	0.96(4)	2.51(3)	3.182(4)	126(3)

This co-crystal is at first sight somewhat puzzling. If there are no arene-perfluoroarene interactions, what is the explanation for the formation of the co-crystal? It would be expected that, after mixing, the molecules would separate into the two individual components to crystallise, but since they actually form the co-crystal, there must be some favourable interaction, but not the arene-perfluoroarene interaction, within the co-crystal to make this situation favourable. The first logical explanation is that the intermolecular interactions between fluorine atoms help to stabilise the structure, but the contacts are Type I contacts and thus give no stabilisation to the structure. It is, however, possible that the short C-H⋯F contacts are acting as a stabilising influence.

Another possible explanation is simply that the (4e) molecules act as 'spacers' for the (4f) molecules. The (4e) molecules could just sit innocently between the (4f) molecules, thus increasing the distance between molecules of (4f) and therefore preventing unfavourable interactions between CF_3 moieties.

A third idea is that the two compounds, when in the original THF solution, actually dissolve in each other. It is known that fluoroalkyl groups can dissolve in each other. This principle forms the basis of fluorous biphase technique for catalysis.[168] If this is the case, the two compounds could potentially form a solution which crystallises on complete evaporation of THF. Although this is an elegant explanation, it may be unlikely because homogeneous fluorous solutions tend to form when the biphase is

heated. The two components separate out again on cooling. To my knowledge, the solution which the crystals grew from was not heated at all. But perhaps some of the principles involved in fluorous biphase chemistry could help to explain the formation of this puzzling co-crystal.

A fourth explanation could be that the structure is stabilised by intermolecular, or other, forces which have not been recognised here. What is clear, however, is that further crystal structures of this type would facilitate a thorough analysis of what is happening here.

Co-crystal 4g:4h

The structure of component MeO-Ph-CC-Ph-CC-Ph-OMe (**4g**) has also been solved[xiii] but not yet published. Unfortunately the full coordinate set is not available for a comparative study. The structure of component MeO-PhF$_4$-CC-PhF$_4$-CC-PhF$_4$-OMe (**4h**) has been solved before[xiv] at 160K, but is also unpublished. It was solved again during this work at 100(2)K. The unit cells were similar, so for comparison purposes the lower temperature structure will be discussed here.

Table 4.7: Unit cell data for 4g, 4h and the co-crystal of 4g:4h.

Compound	(4g)	(4h)	4g:4h
Crystal System	orthorhombic	monoclinic	triclinic
Space Group	*Pbca*	*C2/c*	$P\bar{1}$
Temperature (K)	295	100(2)	100(2)
a (Å)	6.095(1)	28.941(7)	8.5588(6)
b (Å)	40.000(6)	7.7027(18)	9.8957(7)
c (Å)	7.561(1)	8.961(2)	12.7564(9)
α (°)	-	-	89.216(1)
β (°)	-	96.541(4)	76.896(1)
γ (°)	-	-	65.854(1)

Compound (**4g**) crystallises in orthorhombic space group *Pbca* at 295K. The molecule lies on a two-fold rotation axis. The triple bond distance (1.184(4) Å) is slightly shorter than in related structures, but the C-C single bond distances (1.437(4) Å and 1.444(4) Å) are typical. The bond angles at the inner phenyl ring are within 1° of 120°, but at the outer ring are slightly larger than 120°. The methoxy group is bent away from linearity

---

[xiii] By Nick Taylor at the University of Waterloo, Canada.
[xiv] By Andrew Scott, University of Newcastle-upon-Tyne.

by almost 5°. The C-OMe bond distance is 1.374(3) Å, and the O-CH$_3$ bond distance is 1.419(5) Å. The molecules pack in a very similar way to (4f) (see Figure 4.40, Figure 4.41 and Figure 4.42). There is no evidence for any hydrogen bonding.

Compound (4h) crystallises in space group *C2/c* at 100(2)K. The C≡C triple bond length is typical (1.192(3) Å), as are the C-C single bonds distances (1.423(3) Å and 1.425(3) Å for bonds adjacent to inner and outer rings respectively). The bond angles at the phenyl rings are more distorted from 120° than most of the other BPEBs, but by no more than 3°. The greatest distortion is the angle between the outer ring and the methoxy substituent, with bond angles C(8)-C(9)-O(1) and C(10)-C(9)-O(1) measuring 114.87(17)° and 128.65(18)° respectively. The C(9)-O(1)-C(12) bond angle, however, is 120.87(16)°. The molecule is slightly banana-shaped, with a bend at an angle of 3.1° between the inner and outer rings. The methoxy substituent does not lie completely in the plane of the molecule. The angle of the O(1)-C(12) bond to the mean plane of the outer ring is 6.4°.
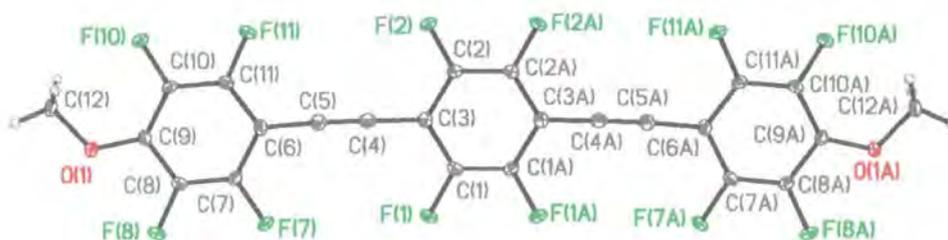
Figure 4.47: Ortep plot for (4h), with thermal ellipsoids shown at 50% probability level. The deviation from linearity is clearly visible.

The molecules stack together in columns where two phenyl rings on one molecule sit directly above two phenyl rings from another. These are separated by a large inter-planar distance of 5.712 Å (see Figure 4.48).
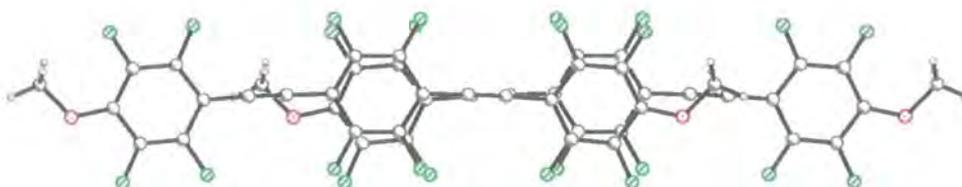
Figure 4.48: Diagram of two molecules of (4h) viewed orthogonal to the central ring.

These columns of stacked molecules are aligned as shown in Figure 4.49.
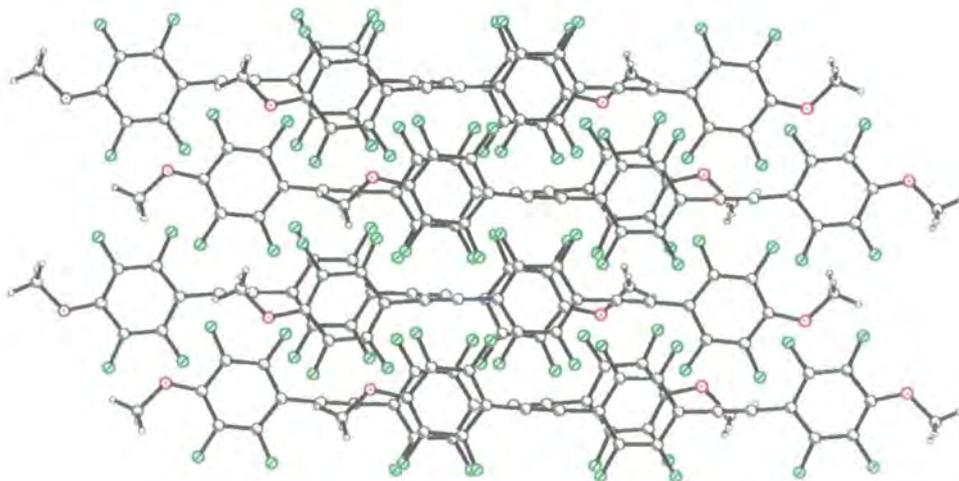
Figure 4.49: Diagram of molecules in (4h), viewed perpendicular to the central ring, demonstrating how the columns pack together.

This elegant packing pattern means that the distance between the mean planes of central

rings of nearest-neighbour molecules is only 2.894 Å, as shown in Figure 4.50.
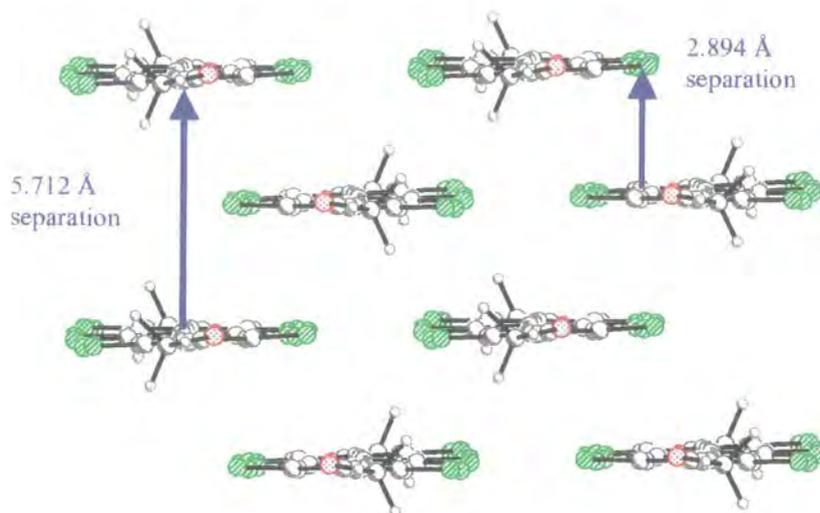
Figure 4.50: Diagram of the molecules in (4h) viewed end on, to show the packing and the distance between the layers.

These columns, shown in the direction of the arrows in Figure 4.50, run parallel to the *c*

axis, as can be seen in Figure 4.51.
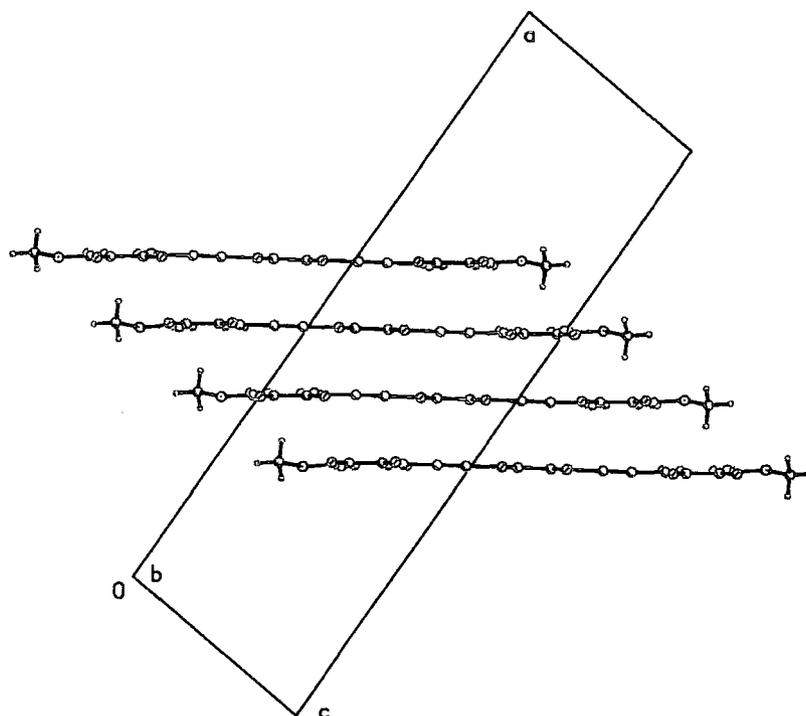
Figure 4.51: Diagram of molecules of (4h), showing how the stacking is parallel to the c axis. Interplanar distance, as seen here, is 2.894 Å.

There are no direct face-to-face interactions at all. There is a short contact of 2.56 Å between H(12A) and F(8), but no classical hydrogen bond formation between methoxy groups on adjacent molecules.

The structure of the co-crystal **4h:4g**, however, does utilise hydrogen bonding. It crystallises in triclinic space group $P\bar{1}$, with each molecule lying on an inversion centre. There are no significant changes in any of the C≡C triple bond or C-C single bond distances on co-crystallisation. The C-OMe and O-CH₃ bond distances also remain the same, as do the major bond angles.
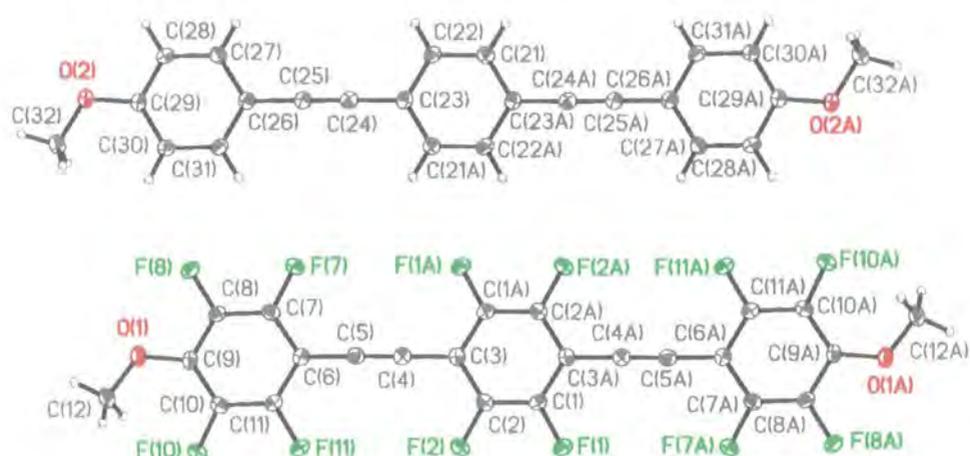
Figure 4.52: Ortep diagram for co-crystal 4g:4h. Thermal ellipsoids are plotted at 50% probability level.

The major change on co-crystallisation is in the angle at which the methoxy group is bent away from the plane in the (**4h**) molecule. In the structure of (**4h**) alone, the O-CH$_3$ bond is at an angle of 10.7° from the plane of the outer ring, but on co-crystallisation, this increases to 23.2° from the plane of the ring (see Figure 4.53).
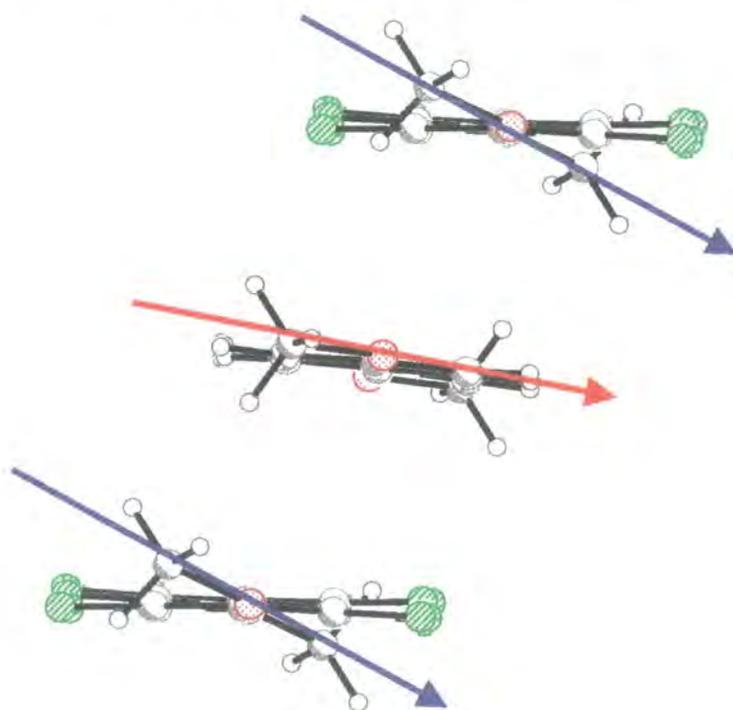
Figure 4.53: Diagram of 4g:4h, viewed down the molecular axis, demonstrating the greater twist out of the plane methoxy group on (4h).

The molecules stack alternately, with two rings of one rod overlapping with two of the one below (illustrated in Figure 4.54). There is a slip to one side of approximately one C-C bond distance.
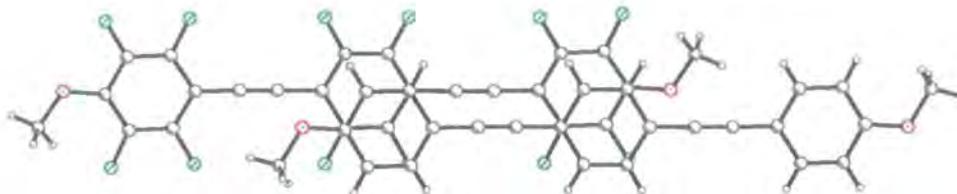
Figure 4.54: Diagram of 4h:4g, viewed perpendicular to the central C_6F_4 ring, showing how the molecules stack.

The distance between the molecules, the inter-planar distance, is 3.308 Å. The inter-centroid distance of overlapping rings is 3.692 Å, inclined at an angle of 25.8°. At first glance, it would appear that the arene-perfluoroarene interaction is influencing the crystal structure since the rings are arranged face-to-face, as seen in previous cases, but the major influence in this case must surely be the hydrogen bonds between the methoxy groups that hold infinite chains of molecules together (see Figure 4.55). The hydrogen bond on the (**4g**) molecule is in the plane of the molecule (the O-CH$_3$ bond is at an angle of only 0.4° to the mean plane of the outer ring). It is between atoms C(32)-H(32)···O(2), at an angle of 143.8° and at a distance of 2.44 Å. The hydrogen bonds that hold the chains of (**4h**) molecules together are out of the plane (the O-CH$_3$ bond is at an angle of 23.2° to the mean plane of the outer ring). The participating atoms are C(12)-H(12B)···O(1), at an angle of 143.8° and a distance of 2.50 Å.
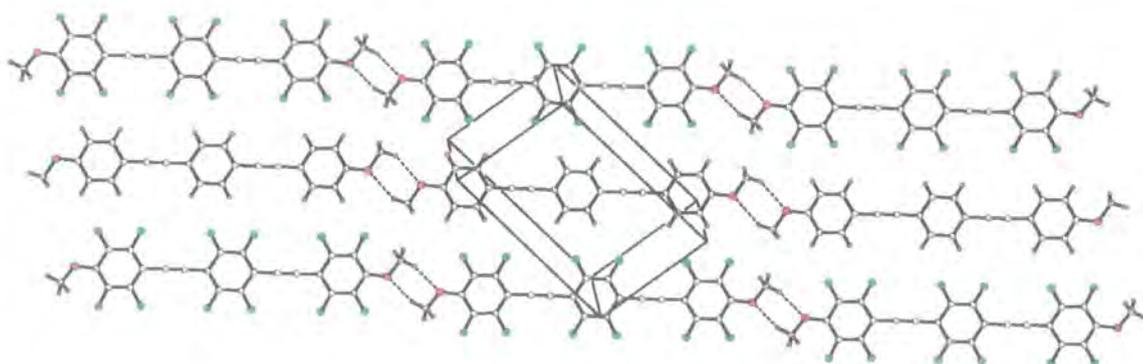
Figure 4.55: Diagram of 4g:4h, viewed perpendicular to the mean plane of the central C_6F_4 ring, showing the hydrogen bonds linking the molecules in chains. The unit cell outline is shown.

There is also a short F···F contact, between F(1) and F(10), at 2.853 Å (the sum of the van der Waals radii is 2.94 Å). All of these forces could contribute stabilising influences on the structure. The (4g) and (4h) units that make up this structure pack in infinite chains and layers, not in sets of three as seen in the case of the parent AAA···BBB co-crystal, and exhibit a 'brick wall' motif (see Figure 4.56). There is very little comparison with the packing of the parent system.
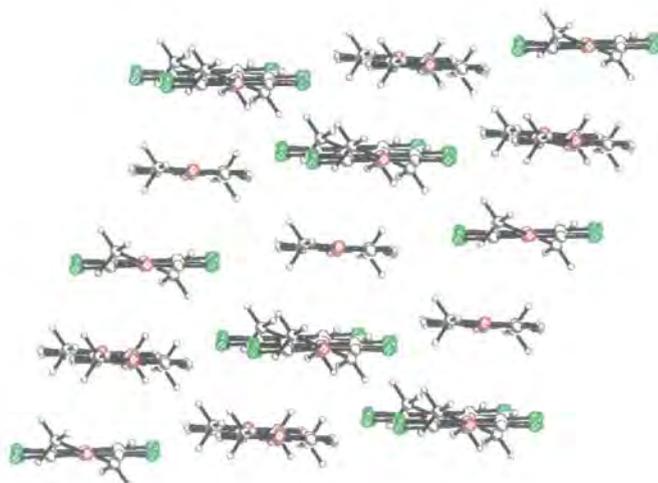
Figure 4.56: Diagram of 4g:4h, viewed down the molecular axis, illustrating the packing in the structure. There are infinite chains of molecules running in the direction of the molecular axes.

Despite all these intermolecular forces, the packing coefficient is still comparable to the other structures seen in this chapter (K = 0.716).

Liquid crystal data

Liquid crystal phase behaviour was again studied for these systems. The preliminary

results for the BPEBs used for these co-crystals are presented in Table 4.8, using the

same abbreviations for liquid crystal phases as given on page 42.

Table 4.8: Preliminary liquid crystal data for selected BPEBs

Sample	Transitions on heating / °C	Transitions on cooling / °C
PhF$_5$-CC-PhF$_4$-CC-PhF$_5$ (4e)	K 226.1 I	
Ph-CC-Ph-CC-Ph	K 181.7 I	I 164.3 N 159.5 K
F$_3$C-Ph-CC-Ph-CC-Ph-CF$_3$ (4f)	K 200.0 S$_b$ 222.3 I	I 172 N 165 K
MeO-Ph-CC-Ph-CC-Ph-OMe (4g)	K 217.6 N ? I	N (184.6) S 170.1 K
MeO-PhF$_4$-CC-PhF$_4$-CC-PhF$_4$-OMe (4h)	K 188.2 N 200.7 I	

Again, the liquid crystal behaviour of the co-crystals was then investigated to ascertain

whether any change in liquid crystal phase behaviour occurs on co-crystallisation. The

preliminary results are given in Table 4.9.

Table 4.9: Preliminary liquid crystal data for AAA···BBB type co-crystals

Sample	Transitions on heating / °C	Transitions on cooling / °C
PhF$_5$-CC-PhF$_4$-CC-PhF$_5$ (**4e**) / Ph-CC-Ph-CC-Ph	There is an effect, but no final results yet!	
4e:4f	K$_1$ 166.1 S$_B$ 203.8 I	I 202.9 [N + S$_B$] 162.6 K
4g:4h	No final results. Preliminary findings suggest it increases smectic stability (probably smectic E) i.e. the temperature region in which these phases are observed is larger than for the individual components.	

* Temperatures have not been detected by DSC and are estimated by polarising light optical microscopy.

It seems that co-crystallisation certainly affects the liquid crystal behaviour, but work in this area is not yet finished. In the case of the parent co-crystal, the behaviour becomes very complex. It would seem that, so far, co-crystallisation allows only very limited control over the crystal and liquid crystal phases.

4.4 Conclusion

ABA···BAB motif co-crystals:

The crystal structures of substituted BPEBs Me-Ph-CC-Ph-CC-Ph-Me (**4b**) and F_3C-Ph-CC-Ph-CC-Ph-CF_3 (**4d**) have been presented and analysed for evidence of arene-perfluoroarene interactions and any interesting features of molecular geometry or packing.

The structure of (**4b**) showed the influence of arene-perfluoroarene interactions, with a phenyl ring and a perfluorophenyl ring of one molecule sitting almost directly over the perfluorophenyl and phenyl ring of an adjacent molecule. There is slight disruption to the interaction because there is a ratio of 2:1 phenyl:perfluorphenyl rings in the crystal, which means that there are some phenyl-phenyl face-to-face interactions.

In contrast, the structure of (**4d**) showed no arene-perfluoroarene interactions. The phenyl rings align to the C≡C triple bond of the adjacent molecule, minimising any face-to-face interactions.

The other two components of the co-crystals presented here were analysed for any key features. It was found that (**4a**) packs in a similar way to (**4d**), with no arene-perfluoroarene interactions, with the C≡C triple bond aligned slightly overlapping the C≡≡C triple bond. The structure of (**4c**) was analagous to that of (**4b**), with an arene-perfluoroarene interaction dictating the packing.

The structure of three new co-crystals has been presented. Co-crystallisation of (**4a**) with (**4b**) resulted in an arene-perfluoroarene stacked co-crystal. Thus co-crystallisation

induces an arene-perfluoroarene interaction which alters the packing type of (4a), but allows (4b) to still utilise an arene-perfluoroarene interaction. The same was found for the co-crystals of 4a:4c and 4a:4d. The arene-perfluoroarene interaction dominates the packing in all of the co-crystals studied in this section. The *para* substituents do not seem to hinder the interaction in any way.

AAA···BBB motif co-crystals:

The new crystal structure of the parent, unsubstituted BPEB, PhF_5-CC-PhF_4-CC-PhF_5 (4e) has been presented, as well as an analysis of the other component of the co-crystal, (4f).

The structure of (4e) was found to be aligned in columns with stacking of parallel molecules, but with the molecules slipped so far as to remove any overlap of the molecules. There are obviously no face-to-face interactions occurring. This is similar to the structures of (4a) and (4d), but with the molecules shifted further apart.

Molecule (4f), in contrast, did not form parallel stacked columns of molecules. There was an edge-to-face arrangement, resulting in a herringbone-type packing pattern.

The new co-crystal system, 4e:4f, has been presented. It was found that although the molecules packed in a parallel fashion, there was no direct overlap of the phenyl and perfluorophenyl rings. This raises questions as to why the co-crystal forms at all, since there appear to be no arene-perfluoroarene interactions occurring. Possible explanations include the presence of other, undetected, stabilising influences, or the possibility that the two components simply dissolved in each other and then crystallised together. More study on these types of systems would be required to generate a general explanation.

The two components of the other new co-crystals presented in this section are MeO-Ph-CC-Ph-CC-Ph-OMe (**4g**) and MeO-PhF$_4$-CC-PhF$_4$-CC-PhF$_4$-OMe (**4h**). The structure of (**4g**) pack in a similar way to those in (**4f**).

The new 100K structure of (**4h**) was presented with analysis of geometry and packing. It was found to align in an elegant way, with molecules stacking in parallel directly on top of each other, with eclipsing rings, but with a large separation (5.712 Å) between the planes of the rings to minimise any repulsions. There is no scope here for any arene-perfluoroarene interactions.

The co-crystal of **4g:4h** packed with another, different motif. It seems that both arene-perfluoroarene interactions and stronger hydrogen bonding dictate the packing, resulting in elegant "chains" of like molecules. These "chains" stack in an alternating perfluoro-perhydro fashion, with rings eclipsing but slightly laterally offset, as is seen in crystals with active arene-perfluoroarene interactions. The hydrogen bonds between the methoxy groups appear to be a strong stabilising force in this structure. The lack of any other AAA···BBB systems, despite trying several samples (see section 4.6, below) could suggest that it is the influence of the strong hydrogen bond, supported by the arene-perfluoroarene interaction, which enables this co-crystal to form.

The two new co-crystal systems presented here, and the parent AAA···BBB co-crystal, are three totally different systems. One has no substituents, one has one *para* substituted molecule and the other has two *para* substituted molecules with hydrogen bonding capability, so it is difficult to compare them directly, or with the ABA···BAB systems. It has been noted, however, that all the co-crystals are in space group $P\bar{1}$.

It is possible that the arene-perfluoroarene interaction only readily stabilises the ABA···BAB structures. The three AAA···BBB systems all seemed to have other favourable interactions such as hydrogen bonding to help stabilise the crystal packing. Perhaps the phenyl-perfluorophenyl interaction is, for some reason, not strong enough for the AAA···BBB systems. More work in this area may lead to further clues as to what is going on in these systems. It is also possible that simple sterics may inhibit the growth of AAA···BBB co-crystals. It seems apparent that any *para* substituent on the perhydrogenated ring would be hindered by the presence of the two *para* fluorine atoms on the perfluorinated molecule. Perhaps it is this which prevents more crystals of this type. Maybe it is only when the two substituents cooperate (e.g. in hydrogen bonding) that the co-crystal can form.

4.5 Related structures

During the course of the work in presented in this chapter, two structures were obtained which, although they are related to the BPEB-type structures, are not directly linked to any of the co-crystal presented above. The two structures to be discussed here are MeO-Ph-CC-PhF$_4$-CC-Ph-OMe (**4i**) and an interesting molecule which has an anthracene moiety rather than a phenyl ring between the triple bonds: MeO$_2$C-Ph-CC-Ant-CC-Ph-CO$_2$Me (**4j**), a substituted bis(phenylethynyl)anthracene (BPEA).

4.5.1 MeO-Ph-CC-PhF$_4$-CC-Ph-OMe (4i)

The structure of (**4i**) has been solved previously[xv] at 180K, but as part of this study the structure was solved at 110(2)K. The unit cell was found to be the same. The data were collected from a crystal grown by slow evaporation from THF.[xvi] It was found to be in monoclinic space group $P2_1/n$ with cell parameters a = 8.5770(16) Å, b = 5.9594(12) Å, c = 18.882(4) Å, β =94.948(4)°. The molecule sits on a 2-fold rotation axis. The C≡C triple bond distance (1.198(2) Å) and C-C single bond distances (1.425(2) Å and 1.433(2) Å) are typical of this class of compounds. The inner and outer rings are at an angle of 4.5°.
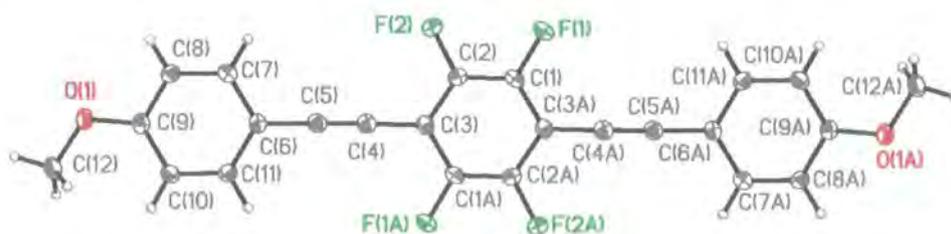
Figure 4.57: Ortep diagram for (4i). Thermal ellipsoids are plotted at 50% probability level.

The angles at the substituent end of the molecule (C(10)-C(9)-O(1) = 124.43(12)° and

C(8)-C(9)-O(1) = 115.42(11)°) show how the methoxy group bends away from trigonal

planarity in a similar way to the other methoxy-BPEBs studied in this chapter ((**4g**) and

(**4h**)). The molecules stack on top of each other in much the same way as the

constituents of co-crystal **4g:4h** (see Figure 4.58). The inter-planar distance between

these molecules is 3.394 Å, with a slightly larger inter-centroid distance (3.729 Å),

inclined at an angle of 26.4°, indicating the slight slip.
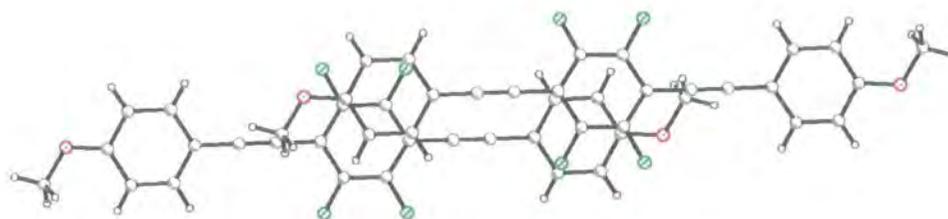
Figure 4.58: Diagram of (4i), viewed perpendicular to the central C_6F_4 ring, showing how the molecules stack.

There is not, however, a 'brick wall' type motif as seen in **4g:4h** since there are columns

of these stacks at a different angles. This can be seen in Figure 4.59.
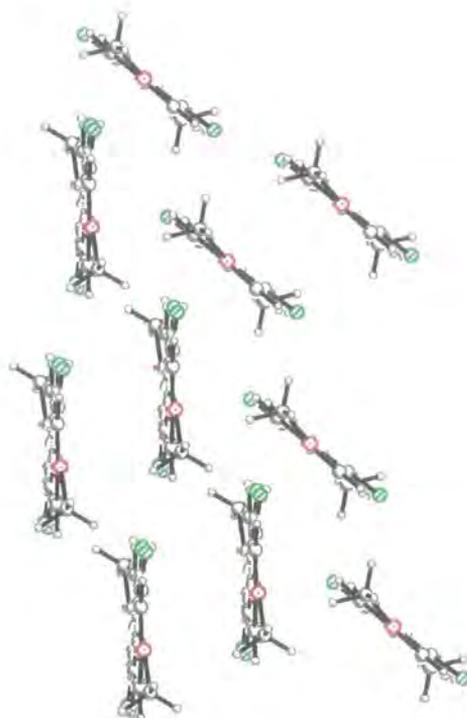
Figure 4.59: Diagram of (4i), viewed down the molecular axis, showing how the columns of molecules pack with respect to each other.

This pattern leads to an attractive herringbone-type packing motif throughout the crystal, as shown in Figure 4.60.
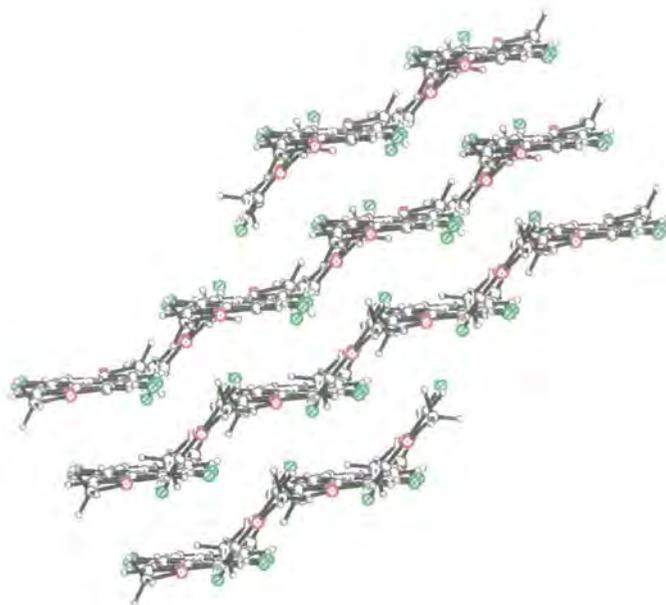
Figure 4.60: Packing diagram for (4i) viewed down the axis of the molecules showing the herringbone-type motif throughout the crystal.
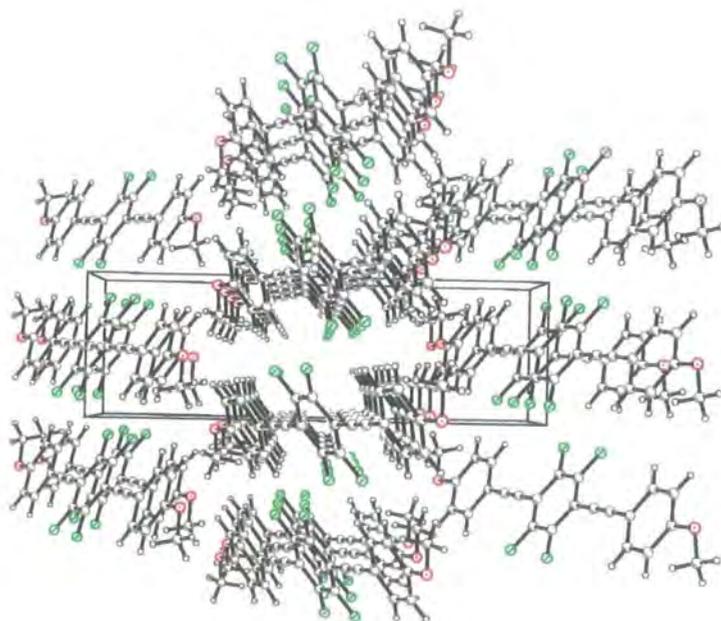
Figure 4.61: Packing diagram for (4i) viewed down the *b* axis of the unit cell showing the herringbone-type motif throughout the crystal.

There is no significant hydrogen bonding interaction between adjacent molecules. The packing coefficient, K, is 0.693. This is smaller than most of the structures seen so far, indicating a less efficiently packed structure.

Many attempts were made to obtain the crystal structure of the ABA···BAB co-crystal using (**4i**). (**4i**) and MeO-PhF$_4$-CC-Ph-CC-PhF$_4$-OMe were mixed together and crystals grown from the mixture, but the unit cell of the crystals tested revealed them to be of only (**4i**). Three different samples were tested, with several crystals used from each sample. Presumably co-crystallisation would so disrupt the packing that it is more favourable for the two components to separate out and crystallise individually. In the structure of (**4i**) a 2:1 ratio of phenyl to perfluorophenyl groups is favourably aligned in the crystal. Addition of the MeO-PhF$_4$-CC-Ph-CC-PhF$_4$-OMe in an attempt to form a co-crystal could disrupt this packing by unbalancing this 2:1 ratio.

4.5.2 MeO$_2$C-Ph-CC-Ant-CC-Ph-CO$_2$Me (4j)

The earliest structure of a 9,10-bis(phenylethynyl)anthracene (BPEA) to appear in the Cambridge Structural Database[73] (in 1993) is the parent, unsubstituted molecule. It appears first as part of a study into porphyrin-based lattice clathrates, and is incorporated into the lattice of a zinc porphyrin.[169]

The structure of the parent compound was presented a year later.[170] It was synthesised, along with other substituted analogues, by cross-coupling a terminal phenyl alkyne with iodoanthracene catalysed by palladium and copper. This group of compounds were being investigated for their fluorescence properties. The parent compound was found to crystallise in orthorhombic space group *Pbcn*, with unit cell parameters a = 24.305(4) Å, b = 11.512(1) Å, c = 7.099(1) Å.

The only other BPEA in the database is the diphenylamino-substituted analogue.[171] This is a monoclinic structure (space group $P2_1/n$) with cell parameters a = 11.582(2) Å, b = 9.407(2) Å, c = 18.429(4) Å, β =108.14(2)°. The anthracene units do not stack face-to-face, but overlap with the planar N atom (at a distance of 4.59 Å, offset angle 11.2°) in the substituent group. The C≡C triple bond distance of 1.192(3) Å and the C-C single bond distances of 1.435(3) Å and 1.433(3) Å are the same as seen in the BPEBs discussed in this chapter.

The structure of the cyano-substituted BPEA has also been solved in Durham but is not yet published. It crystallises in space group $P\bar{1}$, with the molecule lying on a centre of inversion. There is a short C≡C bond distance of 1.131 Å, shorter than is usual in the BPEA structures, but the C-C single bond distances are typical (C_{ant}-C = 1.454(3) Å and C_{Ph}-C = 1.461(3) Å). The aromatic moieties are not co-planar, with a dihedral angle between the mean plane of the anthracene moiety and the phenyl rings of 25.53(7)°. The molecules are not linear, with a bend in the molecules as well as a twist. The C-C≡C bond angles are 173.1(2)° and 174.0(2)°.
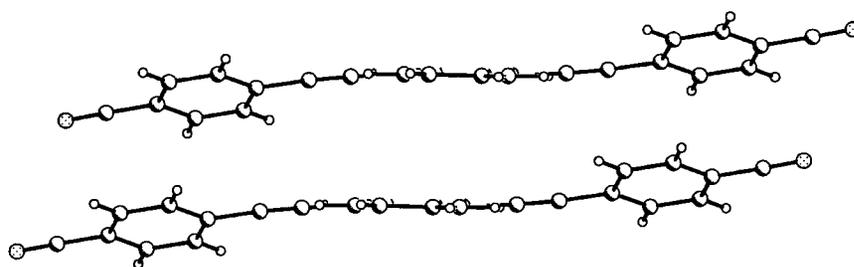
Figure 4.62: Diagram of NC-Ph-CC-Ant-CC-Ph-CN, viewed parallel to the plane of the anthracene moiety, showing the lack of planarity and linearity of the molecule.

The packing coefficient, K, is 0.722, which is consistent with values found for the BPEBs, so the lack of planarity or linearity is not disruptive. In fact, it is likely that the molecule adopts this conformation to maximise favourable interactions (and minimise

unfavourable ones) between arene moieties in adjacent molecules. The molecules stack almost directly on top of each other, with both the phenyl rings and the anthracene moiety slipped by a small amount.
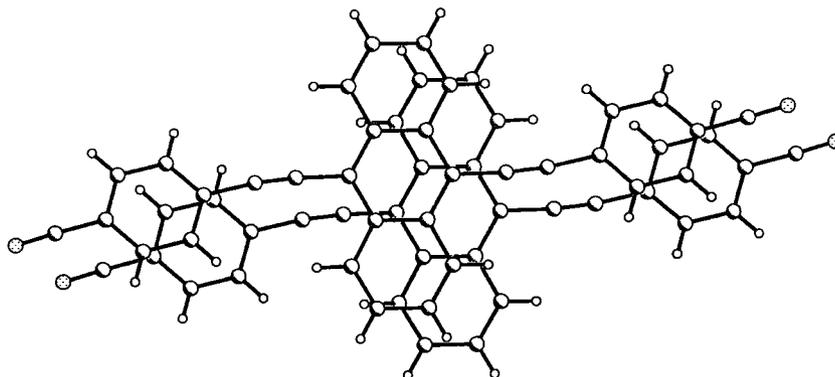
Figure 4.63: Diagram of NC-Ph-CC-Ant-CC-Ph-CN, viewed perpendicular to the mean plane of the anthracene moiety.

Columns of these stacks line up in the direction of the *b* axis, with the anthracene moieties stacking parallel to the *b* axis and the phenyl rings stacking parallel to the *a* axis (see Figure 4.64 and Figure 4.65).
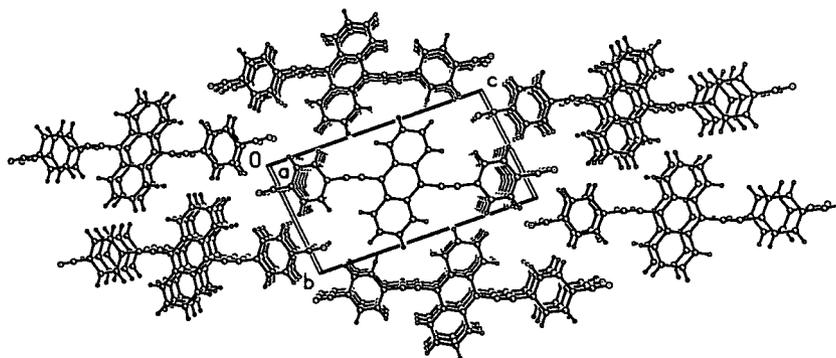
Figure 4.64: Diagram of NC-Ph-CC-Ant-CC-Ph-CN viewed down the *a* axis, showing the alignment of anthracene moieties.
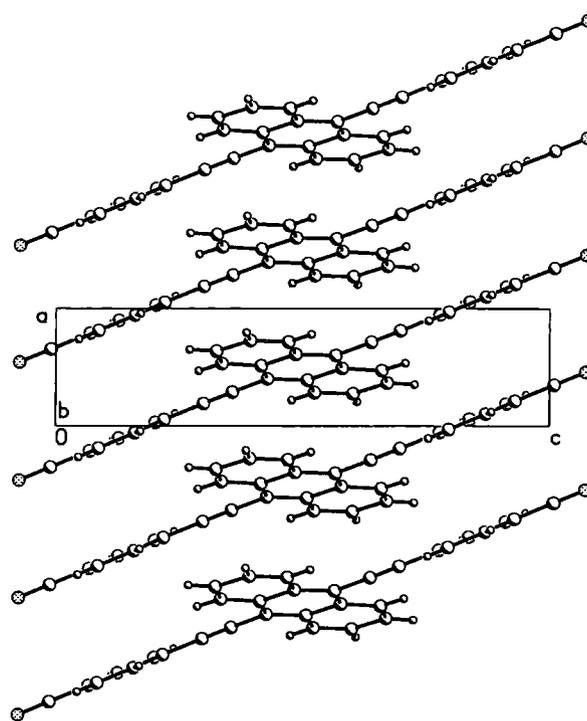
Figure 4.65: Diagram of NC-Ph-CC-Ant-CC-Ph-CN viewed down the *b* axis, showing the alignment of Ph groups parallel to the *a* axis.

There are no significant short contacts in the structure. The inter-centroid distance between adjacent anthracene groups (using the mean plane of the central ring) is 3.854 Å. The inter-planar distance is 3.488 Å. These separations can be seen clearly in Figure 4.65 and Figure 4.66.
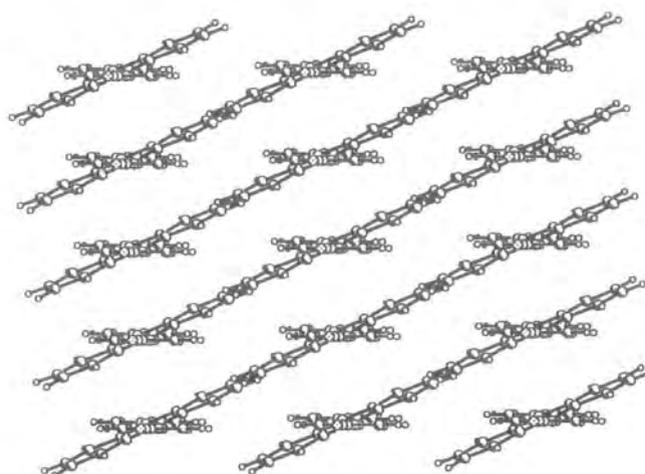
Figure 4.66: Diagram of NC-Ph-CC-Ant-CC-Ph-CN viewed down the molecular axis, showing the alignment of Ph stacks (vertical) and anthracene stacks (diagonal).

The new crystal structure of MeO_2C-Ph-CC-Ant-CC-Ph- CO_2Me (**4j**) is in the same space group as the cyano-substituted analogue ($P\bar{1}$), but the cell dimensions are quite different (see Table 4.10). The compound crystallises with two independent molecules in the unit cell, with each one lying on a centre of inversion. Both C≡C triple bond distances (av. 1.196(2) Å) and C-C single bond distances (1.4291(17) Å to 1.4382(17) Å) are typical. The C-CO_2Me bond distance is slightly longer than the other C-C bond distances, at 1.4917(17) Å (average).
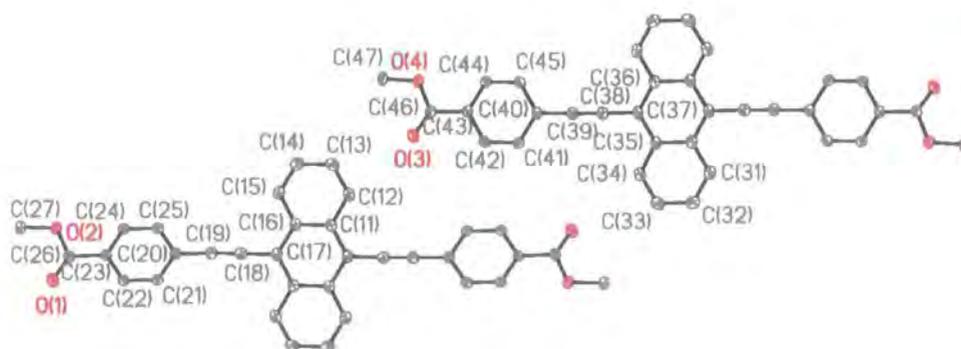
Figure 4.67: Ortep diagram for (4j). Ellipsoids plotted at 50% probability level. Hydrogen atoms have been omitted for clarity.

The most striking feature of this structure is that one of the molecules is almost planar, with a dihedral angle between the anthracene moiety and the phenyl rings of only 5.2°, but the second molecule exhibits a twist, with a dihedral angle between the anthracene and the phenyl ring of 30.9°. This cannot be seen as clearly in Figure 4.68 as it might due to the substituent CO_2Me groups obscuring the view.
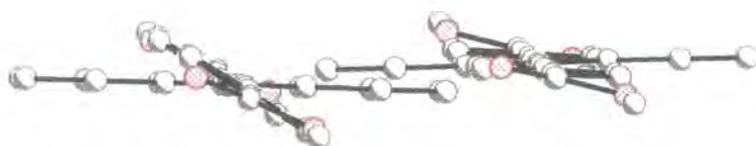
Figure 4.68: Diagram of the two independent molecules in (4j), viewed down the molecular axis, demonstrating the difference in the dihedral angles.

The molecules align themselves in the crystal with the outer rings of anthracene moieties from alternating molecules overlapping, and with phenyl rings in like molecules partially overlapped. The molecules lie almost parallel to the [0 1 1] plane (in bc).
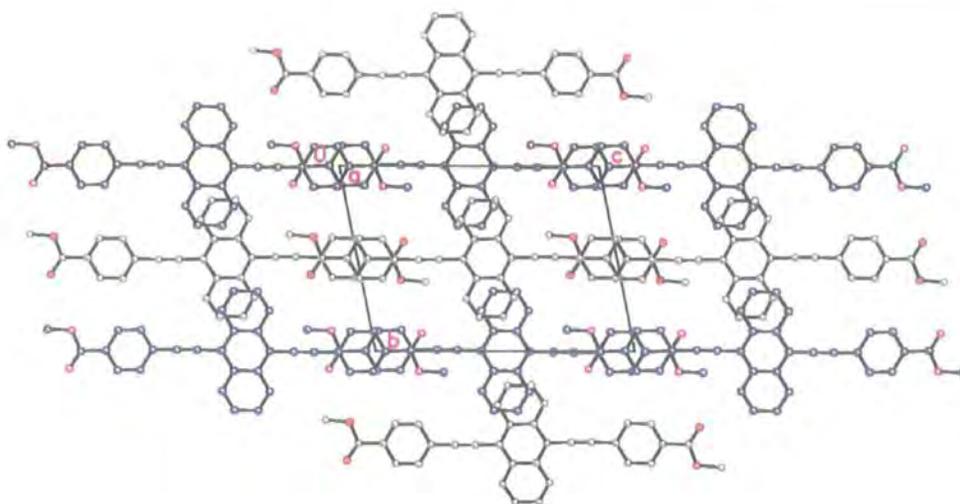
Figure 4.69: Packing diagram for (4j), viewed down the *a* axis to show the slight overlap of anthracene and phenyl moieties. The more planar molecule is depicted with black carbon atoms, the less planar molecule has carbon atoms shown in blue. Hydrogen atoms have been omitted for clarity.

There are rows of like molecules lined up end-to-end, but the two independent units alternate side-by-side. This can be seen in Figure 4.70.
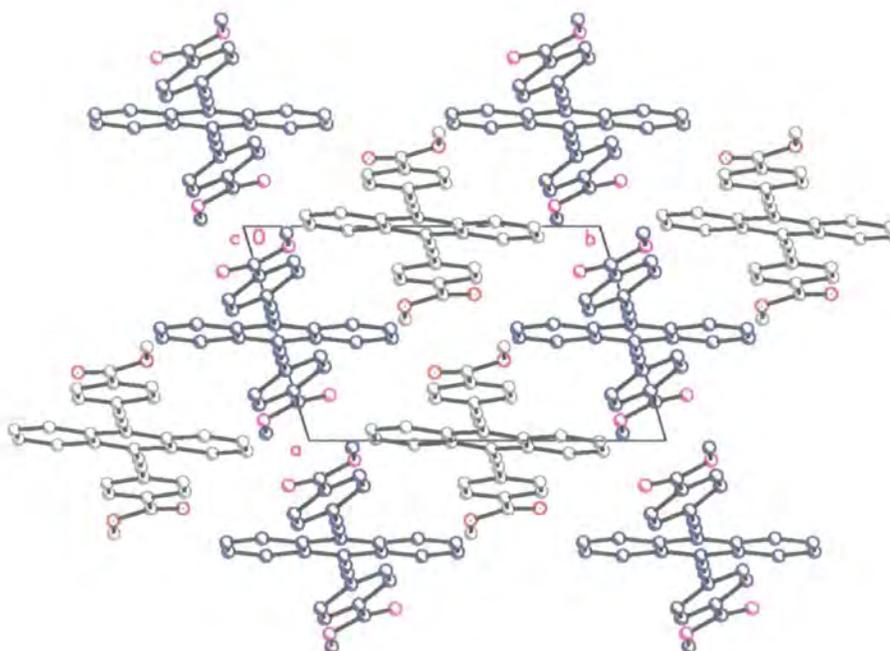
Figure 4.70: Packing diagram for (4j), viewed down the crystallographic *c* axis. The more planar molecule is depicted with black carbon atoms, the less planar molecule has carbon atoms shown in blue. Hydrogen atoms have been omitted for clarity.

The phenyl groups in each independent molecule can be seen to sit above and below of each other, with anthracene groups almost co-planar (see Figure 4.71).
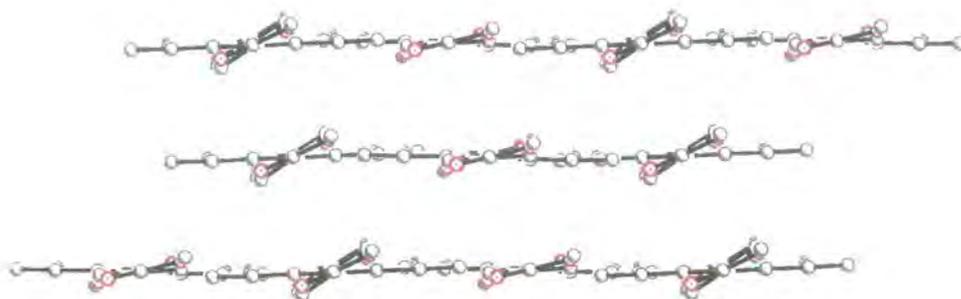
Figure 4.71: Packing diagram of (4j) viewed down the molecular axis, showing almost co-planar anthracene moieties horizontally. The differently tilted phenyl groups can be seen to align above and below each other. Hydrogen atoms have been omitted for clarity.

The packing coefficient, K, is 0.726, which is comparable to that for NC-Ph-CC-Ant-CC-Ph-CN, the other BPEA system which has been analysed. The inter planar distance between the centre phenyl rings in the anthracene moiety is 3.422 Å, and the corresponding inter-centroid distance is 5.834 Å (inclined at an angle of 56.0°).

The space group and unit cell data for all known BPEA structures, including the new one which has been presented in this section, are listed for comparison purposes in Table 4.10.

Table 4.10: Space group and unit cell data for known structures of the type R-Ph-CC-Ant-CC-Ph-R

R	H	NPh_2	CN	CO_2Me (**4j**)
Crystal System	orthorhombic	monoclinic	triclinic	triclinic
Space Group	*Pbcn*	*P2₁/n*	$P\bar{1}$	$P\bar{1}$
a (Å)	24.305(4)	11.582(2)	3.8537(5)	7.2247(4)
b (Å)	11.512(1)	9.407(2)	8.604(1)	11.6597(8)
c (Å)	7.099(1)	18.429(4)	16.130(2)	15.3807(9)
α (°)	90	90	82.682(2)	77.343(1)
β (°)	90	108.14(2)	88.923(3)	83.037(1)
γ (°)	90	90	83.830(2)	72.026(1)

4.6 Other samples tested

Co-crystals

It has proved to be quite difficult to obtain structures of co-crystals of BPEB derivatives. There have been several samples tested that were thought to be co-crystals, but which turned out to be only one single component. This could be a suggestion that the co-crystal in question is reluctant to form possibly due to repulsive forces between the two components, thus it may be interesting to consider these. Of course, the lack of a structure solution could just be down to a lack of decent crystalline samples. Other samples simply didn't contain a crystal of high enough quality for an X-ray diffraction experiment. Listed below are the samples which were tested, with a brief explanation of why the experiment did not proceed.

1. MeO-PhF$_4$-CC-Ph-CC-PhF$_4$-OMe with MeO-Ph-CC-PhF$_4$-CC-Ph-OMe

Three different samples were tested on the diffractometer. All of them gave the cell for the MeO-Ph-CC-PhF$_4$-CC-Ph-OMe component only, despite both components being added to the solution which the crystals were grown from.

2. Py-CC-PyF$_4$-CC-Py with PyF$_4$-CC-Py-CC-PyF$_4$

This failure could have been the result of poor crystals, since neither of the two crystals tried would index.

3. PhF$_5$-CC-PhF$_5$ with Ph-CC-Ph-CC-Ph

None of the crystals provided were of a suitable quality for X-ray diffraction.

4. Me$_2$N-Ph-CC-Ph-CC-Ph-NMe$_2$ with PhF$_5$-CC-PhF$_4$-CC-PhF$_5$

This sample consisted of thin plate crystals. The plates gave few spots, all of which were weak and small. No samples were suitable for an X-ray diffraction experiment.

5. O_2N-Ph-CC-Ph-CC-Ph-NO_2 with PhF_5-CC-PhF_4-CC-PhF_5

Cell proved to be that of F_3C-Ph-CC-PhF_4-Ph-CF_3, which was put down to a labelling mix up by the chemist.

6. Naphthalene with PhF_5-CC-PhF_4-CC-PhF_5

The first sample attempted gave the same unit cell as PhF_4-CC-PhF_4-CC-PhF_5 All crystals had the same morphology thus the sample was abandoned. Several crystals tested from the second sample also gave only the unit cell for the PhF_5-CC-PhF_4-CC-PhF_5 component.

7. MeO_2C-Ph-CC-Ph-CC-Ph-CO_2Me with PhF_5-CC-PhF_4-CC-PhF_5

All the crystals which were tested on the diffractometer gave the unit cell for the PhF_5-CC-PhF_4-CC-PhF_5 component only.

8. MeO-PhF_4-CC-PhF_4-CC-PhF_4-OMe with MeO-Ph-CC-Ph-OMe

When several crystals were tested, the unit cell was consistently the same as that for three-ring component alone.

BPEBs

Ph-CC-Ph-CC-PhF_5 has not been structurally characterised before. The sample tested contained small plate-like crystals that looked beautiful under the microscope. Testing on the diffractometer at 100 K showed that the diffraction was poor and weak, and was strange in that there were some decent-looking spots, but some near the centre of the diffraction pattern which appeared as smudges. A data set was collected but repeated

attempts to solve it failed. In all, five crystals were tested. It was noted that when removed from the diffractometer and warmed back up to room temperature, cracks appeared in the crystal. It has been suggested that this could imply a destructive phase transition, thus if another sample is obtained, higher temperature collections could be attempted to attempt to eliminate any sudden partial phase transitions on cooling destroying the crystal.

Chapter 5: Halogen-substituted tolans – a further look at arene-perfluoroarene interactions

5.1 Introduction

One method of synthesis for the bis(phenylethynyl)benzene compounds discussed in Chapter 4, is via the use of halogen-substituted diphenylacetylenes (tolans). These compounds are also of interest for the structural, electronic, and optical properties they themselves possess. Simple derivatives of the parent tolan are known to exhibit good fluorescent properties,[172] reasonable NLO properties[173] as well as liquid crystalline behaviour.[174] The higher than expected melting point for tolan and derivatives is thought to be due to the planarity of the molecule allowing efficient crystal packing. Tolans with polar substituents can further enhance this by providing extra intermolecular interactions. But not all tolans are planar in the solid state. The angle between the mean planes of the two phenyl groups is due to rotation about the C-C single bonds, which in turn is thought to be dictated by any conjugation of the phenyl rings with the C≡C triple bond.[175] This angle is known as the dihedral angle and the larger this parameter, the more the molecule deviates from planarity. A completely planar molecule will have a dihedral angle of 0.0°

The crystal packing of tolans can be described and compared using a variety of parameters, not just the dihedral angle. The interplanar distance and inter centroid distance between two adjacent stacked molecules has been defined in Chapter 4, as has the packing coefficient, K. A further parameter that can be used, which gives an indication of how linear the molecule is, is the 'distortion' angle of the molecule. This can be defined as the complement of the angle formed between the centroids of the phenyl rings and the centre of the triple bond. The larger the distortion angle, the more the molecule deviates away from linearity.

It is also important to analyse the intermolecular close contacts between atoms or groups, since these are often thought to play a significant role in determining overall structure. A close contact between two atoms is defined here as one which is below the sum of the van der Waals radii of the atoms, as defined by Bondi.[158] Care must be taken when assessing the relevance of close contacts since they can arise merely as a consequence of other packing forces in the crystal, and may not be a driving force behind the particular structure. Because of this, halogen···halogen close contacts have been classified into two types: type I and type II.[161a]

Type I contacts are those which arise merely as a consequence of close packing forces elsewhere in the structure, and can be identified by approximately equal C-X···X angles. They usually arise between molecules related by a centre of inversion. Both types of short contact are illustrated in Figure 5.1.
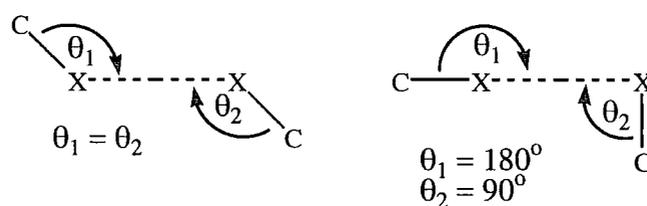
Figure 5.1: Diagram to show the difference between Type I (left) and Type II (right) halogen···halogen short contacts.

Type II contacts, however, have two different C-X···X angles, usually approximately 90° and 180°. These are thought to be caused by polarisation arising between the halogen atoms. Desiraju *et al.* have even suggested that these contacts have covalent character for the larger halogen atoms.[176] It is these, Type II, interactions that can contribute to stabilising certain structures. Thus, only Type II interactions will be considered relevant here. Type II interactions occur much less frequently for fluorine atoms, possibly due to the fact that fluorine is much less polarisable than the other

halogens. It has even been suggested that F···F contacts could be repulsive.[177] Thus, although short F···F contacts will be noted in this study, they will be not considered as a possible means of stabilisation of these structures.

5.1.1 Literature search for crystal structures of tolans

Structures of unsubstituted tolans

The parent tolan, Ph-CC-Ph, is known and six slightly different crystal structures[178] appear in the Cambridge Structural Database[73] (Refcodes DPHACT01-03, DPHACT05-07). It crystallises in space groups $P2_1/a$ and $P2_1/c$, with very similar unit cell parameters. In all six cases, the molecule is planar, with a 'twist' or dihedral angle of 0.0°. The most recent structure,[178e] solved at both 153K and 295K, crystallised in $P2_1/c$. The C≡C triple bond distance is 1.198 Å (averaged for the two independent molecules). The molecule is almost linear, with an average bond angle C_{sp}-C_{sp}≡C_{sp} of 178.03°. There are no arene-arene interactions in the structure.

This tolan has also been published as a co-crystal with octafluoronaphthalene (OFN), which displays arene-perfluorophenyl interactions. Two publications of the same structure were made in the same year, one[179] at 223K and one[180] at 100K. Both structures were in the same space group ($P2_1/n$). The unit cell of the lower temperature structure had slightly smaller unit cell parameters, as expected due to the reduction in thermal motion at lower temperatures. Analysing the low temperature structure, it was found that the co-crystal structure consists of alternating stacks of tolan and OFN molecules, that are only 8.6(1)° away from parallel to one another, as opposed to the structure of the pure components which both display herringbone-type packing. Arene-

perfluoroarene interactions are thought to be responsible for this change in packing. The tolan is linear and planar.

The structure of the fully fluorinated tolan, PhF_5-CC-PhF_5 at 295K (CSD Refcode PFDPAY) is also known.[181] It crystallises in orthorhombic space group *Pbca* with C≡C bond distance 1.198 Å and C-C single bond distances 1.416 Å and 1.422 Å. The molecule is almost planar, with a dihedral angle of just 2.23°, and almost linear (C-C≡C angles 177.80° and 179.45°). The packing is in a herringbone pattern with the molecular axis running parallel to the long *c* axis of the unit cell.

The structure of the Ph-CC-PhF_5 tolan has been solved in Durham but is not yet published. It crystallises in space group $P\bar{1}$ with unit cell parameters a = 6.1305(10), b = 7.2444(12), c = 12.754(2), α = 85.229(4), β = 84.793(4), γ = 85.766(4). There is evidence of arene-perfluoroarene interactions between molecules in the crystal, with a slight offset as seen in the BPEBs of Chapter 4. The molecules can be seen to exhibit a 'head-to-tail' arrangement that allows for the stacking of alternate phenyl-perfluorophenyl rings.

The inter planar distances between molecules are not identical above and below a molecule, the two distances being 3.418 Å and 3.424 Å. The inter centroid distances are 3.700 Å and 3.681 Å. The packing coefficient, K, is 0.701, which is not as large as most of the BPEB structures, but still shows efficient packing in the crystal.

(a)

(b)

(c)
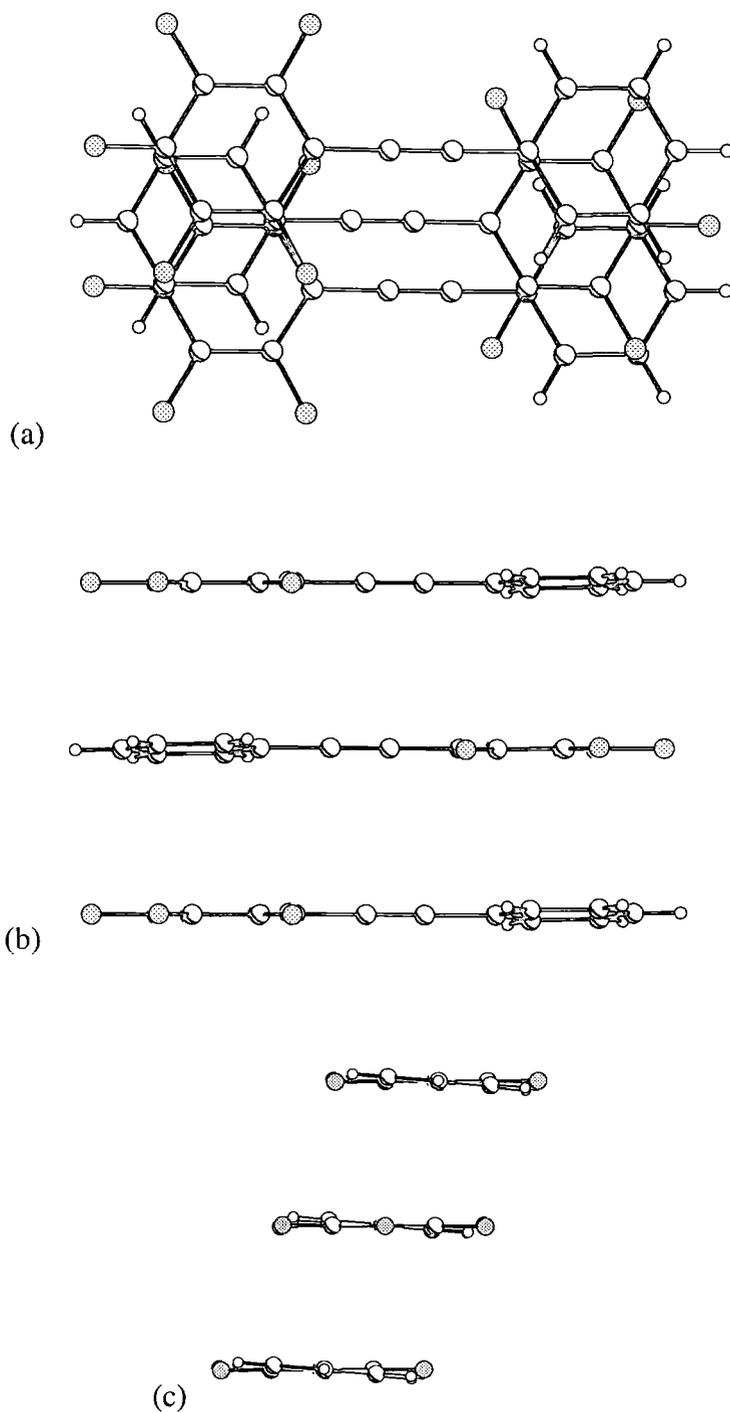
Figure 5.2: Diagram of molecules of Ph-CC-PhF$_5$, viewed (a) perpendicular to the C$_6$F$_5$ ring, and (b) down the plane of the Ph-CC-PhF$_5$ ring and (c) down the molecular axis, showing how they stack on top of each other in an alternating fashion to allow arene-perfluoroarene interactions.

There is an arene-perfluoroarene interaction between molecules that perpetuates parallel to the b axis of the unit cell. There are short H$\cdots$F contacts between H(14) and F(2) of 2.545 Å at an angle of 130.5°, which can be seen in Figure 5.3.
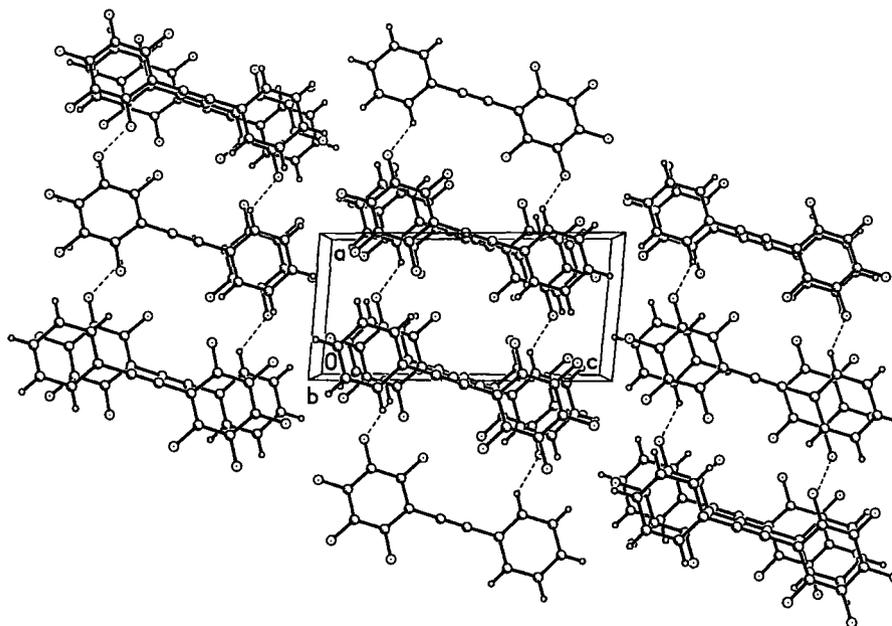
Figure 5.3: Packing diagram for Ph-CC-PhF$_5$, viewed down the b axis of the unit cell, showing the short H$\cdots$F contacts.

The co-crystal of the two parent tolans also exhibits arene-perfluoroarene interactions, and is almost isostructural with the unsymmetrical Ph-CC-PhF$_5$ tolan discussed above. Both the molecules in the co-crystal are perfectly planar, and no significant differences are observed in the geometry of the molecules compared with the structures of the pure components. The structure is comprised of alternate layers of tolan and perfluorotolan molecules. The alternating columns of molecules stack along the b axis. The distances above and below the molecules are not the same. The inter planar distances are 3.452 Å and 3.404 Å, with corresponding inter centroid distances of 3.799 Å and 3.730 Å. The molecules are not stacked directly on top of each other in an eclipsing fashion, but are slipped by approximately one C-C bond distance. This is typical for structures where the arene-perfluoroarene interaction has an influence. There are short H$\cdots$F contacts

ranging from 2.593 Å to 2.741 Å. The packing coefficient, K, is 0.695, which is at the low end of the range expected (compared to co-crystals in Chapter 4).

An elegant example of the arene-perfluoroarene interaction is presented in the structure of a co-crystal of *sym*-triphenethynylbenzene and the perfluorinated analogue *sym*-tris(perfluorophenylethynyl)benzene (see Figure 5.4).
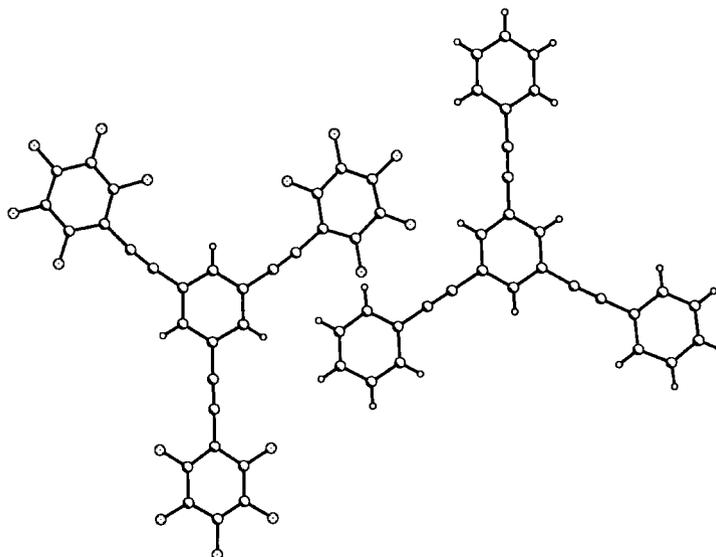
Figure 5.4: Diagram of *sym*-triphenethynylbenzene *sym*-tris(perfluorophenylethynyl)benzene.

The pure components display herringbone packing in the solid state, but when co-crystallised, favourable arene-perfluoroarene interactions cause the molecules to align in alternating fluorinated and non-fluorinated stacks. The different molecules stack over each other with a slight slip, as has been seen previously in structures of this type.
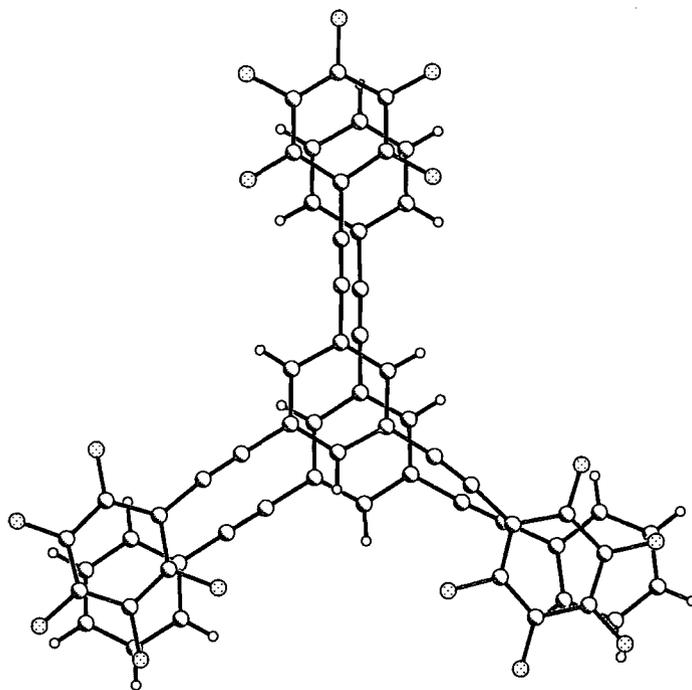
Figure 5.5: Diagram of the co-crystal of *sym*-triphenethynylbenzene *sym*-tris(perfluorophenylethynyl)benzene, viewed perpendicular to the central ring of the fluorinated molecule.

The space group is $P\bar{1}$, which is a common space group for co-crystals of this type (see Chapter 4). There are some short C-H⋯F interactions (2.4-2.7 Å). The molecules in the co-crystal are within 5° of planarity, whereas the pure components demonstrate considerable twist between the central and outer phenyl rings.

Structures of disubstituted tolans

Structures of *para*-disubstituted tolans were searched for in the Cambridge Structural Database.[73] Several were found, including H_2N-Ph-CC-Ph-NO_2 (CSD refcode KEFLOW), H_2CHNCO-Ph-CC-Ph-$CONHCH_2$ (CSD Refcode ZUKKAR) and two carborane containing structures: $1,12$-$C_2B_{10}H_{11}$-Ph-CC-Ph-$(1,12C_2B_{10}H_{11})$ (CSD Refcode NEVCAS) and the monosubstituted analogue $1,12$-$C_2B_{10}H_{11}$-Ph-CC-Ph (CSD Refcode NEVCEW). There were no partially fluorinated tolans of this type found. Several *ortho*- and *meta*-substituted tolans were also found.

Several asymmetrically substituted tolans were investigated[182] as part of a study to find non-centrosymmetric crystal structures. These are of interest because only non-centrosymmetric structures can exhibit the non-linear optical phenomenon of second harmonic generation (SHG). The initial interest in this area began when the disubstituted tolan $MeS-Ph-CC-Ph-NO_2$ proved to have strong SHG capabilities. The compound crystallises in the non-centrosymmetric space group *P1*.

Analysis of the structure shows that the two independent molecules in the unit cell are slightly twisted, with dihedral angles between the phenyl rings of 7.2° and 4.5°. The substituents are slightly out of the planes of the attached phenyl rings. The mean plane of the NO_2 group is at an angle of 3.3° to the phenyl ring, and the MeS has a torsion angle of 4.9°. The different substituents have differing effects on the angles in the phenyl rings. The internal angle at the NO_2 moiety is greater than 120° (average of the two independent units is 123.2(6)°) but at the MeS the angle is less than 120° (117.6(6)° average). This is due to the ability of the substituents to withdraw electrons from or release electrons into the π-system of the phenyl ring. NO_2 is electron withdrawing, causing the angle to be increased above 120°, whereas the MeS is electron releasing so the angle is less than 120°. A further interesting point is that the molecules in the crystal all pack in the same direction, meaning that not only do the molecules have a dipole moment, but also the crystal itself has a net dipole moment. The packing is a herringbone type.

Following the discovery of the non-centrosymmetric space group for the above tolan, more investigations were undertaken in the hope of finding other, related non-centrosymmetric structures. Crystals of $MeO-Ph-CC-Ph-NO_2$ were grown from a variety of solvents in an attempt to isolate a non-centrosymmetric polymorph. Crystals

grown from acetonitrile were in the centrosymmetric space group $P\bar{1}$, with three independent molecules in the asymmetric unit. The same unit cell was found for crystals grown from toluene, DMSO, methyl formamide, methyl acetamide and, by another research group,[183] from ethyl acetate. The only difference was found when the sample was crystallised from cyclohexane. Two different types of crystal were grown. The first were crystalline blocks. The structure of one of these crystals was solved, and found to be a different polymorph of the compound, in space group $P2_1/n$, but unfortunately this is also a centrosymmetric space group so no SHG was observed. The second type of crystals were small needles, which were not suitable for single crystal X-ray diffraction, so no unit cell was found. The sample did, however, exhibit large SHG thus it is likely that these needle crystals were in a non-centrosymmetric space group.

The structure of the two polymorphs of MeO-Ph-CC-Ph-NO_2 have similar C≡C bond distances. The dihedral angle, however, differs quite significantly. The $P2_1/n$ crystals have a dihedral angle of 15.7°, which is greater than any of the three independent molecules in the $P\bar{1}$ structure (12.0°, 8.5° and 1.4°). The angle in the phenyl ring at the NO_2 group in both structures is greater than 120° (122.7(3)° ($P\bar{1}$) and 122.1(2)° ($P2_1/n$)). The angle of the MeO group away from the plane of the phenyl ring is only 1.7° (average) in the $P\bar{1}$ structure and 2.0° for the $P2_1/n$. The torsion angles for the NO_2 groups in $P\bar{1}$ are 4.3°, 5.7° and 17.8° compared to 5.7° in the $P2_1/n$ structure.

The packing in the crystals of the two polymorphs is very different. The $P\bar{1}$ structure exhibits herringbone-type packing whereas the molecules in the $P2_1/n$ structure are packed in columns down the b axis.

The structures of MeS-Ph-CC-Ph-CN and MeO-Ph-CC-Ph-CN were found to be very similar. Both crystallised in the centrosymmetric space group $P2_1/n$ with near-planar molecules (dihedral angles 3.6° and 4.7° respectively). The MeS torsion angle is 6.9°, and the MeO torsion angle is 2.7°. Both structures exhibit herringbone style crystal packing.

Me-Ph-CC-Ph-OMe[184] and MeO-Ph-CC-Ph-OMe both crystallise in centrosymmetric space groups at 148K (orthorhombic $Pna2_1$ and monoclinic $P21/n$ respectively). The molecules are almost planar. Me-Ph-CC-Ph-OMe has a dihedral angle of 6.0° and the two independent molecules in the structure of MeO-Ph-CC-Ph-OMe have dihedral angles of 5.1° and 6.9°. The herringbone type packing is very similar in both structures. There are short C-H⋯C contacts in both structures (2.74 Å and 2.76 Å respectively) that were thought to be C-H⋯π type interactions.

The symmetrical tolan NC-Ph-CC-Ph-CN crystallises in space group $P2_1/c$ with a short a axis. The molecules are perfectly planar. The internal angle of the phenyl ring at the substituents is 120.56(9)°. There is a short contact (2.560 Å) between the C≡N group and the *ortho* hydrogen atom on an adjacent molecule.

Me-Ph-CC-Ph-CC-Me and MeO-Ph-CC-Ph-OMe both crystallise in $P2_1/c$. They are both completely planar. The internal angles of phenyl ring at the substituent are 117.9(1)° and 119.8(1)° respectively, indicating that Me is more electron releasing than MeO.

F_3C-Ph-CC-Ph-CF_3 crystallises in space group Cc. The molecule is not completely planar with a dihedral angle of $3.0(2)°$. The internal angle of phenyl ring at substituent $120.6(3)°$, indicating the slight electron withdrawing ability of the fluoromethyl group.

Monosubstituted tolans

A study of a series of five monosubstituted tolans of the type Ph-CC-PhF_4-O-R (R = Me, ^{n}Pr, ^{i}Pr, CH_2Ph and p-tolyl [4-methylphenyl]) was undertaken[185] to investigate the perturbation effect of the substituent, if any, on the arene-perfluoroarene interaction which influences the structure of the parent compound Ph-CC-PhF_5. The series were synthesised by reacting Ph-CC-PhF_5 with the relevant alcohol with 10% KOH.

Ph-CC-PhF_4-OMe[xvii] crystallises in the monoclinic space group $P2_1/n$. The molecules display the influence of the arene-perfluoroarene interaction in an elegant fashion. Alternating columns of phenyl and perfluorophenyl rings run parallel to the short b axis. The columns interpenetrate since the stacks of molecules are slipped by one ring, resulting in an infinite chain of staggered molecules running throughout the crystal almost perpendicular to the direction of the stacks. There are two very short C-F···H-C contacts with corrected[xviii] distances of 2.476 Å and 2.389 Å. The inter centroid distances are 3.650 Å and 3.763 Å, with inter planar distances of 3.444 Å and 3.558 Å.

The tolan PhF_5-CC-Ph-OMe, which does not strictly belong in this series but is related to the compound above, was synthesised via a cross coupling reaction. C_6F_5-I and MeO-C_6H_5-C≡C-H were reacted in triethylamine, with a palladium and copper catalyst. This

---

[xvii] Structure solved by Simon Borthwick, University of Durham, 1998.
[xviii] C-H distances extended to 1.08 Å consistent with neutron diffraction data for C-H bonds.

isomer is only slightly different in atomic arrangement, but this small change has large

effects on the crystal packing of the structure. The most obvious of the differences is the

dihedral angle. The structure of Ph-CC-PhF$_4$-OMe has a twist of 25.8°, whereas the two

rings in the isomer are almost at 90° to each other (dihedral angle 79.8°). The result of

this is alternating phenyl-perfluorophenyl ring stacking in two directions. The

interplanar distance in the arene-perfluoroarene stack is 3.340 Å, and the inter-centroid

distance is 3.535 Å. This style of packing has the consequence that some

perfluorophenyl groups are also face-to-face, with an interplanar distance of 3.293 Å

and an intercentroid distance of 3.617 Å.

The n-propyl analogue in the series, Ph-CC-PhF$_4$-O-^{n}Pr, crystallises in space group $P\bar{1}$.

Face-to-face π-stacking can be observed in the structure, leaving spaces between the

ends of the molecules for the n-propyl substituent to fold itself into. The interplanar

distance is 3.495 Å with an inter centroid distance of 3.722 Å. The dihedral angle

between the two phenyl rings is just 5.5°. The orientation of the molecules which is

required to create the space for the n-propyl groups again leads to close

perfluorophenyl-perfluorophenyl face-to-face stacking (interplanar distance 3.259 Å and

inter centroid distance 3.501 Å. Short F···H contacts of 2.457 Å (corrected value) are

present in the structure.

The related compound of Ph-CC-PhF$_4$-O^{i}Pr was found[xix] to have a somewhat different

structure. The increased bulk of the *iso*-propyl substituent cannot be accommodated in

the plane of the molecule, nor can it be folded so easily as the n-propyl substituent,

above. The result of this is that the packing of the structure is disrupted. Pairs of

---

[xix] Structure solved by Simon Borthwick, University of Durham, 1998.

molecules, with the phenyl ring face-to-face with the perfluorophenyl ring, make up

units that form the overall structure. There are no infinite arene-perfluoroarene stacks

through the crystal. The interplanar distance between molecules in the pairs is 3.699 Å,

with a corresponding inter-centroid distance of 3.731 Å.

The structure of $Ph-CC-PhF_4-O-CH_2Ph$ is disordered. There are phenyl-perfluorophenyl

interactions utilising the benzyl phenyl ring. Short C-F⋯H-C contacts of 2.332 Å, 2.545

Å and 2.451 Å are present between molecules. The interplanar distances are 3.562 Å

and 3.293 Å, with corresponding inter centroid distances of 3.853 Å and 3.842 Å.

In the structure of $Ph-CC-PhF_4-O-p$-tol, the tolan section aligns so it is stacked above

and below tolan sections of adjacent molecules. At first glance, it looks as though this is

to maximise arene-perfluoroarene interactions in the molecules, as well as

accommodating the bulky p-tolyl substituent outside of the stacks. When viewed from

perpendicular to the plane of the molecule, however, the slip distance is such that the

phenyl and perfluorophenyl rings barely overlap thus it is doubtful that arene-

perfluoroarene interactions are having any effect at all. It may just be that

accommodating the p-tolyl substituent dictates the packing.

Halogen substituted tolans

A search of the Cambridge Structural Database revealed that there are no crystal

structures of partially fluorinated tolans that contain a halogen molecule in the _para_

position. In fact, there is only one structure of a tolan-type molecule which contains

such a halogen (not including fluorine) and it is not fluorinated. The brominated tolan

structure appears as part of a highly substituted diphenylcarbonate,[186] but it is not

discussed and is not central to the study.

This chapter attempts to investigate the effect of a *para*-substituted halogen atom on the arene-perfluoroarene interaction.

5.2 Scope of this Study

This chapter will present the crystal structures of the halogen substituted tolan systems PhF_5-CC-Ph-I (**5a**), PhF_5-CC-Ph-Br (**5b**), PhF_5-CC-Ph-Cl (**5c**) and Ph-CC-Ph F_4-I (**5d**), with discussion of their molecular geometries and crystal packing. Of particular interest is the effect of the halogen substituent on the arene-perfluoroarene interaction which is observed in the structure of the parent Ph-CC-PhF_5 compound.

The structure of a related compound, Ph-CC-PhF_4-CC-$SiMe_3$ will also be presented here, with discussion.

5.3 Results and Discussion

Compounds of type PhF_5-CC-Ph-X (X = I, Br, Cl), (5a), (5b) and (5c), respectively, and Ph-CC-PhF_4-I (5d) were synthesised[187] by Jonathon C. Collings, with crystals obtained by slow evaporation from hexane solution. The crystal structures were solved, and the data is presented in Table 5.1, below. Full refinement and structural data are presented in Appendices A5a to A5d respectively.

Table 5.1: Crystal data for compounds (5a) to (5d)

Compound	(5a)	(5b)	(5c)	(5d)
Formula	$C_{14}H_4F_5I$	$C_{14}H_4F_5Br$	$C_{14}H_4F_5Cl$	$C_{14}H_5F_4I$
Formula weight	394.07	347.08	302.62	376.08
T (K)	105(2)	100(2)	110(2)	100(2)
Crystal system	Monoclinic	Monoclinic	Triclinic	Monoclinic
Space group	$P2_1/c$	$P2_1/c$	$P\bar{1}$	$P2_1/n$
a (Å)	21.417(7)	20.517(1)	6.076(1)	12.668(2)
b (Å)	4.9672(16)	5.181(1)	7.488(1)	5.0744(8)
c (Å)	11.692(4)	11.254(1)	13.168(1)	18.833(3)
α (°)	90	90	85.343(1)	90
β (°)	92.288(5)	96.922(1)	86.054(1)	93.703(4)
γ (°)	90	90	83.332(1)	90
U (Å^3)	1242.9(7)	1187.6(1)	592.1(1)	1208.1(3)
Z	4	4	2	4
D_c (g cm^{-3})	2.106	1.941	1.698	2.068
μ (mm^{-1})	2.623	3.510	0.371	2.682
F(000)	744	672	300	712
Crystal size (mm^3)	0.6 x 0.2 x 0.05	0.6 x 0.3 x 0.05	0.6 x 0.6 x 0.05	0.2 x 0.2 x 0.1

Compound (5a) (1-iodo-4-(pentafluorophenylethynyl)benzene) has a C≡C triple bond distance of 1.205(9) Å, and C-C single bond distances of 1.421(9) Å and 1.429(9) Å for the bonds adjacent to the perfluorophenyl and phenyl rings respectively. The C-I

distance is 2.087(5) Å. The dihedral angle is 9.4° and the distortion angle is 4.7°, indicating slight deviations away from linearity and planarity.
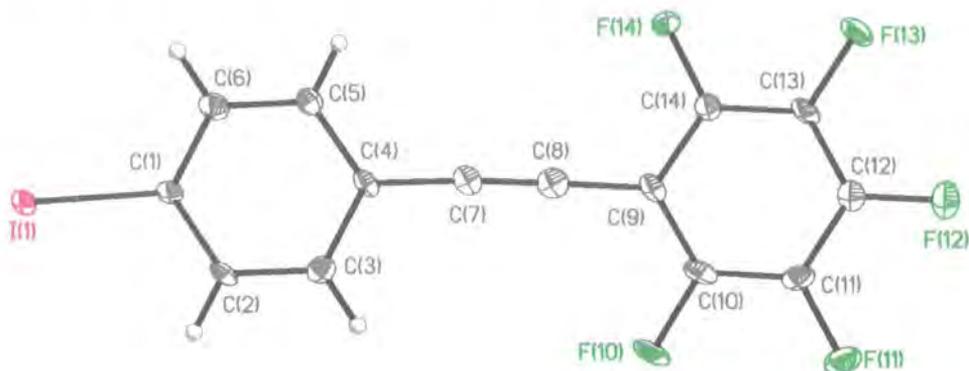
Figure 5.6: Ortep diagram for (5a), viewed perpendicular to the plane of the perfluorophenyl ring. Thermal ellipsoids are plotted to 50% probability level.

There is no arene-perfluoroarene interaction in the crystal, with the molecules stacking almost parallel, the iodine atom pointing the same way and neighbouring molecules slipped so that the phenyl rings are aligned with the C≡C triple bond.
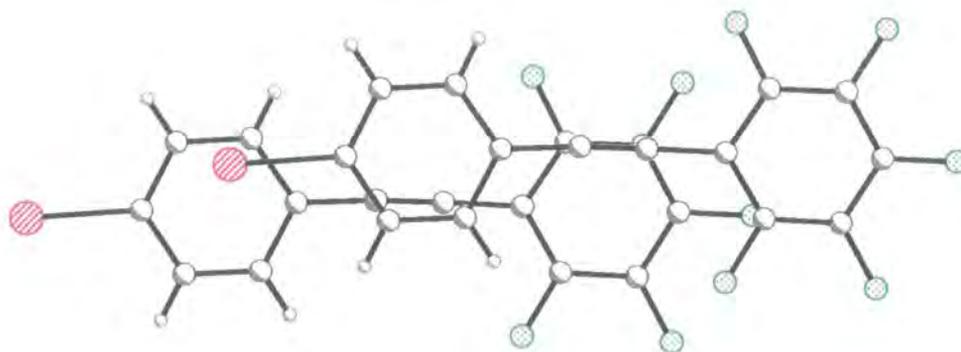
Figure 5.7: Stacking diagram of (5a), viewed perpendicular to the plane of the perfluorophenyl ring.

The molecules stack in a parallel fashion, despite the 'banana' shape of the molecules. The inter planar distance is 3.428 Å, with a large inter centroid distance of 4.859 Å reflecting the large displacement from an eclipsing stack motif.
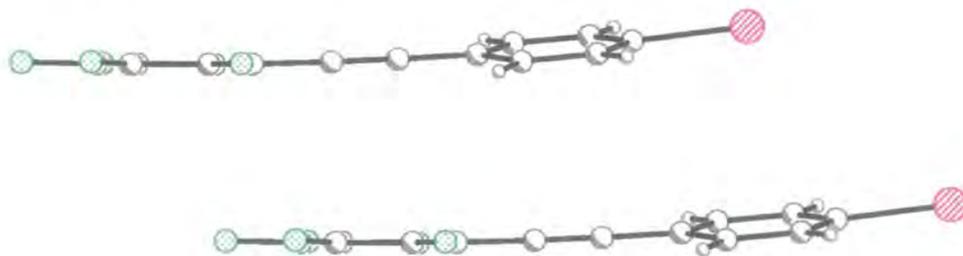
Figure 5.8: Stacking diagram of (5a), viewed side on down the plane of the perfluorophenyl ring.

This packing motif leads to separate columns at almost perpendicular to each other. There is a short F⋯F contacts (2.859(5) Å at 148.4(3)°) between these columns.
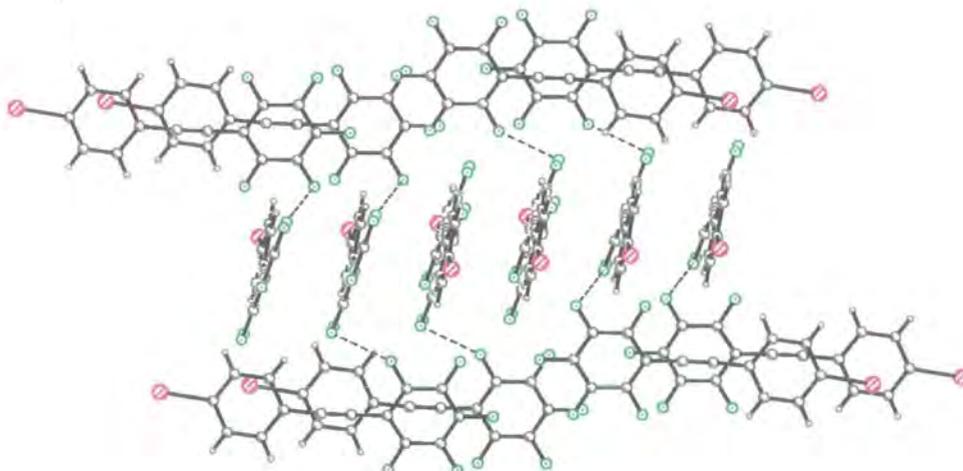
Figure 5.9: Packing diagram of (5a) showing the almost perpendicular columns of molecules. The short F⋯F interaction is visible between the columns.

The columns align themselves so that the perfluorophenyl rings of adjacent columns are adjacent to each other in a 'head-to-head' arrangement.
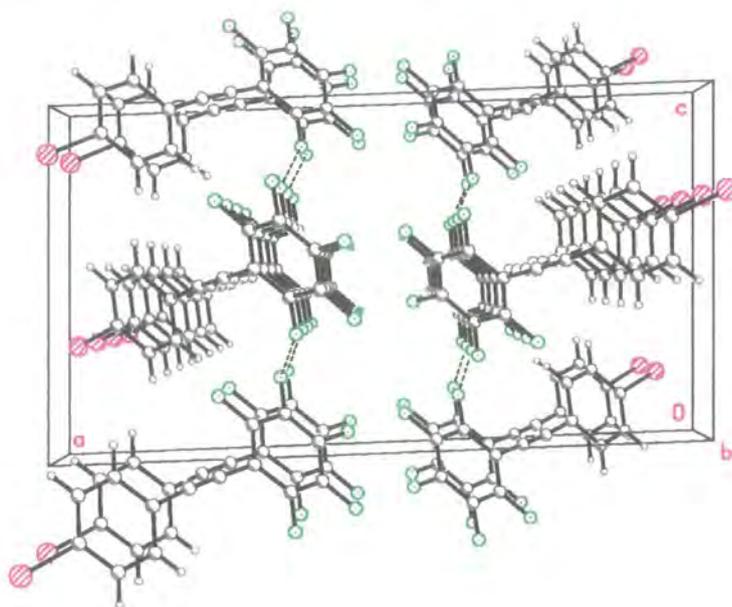
Figure 5.10: Diagram to show the packing of (5a), viewed down the crystallographic *b* axis.

These columns alternate in orientation so that they are almost perpendicular to each other when viewed down the *c* axis.
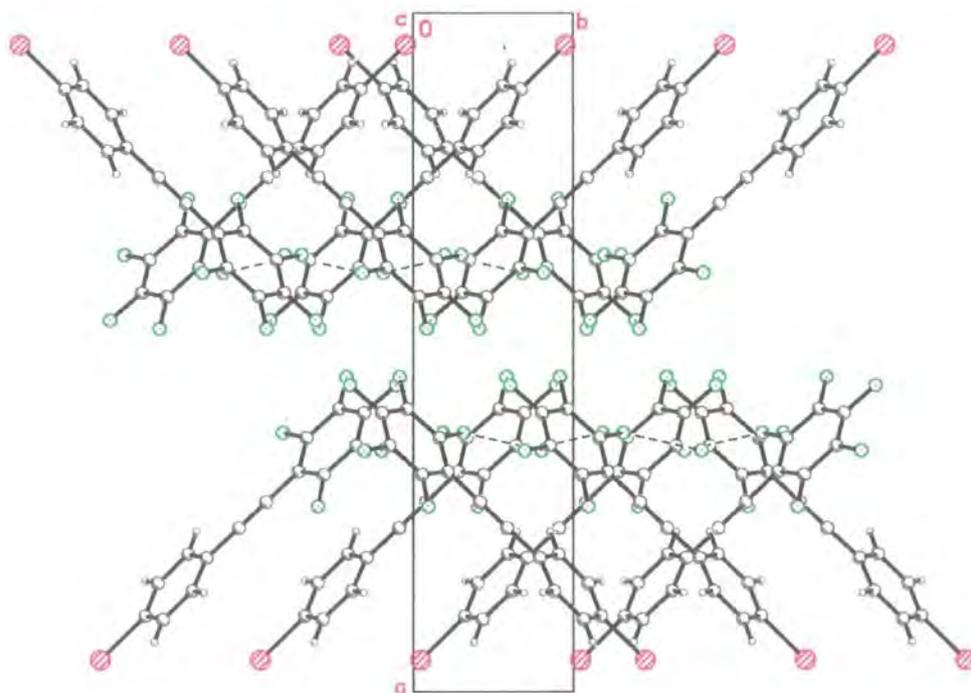
Figure 5.11: Diagram to show the packing of (5a), viewed down the crystallographic *c* axis.

There are very short I···I type II contacts (3.744(2) Å with C-I···I angles of 167.4° and 95.6°) where the iodine ends of the molecules are adjacent. The 'chain' of I···I contacts perpetuates along the crystallographic b axis (vector [0 1 0]). The packing coefficient, K, is quite large at 0.718.
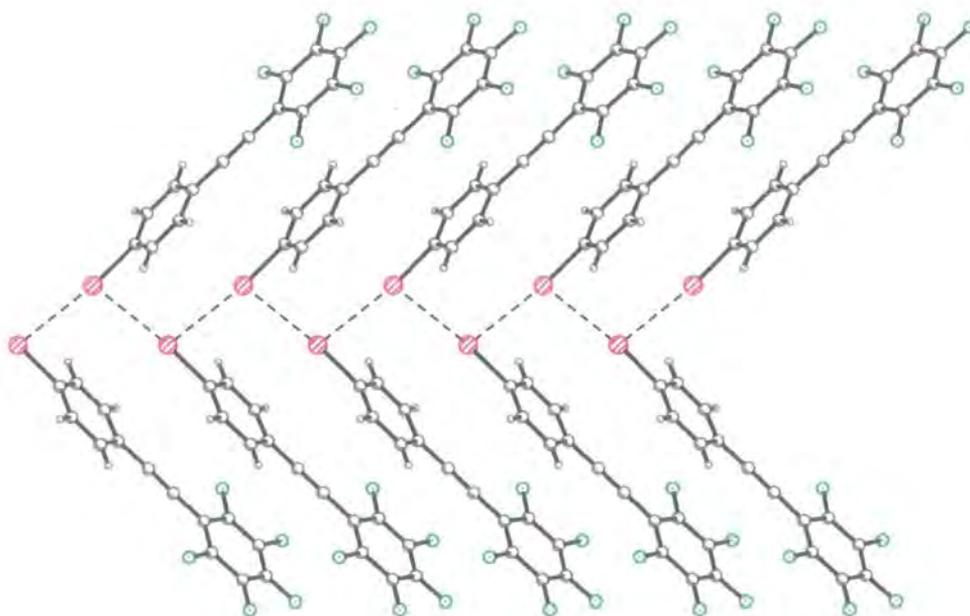
Figure 5.12: Diagram to show the short I···I contacts in the packing of (5a), viewed down the crystallographic c axis.

The structure of compound (5b) (1-bromo-4-(pentafluorophenylethynyl)benzene) proved almost isostructural to (5a). The C≡C triple bond distance (1.203(4) Å) and C-C single bond distances (1.432(4) Å and 1.438(4) Å for the bonds adjacent to the perfluorophenyl and phenyl rings respectively) are not significantly different. The C-Br distance of 1.898(2) Å is shorter than the C-I bond distance in (5a), as expected due to the smaller size of the bromine atom. The deviation from planarity of (5b) (dihedral angle 15.7°) is greater than for (5a). The deviation from linearity is also greater with a distortion angle of 7.8°.
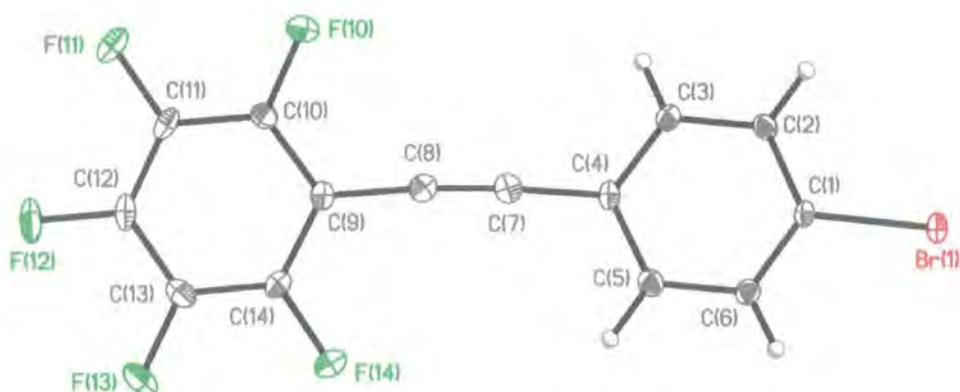
Figure 5.13: Ortep diagram for (5b), viewed perpendicular to the plane of the perfluorophenyl ring. Thermal ellipsoids are plotted to 50% probability level.

Again, there is no arene-perfluoroarene interaction in the crystal. The molecules stack on top of each other as in (5a), with the perfluorophenyl ring slipped so that the phenyl rings sit almost on top of the C≡C triple bond.
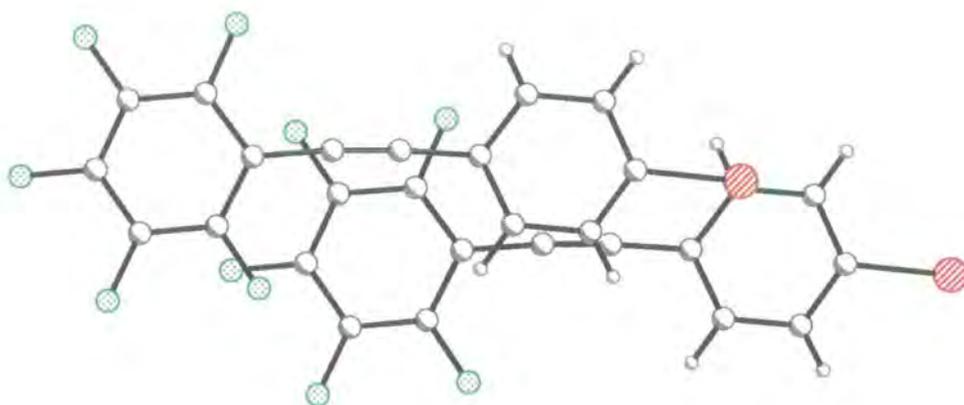
Figure 5.14: Stacking diagram of (5b), viewed perpendicular to the plane of the perfluorophenyl ring.

The molecules again stack in a parallel fashion. The molecules look less 'banana' shaped than (5a) when viewed side on due to the larger dihedral angle. The inter planar distance is very similar at 3.462 Å, with a comparably large inter centroid distance of 4.869 Å, indicating that the slip distance for both (5a) and (5b) are very similar.
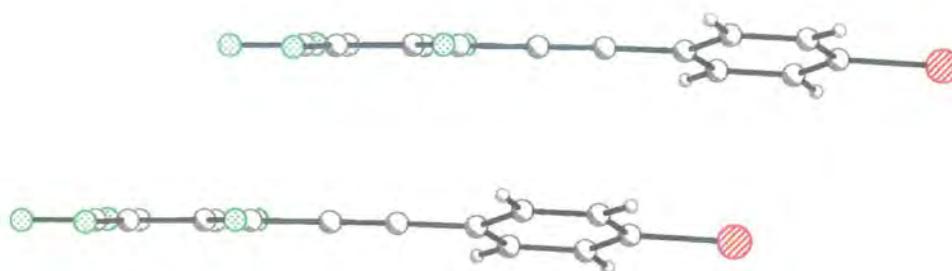
Figure 5.15: Stacking diagram of (5b), viewed side on down the plane of the perfluorophenyl ring.

This similar packing motif to **(5a)** is illustrated in Figure 5.16. Again, separate columns stack almost perpendicular to each other. There are two short F···F contacts (2.731(2) at 160.85(16)° and 2.569(3) Å at 168.79(16)°) and a short C-H···F contact (2.54(3) Å at 134°).
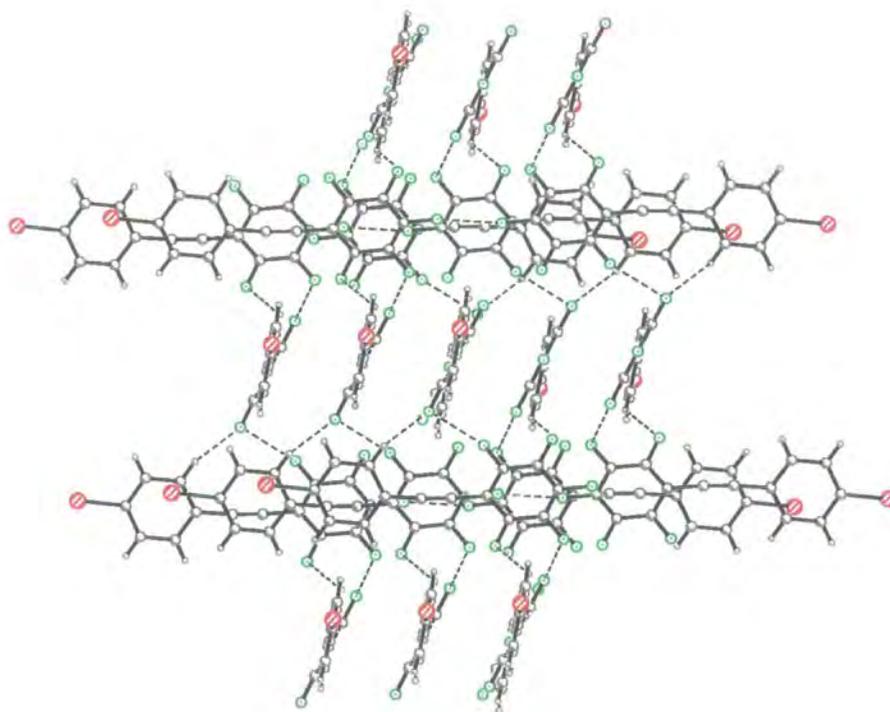
Figure 5.16: Packing diagram of (5b) showing the almost perpendicular columns of molecules. The short F···F and F···H interactions are just visible between the columns.

The short F···F and F···H contacts are illustrated better in Figure 5.17.
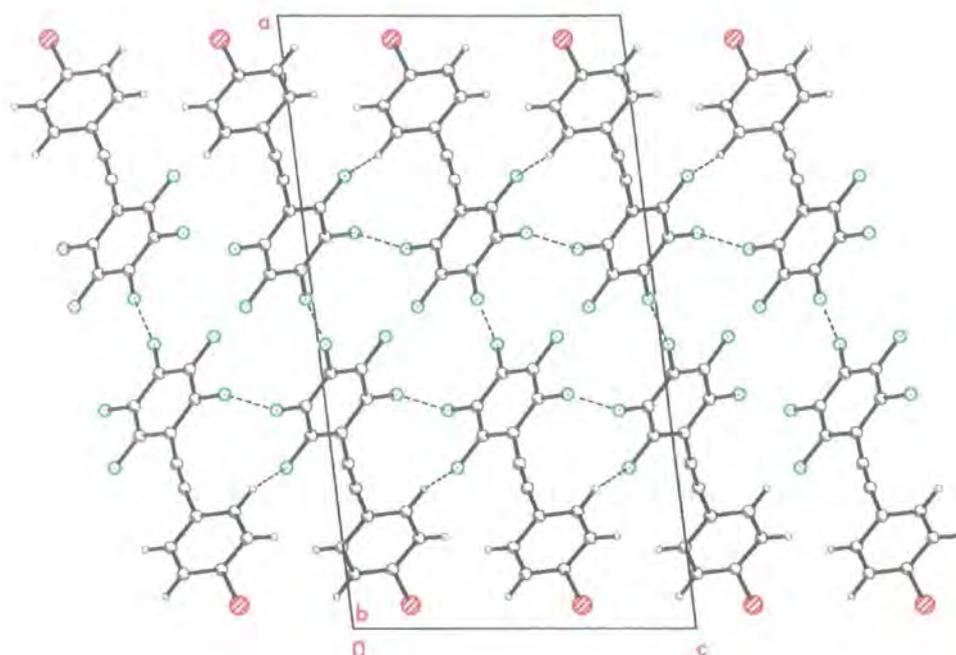
Figure 5.17: Diagram to show the packing of (5b), viewed down the crystallographic *b* axis. The stack is viewed with no perspective to give a clearer view of the short contacts.

The major short contact in the structure is again the halogen···halogen contact. The Br···Br type II contact distance is 3.5574(4) Å (with C-Br···Br angles of 163.7° and 85.5°). Again, these short contacts form a 'chain' parallel to the crystallographic *b* axis.
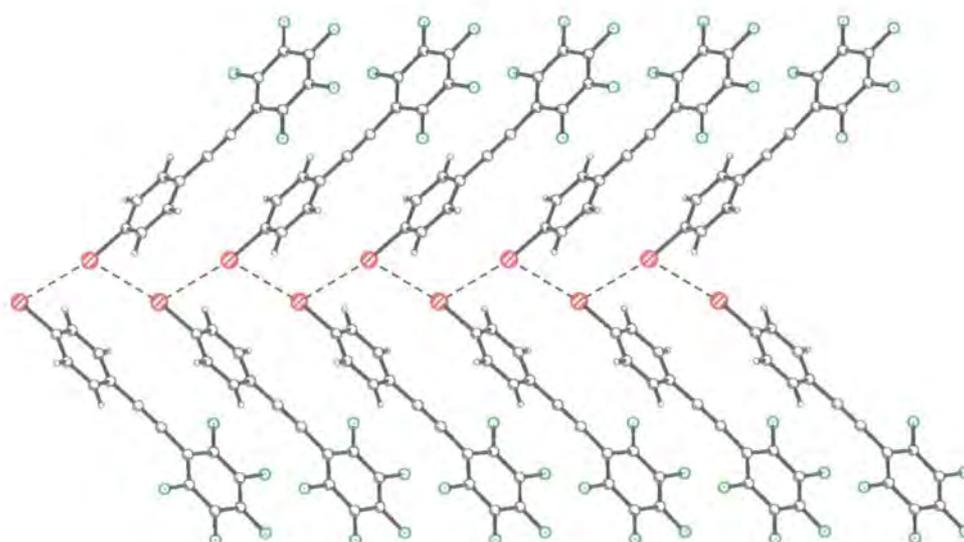
Figure 5.18: Diagram to show the short Br···Br contacts in the packing of (5b), viewed down the crystallographic *c* axis.

The packing coefficient of (**5b**), at 0.728, is slightly larger than that for (**5a**).

The chloro analogue of these structures, PhF_5-CC-Ph-Cl (**5c**) (1-chloro-4-(pentafluorophenylethynyl)benzene) has similar molecular geometry to the bromo and iodo analogues discussed above. The C≡C triple bond distance (1.195(2) Å) and C-C single bond distances (1.422(2) Å and 1.433(2) Å for the bonds adjacent to the perfluorophenyl and phenyl rings respectively) are not significantly different to those for (**5a**) or (**5b**). The C-Cl distance of 1.737(1) Å is shorter than either the C-I bond distance in (**5a**) or the C-Br bond distance in (**5b**), as expected due to the smaller size of the chlorine atom. The first difference in the structure of (**5c**) when compared to (**5a**) and (**5b**) is in the planarity and linearity measurements. The dihedral angle for (**5c**) is only 3.4°, which is very close to planar. The distortion angle is only 3.5°, making this the most linear arrangement in this series.
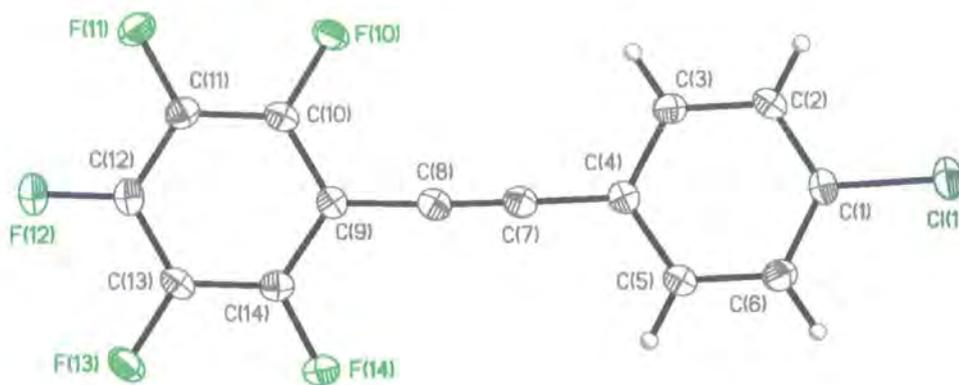
Figure 5.19: Ortep diagram for (5c), viewed perpendicular to the plane of the perfluorophenyl ring. Thermal ellipsoids are plotted to 50% probability level.

The stacking diagram for this structure reveals the major difference from (**5a**) and (**5b**). The molecules line up in a 'head-to-tail' fashion with the phenyl and perfluorophenyl rings stacking alternately. There is a slip distance of approximately one C-C bond distance. This has been commonly seen in the arene-perfluoroarene co-crystals such as

those in Chapter 4. It would seem that (5c), unlike (5a) and (5b), does exhibit an arene-perfluoroarene stacking motif in the structure.
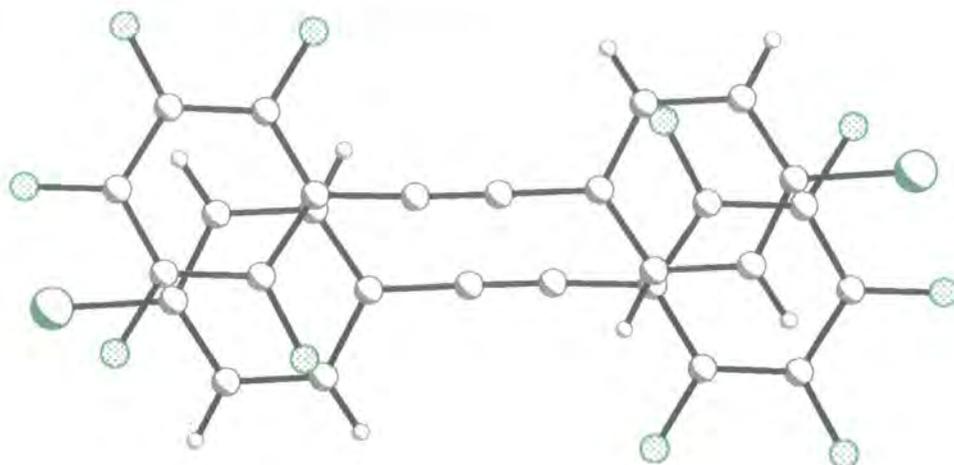
Figure 5.20: Stacking diagram of (5c), viewed perpendicular to the plane of the perfluorophenyl ring.

The molecules again stack almost parallel to each other. The inter-planar distances are almost identical above and below one molecule, at 3.402 Å and 3.395 Å. The inter centroid distances are quite similar to these values (3.761 Å and 3.728 Å), as would be expected for such packing.
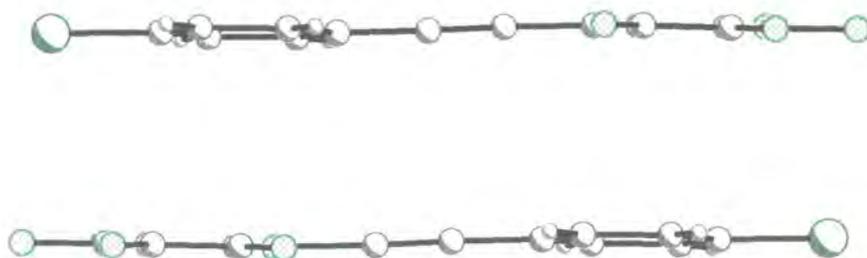
Figure 5.21: Stacking diagram of (5c), viewed side on down the plane of the perfluorophenyl ring.

There are no Cl···Cl contacts less than the sum of the van der Waals radii (3.5 Å). There is, however, a short Cl···F contact (3.212(1) Å) and two short F···F contacts (2.878(1) Å and 2.906(1) Å. These short contacts are illustrated in Figure 5.22.
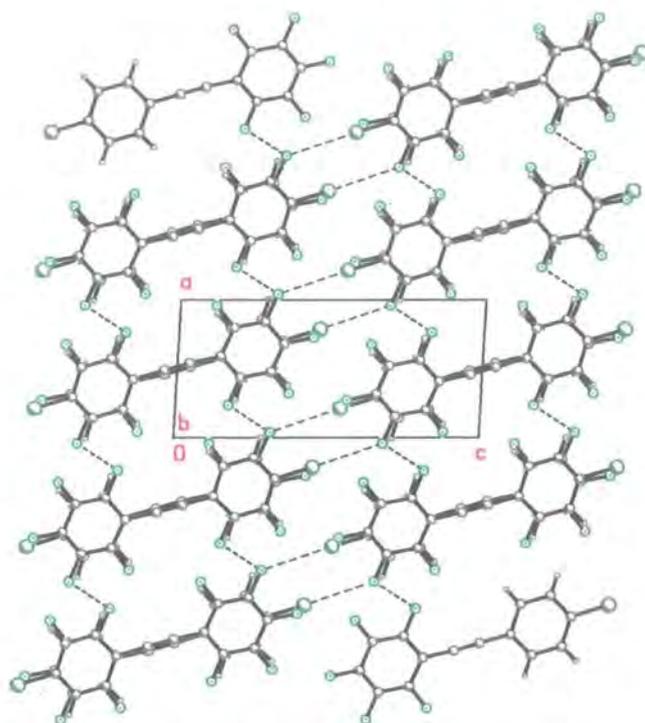
Figure 5.22: Diagram to show the packing of (5c), viewed down the crystallographic *b* axis. The stack is viewed with no perspective to give a clearer view of the short contacts.

An interesting comparison to this series of structures is that of compound Ph-CC-PhF$_4$-I

(5d) (1-iodo-4-(phenylethynyl)tetrafluorobenzene). This is an iodofluorotolan like **(5a)**,

with the exception that the halogen atom is on the fluorinated ring. The C≡C triple bond

distance (1.175(4) Å) and C-C single bond distances (1.438(4) Å and 1.447(4) Å for the

bonds adjacent to the perfluorophenyl and phenyl rings respectively) are not much

different to the other structures presented in this section. The C-I bond distance of

1.2.082(3) Å is the same as that observed in the other iodine containing system **(5a)**.

The deviation from planarity for **(5d)** is greater than for **(5a)**. The dihedral angle is

13.1°. The deviation from linearity, however, is less than in **(5a)**, with the smallest

distortion angle so far in this chapter of 1.1°.
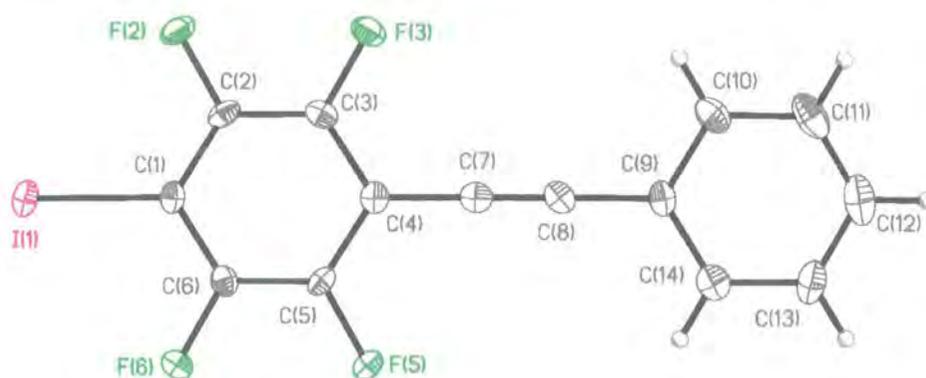
Figure 5.23: Ortep diagram for (5d), viewed perpendicular to the plane of the perfluorophenyl ring. Thermal ellipsoids are plotted to 50% probability level.

The packing structure is also similar to **(5a)** and **(5b)** in that there is no arene-perfluoroarene influence in the crystal structure. The molecules stack on top of each other in the same fashion as for **(5a)** and **(5b)**, with the perfluorophenyl ring slipped so that the phenyl rings sit almost aligned into the C≡C triple bond.
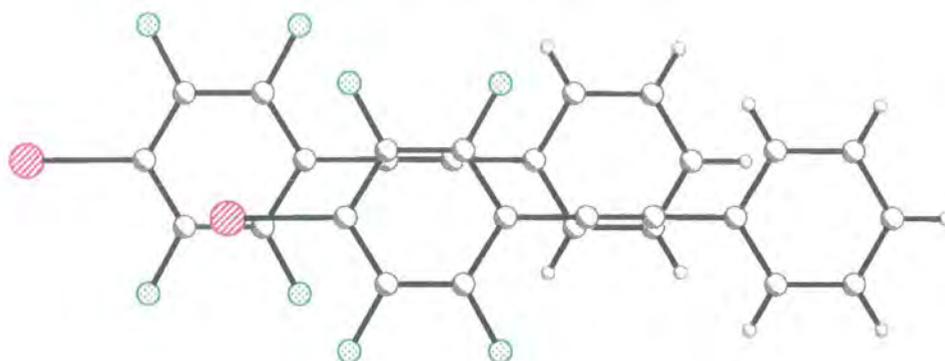
Figure 5.24: Stacking diagram of (5d), viewed perpendicular to the plane of the perfluorophenyl ring.

The molecules stack in a parallel fashion. The inter planar distance is 3.134 Å, with a large inter centroid distance of 5.794 Å reflecting the large displacement from an eclipsing stack motif.
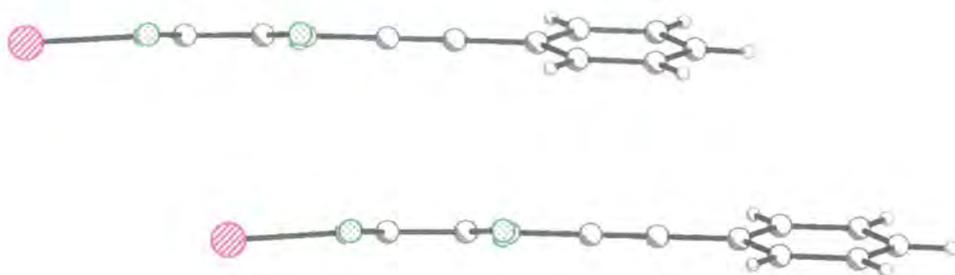
Figure 5.25: Stacking diagram of (5d), viewed side on down the plane of the perfluorophenyl ring.

Like (5a) and (5b), separate columns stack almost perpendicular to each other. There is only one short F⋯F contact (2.887(3) Å).
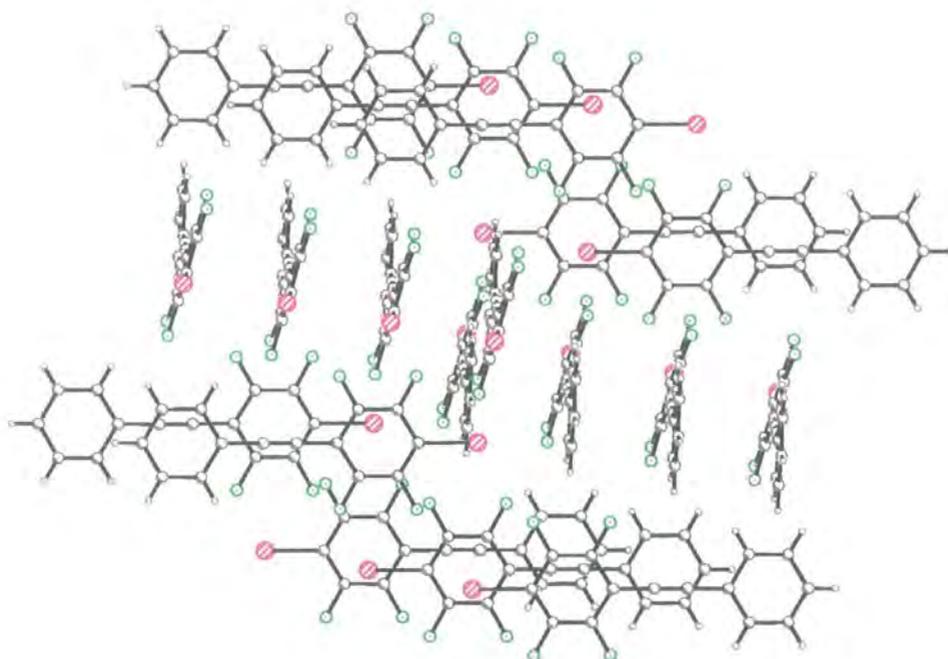
Figure 5.26: Packing diagram of (5d) showing the almost perpendicular columns of molecules

This illustration, however, does not obviously show the main difference between structures (5a) and (5d). In (5a), the columns all line up 'head-to-head', but in (5d)they line up 'head-to-tail'. This is best illustrated in Figure 5.27.

(a)   (b)
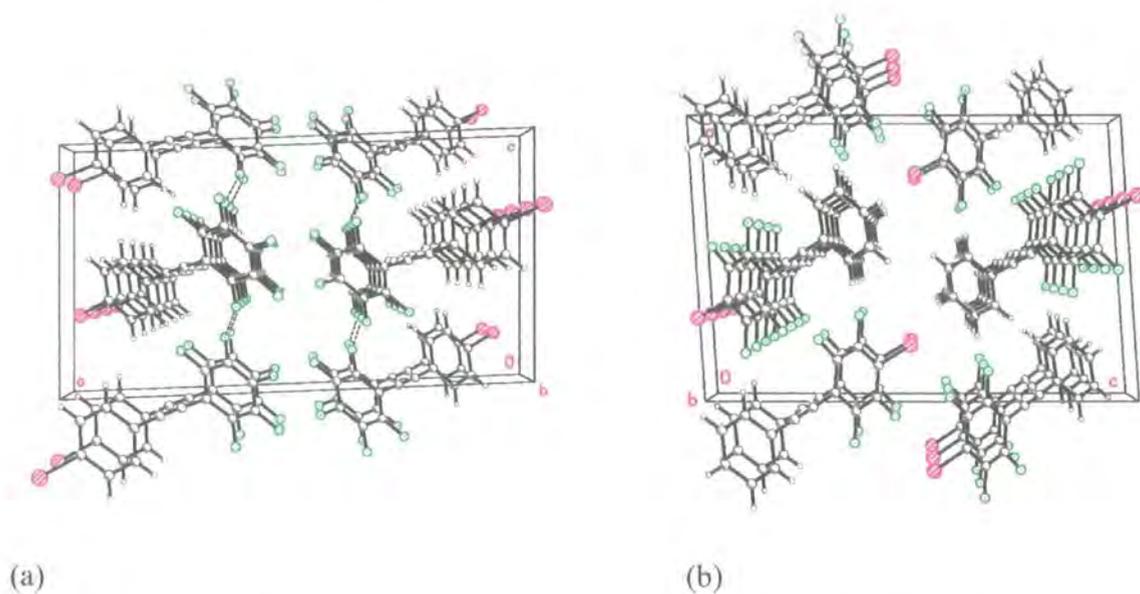
Figure 5.27: Packing diagrams of (5a) (a) and (5d) (b) viewed down the *b* axis.

Other than this, the effect of altering the position of the iodine atom, in this case from one ring to the other, is small. No arene-perfluoroarene interactions are observed, and the packing and overlap diagrams look very similar.

5.4 Related structural studies

The structure of Ph-CC-PhF$_4$-CC-Si(CH$_3$)$_3$ (**5e**) was solved at 110 K and 293 K. Both structures were the same, except for smaller cell parameters at lower temperatures due to both normal contraction and possibly reduced thermal motion at lower temperatures. Only the lower temperature structure will be discussed here. The compound crystallised in monoclinic space group *C2/c* with cell parameters a = 25.2621(9) Å, b = 10.8402(3) Å, c = 13.7269(5) Å, β = 112.203(1)°. The C≡C triple bond lengths are as expected and are very similar (1.204(2) Å near to the TMS group, and 1.192(2) Å between the two phenyl rings), as are the C-C single bond lengths which range from 1.429(2) Å to 1.436(2) Å. The C-Si bond length is 1.857(2) Å.
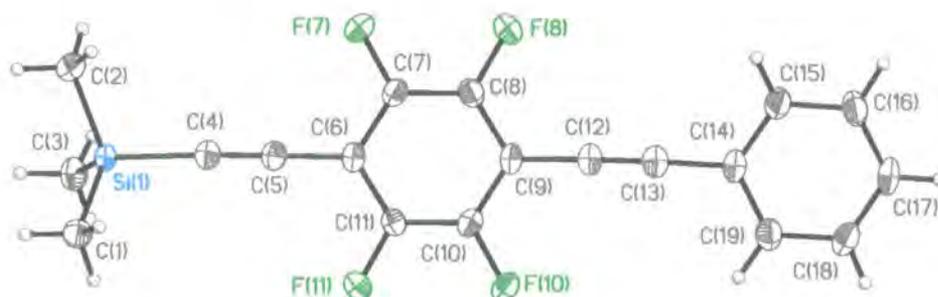
Figure 5.28: Ortep diagram for (5e), with thermal ellipsoids plotted at 50% probability level.

The molecule is almost planar, with a dihedral angle of just 3.73(8)°. Packing seems to be dominated by the need to accommodate the bulky trimethylsilyl groups, with no evidence of arene-perfluoroarene interactions playing any part. When viewed perpendicular to the fluorinated ring, the molecules can be seen to project at right angles to each other, aligned with the fluorinated rings on top of each other, keeping the TMS groups apart.
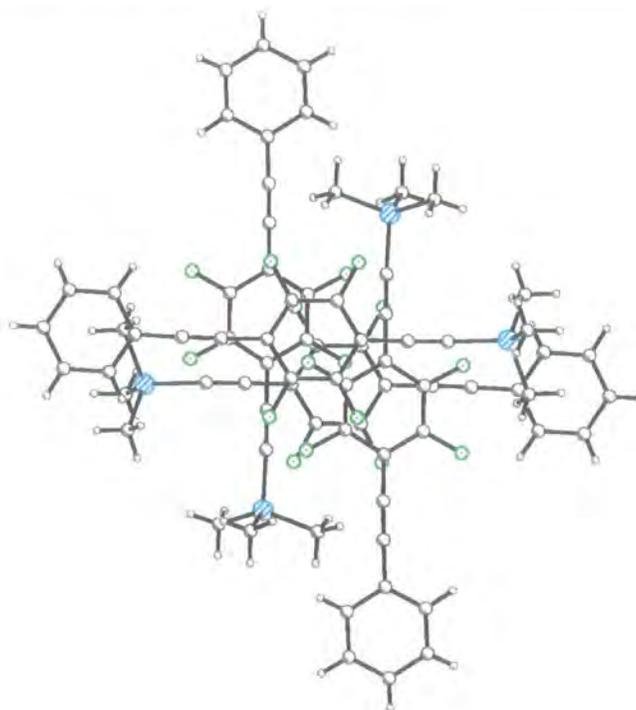
Figure 5.29: Stacking diagram for (5e), viewed perpendicular to the mean plane of the fluorinated ring.

When this stacking motif is viewed down the axis of the middle two molecules, the method adopted to keep the trimethylsilyl moieties apart, with adjacent molecules rotated either 90° or 180° from the nearest neighbours, can clearly be seen.
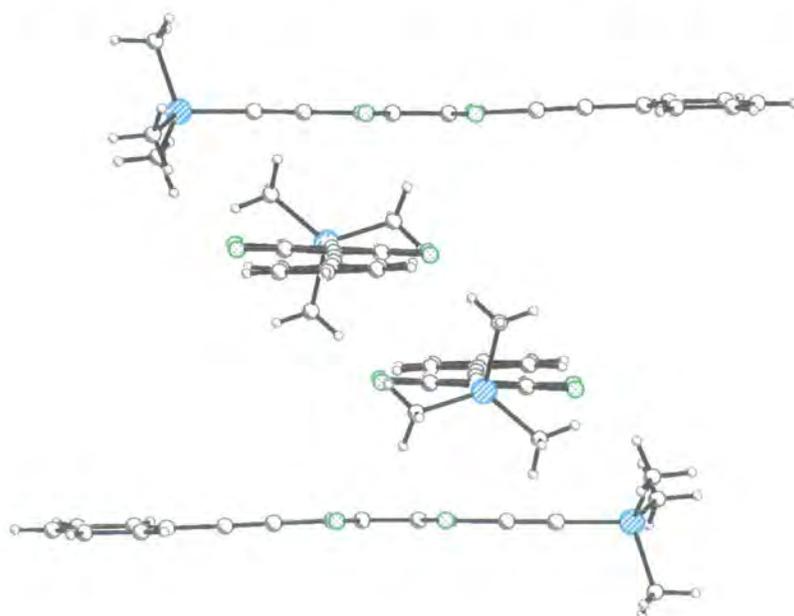
Figure 5.30: Stacking diagram for (5e), viewed down the axis of the central two molecules.

The molecules form parallel stacks running down the c axis.
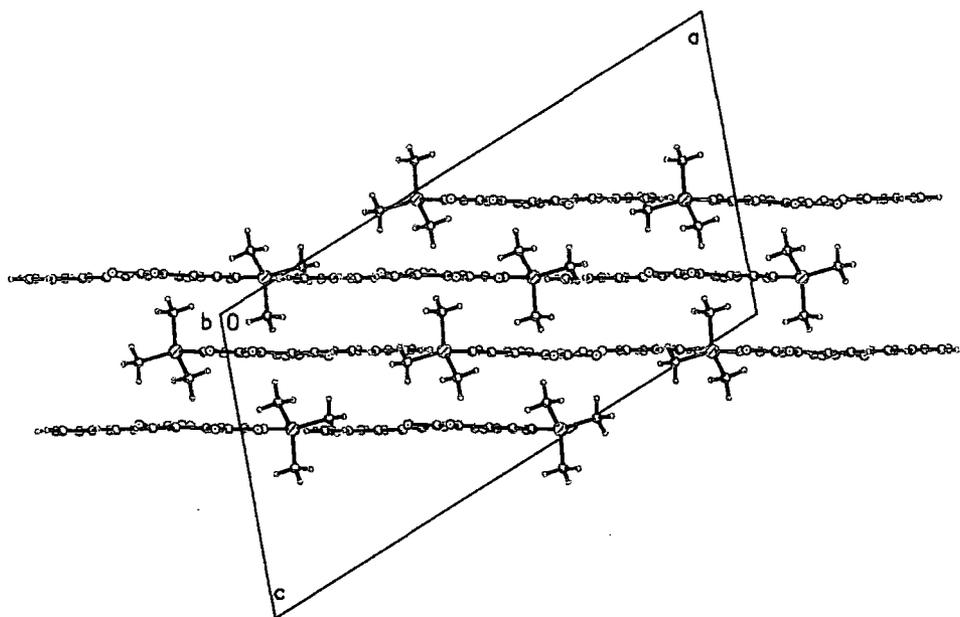
Figure 5.31: Packing diagram for (5e), viewed down the c axis.

Attempts were made to solve the structure of the related compound PhF_5-CC-Ph-CC-$Si(CH_3)_3$. Unfortunately, no diffraction-quality crystals were found in two samples attempted, despite examining many crystals. Under the microscope, the general morphology of the crystals was curved needles, which unsurprisingly would not diffract well when tested on the diffractometer. No other samples were provided, so the experiment was aborted.

5.5 Conclusion

The crystal structures of the series of halogenated tolans of the form Ph-CC-PhF_4-X (X = I, Br, Cl) have been presented. They were analysed for evidence of arene-perfluoroarene interactions and other interesting features in the molecular geometry or packing. The structure of Ph-CC-PhF_4-I and Ph-CC-PhF_4-Br were very similar, consisting of stacks of parallel molecules arranged in layers. There was no evidence of

the arene-perfluoroarene interaction. There were short halogen$\cdots$halogen contacts. In contrast, the structure of Ph-CC-PhF$_4$-Cl shows clear evidence of the interaction, with adjacent molecules stacked in an alternating 'head-to-tail' arrangement. There are no short chlorine$\cdots$chlorine interactions. Thus it can be concluded that the halogen$\cdots$halogen interactions in the bromo and iodo structures are the major influence in determining the packing of the molecules, whereas in the chloro analogue the lack of any short halogen$\cdots$halogen interactions paves the way for the domination of the arene-perfluoroarene interaction in determining the packing. It would seem that arene-perfluoroarene interactions only persist in structures where there are no stronger interactions to prevent them. It could be hypothesised from this evidence that the order of strength of intermolecular interactions observed in this study are I$\cdots$I > Br$\cdots$Br > arene-perfluoroarene > Cl$\cdots$Cl. It could be expected that the structure containing a *para*-substituted fluorine atom would also exhibit arene-perfluoroarene interactions in an analogous way to the chlorine structure.

The crystal structure of Ph-CC-PhF$_4$-I is not so simple to rationalise in this way. The task is also hampered by the absence of the structures of the other halogen analogues. There are neither arene-perfluoroarene interactions nor any short I$\cdots$I contacts observed in the crystal to help explain the orientation of the molecules in the crystal. Evidently, the analogous bromine- and chlorine-containing structures need to be solved to identify any trends in this series.

The structure of Ph-CC-PhF$_4$-CC-TMS shows no short contacts or evidence of the arene-perfluoroarene interaction. It seems that the structure is dominated by the need to accommodate the bulky trimethylsilyl groups.

Chapter 6: References

1 Glusker, J. P., Lewis, M., Rossi, M., "Crystal Structure Analysis for Chemists and Biologists", VCH Publishers, 1994.

2 References used indirectly to help in writing this chapter: (a) Bilton, C., Ph. D. Thesis, University of Durham, UK, (1999), (b) Smith, P. S., 1st year Ph. D. report, University of Durham, UK, (2001), (c) Course notes from BCA School, *Seventh Intensive Course in X-ray Structural Analysis*, attended April 1999, University of Durham.

3 Röntgen, W. C., (1895). *Sitzungsberichte der Wurzburger Physikalischen-Medizinischen Gesellschaft*, 131. English translation: Stanton, A., *Science*, 1896, **3**, 227.

4 Figure taken from http://www.za.iucr.org/craig/diagrams, drawn by Brian Craig Taverner, with thanks.

5 Picture taken, with thanks, from http://www-structure.llnl.gov/xray/101index.html: X-ray 101 - An Interactive Web Tutorial by Bernhard Rupp.

6 Oxford HeliX. Oxford Cryosystems Ltd, Oxford, U.K.

7 SMART-1000 CCD, Bruker AXS, Madison, Wisconsin, U.S.A.

8 SAINTPLUS Version 6.02. Bruker AXS., Madison, Wisconsin, U.S.A.

9 (a) Sheldrick, G.M., (1997). SHELXS-97, SHELXL 97. Program for the Refinement of Crystal Structures. University of Göttingen, Germany. (b) Sheldrick, G. M., (1998). (c) SHELXTL Version 5.1. Bruker AXS., Madison, Wisconsin, U.S.A.

10 (a) Harker, D., Kasper, J. S., 1948, *Acta Crystallogr.*, **1**, 70; (b) Karle, J., Hauptmann, H., *Acta Crystallogr.*, 1950, **3**, 181; (c) Sayre, D., *Acta Crystallogr.*, 1952, **5**, 60.

11   Patterson, A. L., *Phys. Rev.*, 1934, **46**, 372.

12   (a) Legende, A. M., *Appendix. Sur le méthod des moindres quarrés.* In: *Nouvelles Méthodes pour la Détermination des Orbites des Comètes*, 72, Courcier, Paris; (b) Gauss, C. F., (1809). *Theoria Motus Corporum Caelestiun in Sectionibus Conicus Solum Ambientum*, Perthes et Besser: Hamburg. Both taken from *Crystal Structure Analysis for Chemists and Biologists*, 1994, Glusker, J. P., Lewis, M., Rossi, M., Wiley-VCH.

13   http://www.iucr.ac.uk/

14   Spek, A. L., *Acta Cryst.*, 1990, **A46**, C34. PLATON – A Multipurpose Crystallographic Tool, Utrecht University, Utrecht, The Netherlands. Version 290402.

15   Coapes, R. B., Souza, F. E. S., Fox, M. A., Batsanov, A. S., Goeta, A. E., Yufit, D. S., Leech, M. A., Howard, J. A. K., Scott, A. J., Clegg, W., Marder, T. B., *J. Chem. Soc., Dalton Trans.*, 2001, 1201.

16   Synthesis of $Cl_3B \cdot PH_3$ was reported in Besson, A., *Compt. Rend.*, 1890, **160**, 516.

17   (a) Gamble, E. L., Gilmont, P., *J. Am. Chem. Soc.*, 1940, **62**, 717; (b) Phillips, G. M., Hunter, J. S., Sutton, L. E., *J. Chem. Soc. (London)*, 1945, 146.

18   Wagner, R. I., US Patent, 3,092,665, (1963),

19   Muylle, E., van der Kelen, G. P., Claeys, E. G., *Spectrochim. Acta*, 1976, **32A**, 1149.

20   Black, D. L., Taylor, R. C., *Acta Crystallogr.* 1975, **B31**, 1116.

21   Aubauer, C., Davidge, K., Klapötke, T. M., Mayer, P., Piotrowski, H., Schulz, A., *Z. Anorg. Allg. Chem.*, 2000, **626**, 2373.

22   Weller, F., Mohlen, M., Dehnicke, K., *Z. Kristallogr. – New Crystal Structures*, 1997, **212**, 159.

23   Carboni, B., Monnier, L., *Tetrahedron*, 1999, **55**, 1197.

24   Dorn, H., Singh, R. A., Massey, J. A., Lough, A. J., Manners, I., *Angew. Chem., Int. Ed. Engl.*, 1999, **38**, 3321.

25   Dorn, H. Singh, R. A., Massey, J. A., Nelson, J. M., Jaska, C. A., Lough, A. J., Manners, I., *J. Am. Chem. Soc.*, 2000, **122**, 6669.

26   Dorn, H., Jaska, C. A., Singh, R. A., Lough, A. J., Manners, I., *Chem. Commun.*, 2000, 1041.

27   Evans, C. E. B., Lough, A. J., Grondey, H., Manners, I., *New J. Chem.*, 2000, **24**, 447.

28   Starzewski, K. A. O., Kelly, W. M., Stumpf, A., Freitag, D., *Angew. Chem., Int. Ed. Engl.*, 1999, **38**, 2439.

29   Jäkle, F., Mattner, M., Priermeier, T., Wagner, M., *J. Organomet. Chem.*, 1995, **502**, 123.

30   Herdtweck, E., Jäkle, F., Wagner, M., *Organometallics*, 1997, **16**, 4737.

31   Stelck, D. S., Shapiro, P. J., Basickes, N., *Organometallics*, 1997, **16**, 4546.

32   For examples, see (a) Haubold, W., Keller, W., Sawitzki, G., *Angew. Chem., Int. Ed. Engl.*, 1988, **27**, 925; (b) Keller, W., Sawitzki, G., Haubold, W., *Inorg. Chem.*, 2000, **39**, 1282.

33   Holub, J., Jelínek, T., Hnyk, D, Plzák, Z., Císařová, Bakardjiev, M., Stíbr, B., *Chem. Eur. J.*, 2001, **7**, 1546.

34   Marder, T. B., Norman, N. C., *Topics in Catalysis*, 1998, **5**, 63.

35   Einertshöfer, Ph. D. Thesis, Ludwig Maximilians Universität, München, (1992).

36   Coapes, R. B., Souza, F. E. S., Fox, M. A., Batsanov, A. S., Goeta, A. E., Yufit, D. S., Leech, M. A., Howard, J. A. K., Scott, A. J., Clegg, W., Marder, T. B., *J. Chem. Soc., Dalton Trans.*, 2001, 1201.

37   Clegg, W., Dai, C., Lawlor, F., Marder, T. B., Nguyen, P., Norman, N. C., Picket, N. L., Power, W. P., Scott, A. J., *J. Chem. Soc, Dalton Trans.*, 1997, 839.

38   For examples, see (a) Schulz, S., Nieger, M., *J. Chem. Soc., Dalton Trans.*, 2000, 639; (b) Schulz, S., Kuczkowski, A., Nieger, M., *J. Organomet. Chem.*, 2000, **604**, 202.

39   Timoshkin, A. Y., Suvorov, A. V., Bettinger, H. F., Schaefer III, H. F., *J. Am. Chem. Soc.*, 1999, **121**, 5687.

40   Lube, M. S., Wells, R. L., White, P. S., *Inorg. Chem.*, 1996, **35**, 5007.

41   Emsley, J., *"The Elements"*, 2nd Edition, 1991, Clarendon Press, Oxford, p35.

42   (a) Gryff-Keller, A., *Bull. Polish Acad. Sci. – Chem.*, 1998, **46**, 105; (b) Werbelow, L., *J. Magn. Reson.*, 1986, **67**, 66.

43   Packer, K. J., Muetterties, E. L., *J. Am. Chem. Soc.*, 1963, **85**, 3035.

44   Personal communication with A. Kenwright and G. Saunders.

45   Penner, G. H., Wasylishen, R. E., *Can. J. Chem.*, 1989, **67**, 1909.

46   Cotton, F. A., Wilkinson, G., *"Advanced Inorganic Chemistry"*, Wiley-Interscience, New York, 5th Edn., 1988, p. 173.

47   Nöth, H., Wrackmeyer, B., *"Nuclear Magnetic Resonance Spectroscopy of Boron Compounds"*, NMR Series, v.14, Springer-Verlag, New York, (1978).

48   Tolman, C. A., *Chem. Rev.*, 1977, **77**, 313.

49   Orpen, A. G., Brammer, L., Allen, F. H., Kennard, O., Watson, D. G., Taylor, R., *J. Chem. Soc., Dalton Trans.*, 1989, S1.

50   Crystal structure originally appeared Souza, F. S., M. Sc. Thesis, University of Waterloo, Canada, (1997).

51   Weller, F., Mohlen, M., Dehnicke, K., *Z. Kristallogr. – New Crystal Structures*, 1997, **212**, 159.

52   Unless otherwise stated, data taken from: Golovin, M. N., Rahman, Md. M., Belmonte, J. E., Giering, W. P., *Organometallics*, 1985, **4**, 1981.

53   Allman, T., Goel, R. G., *Can. J. Chem.*, 1982, **60**, 716.

54   Henderson, W. A., Streuli, C. A., *J. Am. Chem. Soc.*, 1960, **82**, 5791.

55   pK_a values obtained from Tolman, C. A., *Chem. Rev.*, 1977, **77**, 313.

56   Binder, H. Matheis, W., Heckmann, G., Deiseroth H-J., Fu-Son, H., *Z. Naturforsch.*, 1985, **40B**, 94 and references therein.

57   Schmidbaur, H., Brachthauser, B., Steigelmann O., Beruda, H., *Chem. Ber.*, 1992, **125**, 2705.

58   Greenwood N. N., Earnshaw, A., *Chemistry of the Elements*, Pergamon Press, Oxford, 1997, 2nd Edition, Ch. 6, p. 205 or F. A. Cotton, G. Wilkinson, C. A. Murillo and M. Bochmann, *Advanced Inorganic Chemistry*, Wiley-Interscience, New York, 1999, 6th Edition, Ch. 5, p. 171. See also Pachaly, B. and West, R., *J. Am. Chem. Soc.,* 1985, **107**, 2987 and Ito, M., Tokitoh, N. and Okazaki, R., *Tetrahedron Lett.* 1997, **38**, 4451.

59   Oliver J. P., Kumar, R., *Polyhedron*, 1990, **9**, 409 and references therein. For an exception to this, see Saied, O., Simard, M. and Wuest, J. D., *Organometallics*, 1996, **15**, 2345.

60   (a) Belcher, W. J., Breede, M., Brothers P. J., Rickard, C. E. F., *Angew. Chem., Int. Ed. Engl.*, 1998, **37**, 1112. (b) Bormann, H., Simon A., Vahrenkamp, H., *Angew. Chem., Int. Ed. Engl.*, 1989, **28**, 180. (c) Hanecker, E., Nöth H.,

Wietelmann, U., *Chem. Ber.*, 1986, **119**, 1904. (d) Vorontsova, L. G., Chizhov, O. S., Vasilev, L. S., Veselovskii V. V., Mikhailov, B. M., *Isv. Akad. Nauk. SSSR, Ser. Khim.*, 1981, 353.

61   Belcher, W. J., Breede, M., Brothers P. J., Rickard, C. E. F., *Angew. Chem., Int. Ed. Engl.*, 1998, **37**, 1112.

62   Bormann, H., Simon A., Vahrenkamp, H., *Angew. Chem., Int. Ed. Engl.*, 1989, **28**, 180.

63   Vorontsova, L. G., Chizhov, O. S., Vasilev, L. S., Veselovskii V. V., Mikhailov, B. M., *Isv. Akad. Nauk. SSSR, Ser. Khim.*, 1981, 353.

64   Hanecker, E., Nöth H., Wietelmann, U., *Chem. Ber.*, 1986, **119**, 1904.

65   Sutton, L. R., Blake, A. J., Cooke P. A., Schröder, M., *Chem. Commun.*, 2000, 563.

66   Williams, V. C., Irvine, G. J., Piers, W. E., Li, Z., Collins, S., Clegg, W., Elsegood, M. R. J., Marder, T. B., *Organometallics*, 2000, **19**, 1619.

67   *Ab initio* calculations performed by M. A. Fox, Extended Hückel calculations by A. K. Hughes.

68   (a) EHMO calculations were performed with EH and CACAO; Mealli C., Proserpio, D. M., *J. Chem. Educ.*, 1990, **67**, 399. (b) Hoffmann, R., Lipscomb, W. N. *J. Chem. Phys.*, 1962, **36**, 2179; Hoffmann, R., *J. Chem. Phys.*, 1963, **39**, 1397.

69   Taken from: Burke, J. M., Fox, M. A., Goeta, A. E., Hughes, A. K., Marder, T. B., *Chem. Commun.*, 2000, 2217.

70   *Ab initio* calculations were performed with the GAUSSIAN94 package; GAUSSIAN94, Revision E.2, Frisch, M. J., Trucks, G. W., Schlegel, H. B., Gill, P. M. W., Johnson, B. G., Robb, M. A., Cheeseman, J. R., Keith, T., Petersson,

G. A., Montgomery, J. A., Raghavachari, K., Al-Laham, M. A., Zakrzewski, V. G., Ortiz, J. V., Foresman, J. B., Cioslowski, J., Stefanov, B. B., Nanayakkara, A., Challacombe, M., Peng, C. Y., Ayala, P. Y., Chen, W., Wong, M. W., Andres, J. L., Replogle, E. S., Gomperts, R., Martin, R. L., Fox, D. J., Binkley, J. S., Defrees, D. J., Baker, J., Stewart, J. P., Head-Gordon, M., Gonzalez C., Pople, J. A., Gaussian, Inc., Pittsburgh, PA, 1995.

71   Batsanov, A., Burke, J. M., Clegg, W., Howard, J. A. K., Marder, T. B., Souza, F. S., Wilson, C., Manuscript in preparation.

72   Cameron, T. S., Dahlèn, B., *J. Chem. Soc., Perkin II,* 1975, 1737.

73   Allen, F. H., Davies, J. E., Galloy, J. J., Johnson, O., Kennard, O., Macrae, C. F., Mitchell, E. M., Mitchell, G. F., Smith, J. M., Watson, D. G., *J. Chem. Inf. Comp. Sci.,* 1991, **2**, 187.

74   Hasselgren, C., Dean, P. A. W., Scudder, M. L., Craig, D. C., Dance, I. G., *J. Chem. Soc., Dalton Trans.,* 1997, 2019.

75   Majeste, R. J., Chriss, D., Trefonas, L. M., *Inorg. Chem.,* 1977, **16**, 188.

76   Pangborn, A. B., Giardello, M. A., Grubbs, R. H., Rosen, R. K., Timers, F. J., *Organometallics,* 1996, **15**, 1518.

77   See reference 8.

78   Stone, F. G. A., *Chem. Rev.,* 1958, **58**, 101.

79   Topel, K., Hensen, K., Bats, J. W., *Acta Crystallogr.* 1981, **C40**, 828.

80   Topel, K., Hensen, K., Tromel, M., *Acta Crystallogr.* 1981, **B37**, 969.

81   Iijima, K., Oonishi, I., Shibata, S., *Chem. Lett.,* 1983, 251.

82   (a) Barber, M., Connor, J. A., Guest, M. F., Hillier, I. H., Schwarz, M., Stacey, M., *J. Chem. Soc., Faraday Trans. 2,* 1973, **69**, 551; (b) Hillier, I. H., Vincent,

M. A., Connor, J. A., Guest, M. F., MacDowell, A. A., von Niessen, W., *J. Chem. Soc., Faraday Trans. 2*, 1988, **84**, 409.

83   Haw, J. F., Zhang, J., Shimizu, K., Venktramen, T. N., Luigi, D-P, Song, W., Barich, D. H., Nicholas, J. B., *J. Am. Chem. Soc.*, 2000, **122**, 12561.

84   Powell, P., Nöth, H., *Chem. Commun.*, 1966, 637.

85   Irvine, G. J., Lesley, M. J. G., Marder, T. B., Norman, N. C., Rice, C. R., Robins, E. G., Roper, W. R., Whittell, G. R., Wright, L. J., *Chem. Rev.*, 1998, **98**, 2685.

86   Beilstein Commander 2000, Version 5.0. 1995-2000 MDL Information Systems GmbH.

87   Vasil'ev, A. N., Mushkalo, L. K., *J. Gen. Chem. USSR (Engl. Transl.)*, 1993, **62**, 1718.

88   Lesley, M. J. G., Woodward, A., Taylor, N. J., Marder, T. B., *Chem. Mater.*, 1998, **10**, 1355.

89   Nguyen, P., Dai, C., Taylor, N. J., Power, W. P., Marder, T. B., Pickett, N. L., Norman, N. C., *Inorg. Chem.*, 1995, **34**, 4290.

90   Clegg, W., Dai, C., Lawlor, F. J., Marder, T. B., Nguyen, P., Norman, N. C., Pickett, N. L., Power, W. P., Scott, A. J., *J. Chem. Soc., Dalton Trans.*, 1997, 839.

91   Clegg, W., Scott, A. J., Souza, F. E. S., Marder, T. B., *Acta Crystallogr.* 1999, **C55**, 1885.

92   Koster, R., Seidal, G., Lutz, F., Kruger, C., Kehr, G., Wrackmeyer, B., *Chem. Ber.*, 1994, **127**, 813.

93   Koster, R., Seidel, G., Boese, R., *Chem. Ber.*, 1994, **127**, 2159.

94   a) Malarski, Z., Majerz, I, Lis, T., *J. Mol. Struct.*, 1987, **158**, 369; b) Majerz, I, Malarski, Z., Lis, T., *J. Mol. Struct.*, 1990, **240**, 47.

95   Malarski, Z., Majerz I., Lis T., *J. Mol. Struct.*, 1996, **380**, 249.

96   Biradha K., Zaworotko, M. J, *J. Am. Chem. Soc.*, 1998, **120**, 6431.

97   Bacsa, J., Caira, R. M., Jacobs, A., Nassimbeni, L. R., Toda, F., *Crystal Engineering*, 2000, **3**, 251.

98   Jin, Z. M., Pan, Y. J., Xu, D. J., Xu, Y. Z., *Acta Crystallogr.*, 2000, **C56**, e59.

99   Biswas, S. G. *Indian J. Phys.*, 1961, **35**, 261.

100   Ohms, U., Guth, H., Treutman, W., Dannohl, H., Schweig, A., Heger, G., *J. Chem. Phys.*, 1985, **83**, 273.

101   Healy, P. C., Pakawatchai, C., Raston, C. L., Skelton, B. W., White, A. H., *J. Chem. Soc, Dalton Trans.*, 1983, 1905.

102   Engelhardt, L. M., Junk, P. C., Raston, C. L., Skelton, B. W., White, A. H., *J. Chem. Soc., Dalton Trans.*, 1996, 3297.

103   Steiner, T., Wilson, C. C., Majerz, I., *Chem. Commun.*, 2000, 1231.

104   Cowan, J. A., Ph. D. Thesis, University of Durham, England, 2002.

105   Coapes, R. B., Souza, F. E. S., Fox, M. A., Batsanov, A. S., Goeta, A. E., Yufit, D. S., Leech, M. A., Howard, J. A. K., Scott, A. J., Clegg, W., Marder, T. B., *J. Chem. Soc., Dalton Trans.*, 2001, 1201.

106   (a) Töpel, K., Hensen, K., Tromel, M., *Acta Crystallogr.*, 1981, **B37**, 969 (CSD Refcode CLBNPY); (b) Iijima, K., Oonishi, I., Shibata, S., *Chem. Lett.*, 1983, 251 (CSD Refcode BUNGEW).

107   Cotton, F. A., Wilkinson, G., *"Advanced Inorganic Chemistry"*, 5th Edn., Wiley-Interscience, 1988. Chapter 6, p175.

108   Vasil'ev, A. N., Mushkalo, L. K., *J. Gen. Chem. USSR (Engl. Transl.)*, 1993, **62**, 1718.

109   Töpel, K., Hensen, K., *Acta. Cryst.*, 1981, **B37**, 969.

110   Iijima, K., Oonishi, I., Shibata, S., *Chem. Lett.*, 1983, 251.

111   See reference 41.

112   Black, D. L., Taylor, R. C., *Acta Cryst.*, 1975, **B31**, 1116.

113   Hess, H., *Acta Cryst.*, 1969, **B25**, 2338.

114   Clippard, P. H., Hanson, J. C., Taylor, R. C., *J. Cryst. Mol. Struct.*, 1971, **1**, 363.

115   Engelhardt, L. M., Junk, P. C., Raston, C. L., Skelton, B. W., White, A. H., *J. Chem. Soc., Dalton Trans.*, 1996, 3297.

116   Iijima, K., Oonishi, I., Shibata, S., *Chem. Lett.*, 1983, 251.

117   Töpel, K., Hensen, K., Bats, J. W., *Acta Cryst.*, 1984, **C40**, 828.

118   For examples, see (a) Choon, O. C., McKee, V., Rodley, G. A., *Inorg. Chim. Acta*, 1986, **123**, 11 (CSD Refcode DUJKUO); (b) Steiner, T., Wilson, C. C., Majerz, I., *Chem. Commun.*, 2000, 1231 (CSD Refcode LOLSUA); (c) Bond, D. R., Caira, M. R., Harvey, G. A., Nassimbeni, L. R., Toda, F., *Acta Crystallogr.* 1990, **B46**, 771 (CSD Refcode SIRRAM); (d) Kepert, D. L., Skelton, B. W., Waters, A. F., White, A. H., *Aust. J. Chem.*, 1996, **49**, 47 (CSD Refcode TAPJID).

119   Ohms, U., Guth, H., Treutmann, W., Dannohl, H., Schweig, A., Heger, G., *J. Chem. Phys.*, 1985, **83**, 237 (CSD Refcode ZZZIVG02 and ZZZIVG11).

120   Lide, D. R., *"Handbook of Chemistry and Physics"*, CRC Press, 72nd Edition.

121   See reference 117. CSD Refcode: CEZJIA.

122   See reference 14.

123   Pangborn, A. B., Giardello, M. A., Grubbs, R. H., Rosen, R. K., Timers, F. J., *Organometallics*, 1996, **15**, 1518.

124   SADABS: Area-Detector Absorption Correction; Siemens Industrial Automation, Inc.: Madison, WI, 1996.

125   G.M. Sheldrick, (1997). SHELXS-97, SHELXL 97. Program for the Refinement of Crystal Structures. University of Göttingen, Germany.   G. M. Sheldrick, (1998). SHELXTL Version 5.1. Bruker AXS., Madison, Wisconsin, U.S.A.

126   SAINTPLUS Version 6.02. Bruker AXS., Madison, Wisconsin, U.S.A.

127   Desiraju, G. R., *Chem. Commun.*, 1997, 1475.

128   Desiraju, G. R., Steiner, T., "The Weak Hydrogen Bond in Structural Chemistry and Biology", IUCr Monographs on Crystallography 9, Oxford Science Publications, 1999.

129   Weck, M., Dunn, A. R., Matsumoto, K., Coates, G. W., Lobkovsky, E. B., Grubbs, R. H., *Angew. Chem., Int. Ed. Engl.*, 1999, **38**, 2741.

130   Pietsch, M. A., Rappe, A. K., *J. Am. Chem. Soc.*, 1996, **118**, 10908.

131   Ngola, S. M., Dougherty, D. A., *J. Org. Chem.*, 1998, **63**, 4566.

132   Ma, J. C., Dougherty, D. A., *Chem. Rev.*, 1997, **97**, 1303.

133   Patrick, C. R., Prosser, G. S., *Nature*, 1960, **271**, 1021.

134   (a) Duncan, W. A., F. L. Swinton, *Trans. Faraday Soc.*, 1966, **62**, 1082; (b) E. McLaughlin, C. E. Messer, *J. Chem. Soc. A*, 1966, 1106.

135   Kelly, T, Swinton, F. L., *J. Chem. Thermodynamics*, 1974, **6**, 435.

136   (a) Brennan, J. S., Brown, N. M. D., Swinton, F. L., *Trans. Faraday Soc.*, 1974, **70**, 1965; (b) J. A. Ripmeester, J. A., Wright, D. A., Fyfe, C. A., Boyd, R. K., *J. Chem. Soc. Faraday Trans. 2*, 1978, **74**, 1164.

137   Overell, J. S. W., Pawley, G. S., *Acta Crystallogr.*, 1982, **B38**, 1966.

138   Benzene refcodes: BENZEN, BENZEN01, BENZEN02, BENZEN03, BENZEN04 and BENZEN05. Hexafluorobenzene refcodes: HFBENZ and HFBENZ01.

139   Williams, J. H., Cockcroft, J. K., Fitch, A. N., *Angew. Chem., Int. Ed. Engl.*, 1992, **31**, 1655.

140   Heaton, N. J., Bello, P., Herradon, B., del Campo, A., Jimnenez-Barbero, J., *J. Am. Chem. Soc.*, 1998, **120**, 9632.

141   Gallivan, J. P., Dougherty, D. A., *Org. Lett.*, 1999, **1**, 103.

142   Williams, J. H., *Acc. Chem. Res.*, 1993, **26**, 593.

143   (a) Dahl, T., *Acta Chem. Scand.*, 1971, **25**,1031; (b) Dahl, T., *Acta Chem. Scand.*, 1972, **26**, 1569; (c) Dahl, T., *Acta Chem. Scand.*, 1973, **27**, 1031; (d) Dahl, T. *Acta Chem. Scand. Sect. A.*, 1975, **29**, 170; (e) Dahl, T. *Acta Chem. Scand. Sect. A.*, 1975, **29**, 699, (f) Dahl, T. *Acta Crystallogr. Sect B.*, 1977, **33**, 3021; (g) Dahl, T. *Acta Chem. Scand. Sect. A*, 1979, **33**, 665; (h) T. Dahl, *Acta Crystallogr. Sect. B*, 1981, **37**, 98; (i) Dahl, T. *Acta Crystallogr.*, 1989, **C41**, 931.

144   Naae, D. G., *Acta Crystallogr.*, 1979, **B35**, 2765.

145   For examples see: (a) Hunter, C. A., *Angew. Chem., Int. Ed. Engl.*, 1993, **32**, 1583 (b) Williams, J. H., *Acc. Chem. Res.*, 1993, **26**, 593.

146   Lorenzo, S., Lewis, G. R., Dance, I., *New J. Chem.*, 2000, **24**, 295.

147   Private communications with Todd B. Marder and Stewart Clark (Physics Department, University of Durham, England).

148   Study undertaken by Stewart Clark, Physics Dept., University of Durham, England.

149   Coates, G. W., Dunn, A. R., Henling, Dougherty, D. A., Grubbs, R. H., *Angew Chem., Int. Ed. Engl.*, 1997, **36**, 248.

150   Coates, G. W., Dunn, A. R., Henling, L. M., Ziller, J. W., Lobkovsky, E. B., Grubbs, R. H., *J. Am. Chem. Soc.*, 1998, **120**, 3641.

151   (a) Fugita, M., Nagao, S., Iida, M., Ogata, K., Ogura, K., *J. Am. Chem. Soc.*, 1993, **115**, 1574; (b) Fugita, M., Ibukuro, F., Hagihara, F., Ogura, K., *Nature*, 1994, **367**, 720.

152   Marsella, M. J., Wang, Z. Q., Reid, R. J., Yoon, K., *Org. Lett.*, 2001, 885.

153   Kilbinger, A. F. M., Grubbs, R. H., *Angew. Chem., Int. Ed. Engl.*, 2002, **41**, 1563.

154   Blanchard, M. D., Hughes, R. P., Concolino, T. E., Rheingold, A. L., *Chem. Mater.*, 2000, **12**, 1604.

155   Feast, W. J., Lövenich, P. W., Puschmann, H., Taliani, C., *Chem. Commun.*, 2001, 505.

156   Bartholemew, G. P., Bu, X. H., Bazan, G. C., *Chem. Mater.*, 2000, **12**, 2311.

157   Schwab, P. F. H., Levin, M. D., Michl, J., *Chem. Rev.* 1999, **99**, 1863.

158   Bondi, A., *J. Phys. Chem.*, 1964, **68**, 441.

159   Kitaigorodski, A. I., *Molecular Crystals and Molecules,* New York Academic Press, 1973, 33.

160   See reference 14.

161   See (a) Ramasubbu, N., Parthasarathy, R., Murray-Rust, P., *J. Am. Chem. Soc.*, 1986, **108**, 4308; (b) Peddireddi, V. R., Reddy, D. S., Goud, S., Craig, D. C., Rae, A. D., Desiraju, G. R., *J. Chem. Soc., Perkin Trans 2*, 1994, 2353; (c) Desiraju, G. R., Parthasarathy, R., *J. Am. Chem. Soc.*, 1989, **111**, 8725.

162 Dai, C., Nguyen, P., Marder, T. B., Scott, A. J., Clegg, W., Viney, C., *Chem. Commun.*, 1999, 2493.

163 Watt, S. W., Dai, C., Scott, A. J., Burke, J. M., Thomas, R. Ll., Collings, J. C., Viney, C., Clegg, W., Marder, T. B., Manuscript in preparation.

164 For (**4a**), see Scott, A. J., Ph. D. Thesis, University of Newcastle-upon-Tyne, 1999. (**4b**) was solved by Nick Taylor at the University of Waterloo, Canada. (**4c**) and (**4d**) were originally solved by Andrew Scott at the University of Newcastle-upon-Tyne. All results are as yet unpublished.

165 (a) Desiraju, G. R., Gavezzotti, A., *Acta Crystallogr.*, 1989, **B45**, 473; (b) Desiraju, G. R., Gavezzotti, A., *J. Chem. Soc., Chem. Commun.*, 1989, 621.

166 Feast, W. J., Lövenich, P. W., Puschmann, H., Taliani, C., *Chem. Commun.*, 2001, 505.

167 Scott, A. J., Ph. D. Thesis, University of Newcastle-upon-Tyne, 1999.

168 Hope, E. G., Stuart, A. M., *J. Fluorine Chem.*, 1999, **100**, 75.

169 Byrn, M. P., Curtic, C. J., Hsiou, Y., Khan, S. I., Sawin, P. A., Tendick, S. K., Terzis, A., Strouse, C. E., *J. Am. Chem. Soc.*, 1993, **115**, 9480.

170 Nguyen, P., Todd, S., Van den Biggelaar, D., Taylor, N. J., Marder, T. B., Wittman, F., Friend, R. H., *Synlett*, 1994, 299.

171 Venkataraman, D., Wang, P-W, Moore, J. S., *Acta Crystallogr.*, 1997, **C53**, 241.

172 (a) Khundkar, L. R., Steigman, A. E., Perry, J. W., *J. Phys. Chem.*, 1990, **94**, 1224; (b) Khundar, L. R., Bartlett, J. T., Biswas, M., *J. Phys. Chem.*, 1995, **102**, 6456.

173 (a) Steigman, A. E., Miskowski, V. M., Perry, J. W., Coulter, D. R., *J. Am. Chem. Soc.*, 1987, **109**, 5884; (b) Steigman, A. E., Graham, E., Perry, K. J., Khundkar, L. R., Cheng, L-T, Perry, J. W., *J. Am. Chem. Soc.*, 1991, **113**, 7658;

(c) Barzoukas, M., Fort, A., Klein, G., Boeglin, A., Serbutiviez, C., Oswald, L, Nicould, J. F., *Chem. Phys*, 1991, **153**, 457; (d) Jungbaur, D., Teraoka, I., Yoon, D. Y., Reck, B., Swalen, J. D., Tweig, R., Wilson, C. G., *J. Appl. Phys.*, 1991, **69**, 8011; (e) Dehu, C., Meyers, F.,Bredas, J. L., *J. Am. Chem. Cos.*, 1993, **115**, 6198.

174   Malthete, J., Leclercq, M., Dvolaitzky, M., Gabard, J., Billard, J., Pontikis, V., Jacques, J., *J. Mol. Cryst. Liqu. Cryst.*, 1973, **23**, 233.

175   Dai, C., Doctoral Thesis, University of Waterloo, Canada, (1998).

176   Peddireddi, V. R., Reddy, D. S., Goud, S., Craig, D. C., Rae, A. D., Desiraju, G. R., *J. Chem. Soc., Perkin Trans 2*, 1994, 2353.

177   See reference 161 (a).

178   (a) Samarskaya, V. D., Myasnikova, R. M., Kitaigorodskij, *Kristallografiya*, 1968, **13**, 616; (b) Mavridis, A., Moustakali-Mavridis, I., *Acta Crystallogr.*, 1977, **B33**, 3612; (c) Espiritu, A. A., White, J. G., *Z. Kristallog., Kristallg., Kristallp., Kristallch.*, 1978, **147**, 177; (d) Abramenkov, A. V., Almenningen, A., Cyvin, B. N., Cyvin, S. J., Jonvik, T., Khaikin, L. S., Romming, C., Vilkov, L. V., *Acta Chem. Scand. Ser. A.*, 1988, **42**, 674; (e) Zanin, I. E., Antipin, M. Y., Struchkov, Y. T., *Kristallografiya*, 1991, **36**, 411.

179   Clyburne, J. A. C., Hamilton, T., Jenkins, H. A., *Crystal Engineering*, 2001, **4**, 1.

180   Collings, J. C., Batsanov, A. S., Howard, J. A. K., Marder, T. B., *Acta Crystallogr.*, 2001, **57**, 870.

181   Goodhand, N., Hamor, T. A., *Acta Crystallogr.*, (1979), **B35**, 704.

182   See reference 167.

183   Wang, C., collected abstracts, IUCr, XVII Congress and General Assembly, C272, (1996)

184   Roscoe, K., M. Sci. project report, University of Durham, England, (1999).

185   Smith, P. S., M. Sci. project report, University of Durham, England (2000).

186   Godt, A., Ünsal, Ö., Enkelmann, V., *Chem. Eur. J.*, 2000, **6**, 3522.

187   For details, see Collings, J. C., Ph. D. Thesis, University of Durham, England, (2002).

Appendix A: Crystal Structure Data Tables

Listed in order of A(n), where n is the compound reference code.

Appendix A2: Crystal Structure Data Tables for Structures in Chapter 2

Appendix A2b

Data for the structure of $Cl_3B \cdot PEt_3$ (**2b**)

Crystals grown by the author. Structure solved with help from Dr. Claire Wilson at the University of Durham Crystallography Department (reference code 99srv103).

Table 1. Crystal data and structure refinement for (**2b**).

Identification code	99srv103
Empirical formula	C6 H15 B Cl3 P
Formula weight	235.31
Temperature	150(2) K
Wavelength	0.71073 Å
Crystal system	Orthorhombic
Space group	P2(1)2(1)2(1)
Unit cell dimensions	a = 7.0992(5) Å $\quad$ α= 90°.
	b = 11.8304(8) Å $\quad$ β= 90°.
	c = 13.4392(8) Å $\quad$ γ = 90°.
Volume	1128.71(13) Å^3
Z	4
Density (calculated)	1.385 Mg/m^3
Absorption coefficient	0.896 mm^{-1}
F(000)	488
Crystal size	0.36 x 0.09 x 0.08 mm^3
Theta range for data collection	2.29 to 30.35°.
Index ranges	-9<=h<=8, -16<=k<=16, -12<=l<=18
Reflections collected	9193
Independent reflections	3136 [R(int) = 0.0581]
Completeness to theta = 30.35°	94.9 %
Absorption correction	Has
Max. and min. transmission	0.914 and 0.667
Refinement method	Full-matrix least-squares on F^2
Data / restraints / parameters	3136 / 0 / 160
Goodness-of-fit on F^2	1.016
Final R indices [I>2sigma(I)]	R1 = 0.0421, wR2 = 0.0854
R indices (all data)	R1 = 0.0644, wR2 = 0.0937
Absolute structure parameter	0.410
Largest diff. peak and hole	0.541 and -0.443 e.Å^{-3}

Table 2. Atomic coordinates (x 10^4) and equivalent isotropic displacement parameters (Å^2x 10^3) for (**2b**). U(eq) is defined as one third of the trace of the orthogonalized U^{ij} tensor.

Atom	x	y	z	U(eq)
Cl(1)	723(1)	50(1)	9238(1)	29(1)
P(1)	4873(1)	-125(1)	8570(1)	18(1)
B(1)	2222(4)	-78(3)	8111(2)	22(1)
C(1)	5112(5)	-918(2)	9712(2)	26(1)
Cl(2)	1911(1)	1163(1)	7297(1)	36(1)
C(2)	4459(5)	-2144(3)	9654(3)	34(1)
Cl(3)	1686(1)	-1395(1)	7436(1)	34(1)
C(3)	6414(4)	-795(2)	7670(2)	25(1)
C(4)	6638(6)	-155(4)	6699(3)	41(1)
C(5)	5796(4)	1281(3)	8800(3)	28(1)
C(6)	4665(5)	1978(3)	9546(3)	35(1)

Table 3. Bond lengths [Å] and angles [°] for (**2b**)

Cl(1)-B(1)	1.857(3)	C(5)-H(5A)	0.99(3)
P(1)-C(1)	1.807(3)	C(5)-H(5B)	0.95(4)
P(1)-C(3)	1.814(3)	C(6)-H(6C)	0.98(3)
P(1)-C(5)	1.814(3)	C(6)-H(6B)	1.04(5)
P(1)-B(1)	1.981(3)	C(6)-H(6A)	0.99(5)
B(1)-Cl(3)	1.843(3)		
B(1)-Cl(2)	1.844(3)	C(1)-P(1)-C(3)	106.43(14)
C(1)-C(2)	1.524(4)	C(1)-P(1)-C(5)	107.33(15)
C(1)-H(1B)	0.96(3)	C(3)-P(1)-C(5)	107.25(14)
C(1)-H(1A)	0.92(4)	C(1)-P(1)-B(1)	111.60(14)
C(2)-H(2C)	0.94(4)	C(3)-P(1)-B(1)	112.18(14)
C(2)-H(2B)	0.95(4)	C(5)-P(1)-B(1)	111.74(14)
C(2)-H(2A)	0.98(5)	Cl(3)-B(1)-Cl(2)	110.85(15)
C(3)-C(4)	1.518(5)	Cl(3)-B(1)-Cl(1)	110.63(16)
C(3)-H(3A)	1.05(4)	Cl(2)-B(1)-Cl(1)	110.52(16)
C(3)-H(3B)	0.94(4)	Cl(3)-B(1)-P(1)	109.00(15)
C(4)-H(4C)	1.03(4)	Cl(2)-B(1)-P(1)	108.70(15)
C(4)-H(4B)	0.86(4)	Cl(1)-B(1)-P(1)	107.02(14)
C(4)-H(4A)	0.89(5)	C(2)-C(1)-P(1)	114.9(3)
C(5)-C(6)	1.527(5)	C(2)-C(1)-H(1B)	107.5(19)

P(1)-C(1)-H(1B)	110.1(19)	H(4C)-C(4)-H(4B)	108(3)
C(2)-C(1)-H(1A)	113(2)	C(3)-C(4)-H(4A)	112(3)
P(1)-C(1)-H(1A)	104(2)	H(4C)-C(4)-H(4A)	110(4)
H(1B)-C(1)-H(1A)	106(3)	H(4B)-C(4)-H(4A)	103(4)
C(1)-C(2)-H(2C)	102(2)	C(6)-C(5)-P(1)	114.7(2)
C(1)-C(2)-H(2B)	110(2)	C(6)-C(5)-H(5A)	113.9(19)
H(2C)-C(2)-H(2B)	112(3)	P(1)-C(5)-H(5A)	102.3(19)
C(1)-C(2)-H(2A)	111(2)	C(6)-C(5)-H(5B)	113(2)
H(2C)-C(2)-H(2A)	118(3)	P(1)-C(5)-H(5B)	106(2)
H(2B)-C(2)-H(2A)	104(3)	H(5A)-C(5)-H(5B)	106(3)
C(4)-C(3)-P(1)	114.7(2)	C(5)-C(6)-H(6C)	112(2)
C(4)-C(3)-H(3A)	110(2)	C(5)-C(6)-H(6B)	104(2)
P(1)-C(3)-H(3A)	107(2)	H(6C)-C(6)-H(6B)	111(3)
C(4)-C(3)-H(3B)	112(2)	C(5)-C(6)-H(6A)	110(2)
P(1)-C(3)-H(3B)	100(2)	H(6C)-C(6)-H(6A)	106(3)
H(3A)-C(3)-H(3B)	114(3)	H(6B)-C(6)-H(6A)	113(3)
C(3)-C(4)-H(4C)	113(2)		
C(3)-C(4)-H(4B)	110(3)		

Table 4. Anisotropic displacement parameters (Å^2x 10^3) for (**2b**). The anisotropic displacement factor exponent takes the form: $-2\pi^2[\ h^2\ a^{*2}U^{11} + ... + 2\ h\ k\ a^*\ b^*\ U^{12}\ ]$

Atom	U^{11}	U^{22}	U^{33}	U^{23}	U^{13}	U^{12}
Cl(1)	21(1)	30(1)	37(1)	-4(1)	6(1)	1(1)
P(1)	17(1)	14(1)	23(1)	0(1)	0(1)	0(1)
B(1)	19(1)	18(1)	28(2)	-1(1)	-2(1)	0(1)
C(1)	27(1)	23(1)	27(2)	2(1)	0(1)	2(1)
Cl(2)	36(1)	30(1)	42(1)	11(1)	-13(1)	1(1)
C(2)	34(2)	22(2)	45(2)	12(2)	0(2)	-1(1)
Cl(3)	26(1)	27(1)	49(1)	-16(1)	-5(1)	-1(1)
C(3)	21(1)	24(1)	29(2)	-3(1)	2(1)	2(1)
C(4)	47(2)	42(2)	33(2)	-2(2)	16(2)	1(2)
C(5)	23(1)	20(1)	41(2)	-2(1)	-4(1)	-3(1)
C(6)	36(2)	21(2)	48(2)	-8(2)	-5(2)	0(1)

Table 5.   Hydrogen coordinates (x 10^4) and isotropic displacement parameters (Å^2x 10 ^{3}) for (2b).

Atom	x	y	z	U(eq)
H(2C)	4660(40)	-2400(30)	10310(30)	24(9)
H(3A)	5850(50)	-1600(30)	7530(30)	43(10)
H(4C)	5370(60)	-10(40)	6350(30)	59(12)
H(2B)	5200(50)	-2540(30)	9180(30)	35(10)
H(1B)	4410(40)	-560(30)	10240(20)	24(8)
H(4B)	7340(60)	-530(30)	6300(30)	47(12)
H(5A)	5830(50)	1610(30)	8120(20)	26(8)
H(6C)	4590(40)	1610(30)	10200(30)	24(8)
H(6B)	5390(60)	2740(40)	9580(30)	59(13)
H(1A)	6370(60)	-840(30)	9880(30)	40(10)
H(2A)	3170(70)	-2190(30)	9380(30)	51(12)
H(4A)	7270(60)	490(40)	6780(30)	69(15)
H(6A)	3350(70)	2070(30)	9320(30)	40(10)
H(5B)	7070(50)	1190(30)	8990(30)	42(11)
H(3B)	7550(60)	-810(30)	8040(30)	47(11)

Table 6. Torsion angles [°] for (2b).

C(1)-P(1)-B(1)-Cl(3)	-82.09(18)
C(3)-P(1)-B(1)-Cl(3)	37.2(2)
C(5)-P(1)-B(1)-Cl(3)	157.73(16)
C(1)-P(1)-B(1)-Cl(2)	156.98(15)
C(3)-P(1)-B(1)-Cl(2)	-83.68(18)
C(5)-P(1)-B(1)-Cl(2)	36.8(2)
C(1)-P(1)-B(1)-Cl(1)	37.6(2)
C(3)-P(1)-B(1)-Cl(1)	156.93(15)
C(5)-P(1)-B(1)-Cl(1)	-82.59(19)
C(3)-P(1)-C(1)-C(2)	-63.6(3)
C(5)-P(1)-C(1)-C(2)	-178.2(3)
B(1)-P(1)-C(1)-C(2)	59.1(3)
C(1)-P(1)-C(3)-C(4)	-171.5(3)
C(5)-P(1)-C(3)-C(4)	-56.9(3)
B(1)-P(1)-C(3)-C(4)	66.2(3)
C(1)-P(1)-C(5)-C(6)	-66.0(3)
C(3)-P(1)-C(5)-C(6)	180.0(3)
B(1)-P(1)-C(5)-C(6)	56.6(3)

Appendix A2c

Data for the structure of $Cl_3B \cdot P(^iPr)_3$ (**2c**)

Crystals grown by the author. Structure solved by Dr. A. S. Batsanov at the University

of Durham Crystallography Department (reference code 00srv286).

Table 1. Crystal data and structure refinement for (**2c**).

Identification code	00srv286	
Empirical formula	$C_9 H_{21} B Cl_3 P$	
Formula weight	277.39	
Temperature	110.0(2) K	
Wavelength	0.71073 Å	
Crystal system	Monoclinic	
Space group	$P2_1/c$	
Unit cell dimensions	a = 14.897(1) Å	α= 90°.
	b = 14.008(1) A	β= 116.01(1)°.
	c = 15.076(1) A	γ = 90°.
Volume	2827.5(4) Å^3	
Z	8	
Density (calculated)	1.303 Mg/m^3	
Absorption coefficient	0.726 mm^{-1}	
F(000)	1168	
Crystal size	0.36 x 0.24 x 0.06 mm^3	
Theta range for data collection	1.52 to 30.16°.	
Index ranges	-19<=h<=19, -19<=k<=19, -21<=l<=20	
Reflections collected	32244	
Independent reflections	7617 [R(int) = 0.0799]	
Completeness to theta = 30.16°	91.3 %	
Absorption correction	Not applied	
Max. and min. transmission	0.9577 and 0.7800	
Refinement method	Full-matrix least-squares on F^2	
Data / restraints / parameters	7617 / 0 / 421	
Goodness-of-fit on F^2	1.057	
Final R indices [I>2sigma(I)]	R1 = 0.0515, wR2 = 0.0929	
R indices (all data)	R1 = 0.0899, wR2 = 0.1053	
Largest diff. peak and hole	0.571 and -0.402 e.Å^{-3}	

Appendix A2c

Table 2. Atomic coordinates (x 10^4) and equivalent isotropic displacement parameters ($\mathring{A}^2$x 10^3) for (2c). U(eq) is defined as one third of the trace of the orthogonalized U^{ij} tensor.

Atom	x	y	z	U(eq)
P(1)	428(1)	1901(1)	3242(1)	16(1)
P(2)	5611(1)	1641(1)	8028(1)	17(1)
Cl(1)	-832(1)	3083(1)	1342(1)	34(1)
Cl(2)	173(1)	1251(1)	1169(1)	32(1)
Cl(3)	1415(1)	3014(1)	2063(1)	39(1)
Cl(21)	4509(1)	2876(1)	6071(1)	35(1)
Cl(22)	5357(1)	933(1)	5964(1)	34(1)
Cl(23)	6736(1)	2604(1)	6922(1)	37(1)
B(1)	305(2)	2329(2)	1931(2)	25(1)
B(2)	5544(2)	2029(2)	6716(2)	23(1)
C(1)	-835(2)	1565(2)	3078(2)	19(1)
C(2)	-999(2)	1652(2)	4010(2)	26(1)
C(3)	-1148(2)	585(2)	2606(2)	27(1)
C(4)	1239(2)	845(2)	3678(2)	22(1)
C(5)	1391(2)	523(2)	4702(2)	29(1)
C(6)	2243(2)	941(3)	3622(3)	35(1)
C(7)	843(2)	2845(2)	4186(2)	25(1)
C(8)	211(3)	3744(2)	3797(3)	35(1)
C(9)	1955(3)	3084(3)	4625(3)	45(1)
C(21)	4694(2)	689(2)	7855(2)	21(1)
C(22)	3674(2)	868(2)	6985(2)	27(1)
C(23)	4583(3)	463(3)	8794(2)	39(1)
C(24)	6886(2)	1188(2)	8790(2)	22(1)
C(25)	7149(3)	333(3)	8326(3)	39(1)
C(26)	7147(3)	987(3)	9870(2)	41(1)
C(27)	5435(2)	2619(2)	8754(2)	21(1)
C(28)	4376(2)	3029(2)	8330(3)	31(1)
C(29)	6194(2)	3417(2)	8927(3)	32(1)

Table 3. Bond lengths [Å] and angles [°] for (2c).

P(1)-C(7)	1.838(3)	Cl(2)-B(1)	1.855(3)	C(7)-C(9)	1.528(4)
P(1)-C(4)	1.840(3)	Cl(3)-B(1)	1.845(3)	C(7)-C(8)	1.528(4)
P(1)-C(1)	1.849(2)	Cl(21)-B(2)	1.848(3)	C(21)-C(23)	1.530(4)
P(1)-B(1)	1.996(3)	Cl(22)-B(2)	1.855(3)	C(21)-C(22)	1.531(4)
P(2)-C(27)	1.842(3)	Cl(23)-B(2)	1.848(3)	C(24)-C(25)	1.523(4)
P(2)-C(21)	1.844(3)	C(1)-C(3)	1.523(4)	C(24)-C(26)	1.525(4)
P(2)-C(24)	1.849(3)	C(1)-C(2)	1.534(3)	C(27)-C(29)	1.528(4)
P(2)-B(2)	2.011(3)	C(4)-C(5)	1.526(4)	C(27)-C(28)	1.531(4)
Cl(1)-B(1)	1.859(3)	C(4)-C(6)	1.541(4)		

C(7)-P(1)-C(4)	110.90(13)	Cl(21)-B(2)-P(2)	111.17(15)
C(7)-P(1)-C(1)	105.27(12)	Cl(23)-B(2)-P(2)	108.85(15)
C(4)-P(1)-C(1)	108.25(12)	Cl(22)-B(2)-P(2)	107.89(15)
C(7)-P(1)-B(1)	113.85(13)	C(3)-C(1)-C(2)	111.1(2)
C(4)-P(1)-B(1)	110.87(12)	C(3)-C(1)-P(1)	112.17(18)
C(1)-P(1)-B(1)	107.33(13)	C(2)-C(1)-P(1)	114.78(19)
C(27)-P(2)-C(21)	109.46(12)	C(5)-C(4)-C(6)	111.4(3)
C(27)-P(2)-C(24)	105.14(12)	C(5)-C(4)-P(1)	112.44(19)
C(21)-P(2)-C(24)	109.59(13)	C(6)-C(4)-P(1)	114.2(2)
C(27)-P(2)-B(2)	115.13(13)	C(9)-C(7)-C(8)	110.7(3)
C(21)-P(2)-B(2)	109.97(12)	C(9)-C(7)-P(1)	115.2(2)
C(24)-P(2)-B(2)	107.33(12)	C(8)-C(7)-P(1)	110.8(2)
Cl(3)-B(1)-Cl(2)	109.71(15)	C(23)-C(21)-C(22)	110.9(2)
Cl(3)-B(1)-Cl(1)	109.98(16)	C(23)-C(21)-P(2)	113.1(2)
Cl(2)-B(1)-Cl(1)	109.86(18)	C(22)-C(21)-P(2)	113.45(19)
Cl(3)-B(1)-P(1)	111.14(17)	C(25)-C(24)-C(26)	110.4(3)
Cl(2)-B(1)-P(1)	107.91(15)	C(25)-C(24)-P(2)	112.7(2)
Cl(1)-B(1)-P(1)	108.20(14)	C(26)-C(24)-P(2)	116.0(2)
Cl(21)-B(2)-Cl(23)	109.07(16)	C(29)-C(27)-C(28)	110.3(2)
Cl(21)-B(2)-Cl(22)	110.01(16)	C(29)-C(27)-P(2)	111.00(18)
Cl(23)-B(2)-Cl(22)	109.84(15)	C(28)-C(27)-P(2)	114.8(2)

Table 4.   Anisotropic displacement parameters ($\mathring{A}^2 \times 10^3$) for (2c). The anisotropic displacement factor exponent takes the form: $-2\pi^2[h^2 a^{*2}U^{11} + ... + 2 h k a^* b^* U^{12}]$

Atom	U^{11}	U^{22}	U^{33}	U^{23}	U^{13}	U^{12}
P(1)	17(1)	16(1)	18(1)	1(1)	10(1)	0(1)
P(2)	14(1)	21(1)	15(1)	1(1)	6(1)	1(1)
Cl(1)	47(1)	36(1)	26(1)	15(1)	22(1)	16(1)
Cl(2)	53(1)	27(1)	28(1)	-1(1)	27(1)	0(1)
Cl(3)	51(1)	28(1)	60(1)	2(1)	45(1)	-6(1)
Cl(21)	29(1)	40(1)	29(1)	14(1)	7(1)	5(1)
Cl(22)	37(1)	45(1)	22(1)	-6(1)	16(1)	-2(1)
Cl(23)	25(1)	60(1)	29(1)	7(1)	13(1)	-13(1)
B(1)	33(2)	22(2)	28(2)	5(1)	21(2)	2(1)
B(2)	19(1)	34(2)	16(1)	3(1)	7(1)	-2(1)
C(1)	17(1)	23(1)	19(1)	4(1)	9(1)	1(1)
C(2)	27(2)	33(2)	25(2)	4(1)	19(1)	3(1)
C(3)	20(2)	30(2)	29(2)	-1(1)	9(1)	-5(1)
C(4)	19(1)	21(1)	24(1)	-1(1)	9(1)	2(1)
C(5)	28(2)	29(2)	24(2)	7(1)	7(1)	10(1)
C(6)	23(2)	39(2)	48(2)	3(2)	19(2)	9(1)
C(7)	34(2)	17(1)	25(1)	-5(1)	14(1)	-5(1)
C(8)	58(2)	20(2)	36(2)	2(1)	30(2)	3(2)
C(9)	39(2)	40(2)	51(2)	-19(2)	16(2)	-17(2)
C(21)	20(1)	21(1)	20(1)	0(1)	8(1)	-2(1)
C(22)	20(1)	28(2)	30(2)	0(1)	9(1)	-1(1)
C(23)	42(2)	47(2)	29(2)	5(2)	18(2)	-19(2)
C(24)	17(1)	28(2)	17(1)	2(1)	3(1)	4(1)
C(25)	33(2)	47(2)	26(2)	-3(2)	3(2)	23(2)
C(26)	35(2)	60(2)	20(2)	6(2)	5(1)	23(2)
C(27)	20(1)	24(1)	21(1)	-2(1)	10(1)	2(1)
C(28)	24(2)	31(2)	38(2)	-6(1)	13(1)	6(1)
C(29)	35(2)	25(2)	42(2)	-8(1)	23(2)	-5(1)

Table 5. Hydrogen coordinates (x 10^4) and isotropic displacement parameters (E^2x 10 ^{3})
for (**2c**).

Atom	x	y	z	U(eq)
H(1)	-1250(20)	2025(19)	2600(20)	17(7)
H(4)	831(19)	378(19)	3218(19)	14(6)
H(7)	720(20)	2578(19)	4720(20)	21(7)
H(21)	-1650(20)	1440(20)	3860(20)	24(7)
H(22)	-910(20)	2300(20)	4280(20)	27(8)
H(23)	-550(20)	1220(20)	4540(20)	35(9)
H(31)	-1060(20)	520(20)	2010(20)	31(8)
H(32)	-1830(30)	530(20)	2420(20)	38(9)
H(33)	-830(20)	110(20)	3030(20)	25(8)
H(51)	1830(20)	-50(20)	4900(20)	37(9)
H(52)	1650(30)	1010(20)	5170(30)	43(10)
H(53)	790(30)	400(20)	4710(20)	44(10)
H(61)	2540(20)	300(20)	3770(20)	35(8)
H(62)	2700(30)	1430(20)	4110(20)	41(9)
H(63)	2160(20)	1090(20)	2970(20)	26(8)
H(81)	400(20)	4220(20)	4330(20)	43(9)
H(82)	330(20)	4010(20)	3320(20)	37(9)
H(83)	-480(30)	3630(20)	3520(30)	44(10)
H(91)	2370(30)	2550(30)	4930(20)	39(10)
H(92)	2060(30)	3570(30)	5070(30)	45(10)
H(93)	2120(30)	3320(20)	4110(30)	43(10)
H(211)	4970(20)	120(20)	7680(20)	29(8)
H(221)	3260(20)	330(20)	6930(20)	21(7)
H(222)	3350(30)	1410(20)	7050(20)	41(9)
H(223)	3710(20)	930(20)	6400(30)	43(10)
H(231)	4140(30)	-70(20)	8660(20)	40(9)
H(232)	4240(30)	1010(20)	8940(20)	42(10)
H(233)	5210(30)	360(30)	9370(30)	56(11)
H(241)	7230(20)	1730(19)	8785(18)	13(6)
H(251)	7870(30)	170(20)	8780(20)	40(9)
H(252)	6740(30)	-240(30)	8310(30)	61(12)
H(253)	7040(30)	420(30)	7660(30)	70(13)
H(261)	6830(30)	380(30)	9920(20)	43(10)
H(262)	6980(30)	1470(30)	10140(30)	64(13)
H(263)	7900(30)	860(30)	10260(30)	51(10)
H(271)	5570(20)	2310(20)	9360(20)	27(8)
H(281)	4360(20)	3540(20)	8750(20)	26(8)
H(282)	3910(20)	2580(20)	8300(20)	28(8)

H(283)	4170(30)	3310(20)	7680(30)	45(10)
H(291)	6140(20)	3680(20)	8330(20)	36(9)
H(292)	6080(20)	3880(20)	9290(20)	35(9)
H(293)	6870(30)	3180(20)	9260(20)	40(9)

Table 6. Torsion angles [°] for (2c).

C(7)-P(1)-B(1)-Cl(3)	46.8(2)	C(7)-P(1)-C(4)-C(6)	-78.4(2)
C(4)-P(1)-B(1)-Cl(3)	-79.10(18)	C(1)-P(1)-C(4)-C(6)	166.6(2)
C(1)-P(1)-B(1)-Cl(3)	162.86(14)	B(1)-P(1)-C(4)-C(6)	49.1(3)
C(7)-P(1)-B(1)-Cl(2)	167.11(14)	C(4)-P(1)-C(7)-C(9)	49.7(3)
C(4)-P(1)-B(1)-Cl(2)	41.2(2)	C(1)-P(1)-C(7)-C(9)	166.5(2)
C(1)-P(1)-B(1)-Cl(2)	-76.81(17)	B(1)-P(1)-C(7)-C(9)	-76.2(3)
C(7)-P(1)-B(1)-Cl(1)	-74.07(19)	C(4)-P(1)-C(7)-C(8)	176.3(2)
C(4)-P(1)-B(1)-Cl(1)	160.05(14)	C(1)-P(1)-C(7)-C(8)	-66.8(2)
C(1)-P(1)-B(1)-Cl(1)	42.02(18)	B(1)-P(1)-C(7)-C(8)	50.5(2)
C(27)-P(2)-B(2)-Cl(21)	-42.6(2)	C(27)-P(2)-C(21)-C(23)	-43.6(3)
C(21)-P(2)-B(2)-Cl(21)	81.56(18)	C(24)-P(2)-C(21)-C(23)	71.2(2)
C(24)-P(2)-B(2)-Cl(21)	-159.29(15)	B(2)-P(2)-C(21)-C(23)	-171.0(2)
C(27)-P(2)-B(2)-Cl(23)	77.52(18)	C(27)-P(2)-C(21)-C(22)	83.9(2)
C(21)-P(2)-B(2)-Cl(23)	-158.29(14)	C(24)-P(2)-C(21)-C(22)	-161.27(19)
C(24)-P(2)-B(2)-Cl(23)	-39.13(19)	B(2)-P(2)-C(21)-C(22)	-43.5(2)
C(27)-P(2)-B(2)-Cl(22)	-163.34(13)	C(27)-P(2)-C(24)-C(25)	177.1(2)
C(21)-P(2)-B(2)-Cl(22)	-39.14(18)	C(21)-P(2)-C(24)-C(25)	59.6(3)
C(24)-P(2)-B(2)-Cl(22)	80.01(17)	B(2)-P(2)-C(24)-C(25)	-59.8(3)
C(7)-P(1)-C(1)-C(3)	-160.2(2)	C(27)-P(2)-C(24)-C(26)	48.5(3)
C(4)-P(1)-C(1)-C(3)	-41.5(2)	C(21)-P(2)-C(24)-C(26)	-69.0(3)
B(1)-P(1)-C(1)-C(3)	78.2(2)	B(2)-P(2)-C(24)-C(26)	171.6(3)
C(7)-P(1)-C(1)-C(2)	-32.1(2)	C(21)-P(2)-C(27)-C(29)	179.1(2)
C(4)-P(1)-C(1)-C(2)	86.6(2)	C(24)-P(2)-C(27)-C(29)	61.5(2)
B(1)-P(1)-C(1)-C(2)	-153.7(2)	B(2)-P(2)-C(27)-C(29)	-56.4(2)
C(7)-P(1)-C(4)-C(5)	49.8(2)	C(21)-P(2)-C(27)-C(28)	-54.9(2)
C(1)-P(1)-C(4)-C(5)	-65.2(2)	C(24)-P(2)-C(27)-C(28)	-172.6(2)
B(1)-P(1)-C(4)-C(5)	177.4(2)	B(2)-P(2)-C(27)-C(28)	69.5(2)

Appendix A2d

Data for the structure of $Cl_3B \cdot P(^nBu)_3$ (**2d**).

Crystals grown by the author. Structure solved by Dr. A. S. Batsanov at the University of Durham Crystallography Department (reference code 99srv102).

Table 1. Crystal data and structure refinement for (**2d**).

Identification code	99srv102
Empirical formula	C12 H27 B Cl3 P
Formula weight	319.47
Temperature	120(2) K
Wavelength	0.71073 Å
Crystal system	Rhombohedral
Space group	R3c
Unit cell dimensions	a = 14.990(1) Å $\quad$ α= 90°.
	b = 14.990(1) Å $\quad$ β= 90°.
	c = 13.579(1) Å $\quad$ γ = 120°.
Volume	2642.4(3) Å^3
Z	6
Density (calculated)	1.205 Mg/m^3
Absorption coefficient	0.592 mm^{-1}
F(000)	1020
Crystal size	0.68 x 0.05 x 0.04 mm^3
Theta range for data collection	2.72 to 27.47°.
Index ranges	-19<=h<=18, -19<=k<=16, -17<=l<=16
Reflections collected	5975
Independent reflections	1337 [R(int) = 0.0372]
Completeness to theta = 27.47°	100.0 %
Absorption correction	Multiscan
Max. and min. transmission	1.0000 and 0.8412
Refinement method	Full-matrix least-squares on F^2
Data / restraints / parameters	1337 / 1 / 88
Goodness-of-fit on F^2	1.066
Final R indices [I>2sigma(I)]	R1 = 0.0219, wR2 = 0.0484
R indices (all data)	R1 = 0.0261, wR2 = 0.0502
Absolute structure parameter	0.07(7)
Largest diff. peak and hole	0.162 and -0.136 e.Å^{-3}

Table 2. Atomic coordinates (x 10^4) and equivalent isotropic displacement parameters (Å^2x 10^3) for (**2d**). U(eq) is defined as one third of the trace of the orthogonalized U^{ij} tensor.

Atom	x	y	z	U(eq)
Cl	7760(1)	4573(1)	4254(1)	28(1)
P	6667	3333	2371(1)	18(1)
B	6667	3333	3826(2)	21(1)
C(1)	7961(1)	3853(1)	1881(1)	21(1)
C(2)	8428(1)	3153(1)	1998(1)	26(1)
C(3)	9508(1)	3638(1)	1570(2)	31(1)
C(4)	9983(2)	2955(2)	1691(2)	45(1)

Table 3. Bond lengths [Å] and angles [°] for (**2d**).

Cl-B	1.8526(10)	C(1)#1-P-B	111.50(5)
P-C(1)	1.8171(15)	C(1)#2-P-B	111.50(5)
P-C(1)#1	1.8171(15)	Cl#1-B-Cl	110.63(8)
P-C(1)#2	1.8171(15)	Cl#1-B-Cl#2	110.63(8)
P-B	1.975(3)	Cl-B-Cl#2	110.63(8)
B-Cl#1	1.8526(10)	Cl#1-B-P	108.29(9)
B-Cl#2	1.8526(10)	Cl-B-P	108.29(9)
C(1)-C(2)	1.534(2)	Cl#2-B-P	108.29(9)
C(1)-H(11)	0.949(18)	C(2)-C(1)-P	115.04(11)
C(1)-H(12)	0.96(2)	C(2)-C(1)-H(11)	111.0(11)
C(2)-C(3)	1.520(2)	P-C(1)-H(11)	108.0(10)
C(2)-H(21)	0.95(3)	C(2)-C(1)-H(12)	109.7(11)
C(2)-H(22)	0.95(2)	P-C(1)-H(12)	106.2(11)
C(3)-C(4)	1.520(3)	H(11)-C(1)-H(12)	106.3(15)
C(3)-H(31)	0.98(2)	C(3)-C(2)-C(1)	111.98(13)
C(3)-H(32)	0.96(2)	C(3)-C(2)-H(21)	109.3(15)
C(4)-H(41)	0.98(3)	C(1)-C(2)-H(21)	109.2(15)
C(4)-H(42)	0.96(2)	C(3)-C(2)-H(22)	108.3(12)
C(4)-H(43)	0.92(3)	C(1)-C(2)-H(22)	110.5(12)
		H(21)-C(2)-H(22)	108(2)
C(1)-P-C(1)#1	107.36(6)	C(4)-C(3)-C(2)	112.47(15)
C(1)-P-C(1)#2	107.36(6)	C(4)-C(3)-H(31)	108.8(12)
C(1)#1-P-C(1)#2	107.36(6)	C(2)-C(3)-H(31)	108.3(13)
C(1)-P-B	111.50(5)	C(4)-C(3)-H(32)	110.7(14)

C(2)-C(3)-H(32)	109.6(14)		H(41)-C(4)-H(43)	105(2)
H(31)-C(3)-H(32)	106.8(18)		H(42)-C(4)-H(43)	113(2)
C(3)-C(4)-H(41)	108.8(15)			
C(3)-C(4)-H(42)	110.9(14)		Symmetry transformations used to generate	
H(41)-C(4)-H(42)	111(2)		equivalent atoms:	
C(3)-C(4)-H(43)	107.7(18)		#1 -x+y+1,-x+1,z	#2 -y+1,x-y,z

Table 4. Anisotropic displacement parameters $(\text{Å}^2\text{x } 10^3)$ for (2d). The anisotropic displacement factor exponent takes the form: $-2\pi^2[h^2 a^{*2}U^{11} + ... + 2 h k a^* b^* U^{12}]$

Atom	U^{11}	U^{22}	U^{33}	U^{23}	U^{13}	U^{12}
Cl	28(1)	25(1)	24(1)	-2(1)	-6(1)	8(1)
P	18(1)	18(1)	17(1)	0	0	9(1)
B	22(1)	22(1)	20(2)	0	0	11(1)
C(1)	19(1)	23(1)	21(1)	1(1)	2(1)	10(1)
C(2)	24(1)	24(1)	33(1)	4(1)	5(1)	13(1)
C(3)	22(1)	28(1)	41(1)	4(1)	5(1)	12(1)
C(4)	29(1)	36(1)	72(2)	5(1)	12(1)	19(1)

Table 5. Hydrogen coordinates (x 10^4) and isotropic displacement parameters $(\text{Å}^2\text{x } 10^{3})$ for (2d).

Atom	x	y	z	U(eq)
H(11)	7950(12)	4023(14)	1210(14)	23(4)
H(12)	8379(14)	4490(15)	2217(14)	22(4)
H(21)	7998(18)	2510(20)	1677(19)	52(6)
H(22)	8462(16)	3009(15)	2674(17)	36(5)
H(31)	9943(19)	4293(19)	1911(15)	38(6)
H(32)	9492(17)	3800(17)	886(19)	50(6)
H(41)	9990(20)	2800(20)	2390(20)	68(8)
H(42)	10665(18)	3280(18)	1420(19)	47(6)
H(43)	9540(20)	2330(20)	1400(20)	74(9)

Table 6. Torsion angles [°] for (**2d**).

C(1)-P-B-Cl#1	-77.31(6)
C(1)#1-P-B-Cl#1	42.69(6)
C(1)#2-P-B-Cl#1	162.69(6)
C(1)-P-B-Cl	42.69(6)
C(1)#1-P-B-Cl	162.69(6)
C(1)#2-P-B-Cl	-77.31(6)
C(1)-P-B-Cl#2	162.69(6)
C(1)#1-P-B-Cl#2	-77.31(6)
C(1)#2-P-B-Cl#2	42.69(6)
C(1)#1-P-C(1)-C(2)	-50.31(18)
C(1)#2-P-C(1)-C(2)	-165.49(10)
B-P-C(1)-C(2)	72.10(13)
P-C(1)-C(2)-C(3)	179.90(12)
C(1)-C(2)-C(3)-C(4)	179.42(17)

Symmetry transformations used to generate equivalent atoms:
#1 -x+y+1,-x+1,z   #2 -y+1,x-y,z

Appendix A2e

Data for the structure of $Cl_3B \cdot P(^tBu)_3$ (**2e**).

Crystals grown by the author. Structure solved by Dr. A. S. Batsanov at the University of Durham Crystallography Department (reference 00srv285).

Table 1. Crystal data and structure refinement for (**2e**).

Identification code	00srv285
Empirical formula	C12 H27 B Cl3 P
Formula weight	319.47
Temperature	110(2) K
Wavelength	0.71073 Å
Crystal system	Monoclinic
Space group	Pc
Unit cell dimensions	$a = 14.7580(11)$ Å $\alpha = 90°$.
	$b = 14.0241(12)$ Å $\beta = 90.093(5)°$.
	$c = 16.0336(14)$ Å $\gamma = 90°$.
Volume	$3318.4(5)$ Å^3
Z	8
Density (calculated)	1.279 Mg/m^3
Absorption coefficient	0.628 mm^{-1}
F(000)	1360
Crystal size	$0.40 \times 0.55 \times 0.85$ mm^3
Theta range for data collection	1.38 to 29.01°.
Index ranges	-20<=h<=19, -18<=k<=19, -21<=l<=21
Reflections collected	39666
Independent reflections	16651 [R(int) = 0.0228]
Completeness to theta = 29.01°	99.7 %
Absorption correction	Integration
Max. and min. transmission	0.8324 and 0.6562
Refinement method	Full-matrix least-squares on F^2
Data / restraints / parameters	16651 / 2 / 722
Goodness-of-fit on F^2	1.092
Final R indices [I>2sigma(I)]	R1 = 0.0247, wR2 = 0.0641
R indices (all data)	R1 = 0.0264, wR2 = 0.0651
Absolute structure parameter	0.29(2)
Largest diff. peak and hole	0.347 and -0.218 e.Å^{-3}

Table 2. Atomic coordinates (x 10^4) and equivalent isotropic displacement parameters (Å^2x 10^3) for (**2e**). U(eq) is defined as one third of the trace of the orthogonalized U^{ij} tensor.

Atom	x	y	z	U(eq)
P(1)	2207(1)	4969(1)	4154(1)	13(1)
Cl(1)	4296(1)	4351(1)	3971(1)	26(1)
Cl(2)	3581(1)	5879(1)	2832(1)	27(1)
Cl(3)	3031(1)	3838(1)	2571(1)	26(1)
B(1)	3288(1)	4747(1)	3372(1)	18(1)
C(1)	2380(1)	6125(1)	4768(1)	19(1)
C(2)	2190(1)	7013(1)	4224(1)	26(1)
C(3)	3378(1)	6207(1)	5053(1)	27(1)
C(4)	1764(1)	6196(1)	5540(1)	24(1)
C(5)	2115(1)	3922(1)	4907(1)	21(1)
C(6)	2829(1)	3981(1)	5612(1)	27(1)
C(7)	2306(1)	2984(1)	4432(1)	28(1)
C(8)	1178(1)	3852(1)	5331(1)	27(1)
C(9)	1128(1)	5061(1)	3499(1)	18(1)
C(10)	797(1)	4074(1)	3194(1)	27(1)
C(11)	332(1)	5517(1)	3981(1)	24(1)
C(12)	1313(1)	5656(1)	2710(1)	24(1)
P(2)	4913(1)	-26(1)	8379(1)	14(1)
Cl(4)	6382(1)	-892(1)	9644(1)	33(1)
Cl(5)	6961(1)	760(1)	8572(1)	27(1)
Cl(6)	5679(1)	1073(1)	9993(1)	32(1)
B(2)	5996(1)	233(1)	9153(1)	21(1)
C(13)	3851(1)	-210(1)	9038(1)	19(1)
C(14)	3472(1)	747(1)	9374(1)	29(1)
C(15)	4075(1)	-823(1)	9808(1)	25(1)
C(16)	3076(1)	-695(1)	8550(1)	22(1)
C(17)	5140(1)	-1144(1)	7740(1)	21(1)
C(18)	5010(1)	-2062(1)	8259(1)	28(1)
C(19)	6136(1)	-1142(1)	7443(1)	30(1)
C(20)	4509(1)	-1228(2)	6965(1)	30(1)
C(21)	4753(1)	1041(1)	7652(1)	24(1)
C(22)	4898(1)	1971(1)	8145(1)	34(1)
C(23)	5459(1)	1045(1)	6939(1)	30(1)
C(24)	3805(1)	1074(2)	7246(1)	34(1)
P(3)	7211(1)	4956(1)	5896(1)	14(1)

Cl(7)	8604(1)	4025(1)	7207(1)	26(1)
Cl(8)	8025(1)	6051(1)	7501(1)	24(1)
Cl(9)	9295(1)	5589(1)	6095(1)	24(1)
B(3)	8294(1)	5162(1)	6684(1)	18(1)
C(25)	7397(1)	3813(1)	5271(1)	18(1)
C(26)	7220(1)	2911(1)	5802(1)	25(1)
C(27)	8393(1)	3750(1)	4988(1)	25(1)
C(28)	6778(1)	3746(1)	4496(1)	23(1)
C(29)	6133(1)	4846(1)	6547(1)	20(1)
C(30)	5796(1)	5823(1)	6862(1)	27(1)
C(31)	5340(1)	4392(1)	6058(1)	26(1)
C(32)	6317(1)	4235(1)	7328(1)	25(1)
C(33)	7113(1)	6011(1)	5152(1)	20(1)
C(34)	7828(1)	5975(1)	4449(1)	25(1)
C(35)	7294(1)	6945(1)	5641(1)	27(1)
C(36)	6171(1)	6087(1)	4731(1)	25(1)
P(4)	9903(1)	-88(1)	6699(1)	14(1)
B(4)	10983(1)	-351(1)	5923(1)	22(1)
Cl(10)	11951(1)	-874(1)	6506(1)	28(1)
Cl(11)	11367(1)	773(1)	5428(1)	37(1)
Cl(12)	10657(1)	-1192(1)	5090(1)	34(1)
C(37)	9743(1)	-1149(1)	7432(1)	21(1)
C(38)	8797(1)	-1170(1)	7838(1)	30(1)
C(39)	9873(1)	-2080(1)	6935(1)	30(1)
C(40)	10451(1)	-1161(1)	8141(1)	29(1)
C(41)	8837(1)	92(1)	6040(1)	18(1)
C(42)	8069(1)	580(1)	6532(1)	21(1)
C(43)	8450(1)	-861(1)	5708(1)	27(1)
C(44)	9060(1)	708(1)	5268(1)	26(1)
C(45)	10134(1)	1035(1)	7335(1)	22(1)
C(46)	10009(1)	1950(1)	6811(1)	31(1)
C(47)	11133(1)	1027(1)	7633(1)	31(1)
C(48)	9512(1)	1125(1)	8109(1)	28(1)

Table 3. Bond lengths [Å] and angles [°] for (2e).

P(1)-C(5)	1.9062(16)	Cl(9)-B(3)	1.8539(18)
P(1)-C(9)	1.9112(15)	C(25)-C(27)	1.542(2)
P(1)-C(1)	1.9130(16)	C(25)-C(28)	1.543(2)
P(1)-B(1)	2.0537(17)	C(25)-C(26)	1.547(2)
Cl(1)-B(1)	1.8531(17)	C(29)-C(30)	1.542(2)
Cl(2)-B(1)	1.8610(19)	C(29)-C(32)	1.542(2)
Cl(3)-B(1)	1.8486(18)	C(29)-C(31)	1.545(2)
C(1)-C(4)	1.540(2)	C(33)-C(34)	1.545(2)
C(1)-C(3)	1.545(2)	C(33)-C(36)	1.548(2)
C(1)-C(2)	1.546(2)	C(33)-C(35)	1.549(2)
C(5)-C(8)	1.544(2)	P(4)-C(45)	1.9074(16)
C(5)-C(7)	1.546(2)	P(4)-C(37)	1.9105(16)
C(5)-C(6)	1.547(2)	P(4)-C(41)	1.9105(15)
C(9)-C(12)	1.540(2)	P(4)-B(4)	2.0571(19)
C(9)-C(11)	1.546(2)	B(4)-Cl(12)	1.845(2)
C(9)-C(10)	1.547(2)	B(4)-Cl(11)	1.854(2)
P(2)-C(17)	1.9032(16)	B(4)-Cl(10)	1.8562(19)
P(2)-C(13)	1.9093(16)	C(37)-C(38)	1.542(2)
P(2)-C(21)	1.9102(16)	C(37)-C(40)	1.542(2)
P(2)-B(2)	2.0552(18)	C(37)-C(39)	1.543(2)
Cl(4)-B(2)	1.852(2)	C(41)-C(42)	1.542(2)
Cl(5)-B(2)	1.8564(19)	C(41)-C(44)	1.546(2)
Cl(6)-B(2)	1.8501(19)	C(41)-C(43)	1.547(2)
C(13)-C(15)	1.540(2)	C(45)-C(46)	1.545(2)
C(13)-C(16)	1.543(2)	C(45)-C(48)	1.549(2)
C(13)-C(14)	1.550(2)	C(45)-C(47)	1.550(2)
C(17)-C(19)	1.546(2)		
C(17)-C(18)	1.545(2)	C(5)-P(1)-C(9)	109.84(7)
C(17)-C(20)	1.556(2)	C(5)-P(1)-C(1)	109.66(7)
C(21)-C(22)	1.540(3)	C(9)-P(1)-C(1)	109.64(7)
C(21)-C(24)	1.542(2)	C(5)-P(1)-B(1)	109.02(8)
C(21)-C(23)	1.548(3)	C(9)-P(1)-B(1)	108.79(7)
P(3)-C(33)	1.9063(16)	C(1)-P(1)-B(1)	109.88(7)
P(3)-C(25)	1.9113(15)	Cl(3)-B(1)-Cl(1)	108.47(9)
P(3)-C(29)	1.9114(16)	Cl(3)-B(1)-Cl(2)	108.16(9)
P(3)-B(3)	2.0554(17)	Cl(1)-B(1)-Cl(2)	108.07(9)
Cl(7)-B(3)	1.8576(19)	Cl(3)-B(1)-P(1)	111.76(9)
Cl(8)-B(3)	1.8523(18)	Cl(1)-B(1)-P(1)	110.66(8)

Cl(2)-B(1)-P(1)	109.61(9)	C(19)-C(17)-P(2)	109.48(11)
C(4)-C(1)-C(3)	108.74(13)	C(18)-C(17)-P(2)	111.96(12)
C(4)-C(1)-C(2)	107.14(14)	C(20)-C(17)-P(2)	112.74(12)
C(3)-C(1)-C(2)	106.19(14)	C(22)-C(21)-C(24)	108.42(15)
C(4)-C(1)-P(1)	112.96(11)	C(22)-C(21)-C(23)	106.44(15)
C(3)-C(1)-P(1)	109.97(11)	C(24)-C(21)-C(23)	107.43(15)
C(2)-C(1)-P(1)	111.57(11)	C(22)-C(21)-P(2)	109.43(12)
C(8)-C(5)-C(7)	109.06(14)	C(24)-C(21)-P(2)	113.10(12)
C(8)-C(5)-C(6)	106.97(14)	C(23)-C(21)-P(2)	111.76(12)
C(7)-C(5)-C(6)	106.28(14)	C(33)-P(3)-C(25)	109.49(7)
C(8)-C(5)-P(1)	113.13(11)	C(33)-P(3)-C(29)	109.97(7)
C(7)-C(5)-P(1)	109.29(11)	C(25)-P(3)-C(29)	109.82(7)
C(6)-C(5)-P(1)	111.84(12)	C(33)-P(3)-B(3)	109.48(7)
C(12)-C(9)-C(11)	108.85(13)	C(25)-P(3)-B(3)	109.19(7)
C(12)-C(9)-C(10)	106.35(13)	C(29)-P(3)-B(3)	108.87(7)
C(11)-C(9)-C(10)	106.73(14)	Cl(8)-B(3)-Cl(9)	108.37(9)
C(12)-C(9)-P(1)	109.83(11)	Cl(8)-B(3)-Cl(7)	108.11(9)
C(11)-C(9)-P(1)	112.72(11)	Cl(9)-B(3)-Cl(7)	108.16(9)
C(10)-C(9)-P(1)	112.10(11)	Cl(8)-B(3)-P(3)	111.21(9)
C(17)-P(2)-C(13)	109.42(7)	Cl(9)-B(3)-P(3)	110.62(8)
C(17)-P(2)-C(21)	109.78(8)	Cl(7)-B(3)-P(3)	110.28(9)
C(13)-P(2)-C(21)	110.05(7)	C(27)-C(25)-C(28)	108.84(13)
C(17)-P(2)-B(2)	109.44(8)	C(27)-C(25)-C(26)	106.08(14)
C(13)-P(2)-B(2)	109.14(7)	C(28)-C(25)-C(26)	107.10(13)
C(21)-P(2)-B(2)	109.00(8)	C(27)-C(25)-P(3)	109.84(10)
Cl(6)-B(2)-Cl(4)	108.12(9)	C(28)-C(25)-P(3)	112.83(11)
Cl(6)-B(2)-Cl(5)	107.90(10)	C(26)-C(25)-P(3)	111.87(11)
Cl(4)-B(2)-Cl(5)	108.47(10)	C(30)-C(29)-C(32)	106.52(13)
Cl(6)-B(2)-P(2)	110.79(9)	C(30)-C(29)-C(31)	106.82(14)
Cl(4)-B(2)-P(2)	110.13(9)	C(32)-C(29)-C(31)	108.38(14)
Cl(5)-B(2)-P(2)	111.32(9)	C(30)-C(29)-P(3)	112.12(12)
C(15)-C(13)-C(16)	108.56(13)	C(32)-C(29)-P(3)	110.01(11)
C(15)-C(13)-C(14)	106.42(14)	C(31)-C(29)-P(3)	112.72(11)
C(16)-C(13)-C(14)	106.85(14)	C(34)-C(33)-C(36)	107.30(14)
C(15)-C(13)-P(2)	110.12(11)	C(34)-C(33)-C(35)	106.23(14)
C(16)-C(13)-P(2)	112.74(11)	C(36)-C(33)-C(35)	108.45(14)
C(14)-C(13)-P(2)	111.87(11)	C(34)-C(33)-P(3)	112.31(11)
C(19)-C(17)-C(18)	106.68(15)	C(36)-C(33)-P(3)	113.17(11)
C(19)-C(17)-C(20)	108.79(14)	C(35)-C(33)-P(3)	109.09(11)
C(18)-C(17)-C(20)	106.96(14)	C(45)-P(4)-C(37)	109.62(8)

C(45)-P(4)-C(41)	109.43(7)	C(42)-C(41)-C(44)	108.59(13)
C(37)-P(4)-C(41)	109.94(7)	C(42)-C(41)-C(43)	106.73(14)
C(45)-P(4)-B(4)	109.49(8)	C(44)-C(41)-C(43)	106.66(14)
C(37)-P(4)-B(4)	109.22(8)	C(42)-C(41)-P(4)	112.40(10)
C(41)-P(4)-B(4)	109.12(7)	C(44)-C(41)-P(4)	109.95(11)
Cl(12)-B(4)-Cl(11)	108.24(9)	C(43)-C(41)-P(4)	112.27(11)
Cl(12)-B(4)-Cl(10)	108.14(10)	C(46)-C(45)-C(48)	107.37(14)
Cl(11)-B(4)-Cl(10)	108.45(10)	C(46)-C(45)-C(47)	106.63(15)
Cl(12)-B(4)-P(4)	110.54(10)	C(48)-C(45)-C(47)	108.62(15)
Cl(11)-B(4)-P(4)	110.11(9)	C(46)-C(45)-P(4)	111.94(12)
Cl(10)-B(4)-P(4)	111.27(9)	C(48)-C(45)-P(4)	112.94(12)
C(38)-C(37)-C(40)	107.58(14)	C(47)-C(45)-P(4)	109.10(11)
C(38)-C(37)-C(39)	108.38(15)		
C(40)-C(37)-C(39)	106.65(14)		
C(38)-C(37)-P(4)	112.80(11)		
C(40)-C(37)-P(4)	112.20(12)	Symmetry transformations used to generate
C(39)-C(37)-P(4)	108.98(12)	equivalent atoms:

Table 4. Anisotropic displacement parameters (Å^2x 10^3) for (2e). The anisotropic displacement factor exponent takes the form: $-2\pi^2[$ h^2 $a^{*2}U^{11}$ + ... + 2 h k a^* b^* U^{12}]

Atom	U^{11}	U^{22}	U^{33}	U^{23}	U^{13}	U^{12}
P(1)	12(1)	14(1)	13(1)	0(1)	0(1)	0(1)
Cl(1)	16(1)	37(1)	24(1)	-7(1)	-3(1)	6(1)
Cl(2)	25(1)	31(1)	26(1)	3(1)	10(1)	-4(1)
Cl(3)	24(1)	32(1)	21(1)	-11(1)	-2(1)	5(1)
B(1)	12(1)	24(1)	19(1)	-2(1)	2(1)	1(1)
C(1)	19(1)	18(1)	20(1)	-4(1)	2(1)	-1(1)
C(2)	32(1)	16(1)	31(1)	0(1)	7(1)	1(1)
C(3)	20(1)	30(1)	30(1)	-10(1)	-1(1)	-6(1)
C(4)	25(1)	28(1)	21(1)	-6(1)	4(1)	2(1)
C(5)	25(1)	18(1)	20(1)	5(1)	1(1)	1(1)
C(6)	29(1)	32(1)	21(1)	6(1)	-3(1)	6(1)
C(7)	34(1)	16(1)	34(1)	2(1)	0(1)	2(1)
C(8)	25(1)	29(1)	29(1)	9(1)	5(1)	-4(1)
C(9)	14(1)	24(1)	18(1)	0(1)	-1(1)	0(1)
C(10)	21(1)	31(1)	29(1)	-7(1)	-7(1)	-5(1)
C(11)	16(1)	36(1)	21(1)	0(1)	0(1)	4(1)
C(12)	22(1)	32(1)	17(1)	4(1)	0(1)	6(1)

P(2)	12(1)	15(1)	14(1)	0(1)	2(1)	0(1)
Cl(4)	26(1)	37(1)	35(1)	10(1)	-12(1)	1(1)
Cl(5)	17(1)	39(1)	25(1)	-2(1)	3(1)	-7(1)
Cl(6)	32(1)	40(1)	23(1)	-13(1)	6(1)	-14(1)
B(2)	20(1)	27(1)	17(1)	0(1)	-1(1)	-5(1)
C(13)	15(1)	22(1)	19(1)	1(1)	3(1)	-2(1)
C(14)	22(1)	29(1)	35(1)	-6(1)	10(1)	2(1)
C(15)	22(1)	35(1)	17(1)	5(1)	2(1)	-7(1)
C(16)	14(1)	30(1)	22(1)	3(1)	0(1)	-4(1)
C(17)	19(1)	20(1)	24(1)	-7(1)	4(1)	-1(1)
C(18)	27(1)	17(1)	41(1)	-3(1)	4(1)	0(1)
C(19)	24(1)	31(1)	35(1)	-12(1)	8(1)	1(1)
C(20)	29(1)	40(1)	22(1)	-9(1)	3(1)	-11(1)
C(21)	22(1)	23(1)	26(1)	10(1)	-1(1)	-1(1)
C(22)	32(1)	19(1)	49(1)	7(1)	8(1)	2(1)
C(23)	27(1)	38(1)	25(1)	12(1)	2(1)	-7(1)
C(24)	23(1)	40(1)	37(1)	20(1)	-5(1)	2(1)
P(3)	12(1)	15(1)	13(1)	-1(1)	1(1)	0(1)
Cl(7)	25(1)	29(1)	25(1)	2(1)	-8(1)	3(1)
Cl(8)	22(1)	31(1)	19(1)	-10(1)	3(1)	-4(1)
Cl(9)	14(1)	34(1)	23(1)	-6(1)	4(1)	-5(1)
B(3)	15(1)	22(1)	17(1)	-2(1)	1(1)	-1(1)
C(25)	20(1)	15(1)	19(1)	-4(1)	-1(1)	0(1)
C(26)	30(1)	16(1)	29(1)	0(1)	-3(1)	-2(1)
C(27)	22(1)	24(1)	29(1)	-9(1)	2(1)	5(1)
C(28)	25(1)	23(1)	20(1)	-6(1)	-2(1)	-2(1)
C(29)	15(1)	28(1)	16(1)	-2(1)	3(1)	-2(1)
C(30)	20(1)	35(1)	27(1)	-8(1)	7(1)	4(1)
C(31)	16(1)	40(1)	23(1)	-1(1)	1(1)	-6(1)
C(32)	22(1)	38(1)	16(1)	3(1)	1(1)	-8(1)
C(33)	22(1)	16(1)	21(1)	2(1)	0(1)	-1(1)
C(34)	28(1)	26(1)	22(1)	4(1)	4(1)	-6(1)
C(35)	31(1)	18(1)	32(1)	-2(1)	0(1)	0(1)
C(36)	24(1)	26(1)	26(1)	6(1)	-4(1)	4(1)
P(4)	13(1)	14(1)	14(1)	0(1)	0(1)	0(1)
B(4)	18(1)	30(1)	20(1)	0(1)	2(1)	5(1)
Cl(10)	16(1)	41(1)	27(1)	-3(1)	-2(1)	8(1)
Cl(11)	28(1)	43(1)	40(1)	14(1)	17(1)	1(1)
Cl(12)	32(1)	47(1)	23(1)	-14(1)	-5(1)	17(1)
C(37)	21(1)	20(1)	24(1)	6(1)	-1(1)	1(1)

C(38)	23(1)	34(1)	31(1)	15(1)	5(1)	-1(1)
C(39)	30(1)	17(1)	43(1)	4(1)	-5(1)	2(1)
C(40)	28(1)	37(1)	22(1)	8(1)	-3(1)	7(1)
C(41)	15(1)	22(1)	17(1)	1(1)	-3(1)	3(1)
C(42)	15(1)	28(1)	21(1)	3(1)	1(1)	4(1)
C(43)	23(1)	27(1)	32(1)	-8(1)	-9(1)	1(1)
C(44)	25(1)	34(1)	19(1)	6(1)	2(1)	8(1)
C(45)	19(1)	19(1)	27(1)	-8(1)	0(1)	-2(1)
C(46)	28(1)	16(1)	48(1)	-3(1)	1(1)	-3(1)
C(47)	23(1)	31(1)	39(1)	-13(1)	-6(1)	-3(1)
C(48)	28(1)	33(1)	24(1)	-10(1)	-2(1)	6(1)

Table 5. Hydrogen coordinates (x 10^4) and isotropic displacement parameters ($Å^2$x 10^3) for (**2e**).

Atom	x	y	z	U(eq)
H(21)	2325(9)	7585(7)	4541(5)	34(3)
H(22)	1556(8)	7017(5)	4060(7)	34(3)
H(23)	2567(8)	6993(5)	3729(8)	34(3)
H(31)	3778(6)	6215(10)	4558(7)	37(4)
H(32)	3535(4)	5656(9)	5410(9)	37(4)
H(33)	3459(3)	6805(9)	5373(9)	37(4)
H(41)	1858(7)	6803(9)	5809(6)	36(4)
H(42)	1910(7)	5689(9)	5924(7)	36(4)
H(43)	1139(9)	6141(10)	5371(3)	36(4)
H(61)	2704(6)	4550(10)	5971(7)	40(4)
H(62)	3448(9)	4041(10)	5360(4)	40(4)
H(63)	2801(7)	3388(9)	5959(7)	40(4)
H(71)	2230(9)	2448(7)	4806(5)	36(4)
H(72)	2920(9)	2993(4)	4223(8)	36(4)
H(73)	1888(8)	2925(5)	3970(8)	36(4)
H(81)	1188(3)	3344(10)	5736(8)	37(4)
H(82)	720(7)	3721(10)	4916(6)	37(4)
H(83)	1042(5)	4447(9)	5606(8)	37(4)
H(101)	265(9)	4161(2)	2789(8)	34(3)
H(102)	590(9)	3675(6)	3695(6)	34(3)
H(103)	1317(7)	3731(6)	2896(8)	34(3)
H(111)	491(4)	6189(9)	4135(8)	33(3)
H(112)	213(6)	5139(8)	4501(8)	33(3)
H(113)	-225(8)	5517(9)	3622(6)	33(3)

H(121)	1751(9)	5338(6)	2373(6)	30(3)
H(122)	1538(9)	6268(9)	2866(2)	30(3)
H(123)	764(7)	5729(8)	2402(6)	30(3)
H(141)	2976(9)	624(2)	9739(9)	36(4)
H(142)	3270(9)	1129(7)	8918(6)	36(4)
H(143)	3937(7)	1076(7)	9670(9)	36(4)
H(151)	3525(7)	-917(8)	10139(6)	29(3)
H(152)	4533(9)	-499(6)	10147(6)	29(3)
H(153)	4309(9)	-1444(9)	9628(2)	29(3)
H(161)	3244(4)	-1313(9)	8414(8)	31(3)
H(162)	2961(6)	-354(7)	8064(8)	31(3)
H(163)	2558(8)	-709(9)	8876(5)	31(3)
H(181)	5200(9)	-2605(7)	7938(5)	39(4)
H(182)	4380(9)	-2130(5)	8404(8)	39(4)
H(183)	5368(9)	-2020(4)	8760(8)	39(4)
H(191)	6521(6)	-1144(10)	7905(7)	39(4)
H(192)	6245(3)	-597(9)	7123(9)	39(4)
H(193)	6245(3)	-1684(9)	7120(9)	39(4)
H(201)	4623(6)	-1822(9)	6687(6)	28(3)
H(202)	4627(7)	-710(8)	6590(6)	28(3)
H(203)	3889(8)	-1206(9)	7141(3)	28(3)
H(221)	5492(9)	1999(5)	8337(8)	43(4)
H(222)	4504(9)	1985(5)	8598(9)	43(4)
H(223)	4783(10)	2491(8)	7801(6)	43(4)
H(231)	5381(6)	499(9)	6610(7)	40(4)
H(232)	6044(9)	1048(10)	7165(3)	40(4)
H(233)	5376(6)	1590(9)	6610(7)	40(4)
H(241)	3775(3)	1599(10)	6875(8)	36(4)
H(242)	3359(7)	1144(10)	7665(6)	36(4)
H(243)	3701(4)	501(9)	6948(8)	36(4)
H(261)	6584(8)	2857(5)	5920(7)	34(3)
H(262)	7553(8)	2958(5)	6317(8)	34(3)
H(263)	7418(9)	2357(7)	5499(5)	34(3)
H(271)	8486(3)	3153(9)	4668(9)	37(4)
H(272)	8793(6)	3751(10)	5484(7)	37(4)
H(273)	8540(4)	4305(9)	4630(9)	37(4)
H(281)	6915(6)	4252(9)	4124(6)	29(3)
H(282)	6162(8)	3791(10)	4663(2)	29(3)
H(283)	6875(7)	3154(9)	4225(6)	29(3)
H(301)	5270(9)	5731(2)	7232(9)	38(4)
H(302)	5618(10)	6221(7)	6382(6)	38(4)
H(303)	6287(7)	6142(6)	7174(9)	38(4)
H(311)	5502(4)	3729(9)	5906(7)	30(3)
H(312)	5222(6)	4764(7)	5545(8)	30(3)
H(313)	4790(7)	4388(9)	6410(5)	30(3)

H(321)	6758(8)	4548(6)	7676(6)	23(3)
H(322)	6545(8)	3621(8)	7161(2)	23(3)
H(323)	5763(7)	4153(7)	7635(6)	23(3)
H(341)	7690(6)	5437(10)	4072(7)	38(4)
H(342)	8436(9)	5886(10)	4695(4)	38(4)
H(343)	7813(7)	6578(9)	4131(7)	38(4)
H(351)	7916(8)	6946(4)	5849(7)	32(3)
H(352)	6875(8)	6985(5)	6109(8)	32(3)
H(353)	7204(9)	7491(7)	5273(5)	32(3)
H(361)	6168(3)	6602(10)	4363(8)	37(4)
H(362)	5729(7)	6178(10)	5139(6)	37(4)
H(363)	6048(5)	5526(9)	4438(8)	37(4)
H(381)	8379(6)	-1249(10)	7447(6)	34(4)
H(382)	8700(4)	-625(9)	8102(8)	34(4)
H(383)	8768(3)	-1647(9)	8198(8)	34(4)
H(391)	9720(10)	-2616(8)	7282(6)	38(4)
H(392)	10493(9)	-2133(5)	6759(8)	38(4)
H(393)	9484(9)	-2073(5)	6453(8)	38(4)
H(401)	10367(6)	-605(9)	8496(7)	30(3)
H(402)	11056(8)	-1148(10)	7901(3)	30(3)
H(403)	10377(6)	-1738(9)	8471(7)	30(3)
H(421)	7555(7)	609(8)	6206(5)	24(3)
H(422)	8244(4)	1188(8)	6677(7)	24(3)
H(423)	7949(6)	234(7)	7007(7)	24(3)
H(431)	8257(10)	-1218(7)	6139(6)	37(4)
H(432)	8885(7)	-1177(7)	5430(9)	37(4)
H(433)	7983(9)	-742(2)	5363(9)	37(4)
H(441)	8519(7)	799(7)	4940(6)	24(3)
H(442)	9512(8)	392(6)	4935(6)	24(3)
H(443)	9287(8)	1318(8)	5447(2)	24(3)
H(461)	10175(9)	2482(7)	7128(5)	40(4)
H(462)	9401(9)	2006(5)	6649(8)	40(4)
H(463)	10375(9)	1914(5)	6335(8)	40(4)
H(471)	11518(6)	1023(10)	7167(7)	36(4)
H(472)	11242(3)	480(9)	7956(9)	36(4)
H(473)	11247(3)	1574(9)	7954(9)	36(4)
H(481)	9609(7)	585(9)	8475(7)	35(4)
H(482)	8885(9)	1136(10)	7929(3)	35(4)
H(483)	9651(7)	1709(9)	8405(6)	35(4)

Appendix A2f

$Cl_3B \cdot PCy_3$ (**2f**).

Crystals grown by F. E. S. Souza. Structure solved by Dr. A. Churakov at the University

of Durham Crystallography Department (reference code 97srv146).

Data tables not included, since I was not involved in the structure solution.

Appendix A2g

Structure of $Cl_3B \cdot PMe_2Ph$ (**2g**).

Crystals grown by F. E. S. Souza. Structure solved by Dr. A. Churakov at the University

of Durham Crystallography Department (reference code 97srv145).

Data tables not included, since I was not involved in the structure solution.

Appendix A2i

Structure of $Cl_3B \cdot PPh_3$ (**2i**).

Crystals grown by F. E. S. Souza. Structure solved by Dr. C. W. Lehman at the

University of Durham Crystallography Department (reference code 97srv148).

Data tables not included, since I was not involved in the structure solution.

Appendix A2bb

Data for the structure of $Br_3B \cdot PEt_3$ (**2bb**).

Crystals grown by the author. Structure solved by Dr. D. S. Yufit at the University of Durham Crystallography Department (reference code 00srv287).

Table 1. Crystal data and structure refinement for (**2bb**).

Identification code	s287s
Empirical formula	C6 H15 B Br3 P
Formula weight	368.69
Temperature	110.0(2) K
Wavelength	0.71073 Å
Crystal system	Orthorhombic
Space group	P 212121
Unit cell dimensions	a = 7.2464(2) Å α= 90°.
	b = 12.2020(3) Å β= 90°.
	c = 13.7193(4) Å γ = 90°.
Volume	1213.1(1) Å^3
Z	4
Density (calculated)	2.019 Mg/m^3
Absorption coefficient	10.055 mm^{-1}
F(000)	704
Crystal size	0.61 x 0.06 x 0.04 mm^3
Theta range for data collection	2.23 to 30.18°.
Index ranges	-10<=h<=9, -17<=k<=17, -19<=l<=19
Reflections collected	14311
Independent reflections	3299 [R(int) = 0.0386]
Completeness to theta = 30.18°	94.2 %
Absorption correction	Semi-empirical from equivalents
Max. and min. transmission	0.6892 and 0.0636
Refinement method	Full-matrix least-squares on F^2
Data / restraints / parameters	3299 / 1 / 161
Goodness-of-fit on F^2	1.039
Final R indices [I>2sigma(I)]	R1 = 0.0240, wR2 = 0.0495
R indices (all data)	R1 = 0.0300, wR2 = 0.0514
Absolute structure parameter	0.49(1)
Largest diff. peak and hole	0.497 and -0.388 e.Å^{-3}

Table 2. Atomic coordinates (x 10^4) and equivalent isotropic displacement parameters (Å^2x 10^3) for (2bb). U(eq) is defined as one third of the trace of the orthogonalized U^{ij} tensor.

Atom	x	y	z	U(eq)
Br(1)	1971(1)	-1162(1)	2681(1)	26(1)
Br(2)	1766(1)	1531(1)	2475(1)	23(1)
Br(3)	808(1)	-37(1)	574(1)	20(1)
P(1)	4977(1)	144(1)	1361(1)	14(1)
B(1)	2381(5)	129(3)	1785(2)	16(1)
C(1)	5865(5)	-1229(3)	1165(3)	23(1)
C(2)	4809(6)	-1926(3)	427(3)	30(1)
C(3)	6490(5)	803(3)	2236(2)	20(1)
C(4)	6676(7)	214(4)	3209(3)	35(1)
C(5)	5286(5)	887(3)	229(3)	19(1)
C(6)	4630(6)	2079(3)	245(3)	26(1)

Table 3. Bond lengths [Å] and angles [°] for (2bb).

Br(1)-B(1)	2.020(3)	C(3)-P(1)-B(1)	112.72(15)
Br(2)-B(1)	2.005(3)	C(1)-P(1)-B(1)	111.94(16)
Br(3)-B(1)	2.026(3)	P(1)-B(1)-Br(2)	110.08(17)
P(1)-C(5)	1.812(3)	P(1)-B(1)-Br(1)	109.13(16)
P(1)-C(3)	1.813(3)	Br(2)-B(1)-Br(1)	110.25(15)
P(1)-C(1)	1.815(3)	P(1)-B(1)-Br(3)	107.21(15)
P(1)-B(1)	1.970(3)	Br(2)-B(1)-Br(3)	110.32(16)
C(1)-C(2)	1.528(5)	Br(1)-B(1)-Br(3)	109.80(16)
C(3)-C(4)	1.522(5)	C(2)-C(1)-P(1)	115.8(3)
C(5)-C(6)	1.530(5)	C(4)-C(3)-P(1)	115.1(3)
		C(6)-C(5)-P(1)	115.1(3)

C(5)-P(1)-C(3)	105.70(17)
C(5)-P(1)-C(1)	106.89(16)
C(3)-P(1)-C(1)	107.05(17)
C(5)-P(1)-B(1)	112.10(16)

Symmetry transformations used to generate equivalent atoms:

Table 4.   Anisotropic displacement parameters (Å^2x 10^3) for (2bb). The anisotropic displacement factor exponent takes the form: $-2\pi^2[\ h^2\ a^{*2}U^{11} + ... + 2\ h\ k\ a^*\ b^*\ U^{12}\ ]$

Atom	U^{11}	U^{22}	U^{33}	U^{23}	U^{13}	U^{12}
Br(1)	27(1)	23(1)	28(1)	9(1)	8(1)	-1(1)
Br(2)	19(1)	20(1)	29(1)	-10(1)	2(1)	0(1)
Br(3)	16(1)	22(1)	23(1)	-4(1)	-4(1)	-1(1)
P(1)	13(1)	14(1)	16(1)	1(1)	0(1)	1(1)
B(1)	16(2)	14(2)	17(2)	0(1)	0(1)	1(1)
C(1)	19(2)	17(2)	33(2)	2(1)	4(2)	3(1)
C(2)	34(2)	18(2)	38(2)	-9(2)	8(2)	-1(2)
C(3)	17(2)	24(2)	20(2)	-4(1)	-2(1)	1(1)
C(4)	33(2)	54(3)	19(2)	2(2)	-8(2)	-3(2)
C(5)	17(2)	20(2)	19(2)	4(1)	0(1)	0(1)
C(6)	23(2)	24(2)	30(2)	9(1)	-1(2)	0(1)

Table 5.   Hydrogen coordinates (x 10^4) and isotropic displacement parameters (Å^2x 10 ^{3}) for (2bb).

Atom	x	y	z	U(eq)
H(11)	5920(60)	-1590(30)	1780(30)	43(12)
H(12)	7150(60)	-1100(30)	950(30)	30(11)
H(21)	5470(80)	-2710(30)	350(50)	100(20)
H(22)	3440(70)	-2090(30)	660(30)	47(13)
H(23)	4550(70)	-1590(30)	-290(30)	48(13)
H(31)	7640(50)	890(30)	1910(20)	12(9)
H(32)	5910(50)	1520(30)	2310(30)	30(10)
H(41)	5650(60)	220(30)	3500(30)	34(12)
H(42)	7190(70)	-490(40)	3260(40)	71(18)
H(43)	7440(60)	660(30)	3620(30)	39(12)
H(51)	6430(60)	880(30)	130(30)	23(10)
H(52)	4670(50)	580(30)	-180(30)	20(10)
H(61)	3360(70)	2100(30)	420(30)	37(12)
H(62)	5270(60)	2460(30)	730(30)	36(12)
H(63)	4850(50)	2380(30)	-440(30)	32(11)

Table 6. Torsion angles [°] for (**2bb**).

C(5)-P(1)-B(1)-Br(2)	-81.8(2)
C(3)-P(1)-B(1)-Br(2)	37.4(2)
C(1)-P(1)-B(1)-Br(2)	158.11(16)
C(5)-P(1)-B(1)-Br(1)	157.10(16)
C(3)-P(1)-B(1)-Br(1)	-83.8(2)
C(1)-P(1)-B(1)-Br(1)	37.0(2)
C(5)-P(1)-B(1)-Br(3)	38.2(2)
C(3)-P(1)-B(1)-Br(3)	157.37(16)
C(1)-P(1)-B(1)-Br(3)	-81.9(2)
C(5)-P(1)-C(1)-C(2)	-65.7(3)
C(3)-P(1)-C(1)-C(2)	-178.6(3)
B(1)-P(1)-C(1)-C(2)	57.4(3)
C(5)-P(1)-C(3)-C(4)	-171.5(3)
C(1)-P(1)-C(3)-C(4)	-57.8(3)
B(1)-P(1)-C(3)-C(4)	65.7(3)
C(3)-P(1)-C(5)-C(6)	-65.8(3)
C(1)-P(1)-C(5)-C(6)	-179.6(3)
B(1)-P(1)-C(5)-C(6)	57.4(3)

Symmetry transformations used to generate equivalent atoms:

Appendix A2ii

Structure of $Br_3B \cdot PPh_3$ (**2ii**).

Crystals grown by F. E. S. Souza. Structure solved by Dr. W. Clegg at the University of Newcastle-upon-Tyne

Data tables not included, since I was not involved in the structure solution.

Appendix A2jj

Data for the structure of $Br_3B \cdot P(o\text{-tolyl})_3$ (**2jj**).

Crystals grown and structure solved by the author at the University of Durham Crystallography Department (reference code 01jmb004).

Table 1. Crystal data and structure refinement for (**2jj**).

Identification code	01jmb004
Empirical formula	C21 H21 B Br3 P
Formula weight	554.89
Temperature	110(2) K
Wavelength	0.71073 Å
Crystal system	Orthorhombic
Space group	Pna2(1)
Unit cell dimensions	a = 20.4261(12) Å α= 90°.
	b = 10.1260(6) Å β= 90°.
	c = 10.2236(6) Å γ = 90°.
Volume	2114.6(2) $Å^3$
Z	4
Density (calculated)	1.743 Mg/m^3
Absorption coefficient	5.802 mm^{-1}
F(000)	1088
Crystal size	0.10 x 0.10 x 0.05 mm^3
Theta range for data collection	1.99 to 27.51°.
Index ranges	-26<=h<=26, -13<=k<=13, -13<=l<=13
Reflections collected	21944
Independent reflections	4873 [R(int) = 0.0682]
Completeness to theta = 27.51°	100.0 %
Absorption correction	Semi-empirical from equivalents
Max. and min. transmission	0.746 and 0.595
Refinement method	Full-matrix least-squares on F^2
Data / restraints / parameters	4873 / 1 / 236
Goodness-of-fit on F^2	1.071
Final R indices [I>2sigma(I)]	R1 = 0.0355, wR2 = 0.0676
R indices (all data)	R1 = 0.0419, wR2 = 0.0698
Absolute structure parameter	0.028(10)
Largest diff. peak and hole	0.522 and -0.516 e.$Å^{-3}$

Table 2. Atomic coordinates (x 10^4) and equivalent isotropic displacement parameters ($Å^2$x 10^3) for (**2jj**). U(eq) is defined as one third of the trace of the orthogonalized U^{ij} tensor.

	x	y	z	U(eq)
Br(1)	7938(1)	2013(1)	2610(1)	15(1)
Br(2)	7810(1)	4143(1)	197(1)	15(1)
Br(3)	9001(1)	4431(1)	2345(1)	15(1)
P(1)	9027(1)	1966(1)	197(1)	11(1)
B(1)	8446(3)	3141(6)	1335(6)	14(1)
C(11)	9893(2)	2068(4)	627(5)	12(1)
C(12)	10338(2)	2328(5)	-385(5)	18(1)
C(13)	11008(2)	2437(5)	-144(5)	21(1)
C(14)	11228(2)	2298(5)	1133(5)	20(1)
C(15)	10792(2)	2022(4)	2130(5)	16(1)
C(16)	10126(2)	1863(4)	1902(4)	12(1)
C(17)	9709(2)	1423(5)	3038(5)	17(1)
C(21)	8975(2)	2401(5)	-1527(4)	12(1)
C(22)	8809(2)	1417(5)	-2419(5)	16(1)
C(23)	8754(2)	1684(5)	-3736(5)	21(1)
C(24)	8868(2)	2939(5)	-4188(5)	24(1)
C(25)	9055(2)	3933(5)	-3322(5)	20(1)
C(26)	9118(2)	3684(5)	-1986(5)	15(1)
C(27)	9329(2)	4815(5)	-1131(5)	19(1)
C(31)	8799(2)	224(4)	354(4)	10(1)
C(32)	9288(2)	-656(5)	768(4)	12(1)
C(33)	9142(2)	-1965(5)	1016(4)	17(1)
C(34)	8507(2)	-2416(5)	858(5)	18(1)
C(35)	8028(2)	-1556(5)	408(5)	20(1)
C(36)	8161(2)	-237(5)	127(5)	16(1)
C(37)	7607(2)	573(5)	-424(5)	20(1)

Table 3. Bond lengths [Å] and angles [°] for (**2jj**).

Br(1)-B(1)	2.021(6)	Br(2)-B(1)-Br(1)	109.0(2)
Br(2)-B(1)	2.018(6)	Br(3)-B(1)-P(1)	110.1(2)
Br(3)-B(1)	2.014(6)	Br(2)-B(1)-P(1)	109.8(3)
P(1)-C(21)	1.820(5)	Br(1)-B(1)-P(1)	109.6(3)
P(1)-C(11)	1.825(4)	C(12)-C(11)-C(16)	119.5(4)
P(1)-C(31)	1.831(4)	C(12)-C(11)-P(1)	117.5(4)
P(1)-B(1)	2.044(6)	C(16)-C(11)-P(1)	123.0(3)
C(11)-C(12)	1.403(6)	C(13)-C(12)-C(11)	121.3(5)
C(11)-C(16)	1.404(6)	C(14)-C(13)-C(12)	118.5(5)
C(12)-C(13)	1.395(7)	C(15)-C(14)-C(13)	120.4(4)
C(13)-C(14)	1.388(7)	C(14)-C(15)-C(16)	122.0(5)
C(14)-C(15)	1.382(7)	C(15)-C(16)-C(11)	118.1(4)
C(15)-C(16)	1.390(6)	C(15)-C(16)-C(17)	117.3(4)
C(16)-C(17)	1.508(6)	C(11)-C(16)-C(17)	124.5(4)
C(21)-C(22)	1.393(7)	C(22)-C(21)-C(26)	119.5(4)
C(21)-C(26)	1.412(7)	C(22)-C(21)-P(1)	118.3(4)
C(22)-C(23)	1.378(7)	C(26)-C(21)-P(1)	122.2(4)
C(23)-C(24)	1.373(7)	C(23)-C(22)-C(21)	121.3(5)
C(24)-C(25)	1.393(8)	C(24)-C(23)-C(22)	119.8(5)
C(25)-C(26)	1.395(7)	C(23)-C(24)-C(25)	120.1(5)
C(26)-C(27)	1.504(7)	C(24)-C(25)-C(26)	121.1(5)
C(31)-C(36)	1.403(6)	C(25)-C(26)-C(21)	118.2(5)
C(31)-C(32)	1.404(6)	C(25)-C(26)-C(27)	117.3(5)
C(32)-C(33)	1.382(6)	C(21)-C(26)-C(27)	124.5(4)
C(33)-C(34)	1.385(7)	C(36)-C(31)-C(32)	120.0(4)
C(34)-C(35)	1.388(7)	C(36)-C(31)-P(1)	122.8(3)
C(35)-C(36)	1.393(6)	C(32)-C(31)-P(1)	117.2(3)
C(36)-C(37)	1.508(7)	C(33)-C(32)-C(31)	120.7(4)
		C(32)-C(33)-C(34)	119.8(5)
C(21)-P(1)-C(11)	106.0(2)	C(33)-C(34)-C(35)	119.4(5)
C(21)-P(1)-C(31)	107.7(2)	C(34)-C(35)-C(36)	122.2(4)
C(11)-P(1)-C(31)	106.3(2)	C(35)-C(36)-C(31)	117.7(4)
C(21)-P(1)-B(1)	112.1(2)	C(35)-C(36)-C(37)	116.9(4)
C(11)-P(1)-B(1)	113.1(2)	C(31)-C(36)-C(37)	125.3(4)
C(31)-P(1)-B(1)	111.3(2)		
Br(3)-B(1)-Br(2)	109.4(3)	Symmetry transformations used to generate
Br(3)-B(1)-Br(1)	109.0(3)	equivalent atoms:

Table 4. Anisotropic displacement parameters (Å^2x 10^3) for (**2jj**). The anisotropic displacement factor exponent takes the form: $-2\pi^2[\ h^2\ a^{*2}U^{11} + ... + 2\ h\ k\ a^*\ b^*\ U^{12}\ ]$

	U^{11}	U^{22}	U^{33}	U^{23}	U^{13}	U^{12}
Br(1)	14(1)	19(1)	12(1)	2(1)	2(1)	-1(1)
Br(2)	12(1)	15(1)	18(1)	2(1)	-2(1)	2(1)
Br(3)	17(1)	13(1)	13(1)	-2(1)	-3(1)	-1(1)
P(1)	12(1)	12(1)	9(1)	1(1)	-1(1)	0(1)
B(1)	11(2)	19(3)	13(2)	2(2)	3(2)	0(2)
C(11)	7(2)	11(2)	18(2)	-3(2)	3(2)	0(2)
C(12)	16(2)	22(3)	15(2)	-2(2)	2(2)	0(2)
C(13)	11(2)	29(3)	23(3)	-1(2)	10(2)	-2(2)
C(14)	11(2)	18(3)	30(3)	-3(2)	-4(2)	-2(2)
C(15)	13(2)	16(2)	17(2)	-2(2)	-4(2)	3(2)
C(16)	18(2)	7(2)	12(2)	-4(2)	1(2)	3(2)
C(17)	21(2)	18(3)	13(2)	0(2)	-3(2)	0(2)
C(21)	10(2)	16(2)	9(2)	4(2)	3(2)	6(2)
C(22)	16(2)	17(2)	16(2)	4(2)	5(2)	2(2)
C(23)	22(3)	25(3)	16(3)	-4(2)	-5(2)	4(2)
C(24)	22(3)	34(3)	14(3)	3(2)	-4(2)	12(2)
C(25)	23(3)	18(3)	18(3)	8(2)	3(2)	7(2)
C(26)	14(2)	16(3)	14(2)	2(2)	5(2)	3(2)
C(27)	22(3)	14(3)	21(3)	3(2)	7(2)	0(2)
C(31)	12(2)	11(2)	7(2)	-1(2)	1(2)	0(2)
C(32)	12(2)	15(2)	9(2)	-1(2)	0(2)	1(2)
C(33)	24(3)	14(2)	13(2)	2(2)	-1(2)	2(2)
C(34)	25(3)	12(2)	17(2)	0(2)	4(2)	-6(2)
C(35)	23(2)	21(2)	16(3)	-2(2)	2(2)	-4(2)
C(36)	17(2)	20(2)	13(2)	-2(2)	0(2)	-1(2)
C(37)	17(2)	19(3)	22(3)	-2(2)	-4(2)	-3(2)

Table 5. Hydrogen coordinates (x 10^4) and isotropic displacement parameters (Å^2x 10^3) for (**2jj**).

	x	y	z	U(eq)
H(12A)	10184	2431	-1235	21
H(13A)	11300	2598	-822	26
H(14A)	11671	2392	1319	23
H(15A)	10950	1940	2980	19
H(17A)	9741	2057	3733	26
H(17B)	9859	579	3343	26
H(17C)	9261	1352	2761	26
H(22A)	8735	563	-2120	19
H(23A)	8639	1016	-4317	25
H(24A)	8820	3127	-5073	28
H(25A)	9139	4776	-3641	24
H(27A)	9707	5232	-1507	29
H(27B)	9436	4489	-275	29
H(27C)	8980	5445	-1065	29
H(32A)	9714	-354	876	15
H(33A)	9470	-2541	1288	20
H(34A)	8402	-3288	1052	22
H(35A)	7605	-1871	291	24
H(37D)	7234	509	143	29
H(37A)	7493	247	-1276	29
H(37B)	7740	1480	-491	29

Appendix A2k

Data for the structure of $[B_4O_2F_{10}][HPPh_3]_2$ (**2k**).

Crystals grown by the author. Structure solved by Dr. A. E. Goeta at the University of

Durham Crystallography Department (reference code 00srv068).

Table 1. Crystal data and structure refinement for (**2k**)

Identification code	00srv068
Empirical formula	C18 H16 B2 F5 O P
Formula weight	395.90
Temperature	150(2) K
Wavelength	0.71073 Å
Crystal system	Monoclinic
Space group	P2(1)/n
No. of reflections for cell determination	617
Theta range for cell determination	13.80° - 21.10°
Unit cell dimensions	a = 11.638(3) Å α= 90°.
	b = 12.174(3) Å β= 93.688(3)°.
	c = 13.542(3) Å γ = 90°.
Volume	1914.6(8) Å^3
Z	4
Density (calculated)	1.373 Mg/m^3
Absorption coefficient	0.194 mm^{-1}
F(000)	808
Crystal size	0.34 x 0.22 x 0.18 mm^3
Crystal shape	irregular
Crystal colour	colourless
Diffractometer	Bruker SMART-CCD
Data collection method	ω scans
Theta range for data collection	2.24 to 30.49°.
Index ranges	-16<=h<=16, -17<=k<=17, -18<=l<=18
Reflections collected	22662
Independent reflections	5437 [R(int) = 0.0390]
Completeness to theta = 30.49°	93.1 %
Absorption correction	None
Refinement method	Full-matrix least-squares on F^2
Data / restraints / parameters	5437 / 0 / 248
Goodness-of-fit on F^2	1.032
Final R indices [I>2sigma(I)]	R1 = 0.0482, wR2 = 0.1137
R indices (all data)	R1 = 0.0763, wR2 = 0.1287
Largest diff. peak and hole	0.569 and -0.404 e.Å^{-3}

Table 2. Atomic coordinates (x 10^4) and equivalent isotropic displacement parameters ($Å^2$x 10^3) for (**2k**). U(eq) is defined as one third of the trace of the orthogonalized U^{ij} tensor.

	x	y	z	U(eq)
P(1)	6927(1)	7394(1)	1244(1)	25(1)
C(1)	6161(2)	7432(1)	2342(1)	27(1)
C(2)	5033(2)	7800(2)	2272(2)	49(1)
C(3)	4402(2)	7765(3)	3101(2)	74(1)
C(4)	4904(2)	7392(2)	3995(2)	61(1)
C(5)	6027(2)	7045(2)	4068(2)	44(1)
C(6)	6664(2)	7052(2)	3237(1)	36(1)
C(7)	6776(2)	6079(1)	655(1)	30(1)
C(8)	6349(2)	5184(2)	1149(2)	42(1)
C(9)	6288(2)	4165(2)	692(2)	51(1)
C(10)	6645(2)	4044(2)	-248(2)	51(1)
C(11)	7045(2)	4939(2)	-759(2)	56(1)
C(12)	7107(2)	5965(2)	-307(2)	47(1)
C(13)	8418(2)	7721(1)	1476(1)	27(1)
C(14)	8783(2)	8805(2)	1372(1)	32(1)
C(15)	9940(2)	9057(2)	1560(2)	41(1)
C(16)	10712(2)	8250(2)	1862(2)	45(1)
C(17)	10352(2)	7176(2)	1970(2)	49(1)
C(18)	9204(2)	6902(2)	1772(2)	40(1)
F(1)	12041(1)	6387(1)	4027(1)	51(1)
F(2)	11575(1)	4933(1)	3054(1)	47(1)
F(3)	12643(1)	4686(2)	4498(1)	68(1)
B(1)	11782(2)	5281(2)	4013(2)	33(1)
O(1)	10714(1)	5106(1)	4572(1)	30(1)
B(2)	9504(2)	5534(2)	4508(2)	26(1)
F(4)	9437(1)	6642(1)	4637(1)	41(1)
F(5)	8855(1)	5189(1)	3694(1)	36(1)

Table 3.   Bond lengths [Å] and angles [°] for **(2k)**.

P(1)-C(1)	1.7832(17)	F(2)-B(1)	1.372(2)
P(1)-C(13)	1.7877(19)	F(3)-B(1)	1.369(3)
P(1)-C(7)	1.7922(19)	B(1)-O(1)	1.512(2)
P(1)-H(1P)	1.24(2)	O(1)-B(2)	1.498(2)
C(1)-C(2)	1.384(3)	O(1)-B(2)#1	1.505(2)
C(1)-C(6)	1.390(3)	B(2)-F(5)	1.362(2)
C(2)-C(3)	1.381(3)	B(2)-F(4)	1.362(2)
C(2)-H(2)	0.9300	B(2)-O(1)#1	1.505(2)
C(3)-C(4)	1.385(4)		
C(3)-H(3)	0.9300	C(1)-P(1)-C(13)	112.28(9)
C(4)-C(5)	1.372(3)	C(1)-P(1)-C(7)	110.72(8)
C(4)-H(4)	0.9300	C(13)-P(1)-C(7)	110.09(8)
C(5)-C(6)	1.387(3)	C(1)-P(1)-H(1P)	108.4(10)
C(5)-H(5)	0.9300	C(13)-P(1)-H(1P)	106.8(10)
C(6)-H(6)	0.9300	C(7)-P(1)-H(1P)	108.3(10)
C(7)-C(8)	1.388(3)	C(2)-C(1)-C(6)	120.76(17)
C(7)-C(12)	1.388(3)	C(2)-C(1)-P(1)	118.30(14)
C(8)-C(9)	1.386(3)	C(6)-C(1)-P(1)	120.87(14)
C(8)-H(8)	0.9300	C(3)-C(2)-C(1)	119.1(2)
C(9)-C(10)	1.371(3)	C(3)-C(2)-H(2)	120.5
C(9)-H(9)	0.9300	C(1)-C(2)-H(2)	120.5
C(10)-C(11)	1.387(3)	C(2)-C(3)-C(4)	120.3(2)
C(10)-H(10)	0.9300	C(2)-C(3)-H(3)	119.9
C(11)-C(12)	1.391(3)	C(4)-C(3)-H(3)	119.9
C(11)-H(11)	0.9300	C(5)-C(4)-C(3)	120.6(2)
C(12)-H(12)	0.9300	C(5)-C(4)-H(4)	119.7
C(13)-C(18)	1.395(3)	C(3)-C(4)-H(4)	119.7
C(13)-C(14)	1.397(3)	C(4)-C(5)-C(6)	119.8(2)
C(14)-C(15)	1.388(3)	C(4)-C(5)-H(5)	120.1
C(14)-H(14)	0.9300	C(6)-C(5)-H(5)	120.1
C(15)-C(16)	1.376(3)	C(5)-C(6)-C(1)	119.47(18)
C(15)-H(15)	0.9300	C(5)-C(6)-H(6)	120.3
C(16)-C(17)	1.384(4)	C(1)-C(6)-H(6)	120.3
C(16)-H(16)	0.9300	C(8)-C(7)-C(12)	120.25(18)
C(17)-C(18)	1.386(3)	C(8)-C(7)-P(1)	120.99(15)
C(17)-H(17)	0.9300	C(12)-C(7)-P(1)	118.76(14)
C(18)-H(18)	0.9300	C(9)-C(8)-C(7)	119.8(2)
F(1)-B(1)	1.380(3)	C(9)-C(8)-H(8)	120.1

C(7)-C(8)-H(8)	120.1	C(16)-C(17)-C(18)	120.1(2)
C(10)-C(9)-C(8)	120.1(2)	C(16)-C(17)-H(17)	119.9
C(10)-C(9)-H(9)	120.0	C(18)-C(17)-H(17)	119.9
C(8)-C(9)-H(9)	120.0	C(17)-C(18)-C(13)	119.3(2)
C(9)-C(10)-C(11)	120.6(2)	C(17)-C(18)-H(18)	120.3
C(9)-C(10)-H(10)	119.7	C(13)-C(18)-H(18)	120.3
C(11)-C(10)-H(10)	119.7	F(3)-B(1)-F(2)	111.71(17)
C(10)-C(11)-C(12)	119.7(2)	F(3)-B(1)-F(1)	110.9(2)
C(10)-C(11)-H(11)	120.1	F(2)-B(1)-F(1)	109.82(17)
C(12)-C(11)-H(11)	120.1	F(3)-B(1)-O(1)	106.56(16)
C(7)-C(12)-C(11)	119.5(2)	F(2)-B(1)-O(1)	109.31(17)
C(7)-C(12)-H(12)	120.2	F(1)-B(1)-O(1)	108.45(15)
C(11)-C(12)-H(12)	120.2	B(2)-O(1)-B(2)#1	91.17(12)
C(18)-C(13)-C(14)	120.43(18)	B(2)-O(1)-B(1)	136.21(14)
C(18)-C(13)-P(1)	120.18(15)	B(2)#1-O(1)-B(1)	132.48(14)
C(14)-C(13)-P(1)	119.38(14)	F(5)-B(2)-F(4)	112.06(15)
C(15)-C(14)-C(13)	119.21(18)	F(5)-B(2)-O(1)	114.18(15)
C(15)-C(14)-H(14)	120.4	F(4)-B(2)-O(1)	113.49(16)
C(13)-C(14)-H(14)	120.4	F(5)-B(2)-O(1)#1	113.33(15)
C(16)-C(15)-C(14)	120.3(2)	F(4)-B(2)-O(1)#1	113.09(15)
C(16)-C(15)-H(15)	119.9	O(1)-B(2)-O(1)#1	88.83(12)
C(14)-C(15)-H(15)	119.9		
C(15)-C(16)-C(17)	120.6(2)		
C(15)-C(16)-H(16)	119.7		
C(17)-C(16)-H(16)	119.7		

Symmetry transformations used to generate equivalent atoms:

#1 -x+2,-y+1,-z+1

Table 4. Anisotropic displacement parameters $(\text{Å}^2 \times 10^3)$ for (2k). The anisotropic displacement factor exponent takes the form: $-2\pi^2[\ h^2\ a^{*2}U^{11} + ... + 2\ h\ k\ a^*\ b^*\ U^{12}\ ]$

	U^{11}	U^{22}	U^{33}	U^{23}	U^{13}	U^{12}
P(1)	28(1)	25(1)	24(1)	4(1)	7(1)	0(1)
C(1)	30(1)	27(1)	26(1)	5(1)	9(1)	2(1)
C(2)	36(1)	76(2)	35(1)	23(1)	12(1)	20(1)
C(3)	46(1)	130(3)	49(2)	37(2)	24(1)	42(2)
C(4)	59(2)	86(2)	39(1)	25(1)	27(1)	28(1)
C(5)	52(1)	55(1)	27(1)	13(1)	9(1)	14(1)
C(6)	34(1)	46(1)	29(1)	6(1)	6(1)	9(1)
C(7)	31(1)	29(1)	31(1)	1(1)	7(1)	-2(1)
C(8)	57(1)	31(1)	38(1)	5(1)	12(1)	-4(1)
C(9)	70(2)	29(1)	55(1)	3(1)	10(1)	-8(1)
C(10)	61(2)	34(1)	59(2)	-12(1)	9(1)	-5(1)
C(11)	76(2)	47(1)	48(1)	-15(1)	25(1)	-11(1)
C(12)	64(2)	39(1)	41(1)	-5(1)	25(1)	-14(1)
C(13)	27(1)	33(1)	23(1)	2(1)	8(1)	0(1)
C(14)	33(1)	33(1)	32(1)	-4(1)	7(1)	1(1)
C(15)	38(1)	46(1)	40(1)	-6(1)	7(1)	-10(1)
C(16)	29(1)	71(2)	36(1)	4(1)	4(1)	-6(1)
C(17)	36(1)	67(2)	44(1)	21(1)	3(1)	11(1)
C(18)	37(1)	43(1)	41(1)	16(1)	7(1)	4(1)
F(1)	53(1)	50(1)	54(1)	-15(1)	23(1)	-20(1)
F(2)	62(1)	49(1)	31(1)	-11(1)	13(1)	-8(1)
F(3)	42(1)	109(1)	54(1)	28(1)	17(1)	36(1)
B(1)	32(1)	41(1)	27(1)	2(1)	8(1)	6(1)
O(1)	27(1)	35(1)	29(1)	10(1)	5(1)	7(1)
B(2)	29(1)	25(1)	25(1)	5(1)	2(1)	6(1)
F(4)	51(1)	23(1)	49(1)	3(1)	-1(1)	8(1)
F(5)	35(1)	42(1)	29(1)	1(1)	-4(1)	4(1)

Table 5. Hydrogen coordinates (x 10^4) and isotropic displacement parameters (Å^2x 10^3) for (**2k**).

	x	y	z	U(eq)
H(1P)	6516(18)	8099(18)	665(16)	39(6)
H(2)	4705	8067	1675	58
H(3)	3638	7993	3060	89
H(4)	4474	7377	4550	73
H(5)	6361	6806	4672	53
H(6)	7422	6805	3278	43
H(8)	6104	5267	1785	50
H(9)	6006	3563	1022	61
H(10)	6618	3355	-545	62
H(11)	7271	4854	-1400	67
H(12)	7367	6571	-646	57
H(14)	8258	9352	1179	39
H(15)	10194	9774	1480	49
H(16)	11484	8429	1996	54
H(17)	10882	6637	2174	59
H(18)	8961	6179	1837	48

Table 6. Torsion angles [°] for (2k).

C(13)-P(1)-C(1)-C(2)	144.73(17)	C(7)-P(1)-C(13)-C(14)	142.91(15)
C(7)-P(1)-C(1)-C(2)	-91.77(19)	C(18)-C(13)-C(14)-C(15)	0.5(3)
C(13)-P(1)-C(1)-C(6)	-38.26(19)	P(1)-C(13)-C(14)-C(15)	179.55(14)
C(7)-P(1)-C(1)-C(6)	85.24(18)	C(13)-C(14)-C(15)-C(16)	-1.2(3)
C(6)-C(1)-C(2)-C(3)	-1.3(4)	C(14)-C(15)-C(16)-C(17)	1.0(3)
P(1)-C(1)-C(2)-C(3)	175.7(2)	C(15)-C(16)-C(17)-C(18)	0.0(3)
C(1)-C(2)-C(3)-C(4)	1.6(5)	C(16)-C(17)-C(18)-C(13)	-0.7(3)
C(2)-C(3)-C(4)-C(5)	-0.5(5)		
C(3)-C(4)-C(5)-C(6)	-0.9(5)	C(14)-C(13)-C(18)-C(17)	0.5(3)
C(4)-C(5)-C(6)-C(1)	1.2(4)	P(1)-C(13)-C(18)-C(17)	-178.60(16)
C(2)-C(1)-C(6)-C(5)	-0.1(3)	F(3)-B(1)-O(1)-B(2)	175.83(19)
P(1)-C(1)-C(6)-C(5)	-177.02(17)	F(2)-B(1)-O(1)-B(2)	-63.3(3)
C(1)-P(1)-C(7)-C(8)	-13.9(2)	F(1)-B(1)-O(1)-B(2)	56.4(3)
C(13)-P(1)-C(7)-C(8)	110.84(18)	F(3)-B(1)-O(1)-B(2)#1	1.4(3)
C(1)-P(1)-C(7)-C(12)	166.80(17)	F(2)-B(1)-O(1)-B(2)#1	122.3(2)
C(13)-P(1)-C(7)-C(12)	-68.44(19)	F(1)-B(1)-O(1)-B(2)#1	-118.0(2)
C(12)-C(7)-C(8)-C(9)	2.1(3)	B(2)#1-O(1)-B(2)-F(5)	-115.15(18)
P(1)-C(7)-C(8)-C(9)	-177.17(18)	B(1)-O(1)-B(2)-F(5)	69.0(3)
C(7)-C(8)-C(9)-C(10)	-0.3(4)	B(2)#1-O(1)-B(2)-F(4)	114.75(19)
C(8)-C(9)-C(10)-C(11)	-1.4(4)	B(1)-O(1)-B(2)-F(4)	-61.1(3)
C(9)-C(10)-C(11)-C(12)	1.3(4)	B(2)#1-O(1)-B(2)-O(1)#1	0.0
C(8)-C(7)-C(12)-C(11)	-2.2(4)	B(1)-O(1)-B(2)-O(1)#1	-175.9(2)
P(1)-C(7)-C(12)-C(11)	177.0(2)		
C(10)-C(11)-C(12)-C(7)	0.6(4)		
C(1)-P(1)-C(13)-C(18)	85.83(17)		
C(7)-P(1)-C(13)-C(18)	-38.03(18)		
C(1)-P(1)-C(13)-C(14)	-93.24(16)		

Symmetry transformations used to generate equivalent atoms:

#1 -x+2,-y+1,-z+1

Appendix A2l

Data for the structure of HP(*o*-tolyl)₃BCl₄ (**2l**).

Crystals grown by the author. Structure solved with help from Dr. Claire Wilson at the University of Durham Crystallography Department (reference code 99srv157).

Table 1. Crystal data and structure refinement for (**2l**).

Identification code	157abs
Empirical formula	C21 H22 B Cl4 P
Formula weight	457.97
Temperature	100(2) K
Wavelength	0.71073 Å
Crystal system	Triclinic
Space group	P-1
Unit cell dimensions	a = 9.4160(3) Å α= 118.2810(10)°.
	b = 11.4361(3) Å β= 90.1140(10)°.
	c = 11.5642(3) Å γ = 93.4440(10)°.
Volume	1093.98(5) Å³
Z	2
Density (calculated)	1.390 Mg/m³
Absorption coefficient	0.619 mm⁻¹
F(000)	472
Crystal size	0.48 x 0.18 x 0.10 mm³
Theta range for data collection	2.00 to 30.47°.
Index ranges	-12<=h<=13, -15<=k<=15, -16<=l<=16
Reflections collected	14295
Independent reflections	6059 [R(int) = 0.0421]
Completeness to theta = 30.47°	90.7 %
Absorption correction	Empirical
Max. and min. transmission	0.96162 and 0.81438
Refinement method	Full-matrix least-squares on F^2
Data / restraints / parameters	6059 / 0 / 332
Goodness-of-fit on F^2	1.001
Final R indices [I>2sigma(I)]	R1 = 0.0392, wR2 = 0.0807
R indices (all data)	R1 = 0.0698, wR2 = 0.0895
Largest diff. peak and hole	0.432 and -0.381 e.Å⁻³

Table 2. Atomic coordinates (x 10^4) and equivalent isotropic displacement parameters ($\mathring{A}^2$x 10^3) for (2I). U(eq) is defined as one third of the trace of the orthogonalized U^{ij} tensor.

Atom	x	y	z	U(eq)
P(1)	1258(1)	2891(1)	1372(1)	15(1)
C(1)	1399(2)	2334(2)	-361(2)	16(1)
C(2)	186(2)	1715(2)	-1186(2)	20(1)
C(3)	264(2)	1250(2)	-2527(2)	27(1)
C(4)	1558(2)	1388(2)	-3047(2)	29(1)
C(5)	2758(2)	2001(2)	-2237(2)	26(1)
C(6)	2707(2)	2495(2)	-878(2)	20(1)
C(7)	4021(2)	3179(2)	-6(2)	26(1)
C(8)	-573(2)	2890(2)	1810(2)	16(1)
C(9)	-1087(2)	1964(2)	2211(2)	20(1)
C(10)	-2489(2)	1955(2)	2576(2)	25(1)
C(11)	-3370(2)	2864(2)	2539(2)	27(1)
C(12)	-2873(2)	3775(2)	2134(2)	24(1)
C(13)	-1465(2)	3813(2)	1755(2)	18(1)
C(14)	-967(2)	4789(2)	1293(2)	22(1)
C(15)	2240(2)	1866(2)	1831(2)	16(1)
C(16)	2712(2)	680(2)	823(2)	20(1)
C(17)	3474(2)	-151(2)	1116(2)	24(1)
C(18)	3773(2)	200(2)	2422(2)	24(1)
C(19)	3311(2)	1373(2)	3428(2)	22(1)
C(20)	2534(2)	2235(2)	3167(2)	17(1)
C(21)	2057(2)	3495(2)	4286(2)	23(1)
B(1)	2995(2)	7055(2)	3632(2)	18(1)
Cl(1)	4320(1)	5957(1)	3733(1)	26(1)
Cl(2)	2777(1)	6685(1)	1885(1)	23(1)
Cl(3)	3642(1)	8810(1)	4651(1)	24(1)
Cl(4)	1257(1)	6718(1)	4202(1)	24(1)

Table 3. Bond lengths [Å] and angles [°] for (21).

P(1)-C(15)	1.7968(18)	C(18)-C(19)	1.391(3)
P(1)-C(8)	1.7977(18)	C(18)-H(18A)	1.00(2)
P(1)-C(1)	1.8009(18)	C(19)-C(20)	1.402(3)
P(1)-H(1)	1.289(19)	C(19)-H(19A)	0.92(2)
C(1)-C(2)	1.405(3)	C(20)-C(21)	1.505(3)
C(1)-C(6)	1.411(3)	C(21)-H(21C)	0.90(3)
C(2)-C(3)	1.384(3)	C(21)-H(21A)	0.88(3)
C(2)-H(2A)	0.90(2)	C(21)-H(21B)	0.91(3)
C(3)-C(4)	1.393(3)	B(1)-Cl(3)	1.843(2)
C(3)-H(3A)	0.96(2)	B(1)-Cl(4)	1.853(2)
C(4)-C(5)	1.387(3)	B(1)-Cl(1)	1.864(2)
C(4)-H(4A)	0.93(2)	B(1)-Cl(2)	1.865(2)
C(5)-C(6)	1.397(3)		
C(5)-H(5A)	0.95(2)	C(15)-P(1)-C(8)	111.09(9)
C(6)-C(7)	1.513(3)	C(15)-P(1)-C(1)	109.90(8)
C(7)-H(7C)	0.96(2)	C(8)-P(1)-C(1)	111.07(8)
C(7)-H(7B)	0.95(3)	C(15)-P(1)-H(1)	109.1(8)
C(7)-H(7A)	1.00(2)	C(8)-P(1)-H(1)	107.8(8)
C(8)-C(9)	1.405(3)	C(1)-P(1)-H(1)	107.8(8)
C(8)-C(13)	1.413(3)	C(2)-C(1)-C(6)	120.91(17)
C(9)-C(10)	1.388(3)	C(2)-C(1)-P(1)	118.57(14)
C(9)-H(9A)	0.96(2)	C(6)-C(1)-P(1)	120.51(14)
C(10)-C(11)	1.384(3)	C(3)-C(2)-C(1)	120.09(19)
C(10)-H(10A)	0.98(2)	C(3)-C(2)-H(2A)	118.8(13)
C(11)-C(12)	1.389(3)	C(1)-C(2)-H(2A)	121.1(13)
C(11)-H(11A)	0.89(3)	C(2)-C(3)-C(4)	119.3(2)
C(12)-C(13)	1.402(3)	C(2)-C(3)-H(3A)	121.5(14)
C(12)-H(12A)	0.97(2)	C(4)-C(3)-H(3A)	119.2(14)
C(13)-C(14)	1.502(3)	C(5)-C(4)-C(3)	120.8(2)
C(14)-H(14C)	0.92(2)	C(5)-C(4)-H(4A)	119.9(14)
C(14)-H(14A)	0.94(3)	C(3)-C(4)-H(4A)	119.3(14)
C(14)-H(14B)	0.95(3)	C(4)-C(5)-C(6)	121.2(2)
C(15)-C(16)	1.404(3)	C(4)-C(5)-H(5A)	118.5(14)
C(15)-C(20)	1.416(2)	C(6)-C(5)-H(5A)	120.2(14)
C(16)-C(17)	1.385(3)	C(5)-C(6)-C(1)	117.68(18)
C(16)-H(16A)	0.88(2)	C(5)-C(6)-C(7)	120.46(18)
C(17)-C(18)	1.389(3)	C(1)-C(6)-C(7)	121.86(18)
C(17)-H(17A)	0.95(2)	C(6)-C(7)-H(7C)	113.9(15)

C(6)-C(7)-H(7B)	110.6(15)	C(17)-C(16)-C(15)	120.58(19)
H(7C)-C(7)-H(7B)	108(2)	C(17)-C(16)-H(16A)	119.7(13)
C(6)-C(7)-H(7A)	114.0(15)	C(15)-C(16)-H(16A)	119.7(13)
H(7C)-C(7)-H(7A)	104(2)	C(16)-C(17)-C(18)	119.39(19)
H(7B)-C(7)-H(7A)	105.6(19)	C(16)-C(17)-H(17A)	118.9(13)
C(9)-C(8)-C(13)	121.13(16)	C(18)-C(17)-H(17A)	121.7(13)
C(9)-C(8)-P(1)	118.82(14)	C(17)-C(18)-C(19)	120.46(18)
C(13)-C(8)-P(1)	120.05(14)	C(17)-C(18)-H(18A)	119.8(13)
C(10)-C(9)-C(8)	120.08(18)	C(19)-C(18)-H(18A)	119.7(13)
C(10)-C(9)-H(9A)	118.1(12)	C(18)-C(19)-C(20)	121.67(19)
C(8)-C(9)-H(9A)	121.8(12)	C(18)-C(19)-H(19A)	120.4(13)
C(11)-C(10)-C(9)	119.33(19)	C(20)-C(19)-H(19A)	117.9(13)
C(11)-C(10)-H(10A)	121.8(12)	C(19)-C(20)-C(15)	117.21(17)
C(9)-C(10)-H(10A)	118.8(12)	C(19)-C(20)-C(21)	119.87(18)
C(10)-C(11)-C(12)	120.96(19)	C(15)-C(20)-C(21)	122.92(17)
C(10)-C(11)-H(11A)	118.5(16)	C(20)-C(21)-H(21C)	113.4(19)
C(12)-C(11)-H(11A)	120.5(16)	C(20)-C(21)-H(21A)	112.0(17)
C(11)-C(12)-C(13)	121.40(19)	H(21C)-C(21)-H(21A)	108(3)
C(11)-C(12)-H(12A)	121.6(13)	C(20)-C(21)-H(21B)	111(2)
C(13)-C(12)-H(12A)	117.0(13)	H(21C)-C(21)-H(21B)	110(3)
C(12)-C(13)-C(8)	117.09(17)	H(21A)-C(21)-H(21B)	102(3)
C(12)-C(13)-C(14)	120.21(17)	Cl(3)-B(1)-Cl(4)	110.40(11)
C(8)-C(13)-C(14)	122.69(17)	Cl(3)-B(1)-Cl(1)	109.36(11)
C(13)-C(14)-H(14C)	112.2(15)	Cl(4)-B(1)-Cl(1)	109.68(11)
C(13)-C(14)-H(14A)	113.4(17)	Cl(3)-B(1)-Cl(2)	109.66(11)
H(14C)-C(14)-H(14A)	112(2)	Cl(4)-B(1)-Cl(2)	108.94(10)
C(13)-C(14)-H(14B)	112.7(18)	Cl(1)-B(1)-Cl(2)	108.78(11)
H(14C)-C(14)-H(14B)	104(2)		
H(14A)-C(14)-H(14B)	102(2)		
C(16)-C(15)-C(20)	120.69(17)		
C(16)-C(15)-P(1)	117.95(14)		
C(20)-C(15)-P(1)	121.36(14)		

Symmetry transformations used to generate equivalent atoms:

Table 4. Anisotropic displacement parameters $(\mathring{A}^2 x\ 10^3)$ for **(2l)**. The anisotropic displacement factor exponent takes the form: $-2\pi^2[\ h^2\ a^{*2}U^{11} + ... + 2\ h\ k\ a^*\ b^*\ U^{12}\ ]$

Atom	U^{11}	U^{22}	U^{33}	U^{23}	U^{13}	U^{12}
P(1)	11(1)	17(1)	17(1)	8(1)	1(1)	2(1)
C(1)	15(1)	18(1)	19(1)	11(1)	4(1)	4(1)
C(2)	18(1)	22(1)	22(1)	10(1)	1(1)	4(1)
C(3)	25(1)	33(1)	21(1)	10(1)	-1(1)	8(1)
C(4)	35(1)	34(1)	19(1)	12(1)	8(1)	14(1)
C(5)	25(1)	31(1)	27(1)	17(1)	12(1)	14(1)
C(6)	18(1)	21(1)	25(1)	13(1)	7(1)	8(1)
C(7)	15(1)	30(1)	33(1)	15(1)	7(1)	1(1)
C(8)	13(1)	19(1)	14(1)	6(1)	2(1)	2(1)
C(9)	18(1)	24(1)	17(1)	10(1)	0(1)	-1(1)
C(10)	21(1)	35(1)	19(1)	15(1)	0(1)	-8(1)
C(11)	13(1)	41(1)	21(1)	9(1)	3(1)	-2(1)
C(12)	15(1)	28(1)	22(1)	6(1)	-1(1)	4(1)
C(13)	15(1)	19(1)	14(1)	4(1)	-1(1)	2(1)
C(14)	21(1)	20(1)	25(1)	11(1)	-2(1)	3(1)
C(15)	10(1)	19(1)	21(1)	11(1)	-1(1)	-1(1)
C(16)	16(1)	22(1)	21(1)	10(1)	0(1)	1(1)
C(17)	21(1)	21(1)	30(1)	12(1)	2(1)	5(1)
C(18)	18(1)	26(1)	35(1)	20(1)	-2(1)	2(1)
C(19)	16(1)	29(1)	24(1)	16(1)	-4(1)	-3(1)
C(20)	11(1)	20(1)	21(1)	11(1)	0(1)	-3(1)
C(21)	20(1)	28(1)	21(1)	12(1)	0(1)	1(1)
B(1)	15(1)	20(1)	18(1)	8(1)	0(1)	-1(1)
Cl(1)	20(1)	25(1)	32(1)	13(1)	0(1)	6(1)
Cl(2)	20(1)	31(1)	18(1)	11(1)	2(1)	0(1)
Cl(3)	26(1)	18(1)	23(1)	8(1)	-3(1)	-3(1)
Cl(4)	15(1)	34(1)	22(1)	12(1)	3(1)	-2(1)

Table 5.   Hydrogen coordinates (x 10⁴) and isotropic displacement parameters (Å²x 10 ³) for (**2l**).

Atom	x	y	z	U(eq)
H(1)	1800(20)	4099(18)	1992(19)	16(5)
H(2A)	-650(20)	1594(19)	-860(20)	17(5)
H(3A)	-550(30)	840(20)	-3100(20)	35(6)
H(4A)	1610(20)	1070(20)	-3950(20)	26(6)
H(5A)	3610(30)	2130(20)	-2620(20)	33(6)
H(7C)	3900(30)	4080(30)	650(30)	40(7)
H(7B)	4810(30)	3190(20)	-520(20)	37(7)
H(7A)	4340(30)	2730(20)	510(20)	43(7)
H(9A)	-480(20)	1343(19)	2270(19)	15(5)
H(10A)	-2830(20)	1300(20)	2847(19)	18(5)
H(11A)	-4260(30)	2860(20)	2790(20)	46(7)
H(12A)	-3470(20)	4430(20)	2130(20)	25(6)
H(14C)	-780(30)	4380(20)	410(30)	36(7)
H(14A)	-1570(30)	5490(30)	1520(30)	55(8)
H(14B)	-90(30)	5270(30)	1710(30)	69(9)
H(16A)	2520(20)	465(19)	0(20)	12(5)
H(17A)	3750(20)	-970(20)	410(20)	22(5)
H(18A)	4320(20)	-390(20)	2640(20)	30(6)
H(19A)	3530(20)	1610(20)	4290(20)	25(6)
H(21C)	1130(30)	3620(30)	4210(30)	65(9)
H(21A)	2190(30)	3520(30)	5050(30)	53(8)
H(21B)	2610(40)	4210(30)	4370(30)	72(10)

Table 6. Torsion angles [°] for (**2l**).

C(15)-P(1)-C(1)-C(2)	109.96(15)
C(8)-P(1)-C(1)-C(2)	-13.39(17)
C(15)-P(1)-C(1)-C(6)	-68.78(17)
C(8)-P(1)-C(1)-C(6)	167.88(14)
C(6)-C(1)-C(2)-C(3)	0.1(3)
P(1)-C(1)-C(2)-C(3)	-178.60(15)
C(1)-C(2)-C(3)-C(4)	0.7(3)
C(2)-C(3)-C(4)-C(5)	-0.8(3)
C(3)-C(4)-C(5)-C(6)	0.0(3)
C(4)-C(5)-C(6)-C(1)	0.8(3)
C(4)-C(5)-C(6)-C(7)	-179.02(19)

C(2)-C(1)-C(6)-C(5)	-0.9(3)
P(1)-C(1)-C(6)-C(5)	177.82(14)
C(2)-C(1)-C(6)-C(7)	178.93(18)
P(1)-C(1)-C(6)-C(7)	-2.4(3)
C(15)-P(1)-C(8)-C(9)	-11.11(17)
C(1)-P(1)-C(8)-C(9)	111.54(15)
C(15)-P(1)-C(8)-C(13)	168.58(14)
C(1)-P(1)-C(8)-C(13)	-68.77(16)
C(13)-C(8)-C(9)-C(10)	-0.7(3)
P(1)-C(8)-C(9)-C(10)	178.95(14)
C(8)-C(9)-C(10)-C(11)	0.0(3)
C(9)-C(10)-C(11)-C(12)	0.5(3)
C(10)-C(11)-C(12)-C(13)	-0.4(3)
C(11)-C(12)-C(13)-C(8)	-0.4(3)
C(11)-C(12)-C(13)-C(14)	178.68(18)
C(9)-C(8)-C(13)-C(12)	0.9(3)
P(1)-C(8)-C(13)-C(12)	-178.79(13)
C(9)-C(8)-C(13)-C(14)	-178.11(17)
P(1)-C(8)-C(13)-C(14)	2.2(2)
C(8)-P(1)-C(15)-C(16)	111.14(15)
C(1)-P(1)-C(15)-C(16)	-12.19(17)
C(8)-P(1)-C(15)-C(20)	-68.95(16)
C(1)-P(1)-C(15)-C(20)	167.73(14)
C(20)-C(15)-C(16)-C(17)	0.1(3)
P(1)-C(15)-C(16)-C(17)	-179.99(15)
C(15)-C(16)-C(17)-C(18)	-0.2(3)
C(16)-C(17)-C(18)-C(19)	0.1(3)
C(17)-C(18)-C(19)-C(20)	0.0(3)
C(18)-C(19)-C(20)-C(15)	-0.1(3)
C(18)-C(19)-C(20)-C(21)	-179.95(19)
C(16)-C(15)-C(20)-C(19)	0.1(3)
P(1)-C(15)-C(20)-C(19)	-179.84(14)
C(16)-C(15)-C(20)-C(21)	179.88(18)
P(1)-C(15)-C(20)-C(21)	0.0(2)

Symmetry transformations used to generate equivalent atoms:

Appendix A3: Crystal Structure Data Tables for Structures in Chapter 3

Appendix A3b

Data for the structure of $Cl_3B \cdot 2$-picoline (**3b**).

Crystals grown by the author. Structure solved by Andrei S. Batsanov at the University of Durham Crystallography Department (reference code 00srv291).

Table 1. Crystal data and structure refinement for (**3b**).

Identification code	00srv291
Empirical formula	C6 H7 B Cl3 N
Formula weight	210.29
Temperature	110(2) K
Wavelength	0.71073 Å
Crystal system	Orthorhombic
Space group	Pnma
Unit cell dimensions	a = 10.0304(9) Å $\quad\quad$ α= 90°.
	b = 6.8481(5) Å $\quad\quad$ β= 90°.
	c = 12.8675(10) Å $\quad\quad$ γ = 90°.
Volume	883.86(12) Å^3
Z	4
Density (calculated)	1.580 Mg/m^3
Absorption coefficient	0.966 mm^{-1}
F(000)	424
Crystal size	0.40 x 0.42 x 0.60 mm^3
Theta range for data collection	2.57 to 28.98°.
Index ranges	-13<=h<=13, -9<=k<=9, -17<=l<=17
Reflections collected	10143
Independent reflections	1259 [R(int) = 0.0254]
Completeness to theta = 28.98°	99.4 %
Absorption correction	Integration
Max. and min. transmission	0.7323 and 0.6171
Refinement method	Full-matrix least-squares on F^2
Data / restraints / parameters	1259 / 0 / 83
Goodness-of-fit on F^2	1.098
Final R indices [I>2sigma(I)]	R1 = 0.0258, wR2 = 0.0681
R indices (all data)	R1 = 0.0265, wR2 = 0.0688
Largest diff. peak and hole	0.329 and -0.386 e.Å^{-3}

Table 2. Atomic coordinates (x 10^4) and equivalent isotropic displacement parameters (Å^2x 10^3) for (**3b**). U(eq) is defined as one third of the trace of the orthogonalized U^{ij} tensor.

Atom	x	y	z	U(eq)
Cl(1)	1355(1)	254(1)	3770(1)	29(1)
Cl(2)	3110(1)	2500	2322(1)	36(1)
N	3488(1)	2500	4517(1)	15(1)
B	2357(2)	2500	3629(1)	20(1)
C(1)	1763(2)	2500	5942(1)	27(1)
C(2)	3174(1)	2500	5554(1)	18(1)
C(3)	4198(2)	2500	6287(1)	23(1)
C(4)	5523(2)	2500	5992(1)	25(1)
C(5)	5826(2)	2500	4941(1)	21(1)
C(6)	4800(1)	2500	4232(1)	18(1)

Table 3. Bond lengths [Å] and angles [°] for (**3b**).

Cl(1)-B	1.8466(10)	C(6)-N-B	119.24(12)
Cl(2)-B	1.8437(17)	C(2)-N-B	121.93(12)
N-C(6)	1.3667(17)	N-B-Cl(2)	111.00(10)
N-C(2)	1.3719(18)	N-B-Cl(1)	108.29(6)
N-B	1.609(2)	Cl(2)-B-Cl(1)	108.22(6)
B-Cl(1)#1	1.8466(10)	N-B-Cl(1)#1	108.29(6)
C(1)-C(2)	1.500(2)	Cl(2)-B-Cl(1)#1	108.22(6)
C(1)-H(13)	0.9601	Cl(1)-B-Cl(1)#1	112.84(9)
C(1)-H(14)	0.9600	C(2)-C(1)-H(13)	106.4
C(1)-H(11)	0.96(4)	C(2)-C(1)-H(14)	103.7
C(1)-H(12)	0.96(4)	H(13)-C(1)-H(14)	103.8
C(2)-C(3)	1.394(2)	C(2)-C(1)-H(11)	115(2)
C(3)-C(4)	1.382(2)	H(13)-C(1)-H(11)	66.2
C(3)-H(3)	0.91(3)	H(14)-C(1)-H(11)	141.3
C(4)-C(5)	1.386(2)	C(2)-C(1)-H(12)	110.1(19)
C(4)-H(4)	0.92(2)	H(13)-C(1)-H(12)	48.7
C(5)-C(6)	1.376(2)	H(14)-C(1)-H(12)	55.4
C(5)-H(5)	0.93(2)	H(11)-C(1)-H(12)	108(2)
C(6)-H(6)	0.94(2)	N-C(2)-C(3)	119.29(13)
		N-C(2)-C(1)	122.68(14)
C(6)-N-C(2)	118.83(12)	C(3)-C(2)-C(1)	118.02(14)

C(4)-C(3)-C(2)	121.51(14)	C(4)-C(5)-H(5)	122.0(14)
C(4)-C(3)-H(3)	120.4(16)	N-C(6)-C(5)	122.85(13)
C(2)-C(3)-H(3)	118.0(16)	N-C(6)-H(6)	116.1(13)
C(3)-C(4)-C(5)	118.61(14)	C(5)-C(6)-H(6)	121.1(14)
C(3)-C(4)-H(4)	123.3(15)		
C(5)-C(4)-H(4)	118.1(15)	Symmetry transformations used to generate	
C(6)-C(5)-C(4)	118.90(14)	equivalent atoms:	
C(6)-C(5)-H(5)	119.1(14)	#1 x,-y+1/2,z	

Table 4.   Anisotropic displacement parameters (Å^2x 10^3) for (3b). The anisotropic displacement factor exponent takes the form: $-2\pi^2[h^2 a^{*2}U^{11} + ... + 2 h k a^* b^* U^{12}]$

Atom	U^{11}	U^{22}	U^{33}	U^{23}	U^{13}	U^{12}
Cl(1)	23(1)	23(1)	42(1)	-2(1)	-9(1)	-6(1)
Cl(2)	31(1)	62(1)	16(1)	0	-2(1)	0
N	15(1)	14(1)	17(1)	0	0(1)	0
B	17(1)	22(1)	20(1)	0	-4(1)	0
C(1)	24(1)	33(1)	26(1)	0	9(1)	0
C(2)	21(1)	15(1)	18(1)	0	3(1)	0
C(3)	30(1)	23(1)	16(1)	0	-2(1)	0
C(4)	26(1)	22(1)	25(1)	0	-10(1)	0
C(5)	16(1)	20(1)	28(1)	0	-3(1)	0
C(6)	17(1)	17(1)	19(1)	0	2(1)	0

Table 5.   Hydrogen coordinates (x 10^4) and isotropic displacement parameters (Å^2x 10^3) for (3b).

Atom	x	y	z	U(eq)
H(13)	1408	1230	5791	33
H(14)	1858	2500	6685	33
H(11)	1090(40)	2500	5410(30)	37(9)
H(12)	1610(30)	1380(50)	6380(20)	58(9)
H(3)	3970(20)	2500	6970(20)	33(6)
H(4)	6210(20)	2500	6457(19)	33(6)
H(5)	6700(20)	2500	4701(17)	23(5)
H(6)	4970(20)	2500	3510(17)	24(5)

Appendix A3c1

Data for the structure of $Cl_3B \cdot 4$-picoline (**3c1**).

Crystals grown by the author. Structure solved at 100(2)K by Andrei S. Batsanov at the University of Durham Crystallography Department (reference code 00srv292).

Table 1. Crystal data and structure refinement for (**3c1**).

Identification code	00srv292
Empirical formula	C6 H7 B Cl3 N
Formula weight	210.29
Temperature	100(2) K
Wavelength	0.71073 Å
Crystal system	Monoclinic
Space group	P2(1)/n
Unit cell dimensions	a = 7.214(1) Å α= 90°.
	b = 8.954(1) Å β= 94.65(2)°.
	c = 13.963(2) Å γ = 90°.
Volume	899.0(2) Å^3
Z	4
Density (calculated)	1.554 Mg/m^3
Absorption coefficient	0.949 mm^{-1}
F(000)	424
Crystal size	0.43 x 0.36 x 0.21 mm^3
Theta range for data collection	2.70 to 29.09°.
Index ranges	-9<=h<=9, -12<=k<=12, -18<=l<=19
Reflections collected	6716
Independent reflections	2367 [R(int) = 0.0653]
Completeness to theta = 29.09°	98.6 %
Absorption correction	Integration
Max. and min. transmission	0.8404 and 0.7064
Refinement method	Full-matrix least-squares on F^2
Data / restraints / parameters	2367 / 0 / 102
Goodness-of-fit on F^2	1.166
Final R indices [I>2sigma(I)]	R1 = 0.1160, wR2 = 0.3358
R indices (all data)	R1 = 0.1207, wR2 = 0.3380
Largest diff. peak and hole	2.035 and -2.008 e.Å^{-3}

Table 2. Atomic coordinates (x 10^4) and equivalent isotropic displacement parameters ($\mathring{A}^2$x 10^3) for (**3c1**). U(eq) is defined as one third of the trace of the orthogonalized U^{ij} tensor.

Atom	x	y	z	U(eq)
Cl(1)	426(2)	748(2)	7028(1)	26(1)
Cl(2)	4657(2)	658(2)	7070(1)	29(1)
Cl(3)	2302(3)	-1143(2)	5601(1)	27(1)
B	2442(10)	593(7)	6305(4)	17(1)
N(1)	2467(7)	1997(5)	5607(3)	16(1)
C(1)	2722(9)	5980(6)	3899(4)	18(1)
C(2)	2660(8)	1906(6)	4649(4)	17(1)
C(3)	2752(9)	3169(7)	4096(4)	18(1)
C(4)	2646(8)	4587(6)	4488(4)	15(1)
C(5)	2412(9)	4661(6)	5475(4)	18(1)
C(6)	2342(8)	3382(6)	6016(4)	16(1)

Table 3. Bond lengths [$\mathring{A}$] and angles [°] for 00srv292.

Cl(1)-B	1.841(7)	Cl(1)-B-Cl(2)	111.4(3)
Cl(2)-B	1.850(7)	C(2)-N(1)-C(6)	118.7(5)
Cl(3)-B	1.838(7)	C(2)-N(1)-B	124.3(5)
B-N(1)	1.592(7)	C(6)-N(1)-B	117.0(4)
N(1)-C(2)	1.358(7)	N(1)-C(2)-C(3)	121.2(5)
N(1)-C(6)	1.371(7)	C(2)-C(3)-C(4)	121.6(5)
C(1)-C(4)	1.497(7)	C(3)-C(4)-C(5)	116.4(5)
C(2)-C(3)	1.374(8)	C(3)-C(4)-C(1)	122.7(5)
C(3)-C(4)	1.387(8)	C(5)-C(4)-C(1)	120.8(5)
C(4)-C(5)	1.405(8)	C(6)-C(5)-C(4)	120.8(5)
C(5)-C(6)	1.375(7)	N(1)-C(6)-C(5)	121.2(5)

N(1)-B-Cl(3)	110.0(4)
N(1)-B-Cl(1)	108.9(4)
Cl(3)-B-Cl(1)	110.2(3)
N(1)-B-Cl(2)	106.1(4)
Cl(3)-B-Cl(2)	110.1(3)

Symmetry transformations used to generate equivalent atoms:

Table 4.   Anisotropic displacement parameters ($\text{Å}^2 \times 10^3$) for (**3c1**). The anisotropic displacement factor exponent takes the form: $-2\pi^2[\ h^2\ a^{*2}U^{11} + ...\ + 2\ h\ k\ a^*\ b^*\ U^{12}\ ]$

Atom	U^{11}	U^{22}	U^{33}	U^{23}	U^{13}	U^{12}
Cl(1)	31(1)	22(1)	27(1)	7(1)	15(1)	3(1)
Cl(2)	27(1)	29(1)	29(1)	11(1)	-4(1)	-2(1)
Cl(3)	45(1)	9(1)	26(1)	0(1)	9(1)	-1(1)
B	24(3)	10(3)	18(3)	6(2)	6(3)	-1(3)
N(1)	26(3)	11(2)	12(2)	0(2)	2(2)	-2(2)
C(1)	26(3)	10(2)	17(3)	2(2)	7(2)	-2(2)
C(2)	24(3)	11(2)	17(3)	-4(2)	3(2)	3(2)
C(3)	23(3)	20(3)	12(2)	4(2)	4(2)	-2(2)
C(4)	17(2)	15(3)	13(2)	3(2)	5(2)	0(2)
C(5)	28(3)	8(2)	20(3)	0(2)	4(2)	-1(2)
C(6)	22(3)	14(3)	11(2)	-2(2)	3(2)	-1(2)

Table 5.   Hydrogen coordinates (x 10^4) and isotropic displacement parameters ($\text{Å}^2 \times 10^3$) for (**3c1**).

Atom	x	y	z	U(eq)
H(101)	3385	5761	3329	26
H(102)	3385	6762	4279	26
H(103)	1460	6323	3697	26
H(2)	2733	952	4357	21
H(3)	2893	3069	3428	22
H(5)	2299	5607	5774	22
H(6)	2207	3458	6685	19

Appendix A3c2

Data for the structure of $Cl_3B\cdot4$-picoline (**3c2**).

Crystals grown by the author. Structure solved at 180(2)K by Andrei S. Batsanov at the

University of Durham Crystallography Department (reference code 00srv296).

Table 1. Crystal data and structure refinement for(**3c2**).

Identification code	00srv296
Empirical formula	C6 H7 B Cl3 N
Formula weight	210.29
Temperature	180(2) K
Wavelength	0.71073 Å
Crystal system	Orthorhombic
Space group	Pnma
Unit cell dimensions	a = 8.990(1) Å α= 90°.
	b = 7.256(1) Å β= 90°.
	c = 14.076(2) Å γ = 90°.
Volume	918.2(2) Å^3
Z	4
Density (calculated)	1.521 Mg/m^3
Absorption coefficient	0.929 mm^{-1}
F(000)	424
Crystal size	0.21 x 0.36 x 0.43 mm^3
Theta range for data collection	2.69 to 28.99°.
Index ranges	-12<=h<=12, -9<=k<=9, -19<=l<=19
Reflections collected	11250
Independent reflections	1312 [R(int) = 0.0355]
Completeness to theta = 28.99°	100.0 %
Absorption correction	Integration
Max. and min. transmission	0.8497 and 0.6913
Refinement method	Full-matrix least-squares on F^2
Data / restraints / parameters	1312 / 1 / 73
Goodness-of-fit on F^2	1.051
Final R indices [I>2sigma(I)]	R1 = 0.0297, wR2 = 0.0867
R indices (all data)	R1 = 0.0327, wR2 = 0.0893
Extinction coefficient	0.005(2)
Largest diff. peak and hole	0.283 and -0.222 e.Å^{-3}

Table 2. Atomic coordinates (x 10^4) and equivalent isotropic displacement parameters (Å^2x 10^3) for (3c2). U(eq) is defined as one third of the trace of the orthogonalized U^{ij} tensor.

Atom	x	y	z	U(eq)
Cl(1)	4279(1)	393(1)	7029(1)	52(1)
Cl(2)	6119(1)	2500	5618(1)	56(1)
Cl(3)	3880(8)	819(9)	7293(5)	29(2)
Cl(4)	6042(15)	1690(20)	5789(11)	36(3)
B	4376(2)	2500	6300(2)	36(1)
N(1)	2980(2)	2500	5612(1)	30(1)
C(1)	-953(2)	2500	3878(1)	40(1)
C(2)	3086(2)	2500	4657(1)	37(1)
C(3)	1835(2)	2500	4089(1)	40(1)
C(4)	418(2)	2500	4485(1)	30(1)
C(5)	332(2)	2500	5474(1)	35(1)
C(6)	1607(2)	2500	6014(1)	35(1)

Table 3. Bond lengths [Å] and angles [°] for (3c2).

Cl(1)-B	1.8433(13)	Cl(4)-B-Cl(3)#1	135.3(6)
Cl(2)-B	1.838(2)	Cl(2)-B-Cl(3)#1	125.6(2)
Cl(3)-B	1.908(7)	Cl(1)-B-Cl(3)#1	96.4(2)
Cl(4)-B	1.763(13)	N(1)-B-Cl(3)	105.2(2)
B-N(1)	1.585(2)	Cl(4)-B-Cl(3)	106.5(5)
N(1)-C(2)	1.348(2)	Cl(2)-B-Cl(3)	125.6(2)
N(1)-C(6)	1.357(2)	Cl(1)-B-Cl(3)	18.4(2)
C(1)-C(4)	1.499(2)	C(2)-N(1)-C(6)	118.65(15)
C(2)-C(3)	1.380(3)	C(2)-N(1)-B	123.61(15)
C(3)-C(4)	1.391(3)	C(6)-N(1)-B	117.74(15)
C(4)-C(5)	1.394(3)	N(1)-C(2)-C(3)	121.35(17)
C(5)-C(6)	1.376(3)	C(2)-C(3)-C(4)	120.96(17)
		C(3)-C(4)-C(5)	116.81(16)
N(1)-B-Cl(4)	115.0(5)	C(3)-C(4)-C(1)	121.65(17)
N(1)-B-Cl(2)	110.82(13)	C(5)-C(4)-C(1)	121.55(17)
Cl(4)-B-Cl(2)	20.3(5)	C(6)-C(5)-C(4)	120.36(17)
N(1)-B-Cl(1)	107.62(8)	N(1)-C(6)-C(5)	121.87(16)
Cl(4)#1-B-Cl(1)	123.0(5)		
Cl(4)-B-Cl(1)	89.4(5)		
Cl(2)-B-Cl(1)	109.32(7)	Symmetry transformations used to generate
Cl(1)#1-B-Cl(1)	112.12(12)	equivalent atoms:
Cl(4)#1-B-Cl(3)#1	106.5(5)	#1 x,-y+1/2,z

Table 4.   Anisotropic displacement parameters $(\text{Å}^2 \times 10^3)$ for (3c2). The anisotropic
displacement factor exponent takes the form: $-2\pi^2[\ h^2\ a^{*2}U^{11} + ...\ + 2\ h\ k\ a^*\ b^*\ U^{12}\ ]$

Atom	U^{11}	U^{22}	U^{33}	U^{23}	U^{13}	U^{12}
Cl(1)	47(1)	55(1)	55(1)	16(1)	-16(1)	-1(1)
Cl(2)	22(1)	91(1)	55(1)	0	0(1)	0
B	26(1)	45(1)	37(1)	0	-5(1)	0
N(1)	23(1)	37(1)	29(1)	0	-1(1)	0
C(1)	28(1)	51(1)	40(1)	0	-6(1)	0
C(2)	25(1)	56(1)	31(1)	0	2(1)	0
C(3)	29(1)	61(1)	29(1)	0	1(1)	0
C(4)	26(1)	32(1)	33(1)	0	-3(1)	0
C(5)	23(1)	47(1)	34(1)	0	3(1)	0
C(6)	26(1)	50(1)	29(1)	0	1(1)	0

Table 5.   Hydrogen coordinates (x 10^4) and isotropic displacement parameters $(\text{Å}^2 \times 10^3)$
for (3c2).

Atom	x	y	z	U(eq)
H(11)	-769	2500	3272	59
H(12)	-1567	1700	4065	59
H(2)	4041	2500	4368	45
H(3)	1943	2500	3417	48
H(5)	-612	2500	5778	42
H(6)	1525	2500	6687	42

Appendix A3e

Data for the structure of $Br_3B\cdot2$-picoline (**3e**).

Crystals grown by the author. Structure solved by Andrei S. Batsanov at the University of Durham Crystallography Department (reference code 00srv294).

Table 1. Crystal data and structure refinement for (**3e**).

Identification code	00srv294
Empirical formula	C6 H7 B Br3 N
Formula weight	343.67
Temperature	110(2) K
Wavelength	0.71073 Å
Crystal system	Monoclinic
Space group	P2(1)/m
Unit cell dimensions	$a = 6.4829(4)$ Å $\alpha= 90°.$
	$b = 9.8812(6)$ Å $\beta= 91.145(4)°.$
	$c = 7.7791(4)$ Å $\gamma = 90°.$
Volume	498.22(5) Å^3
Z	2
Density (calculated)	2.291 Mg/m^3
Absorption coefficient	12.083 mm^{-1}
F(000)	320
Crystal size	0.18 x 0.30 x 0.30 mm^3
Theta range for data collection	2.62 to 28.97°.
Index ranges	-8<=h<=8, -11<=k<=13, -10<=l<=10
Reflections collected	4232
Independent reflections	1379 [R(int) = 0.0360]
Completeness to theta = 28.97°	98.6 %
Absorption correction	Semi-empirical from equivalents
Max. and min. transmission	0.2103 and 0.1087
Refinement method	Full-matrix least-squares on F^2
Data / restraints / parameters	1379 / 0 / 74
Goodness-of-fit on F^2	1.064
Final R indices [I>2sigma(I)]	R1 = 0.0262, wR2 = 0.0668
R indices (all data)	R1 = 0.0302, wR2 = 0.0686
Extinction coefficient	0.0151(15)
Largest diff. peak and hole	0.631 and -0.680 e.Å^{-3}

Table 2. Atomic coordinates (x 10^4) and equivalent isotropic displacement parameters ($Å^2$x 10^3) for (**3e**). U(eq) is defined as one third of the trace of the orthogonalized U^{ij} tensor.

Atom	x	y	z	U(eq)
Br(1)	-2244(1)	2500	4249(1)	21(1)
Br(2)	1129(1)	848(1)	1923(1)	25(1)
N(1)	2153(5)	2500	5001(4)	18(1)
B	673(7)	2500	3359(5)	17(1)
C(1)	5921(7)	2500	9606(6)	29(1)
C(2)	2708(4)	1317(3)	5776(4)	21(1)
C(3)	3891(5)	1303(3)	7267(4)	24(1)
C(4)	4551(6)	2500	8032(5)	21(1)

Table 3. Bond lengths [Å] and angles [°] for (**3e**).

Br(1)-B	2.027(4)	N(1)-B-Br(2)#1	110.86(16)
Br(2)-B	2.003(2)	Br(2)-B-Br(2)#1	109.15(19)
N(1)-C(2)#1	1.360(3)	N(1)-B-Br(1)	106.2(2)
N(1)-C(2)	1.360(3)	Br(2)-B-Br(1)	109.85(14)
N(1)-B	1.582(5)	Br(2)#1-B-Br(1)	109.85(14)
B-Br(2)#1	2.003(2)	N(1)-C(2)-C(3)	121.3(3)
C(1)-C(4)	1.498(5)	C(2)-C(3)-C(4)	120.9(3)
C(2)-C(3)	1.378(4)	C(3)-C(4)-C(3)#1	116.9(4)
C(3)-C(4)	1.388(4)	C(3)-C(4)-C(1)	121.56(18)
C(4)-C(3)#1	1.388(4)	C(3)#1-C(4)-C(1)	121.56(18)

C(2)#1-N(1)-C(2)	118.4(3)		
C(2)#1-N(1)-B	120.58(17)	Symmetry transformations used to generate	
C(2)-N(1)-B	120.58(17)	equivalent atoms:	
N(1)-B-Br(2)	110.86(16)	#1	x,-y+1/2,z

Table 4.   Anisotropic displacement parameters (Å^2x 10^3) for (3e). The anisotropic displacement factor exponent takes the form: $-2\pi^2[\ h^2\ a^{*2}U^{11} + ...\ + 2\ h\ k\ a^*\ b^*\ U^{12}\ ]$

Atom	U^{11}	U^{22}	U^{33}	U^{23}	U^{13}	U^{12}
Br(1)	18(1)	21(1)	25(1)	0	1(1)	0
Br(2)	29(1)	24(1)	22(1)	-8(1)	-2(1)	3(1)
N(1)	17(1)	18(2)	18(1)	0	-1(1)	0
B	18(2)	18(2)	15(2)	0	-3(1)	0
C(1)	29(2)	35(2)	22(2)	0	-7(2)	0
C(2)	23(1)	17(1)	24(1)	1(1)	-4(1)	-4(1)
C(3)	27(1)	20(1)	24(1)	6(1)	-3(1)	1(1)
C(4)	16(2)	29(2)	18(2)	0	-1(1)	0

Table 5.   Hydrogen coordinates (x 10^4) and isotropic displacement parameters (Å^2x 10^3) for (3e).

Atom	x	y	z	U(eq)
H(13)	7619	2500	9550	34
H(14)	5545	1721	10268	34
H(11)	5210(110)	2500	10690(90)	29(18)
H(12)	6620(90)	1590(60)	9710(70)	41(15)
H(2)	2280(60)	630(40)	5190(50)	26(9)
H(3)	4300(50)	470(40)	7720(40)	26(9)

Appendix A4: Crystal Structure Data Tables for Structures in Chapter 4

Appendix A4b

Data for the structure of CH_3-Ph-CC-PhF$_4$-CC-Ph- CH_3 (**4b**).

Crystals grown by Stephen Watt at Heriot Watt University. Structure solved at 110(2)K by the author at the University of Durham Crystallography Department (reference code 01jmb006).

Table 1. Crystal data and structure refinement for (**4b**).

Identification code	01jmb006	
Empirical formula	C24 H14 F4	
Formula weight	378.35	
Temperature	110(2) K	
Wavelength	0.71073 Å	
Crystal system	Triclinic	
Space group	P-1	
Unit cell dimensions	a = 6.1102(6) Å	α= 81.971(2)°.
	b = 8.0296(7) Å	β= 82.178(2)°.
	c = 9.3699(9) Å	γ = 75.552(2)°.
Volume	438.34(7) Å^3	
Z	1	
Density (calculated)	1.433 Mg/m^3	
Absorption coefficient	0.112 mm^{-1}	
F(000)	194	
Crystal size	0.6 x 0.3 x 0.05 mm^3	
Theta range for data collection	2.21 to 27.49°.	
Index ranges	-7<=h<=7, -10<=k<=10, -12<=l<=12	
Reflections collected	4672	
Independent reflections	2005 [R(int) = 0.0284]	
Completeness to theta = 27.49°	99.4 %	
Absorption correction	Semi-empirical from equivalents	
Max. and min. transmission	0.9889 and 0.9566	
Refinement method	Full-matrix least-squares on F^2	
Data / restraints / parameters	2005 / 0 / 144	
Goodness-of-fit on F^2	1.029	
Final R indices [I>2sigma(I)]	R1 = 0.0452, wR2 = 0.1148	
R indices (all data)	R1 = 0.0698, wR2 = 0.1271	
Extinction coefficient	.	
Largest diff. peak and hole	0.253 and -0.339 e.Å^{-3}	

Table 2. Atomic coordinates (x 10^4) and equivalent isotropic displacement parameters (Å^2x 10^3) for (4b). U(eq) is defined as one third of the trace of the orthogonalized U^{ij} tensor.

Atom	x	y	z	U(eq)
C(1)	2029(3)	-534(2)	595(2)	20(1)
C(2)	253(3)	636(2)	1239(2)	20(1)
C(3)	-1837(3)	1215(2)	661(2)	19(1)
C(4)	-3675(3)	2461(2)	1300(2)	22(1)
C(5)	-5241(3)	3523(2)	1798(2)	21(1)
C(6)	-7125(3)	4781(2)	2391(2)	19(1)
C(7)	-6870(3)	5680(2)	3515(2)	22(1)
C(8)	-8714(3)	6876(2)	4097(2)	22(1)
C(9)	-10830(3)	7240(2)	3570(2)	21(1)
C(10)	-11060(3)	6349(2)	2439(2)	21(1)
C(11)	-9244(3)	5124(2)	1868(2)	20(1)
C(12)	-12821(3)	8534(2)	4222(2)	28(1)
F(1)	3989(2)	-1039(1)	1205(1)	24(1)
F(2)	527(2)	1216(1)	2466(1)	25(1)

Table 3. Bond lengths [Å] and angles [°] for (4b).

C(1)-F(1)	1.343(2)	C(10)-H(10)	0.96(2)
C(1)-C(2)	1.377(2)	C(11)-H(11)	0.98(2)
C(1)-C(3)#1	1.395(2)	C(12)-H(12A)	0.9800
C(2)-F(2)	1.3445(19)	C(12)-H(12B)	0.9800
C(2)-C(3)	1.401(3)	C(12)-H(12C)	0.9800
C(3)-C(1)#1	1.395(2)		
C(3)-C(4)	1.429(2)	F(1)-C(1)-C(2)	118.77(15)
C(4)-C(5)	1.201(2)	F(1)-C(1)-C(3)#1	119.43(15)
C(5)-C(6)	1.434(2)	C(2)-C(1)-C(3)#1	121.79(16)
C(6)-C(11)	1.396(3)	F(2)-C(2)-C(1)	118.96(16)
C(6)-C(7)	1.403(2)	F(2)-C(2)-C(3)	119.30(15)
C(7)-C(8)	1.389(2)	C(1)-C(2)-C(3)	121.73(16)
C(7)-H(7)	0.97(2)	C(1)#1-C(3)-C(2)	116.48(15)
C(8)-C(9)	1.395(3)	C(1)#1-C(3)-C(4)	121.30(16)
C(8)-H(8)	0.96(2)	C(2)-C(3)-C(4)	122.22(16)
C(9)-C(10)	1.399(2)	C(5)-C(4)-C(3)	178.06(19)
C(9)-C(12)	1.509(2)	C(4)-C(5)-C(6)	179.43(19)
C(10)-C(11)	1.388(2)	C(11)-C(6)-C(7)	118.90(15)

C(11)-C(6)-C(5)	120.71(16)	C(10)-C(11)-C(6)	120.55(16)
C(7)-C(6)-C(5)	120.39(16)	C(10)-C(11)-H(11)	120.2(11)
C(8)-C(7)-C(6)	119.96(17)	C(6)-C(11)-H(11)	119.2(11)
C(8)-C(7)-H(7)	118.7(11)	C(9)-C(12)-H(12A)	109.5
C(6)-C(7)-H(7)	121.3(11)	C(9)-C(12)-H(12B)	109.5
C(7)-C(8)-C(9)	121.48(16)	H(12A)-C(12)-H(12B)	109.5
C(7)-C(8)-H(8)	118.4(13)	C(9)-C(12)-H(12C)	109.5
C(9)-C(8)-H(8)	120.1(13)	H(12A)-C(12)-H(12C)	109.5
C(8)-C(9)-C(10)	118.08(16)	H(12B)-C(12)-H(12C)	109.5
C(8)-C(9)-C(12)	120.81(16)		
C(10)-C(9)-C(12)	121.10(17)		
C(11)-C(10)-C(9)	121.02(17)	Symmetry transformations used to generate equivalent atoms:	
C(11)-C(10)-H(10)	118.2(13)	#1	-x,-y,-z
C(9)-C(10)-H(10)	120.8(13)		

Table 4. Anisotropic displacement parameters ($\text{Å}^2 \times 10^3$) for (**4b**). The anisotropic displacement factor exponent takes the form: $-2\pi^2[\,h^2\,a^{*2}U^{11} + \ldots + 2\,h\,k\,a^*\,b^*\,U^{12}\,]$

Atom	U^{11}	U^{22}	U^{33}	U^{23}	U^{13}	U^{12}
C(1)	14(1)	18(1)	25(1)	1(1)	-2(1)	-1(1)
C(2)	21(1)	18(1)	21(1)	-5(1)	1(1)	-4(1)
C(3)	16(1)	14(1)	25(1)	-2(1)	1(1)	-1(1)
C(4)	19(1)	19(1)	25(1)	-2(1)	1(1)	-2(1)
C(5)	19(1)	20(1)	23(1)	-3(1)	-1(1)	0(1)
C(6)	17(1)	15(1)	21(1)	-3(1)	1(1)	1(1)
C(7)	18(1)	23(1)	25(1)	-3(1)	-2(1)	-3(1)
C(8)	23(1)	21(1)	23(1)	-8(1)	0(1)	-2(1)
C(9)	20(1)	15(1)	24(1)	-2(1)	4(1)	-1(1)
C(10)	17(1)	20(1)	25(1)	-1(1)	-2(1)	1(1)
C(11)	22(1)	17(1)	20(1)	-5(1)	-1(1)	-2(1)
C(12)	23(1)	23(1)	31(1)	-6(1)	6(1)	4(1)
F(1)	16(1)	25(1)	30(1)	-2(1)	-6(1)	1(1)
F(2)	27(1)	25(1)	25(1)	-10(1)	-3(1)	-3(1)

Table 5. Hydrogen coordinates (x 10^4) and isotropic displacement parameters ($Å^2$x 10^3) for (**4b**).

Atom	x	y	z	U(eq)
H(12A)	-12297	9515	4450	42
H(12B)	-13505	7981	5111	42
H(12C)	-13954	8947	3527	42
H(7)	-5410(40)	5500(30)	3890(20)	24(5)
H(8)	-8490(40)	7490(30)	4850(20)	33(6)
H(10)	-12480(40)	6570(30)	2040(20)	35(6)
H(11)	-9430(30)	4490(20)	1090(20)	23(5)

Table 6. Torsion angles [°] for (**4b**).

F(1)-C(1)-C(2)-F(2)	-0.9(2)
C(3)#1-C(1)-C(2)-F(2)	178.60(15)
F(1)-C(1)-C(2)-C(3)	-179.94(16)
C(3)#1-C(1)-C(2)-C(3)	-0.4(3)
F(2)-C(2)-C(3)-C(1)#1	-178.62(15)
C(1)-C(2)-C(3)-C(1)#1	0.4(3)
F(2)-C(2)-C(3)-C(4)	2.5(3)
C(1)-C(2)-C(3)-C(4)	-178.47(16)
C(1)#1-C(3)-C(4)-C(5)	-27(6)
C(2)-C(3)-C(4)-C(5)	151(6)
C(3)-C(4)-C(5)-C(6)	78(21)
C(4)-C(5)-C(6)-C(11)	-41(20)
C(4)-C(5)-C(6)-C(7)	139(20)
C(11)-C(6)-C(7)-C(8)	0.6(3)
C(5)-C(6)-C(7)-C(8)	-179.01(16)
C(6)-C(7)-C(8)-C(9)	-1.4(3)
C(7)-C(8)-C(9)-C(10)	0.7(3)
C(7)-C(8)-C(9)-C(12)	179.57(16)
C(8)-C(9)-C(10)-C(11)	0.7(3)
C(12)-C(9)-C(10)-C(11)	-178.17(16)
C(9)-C(10)-C(11)-C(6)	-1.4(3)
C(7)-C(6)-C(11)-C(10)	0.7(3)
C(5)-C(6)-C(11)-C(10)	-179.61(16)

Symmetry transformations used to generate equivalent atoms:

#1 -x,-y,-z

Appendix A4d

Data for the structure of CF_3-Ph-CC-PhF_4-CC-Ph- CF_3 (**4d**).

Crystals grown by Stephen Watt at Heriot Watt University. Structure solved at 100(2)K

by the author at the University of Durham Crystallography Department (reference code

01srv071).

Table 1. Crystal data and structure refinement for (**4d**).

Identification code	01srv071
Empirical formula	C24 H8 F10
Formula weight	486.30
Temperature	100(2) K
Wavelength	0.71073 Å
Crystal system	Monoclinic
Space group	P2(1)/c
Unit cell dimensions	a = 16.924(5) Å α= 90°.
	b = 4.9358(14) Å β= 103.328(4)°.
	c = 11.498(3) Å γ = 90°.
Volume	934.6(5) Å^3
Z	2
Density (calculated)	1.728 Mg/m^3
Absorption coefficient	0.170 mm^{-1}
F(000)	484
Crystal size	0.6 x 0.6 x 0.1 mm^3
Theta range for data collection	1.24 to 27.48°.
Index ranges	-21<=h<=21, -6<=k<=6, -14<=l<=14
Reflections collected	9320
Independent reflections	2152 [R(int) = 0.0436]
Completeness to theta = 27.48°	100.0 %
Absorption correction	Semi-empirical from equivalents
Max. and min. transmission	0.74555 and 0.52789
Refinement method	Full-matrix least-squares on F^2
Data / restraints / parameters	2152 / 0 / 170
Goodness-of-fit on F^2	1.117
Final R indices [I>2sigma(I)]	R1 = 0.0489, wR2 = 0.1256
R indices (all data)	R1 = 0.0738, wR2 = 0.1515
Extinction coefficient	.
Largest diff. peak and hole	0.382 and -0.334 e.Å^{-3}

Table 2. Atomic coordinates (x 10^4) and equivalent isotropic displacement parameters (Å^2x 10^3) for (**4d**). U(eq) is defined as one third of the trace of the orthogonalized U^{ij} tensor.

Atom	x	y	z	U(eq)
C(1)	4364(1)	-435(4)	5528(2)	14(1)
C(2)	4919(1)	1566(4)	5945(2)	14(1)
C(3)	5577(1)	2072(4)	5438(2)	14(1)
C(4)	6161(1)	4133(4)	5882(2)	16(1)
C(5)	6653(1)	5837(5)	6274(2)	16(1)
C(6)	7241(1)	7857(4)	6775(2)	16(1)
C(7)	7883(1)	8453(5)	6239(2)	19(1)
C(8)	8467(2)	10325(5)	6751(2)	19(1)
C(9)	8414(1)	11625(4)	7803(2)	16(1)
C(10)	7771(1)	11099(5)	8325(2)	17(1)
C(11)	7184(1)	9233(5)	7817(2)	18(1)
C(12)	9080(1)	13491(5)	8411(2)	20(1)
F(1)	3739(1)	-791(3)	6045(1)	20(1)
F(2)	4810(1)	3133(3)	6853(1)	20(1)
F(12A)	8804(1)	15525(3)	8982(1)	26(1)
F(12B)	9640(1)	12192(3)	9235(2)	38(1)
F(12C)	9477(1)	14621(3)	7656(1)	30(1)

Table 3. Bond lengths [Å] and angles [°] for (**4d**).

C(1)-F(1)	1.339(3)	C(9)-C(12)	1.497(3)
C(1)-C(2)	1.371(3)	C(10)-C(11)	1.382(3)
C(1)-C(3)#1	1.395(3)	C(12)-F(12C)	1.336(3)
C(2)-F(2)	1.346(2)	C(12)-F(12B)	1.340(3)
C(2)-C(3)	1.394(3)	C(12)-F(12A)	1.341(3)
C(3)-C(1)#1	1.395(3)		
C(3)-C(4)	1.428(3)	F(1)-C(1)-C(2)	119.1(2)
C(4)-C(5)	1.197(3)	F(1)-C(1)-C(3)#1	119.06(19)
C(5)-C(6)	1.432(3)	C(2)-C(1)-C(3)#1	121.8(2)
C(6)-C(7)	1.398(3)	F(2)-C(2)-C(1)	118.7(2)
C(6)-C(11)	1.400(3)	F(2)-C(2)-C(3)	119.16(19)
C(7)-C(8)	1.383(3)	C(1)-C(2)-C(3)	122.1(2)
C(8)-C(9)	1.390(3)	C(2)-C(3)-C(1)#1	116.1(2)
C(9)-C(10)	1.384(3)	C(2)-C(3)-C(4)	122.1(2)

C(1)#1-C(3)-C(4)	121.8(2)
C(5)-C(4)-C(3)	178.8(2)
C(4)-C(5)-C(6)	178.5(2)
C(7)-C(6)-C(11)	119.3(2)
C(7)-C(6)-C(5)	120.5(2)
C(11)-C(6)-C(5)	120.2(2)
C(8)-C(7)-C(6)	120.3(2)
C(7)-C(8)-C(9)	119.7(2)
C(10)-C(9)-C(8)	120.4(2)
C(10)-C(9)-C(12)	119.7(2)
C(8)-C(9)-C(12)	119.9(2)
C(11)-C(10)-C(9)	120.1(2)

C(10)-C(11)-C(6)	120.1(2)
F(12C)-C(12)-F(12B)	106.2(2)
F(12C)-C(12)-F(12A)	106.83(19)
F(12B)-C(12)-F(12A)	106.3(2)
F(12C)-C(12)-C(9)	113.0(2)
F(12B)-C(12)-C(9)	111.7(2)
F(12A)-C(12)-C(9)	112.35(19)

Symmetry transformations used to generate equivalent atoms:

#1   -x+1,-y,-z+1

Table 4.   Anisotropic displacement parameters ($\mathring{A}^2 \times 10^3$) for (4d). The anisotropic displacement factor exponent takes the form: $-2\pi^2[h^2 a^{*2}U^{11} + ... + 2 h k a^* b^* U^{12}]$

Atom	U^{11}	U^{22}	U^{33}	U^{23}	U^{13}	U^{12}
C(1)	17(1)	16(1)	12(1)	3(1)	6(1)	-2(1)
C(2)	22(1)	13(1)	9(1)	-2(1)	4(1)	2(1)
C(3)	18(1)	12(1)	12(1)	1(1)	1(1)	0(1)
C(4)	22(1)	14(1)	12(1)	2(1)	5(1)	1(1)
C(5)	19(1)	18(1)	12(1)	1(1)	3(1)	0(1)
C(6)	19(1)	12(1)	16(1)	3(1)	1(1)	0(1)
C(7)	23(1)	20(1)	14(1)	-2(1)	5(1)	-1(1)
C(8)	20(1)	20(1)	17(1)	2(1)	7(1)	-1(1)
C(9)	18(1)	13(1)	15(1)	2(1)	1(1)	1(1)
C(10)	21(1)	16(1)	14(1)	-1(1)	3(1)	2(1)
C(11)	19(1)	17(1)	17(1)	3(1)	5(1)	0(1)
C(12)	20(1)	17(1)	21(1)	0(1)	4(1)	0(1)
F(1)	22(1)	24(1)	19(1)	-2(1)	11(1)	-5(1)
F(2)	29(1)	20(1)	14(1)	-6(1)	9(1)	-1(1)
F(12A)	29(1)	21(1)	27(1)	-9(1)	7(1)	-5(1)
F(12B)	32(1)	25(1)	42(1)	5(1)	-18(1)	-2(1)
F(12C)	29(1)	29(1)	35(1)	-6(1)	13(1)	-13(1)

Table 5. Hydrogen coordinates (x 10⁴) and isotropic displacement parameters (Å^2x 10 ³) for (**4d**).

Atom	x	y	z	U(eq)
H(7)	7948(17)	7450(60)	5560(30)	27(8)
H(8)	8897(18)	10600(60)	6450(30)	26(8)
H(10)	7751(18)	12050(70)	9050(30)	38(9)
H(11)	6753(18)	8770(60)	8170(30)	28(8)

Table 6. Torsion angles [°] for (**4d**).

F(1)-C(1)-C(2)-F(2)	-0.8(3)
C(3)#1-C(1)-C(2)-F(2)	177.71(19)
F(1)-C(1)-C(2)-C(3)	-179.08(19)
C(3)#1-C(1)-C(2)-C(3)	-0.5(4)
F(2)-C(2)-C(3)-C(1)#1	-177.73(18)
C(1)-C(2)-C(3)-C(1)#1	0.5(4)
F(2)-C(2)-C(3)-C(4)	2.6(3)
C(1)-C(2)-C(3)-C(4)	-179.2(2)
C(2)-C(3)-C(4)-C(5)	61(12)
C(1)#1-C(3)-C(4)-C(5)	-119(12)
C(3)-C(4)-C(5)-C(6)	-23(19)
C(4)-C(5)-C(6)-C(7)	146(9)
C(4)-C(5)-C(6)-C(11)	-33(9)
C(11)-C(6)-C(7)-C(8)	1.8(3)
C(5)-C(6)-C(7)-C(8)	-177.3(2)
C(6)-C(7)-C(8)-C(9)	-0.2(4)
C(7)-C(8)-C(9)-C(10)	-1.4(3)
C(7)-C(8)-C(9)-C(12)	175.3(2)
C(8)-C(9)-C(10)-C(11)	1.3(3)
C(12)-C(9)-C(10)-C(11)	-175.4(2)
C(9)-C(10)-C(11)-C(6)	0.3(3)
C(7)-C(6)-C(11)-C(10)	-1.9(3)
C(5)-C(6)-C(11)-C(10)	177.3(2)
C(10)-C(9)-C(12)-F(12C)	-156.0(2)
C(8)-C(9)-C(12)-F(12C)	27.3(3)
C(10)-C(9)-C(12)-F(12B)	84.3(3)
C(8)-C(9)-C(12)-F(12B)	-92.4(3)
C(10)-C(9)-C(12)-F(12A)	-35.0(3)
C(8)-C(9)-C(12)-F(12A)	148.2(2)

Symmetry transformations used to generate equivalent atoms: #1 -x+1,-y,-z+1

Appendix A4e

Data for the structure of PhF_5-CC-PhF_4-CC-PhF_5 (**4e**).

Crystals grown by Stephen Watt at Heriot Watt University. Structure solved at 100(2)K

by the author at the University of Durham Crystallography Department (reference code

01srv061).

Table 1. Crystal data and structure refinement for (**4e**).

Identification code	global	
Empirical formula	C22 F14	
Formula weight	530.22	
Temperature	100(2) K	
Wavelength	0.71073 Å	
Crystal system	Monoclinic	
Space group	C2/m	
Unit cell dimensions	a = 8.9294(7) Å	α= 90°.
	b = 7.6605(7) Å	β= 99.437(2)°.
	c = 13.2005(11) Å	γ = 90°.
Volume	890.74(13) Å^3	
Z	2	
Density (calculated)	1.977 Mg/m^3	
Absorption coefficient	0.219 mm^{-1}	
F(000)	516	
Crystal size	0.5 x 0.5 x 0.06 mm^3	
Theta range for data collection	1.56 to 27.50°.	
Index ranges	-11<=h<=11, -9<=k<=9, -17<=l<=17	
Reflections collected	4717	
Independent reflections	1102 [R(int) = 0.0420]	
Completeness to theta = 27.50°	100.0 %	
Absorption correction	None	
Max. and min. transmission	. and .	
Refinement method	Full-matrix least-squares on F^2	
Data / restraints / parameters	1102 / 0 / 91	
Goodness-of-fit on F^2	1.075	
Final R indices [I>2sigma(I)]	R1 = 0.0311, wR2 = 0.0955	
R indices (all data)	R1 = 0.0375, wR2 = 0.1028	
Largest diff. peak and hole	0.409 and -0.271 e.Å^{-3}	

Table 2. Atomic coordinates (x 10^4) and equivalent isotropic displacement parameters (Å^2x 10^3) for (**4e**). U(eq) is defined as one third of the trace of the orthogonalized U^{ij} tensor.

Atom	x	y	z	U(eq)
C(1)	9482(1)	-1560(1)	336(1)	14(1)
C(2)	8942(2)	0	691(1)	14(1)
C(3)	7872(2)	0	1384(1)	16(1)
C(4)	6979(2)	0	1962(1)	16(1)
C(5)	5902(2)	0	2650(1)	14(1)
C(6)	5353(1)	-1557(1)	2998(1)	15(1)
C(7)	4293(1)	-1569(2)	3655(1)	17(1)
C(8)	3756(2)	0	3972(1)	18(1)
F(1)	8992(1)	-3078(1)	654(1)	18(1)
F(6)	5858(1)	-3077(1)	2692(1)	20(1)
F(7)	3789(1)	-3069(1)	3981(1)	24(1)
F(8)	2730(1)	0	4600(1)	26(1)

Table 3. Bond lengths [Å] and angles [°] for (**4e**).

C(1)-F(1)	1.3346(12)	C(1)#2-C(2)-C(3)	121.25(7)
C(1)-C(1)#1	1.383(2)	C(1)-C(2)-C(3)	121.25(7)
C(1)-C(2)	1.3978(13)	C(4)-C(3)-C(2)	179.90(17)
C(2)-C(1)#2	1.3978(13)	C(3)-C(4)-C(5)	179.73(17)
C(2)-C(3)	1.427(2)	C(6)#2-C(5)-C(6)	117.42(14)
C(3)-C(4)	1.190(2)	C(6)#2-C(5)-C(4)	121.29(7)
C(4)-C(5)	1.426(2)	C(6)-C(5)-C(4)	121.29(7)
C(5)-C(6)#2	1.3959(13)	F(6)-C(6)-C(7)	118.88(10)
C(5)-C(6)	1.3959(13)	F(6)-C(6)-C(5)	119.46(10)
C(6)-F(6)	1.3350(13)	C(7)-C(6)-C(5)	121.66(10)
C(6)-C(7)	1.3853(17)	F(7)-C(7)-C(8)	120.04(11)
C(7)-F(7)	1.3310(13)	F(7)-C(7)-C(6)	120.64(10)
C(7)-C(8)	1.3836(14)	C(8)-C(7)-C(6)	119.32(10)
C(8)-F(8)	1.3327(17)	F(8)-C(8)-C(7)#2	119.70(7)
C(8)-C(7)#2	1.3836(14)	F(8)-C(8)-C(7)	119.70(7)
		C(7)#2-C(8)-C(7)	120.60(14)

F(1)-C(1)-C(1)#1	119.37(5)
F(1)-C(1)-C(2)	119.39(10)
C(1)#1-C(1)-C(2)	121.25(7)
C(1)#2-C(2)-C(1)	117.51(14)

Symmetry transformations used to generate equivalent atoms:
#1   -x+2,y,-z   #2   x,-y,z

Table 4.   Anisotropic displacement parameters ($\text{Å}^2 \times 10^3$) for (**4e**). The anisotropic displacement factor exponent takes the form: $-2\pi^2[\ h^2\ a^{*2}U^{11} + ... + 2\ h\ k\ a^*\ b^*\ U^{12}\ ]$

Atom	U^{11}	U^{22}	U^{33}	U^{23}	U^{13}	U^{12}
C(1)	13(1)	13(1)	16(1)	2(1)	3(1)	-1(1)
C(2)	11(1)	15(1)	15(1)	0	3(1)	0
C(3)	14(1)	17(1)	17(1)	0	3(1)	0
C(4)	14(1)	15(1)	17(1)	0	3(1)	0
C(5)	11(1)	16(1)	15(1)	0	2(1)	0
C(6)	13(1)	15(1)	17(1)	-1(1)	2(1)	0(1)
C(7)	14(1)	19(1)	17(1)	3(1)	3(1)	-5(1)
C(8)	12(1)	27(1)	15(1)	0	5(1)	0
F(1)	19(1)	13(1)	23(1)	3(1)	7(1)	-3(1)
F(6)	22(1)	13(1)	26(1)	-2(1)	5(1)	1(1)
F(7)	23(1)	24(1)	27(1)	7(1)	7(1)	-8(1)
F(8)	18(1)	41(1)	24(1)	0	14(1)	0

Table 5.   Torsion angles [°] for (**4e**).

F(1)-C(1)-C(2)-C(1)#2	-179.86(7)
C(1)#1-C(1)-C(2)-C(1)#2	0.2(2)
F(1)-C(1)-C(2)-C(3)	-0.12(19)
C(1)#1-C(1)-C(2)-C(3)	179.96(13)
C(1)#2-C(2)-C(3)-C(4)	90(100)
C(1)-C(2)-C(3)-C(4)	-90(100)
C(2)-C(3)-C(4)-C(5)	0(100)
C(3)-C(4)-C(5)-C(6)#2	-89.87(15)
C(3)-C(4)-C(5)-C(6)	89.87(15)
C(6)#2-C(5)-C(6)-F(6)	-179.36(7)
C(4)-C(5)-C(6)-F(6)	0.89(19)
C(6)#2-C(5)-C(6)-C(7)	0.6(2)
C(4)-C(5)-C(6)-C(7)	-179.14(12)
F(6)-C(6)-C(7)-F(7)	0.25(16)
C(5)-C(6)-C(7)-F(7)	-179.72(10)
F(6)-C(6)-C(7)-C(8)	-179.69(10)
C(5)-C(6)-C(7)-C(8)	0.34(19)
F(7)-C(7)-C(8)-F(8)	-0.3(2)
C(6)-C(7)-C(8)-F(8)	179.63(11)
F(7)-C(7)-C(8)-C(7)#2	178.73(8)
C(6)-C(7)-C(8)-C(7)#2	-1.3(2)

Symmetry transformations used to generate equivalent atoms: #1 -x+2,y,-z   #2 x,-y,z

Appendix A4h

Data for the structure of MeO-PhF$_4$-CC-PhF$_4$-CC-PhF$_4$-OMe (**4h**).

Crystals grown by Stephen Watt at Heriot Watt University. Structure solved at 100(2)K by the author at the University of Durham Crystallography Department (reference code 01srv097).

Table 1. Crystal data and structure refinement for (**4h**).

Identification code	01srv097
Empirical formula	C24 H6 F12 O2
Formula weight	554.29
Temperature	100(2) K
Wavelength	0.71073 Å
Crystal system	Monoclinic
Space group	C2/c
Unit cell dimensions	a = 28.941(7) Å α= 90°.
	b = 7.7027(18) Å β= 96.541(4)°.
	c = 8.961(2) Å γ = 90°.
Volume	1984.6(8) Å^3
Z	4
Density (calculated)	1.855 Mg/m^3
Absorption coefficient	0.194 mm^{-1}
F(000)	1096
Crystal size	0.5 x 0.2 x 0.1 mm^3
Theta range for data collection	2.74 to 27.48°.
Index ranges	-37<=h<=37, -10<=k<=10, -11<=l<=11
Reflections collected	10047
Independent reflections	2273 [R(int) = 0.0403]
Completeness to theta = 27.48°	99.9 %
Absorption correction	Semi-empirical from equivalents
Max. and min. transmission	0.9809 and 0.9092
Refinement method	Full-matrix least-squares on F^2
Data / restraints / parameters	2273 / 0 / 172
Goodness-of-fit on F^2	1.135
Final R indices [I>2sigma(I)]	R1 = 0.0488, wR2 = 0.1271
R indices (all data)	R1 = 0.0602, wR2 = 0.1330
Extinction coefficient	.
Largest diff. peak and hole	0.416 and -0.401 e.Å^{-3}

Table 2. Atomic coordinates (x 10^4) and equivalent isotropic displacement parameters (Å^2x 10^3) for (**4h**). U(eq) is defined as one third of the trace of the orthogonalized U^{ij} tensor.

Atom	x	y	z	U(eq)
C(1)	4850(1)	-1019(3)	6848(2)	13(1)
C(2)	4849(1)	-4115(3)	6845(2)	13(1)
C(3)	4690(1)	-2567(3)	6153(2)	13(1)
C(4)	4379(1)	-2542(3)	4805(2)	14(1)
C(5)	4118(1)	-2483(3)	3675(2)	15(1)
C(6)	3800(1)	-2329(3)	2346(2)	13(1)
C(7)	3648(1)	-709(3)	1789(2)	13(1)
C(8)	3333(1)	-546(3)	530(2)	14(1)
C(9)	3145(1)	-1995(3)	-269(2)	14(1)
C(10)	3302(1)	-3614(3)	264(2)	14(1)
C(11)	3618(1)	-3763(3)	1533(2)	14(1)
C(12)	2651(1)	-2953(3)	-2480(2)	19(1)
O(1)	2825(1)	-1624(2)	-1437(2)	21(1)
F(1)	4706(1)	495(2)	6225(1)	17(1)
F(2)	4705(1)	-5629(2)	6223(1)	17(1)
F(7)	3811(1)	732(2)	2504(1)	17(1)
F(8)	3193(1)	1040(2)	51(1)	19(1)
F(10)	3143(1)	-5095(2)	-418(1)	21(1)
F(11)	3748(1)	-5362(2)	2007(1)	18(1)

Table 3. Bond lengths [Å] and angles [°] for (**4h**).

C(1)-F(1)	1.338(2)	C(9)-O(1)	1.347(2)
C(1)-C(1)#1	1.375(4)	C(9)-C(10)	1.393(3)
C(1)-C(3)	1.399(3)	C(10)-F(10)	1.350(2)
C(2)-F(2)	1.339(2)	C(10)-C(11)	1.380(3)
C(2)-C(2)#1	1.380(4)	C(11)-F(11)	1.343(2)
C(2)-C(3)	1.398(3)	C(12)-O(1)	1.439(2)
C(3)-C(4)	1.423(3)		
C(4)-C(5)	1.192(3)	F(1)-C(1)-C(1)#1	119.40(10)
C(5)-C(6)	1.425(3)	F(1)-C(1)-C(3)	119.06(17)
C(6)-C(11)	1.393(3)	C(1)#1-C(1)-C(3)	121.54(11)
C(6)-C(7)	1.396(3)	F(2)-C(2)-C(2)#1	119.42(10)
C(7)-F(7)	1.340(2)	F(2)-C(2)-C(3)	119.14(17)
C(7)-C(8)	1.372(3)	C(2)#1-C(2)-C(3)	121.45(11)
C(8)-F(8)	1.342(2)	C(2)-C(3)-C(1)	117.01(17)
C(8)-C(9)	1.402(3)	C(2)-C(3)-C(4)	122.21(18)

C(1)-C(3)-C(4)	120.78(18)	O(1)-C(9)-C(8)	114.87(17)
C(5)-C(4)-C(3)	178.6(2)	C(10)-C(9)-C(8)	116.45(18)
C(4)-C(5)-C(6)	177.2(2)	F(10)-C(10)-C(11)	117.53(17)
C(11)-C(6)-C(7)	115.86(17)	F(10)-C(10)-C(9)	121.37(17)
C(11)-C(6)-C(5)	122.74(18)	C(11)-C(10)-C(9)	121.08(18)
C(7)-C(6)-C(5)	121.40(18)	F(11)-C(11)-C(10)	118.22(17)
F(7)-C(7)-C(8)	118.78(17)	F(11)-C(11)-C(6)	119.06(17)
F(7)-C(7)-C(6)	119.31(17)	C(10)-C(11)-C(6)	122.71(18)
C(8)-C(7)-C(6)	121.91(17)	C(9)-O(1)-C(12)	120.87(16)
F(8)-C(8)-C(7)	119.61(17)		
F(8)-C(8)-C(9)	118.41(17)		
C(7)-C(8)-C(9)	121.97(18)		
O(1)-C(9)-C(10)	128.65(18)		

Symmetry transformations used to generate equivalent atoms: #1 -x+1,y,-z+3/2

Table 4. Anisotropic displacement parameters ($Å^2$x 10^3) for (**4h**). The anisotropic displacement factor exponent takes the form: $-2\pi^2[h^2 a^{*2}U^{11} + ... + 2 h k a^* b^* U^{12}]$

Atom	U^{11}	U^{22}	U^{33}	U^{23}	U^{13}	U^{12}
C(1)	15(1)	11(1)	14(1)	3(1)	2(1)	2(1)
C(2)	15(1)	10(1)	14(1)	-1(1)	1(1)	0(1)
C(3)	13(1)	14(1)	12(1)	0(1)	1(1)	0(1)
C(4)	16(1)	13(1)	15(1)	0(1)	2(1)	-1(1)
C(5)	17(1)	15(1)	14(1)	-1(1)	1(1)	0(1)
C(6)	14(1)	16(1)	11(1)	1(1)	0(1)	-1(1)
C(7)	14(1)	12(1)	12(1)	-2(1)	1(1)	-3(1)
C(8)	15(1)	11(1)	15(1)	2(1)	1(1)	0(1)
C(9)	15(1)	15(1)	13(1)	2(1)	-2(1)	-1(1)
C(10)	16(1)	10(1)	15(1)	-2(1)	0(1)	-3(1)
C(11)	16(1)	10(1)	15(1)	2(1)	2(1)	0(1)
C(12)	20(1)	21(1)	14(1)	-4(1)	-6(1)	1(1)
O(1)	26(1)	13(1)	21(1)	-1(1)	-12(1)	1(1)
F(1)	22(1)	10(1)	18(1)	4(1)	-1(1)	3(1)
F(2)	21(1)	10(1)	18(1)	-4(1)	-1(1)	-3(1)
F(7)	21(1)	12(1)	17(1)	-5(1)	-2(1)	-4(1)
F(8)	24(1)	9(1)	22(1)	3(1)	-3(1)	3(1)
F(10)	31(1)	11(1)	19(1)	-2(1)	-7(1)	-5(1)
F(11)	23(1)	10(1)	20(1)	4(1)	-2(1)	3(1)

Table 5.   Hydrogen coordinates (x 10^4) and isotropic displacement parameters ($Å^2$x 10 ^{3}) for (**4h**).

Atom	x	y	z	U(eq)
H(12A)	2429	-2442	-3266	29
H(12B)	2495	-3852	-1948	29
H(12C)	2910	-3471	-2938	29

Table 6. Torsion angles [°] for (**4h**).

F(2)-C(2)-C(3)-C(1)	179.81(17)
C(2)#1-C(2)-C(3)-C(1)	0.0(3)
F(2)-C(2)-C(3)-C(4)	-0.1(3)
C(2)#1-C(2)-C(3)-C(4)	-179.9(2)
F(1)-C(1)-C(3)-C(2)	179.99(17)
C(1)#1-C(1)-C(3)-C(2)	0.2(3)
F(1)-C(1)-C(3)-C(4)	-0.2(3)
C(1)#1-C(1)-C(3)-C(4)	-180.0(2)
C(2)-C(3)-C(4)-C(5)	178(100)
C(1)-C(3)-C(4)-C(5)	-1(9)
C(3)-C(4)-C(5)-C(6)	-21(13)
C(4)-C(5)-C(6)-C(11)	-159(5)
C(4)-C(5)-C(6)-C(7)	20(5)
C(11)-C(6)-C(7)-F(7)	-179.48(17)
C(5)-C(6)-C(7)-F(7)	1.3(3)
C(11)-C(6)-C(7)-C(8)	0.9(3)
C(5)-C(6)-C(7)-C(8)	-178.41(19)
F(7)-C(7)-C(8)-F(8)	-0.5(3)
C(6)-C(7)-C(8)-F(8)	179.14(18)
F(7)-C(7)-C(8)-C(9)	-179.52(18)
C(6)-C(7)-C(8)-C(9)	0.1(3)
F(8)-C(8)-C(9)-O(1)	-1.9(3)
C(7)-C(8)-C(9)-O(1)	177.06(18)
F(8)-C(8)-C(9)-C(10)	179.72(17)
C(7)-C(8)-C(9)-C(10)	-1.3(3)
O(1)-C(9)-C(10)-F(10)	1.8(3)
C(8)-C(9)-C(10)-F(10)	179.84(18)

O(1)-C(9)-C(10)-C(11)	-176.7(2)
C(8)-C(9)-C(10)-C(11)	1.4(3)
F(10)-C(10)-C(11)-F(11)	0.2(3)
C(9)-C(10)-C(11)-F(11)	178.74(17)
F(10)-C(10)-C(11)-C(6)	-178.93(18)
C(9)-C(10)-C(11)-C(6)	-0.4(3)
C(7)-C(6)-C(11)-F(11)	-179.88(17)
C(5)-C(6)-C(11)-F(11)	-0.6(3)
C(7)-C(6)-C(11)-C(10)	-0.7(3)
C(5)-C(6)-C(11)-C(10)	178.54(19)
C(10)-C(9)-O(1)-C(12)	-10.7(3)
C(8)-C(9)-O(1)-C(12)	171.24(18)

Symmetry transformations used to generate equivalent atoms:

#1 -x+1,y,-z+3/2

Appendix A4i

Data for the structure of MeO-Ph-CC-PhF$_4$-CC-Ph-OMe (**4i**).

Crystals grown by Stephen Watt at Heriot Watt University. Structure solved at 100(2)K

by the author at the University of Durham Crystallography Department (reference code

01jmb001).

Table 1. Crystal data and structure refinement for (**4i**).

Identification code	01jmb001a
Empirical formula	C24 H14 F4 O2
Formula weight	410.35
Temperature	383(2) K
Wavelength	0.71073 Å
Crystal system	Monoclinic
Space group	P2$_1$/n
Unit cell dimensions	a = 8.5770(16) Å α= 90°.
	b = 5.9594(12) Å β= 94.948(4)°.
	c = 18.882(4) Å γ = 90°.
Volume	961.5(3) Å^3
Z	2
Density (calculated)	1.417 Mg/m^3
Absorption coefficient	0.116 mm^{-1}
F(000)	420
Crystal size	? x ? x ? mm^3
Theta range for data collection	2.17 to 27.49°.
Index ranges	-10<=h<=11, -7<=k<=7, -24<=l<=24
Reflections collected .	9658
Independent reflections	2206 [R(int) = 0.0537]
Completeness to theta = 27.49°	100.0 %
Refinement method	Full-matrix least-squares on F^2
Data / restraints / parameters	2206 / 0 / 164
Goodness-of-fit on F^2	1.082
Final R indices [I>2sigma(I)]	R1 = 0.0371, wR2 = 0.0975
R indices (all data)	R1 = 0.0442, wR2 = 0.1032
Largest diff. peak and hole	0.247 and -0.229 e.Å^{-3}

Table 2. Atomic coordinates (x 10^4) and equivalent isotropic displacement parameters (Å^2x 10^3) for (**4i**). U(eq) is defined as one third of the trace of the orthogonalized U^{ij} tensor.

Atom	x	y	z	U(eq)
C(1)	4053(2)	3212(2)	120(1)	20(1)
C(2)	5549(2)	3302(2)	444(1)	20(1)
C(3)	6557(1)	5087(2)	334(1)	19(1)
C(4)	8123(2)	5160(2)	654(1)	21(1)
C(5)	9451(2)	5241(2)	908(1)	21(1)
C(6)	11031(1)	5365(2)	1221(1)	19(1)
C(7)	11696(2)	3591(2)	1634(1)	21(1)
C(8)	13203(2)	3752(2)	1949(1)	21(1)
C(9)	14089(2)	5686(2)	1858(1)	20(1)
C(10)	13460(2)	7447(2)	1438(1)	21(1)
C(11)	11940(2)	7279(2)	1124(1)	20(1)
C(12)	16443(2)	7724(2)	2192(1)	28(1)
O(1)	15551(1)	5696(2)	2207(1)	25(1)
F(1)	3145(1)	1438(1)	245(1)	25(1)
F(2)	6055(1)	1624(1)	883(1)	26(1)

Table 3.   Bond lengths [Å] and angles [°] for (4i).

C(1)-F(1)	1.3460(14)	F(2)-C(2)-C(3)	119.08(11)
C(1)-C(2)	1.3745(19)	C(1)-C(2)-C(3)	121.94(12)
C(1)-C(3)#1	1.3984(18)	C(2)-C(3)-C(1)#1	116.06(12)
C(2)-F(2)	1.3464(15)	C(2)-C(3)-C(4)	122.18(12)
C(2)-C(3)	1.3977(18)	C(1)#1-C(3)-C(4)	121.75(12)
C(3)-C(1)#1	1.3984(18)	C(5)-C(4)-C(3)	178.46(14)
C(3)-C(4)	1.4250(18)	C(4)-C(5)-C(6)	179.02(15)
C(4)-C(5)	1.1983(19)	C(11)-C(6)-C(7)	118.71(12)
C(5)-C(6)	1.4330(17)	C(11)-C(6)-C(5)	120.38(12)
C(6)-C(11)	1.4017(18)	C(7)-C(6)-C(5)	120.91(12)
C(6)-C(7)	1.4055(18)	C(8)-C(7)-C(6)	120.52(12)
C(7)-C(8)	1.3796(19)	C(7)-C(8)-C(9)	120.15(12)
C(8)-C(9)	1.3996(18)	O(1)-C(9)-C(10)	124.43(12)
C(9)-O(1)	1.3651(15)	O(1)-C(9)-C(8)	115.42(11)
C(9)-C(10)	1.3958(18)	C(10)-C(9)-C(8)	120.14(12)
C(10)-C(11)	1.3880(18)	C(11)-C(10)-C(9)	119.39(12)
C(12)-O(1)	1.4320(17)	C(10)-C(11)-C(6)	121.06(12)
F(1)-C(1)-C(2)	118.95(11)	C(9)-O(1)-C(12)	117.64(10)
F(1)-C(1)-C(3)#1	119.05(11)		
C(2)-C(1)-C(3)#1	122.00(12)		
F(2)-C(2)-C(1)	118.98(11)		

Symmetry   transformations   used   to   generate
equivalent   atoms: #1   -x+1,-y+1,-z

Table 4. Anisotropic displacement parameters $(\text{Å}^2 \times 10^3)$ for (4i). The anisotropic displacement factor exponent takes the form: $-2\pi^2[\, h^2 \, a^{*2}U^{11} + ... + 2\, h\, k\, a^*\, b^*\, U^{12}\,]$

Atom	U^{11}	U^{22}	U^{33}	U^{23}	U^{13}	U^{12}
C(1)	20(1)	19(1)	22(1)	-1(1)	5(1)	-5(1)
C(2)	21(1)	19(1)	19(1)	2(1)	2(1)	2(1)
C(3)	17(1)	21(1)	19(1)	-2(1)	3(1)	-1(1)
C(4)	21(1)	23(1)	20(1)	-1(1)	3(1)	-1(1)
C(5)	21(1)	23(1)	20(1)	0(1)	3(1)	-2(1)
C(6)	17(1)	23(1)	18(1)	-2(1)	2(1)	-1(1)
C(7)	21(1)	20(1)	22(1)	-1(1)	4(1)	-3(1)
C(8)	21(1)	19(1)	22(1)	1(1)	1(1)	2(1)
C(9)	17(1)	21(1)	21(1)	-4(1)	1(1)	1(1)
C(10)	20(1)	19(1)	24(1)	0(1)	3(1)	-2(1)
C(11)	20(1)	20(1)	21(1)	2(1)	2(1)	1(1)
C(12)	19(1)	25(1)	40(1)	-4(1)	-2(1)	-3(1)
O(1)	17(1)	23(1)	34(1)	1(1)	-5(1)	0(1)
F(1)	24(1)	22(1)	31(1)	3(1)	3(1)	-8(1)
F(2)	26(1)	23(1)	28(1)	8(1)	-1(1)	0(1)

Table 5. Hydrogen coordinates ($\times 10^4$) and isotropic displacement parameters $(\text{Å}^2 \times 10^3)$ for (4i).

Atom	x	y	z	U(eq)
H(7)	11080(20)	2270(30)	1698(9)	29(4)
H(8)	13640(20)	2590(30)	2247(9)	30(4)
H(10)	14040(20)	8780(30)	1370(9)	32(5)
H(11)	11497(19)	8540(30)	849(9)	25(4)
H(1)	16760(20)	8020(30)	1705(11)	37(5)
H(2)	15810(20)	9000(30)	2355(9)	29(4)
H(3)	17400(20)	7460(30)	2495(11)	37(5)

Appendix A4j

Data for the structure of MeO$_2$C-Ph-CC-Ant-CC-Ph-CO$_2$Me (**4j**).

Crystals grown by Stephen Watt at Heriot Watt University. Structure solved at 100(2)K

by the author at the University of Durham Crystallography Department (reference code

01jmb005).

Table 1. Crystal data and structure refinement for (**4j**).

Identification code	01jmb005
Empirical formula	C34 H22 O4
Formula weight	494.52
Temperature	110(2) K
Wavelength	0.71073 Å
Crystal system	Triclinic
Space group	P-1
Unit cell dimensions	a = 7.2247(4) Å α= 77.3430(10)°.
	b = 11.6597(8) Å β= 83.0370(10)°.
	c = 15.3807(9) Å γ = 72.0260(10)°.
Volume	1200.45(13) Å^3
Z	2
Density (calculated)	1.368 Mg/m^3
Absorption coefficient	0.089 mm^{-1}
F(000)	516
Crystal size	0.6 x 0.35 x 0.1 mm^3
Theta range for data collection	1.87 to 27.49°.
Index ranges	-9<=h<=9, -15<=k<=14, -19<=l<=19
Reflections collected	12771
Independent reflections	5483 [R(int) = 0.0208]
Completeness to theta = 27.49°	99.4 %
Absorption correction	Semi-empirical from equivalents
Max. and min. transmission	0.9911 and 0.9485
Refinement method	Full-matrix least-squares on F^2
Data / restraints / parameters	5483 / 0 / 431
Goodness-of-fit on F^2	0.966
Final R indices [I>2sigma(I)]	R1 = 0.0397, wR2 = 0.1047
R indices (all data)	R1 = 0.0586, wR2 = 0.1182
Extinction coefficient	.
Largest diff. peak and hole	0.314 and -0.253 e.Å^{-3}

Table 2. Atomic coordinates (x 10^4) and equivalent isotropic displacement parameters (Å^2x 10^3) for (**4j**). U(eq) is defined as one third of the trace of the orthogonalized U^{ij} tensor.

Atom	x	y	z	U(eq)
C(11)	4787(2)	8930(1)	-4387(1)	20(1)
C(12)	4583(2)	7838(1)	-3795(1)	23(1)
C(13)	4771(2)	6800(1)	-4106(1)	27(1)
C(14)	5195(2)	6774(1)	-5029(1)	28(1)
C(15)	5398(2)	7797(1)	-5614(1)	24(1)
C(16)	5195(2)	8909(1)	-5317(1)	20(1)
C(17)	5402(2)	9976(1)	-5921(1)	20(1)
C(18)	5833(2)	9946(1)	-6849(1)	22(1)
C(19)	6227(2)	9932(1)	-7624(1)	22(1)
C(20)	6729(2)	9942(1)	-8559(1)	19(1)
C(21)	6094(2)	11034(1)	-9186(1)	21(1)
C(22)	6560(2)	11054(1)	-10088(1)	20(1)
C(23)	7690(2)	9984(1)	-10381(1)	18(1)
C(24)	8336(2)	8897(1)	-9757(1)	20(1)
C(25)	7858(2)	8871(1)	-8856(1)	21(1)
C(26)	8195(2)	10032(1)	-11354(1)	20(1)
C(27)	9666(2)	8854(1)	-12461(1)	26(1)
C(31)	-210(2)	7094(1)	5719(1)	25(1)
C(32)	68(2)	8128(1)	5174(1)	28(1)
C(33)	496(2)	8161(1)	4248(1)	28(1)
C(34)	616(2)	7171(1)	3886(1)	24(1)
C(35)	320(2)	6076(1)	4433(1)	21(1)
C(36)	90(2)	3967(1)	4627(1)	21(1)
C(37)	403(2)	5040(1)	4071(1)	20(1)
C(38)	847(2)	5071(1)	3137(1)	22(1)
C(39)	1246(2)	5076(1)	2358(1)	21(1)
C(40)	1743(2)	5050(1)	1428(1)	19(1)
C(41)	1957(2)	6105(1)	826(1)	21(1)
C(42)	2405(2)	6072(1)	-70(1)	20(1)
C(43)	2680(2)	4993(1)	-383(1)	18(1)
C(44)	2491(2)	3941(1)	214(1)	20(1)
C(45)	2011(2)	3970(1)	1109(1)	22(1)
C(46)	3205(2)	4987(1)	-1351(1)	20(1)
C(47)	4359(2)	3730(1)	-2434(1)	27(1)
O(1)	7882(1)	10965(1)	-11914(1)	28(1)

O(2)	9060(1)	8905(1)	-11534(1)	24(1)
O(3)	3180(2)	5890(1)	-1917(1)	29(1)
O(4)	3734(1)	3842(1)	-1518(1)	24(1)

Table 3. Bond lengths [Å] and angles [°] for **(4j)**.

C(11)-C(17)#1	1.4189(18)	C(31)-C(32)	1.364(2)
C(11)-C(16)	1.4289(17)	C(31)-C(36)#2	1.4257(19)
C(11)-C(12)	1.4309(17)	C(31)-H(31)	0.960(16)
C(12)-C(13)	1.360(2)	C(32)-C(33)	1.4164(19)
C(12)-H(12)	0.946(16)	C(32)-H(32)	1.001(16)
C(13)-C(14)	1.4207(19)	C(33)-C(34)	1.362(2)
C(13)-H(13)	0.988(16)	C(33)-H(33)	0.983(18)
C(14)-C(15)	1.3633(19)	C(34)-C(35)	1.4280(18)
C(14)-H(14)	0.991(16)	C(34)-H(34)	0.991(17)
C(15)-C(16)	1.4261(19)	C(35)-C(37)	1.4188(18)
C(15)-H(15)	0.962(17)	C(35)-C(36)#2	1.4329(17)
C(16)-C(17)	1.4165(17)	C(36)-C(37)	1.4165(18)
C(17)-C(11)#1	1.4189(18)	C(36)-C(31)#2	1.4256(19)
C(17)-C(18)	1.4298(17)	C(36)-C(35)#2	1.4329(17)
C(18)-C(19)	1.1945(18)	C(37)-C(38)	1.4290(17)
C(19)-C(20)	1.4383(16)	C(38)-C(39)	1.1965(18)
C(20)-C(25)	1.4009(18)	C(39)-C(40)	1.4368(16)
C(20)-C(21)	1.4038(17)	C(40)-C(45)	1.4016(18)
C(21)-C(22)	1.3833(17)	C(40)-C(41)	1.4061(17)
C(21)-H(21)	0.990(15)	C(41)-C(42)	1.3821(17)
C(22)-C(23)	1.3978(18)	C(41)-H(41)	0.963(15)
C(22)-H(22)	0.953(14)	C(42)-C(43)	1.3938(18)
C(23)-C(24)	1.3980(17)	C(42)-H(42)	0.941(16)
C(23)-C(26)	1.4905(16)	C(43)-C(44)	1.3947(17)
C(24)-C(25)	1.3838(17)	C(43)-C(46)	1.4928(16)
C(24)-H(24)	0.961(15)	C(44)-C(45)	1.3833(17)
C(25)-H(25)	0.978(15)	C(44)-H(44)	0.945(16)
C(26)-O(1)	1.2083(15)	C(45)-H(45)	0.974(15)
C(26)-O(2)	1.3439(15)	C(46)-O(3)	1.2066(15)
C(27)-O(2)	1.4482(15)	C(46)-O(4)	1.3438(15)
C(27)-H(27A)	0.981(16)	C(47)-O(4)	1.4476(15)
C(27)-H(27B)	0.965(16)	C(47)-H(47A)	0.987(17)
C(27)-H(27C)	0.960(16)	C(47)-H(47B)	0.946(16)

C(47)-H(47C)	0.968(16)	C(24)-C(25)-C(20)	120.07(11)
		C(24)-C(25)-H(25)	119.4(9)
C(17)#1-C(11)-C(16)	119.34(11)	C(20)-C(25)-H(25)	120.5(9)
C(17)#1-C(11)-C(12)	122.05(11)	O(1)-C(26)-O(2)	123.91(11)
C(16)-C(11)-C(12)	118.60(12)	O(1)-C(26)-C(23)	124.62(12)
C(13)-C(12)-C(11)	120.97(12)	O(2)-C(26)-C(23)	111.47(10)
C(13)-C(12)-H(12)	120.2(10)	O(2)-C(27)-H(27A)	108.9(9)
C(11)-C(12)-H(12)	118.8(10)	O(2)-C(27)-H(27B)	109.4(9)
C(12)-C(13)-C(14)	120.47(12)	H(27A)-C(27)-H(27B)	111.5(13)
C(12)-C(13)-H(13)	118.5(9)	O(2)-C(27)-H(27C)	103.8(9)
C(14)-C(13)-H(13)	121.0(9)	H(27A)-C(27)-H(27C)	110.5(13)
C(15)-C(14)-C(13)	120.18(13)	H(27B)-C(27)-H(27C)	112.6(13)
C(15)-C(14)-H(14)	122.2(9)	C(32)-C(31)-C(36)#2	121.23(12)
C(13)-C(14)-H(14)	117.6(9)	C(32)-C(31)-H(31)	121.7(10)
C(14)-C(15)-C(16)	121.21(12)	C(36)#2-C(31)-H(31)	117.0(10)
C(14)-C(15)-H(15)	117.9(10)	C(31)-C(32)-C(33)	120.11(13)
C(16)-C(15)-H(15)	120.8(10)	C(31)-C(32)-H(32)	119.6(9)
C(17)-C(16)-C(15)	121.53(11)	C(33)-C(32)-H(32)	120.3(9)
C(17)-C(16)-C(11)	119.91(12)	C(34)-C(33)-C(32)	120.77(13)
C(15)-C(16)-C(11)	118.56(12)	C(34)-C(33)-H(33)	120.5(10)
C(16)-C(17)-C(11)#1	120.75(11)	C(32)-C(33)-H(33)	118.7(10)
C(16)-C(17)-C(18)	119.70(12)	C(33)-C(34)-C(35)	120.74(12)
C(11)#1-C(17)-C(18)	119.55(11)	C(33)-C(34)-H(34)	120.2(10)
C(19)-C(18)-C(17)	178.49(14)	C(35)-C(34)-H(34)	119.0(10)
C(18)-C(19)-C(20)	178.40(14)	C(37)-C(35)-C(34)	121.90(11)
C(25)-C(20)-C(21)	119.22(11)	C(37)-C(35)-C(36)#2	119.40(11)
C(25)-C(20)-C(19)	120.78(11)	C(34)-C(35)-C(36)#2	118.70(12)
C(21)-C(20)-C(19)	120.00(11)	C(37)-C(36)-C(31)#2	121.79(11)
C(22)-C(21)-C(20)	120.56(12)	C(37)-C(36)-C(35)#2	119.75(12)
C(22)-C(21)-H(21)	120.2(8)	C(31)#2-C(36)-C(35)#2	118.45(12)
C(20)-C(21)-H(21)	119.2(8)	C(36)-C(37)-C(35)	120.85(11)
C(21)-C(22)-C(23)	120.03(11)	C(36)-C(37)-C(38)	119.57(12)
C(21)-C(22)-H(22)	119.0(8)	C(35)-C(37)-C(38)	119.57(11)
C(23)-C(22)-H(22)	120.9(8)	C(39)-C(38)-C(37)	178.78(15)
C(22)-C(23)-C(24)	119.55(11)	C(38)-C(39)-C(40)	178.58(14)
C(22)-C(23)-C(26)	119.03(11)	C(45)-C(40)-C(41)	119.09(11)
C(24)-C(23)-C(26)	121.42(11)	C(45)-C(40)-C(39)	120.18(11)
C(25)-C(24)-C(23)	120.57(12)	C(41)-C(40)-C(39)	120.74(11)
C(25)-C(24)-H(24)	120.8(9)	C(42)-C(41)-C(40)	120.12(12)
C(23)-C(24)-H(24)	118.6(9)	C(42)-C(41)-H(41)	118.7(9)

C(40)-C(41)-H(41)	121.2(9)	O(3)-C(46)-C(43)	124.71(12)
C(41)-C(42)-C(43)	120.54(12)	O(4)-C(46)-C(43)	111.48(10)
C(41)-C(42)-H(42)	120.1(9)	O(4)-C(47)-H(47A)	110.4(9)
C(43)-C(42)-H(42)	119.4(9)	O(4)-C(47)-H(47B)	104.8(9)
C(42)-C(43)-C(44)	119.56(11)	H(47A)-C(47)-H(47B)	110.2(13)
C(42)-C(43)-C(46)	118.92(11)	O(4)-C(47)-H(47C)	109.6(9)
C(44)-C(43)-C(46)	121.51(11)	H(47A)-C(47)-H(47C)	110.9(13)
C(45)-C(44)-C(43)	120.33(12)	H(47B)-C(47)-H(47C)	110.8(13)
C(45)-C(44)-H(44)	118.8(9)	C(26)-O(2)-C(27)	115.87(10)
C(43)-C(44)-H(44)	120.8(9)	C(46)-O(4)-C(47)	115.86(10)
C(44)-C(45)-C(40)	120.35(12)		
C(44)-C(45)-H(45)	119.8(8)	Symmetry transformations used to generate
C(40)-C(45)-H(45)	119.9(8)	equivalent atoms:
O(3)-C(46)-O(4)	123.80(11)	#1 -x+1,-y+2,-z-1 #2 -x,-y+1,-z+1

Table 4. Anisotropic displacement parameters ($\text{Å}^2 \times 10^3$) for (**4j**). The anisotropic displacement factor exponent takes the form: $-2\pi^2[\, h^2\, a^{*2} U^{11} + \ldots + 2\, h\, k\, a^*\, b^*\, U^{12}\,]$

Atom	U^{11}	U^{22}	U^{33}	U^{23}	U^{13}	U^{12}
C(11)	16(1)	25(1)	19(1)	-3(1)	-2(1)	-5(1)
C(12)	21(1)	27(1)	19(1)	-1(1)	0(1)	-6(1)
C(13)	24(1)	23(1)	29(1)	1(1)	-1(1)	-6(1)
C(14)	27(1)	25(1)	31(1)	-8(1)	-2(1)	-6(1)
C(15)	24(1)	27(1)	22(1)	-7(1)	-2(1)	-6(1)
C(16)	17(1)	25(1)	18(1)	-4(1)	-2(1)	-4(1)
C(17)	17(1)	25(1)	17(1)	-4(1)	-1(1)	-5(1)
C(18)	20(1)	23(1)	22(1)	-4(1)	-2(1)	-5(1)
C(19)	22(1)	23(1)	20(1)	-4(1)	-2(1)	-6(1)
C(20)	21(1)	23(1)	17(1)	-5(1)	-1(1)	-8(1)
C(21)	23(1)	19(1)	20(1)	-5(1)	-1(1)	-5(1)
C(22)	22(1)	19(1)	19(1)	-1(1)	-2(1)	-7(1)
C(23)	20(1)	20(1)	16(1)	-3(1)	-1(1)	-8(1)
C(24)	20(1)	18(1)	21(1)	-5(1)	-1(1)	-3(1)
C(25)	23(1)	19(1)	18(1)	0(1)	-3(1)	-5(1)
C(26)	20(1)	22(1)	19(1)	-3(1)	-1(1)	-8(1)
C(27)	33(1)	30(1)	18(1)	-8(1)	4(1)	-10(1)
C(31)	25(1)	29(1)	20(1)	-7(1)	-1(1)	-6(1)
C(32)	30(1)	26(1)	31(1)	-9(1)	-3(1)	-7(1)
C(33)	26(1)	26(1)	28(1)	0(1)	-2(1)	-7(1)

C(34)	22(1)	28(1)	19(1)	-2(1)	-1(1)	-6(1)
C(35)	17(1)	25(1)	17(1)	-3(1)	-1(1)	-4(1)
C(36)	17(1)	26(1)	19(1)	-4(1)	-2(1)	-5(1)
C(37)	17(1)	27(1)	16(1)	-3(1)	-1(1)	-4(1)
C(38)	20(1)	24(1)	21(1)	-4(1)	-2(1)	-4(1)
C(39)	21(1)	23(1)	19(1)	-4(1)	-2(1)	-5(1)
C(40)	17(1)	22(1)	16(1)	-4(1)	-2(1)	-3(1)
C(41)	22(1)	19(1)	20(1)	-5(1)	-2(1)	-4(1)
C(42)	21(1)	18(1)	20(1)	-1(1)	-1(1)	-5(1)
C(43)	15(1)	21(1)	17(1)	-3(1)	-1(1)	-3(1)
C(44)	22(1)	19(1)	20(1)	-5(1)	0(1)	-5(1)
C(45)	24(1)	22(1)	19(1)	-1(1)	0(1)	-7(1)
C(46)	20(1)	22(1)	18(1)	-4(1)	-1(1)	-4(1)
C(47)	32(1)	29(1)	17(1)	-9(1)	2(1)	-5(1)
O(1)	34(1)	25(1)	19(1)	1(1)	0(1)	-5(1)
O(2)	33(1)	23(1)	17(1)	-6(1)	4(1)	-8(1)
O(3)	40(1)	24(1)	18(1)	-1(1)	3(1)	-5(1)
O(4)	32(1)	22(1)	16(1)	-6(1)	1(1)	-6(1)

Table 5. Hydrogen coordinates (x 10^4) and isotropic displacement parameters ($\AA^2$x 10^3) for (**4j**).

Atom	x	y	z	U(eq)
H(12)	4330(20)	7847(14)	-3178(11)	29(4)
H(13)	4620(20)	6064(15)	-3675(10)	32(4)
H(14)	5320(20)	5997(15)	-5224(10)	33(4)
H(15)	5730(30)	7739(16)	-6231(11)	38(4)
H(21)	5270(20)	11785(14)	-8978(9)	24(4)
H(22)	6040(20)	11792(13)	-10503(9)	20(3)
H(24)	9160(20)	8177(14)	-9966(9)	27(4)
H(25)	8320(20)	8102(14)	-8430(10)	27(4)
H(27A)	8500(20)	9094(14)	-12805(10)	29(4)
H(27B)	10480(20)	9389(14)	-12680(10)	27(4)
H(27C)	10360(20)	8004(15)	-12448(10)	29(4)
H(31)	-520(20)	7053(15)	6348(11)	34(4)
H(32)	-20(20)	8860(15)	5435(10)	29(4)
H(33)	690(30)	8915(16)	3868(11)	41(5)
H(34)	900(20)	7205(16)	3236(11)	39(4)

H(41)	1820(20)	6855(14)	1025(9)	29(4)
H(42)	2550(20)	6778(15)	-473(10)	32(4)
H(44)	2640(20)	3206(15)	12(9)	28(4)
H(45)	1870(20)	3232(14)	1520(9)	25(4)
H(47A)	5440(20)	4096(15)	-2640(10)	32(4)
H(47B)	4800(20)	2873(15)	-2422(10)	29(4)
H(47C)	3270(20)	4122(15)	-2809(10)	31(4)

Table 6. Torsion angles [°] for (**4j**).

C(17)#1-C(11)-C(12)-C(13)	-179.99(12)
C(16)-C(11)-C(12)-C(13)	0.01(19)
C(11)-C(12)-C(13)-C(14)	0.6(2)
C(12)-C(13)-C(14)-C(15)	-0.6(2)
C(13)-C(14)-C(15)-C(16)	0.1(2)
C(14)-C(15)-C(16)-C(17)	-179.92(12)
C(14)-C(15)-C(16)-C(11)	0.52(19)
C(17)#1-C(11)-C(16)-C(17)	-0.11(19)
C(12)-C(11)-C(16)-C(17)	179.89(11)
C(17)#1-C(11)-C(16)-C(15)	179.45(12)
C(12)-C(11)-C(16)-C(15)	-0.55(17)
C(15)-C(16)-C(17)-C(11)#1	-179.43(12)
C(11)-C(16)-C(17)-C(11)#1	0.12(19)
C(15)-C(16)-C(17)-C(18)	-0.27(18)
C(11)-C(16)-C(17)-C(18)	179.28(11)
C(16)-C(17)-C(18)-C(19)	-130(6)
C(11)#1-C(17)-C(18)-C(19)	49(6)
C(17)-C(18)-C(19)-C(20)	-21(10)
C(18)-C(19)-C(20)-C(25)	121(5)
C(18)-C(19)-C(20)-C(21)	-59(5)
C(25)-C(20)-C(21)-C(22)	0.60(19)
C(19)-C(20)-C(21)-C(22)	-179.69(12)
C(20)-C(21)-C(22)-C(23)	-0.74(19)
C(21)-C(22)-C(23)-C(24)	0.28(18)
C(21)-C(22)-C(23)-C(26)	-179.14(12)
C(22)-C(23)-C(24)-C(25)	0.31(19)
C(26)-C(23)-C(24)-C(25)	179.72(12)
C(23)-C(24)-C(25)-C(20)	-0.45(19)
C(21)-C(20)-C(25)-C(24)	0.00(19)
C(19)-C(20)-C(25)-C(24)	-179.71(12)
C(22)-C(23)-C(26)-O(1)	8.50(19)
C(24)-C(23)-C(26)-O(1)	-170.91(13)

C(22)-C(23)-C(26)-O(2)	-171.88(11)
C(24)-C(23)-C(26)-O(2)	8.70(17)
C(36)#2-C(31)-C(32)-C(33)	-0.4(2)
C(31)-C(32)-C(33)-C(34)	0.7(2)
C(32)-C(33)-C(34)-C(35)	-0.3(2)
C(33)-C(34)-C(35)-C(37)	178.86(13)
C(33)-C(34)-C(35)-C(36)#2	-0.47(19)
C(31)#2-C(36)-C(37)-C(35)	-178.53(12)
C(35)#2-C(36)-C(37)-C(35)	0.2(2)
C(31)#2-C(36)-C(37)-C(38)	0.12(18)
C(35)#2-C(36)-C(37)-C(38)	178.85(11)
C(34)-C(35)-C(37)-C(36)	-179.53(12)
C(36)#2-C(35)-C(37)-C(36)	-0.2(2)
C(34)-C(35)-C(37)-C(38)	1.82(18)
C(36)#2-C(35)-C(37)-C(38)	-178.85(11)
C(36)-C(37)-C(38)-C(39)	-52(7)
C(35)-C(37)-C(38)-C(39)	126(7)
C(37)-C(38)-C(39)-C(40)	29(11)
C(38)-C(39)-C(40)-C(45)	19(6)
C(38)-C(39)-C(40)-C(41)	-161(6)
C(45)-C(40)-C(41)-C(42)	0.68(18)
C(39)-C(40)-C(41)-C(42)	-178.95(12)
C(40)-C(41)-C(42)-C(43)	-1.07(19)
C(41)-C(42)-C(43)-C(44)	0.36(18)
C(41)-C(42)-C(43)-C(46)	-178.66(11)
C(42)-C(43)-C(44)-C(45)	0.75(19)
C(46)-C(43)-C(44)-C(45)	179.74(11)
C(43)-C(44)-C(45)-C(40)	-1.14(19)
C(41)-C(40)-C(45)-C(44)	0.43(19)
C(39)-C(40)-C(45)-C(44)	-179.95(12)
C(42)-C(43)-C(46)-O(3)	-9.66(19)
C(44)-C(43)-C(46)-O(3)	171.34(13)
C(42)-C(43)-C(46)-O(4)	169.68(11)
C(44)-C(43)-C(46)-O(4)	-9.32(17)
O(1)-C(26)-O(2)-C(27)	1.46(19)
C(23)-C(26)-O(2)-C(27)	-178.16(11)
O(3)-C(46)-O(4)-C(47)	2.10(18)
C(43)-C(46)-O(4)-C(47)	-177.24(11)

Symmetry transformations used to generate equivalent atoms:

#1 -x+1,-y+2,-z-1   #2 -x,-y+1,-z+1

Appendix A4ab

Data for the structure of the 1:1 co-crystal of PhF_5-CC-Ph-CC-PhF_5 with

CH_3-Ph-CC-PhF_4-CC-Ph-CH_3 (**4ab**).

Crystals grown by Stephen Watt at Heriot Watt University. Structure solved by the

author at the University of Durham Crystallography Department (reference code

01srv016).

Table 1. Crystal data and structure refinement for (**4ab**).

Identification code	01srv016
Empirical formula	C46 H18 F14
Formula weight	836.60
Temperature	100(2) K
Wavelength	0.71073 Å
Crystal system	Triclinic
Space group	P-1
Unit cell dimensions	a = 6.0725(11) Å α= 94.440(4)°.
	b = 7.4054(13) Å β= 96.620(4)°.
	c = 20.031(4) Å γ = 96.242(4)°.
Volume	885.8(3) Å^3
Z	1
Density (calculated)	1.568 Mg/m^3
Absorption coefficient	0.142 mm^{-1}
F(000)	420
Crystal size	0.40 x 0.40 x 0.05 mm^3
Theta range for data collection	1.03 to 27.48°.
Index ranges	-7<=h<=7, -9<=k<=9, -26<=l<=26
Reflections collected	9457
Independent reflections	4034 [R(int) = 0.0355]
Completeness to theta = 27.48°	99.5 %
Absorption correction	None
Max. and min. transmission	. and .
Refinement method	Full-matrix least-squares on F^2
Data / restraints / parameters	4034 / 0 / 295
Goodness-of-fit on F^2	1.025
Final R indices [I>2sigma(I)]	R1 = 0.0523, wR2 = 0.1356
R indices (all data)	R1 = 0.0889, wR2 = 0.1582
Largest diff. peak and hole	0.365 and -0.350 e.Å^{-3}

Table 2. Atomic coordinates (x 10^4) and equivalent isotropic displacement parameters (Å^2x 10^3) for (**4ab**). U(eq) is defined as one third of the trace of the orthogonalized U^{ij} tensor.

Atom	x	y	z	U(eq)
F(1)	1050(2)	3845(2)	431(1)	21(1)
F(2)	1690(2)	2954(2)	-850(1)	22(1)
C(1)	3011(3)	4434(3)	222(1)	16(1)
C(2)	3337(3)	3964(3)	-434(1)	17(1)
C(3)	5359(3)	4504(3)	-678(1)	17(1)
C(4)	5744(3)	3971(3)	-1349(1)	18(1)
C(5)	6119(3)	3497(3)	-1905(1)	19(1)
C(6)	6565(3)	3003(3)	-2577(1)	16(1)
C(7)	8669(3)	3507(3)	-2773(1)	20(1)
C(8)	9053(3)	3094(3)	-3434(1)	20(1)
C(9)	7377(3)	2185(3)	-3916(1)	20(1)
C(10)	5290(3)	1663(3)	-3713(1)	19(1)
C(11)	4880(3)	2061(3)	-3053(1)	19(1)
C(12)	7811(4)	1761(3)	-4636(1)	27(1)
F(27)	20296(2)	9562(2)	-2411(1)	23(1)
F(28)	20823(2)	8684(2)	-3713(1)	24(1)
F(29)	17479(2)	6635(2)	-4550(1)	27(1)
F(30)	13567(2)	5520(2)	-4089(1)	23(1)
F(31)	13008(2)	6418(2)	-2790(1)	22(1)
C(21)	16676(3)	10994(3)	466(1)	18(1)
C(22)	17094(3)	10534(3)	-189(1)	18(1)
C(23)	15437(3)	9533(3)	-659(1)	17(1)
C(24)	15893(3)	9018(3)	-1329(1)	17(1)
C(25)	16274(3)	8562(3)	-1886(1)	18(1)
C(26)	16621(3)	8031(3)	-2563(1)	16(1)
C(27)	18618(3)	8571(3)	-2816(1)	17(1)
C(28)	18900(3)	8112(3)	-3478(1)	19(1)
C(29)	17202(3)	7090(3)	-3907(1)	19(1)
C(30)	15214(3)	6514(3)	-3672(1)	18(1)
C(31)	14947(3)	6988(3)	-3010(1)	17(1)

Table 3. Bond lengths [Å] and angles [°] for (4ab).

F(1)-C(1)	1.347(2)	C(26)-C(27)	1.398(3)
F(2)-C(2)	1.343(2)	C(27)-C(28)	1.378(3)
C(1)-C(2)	1.375(3)	C(28)-C(29)	1.378(3)
C(1)-C(3)#1	1.394(3)	C(29)-C(30)	1.382(3)
C(2)-C(3)	1.403(3)	C(30)-C(31)	1.378(3)
C(3)-C(1)#1	1.394(3)		
C(3)-C(4)	1.425(3)	F(1)-C(1)-C(2)	118.81(17)
C(4)-C(5)	1.196(3)	F(1)-C(1)-C(3)#1	118.92(17)
C(5)-C(6)	1.430(3)	C(2)-C(1)-C(3)#1	122.27(18)
C(6)-C(11)	1.400(3)	F(2)-C(2)-C(1)	119.36(18)
C(6)-C(7)	1.401(3)	F(2)-C(2)-C(3)	119.16(18)
C(7)-C(8)	1.387(3)	C(1)-C(2)-C(3)	121.48(18)
C(7)-H(7)	0.91(3)	C(1)#1-C(3)-C(2)	116.24(18)
C(8)-C(9)	1.395(3)	C(1)#1-C(3)-C(4)	121.75(18)
C(8)-H(8)	0.97(3)	C(2)-C(3)-C(4)	121.99(18)
C(9)-C(10)	1.399(3)	C(5)-C(4)-C(3)	178.1(2)
C(9)-C(12)	1.510(3)	C(4)-C(5)-C(6)	177.7(2)
C(10)-C(11)	1.389(3)	C(11)-C(6)-C(7)	119.06(19)
C(10)-H(10)	0.94(2)	C(11)-C(6)-C(5)	120.40(18)
C(11)-H(11)	0.99(3)	C(7)-C(6)-C(5)	120.50(18)
C(12)-H(12A)	0.9800	C(8)-C(7)-C(6)	120.0(2)
C(12)-H(12B)	0.9800	C(8)-C(7)-H(7)	123.3(16)
C(12)-H(12C)	0.9800	C(6)-C(7)-H(7)	116.7(16)
F(27)-C(27)	1.338(2)	C(7)-C(8)-C(9)	121.44(19)
F(28)-C(28)	1.347(2)	C(7)-C(8)-H(8)	117.5(16)
F(29)-C(29)	1.341(2)	C(9)-C(8)-H(8)	121.1(16)
F(30)-C(30)	1.339(2)	C(8)-C(9)-C(10)	118.16(19)
F(31)-C(31)	1.342(2)	C(8)-C(9)-C(12)	120.88(19)
C(21)-C(22)	1.388(3)	C(10)-C(9)-C(12)	120.96(19)
C(21)-C(23)#2	1.407(3)	C(11)-C(10)-C(9)	121.1(2)
C(21)-H(21)	0.94(3)	C(11)-C(10)-H(10)	120.6(13)
C(22)-C(23)	1.400(3)	C(9)-C(10)-H(10)	118.2(13)
C(22)-H(22)	0.96(2)	C(10)-C(11)-C(6)	120.17(19)
C(23)-C(21)#2	1.407(3)	C(10)-C(11)-H(11)	120.0(15)
C(23)-C(24)	1.433(3)	C(6)-C(11)-H(11)	119.8(15)
C(24)-C(25)	1.196(3)	C(9)-C(12)-H(12A)	109.5
C(25)-C(26)	1.428(3)	C(9)-C(12)-H(12B)	109.5
C(26)-C(31)	1.394(3)	H(12A)-C(12)-H(12B)	109.5

C(9)-C(12)-H(12C)	109.5
H(12A)-C(12)-H(12C)	109.5
H(12B)-C(12)-H(12C)	109.5
C(22)-C(21)-C(23)#2	119.86(19)
C(22)-C(21)-H(21)	122.1(15)
C(23)#2-C(21)-H(21)	118.1(15)
C(21)-C(22)-C(23)	120.65(19)
C(21)-C(22)-H(22)	118.9(14)
C(23)-C(22)-H(22)	120.4(14)
C(22)-C(23)-C(21)#2	119.49(19)
C(22)-C(23)-C(24)	120.49(18)
C(21)#2-C(23)-C(24)	120.01(18)
C(25)-C(24)-C(23)	179.0(2)
C(24)-C(25)-C(26)	177.2(2)
C(31)-C(26)-C(27)	116.83(18)
C(31)-C(26)-C(25)	121.21(18)
C(27)-C(26)-C(25)	121.94(18)
F(27)-C(27)-C(28)	118.89(17)
F(27)-C(27)-C(26)	119.70(18)

C(28)-C(27)-C(26)	121.41(18)
F(28)-C(28)-C(29)	119.61(18)
F(28)-C(28)-C(27)	120.23(18)
C(29)-C(28)-C(27)	120.15(18)
F(29)-C(29)-C(28)	120.20(18)
F(29)-C(29)-C(30)	119.78(18)
C(28)-C(29)-C(30)	120.02(19)
F(30)-C(30)-C(31)	120.77(18)
F(30)-C(30)-C(29)	119.92(18)
C(31)-C(30)-C(29)	119.31(19)
F(31)-C(31)-C(30)	118.57(17)
F(31)-C(31)-C(26)	119.16(18)
C(30)-C(31)-C(26)	122.27(18)

Symmetry transformations used to generate equivalent atoms:

#1 -x+1,-y+1,-z

#2 -x+3,-y+2,-z

Table 4. Anisotropic displacement parameters (Å^2x 10^3) for (**4ab**). The anisotropic displacement factor exponent takes the form: $-2\pi^2[\ h^2\ a^{*2}U^{11} + ... + 2\ h\ k\ a^*\ b^*\ U^{12}\ ]$

Atom	U^{11}	U^{22}	U^{33}	U^{23}	U^{13}	U^{12}
F(1)	14(1)	25(1)	24(1)	3(1)	7(1)	-1(1)
F(2)	18(1)	24(1)	22(1)	-3(1)	-2(1)	-3(1)
C(1)	13(1)	16(1)	21(1)	4(1)	5(1)	1(1)
C(2)	15(1)	16(1)	20(1)	0(1)	-1(1)	0(1)
C(3)	16(1)	17(1)	18(1)	3(1)	3(1)	5(1)
C(4)	18(1)	17(1)	21(1)	2(1)	3(1)	2(1)
C(5)	18(1)	15(1)	22(1)	3(1)	1(1)	1(1)
C(6)	17(1)	14(1)	18(1)	3(1)	3(1)	2(1)
C(7)	18(1)	20(1)	21(1)	2(1)	0(1)	1(1)
C(8)	17(1)	20(1)	24(1)	4(1)	6(1)	1(1)
C(9)	22(1)	19(1)	19(1)	3(1)	5(1)	6(1)
C(10)	18(1)	20(1)	19(1)	-1(1)	-1(1)	1(1)
C(11)	17(1)	18(1)	23(1)	5(1)	4(1)	2(1)
C(12)	31(1)	29(1)	22(1)	0(1)	8(1)	3(1)

F(27)	17(1)	25(1)	26(1)	-2(1)	-1(1)	-4(1)
F(28)	16(1)	31(1)	28(1)	6(1)	11(1)	1(1)
F(29)	30(1)	32(1)	18(1)	-1(1)	7(1)	2(1)
F(30)	21(1)	25(1)	21(1)	0(1)	-3(1)	-3(1)
F(31)	14(1)	26(1)	24(1)	3(1)	6(1)	-2(1)
C(21)	16(1)	18(1)	19(1)	0(1)	1(1)	-1(1)
C(22)	14(1)	18(1)	22(1)	1(1)	3(1)	4(1)
C(23)	20(1)	14(1)	18(1)	2(1)	4(1)	2(1)
C(24)	15(1)	15(1)	23(1)	2(1)	3(1)	1(1)
C(25)	17(1)	15(1)	21(1)	3(1)	2(1)	1(1)
C(26)	16(1)	14(1)	18(1)	1(1)	3(1)	4(1)
C(27)	15(1)	15(1)	20(1)	1(1)	-1(1)	1(1)
C(28)	16(1)	19(1)	23(1)	6(1)	7(1)	3(1)
C(29)	23(1)	19(1)	16(1)	2(1)	6(1)	5(1)
C(30)	17(1)	15(1)	21(1)	2(1)	-1(1)	3(1)
C(31)	13(1)	19(1)	21(1)	5(1)	4(1)	2(1)

Table 5. Hydrogen coordinates (x 10^4) and isotropic displacement parameters (Å^2x 10^3) for (**4ab**).

Atom	x	y	z	U(eq)
H(12A)	8970	2675	-4748	41
H(12B)	6433	1783	-4941	41
H(12C)	8310	548	-4686	41
H(7)	9740(40)	4060(40)	-2447(13)	35(7)
H(8)	10510(50)	3500(40)	-3554(13)	39(7)
H(10)	4150(40)	1070(30)	-4041(11)	19(6)
H(11)	3420(40)	1620(40)	-2912(13)	34(7)
H(21)	17780(40)	11650(40)	793(13)	34(7)
H(22)	18530(40)	10950(30)	-320(12)	25(6)

Table 6. Torsion angles [°] for (4ab).

F(1)-C(1)-C(2)-F(2)	0.8(3)
C(3)#1-C(1)-C(2)-F(2)	-179.27(17)
F(1)-C(1)-C(2)-C(3)	-178.70(18)
C(3)#1-C(1)-C(2)-C(3)	1.2(3)
F(2)-C(2)-C(3)-C(1)#1	179.34(17)
C(1)-C(2)-C(3)-C(1)#1	-1.1(3)
F(2)-C(2)-C(3)-C(4)	-1.8(3)
C(1)-C(2)-C(3)-C(4)	177.7(2)
C(1)#1-C(3)-C(4)-C(5)	61(7)
C(2)-C(3)-C(4)-C(5)	-118(7)
C(3)-C(4)-C(5)-C(6)	-132(6)
C(4)-C(5)-C(6)-C(11)	-105(5)
C(4)-C(5)-C(6)-C(7)	73(5)
C(11)-C(6)-C(7)-C(8)	0.9(3)
C(5)-C(6)-C(7)-C(8)	-177.0(2)
C(6)-C(7)-C(8)-C(9)	0.2(3)
C(7)-C(8)-C(9)-C(10)	-1.2(3)
C(7)-C(8)-C(9)-C(12)	179.4(2)
C(8)-C(9)-C(10)-C(11)	1.0(3)
C(12)-C(9)-C(10)-C(11)	-179.6(2)
C(9)-C(10)-C(11)-C(6)	0.1(3)
C(7)-C(6)-C(11)-C(10)	-1.1(3)
C(5)-C(6)-C(11)-C(10)	176.83(19)
C(23)#2-C(21)-C(22)-C(23)	-0.5(3)
C(21)-C(22)-C(23)-C(21)#2	0.5(3)
C(21)-C(22)-C(23)-C(24)	-178.3(2)
C(22)-C(23)-C(24)-C(25)	108(12)
C(21)#2-C(23)-C(24)-C(25)	-71(12)
C(23)-C(24)-C(25)-C(26)	109(12)
C(24)-C(25)-C(26)-C(31)	-39(5)
C(24)-C(25)-C(26)-C(27)	139(4)
C(31)-C(26)-C(27)-F(27)	-179.46(17)
C(25)-C(26)-C(27)-F(27)	2.3(3)
C(31)-C(26)-C(27)-C(28)	0.9(3)
C(25)-C(26)-C(27)-C(28)	-177.33(19)
F(27)-C(27)-C(28)-F(28)	-1.1(3)
C(26)-C(27)-C(28)-F(28)	178.48(18)
F(27)-C(27)-C(28)-C(29)	179.88(18)

C(26)-C(27)-C(28)-C(29)	-0.5(3)
F(28)-C(28)-C(29)-F(29)	1.4(3)
C(27)-C(28)-C(29)-F(29)	-179.64(19)
F(28)-C(28)-C(29)-C(30)	-179.30(19)
C(27)-C(28)-C(29)-C(30)	-0.3(3)
F(29)-C(29)-C(30)-F(30)	-0.6(3)
C(28)-C(29)-C(30)-F(30)	-179.97(17)
F(29)-C(29)-C(30)-C(31)	179.98(18)
C(28)-C(29)-C(30)-C(31)	0.7(3)
F(30)-C(30)-C(31)-F(31)	0.7(3)
C(29)-C(30)-C(31)-F(31)	-179.98(18)
F(30)-C(30)-C(31)-C(26)	-179.57(18)
C(29)-C(30)-C(31)-C(26)	-0.2(3)
C(27)-C(26)-C(31)-F(31)	179.21(17)
C(25)-C(26)-C(31)-F(31)	-2.5(3)
C(27)-C(26)-C(31)-C(30)	-0.6(3)
C(25)-C(26)-C(31)-C(30)	177.69(19)

Symmetry transformations used to generate equivalent atoms:

#1 -x+1,-y+1,-z   #2 -x+3,-y+2,-z

Appendix A4ac

Data for the structure of the 1:1 co-crystal of PhF_5-CC-Ph-CC-PhF_5 with

CH_3-S-Ph-CC-PhF_4-CC-Ph-S-CH_3 (**4ac**).

Crystals grown by Stephen Watt at Heriot Watt University. Structure solved by the author at the University of Durham Crystallography Department (reference code 01srv035).

Table 1. Crystal data and structure refinement for (**4ac**).

Identification code	01srv035
Empirical formula	C46 H18 F14 S2
Formula weight	900.72
Temperature	100(2) K
Wavelength	0.71073 Å
Crystal system	Triclinic
Space group	P-1
Unit cell dimensions	a = 5.8227(15) Å α= 90.499(4)°.
	b = 7.4882(19) Å β= 95.599(5)°.
	c = 22.108(6) Å γ = 92.675(5)°.
Volume	958.2(4) Å^3
Z	1
Density (calculated)	1.561 Mg/m^3
Absorption coefficient	0.243 mm^{-1}
F(000)	452
Crystal size	0.4 x 0.4 x 0.05 mm^3
Theta range for data collection	0.93 to 27.48°.
Index ranges	-7<=h<=7, -9<=k<=9, -28<=l<=28
Reflections collected	10190
Independent reflections	4385 [R(int) = 0.0311]
Completeness to theta = 27.48°	99.4 %
Absorption correction	None
Max. and min. transmission	. and .
Refinement method	Full-matrix least-squares on F^2
Data / restraints / parameters	4385 / 0 / 316
Goodness-of-fit on F^2	1.054
Final R indices [I>2sigma(I)]	R1 = 0.0436, wR2 = 0.1050
R indices (all data)	R1 = 0.0678, wR2 = 0.1190
Largest diff. peak and hole	0.358 and -0.245 e.Å^{-3}

Table 2. Atomic coordinates (x 10^4) and equivalent isotropic displacement parameters ($Å^2$x 10^3) for (**4ac**). U(eq) is defined as one third of the trace of the orthogonalized U^{ij} tensor.

Atom	x	y	z	U(eq)
S(1)	4207(1)	3218(1)	4400(1)	25(1)
F(1)	-3129(2)	-1107(2)	772(1)	22(1)
F(2)	3987(2)	1826(2)	422(1)	21(1)
F(27)	-1423(2)	-4691(2)	2591(1)	22(1)
F(28)	-644(2)	-3973(2)	3794(1)	26(1)
F(29)	3256(2)	-2057(2)	4242(1)	27(1)
F(30)	6481(2)	-1015(2)	3487(1)	25(1)
F(31)	5716(2)	-1728(2)	2281(1)	23(1)
C(1)	-1572(3)	-543(3)	395(1)	17(1)
C(2)	2012(3)	918(3)	218(1)	16(1)
C(3)	452(3)	396(3)	634(1)	17(1)
C(4)	904(3)	831(3)	1265(1)	18(1)
C(5)	1345(3)	1249(3)	1790(1)	18(1)
C(6)	1953(3)	1716(2)	2417(1)	16(1)
C(7)	427(3)	1340(3)	2853(1)	18(1)
C(8)	1034(3)	1765(3)	3463(1)	18(1)
C(9)	3206(3)	2587(3)	3647(1)	17(1)
C(10)	4741(3)	2973(3)	3210(1)	19(1)
C(11)	4126(3)	2547(3)	2603(1)	18(1)
C(12)	1876(5)	2484(4)	4829(1)	36(1)
C(21)	1556(3)	-4594(3)	-426(1)	18(1)
C(22)	2156(3)	-4156(3)	178(1)	18(1)
C(23)	609(3)	-4562(3)	614(1)	17(1)
C(24)	1210(3)	-4090(3)	1240(1)	19(1)
C(25)	1688(3)	-3669(3)	1766(1)	18(1)
C(26)	2125(3)	-3238(2)	2397(1)	16(1)
C(27)	531(3)	-3773(3)	2802(1)	17(1)
C(28)	912(3)	-3412(3)	3419(1)	18(1)
C(29)	2915(4)	-2469(3)	3647(1)	20(1)
C(30)	4529(3)	-1924(3)	3261(1)	19(1)
C(31)	4127(3)	-2298(3)	2645(1)	18(1)

Table 3.   Bond lengths [Å] and angles [°] for (**4ac**).

S(1)-C(9)	1.7623(19)	F(1)-C(1)-C(3)	119.46(16)
S(1)-C(12)	1.799(3)	C(2)#1-C(1)-C(3)	121.68(18)
F(1)-C(1)	1.346(2)	F(2)-C(2)-C(1)#1	119.07(17)
F(2)-C(2)	1.344(2)	F(2)-C(2)-C(3)	119.08(16)
F(27)-C(27)	1.342(2)	C(1)#1-C(2)-C(3)	121.85(18)
F(28)-C(28)	1.343(2)	C(1)-C(3)-C(2)	116.47(17)
F(29)-C(29)	1.343(2)	C(1)-C(3)-C(4)	122.28(18)
F(30)-C(30)	1.348(2)	C(2)-C(3)-C(4)	121.24(17)
F(31)-C(31)	1.341(2)	C(5)-C(4)-C(3)	177.5(2)
C(1)-C(2)#1	1.379(3)	C(4)-C(5)-C(6)	177.8(2)
C(1)-C(3)	1.398(3)	C(7)-C(6)-C(11)	118.92(17)
C(2)-C(1)#1	1.379(3)	C(7)-C(6)-C(5)	121.00(18)
C(2)-C(3)	1.400(3)	C(11)-C(6)-C(5)	120.07(17)
C(3)-C(4)	1.426(3)	C(8)-C(7)-C(6)	120.97(19)
C(4)-C(5)	1.201(3)	C(7)-C(8)-C(9)	119.93(18)
C(5)-C(6)	1.432(3)	C(8)-C(9)-C(10)	119.25(17)
C(6)-C(7)	1.396(3)	C(8)-C(9)-S(1)	125.07(15)
C(6)-C(11)	1.406(3)	C(10)-C(9)-S(1)	115.67(15)
C(7)-C(8)	1.391(3)	C(11)-C(10)-C(9)	120.56(18)
C(8)-C(9)	1.402(3)	C(10)-C(11)-C(6)	120.37(18)
C(9)-C(10)	1.402(3)	C(22)-C(21)-C(23)#2	120.49(18)
C(10)-C(11)	1.385(3)	C(21)-C(22)-C(23)	120.16(19)
C(21)-C(22)	1.380(3)	C(21)#2-C(23)-C(22)	119.34(17)
C(21)-C(23)#2	1.407(3)	C(21)#2-C(23)-C(24)	120.23(18)
C(22)-C(23)	1.408(3)	C(22)-C(23)-C(24)	120.42(18)
C(23)-C(21)#2	1.407(3)	C(25)-C(24)-C(23)	178.9(2)
C(23)-C(24)	1.432(3)	C(24)-C(25)-C(26)	176.3(2)
C(24)-C(25)	1.203(3)	C(31)-C(26)-C(27)	116.80(17)
C(25)-C(26)	1.427(3)	C(31)-C(26)-C(25)	122.82(17)
C(26)-C(31)	1.395(3)	C(27)-C(26)-C(25)	120.38(17)
C(26)-C(27)	1.398(3)	F(27)-C(27)-C(28)	118.34(17)
C(27)-C(28)	1.382(3)	F(27)-C(27)-C(26)	119.54(16)
C(28)-C(29)	1.384(3)	C(28)-C(27)-C(26)	122.12(18)
C(29)-C(30)	1.380(3)	F(28)-C(28)-C(27)	120.37(18)
C(30)-C(31)	1.384(3)	F(28)-C(28)-C(29)	120.20(17)
		C(27)-C(28)-C(29)	119.43(18)
C(9)-S(1)-C(12)	103.58(11)	F(29)-C(29)-C(30)	120.28(18)
F(1)-C(1)-C(2)#1	118.86(17)	F(29)-C(29)-C(28)	119.71(18)

C(30)-C(29)-C(28)	120.00(17)	C(30)-C(31)-C(26)	121.70(18)
F(30)-C(30)-C(29)	119.63(17)		
F(30)-C(30)-C(31)	120.42(18)		
C(29)-C(30)-C(31)	119.95(18)		
F(31)-C(31)-C(30)	118.41(17)		
F(31)-C(31)-C(26)	119.89(17)		

Symmetry transformations used to generate equivalent atoms:

#1   -x,-y,-z   #2   -x,-y-1,-z

Table 4.   Anisotropic displacement parameters (Å^2x 10^3) for (**4ac**). The anisotropic displacement factor exponent takes the form: $-2\pi^2[\ h^2\ a^{*2}U^{11} + ... + 2\ h\ k\ a^*\ b^*\ U^{12}\ ]$

Atom	U^{11}	U^{22}	U^{33}	U^{23}	U^{13}	U^{12}
S(1)	29(1)	32(1)	13(1)	-4(1)	-1(1)	-4(1)
F(1)	23(1)	25(1)	18(1)	2(1)	7(1)	-4(1)
F(2)	19(1)	22(1)	21(1)	-1(1)	-1(1)	-7(1)
F(27)	19(1)	23(1)	23(1)	1(1)	1(1)	-5(1)
F(28)	30(1)	29(1)	19(1)	3(1)	11(1)	-1(1)
F(29)	41(1)	29(1)	12(1)	-3(1)	-1(1)	1(1)
F(30)	24(1)	24(1)	26(1)	-1(1)	-5(1)	-5(1)
F(31)	22(1)	25(1)	24(1)	4(1)	6(1)	-4(1)
C(1)	17(1)	16(1)	16(1)	2(1)	4(1)	1(1)
C(2)	17(1)	14(1)	18(1)	-1(1)	-2(1)	0(1)
C(3)	20(1)	14(1)	16(1)	0(1)	1(1)	1(1)
C(4)	20(1)	14(1)	19(1)	1(1)	0(1)	0(1)
C(5)	20(1)	16(1)	18(1)	1(1)	2(1)	0(1)
C(6)	19(1)	13(1)	14(1)	1(1)	0(1)	2(1)
C(7)	19(1)	17(1)	18(1)	0(1)	2(1)	-2(1)
C(8)	20(1)	20(1)	16(1)	1(1)	3(1)	-1(1)
C(9)	22(1)	16(1)	14(1)	-1(1)	0(1)	2(1)
C(10)	18(1)	19(1)	18(1)	1(1)	0(1)	-1(1)
C(11)	20(1)	17(1)	17(1)	1(1)	4(1)	-1(1)
C(12)	38(2)	55(2)	14(1)	-3(1)	5(1)	-3(1)
C(21)	18(1)	18(1)	18(1)	1(1)	5(1)	-1(1)
C(22)	18(1)	16(1)	20(1)	2(1)	1(1)	-1(1)
C(23)	20(1)	14(1)	17(1)	0(1)	2(1)	2(1)
C(24)	20(1)	16(1)	20(1)	2(1)	2(1)	-1(1)
C(25)	20(1)	16(1)	19(1)	1(1)	3(1)	0(1)
C(26)	21(1)	12(1)	15(1)	2(1)	2(1)	2(1)
C(27)	17(1)	15(1)	19(1)	0(1)	0(1)	1(1)
C(28)	23(1)	17(1)	16(1)	2(1)	7(1)	2(1)

C(29)	27(1)	18(1)	15(1)	-2(1)	-1(1)	4(1)
C(30)	20(1)	15(1)	19(1)	-1(1)	-3(1)	0(1)
C(31)	19(1)	15(1)	20(1)	3(1)	4(1)	1(1)

Table 5.   Hydrogen coordinates (x 10^4) and isotropic displacement parameters (Å^2x 10 ^{3}) for (**4ac**).

Atom	x	y	z	U(eq)
H(7)	-1030(40)	750(30)	2744(9)	15(5)
H(8)	-20(40)	1530(30)	3757(10)	17(5)
H(10)	6260(40)	3580(30)	3319(11)	26(6)
H(11)	5230(40)	2780(30)	2294(10)	19(6)
H(12A)	2400(50)	2820(40)	5210(15)	56(9)
H(12B)	1640(50)	1150(40)	4833(13)	47(8)
H(12C)	350(50)	3070(40)	4693(12)	42(8)
H(21)	2600(40)	-4340(30)	-732(11)	24(6)
H(22)	3660(40)	-3550(30)	283(11)	27(6)

Table 6. Torsion angles [°] for (**4ac**).

F(1)-C(1)-C(3)-C(2)	179.04(16)
C(2)#1-C(1)-C(3)-C(2)	-0.6(3)
F(1)-C(1)-C(3)-C(4)	-1.9(3)
C(2)#1-C(1)-C(3)-C(4)	178.45(19)
F(2)-C(2)-C(3)-C(1)	179.96(16)
C(1)#1-C(2)-C(3)-C(1)	0.6(3)
F(2)-C(2)-C(3)-C(4)	0.9(3)
C(1)#1-C(2)-C(3)-C(4)	-178.46(19)
C(1)-C(3)-C(4)-C(5)	-159(5)
C(2)-C(3)-C(4)-C(5)	20(5)
C(3)-C(4)-C(5)-C(6)	-75(8)
C(4)-C(5)-C(6)-C(7)	-130(6)
C(4)-C(5)-C(6)-C(11)	49(6)
C(11)-C(6)-C(7)-C(8)	-0.3(3)
C(5)-C(6)-C(7)-C(8)	178.87(19)
C(6)-C(7)-C(8)-C(9)	0.1(3)
C(7)-C(8)-C(9)-C(10)	0.1(3)
C(7)-C(8)-C(9)-S(1)	179.54(16)
C(12)-S(1)-C(9)-C(8)	2.0(2)

C(12)-S(1)-C(9)-C(10)	-178.60(17)
C(8)-C(9)-C(10)-C(11)	-0.1(3)
S(1)-C(9)-C(10)-C(11)	-179.56(16)
C(9)-C(10)-C(11)-C(6)	-0.1(3)
C(7)-C(6)-C(11)-C(10)	0.3(3)
C(5)-C(6)-C(11)-C(10)	-178.84(19)
C(23)#2-C(21)-C(22)-C(23)	0.5(3)
C(21)-C(22)-C(23)-C(21)#2	-0.5(3)
C(21)-C(22)-C(23)-C(24)	-179.18(19)
C(21)#2-C(23)-C(24)-C(25)	-72(12)
C(22)-C(23)-C(24)-C(25)	107(12)
C(23)-C(24)-C(25)-C(26)	83(12)
C(24)-C(25)-C(26)-C(31)	173(3)
C(24)-C(25)-C(26)-C(27)	-6(3)
C(31)-C(26)-C(27)-F(27)	-179.63(17)
C(25)-C(26)-C(27)-F(27)	-0.3(3)
C(31)-C(26)-C(27)-C(28)	-0.6(3)
C(25)-C(26)-C(27)-C(28)	178.71(19)
F(27)-C(27)-C(28)-F(28)	0.1(3)
C(26)-C(27)-C(28)-F(28)	-178.94(17)
F(27)-C(27)-C(28)-C(29)	179.96(17)
C(26)-C(27)-C(28)-C(29)	0.9(3)
F(28)-C(28)-C(29)-F(29)	-2.6(3)
C(27)-C(28)-C(29)-F(29)	177.55(18)
F(28)-C(28)-C(29)-C(30)	178.77(17)
C(27)-C(28)-C(29)-C(30)	-1.1(3)
F(29)-C(29)-C(30)-F(30)	1.7(3)
C(28)-C(29)-C(30)-F(30)	-179.63(18)
F(29)-C(29)-C(30)-C(31)	-177.65(18)
C(28)-C(29)-C(30)-C(31)	1.0(3)
F(30)-C(30)-C(31)-F(31)	-0.3(3)
C(29)-C(30)-C(31)-F(31)	179.08(17)
F(30)-C(30)-C(31)-C(26)	179.93(17)
C(29)-C(30)-C(31)-C(26)	-0.7(3)
C(27)-C(26)-C(31)-F(31)	-179.28(17)
C(25)-C(26)-C(31)-F(31)	1.4(3)
C(27)-C(26)-C(31)-C(30)	0.5(3)
C(25)-C(26)-C(31)-C(30)	-178.81(19)

Symmetry transformations used to generate equivalent atoms:

#1 -x,-y,-z   #2 -x,-y-1,-z

Appendix A4ad

Data for the structure of the 1:1 co-crystal of $PhF_5-CC-Ph-CC-PhF_5$ with

$CF_3-Ph-CC-PhF_4-CC-Ph-CF_3$ (**4ad**).

Crystals grown by Stephen Watt at Heriot Watt University. Structure solved by the

author at the University of Durham Crystallography Department (reference code

01srv039).

Table 1. Crystal data and structure refinement for (**4ad**).

Identification code	01srv039
Empirical formula	C46 H12 F20
Formula weight	944.56
Temperature	100(2) K
Wavelength	0.71073 Å
Crystal system	Triclinic
Space group	P-1
Unit cell dimensions	a = 6.1246(8) Å α= 84.283(4)°.
	b = 7.6693(11) Å β= 81.508(2)°.
	c = 20.125(3) Å γ = 82.373(3)°.
Volume	923.6(2) Å^3
Z	1
Density (calculated)	1.698 Mg/m^3
Absorption coefficient	0.170 mm^{-1}
F(000)	468
Crystal size	0.5 x 0.2 x 0.05 mm^3
Theta range for data collection	1.03 to 25.00°.
Index ranges	-7<=h<=7, -9<=k<=9, -23<=l<=23
Reflections collected	8021
Independent reflections	3261 [R(int) = 0.0546]
Completeness to theta = 25.00°	100.0 %
Absorption correction	None
Max. and min. transmission	. and .
Refinement method	Full-matrix least-squares on F^2
Data / restraints / parameters	3261 / 0 / 322
Goodness-of-fit on F^2	1.084
Final R indices [I>2sigma(I)]	R1 = 0.0574, wR2 = 0.1424
R indices (all data)	R1 = 0.1009, wR2 = 0.1786
Largest diff. peak and hole	0.422 and -0.412 e.Å^{-3}

Table 2. Atomic coordinates (x 10^4) and equivalent isotropic displacement parameters (Å^2x 10^3) for (**4ad**). U(eq) is defined as one third of the trace of the orthogonalized U^{ij} tensor.

Atom	x	y	z	U(eq)
C(1)	6260(6)	3931(5)	5429(2)	17(1)
C(2)	7191(6)	4442(5)	4785(2)	16(1)
C(3)	5980(6)	5548(4)	4339(2)	14(1)
C(4)	7005(6)	6128(5)	3684(2)	18(1)
C(5)	7944(6)	6622(5)	3141(2)	17(1)
C(6)	9083(6)	7113(4)	2493(2)	16(1)
C(7)	11363(6)	6538(5)	2336(2)	17(1)
C(8)	12452(6)	6905(5)	1695(2)	18(1)
C(9)	11297(6)	7867(5)	1209(2)	16(1)
C(10)	9046(6)	8490(5)	1360(2)	18(1)
C(11)	7955(6)	8127(5)	1998(2)	17(1)
C(12)	12473(6)	8236(5)	503(2)	19(1)
F(1)	7516(3)	2886(3)	5838(1)	22(1)
F(2)	9337(3)	3873(3)	4581(1)	21(1)
F(12A)	12446(4)	9979(3)	330(1)	36(1)
F(12B)	11492(4)	7626(3)	38(1)	40(1)
F(12C)	14569(4)	7551(4)	427(1)	51(1)
C(21)	2735(6)	570(5)	5160(2)	18(1)
C(22)	3827(6)	1031(5)	4528(2)	20(1)
C(23)	6109(6)	488(5)	4364(2)	16(1)
C(24)	7259(6)	1014(5)	3713(2)	18(1)
C(25)	8201(6)	1485(5)	3173(2)	16(1)
C(26)	9211(5)	2058(4)	2515(2)	14(1)
C(27)	11447(6)	1538(5)	2268(2)	17(1)
C(28)	12371(6)	2059(5)	1622(2)	17(1)
C(29)	11076(6)	3164(5)	1201(2)	17(1)
C(30)	8866(6)	3701(5)	1426(2)	16(1)
C(31)	7982(6)	3165(5)	2074(2)	15(1)
F(27)	12719(3)	477(3)	2668(1)	24(1)
F(28)	14497(3)	1509(3)	1402(1)	24(1)
F(29)	11985(3)	3702(3)	585(1)	23(1)
F(30)	7616(3)	4759(3)	1022(1)	21(1)
F(31)	5833(3)	3722(3)	2284(1)	22(1)

Table 3.   Bond lengths [Å] and angles [°] for (**4ad**).

C(1)-F(1)	1.343(4)	F(1)-C(1)-C(2)	119.3(3)
C(1)-C(2)	1.377(5)	F(1)-C(1)-C(3)#1	119.4(3)
C(1)-C(3)#1	1.401(5)	C(2)-C(1)-C(3)#1	121.3(3)
C(2)-F(2)	1.346(4)	F(2)-C(2)-C(1)	119.1(3)
C(2)-C(3)	1.397(5)	F(2)-C(2)-C(3)	118.9(3)
C(3)-C(1)#1	1.401(5)	C(1)-C(2)-C(3)	122.0(3)
C(3)-C(4)	1.431(5)	C(2)-C(3)-C(1)#1	116.7(3)
C(4)-C(5)	1.207(5)	C(2)-C(3)-C(4)	121.1(3)
C(5)-C(6)	1.425(5)	C(1)#1-C(3)-C(4)	122.2(3)
C(6)-C(7)	1.407(5)	C(5)-C(4)-C(3)	177.4(4)
C(6)-C(11)	1.409(5)	C(4)-C(5)-C(6)	177.0(4)
C(7)-C(8)	1.384(5)	C(7)-C(6)-C(11)	119.1(3)
C(8)-C(9)	1.386(5)	C(7)-C(6)-C(5)	119.7(3)
C(9)-C(10)	1.397(5)	C(11)-C(6)-C(5)	121.2(3)
C(9)-C(12)	1.514(5)	C(8)-C(7)-C(6)	120.2(4)
C(10)-C(11)	1.376(5)	C(7)-C(8)-C(9)	119.8(3)
C(12)-F(12C)	1.314(4)	C(8)-C(9)-C(10)	120.9(3)
C(12)-F(12B)	1.336(4)	C(8)-C(9)-C(12)	119.9(3)
C(12)-F(12A)	1.346(4)	C(10)-C(9)-C(12)	119.3(3)
C(21)-C(22)	1.383(5)	C(11)-C(10)-C(9)	119.5(4)
C(21)-C(23)#2	1.404(5)	C(10)-C(11)-C(6)	120.5(3)
C(22)-C(23)	1.404(5)	F(12C)-C(12)-F(12B)	107.5(3)
C(23)-C(21)#2	1.404(5)	F(12C)-C(12)-F(12A)	106.7(3)
C(23)-C(24)	1.439(5)	F(12B)-C(12)-F(12A)	105.2(3)
C(24)-C(25)	1.199(5)	F(12C)-C(12)-C(9)	113.0(3)
C(25)-C(26)	1.430(5)	F(12B)-C(12)-C(9)	112.2(3)
C(26)-C(31)	1.397(5)	F(12A)-C(12)-C(9)	111.7(3)
C(26)-C(27)	1.405(5)	C(22)-C(21)-C(23)#2	120.1(4)
C(27)-F(27)	1.342(4)	C(21)-C(22)-C(23)	120.4(4)
C(27)-C(28)	1.382(5)	C(21)#2-C(23)-C(22)	119.5(3)
C(28)-F(28)	1.338(4)	C(21)#2-C(23)-C(24)	120.1(3)
C(28)-C(29)	1.394(5)	C(22)-C(23)-C(24)	120.4(3)
C(29)-F(29)	1.331(4)	C(25)-C(24)-C(23)	178.8(4)
C(29)-C(30)	1.384(5)	C(24)-C(25)-C(26)	176.9(4)
C(30)-F(30)	1.338(4)	C(31)-C(26)-C(27)	116.2(3)
C(30)-C(31)	1.381(5)	C(31)-C(26)-C(25)	120.8(3)
C(31)-F(31)	1.347(4)	C(27)-C(26)-C(25)	123.0(3)
		F(27)-C(27)-C(28)	118.8(3)

F(27)-C(27)-C(26)	119.1(3)	F(30)-C(30)-C(29)	120.1(3)
C(28)-C(27)-C(26)	122.1(3)	C(31)-C(30)-C(29)	119.3(3)
F(28)-C(28)-C(27)	120.3(3)	F(31)-C(31)-C(30)	118.2(3)
F(28)-C(28)-C(29)	120.1(3)	F(31)-C(31)-C(26)	118.9(3)
C(27)-C(28)-C(29)	119.6(3)	C(30)-C(31)-C(26)	122.8(3)
F(29)-C(29)-C(30)	120.5(3)		
F(29)-C(29)-C(28)	119.5(3)		
C(30)-C(29)-C(28)	119.9(3)		
F(30)-C(30)-C(31)	120.5(3)		

Symmetry transformations used to generate equivalent atoms:

#1   -x+1,-y+1,-z+1   #2   -x+1,-y,-z+1

Table 4.   Hydrogen coordinates (x 10^4) and isotropic displacement parameters (Å^2x 10^3) for (4ad).

Atom	x	y	z	U(eq)
H(7)	12130(70)	5940(60)	2680(20)	29(11)
H(8)	13940(80)	6530(60)	1630(20)	36(12)
H(10)	8320(70)	9050(60)	1040(20)	30(12)
H(11)	6310(60)	8530(50)	2118(18)	15(9)
H(21)	1180(70)	870(60)	5260(20)	26(11)
H(22)	3040(80)	1720(60)	4210(20)	40(13)

Table 5.   Anisotropic displacement parameters (Å^2x 10^3) for (4ad). The anisotropic displacement factor exponent takes the form: $-2\pi^2[h^2 a^{*2}U^{11} + ... + 2 h k a^* b^* U^{12}]$

Atom	U^{11}	U^{22}	U^{33}	U^{23}	U^{13}	U^{12}
C(1)	19(2)	11(2)	20(2)	0(1)	-5(2)	0(2)
C(2)	10(2)	16(2)	22(2)	-7(2)	2(1)	-3(1)
C(3)	16(2)	10(2)	19(2)	-4(1)	-2(1)	-3(1)
C(4)	15(2)	14(2)	24(2)	-5(2)	-2(2)	0(2)
C(5)	16(2)	12(2)	22(2)	-5(1)	-2(2)	1(2)
C(6)	21(2)	10(2)	18(2)	-4(1)	0(2)	-3(2)
C(7)	17(2)	16(2)	17(2)	1(2)	-2(2)	-3(2)
C(8)	14(2)	19(2)	20(2)	-3(2)	-2(2)	-1(2)
C(9)	16(2)	11(2)	20(2)	-4(1)	1(2)	-4(2)
C(10)	19(2)	17(2)	17(2)	-2(2)	-3(2)	1(2)
C(11)	16(2)	11(2)	25(2)	-3(2)	1(2)	0(2)
C(12)	18(2)	15(2)	21(2)	-1(2)	1(2)	2(2)
F(1)	20(1)	21(1)	23(1)	2(1)	-4(1)	5(1)
F(2)	11(1)	23(1)	26(1)	-4(1)	3(1)	2(1)
F(12A)	62(2)	16(1)	26(1)	0(1)	11(1)	-13(1)

F(12B)	59(2)	48(2)	19(1)	-12(1)	2(1)	-27(1)
F(12C)	25(1)	77(2)	33(1)	23(1)	16(1)	21(1)
C(21)	15(2)	13(2)	27(2)	-5(2)	-1(2)	0(2)
C(22)	20(2)	15(2)	24(2)	0(2)	-3(2)	-2(2)
C(23)	18(2)	11(2)	19(2)	-3(1)	-1(2)	-2(2)
C(24)	15(2)	13(2)	24(2)	-5(2)	-2(2)	1(2)
C(25)	15(2)	10(2)	24(2)	-6(2)	-3(2)	2(2)
C(26)	12(2)	10(2)	20(2)	-5(1)	0(1)	-3(1)
C(27)	16(2)	15(2)	22(2)	-3(2)	-6(2)	0(2)
C(28)	11(2)	17(2)	24(2)	-7(2)	1(1)	1(2)
C(29)	22(2)	16(2)	15(2)	-5(1)	1(2)	-6(2)
C(30)	17(2)	10(2)	23(2)	-3(1)	-5(2)	0(2)
C(31)	10(2)	14(2)	22(2)	-6(1)	3(1)	-3(1)
F(27)	20(1)	23(1)	26(1)	0(1)	-6(1)	7(1)
F(28)	11(1)	28(1)	30(1)	-8(1)	3(1)	0(1)
F(29)	28(1)	22(1)	18(1)	-1(1)	5(1)	-6(1)
F(30)	23(1)	18(1)	21(1)	0(1)	-6(1)	4(1)
F(31)	14(1)	24(1)	25(1)	-5(1)	1(1)	2(1)

Table 6.   Torsion angles [°] for (**4ad**).

F(1)-C(1)-C(2)-F(2)	0.3(5)
C(3)#1-C(1)-C(2)-F(2)	-178.5(3)
F(1)-C(1)-C(2)-C(3)	-179.1(3)
C(3)#1-C(1)-C(2)-C(3)	2.1(6)
F(2)-C(2)-C(3)-C(1)#1	178.6(3)
C(1)-C(2)-C(3)-C(1)#1	-2.0(6)
F(2)-C(2)-C(3)-C(4)	-2.2(5)
C(1)-C(2)-C(3)-C(4)	177.1(3)
C(2)-C(3)-C(4)-C(5)	-37(9)
C(1)#1-C(3)-C(4)-C(5)	142(8)
C(3)-C(4)-C(5)-C(6)	96(11)
C(4)-C(5)-C(6)-C(7)	-61(8)
C(4)-C(5)-C(6)-C(11)	117(8)
C(11)-C(6)-C(7)-C(8)	-2.7(5)
C(5)-C(6)-C(7)-C(8)	175.7(3)
C(6)-C(7)-C(8)-C(9)	1.1(6)
C(7)-C(8)-C(9)-C(10)	0.7(6)
C(7)-C(8)-C(9)-C(12)	-178.7(3)
C(8)-C(9)-C(10)-C(11)	-0.7(6)
C(12)-C(9)-C(10)-C(11)	178.6(3)
C(9)-C(10)-C(11)-C(6)	-1.0(6)
C(7)-C(6)-C(11)-C(10)	2.6(5)

C(5)-C(6)-C(11)-C(10)	-175.7(3)
C(8)-C(9)-C(12)-F(12C)	0.5(5)
C(10)-C(9)-C(12)-F(12C)	-178.9(3)
C(8)-C(9)-C(12)-F(12B)	122.2(4)
C(10)-C(9)-C(12)-F(12B)	-57.2(4)
C(8)-C(9)-C(12)-F(12A)	-119.9(4)
C(10)-C(9)-C(12)-F(12A)	60.7(4)
C(23)#2-C(21)-C(22)-C(23)	-1.8(6)
C(21)-C(22)-C(23)-C(21)#2	1.8(6)
C(21)-C(22)-C(23)-C(24)	-178.0(3)
C(21)#2-C(23)-C(24)-C(25)	-131(19)
C(22)-C(23)-C(24)-C(25)	49(19)
C(23)-C(24)-C(25)-C(26)	-73(22)
C(24)-C(25)-C(26)-C(31)	27(7)
C(24)-C(25)-C(26)-C(27)	-152(7)
C(31)-C(26)-C(27)-F(27)	179.9(3)
C(25)-C(26)-C(27)-F(27)	-1.0(5)
C(31)-C(26)-C(27)-C(28)	-1.3(5)
C(25)-C(26)-C(27)-C(28)	177.8(3)
F(27)-C(27)-C(28)-F(28)	0.0(5)
C(26)-C(27)-C(28)-F(28)	-178.7(3)
F(27)-C(27)-C(28)-C(29)	-179.9(3)
C(26)-C(27)-C(28)-C(29)	1.3(6)
F(28)-C(28)-C(29)-F(29)	-1.7(5)
C(27)-C(28)-C(29)-F(29)	178.2(3)
F(28)-C(28)-C(29)-C(30)	178.7(3)
C(27)-C(28)-C(29)-C(30)	-1.4(5)
F(29)-C(29)-C(30)-F(30)	0.5(5)
C(28)-C(29)-C(30)-F(30)	-179.9(3)
F(29)-C(29)-C(30)-C(31)	-178.1(3)
C(28)-C(29)-C(30)-C(31)	1.5(5)
F(30)-C(30)-C(31)-F(31)	0.6(5)
C(29)-C(30)-C(31)-F(31)	179.2(3)
F(30)-C(30)-C(31)-C(26)	179.8(3)
C(29)-C(30)-C(31)-C(26)	-1.5(5)
C(27)-C(26)-C(31)-F(31)	-179.3(3)
C(25)-C(26)-C(31)-F(31)	1.5(5)
C(27)-C(26)-C(31)-C(30)	1.4(5)
C(25)-C(26)-C(31)-C(30)	-177.7(3)

Symmetry transformations used to generate equivalent atoms:

#1 -x+1,-y+1,-z+1   #2 -x+1,-y,-z+1

Appendix A4ef

Data for the structure of the 1:1 co-crystal of PhF_5-CC-PhF_4-CC-PhF_5 with

CF_3-Ph-CC-Ph-CC-Ph-CF_3 (**4ef**).

Crystals grown by Stephen Watt at Heriot Watt University. Structure solved by the

author at the University of Durham Crystallography Department (reference code

01srv102).

Table 1. Crystal data and structure refinement for (**4ef**).

Identification code	01srv102
Empirical formula	C46 H12 F20
Formula weight	944.56
Temperature	100(2) K
Wavelength	0.71073 Å
Crystal system	Triclinic
Space group	P-1
Unit cell dimensions	a = 5.984(3) Å α= 92.072(8)°.
	b = 8.867(4) Å β= 90.617(7)°.
	c = 17.592(8) Å γ = 98.555(8)°.
Volume	922.3(7) Å^3
Z	1
Density (calculated)	1.701 Mg/m^3
Absorption coefficient	0.170 mm^{-1}
F(000)	468
Crystal size	0.5 x 0.3 x 0.02 mm^3
Theta range for data collection	1.16 to 27.48°.
Index ranges	-7<=h<=7, -11<=k<=11, -22<=l<=22
Reflections collected	8581
Independent reflections	4186 [R(int) = 0.04711]
Completeness to theta = 27.48°	98.9 %
Absorption correction	Semi-empirical from equivalents
Max. and min. transmission	0.9966 and 0.9199
Refinement method	Full-matrix least-squares on F^2
Data / restraints / parameters	4186 / 0 / 322
Goodness-of-fit on F^2	0.987
Final R indices [I>2sigma(I)]	R1 = 0.0519, wR2 = 0.1277
R indices (all data)	R1 = 0.1143, wR2 = 0.1691
Largest diff. peak and hole	0.400 and -0.359 e.Å^{-3}

Table 2. Atomic coordinates (x 10^4) and equivalent isotropic displacement parameters ($\AA^2$x 10^3) for (**4ef**). U(eq) is defined as one third of the trace of the orthogonalized U^{ij} tensor.

Atom	x	y	z	U(eq)
C(1)	2772(5)	-646(3)	130(2)	17(1)
C(2)	3911(5)	-1178(3)	-486(2)	17(1)
C(3)	6167(5)	-538(3)	-621(2)	17(1)
C(4)	7377(5)	-1087(3)	-1250(2)	18(1)
C(5)	8398(5)	-1548(3)	-1773(2)	18(1)
C(6)	9578(5)	-2064(3)	-2423(2)	16(1)
C(7)	11808(5)	-1405(3)	-2573(2)	19(1)
C(8)	12867(5)	-1860(3)	-3226(2)	17(1)
C(9)	11728(5)	-2972(3)	-3726(2)	16(1)
C(10)	9526(5)	-3656(3)	-3572(2)	19(1)
C(11)	8464(5)	-3217(3)	-2922(2)	18(1)
C(12)	12795(5)	-3392(3)	-4458(2)	19(1)
F(12A)	15058(3)	-2997(2)	-4437(1)	32(1)
F(12B)	12024(3)	-2727(2)	-5061(1)	32(1)
F(12C)	12401(3)	-4909(2)	-4624(1)	28(1)
C(21)	2827(4)	4321(3)	142(2)	18(1)
C(22)	3958(5)	3825(3)	-478(2)	18(1)
C(23)	6171(5)	4489(3)	-638(2)	18(1)
C(24)	7365(5)	3969(3)	-1273(2)	19(1)
C(25)	8384(5)	3520(3)	-1799(2)	19(1)
C(26)	9518(4)	2962(3)	-2437(2)	17(1)
C(27)	11726(5)	3592(3)	-2628(2)	19(1)
C(28)	12793(5)	3052(3)	-3251(2)	20(1)
C(29)	11690(5)	1852(3)	-3700(2)	22(1)
C(30)	9524(5)	1196(3)	-3528(2)	20(1)
C(31)	8469(5)	1750(3)	-2907(2)	19(1)
F(21)	700(3)	3651(2)	271(1)	21(1)
F(22)	2926(3)	2664(2)	-929(1)	23(1)
F(27)	12813(3)	4782(2)	-2206(1)	24(1)
F(28)	14907(3)	3705(2)	-3425(1)	28(1)
F(29)	12751(3)	1307(2)	-4300(1)	34(1)
F(30)	8447(3)	25(2)	-3964(1)	28(1)
F(31)	6349(3)	1104(2)	-2749(1)	23(1)

Table 3. Bond lengths [Å] and angles [°] for (**4ef**).

C(1)-C(2)	1.392(4)	C(29)-F(29)	1.349(3)
C(1)-C(3)#1	1.405(4)	C(29)-C(30)	1.381(4)
C(1)-H(1)	0.91(4)	C(30)-F(30)	1.347(3)
C(2)-C(3)	1.410(4)	C(30)-C(31)	1.380(4)
C(2)-H(2)	0.91(3)	C(31)-F(31)	1.348(3)
C(3)-C(1)#1	1.405(4)		
C(3)-C(4)	1.439(4)	C(2)-C(1)-C(3)#1	120.9(3)
C(4)-C(5)	1.202(4)	C(2)-C(1)-H(1)	120(2)
C(5)-C(6)	1.446(4)	C(3)#1-C(1)-H(1)	119(2)
C(6)-C(7)	1.406(4)	C(1)-C(2)-C(3)	120.0(3)
C(6)-C(11)	1.407(4)	C(1)-C(2)-H(2)	120.4(19)
C(7)-C(8)	1.394(4)	C(3)-C(2)-H(2)	119.6(19)
C(7)-H(7)	1.02(3)	C(1)#1-C(3)-C(2)	119.1(3)
C(8)-C(9)	1.390(4)	C(1)#1-C(3)-C(4)	120.2(3)
C(8)-H(8)	0.96(4)	C(2)-C(3)-C(4)	120.7(3)
C(9)-C(10)	1.399(4)	C(5)-C(4)-C(3)	179.6(3)
C(9)-C(12)	1.503(4)	C(4)-C(5)-C(6)	177.6(3)
C(10)-C(11)	1.385(4)	C(7)-C(6)-C(11)	119.5(3)
C(10)-H(10)	0.91(3)	C(7)-C(6)-C(5)	120.9(3)
C(11)-H(11)	1.01(3)	C(11)-C(6)-C(5)	119.6(3)
C(12)-F(12B)	1.343(3)	C(8)-C(7)-C(6)	119.9(3)
C(12)-F(12A)	1.347(3)	C(8)-C(7)-H(7)	121.6(17)
C(12)-F(12C)	1.351(3)	C(6)-C(7)-H(7)	118.5(17)
C(21)-F(21)	1.348(3)	C(9)-C(8)-C(7)	120.1(3)
C(21)-C(22)	1.381(4)	C(9)-C(8)-H(8)	122.1(19)
C(21)-C(23)#2	1.403(4)	C(7)-C(8)-H(8)	118(2)
C(22)-F(22)	1.346(3)	C(8)-C(9)-C(10)	120.4(3)
C(22)-C(23)	1.403(4)	C(8)-C(9)-C(12)	120.4(3)
C(23)-C(21)#2	1.403(4)	C(10)-C(9)-C(12)	119.1(2)
C(23)-C(24)	1.432(4)	C(11)-C(10)-C(9)	120.0(3)
C(24)-C(25)	1.201(4)	C(11)-C(10)-H(10)	121(2)
C(25)-C(26)	1.428(4)	C(9)-C(10)-H(10)	119(2)
C(26)-C(31)	1.398(4)	C(10)-C(11)-C(6)	120.1(3)
C(26)-C(27)	1.405(4)	C(10)-C(11)-H(11)	120.5(18)
C(27)-F(27)	1.348(3)	C(6)-C(11)-H(11)	119.2(18)
C(27)-C(28)	1.381(4)	F(12B)-C(12)-F(12A)	106.8(2)
C(28)-F(28)	1.354(3)	F(12B)-C(12)-F(12C)	105.9(2)
C(28)-C(29)	1.383(4)	F(12A)-C(12)-F(12C)	106.2(2)

F(12B)-C(12)-C(9)	112.9(2)	F(27)-C(27)-C(26)	119.3(3)
F(12A)-C(12)-C(9)	112.1(2)	C(28)-C(27)-C(26)	121.7(3)
F(12C)-C(12)-C(9)	112.4(2)	F(28)-C(28)-C(27)	120.0(3)
F(21)-C(21)-C(22)	119.2(2)	F(28)-C(28)-C(29)	120.1(3)
F(21)-C(21)-C(23)#2	119.1(3)	C(27)-C(28)-C(29)	119.8(3)
C(22)-C(21)-C(23)#2	121.8(3)	F(29)-C(29)-C(30)	120.0(3)
F(22)-C(22)-C(21)	119.2(2)	F(29)-C(29)-C(28)	119.8(3)
F(22)-C(22)-C(23)	119.4(3)	C(30)-C(29)-C(28)	120.2(3)
C(21)-C(22)-C(23)	121.4(3)	F(30)-C(30)-C(31)	120.2(3)
C(22)-C(23)-C(21)#2	116.9(3)	F(30)-C(30)-C(29)	120.3(3)
C(22)-C(23)-C(24)	121.7(3)	C(31)-C(30)-C(29)	119.5(3)
C(21)#2-C(23)-C(24)	121.4(3)	F(31)-C(31)-C(30)	118.8(2)
C(25)-C(24)-C(23)	179.0(3)	F(31)-C(31)-C(26)	118.9(3)
C(24)-C(25)-C(26)	177.9(3)	C(30)-C(31)-C(26)	122.3(3)
C(31)-C(26)-C(27)	116.5(3)		
C(31)-C(26)-C(25)	121.2(3)	Symmetry transformations used to generate
C(27)-C(26)-C(25)	122.3(3)	equivalent atoms:
F(27)-C(27)-C(28)	118.9(2)	#1 -x+1,-y,-z #2 -x+1,-y+1,-z

Table 4.   Anisotropic displacement parameters ($\AA^2$x 10^3) for **(4ef)**. The anisotropic
displacement factor exponent takes the form: $-2\pi^2[$ h^2 $a^{*2}U^{11}$ + ... + 2 h k a* b* U^{12}]

Atom	U^{11}	U^{22}	U^{33}	U^{23}	U^{13}	U^{12}
C(1)	11(1)	17(1)	24(2)	2(1)	0(1)	2(1)
C(2)	16(2)	14(1)	20(2)	0(1)	-1(1)	1(1)
C(3)	18(2)	17(1)	17(2)	3(1)	2(1)	5(1)
C(4)	15(1)	17(1)	22(2)	1(1)	1(1)	5(1)
C(5)	15(1)	16(1)	22(2)	2(1)	-3(1)	2(1)
C(6)	17(1)	13(1)	20(2)	1(1)	0(1)	6(1)
C(7)	18(2)	17(1)	22(2)	-2(1)	-2(1)	2(1)
C(8)	11(1)	16(1)	24(2)	1(1)	3(1)	2(1)
C(9)	13(1)	17(1)	18(2)	2(1)	1(1)	6(1)
C(10)	16(1)	17(2)	23(2)	-3(1)	-2(1)	2(1)
C(11)	12(1)	19(2)	24(2)	2(1)	1(1)	3(1)
C(12)	14(1)	19(2)	23(2)	0(1)	0(1)	3(1)
F(12A)	13(1)	51(1)	32(1)	-12(1)	7(1)	2(1)
F(12B)	37(1)	42(1)	22(1)	7(1)	3(1)	17(1)
F(12C)	31(1)	26(1)	30(1)	-6(1)	5(1)	10(1)

C(21)	8(1)	18(1)	28(2)	6(1)	-2(1)	1(1)
C(22)	14(1)	17(1)	22(2)	1(1)	-5(1)	2(1)
C(23)	13(1)	19(1)	23(2)	4(1)	-2(1)	5(1)
C(24)	13(1)	18(2)	26(2)	5(1)	-3(1)	0(1)
C(25)	14(1)	19(2)	24(2)	4(1)	-4(1)	2(1)
C(26)	12(1)	18(1)	21(2)	4(1)	0(1)	4(1)
C(27)	15(1)	16(1)	25(2)	4(1)	-3(1)	1(1)
C(28)	10(1)	20(2)	31(2)	9(1)	1(1)	1(1)
C(29)	23(2)	21(2)	24(2)	5(1)	5(1)	9(1)
C(30)	22(2)	13(1)	25(2)	2(1)	-4(1)	3(1)
C(31)	12(1)	16(1)	29(2)	7(1)	-1(1)	1(1)
F(21)	8(1)	22(1)	32(1)	4(1)	0(1)	-2(1)
F(22)	17(1)	20(1)	29(1)	-4(1)	-3(1)	-2(1)
F(27)	16(1)	22(1)	33(1)	0(1)	-5(1)	-4(1)
F(28)	12(1)	29(1)	41(1)	9(1)	6(1)	0(1)
F(29)	35(1)	34(1)	34(1)	1(1)	14(1)	10(1)
F(30)	30(1)	23(1)	31(1)	-5(1)	-3(1)	-2(1)
F(31)	10(1)	20(1)	38(1)	4(1)	2(1)	-4(1)

Table 5. Hydrogen coordinates (x 10^4) and isotropic displacement parameters ($\mathring{A}^2$x 10^{3}) for (**4ef**).

Atom	x	y	z	U(eq)
H(1)	1350(60)	-1090(40)	236(19)	36(10)
H(2)	3210(50)	-1940(30)	-805(17)	18(8)
H(7)	12610(50)	-600(30)	-2197(17)	21(8)
H(8)	14410(60)	-1410(40)	-3305(19)	33(9)
H(10)	8820(60)	-4400(40)	-3902(19)	31(9)
H(11)	6930(60)	-3760(40)	-2785(18)	30(9)

Table 6. Torsion angles [°] for (**4ef**).

C(3)#1-C(1)-C(2)-C(3)	0.6(5)
C(1)-C(2)-C(3)-C(1)#1	-0.6(5)
C(1)-C(2)-C(3)-C(4)	179.2(3)
C(1)#1-C(3)-C(4)-C(5)	58(50)
C(2)-C(3)-C(4)-C(5)	-122(50)
C(3)-C(4)-C(5)-C(6)	-158(46)
C(4)-C(5)-C(6)-C(7)	100(7)
C(4)-C(5)-C(6)-C(11)	-79(7)
C(11)-C(6)-C(7)-C(8)	2.2(4)
C(5)-C(6)-C(7)-C(8)	-176.4(3)
C(6)-C(7)-C(8)-C(9)	-0.5(4)
C(7)-C(8)-C(9)-C(10)	-0.8(4)
C(7)-C(8)-C(9)-C(12)	175.8(3)
C(8)-C(9)-C(10)-C(11)	0.5(4)
C(12)-C(9)-C(10)-C(11)	-176.2(3)
C(9)-C(10)-C(11)-C(6)	1.2(4)
C(7)-C(6)-C(11)-C(10)	-2.5(4)
C(5)-C(6)-C(11)-C(10)	176.0(3)
C(8)-C(9)-C(12)-F(12B)	-100.0(3)
C(10)-C(9)-C(12)-F(12B)	76.6(3)
C(8)-C(9)-C(12)-F(12A)	20.7(4)
C(10)-C(9)-C(12)-F(12A)	-162.6(2)
C(8)-C(9)-C(12)-F(12C)	140.3(3)
C(10)-C(9)-C(12)-F(12C)	-43.0(4)
F(21)-C(21)-C(22)-F(22)	-1.3(4)
C(23)#2-C(21)-C(22)-F(22)	179.1(2)
F(21)-C(21)-C(22)-C(23)	179.7(2)
C(23)#2-C(21)-C(22)-C(23)	0.2(5)
F(22)-C(22)-C(23)-C(21)#2	-179.1(2)
C(21)-C(22)-C(23)-C(21)#2	-0.2(5)
F(22)-C(22)-C(23)-C(24)	0.3(4)
C(21)-C(22)-C(23)-C(24)	179.2(3)
C(22)-C(23)-C(24)-C(25)	-100(19)
C(21)#2-C(23)-C(24)-C(25)	79(19)
C(23)-C(24)-C(25)-C(26)	121(18)
C(24)-C(25)-C(26)-C(31)	-21(8)
C(24)-C(25)-C(26)-C(27)	159(8)
C(31)-C(26)-C(27)-F(27)	178.7(2)

C(25)-C(26)-C(27)-F(27)	-1.2(4)
C(31)-C(26)-C(27)-C(28)	0.6(4)
C(25)-C(26)-C(27)-C(28)	-179.3(3)
F(27)-C(27)-C(28)-F(28)	0.8(4)
C(26)-C(27)-C(28)-F(28)	178.9(2)
F(27)-C(27)-C(28)-C(29)	-178.7(3)
C(26)-C(27)-C(28)-C(29)	-0.6(4)
F(28)-C(28)-C(29)-F(29)	1.8(4)
C(27)-C(28)-C(29)-F(29)	-178.7(3)
F(28)-C(28)-C(29)-C(30)	-179.3(3)
C(27)-C(28)-C(29)-C(30)	0.2(4)
F(29)-C(29)-C(30)-F(30)	-0.9(4)
C(28)-C(29)-C(30)-F(30)	-179.9(3)
F(29)-C(29)-C(30)-C(31)	179.1(3)
C(28)-C(29)-C(30)-C(31)	0.2(4)
F(30)-C(30)-C(31)-F(31)	-0.4(4)
C(29)-C(30)-C(31)-F(31)	179.6(2)
F(30)-C(30)-C(31)-C(26)	179.9(3)
C(29)-C(30)-C(31)-C(26)	-0.1(4)
C(27)-C(26)-C(31)-F(31)	-180.0(2)
C(25)-C(26)-C(31)-F(31)	-0.1(4)
C(27)-C(26)-C(31)-C(30)	-0.2(4)
C(25)-C(26)-C(31)-C(30)	179.7(3)

Symmetry transformations used to generate equivalent atoms:

#1 -x+1,-y,-z   #2 -x+1,-y+1,-z

Appendix A4gh

Data for the structure of the 1:1 co-crystal of MeO-PhF$_5$-CC-PhF$_4$-CC-PhF$_5$-OMe with

MeO-Ph-CC-Ph-CC-Ph-MeO (**4gh**).

Crystals grown by Stephen Watt at Heriot Watt University. Structure solved by the

author at the University of Durham Crystallography Department (reference code

01srv025).

Table 1. Crystal data and structure refinement for (**4gh**).

Identification code	01srv025
Empirical formula	C48 H24 F12 O4
Formula weight	892.67
Temperature	100(2) K
Wavelength	0.71073 Å
Crystal system	Triclinic
Space group	P-1
Unit cell dimensions	a = 8.5588(6) Å α= 89.2160(10)°.
	b = 9.8957(7) Å β= 76.8960(10)°.
	c = 12.7564(9) Å γ = 65.8540(10)°.
Volume	956.40(12) Å^3
Z	1
Density (calculated)	1.550 Mg/m^3
Absorption coefficient	0.137 mm^{-1}
F(000)	452
Crystal size	0.5 x 0.5 x 0.3 mm^3
Theta range for data collection	1.65 to 27.49°.
Index ranges	-11<=h<=11, -12<=k<=12, -16<=l<=16
Reflections collected	10199
Independent reflections	4369 [R(int) = 0.0252]
Completeness to theta = 27.49°	99.6 %
Absorption correction	None
Max. and min. transmission	. and .
Refinement method	Full-matrix least-squares on F^2
Data / restraints / parameters	4369 / 0 / 337
Goodness-of-fit on F^2	1.023
Final R indices [I>2sigma(I)]	R1 = 0.0421, wR2 = 0.1125
R indices (all data)	R1 = 0.0615, wR2 = 0.1267
Extinction coefficient	.
Largest diff. peak and hole	0.319 and -0.254 e.Å^{-3}

Table 2. Atomic coordinates (x 10^4) and equivalent isotropic displacement parameters (Å^2x 10^3) for (**4gh**). U(eq) is defined as one third of the trace of the orthogonalized U^{ij} tensor.

Atom	x	y	z	U(eq)
C(1)	-456(2)	4654(2)	11036(1)	19(1)
C(2)	-1735(2)	5301(2)	10472(1)	20(1)
C(3)	-1319(2)	5669(2)	9415(1)	19(1)
C(4)	-2624(2)	6320(2)	8820(1)	21(1)
C(5)	-3721(2)	6843(2)	8315(1)	20(1)
C(6)	-5051(2)	7461(2)	7733(1)	19(1)
C(7)	-4688(2)	7779(2)	6658(1)	19(1)
C(8)	-5999(2)	8374(2)	6110(1)	19(1)
C(9)	-7750(2)	8669(2)	6587(1)	19(1)
C(10)	-8140(2)	8402(2)	7670(1)	20(1)
C(11)	-6814(2)	7807(2)	8213(1)	20(1)
C(12)	-10546(2)	9094(2)	6218(2)	36(1)
C(21)	6733(2)	4791(2)	4547(1)	21(1)
C(22)	5458(2)	5425(2)	3970(1)	21(1)
C(23)	3702(2)	5645(2)	4416(1)	20(1)
C(24)	2386(2)	6296(2)	3819(1)	22(1)
C(25)	1273(2)	6826(2)	3320(1)	21(1)
C(26)	-60(2)	7435(2)	2728(1)	20(1)
C(27)	361(2)	7778(2)	1654(1)	21(1)
C(28)	-930(2)	8340(2)	1085(1)	21(1)
C(29)	-2663(2)	8563(2)	1563(1)	19(1)
C(30)	-3113(2)	8248(2)	2629(1)	20(1)
C(31)	-1807(2)	7690(2)	3201(1)	21(1)
C(32)	-5609(2)	9318(2)	1368(1)	27(1)
F(1)	-934(1)	4337(1)	12051(1)	25(1)
F(2)	-3414(1)	5589(1)	10953(1)	25(1)
F(7)	-3022(1)	7504(1)	6143(1)	26(1)
F(8)	-5581(1)	8678(1)	5081(1)	25(1)
F(10)	-9808(1)	8739(1)	8229(1)	25(1)
F(11)	-7275(1)	7589(1)	9259(1)	27(1)
O(2)	-3819(1)	9079(1)	916(1)	24(1)
O(1)	-8888(1)	9223(1)	5955(1)	25(1)

Table 3. Bond lengths [Å] and angles [°] for (**4gh**).

C(1)-F(1)	1.3405(16)	F(1)-C(1)-C(3)#1	119.12(12)
C(1)-C(2)	1.378(2)	C(2)-C(1)-C(3)#1	121.97(13)
C(1)-C(3)#1	1.397(2)	F(2)-C(2)-C(1)	118.99(12)
C(2)-F(2)	1.3392(16)	F(2)-C(2)-C(3)	119.53(12)
C(2)-C(3)	1.397(2)	C(1)-C(2)-C(3)	121.48(13)
C(3)-C(1)#1	1.397(2)	C(2)-C(3)-C(1)#1	116.55(13)
C(3)-C(4)	1.422(2)	C(2)-C(3)-C(4)	121.97(13)
C(4)-C(5)	1.196(2)	C(1)#1-C(3)-C(4)	121.47(13)
C(5)-C(6)	1.422(2)	C(5)-C(4)-C(3)	178.86(16)
C(6)-C(11)	1.391(2)	C(4)-C(5)-C(6)	178.76(16)
C(6)-C(7)	1.397(2)	C(11)-C(6)-C(7)	115.68(13)
C(7)-F(7)	1.3423(16)	C(11)-C(6)-C(5)	121.54(13)
C(7)-C(8)	1.377(2)	C(7)-C(6)-C(5)	122.77(13)
C(8)-F(8)	1.3443(16)	F(7)-C(7)-C(8)	118.95(12)
C(8)-C(9)	1.391(2)	F(7)-C(7)-C(6)	119.33(13)
C(9)-O(1)	1.3446(17)	C(8)-C(7)-C(6)	121.71(13)
C(9)-C(10)	1.393(2)	F(8)-C(8)-C(7)	119.24(13)
C(10)-F(10)	1.3471(16)	F(8)-C(8)-C(9)	118.66(13)
C(10)-C(11)	1.383(2)	C(7)-C(8)-C(9)	122.10(13)
C(11)-F(11)	1.3434(16)	O(1)-C(9)-C(8)	115.93(13)
C(12)-O(1)	1.4392(18)	O(1)-C(9)-C(10)	127.28(14)
C(21)-C(22)	1.385(2)	C(8)-C(9)-C(10)	116.76(13)
C(21)-C(23)#2	1.404(2)	F(10)-C(10)-C(11)	117.69(13)
C(22)-C(23)	1.406(2)	F(10)-C(10)-C(9)	121.67(13)
C(23)-C(21)#2	1.404(2)	C(11)-C(10)-C(9)	120.63(13)
C(23)-C(24)	1.430(2)	F(11)-C(11)-C(10)	117.86(13)
C(24)-C(25)	1.203(2)	F(11)-C(11)-C(6)	119.09(12)
C(25)-C(26)	1.432(2)	C(10)-C(11)-C(6)	123.03(13)
C(26)-C(31)	1.396(2)	C(22)-C(21)-C(23)#2	120.62(14)
C(26)-C(27)	1.409(2)	C(21)-C(22)-C(23)	120.50(14)
C(27)-C(28)	1.380(2)	C(21)#2-C(23)-C(22)	118.87(13)
C(28)-C(29)	1.395(2)	C(21)#2-C(23)-C(24)	120.63(13)
C(29)-O(2)	1.3661(17)	C(22)-C(23)-C(24)	120.49(13)
C(29)-C(30)	1.394(2)	C(25)-C(24)-C(23)	179.05(16)
C(30)-C(31)	1.392(2)	C(24)-C(25)-C(26)	178.96(16)
C(32)-O(2)	1.4290(18)	C(31)-C(26)-C(27)	118.49(13)
		C(31)-C(26)-C(25)	120.62(13)
F(1)-C(1)-C(2)	118.91(13)	C(27)-C(26)-C(25)	120.88(13)

C(28)-C(27)-C(26)	120.38(14)
C(27)-C(28)-C(29)	120.40(14)
O(2)-C(29)-C(30)	124.36(13)
O(2)-C(29)-C(28)	115.49(13)
C(30)-C(29)-C(28)	120.15(14)
C(31)-C(30)-C(29)	119.15(14)
C(30)-C(31)-C(26)	121.41(14)

| C(29)-O(2)-C(32) | 117.62(12) |
| C(9)-O(1)-C(12) | 119.82(12) |

Symmetry transformations used to generate equivalent atoms:

#1 -x,-y+1,-z+2   #2 -x+1,-y+1,-z+1

Table 4. Hydrogen coordinates (x 10^4) and isotropic displacement parameters ($\mathring{A}^2$x 10 ^{3}) for (**4gh**).

Atom	x	y	z	U(eq)
H(12A)	-10460(20)	8150(20)	6537(15)	35(5)
H(12B)	-10910(30)	9200(20)	5545(18)	52(6)
H(12C)	-11400(30)	9940(20)	6746(18)	52(6)
H(21)	7930(20)	4640(19)	4248(14)	27(4)
H(22)	5790(20)	5700(20)	3263(16)	33(5)
H(27)	1540(20)	7616(19)	1319(14)	26(4)
H(28)	-630(30)	8540(20)	338(16)	36(5)
H(30)	-4280(20)	8369(19)	2967(14)	28(5)
H(31)	-2100(20)	7480(18)	3922(15)	27(4)
H(32A)	-5680(20)	8419(17)	1624(12)	16(4)
H(32B)	-6150(20)	10100(20)	1944(16)	36(5)
H(32C)	-6210(20)	9640(20)	790(16)	38(5)

Table 5. Anisotropic displacement parameters $(\text{Å}^2 \times 10^3)$ for (4gh). The anisotropic displacement factor exponent takes the form: $-2\pi^2[\ h^2\ a^{*2}U^{11} + \ldots + 2\ h\ k\ a^*\ b^*\ U^{12}\ ]$

Atom	U^{11}	U^{22}	U^{33}	U^{23}	U^{13}	U^{12}
C(1)	22(1)	18(1)	17(1)	2(1)	-4(1)	-9(1)
C(2)	18(1)	19(1)	21(1)	0(1)	-4(1)	-8(1)
C(3)	19(1)	16(1)	21(1)	1(1)	-7(1)	-7(1)
C(4)	22(1)	21(1)	20(1)	2(1)	-5(1)	-9(1)
C(5)	20(1)	21(1)	20(1)	1(1)	-4(1)	-9(1)
C(6)	21(1)	17(1)	19(1)	2(1)	-6(1)	-8(1)
C(7)	18(1)	20(1)	21(1)	0(1)	-3(1)	-9(1)
C(8)	23(1)	21(1)	16(1)	4(1)	-4(1)	-12(1)
C(9)	21(1)	19(1)	22(1)	4(1)	-10(1)	-9(1)
C(10)	17(1)	19(1)	23(1)	1(1)	-3(1)	-8(1)
C(11)	22(1)	21(1)	16(1)	3(1)	-4(1)	-10(1)
C(12)	23(1)	58(1)	36(1)	20(1)	-15(1)	-23(1)
C(21)	20(1)	23(1)	22(1)	3(1)	-6(1)	-10(1)
C(22)	24(1)	21(1)	18(1)	5(1)	-6(1)	-10(1)
C(23)	22(1)	17(1)	20(1)	1(1)	-7(1)	-8(1)
C(24)	23(1)	22(1)	20(1)	2(1)	-5(1)	-10(1)
C(25)	21(1)	23(1)	20(1)	2(1)	-6(1)	-9(1)
C(26)	21(1)	18(1)	20(1)	1(1)	-6(1)	-7(1)
C(27)	18(1)	22(1)	21(1)	0(1)	-5(1)	-8(1)
C(28)	22(1)	23(1)	16(1)	3(1)	-3(1)	-10(1)
C(29)	20(1)	18(1)	20(1)	2(1)	-8(1)	-7(1)
C(30)	20(1)	22(1)	19(1)	3(1)	-4(1)	-10(1)
C(31)	24(1)	23(1)	16(1)	4(1)	-6(1)	-10(1)
C(32)	20(1)	33(1)	29(1)	7(1)	-9(1)	-11(1)
F(1)	27(1)	28(1)	18(1)	7(1)	-4(1)	-12(1)
F(2)	16(1)	30(1)	26(1)	4(1)	-3(1)	-9(1)
F(7)	18(1)	35(1)	25(1)	4(1)	-3(1)	-13(1)
F(8)	27(1)	33(1)	17(1)	7(1)	-6(1)	-16(1)
F(10)	17(1)	32(1)	25(1)	3(1)	-2(1)	-10(1)
F(11)	26(1)	35(1)	17(1)	7(1)	-4(1)	-12(1)
O(2)	20(1)	33(1)	20(1)	6(1)	-9(1)	-9(1)
O(1)	23(1)	32(1)	26(1)	11(1)	-14(1)	-14(1)

Appendix A5: Crystal Structure Data Tables for Structures in Chapter 5

Appendix A5a

Data for the structure of PhF_5-CC-Ph-I (**5a**).

Crystals grown by Jonathan C. Collings. Structure solved by the author at the University

of Durham Crystallography Department (reference code 01srv103).

Table 1. Crystal data and structure refinement for (**5a**).

Identification code	01srv103
Empirical formula	C14 H4 F5 I
Formula weight	394.07
Temperature	105(2) K
Wavelength	0.71073 Å
Crystal system	Monoclinic
Space group	P2(1)/c
Unit cell dimensions	a = 21.417(7) Å α= 90°.
	b = 4.9672(16) Å β= 92.288(5)°.
	c = 11.692(4) Å γ = 90°.
Volume	1242.9(7) Å^3
Z	4
Density (calculated)	2.106 Mg/m^3
Absorption coefficient	2.623 mm^{-1}
F(000)	744
Crystal size	0.6 x 0.2 x 0.05 mm^3
Theta range for data collection	0.95 to 27.48°.
Index ranges	-27<=h<=27, -6<=k<=6, -15<=l<=15
Reflections collected	11360
Independent reflections	2850 [R(int) = 0.0524]
Completeness to theta = 27.48°	99.7 %
Absorption correction	Semi-empirical from equivalents
Max. and min. transmission	0.8800 and 0.3021
Refinement method	Full-matrix least-squares on F^2
Data / restraints / parameters	2850 / 6 / 181
Goodness-of-fit on F^2	1.148
Final R indices [I>2sigma(I)]	R1 = 0.0526, wR2 = 0.1320
R indices (all data)	R1 = 0.0612, wR2 = 0.1432
Largest diff. peak and hole	2.293 and -4.715 e.Å^{-3}

Table 2. Atomic coordinates (x 10^4) and equivalent isotropic displacement parameters (Å^2x 10^3) for (**5a**). U(eq) is defined as one third of the trace of the orthogonalized U^{ij} tensor.

	x	y	z	U(eq)
C(1)	1119(2)	8240(11)	1133(4)	13(1)
C(2)	1604(3)	9034(12)	1893(5)	14(1)
C(3)	2034(3)	10929(12)	1564(5)	16(1)
C(4)	1980(3)	12093(11)	467(4)	12(1)
C(5)	1493(3)	11201(12)	-301(5)	15(1)
C(6)	1070(3)	9351(12)	36(5)	19(1)
C(7)	2418(3)	14110(12)	157(5)	14(1)
C(8)	2801(3)	15809(12)	-39(5)	17(1)
C(9)	3251(3)	17835(11)	-245(4)	13(1)
C(10)	3747(3)	18352(12)	515(4)	17(1)
C(11)	4174(3)	20380(12)	340(5)	18(1)
C(12)	4114(3)	21942(12)	-641(4)	16(1)
C(13)	3632(3)	21464(12)	-1416(4)	16(1)
C(14)	3205(3)	19442(11)	-1223(5)	15(1)
F(10)	3821(2)	16851(8)	1468(3)	24(1)
F(11)	4644(2)	20849(8)	1108(3)	25(1)
F(12)	4519(2)	23925(8)	-812(3)	23(1)
F(13)	3559(2)	23034(7)	-2350(3)	22(1)
F(14)	2736(2)	19055(7)	-1990(3)	20(1)
I(1)	469(1)	5460(1)	1700(1)	12(1)

Table 3.   Bond lengths [Å] and angles [°] for (5a).

C(1)-C(6)	1.396(7)	C(4)-C(3)-H(3A)	119.9
C(1)-C(2)	1.397(7)	C(3)-C(4)-C(5)	118.7(5)
C(1)-I(1)	2.087(5)	C(3)-C(4)-C(7)	119.2(5)
C(2)-C(3)	1.382(8)	C(5)-C(4)-C(7)	122.1(5)
C(2)-H(2A)	0.9500	C(6)-C(5)-C(4)	120.5(5)
C(3)-C(4)	1.407(7)	C(6)-C(5)-H(5A)	119.7
C(3)-H(3A)	0.9500	C(4)-C(5)-H(5A)	119.7
C(4)-C(5)	1.420(7)	C(5)-C(6)-C(1)	120.5(5)
C(4)-C(7)	1.430(8)	C(5)-C(6)-H(6A)	119.8
C(5)-C(6)	1.360(9)	C(1)-C(6)-H(6A)	119.8
C(5)-H(5A)	0.9500	C(8)-C(7)-C(4)	176.2(6)
C(6)-H(6A)	0.9500	C(7)-C(8)-C(9)	178.7(6)
C(7)-C(8)	1.205(9)	C(10)-C(9)-C(14)	116.6(5)
C(8)-C(9)	1.420(8)	C(10)-C(9)-C(8)	122.1(5)
C(9)-C(10)	1.382(8)	C(14)-C(9)-C(8)	121.3(5)
C(9)-C(14)	1.395(8)	F(10)-C(10)-C(11)	118.0(5)
C(10)-F(10)	1.346(6)	F(10)-C(10)-C(9)	119.5(5)
C(10)-C(11)	1.381(9)	C(11)-C(10)-C(9)	122.5(5)
C(11)-F(11)	1.342(7)	F(11)-C(11)-C(10)	120.8(5)
C(11)-C(12)	1.387(8)	F(11)-C(11)-C(12)	119.9(5)
C(12)-F(12)	1.333(7)	C(10)-C(11)-C(12)	119.3(5)
C(12)-C(13)	1.367(8)	F(12)-C(12)-C(13)	120.5(5)
C(13)-F(13)	1.346(6)	F(12)-C(12)-C(11)	119.9(5)
C(13)-C(14)	1.383(8)	C(13)-C(12)-C(11)	119.6(5)
C(14)-F(14)	1.335(7)	F(13)-C(13)-C(12)	119.8(5)
		F(13)-C(13)-C(14)	119.8(5)
C(6)-C(1)-C(2)	120.0(5)	C(12)-C(13)-C(14)	120.3(5)
C(6)-C(1)-I(1)	121.8(4)	F(14)-C(14)-C(13)	118.7(5)
C(2)-C(1)-I(1)	118.2(4)	F(14)-C(14)-C(9)	119.6(5)
C(3)-C(2)-C(1)	120.1(5)	C(13)-C(14)-C(9)	121.7(5)
C(3)-C(2)-H(2A)	119.9		
C(1)-C(2)-H(2A)	119.9		
C(2)-C(3)-C(4)	120.1(5)	Symmetry transformations used to generate	
C(2)-C(3)-H(3A)	119.9	equivalent atoms:	

Table 4. Anisotropic displacement parameters ($\text{Å}^2 \times 10^3$) for (5a). The anisotropic displacement factor exponent takes the form: $-2\pi^2[\ h^2\ a^{*2}U^{11} + ... + 2\ h\ k\ a^*\ b^*\ U^{12}\ ]$

	U^{11}	U^{22}	U^{33}	U^{23}	U^{13}	U^{12}
C(1)	18(3)	15(3)	5(2)	-2(2)	2(2)	-2(2)
C(2)	20(3)	15(3)	8(2)	4(2)	4(2)	1(2)
C(3)	16(3)	19(3)	12(3)	-3(2)	1(2)	-1(2)
C(4)	20(3)	11(3)	7(2)	-1(2)	7(2)	0(2)
C(5)	16(1)	16(1)	13(1)	1(1)	3(1)	0(1)
C(6)	26(3)	22(3)	9(3)	-1(2)	2(2)	-3(2)
C(7)	21(3)	13(3)	10(2)	-5(2)	6(2)	2(2)
C(8)	18(3)	22(3)	13(3)	-4(2)	6(2)	2(2)
C(9)	22(3)	11(2)	7(2)	-2(2)	7(2)	0(2)
C(10)	26(3)	19(3)	5(2)	0(2)	3(2)	4(2)
C(11)	17(3)	28(3)	9(3)	-4(2)	0(2)	-1(2)
C(12)	19(3)	16(3)	12(2)	-4(2)	6(2)	-2(2)
C(13)	27(3)	17(3)	5(2)	1(2)	5(2)	-2(2)
C(14)	19(3)	15(3)	11(3)	-2(2)	2(2)	-2(2)
F(10)	36(2)	27(2)	9(2)	8(1)	1(1)	0(2)
F(11)	24(2)	32(2)	17(2)	-4(2)	-6(1)	-3(2)
F(12)	26(2)	21(2)	24(2)	-3(2)	6(1)	-7(2)
F(13)	31(2)	22(2)	13(2)	7(1)	2(1)	-3(2)
F(14)	23(2)	25(2)	11(2)	1(1)	-5(1)	-9(2)
I(1)	16(1)	14(1)	6(1)	-1(1)	5(1)	-2(1)

Table 5. Hydrogen coordinates ($\times 10^4$) and isotropic displacement parameters ($\text{Å}^2 \times 10^3$) for (5a).

	x	y	z	U(eq)
H(2A)	1638	8270	2638	17
H(3A)	2366	11447	2079	19
H(5A)	1462	11901	-1058	18
H(6A)	739	8811	-478	23

Table 6. Torsion angles [°] for (**5a**).

C(6)-C(1)-C(2)-C(3)	0.4(9)
I(1)-C(1)-C(2)-C(3)	-178.1(4)
C(1)-C(2)-C(3)-C(4)	0.8(9)
C(2)-C(3)-C(4)-C(5)	-2.5(8)
C(2)-C(3)-C(4)-C(7)	178.1(6)
C(3)-C(4)-C(5)-C(6)	3.1(9)
C(7)-C(4)-C(5)-C(6)	-177.6(6)
C(4)-C(5)-C(6)-C(1)	-1.9(9)
C(2)-C(1)-C(6)-C(5)	0.2(9)
I(1)-C(1)-C(6)-C(5)	178.6(5)
C(3)-C(4)-C(7)-C(8)	-8(10)
C(5)-C(4)-C(7)-C(8)	173(9)
C(4)-C(7)-C(8)-C(9)	-33(37)
C(7)-C(8)-C(9)-C(10)	48(30)
C(7)-C(8)-C(9)-C(14)	-131(30)
C(14)-C(9)-C(10)-F(10)	-179.2(5)
C(8)-C(9)-C(10)-F(10)	1.9(8)
C(14)-C(9)-C(10)-C(11)	1.2(8)
C(8)-C(9)-C(10)-C(11)	-177.7(6)
F(10)-C(10)-C(11)-F(11)	-0.7(9)
C(9)-C(10)-C(11)-F(11)	178.9(5)
F(10)-C(10)-C(11)-C(12)	179.2(5)
C(9)-C(10)-C(11)-C(12)	-1.2(9)
F(11)-C(11)-C(12)-F(12)	-0.9(8)
C(10)-C(11)-C(12)-F(12)	179.2(5)
F(11)-C(11)-C(12)-C(13)	-179.6(5)
C(10)-C(11)-C(12)-C(13)	0.5(9)
F(12)-C(12)-C(13)-F(13)	-1.1(8)
C(11)-C(12)-C(13)-F(13)	177.7(5)
F(12)-C(12)-C(13)-C(14)	-178.6(5)
C(11)-C(12)-C(13)-C(14)	0.1(9)
F(13)-C(13)-C(14)-F(14)	1.5(8)
C(12)-C(13)-C(14)-F(14)	179.1(5)
F(13)-C(13)-C(14)-C(9)	-177.6(5)
C(12)-C(13)-C(14)-C(9)	-0.1(9)
C(10)-C(9)-C(14)-F(14)	-179.7(5)
C(8)-C(9)-C(14)-F(14)	-0.8(8)
C(10)-C(9)-C(14)-C(13)	-0.6(8)
C(8)-C(9)-C(14)-C(13)	178.3(5)

Appendix A5b

Data for the structure of PhF$_5$-CC-Ph-Br (**5b**).

Crystals grown by Jonathan C. Collings. Structure solved by the author at the University of Durham Crystallography Department (reference code 01srv111).

Table 1. Crystal data and structure refinement for (**5b**).

Identification code	01srv111
Empirical formula	C14 H4 Br F5
Formula weight	347.08
Temperature	100(2) K
Wavelength	0.71073 Å
Crystal system	Monoclinic
Space group	P2(1)/c
Unit cell dimensions	a = 20.5178(16) Å $\quad$ α= 90°.
	b = 5.1812(4) Å $\quad$ β= 96.9220(10)°.
	c = 11.2539(9) Å $\quad$ γ = 90°.
Volume	1187.65(16) Å^3
Z	4
Density (calculated)	1.941 Mg/m^3
Absorption coefficient	3.510 mm^{-1}
F(000)	672
Crystal size	0.60 x 0.30 x 0.05 mm^3
Theta range for data collection	2.00 to 27.50°.
Index ranges	-26<=h<=26, -6<=k<=6, -14<=l<=14
Reflections collected	10137
Independent reflections	2697 [R(int) = 0.0389]
Completeness to theta = 27.50°	98.9 %
Absorption correction	Semi-empirical from equivalents
Max. and min. transmission	0.8441 and 0.2272
Refinement method	Full-matrix least-squares on F^2
Data / restraints / parameters	2697 / 0 / 197
Goodness-of-fit on F^2	1.051
Final R indices [I>2sigma(I)]	R1 = 0.0295, wR2 = 0.0793
R indices (all data)	R1 = 0.0356, wR2 = 0.0821
Largest diff. peak and hole	0.568 and -0.494 e.Å^{-3}

Table 2. Atomic coordinates (x 10^4) and equivalent isotropic displacement parameters (Å^2x 10^3) for (**5b**). U(eq) is defined as one third of the trace of the orthogonalized U^{ij} tensor.

Atom	x	y	z	U(eq)
C(1)	970(1)	1791(5)	6358(2)	10(1)
C(2)	894(1)	686(5)	5221(2)	13(1)
C(3)	1324(1)	-1231(5)	4955(2)	14(1)
C(4)	1833(1)	-2039(5)	5817(2)	12(1)
C(5)	1906(1)	-870(5)	6951(2)	15(1)
C(6)	1474(1)	1035(5)	7226(2)	14(1)
C(7)	2287(1)	-4030(5)	5572(2)	15(1)
C(8)	2684(1)	-5680(5)	5438(2)	15(1)
C(9)	3185(1)	-7578(5)	5362(2)	12(1)
C(10)	3140(1)	-9423(5)	4456(2)	13(1)
C(11)	3620(1)	-11287(5)	4404(2)	15(1)
C(12)	4159(1)	-11314(5)	5253(2)	17(1)
C(13)	4224(1)	-9506(5)	6163(2)	18(1)
C(14)	3740(1)	-7680(5)	6209(2)	15(1)
F(10)	2620(1)	-9417(3)	3614(1)	21(1)
F(11)	3552(1)	-13080(3)	3536(1)	22(1)
F(12)	4627(1)	-13103(4)	5211(2)	29(1)
F(13)	4755(1)	-9536(4)	6981(2)	32(1)
F(14)	3814(1)	-5930(3)	7092(2)	24(1)
Br(1)	385(1)	4403(1)	6755(1)	13(1)

Table 3. Bond lengths [Å] and angles [°] for (5b).

C(1)-C(6)	1.390(3)	C(4)-C(3)-H(3)	120.3(18)
C(1)-C(2)	1.393(3)	C(3)-C(4)-C(5)	119.3(2)
C(1)-Br(1)	1.898(2)	C(3)-C(4)-C(7)	121.8(2)
C(2)-C(3)	1.386(4)	C(5)-C(4)-C(7)	118.9(2)
C(2)-H(2)	0.98(3)	C(6)-C(5)-C(4)	120.6(2)
C(3)-C(4)	1.401(3)	C(6)-C(5)-H(5)	119.3(18)
C(3)-H(3)	0.91(3)	C(4)-C(5)-H(5)	120.1(18)
C(4)-C(5)	1.405(3)	C(5)-C(6)-C(1)	119.1(2)
C(4)-C(7)	1.438(3)	C(5)-C(6)-H(6)	121(2)
C(5)-C(6)	1.386(4)	C(1)-C(6)-H(6)	120(2)
C(5)-H(5)	0.99(3)	C(8)-C(7)-C(4)	176.0(3)
C(6)-H(6)	0.94(3)	C(7)-C(8)-C(9)	175.6(3)
C(7)-C(8)	1.203(4)	C(10)-C(9)-C(14)	116.8(2)
C(8)-C(9)	1.432(3)	C(10)-C(9)-C(8)	122.1(2)
C(9)-C(10)	1.393(3)	C(14)-C(9)-C(8)	121.2(2)
C(9)-C(14)	1.396(3)	F(10)-C(10)-C(11)	118.8(2)
C(10)-F(10)	1.339(3)	F(10)-C(10)-C(9)	119.5(2)
C(10)-C(11)	1.386(4)	C(11)-C(10)-C(9)	121.7(2)
C(11)-F(11)	1.343(3)	F(11)-C(11)-C(12)	120.2(2)
C(11)-C(12)	1.372(4)	F(11)-C(11)-C(10)	120.0(2)
C(12)-F(12)	1.340(3)	C(12)-C(11)-C(10)	119.7(2)
C(12)-C(13)	1.382(4)	F(12)-C(12)-C(11)	120.3(2)
C(13)-F(13)	1.340(3)	F(12)-C(12)-C(13)	119.3(2)
C(13)-C(14)	1.377(4)	C(11)-C(12)-C(13)	120.4(2)
C(14)-F(14)	1.340(3)	F(13)-C(13)-C(14)	120.8(2)
		F(13)-C(13)-C(12)	119.9(2)
C(6)-C(1)-C(2)	121.4(2)	C(14)-C(13)-C(12)	119.3(2)
C(6)-C(1)-Br(1)	118.29(18)	F(14)-C(14)-C(13)	118.5(2)
C(2)-C(1)-Br(1)	120.30(18)	F(14)-C(14)-C(9)	119.3(2)
C(3)-C(2)-C(1)	119.3(2)	C(13)-C(14)-C(9)	122.2(2)
C(3)-C(2)-H(2)	120.2(17)		
C(1)-C(2)-H(2)	120.5(17)		
C(2)-C(3)-C(4)	120.4(2)	Symmetry transformations used to generate
C(2)-C(3)-H(3)	119.2(19)	equivalent atoms:

Table 4.   Anisotropic displacement parameters (Å^2x 10^3) for **(5b)**. The anisotropic displacement factor exponent takes the form: $-2\pi^2[\ h^2\ a^{*2}U^{11} + ... + 2\ h\ k\ a^*\ b^*\ U^{12}\ ]$

Atom	U^{11}	U^{22}	U^{33}	U^{23}	U^{13}	U^{12}
C(1)	10(1)	7(1)	15(1)	1(1)	4(1)	-1(1)
C(2)	13(1)	16(1)	11(1)	1(1)	1(1)	2(1)
C(3)	15(1)	15(1)	12(1)	-2(1)	3(1)	2(1)
C(4)	11(1)	9(1)	17(1)	2(1)	5(1)	0(1)
C(5)	14(1)	14(1)	16(1)	2(1)	1(1)	1(1)
C(6)	15(1)	11(1)	14(1)	-1(1)	2(1)	0(1)
C(7)	14(1)	14(1)	16(1)	3(1)	4(1)	-1(1)
C(8)	15(1)	15(1)	15(1)	0(1)	4(1)	-2(1)
C(9)	12(1)	11(1)	15(1)	2(1)	5(1)	-1(1)
C(10)	13(1)	14(1)	13(1)	2(1)	1(1)	0(1)
C(11)	22(1)	9(1)	16(1)	-2(1)	8(1)	0(1)
C(12)	16(1)	12(1)	25(1)	2(1)	8(1)	5(1)
C(13)	14(1)	20(1)	20(1)	2(1)	-2(1)	1(1)
C(14)	18(1)	14(1)	14(1)	-3(1)	3(1)	0(1)
F(10)	20(1)	23(1)	19(1)	-3(1)	-5(1)	1(1)
F(11)	32(1)	15(1)	21(1)	-6(1)	8(1)	1(1)
F(12)	24(1)	22(1)	41(1)	-1(1)	7(1)	13(1)
F(13)	21(1)	34(1)	37(1)	-3(1)	-13(1)	8(1)
F(14)	27(1)	24(1)	21(1)	-10(1)	-2(1)	3(1)
Br(1)	13(1)	11(1)	15(1)	1(1)	5(1)	4(1)

Table 5.   Hydrogen coordinates (x 10^4) and isotropic displacement parameters (Å^2x 10 ^{3}) for **(5b)**.

Atom	x	y	z	U(eq)
H(2)	522(15)	1180(60)	4630(30)	12(7)
H(3)	1286(14)	-1900(60)	4200(30)	12(7)
H(5)	2274(15)	-1380(60)	7560(30)	17(8)
H(6)	1499(15)	1740(70)	8000(30)	23(8)

Table 6. Torsion angles [°] for (5b).

C(6)-C(1)-C(2)-C(3)	0.8(4)
Br(1)-C(1)-C(2)-C(3)	-179.55(19)
C(1)-C(2)-C(3)-C(4)	-0.3(4)
C(2)-C(3)-C(4)-C(5)	-0.5(4)
C(2)-C(3)-C(4)-C(7)	179.7(2)
C(3)-C(4)-C(5)-C(6)	1.0(4)
C(7)-C(4)-C(5)-C(6)	-179.2(2)
C(4)-C(5)-C(6)-C(1)	-0.6(4)
C(2)-C(1)-C(6)-C(5)	-0.3(4)
Br(1)-C(1)-C(6)-C(5)	180.00(19)
C(3)-C(4)-C(7)-C(8)	-178(100)
C(5)-C(4)-C(7)-C(8)	2(4)
C(4)-C(7)-C(8)-C(9)	-15(7)
C(7)-C(8)-C(9)-C(10)	177(4)
C(7)-C(8)-C(9)-C(14)	-2(4)
C(14)-C(9)-C(10)-F(10)	-179.7(2)
C(8)-C(9)-C(10)-F(10)	1.1(4)
C(14)-C(9)-C(10)-C(11)	0.6(4)
C(8)-C(9)-C(10)-C(11)	-178.6(2)
F(10)-C(10)-C(11)-F(11)	-1.5(4)
C(9)-C(10)-C(11)-F(11)	178.2(2)
F(10)-C(10)-C(11)-C(12)	179.5(2)
C(9)-C(10)-C(11)-C(12)	-0.8(4)
F(11)-C(11)-C(12)-F(12)	1.1(4)
C(10)-C(11)-C(12)-F(12)	-179.9(2)
F(11)-C(11)-C(12)-C(13)	-178.6(2)
C(10)-C(11)-C(12)-C(13)	0.4(4)
F(12)-C(12)-C(13)-F(13)	0.9(4)
C(11)-C(12)-C(13)-F(13)	-179.4(2)
F(12)-C(12)-C(13)-C(14)	-179.6(2)
C(11)-C(12)-C(13)-C(14)	0.1(4)
F(13)-C(13)-C(14)-F(14)	0.1(4)
C(12)-C(13)-C(14)-F(14)	-179.5(2)
F(13)-C(13)-C(14)-C(9)	179.2(2)
C(12)-C(13)-C(14)-C(9)	-0.3(4)
C(10)-C(9)-C(14)-F(14)	179.1(2)
C(8)-C(9)-C(14)-F(14)	-1.7(4)
C(10)-C(9)-C(14)-C(13)	0.0(4)
C(8)-C(9)-C(14)-C(13)	179.2(2)

Appendix A5c

Data for the structure of PhF$_5$-CC-Ph-Cl (**5c**).

Crystals grown by Jonathan C. Collings. Structure solved by the author at the University of Durham Crystallography Department (reference code 01srv140).

Table 1. Crystal data and structure refinement for (**5c**).

Identification code	01srv140
Empirical formula	C14 H4 Cl F5
Formula weight	302.62
Temperature	110(2) K
Wavelength	0.71073 Å
Crystal system	Triclinic
Space group	P-1
Unit cell dimensions	a = 6.0762(4) Å α= 85.3430(10)°.
	b = 7.4882(5) Å β= 86.0540(10)°.
	c = 13.1681(9) Å γ = 83.3320(10)°.
Volume	592.06(7) Å^3
Z	2
Density (calculated)	1.698 Mg/m^3
Absorption coefficient	0.371 mm^{-1}
F(000)	300
Crystal size	0.6 x 0.6 x 0.05 mm^3
Theta range for data collection	1.55 to 27.49°.
Index ranges	-7<=h<=7, -9<=k<=9, -17<=l<=17
Reflections collected	6110
Independent reflections	2698 [R(int) = 0.0158]
Completeness to theta = 27.49°	99.4 %
Absorption correction	Semi-empirical from equivalents
Max. and min. transmission	0.9817 and 0.8080
Refinement method	Full-matrix least-squares on F^2
Data / restraints / parameters	2698 / 0 / 181
Goodness-of-fit on F^2	1.030
Final R indices [I>2sigma(I)]	R1 = 0.0301, wR2 = 0.0853
R indices (all data)	R1 = 0.0340, wR2 = 0.0883
Extinction coefficient	.
Largest diff. peak and hole	0.401 and -0.219 e.Å^{-3}

Table 2. Atomic coordinates (x 10^4) and equivalent isotropic displacement parameters (Å^2x 10^3) for (**5c**). U(eq) is defined as one third of the trace of the orthogonalized U^{ij} tensor.

Atom	x	y	z	U(eq)
C(1)	2960(2)	1784(2)	6616(1)	21(1)
C(2)	1430(2)	2569(2)	7323(1)	22(1)
C(3)	2055(2)	2732(2)	8301(1)	22(1)
C(4)	4221(2)	2117(2)	8567(1)	19(1)
C(5)	5732(2)	1324(2)	7839(1)	21(1)
C(6)	5115(2)	1166(2)	6859(1)	23(1)
C(7)	4879(2)	2342(2)	9569(1)	21(1)
C(8)	5412(2)	2578(2)	10400(1)	21(1)
C(9)	5920(2)	2847(2)	11411(1)	19(1)
C(10)	4355(2)	3731(2)	12079(1)	19(1)
C(11)	4773(2)	3949(2)	13073(1)	21(1)
C(12)	6824(2)	3288(2)	13434(1)	22(1)
C(13)	8418(2)	2419(2)	12791(1)	21(1)
C(14)	7981(2)	2216(2)	11796(1)	20(1)
F(10)	2366(1)	4391(1)	11747(1)	25(1)
F(11)	3232(1)	4816(1)	13682(1)	27(1)
F(12)	7257(1)	3504(1)	14390(1)	30(1)
F(13)	10404(1)	1771(1)	13138(1)	27(1)
F(14)	9562(1)	1377(1)	11192(1)	26(1)
Cl(1)	2129(1)	1556(1)	5401(1)	31(1)

Table 3. Bond lengths [Å] and angles [°] for **(5c)**.

C(1)-C(2)	1.3852(18)	C(5)-C(4)-C(7)	120.82(11)
C(1)-C(6)	1.3877(18)	C(3)-C(4)-C(7)	119.86(11)
C(1)-Cl(1)	1.7366(12)	C(6)-C(5)-C(4)	120.74(11)
C(2)-C(3)	1.3868(18)	C(5)-C(6)-C(1)	118.82(12)
C(3)-C(4)	1.4014(17)	C(8)-C(7)-C(4)	178.22(13)
C(4)-C(5)	1.4000(18)	C(7)-C(8)-C(9)	176.69(13)
C(4)-C(7)	1.4325(17)	C(10)-C(9)-C(14)	116.55(11)
C(5)-C(6)	1.3856(18)	C(10)-C(9)-C(8)	121.25(11)
C(7)-C(8)	1.1950(19)	C(14)-C(9)-C(8)	122.19(11)
C(8)-C(9)	1.4225(17)	F(10)-C(10)-C(11)	118.39(11)
C(9)-C(10)	1.3959(17)	F(10)-C(10)-C(9)	119.15(11)
C(9)-C(14)	1.3997(17)	C(11)-C(10)-C(9)	122.46(11)
C(10)-F(10)	1.3401(14)	F(11)-C(11)-C(10)	120.37(11)
C(10)-C(11)	1.3760(18)	F(11)-C(11)-C(12)	120.06(11)
C(11)-F(11)	1.3348(14)	C(10)-C(11)-C(12)	119.56(11)
C(11)-C(12)	1.3876(18)	F(12)-C(12)-C(13)	120.36(11)
C(12)-F(12)	1.3288(14)	F(12)-C(12)-C(11)	120.17(11)
C(12)-C(13)	1.3820(18)	C(13)-C(12)-C(11)	119.47(12)
C(13)-F(13)	1.3434(14)	F(13)-C(13)-C(14)	119.93(11)
C(13)-C(14)	1.3780(17)	F(13)-C(13)-C(12)	119.69(11)
C(14)-F(14)	1.3367(14)	C(14)-C(13)-C(12)	120.38(11)
		F(14)-C(14)-C(13)	118.89(11)
C(2)-C(1)-C(6)	121.61(12)	F(14)-C(14)-C(9)	119.54(11)
C(2)-C(1)-Cl(1)	118.68(10)	C(13)-C(14)-C(9)	121.56(11)
C(6)-C(1)-Cl(1)	119.70(10)		
C(1)-C(2)-C(3)	119.44(11)		
C(2)-C(3)-C(4)	120.08(12)		
C(5)-C(4)-C(3)	119.30(11)		

Symmetry transformations used to generate equivalent atoms:

Table 4.   Anisotropic displacement parameters (Å^2x 10^3) for (5c). The anisotropic displacement factor exponent takes the form: $-2\pi^2[\, h^2\, a^{*2}U^{11} + \ldots + 2\, h\, k\, a^*\, b^*\, U^{12}\,]$

Atom	U^{11}	U^{22}	U^{33}	U^{23}	U^{13}	U^{12}
C(1)	25(1)	20(1)	19(1)	1(1)	-5(1)	-5(1)
C(2)	18(1)	23(1)	25(1)	1(1)	-5(1)	-1(1)
C(3)	20(1)	22(1)	23(1)	-1(1)	0(1)	-1(1)
C(4)	21(1)	16(1)	20(1)	0(1)	-2(1)	-4(1)
C(5)	18(1)	21(1)	24(1)	0(1)	-3(1)	-2(1)
C(6)	23(1)	22(1)	22(1)	-2(1)	1(1)	-1(1)
C(7)	20(1)	18(1)	23(1)	1(1)	-2(1)	-2(1)
C(8)	20(1)	18(1)	24(1)	0(1)	-2(1)	-3(1)
C(9)	20(1)	17(1)	20(1)	1(1)	-2(1)	-4(1)
C(10)	16(1)	18(1)	23(1)	2(1)	-2(1)	-2(1)
C(11)	22(1)	19(1)	21(1)	-1(1)	2(1)	-2(1)
C(12)	26(1)	22(1)	18(1)	0(1)	-4(1)	-6(1)
C(13)	17(1)	22(1)	24(1)	3(1)	-5(1)	-3(1)
C(14)	19(1)	18(1)	22(1)	0(1)	0(1)	-2(1)
F(10)	18(1)	28(1)	27(1)	1(1)	-5(1)	2(1)
F(11)	27(1)	30(1)	23(1)	-4(1)	4(1)	2(1)
F(12)	35(1)	37(1)	19(1)	-4(1)	-8(1)	-3(1)
F(13)	20(1)	34(1)	28(1)	2(1)	-8(1)	0(1)
F(14)	22(1)	29(1)	26(1)	-4(1)	1(1)	3(1)
Cl(1)	35(1)	37(1)	20(1)	-2(1)	-9(1)	-4(1)

Table 5.   Hydrogen coordinates (x 10^4) and isotropic displacement parameters (Å^2x 10 ^{3}) for (5c).

Atom	x	y	z	U(eq)
H(2A)	-34	2992	7139	26
H(3A)	1012	3261	8792	26
H(5A)	7196	889	8018	25
H(6A)	6150	643	6363	27

Table 6. Torsion angles [°] for (5c).

C(6)-C(1)-C(2)-C(3)	-0.49(19)
Cl(1)-C(1)-C(2)-C(3)	178.88(9)
C(1)-C(2)-C(3)-C(4)	0.43(19)
C(2)-C(3)-C(4)-C(5)	-0.65(18)
C(2)-C(3)-C(4)-C(7)	178.00(11)
C(3)-C(4)-C(5)-C(6)	0.92(18)
C(7)-C(4)-C(5)-C(6)	-177.71(11)
C(4)-C(5)-C(6)-C(1)	-0.97(19)
C(2)-C(1)-C(6)-C(5)	0.76(19)
Cl(1)-C(1)-C(6)-C(5)	-178.61(9)
C(5)-C(4)-C(7)-C(8)	121(4)
C(3)-C(4)-C(7)-C(8)	-58(4)
C(4)-C(7)-C(8)-C(9)	91(5)
C(7)-C(8)-C(9)-C(10)	-35(2)
C(7)-C(8)-C(9)-C(14)	144(2)
C(14)-C(9)-C(10)-F(10)	178.89(10)
C(8)-C(9)-C(10)-F(10)	-2.32(17)
C(14)-C(9)-C(10)-C(11)	-1.28(18)
C(8)-C(9)-C(10)-C(11)	177.51(11)
F(10)-C(10)-C(11)-F(11)	-0.65(17)
C(9)-C(10)-C(11)-F(11)	179.52(10)
F(10)-C(10)-C(11)-C(12)	-179.65(10)
C(9)-C(10)-C(11)-C(12)	0.52(19)
F(11)-C(11)-C(12)-F(12)	0.39(18)
C(10)-C(11)-C(12)-F(12)	179.39(10)
F(11)-C(11)-C(12)-C(13)	-178.96(11)
C(10)-C(11)-C(12)-C(13)	0.03(18)
F(12)-C(12)-C(13)-F(13)	0.84(18)
C(11)-C(12)-C(13)-F(13)	-179.81(10)
F(12)-C(12)-C(13)-C(14)	-179.12(10)
C(11)-C(12)-C(13)-C(14)	0.23(19)
F(13)-C(13)-C(14)-F(14)	-0.29(17)
C(12)-C(13)-C(14)-F(14)	179.67(10)
F(13)-C(13)-C(14)-C(9)	178.99(10)
C(12)-C(13)-C(14)-C(9)	-1.05(19)
C(10)-C(9)-C(14)-F(14)	-179.20(10)
C(8)-C(9)-C(14)-F(14)	2.03(17)
C(10)-C(9)-C(14)-C(13)	1.53(17)
C(8)-C(9)-C(14)-C(13)	-177.24(11)

Appendix A5d

Data for the structure of Ph-CC-Ph F_4-I (**5d**).

Crystals grown by Jonathan C. Collings. Structure solved by the author at the University of Durham Crystallography Department (reference code 01srv074).

Table 1. Crystal data and structure refinement for (**5d**).

Identification code	01srv074
Empirical formula	C14 H5 F4 I
Formula weight	376.08
Temperature	100(2) K
Wavelength	0.71073 Å
Crystal system	Monoclinic
Space group	P2(1)/n
Unit cell dimensions	a = 12.668(2) Å $\quad$ α= 90°.
	b = 5.0744(8) Å $\quad$ β= 93.703(4)°.
	c = 18.833(3) Å $\quad$ γ = 90°.
Volume	1208.1(3) Å^3
Z	4
Density (calculated)	2.068 Mg/m^3
Absorption coefficient	2.682 mm^{-1}
F(000)	712
Crystal size	0.2 x 0.2 x 0.1 mm^3
Theta range for data collection	1.88 to 27.49°.
Index ranges	-16<=h<=16, -6<=k<=6, -24<=l<=24
Reflections collected	11022
Independent reflections	2769 [R(int) = 0.0387]
Completeness to theta = 27.49°	99.6 %
Absorption correction	Semi-empirical from equivalents
Max. and min. transmission	0.7753 and 0.6161
Refinement method	Full-matrix least-squares on F^2
Data / restraints / parameters	2769 / 0 / 172
Goodness-of-fit on F^2	1.094
Final R indices [I>2sigma(I)]	R1 = 0.0268, wR2 = 0.0540
R indices (all data)	R1 = 0.0362, wR2 = 0.0572
Extinction coefficient	.
Largest diff. peak and hole	0.643 and -0.885 e.Å^{-3}

Table 2. Atomic coordinates (x 10^4) and equivalent isotropic displacement parameters (Å^2x 10^3) for (**5d**). U(eq) is defined as one third of the trace of the orthogonalized U^{ij} tensor.

Atom	x	y	z	U(eq)
I(1)	1994(1)	1407(1)	4825(1)	19(1)
C(1)	1374(2)	4095(6)	4074(2)	15(1)
C(2)	302(2)	4600(7)	3991(2)	18(1)
C(3)	-95(2)	6487(7)	3524(2)	17(1)
C(4)	558(2)	7991(6)	3113(2)	16(1)
C(5)	1638(2)	7427(6)	3200(2)	15(1)
C(6)	2029(2)	5520(6)	3662(2)	17(1)
C(7)	145(2)	10027(6)	2642(2)	17(1)
C(8)	-191(2)	11689(6)	2256(2)	17(1)
C(9)	-594(2)	13750(6)	1782(2)	18(1)
C(10)	-1634(3)	14659(7)	1821(2)	24(1)
C(11)	-2014(3)	16649(7)	1375(2)	30(1)
C(12)	-1366(3)	17752(7)	887(2)	31(1)
C(13)	-343(3)	16857(7)	839(2)	28(1)
C(14)	51(3)	14878(7)	1286(2)	23(1)
F(2)	-382(2)	3217(4)	4367(1)	25(1)
F(3)	-1143(1)	6898(4)	3456(1)	25(1)
F(5)	2321(1)	8861(4)	2838(1)	23(1)
F(6)	3082(1)	5130(4)	3732(1)	24(1)

Table 3. Bond lengths [Å] and angles [°] for (**5d**).

I(1)-C(1)	2.082(3)	C(3)-C(2)-C(1)	121.2(3)
C(1)-C(6)	1.377(4)	F(3)-C(3)-C(2)	119.2(3)
C(1)-C(2)	1.381(4)	F(3)-C(3)-C(4)	118.7(3)
C(2)-F(2)	1.351(3)	C(2)-C(3)-C(4)	122.1(3)
C(2)-C(3)	1.373(5)	C(3)-C(4)-C(5)	115.7(3)
C(3)-F(3)	1.342(3)	C(3)-C(4)-C(7)	122.0(3)
C(3)-C(4)	1.396(4)	C(5)-C(4)-C(7)	122.3(3)
C(4)-C(5)	1.397(4)	F(5)-C(5)-C(6)	119.0(3)
C(4)-C(7)	1.438(4)	F(5)-C(5)-C(4)	119.0(3)
C(5)-F(5)	1.348(3)	C(6)-C(5)-C(4)	122.0(3)
C(5)-C(6)	1.372(4)	F(6)-C(6)-C(5)	118.7(3)
C(6)-F(6)	1.347(3)	F(6)-C(6)-C(1)	119.8(3)
C(7)-C(8)	1.175(4)	C(5)-C(6)-C(1)	121.4(3)
C(8)-C(9)	1.446(4)	C(8)-C(7)-C(4)	179.9(4)
C(9)-C(14)	1.402(5)	C(7)-C(8)-C(9)	179.4(4)
C(9)-C(10)	1.402(4)	C(14)-C(9)-C(10)	119.4(3)
C(10)-C(11)	1.380(5)	C(14)-C(9)-C(8)	120.6(3)
C(11)-C(12)	1.388(6)	C(10)-C(9)-C(8)	120.0(3)
C(12)-C(13)	1.381(5)	C(11)-C(10)-C(9)	120.1(3)
C(13)-C(14)	1.384(5)	C(10)-C(11)-C(12)	120.0(3)
		C(13)-C(12)-C(11)	120.5(3)
C(6)-C(1)-C(2)	117.6(3)	C(12)-C(13)-C(14)	120.1(3)
C(6)-C(1)-I(1)	120.8(2)	C(13)-C(14)-C(9)	119.9(3)
C(2)-C(1)-I(1)	121.6(2)		
F(2)-C(2)-C(3)	118.6(3)	Symmetry transformations used to generate
F(2)-C(2)-C(1)	120.2(3)	equivalent atoms:

Table 4. Anisotropic displacement parameters $(\mathring{A}^2 \times 10^3)$ for (5d). The anisotropic displacement factor exponent takes the form: $-2\pi^2[h^2 a^{*2}U^{11} + ... + 2 h k a^* b^* U^{12}]$

Atom	U^{11}	U^{22}	U^{33}	U^{23}	U^{13}	U^{12}
I(1)	28(1)	15(1)	16(1)	2(1)	-3(1)	-2(1)
C(1)	21(2)	10(2)	13(1)	-1(1)	-2(1)	0(1)
C(2)	20(2)	19(2)	15(1)	0(1)	2(1)	-9(1)
C(3)	15(1)	19(2)	17(1)	-5(1)	1(1)	1(1)
C(4)	21(2)	14(2)	14(1)	-4(1)	-2(1)	-1(1)
C(5)	20(2)	12(2)	14(1)	1(1)	4(1)	-3(1)
C(6)	18(2)	14(2)	17(1)	-2(1)	1(1)	4(1)
C(7)	19(2)	18(2)	15(1)	-5(1)	0(1)	-2(1)
C(8)	18(2)	16(2)	17(1)	-6(1)	-2(1)	2(1)
C(9)	23(2)	14(2)	17(1)	-2(1)	-4(1)	2(1)
C(10)	20(2)	26(2)	24(2)	-6(2)	-4(1)	4(1)
C(11)	29(2)	26(2)	33(2)	-11(2)	-13(2)	9(2)
C(12)	43(2)	18(2)	29(2)	-4(2)	-16(2)	3(2)
C(13)	38(2)	21(2)	23(2)	5(1)	-6(2)	-3(2)
C(14)	24(2)	21(2)	24(2)	-3(1)	-2(1)	1(1)
F(2)	22(1)	31(1)	23(1)	10(1)	4(1)	-8(1)
F(3)	15(1)	34(1)	25(1)	3(1)	0(1)	2(1)
F(5)	21(1)	23(1)	26(1)	10(1)	6(1)	-2(1)
F(6)	15(1)	27(1)	28(1)	7(1)	2(1)	3(1)

Table 5. Hydrogen coordinates (x 10^4) and isotropic displacement parameters $(\mathring{A}^2 \times 10^3)$ for (5d).

Atom	x	y	z	U(eq)
H(10A)	-2077	13905	2155	28
H(11A)	-2719	17262	1401	36
H(12A)	-1628	19135	585	37
H(13A)	90	17601	497	33
H(14A)	758	14284	1258	28

Table 6. Torsion angles [°] for (5d).

C(6)-C(1)-C(2)-F(2)	178.3(3)
I(1)-C(1)-C(2)-F(2)	-4.4(4)
C(6)-C(1)-C(2)-C(3)	-1.1(5)
I(1)-C(1)-C(2)-C(3)	176.1(2)
F(2)-C(2)-C(3)-F(3)	0.0(4)
C(1)-C(2)-C(3)-F(3)	179.4(3)
F(2)-C(2)-C(3)-C(4)	-179.7(3)
C(1)-C(2)-C(3)-C(4)	-0.3(5)
F(3)-C(3)-C(4)-C(5)	-178.8(3)
C(2)-C(3)-C(4)-C(5)	0.9(5)
F(3)-C(3)-C(4)-C(7)	2.4(4)
C(2)-C(3)-C(4)-C(7)	-177.9(3)
C(3)-C(4)-C(5)-F(5)	-177.9(3)
C(7)-C(4)-C(5)-F(5)	1.0(4)
C(3)-C(4)-C(5)-C(6)	-0.2(4)
C(7)-C(4)-C(5)-C(6)	178.6(3)
F(5)-C(5)-C(6)-F(6)	-0.6(4)
C(4)-C(5)-C(6)-F(6)	-178.2(3)
F(5)-C(5)-C(6)-C(1)	176.4(3)
C(4)-C(5)-C(6)-C(1)	-1.2(5)
C(2)-C(1)-C(6)-F(6)	178.9(3)
I(1)-C(1)-C(6)-F(6)	1.6(4)
C(2)-C(1)-C(6)-C(5)	1.8(5)
I(1)-C(1)-C(6)-C(5)	-175.4(2)
C(3)-C(4)-C(7)-C(8)	-148(100)
C(5)-C(4)-C(7)-C(8)	33(100)
C(4)-C(7)-C(8)-C(9)	-58(100)
C(7)-C(8)-C(9)-C(14)	38(31)
C(7)-C(8)-C(9)-C(10)	-141(31)
C(14)-C(9)-C(10)-C(11)	-0.1(5)
C(8)-C(9)-C(10)-C(11)	179.2(3)
C(9)-C(10)-C(11)-C(12)	-0.1(5)
C(10)-C(11)-C(12)-C(13)	0.7(5)
C(11)-C(12)-C(13)-C(14)	-1.2(5)
C(12)-C(13)-C(14)-C(9)	1.0(5)
C(10)-C(9)-C(14)-C(13)	-0.4(5)
C(8)-C(9)-C(14)-C(13)	-179.7(3)

Appendix A5e

Data for the structure of Ph-CC-Ph F_4-SiMe$_3$ (**5e**).

Crystals grown by Jonathan C. Collings. Structure solved by the author at the University of Durham Crystallography Department (reference code 01srv128).

Table 1. Crystal data and structure refinement for (**5e**).

Identification code	01srv128
Empirical formula	C19 H14 F4 Si
Formula weight	346.39
Temperature	110(2) K
Wavelength	0.71073 Å
Crystal system	Monoclinic
Space group	C2/c
Unit cell dimensions	a = 25.2621(9) Å α= 90°.
	b = 10.8402(3) Å β= 112.2030(10)°.
	c = 13.7269(5) Å γ = 90°.
Volume	3480.3(2) Å^3
Z	8
Density (calculated)	1.322 Mg/m^3
Absorption coefficient	0.171 mm^{-1}
F(000)	1424
Crystal size	0.5 x 0.5 x 0.3 mm^3
Theta range for data collection	1.74 to 27.45°.
Index ranges	-32<=h<=32, -14<=k<=14, -17<=l<=17
Reflections collected	18737
Independent reflections	3973 [R(int) = 0.0302]
Completeness to theta = 27.45°	100.0 %
Absorption correction	Semi-empirical from equivalents
Max. and min. transmission	0.9505 and 0.9194
Refinement method	Full-matrix least-squares on F^2
Data / restraints / parameters	3973 / 0 / 273
Goodness-of-fit on F^2	1.085
Final R indices [I>2sigma(I)]	R1 = 0.0370, wR2 = 0.0945
R indices (all data)	R1 = 0.0482, wR2 = 0.1021
Extinction coefficient	.
Largest diff. peak and hole	0.318 and -0.246 e.Å^{-3}

Table 2. Atomic coordinates (x 10^4) and equivalent isotropic displacement parameters (Å^{2}x 10^3)

for (**5e**). U(eq) is defined as one third of the trace of the orthogonalized U^{ij} tensor.

Atom	x	y	z	U(eq)
Si(1)	4049(1)	5772(1)	266(1)	22(1)
C(1)	4211(1)	4570(2)	1302(1)	32(1)
C(2)	3321(1)	6438(2)	-106(2)	34(1)
C(3)	4132(1)	5158(2)	-931(1)	32(1)
C(4)	4577(1)	7030(2)	805(1)	26(1)
C(5)	4933(1)	7816(1)	1182(1)	25(1)
C(6)	5360(1)	8747(1)	1635(1)	24(1)
C(7)	5228(1)	10000(2)	1471(1)	26(1)
C(8)	5632(1)	10905(1)	1891(1)	27(1)
C(9)	6203(1)	10608(1)	2497(1)	24(1)
C(10)	6334(1)	9360(2)	2673(1)	25(1)
C(11)	5926(1)	8458(1)	2257(1)	24(1)
C(12)	6631(1)	11541(2)	2888(1)	28(1)
C(13)	6998(1)	12298(2)	3214(1)	28(1)
C(14)	7447(1)	13190(2)	3637(1)	27(1)
C(15)	7331(1)	14448(2)	3530(2)	34(1)
C(16)	7768(1)	15302(2)	3963(2)	37(1)
C(17)	8324(1)	14901(2)	4509(1)	32(1)
C(18)	8444(1)	13650(2)	4612(1)	34(1)
C(19)	8010(1)	12793(2)	4180(1)	31(1)
F(7)	4688(1)	10336(1)	884(1)	37(1)
F(8)	5477(1)	12092(1)	1709(1)	39(1)
F(10)	6873(1)	9018(1)	3242(1)	35(1)
F(11)	6081(1)	7271(1)	2446(1)	33(1)

Table 3. Bond lengths [Å] and angles [°] for (**5e**).

Si(1)-C(4)	1.8560(16)	C(19)-H(19)	0.97(2)
Si(1)-C(3)	1.8563(18)		
Si(1)-C(1)	1.8568(17)	C(4)-Si(1)-C(3)	108.14(8)
Si(1)-C(2)	1.8589(17)	C(4)-Si(1)-C(1)	107.03(8)
C(1)-H(1A)	0.97(2)	C(3)-Si(1)-C(1)	111.12(9)
C(1)-H(1B)	0.98(2)	C(4)-Si(1)-C(2)	108.18(8)
C(1)-H(1C)	0.96(2)	C(3)-Si(1)-C(2)	109.14(9)
C(2)-H(2A)	0.98(2)	C(1)-Si(1)-C(2)	113.06(9)
C(2)-H(2B)	0.98(2)	Si(1)-C(1)-H(1A)	110.6(14)
C(2)-H(2C)	0.97(3)	Si(1)-C(1)-H(1B)	110.3(13)
C(3)-H(3A)	0.95(2)	H(1A)-C(1)-H(1B)	109.6(18)
C(3)-H(3B)	0.93(2)	Si(1)-C(1)-H(1C)	110.9(14)
C(3)-H(3C)	0.98(2)	H(1A)-C(1)-H(1C)	108.5(19)
C(4)-C(5)	1.204(2)	H(1B)-C(1)-H(1C)	106.8(18)
C(5)-C(6)	1.436(2)	Si(1)-C(2)-H(2A)	108.9(12)
C(6)-C(11)	1.395(2)	Si(1)-C(2)-H(2B)	113.5(12)
C(6)-C(7)	1.397(2)	H(2A)-C(2)-H(2B)	107.3(17)
C(7)-F(7)	1.3466(17)	Si(1)-C(2)-H(2C)	111.2(15)
C(7)-C(8)	1.376(2)	H(2A)-C(2)-H(2C)	107.7(19)
C(8)-F(8)	1.3404(18)	H(2B)-C(2)-H(2C)	107.9(19)
C(8)-C(9)	1.402(2)	Si(1)-C(3)-H(3A)	109.5(14)
C(9)-C(10)	1.392(2)	Si(1)-C(3)-H(3B)	111.3(14)
C(9)-C(12)	1.429(2)	H(3A)-C(3)-H(3B)	110(2)
C(10)-F(10)	1.3415(17)	Si(1)-C(3)-H(3C)	109.9(12)
C(10)-C(11)	1.379(2)	H(3A)-C(3)-H(3C)	108.4(18)
C(11)-F(11)	1.3410(18)	H(3B)-C(3)-H(3C)	107.9(18)
C(12)-C(13)	1.192(2)	C(5)-C(4)-Si(1)	177.58(15)
C(13)-C(14)	1.436(2)	C(4)-C(5)-C(6)	179.6(2)
C(14)-C(15)	1.391(2)	C(11)-C(6)-C(7)	116.40(13)
C(14)-C(19)	1.399(2)	C(11)-C(6)-C(5)	122.35(14)
C(15)-C(16)	1.390(2)	C(7)-C(6)-C(5)	121.25(14)
C(15)-H(15)	0.92(2)	F(7)-C(7)-C(8)	118.81(14)
C(16)-C(17)	1.389(3)	F(7)-C(7)-C(6)	119.09(13)
C(16)-H(16)	0.97(2)	C(8)-C(7)-C(6)	122.10(14)
C(17)-C(18)	1.385(3)	F(8)-C(8)-C(7)	119.18(14)
C(17)-H(17)	0.91(2)	F(8)-C(8)-C(9)	119.57(13)
C(18)-C(19)	1.387(2)	C(7)-C(8)-C(9)	121.25(14)
C(18)-H(18)	0.88(2)	C(10)-C(9)-C(8)	116.75(13)

C(10)-C(9)-C(12)	121.69(14)	C(17)-C(16)-H(16)	122.1(13)
C(8)-C(9)-C(12)	121.53(15)	C(15)-C(16)-H(16)	117.7(13)
F(10)-C(10)-C(11)	118.77(14)	C(18)-C(17)-C(16)	119.85(15)
F(10)-C(10)-C(9)	119.51(13)	C(18)-C(17)-H(17)	120.5(13)
C(11)-C(10)-C(9)	121.71(14)	C(16)-C(17)-H(17)	119.6(13)
F(11)-C(11)-C(10)	118.77(13)	C(17)-C(18)-C(19)	120.38(17)
F(11)-C(11)-C(6)	119.46(13)	C(17)-C(18)-H(18)	123.0(15)
C(10)-C(11)-C(6)	121.77(14)	C(19)-C(18)-H(18)	116.7(15)
C(13)-C(12)-C(9)	178.38(18)	C(18)-C(19)-C(14)	120.07(17)
C(12)-C(13)-C(14)	178.23(19)	C(18)-C(19)-H(19)	121.5(13)
C(15)-C(14)-C(19)	119.27(15)	C(14)-C(19)-H(19)	118.4(13)
C(15)-C(14)-C(13)	120.97(15)		
C(19)-C(14)-C(13)	119.75(15)		
C(16)-C(15)-C(14)	120.36(17)		
C(16)-C(15)-H(15)	119.3(13)		
C(14)-C(15)-H(15)	120.2(13)		
C(17)-C(16)-C(15)	120.06(17)		

Symmetry transformations used to generate equivalent atoms:

Table 4. Anisotropic displacement parameters ($\mathring{A}^2$x 10^3) for (**5e**). The anisotropic displacement factor exponent takes the form: $-2\pi^2[\ h^2\ a^{*2}U^{11} + ... + 2\ h\ k\ a^*\ b^*\ U^{12}\ ]$

Atom	U^{11}	U^{22}	U^{33}	U^{23}	U^{13}	U^{12}
Si(1)	20(1)	20(1)	24(1)	-3(1)	5(1)	-4(1)
C(1)	31(1)	30(1)	30(1)	4(1)	8(1)	-2(1)
C(2)	23(1)	32(1)	42(1)	-2(1)	7(1)	2(1)
C(3)	35(1)	32(1)	30(1)	-8(1)	11(1)	-7(1)
C(4)	25(1)	27(1)	26(1)	-4(1)	9(1)	-4(1)
C(5)	25(1)	27(1)	23(1)	-3(1)	10(1)	-4(1)
C(6)	24(1)	26(1)	22(1)	-4(1)	9(1)	-7(1)
C(7)	21(1)	29(1)	24(1)	-1(1)	5(1)	-3(1)
C(8)	29(1)	22(1)	28(1)	0(1)	10(1)	-3(1)
C(9)	24(1)	26(1)	23(1)	-5(1)	9(1)	-8(1)
C(10)	20(1)	30(1)	24(1)	-4(1)	7(1)	-3(1)
C(11)	27(1)	21(1)	24(1)	-3(1)	10(1)	-2(1)
C(12)	27(1)	28(1)	28(1)	-5(1)	11(1)	-7(1)
C(13)	29(1)	29(1)	28(1)	-4(1)	13(1)	-6(1)
C(14)	27(1)	31(1)	25(1)	-6(1)	11(1)	-10(1)
C(15)	24(1)	33(1)	45(1)	-7(1)	12(1)	-6(1)
C(16)	35(1)	28(1)	51(1)	-10(1)	20(1)	-10(1)
C(17)	29(1)	38(1)	32(1)	-10(1)	14(1)	-17(1)
C(18)	24(1)	42(1)	31(1)	0(1)	6(1)	-8(1)
C(19)	31(1)	30(1)	32(1)	-1(1)	11(1)	-7(1)
F(7)	24(1)	35(1)	42(1)	2(1)	0(1)	0(1)
F(8)	39(1)	22(1)	49(1)	2(1)	9(1)	-3(1)
F(10)	21(1)	36(1)	40(1)	-4(1)	3(1)	-1(1)
F(11)	32(1)	22(1)	41(1)	-3(1)	9(1)	0(1)

Table 5.   Hydrogen coordinates (x 10^4) and isotropic displacement parameters (Å^{2}x 10 ^{3})
for (**5e**).

Atom	x	y	z	U(eq)
H(1A)	4581(10)	4200(20)	1436(18)	55(6)
H(1B)	4205(9)	4930(20)	1954(18)	53(6)
H(1C)	3928(10)	3930(20)	1095(18)	55(6)
H(2A)	3040(9)	5770(20)	-324(17)	46(6)
H(2B)	3264(9)	6880(20)	472(17)	46(6)
H(2C)	3234(11)	7000(20)	-690(20)	65(7)
H(3A)	4077(10)	5810(20)	-1428(19)	55(6)
H(3B)	4489(10)	4810(20)	-771(18)	58(7)
H(3C)	3843(9)	4520(20)	-1254(16)	44(5)
H(15)	6961(9)	14720(20)	3203(16)	44(6)
H(16)	7665(9)	16170(20)	3909(16)	47(6)
H(17)	8607(9)	15465(19)	4806(15)	37(5)
H(18)	8788(10)	13360(20)	4946(18)	52(6)
H(19)	8082(9)	11910(20)	4273(16)	45(6)

Table 6. Torsion angles [°] for (**5e**).

C(3)-Si(1)-C(4)-C(5)	-100(4)
C(1)-Si(1)-C(4)-C(5)	19(4)
C(2)-Si(1)-C(4)-C(5)	142(4)
Si(1)-C(4)-C(5)-C(6)	12(29)
C(4)-C(5)-C(6)-C(11)	7(27)
C(4)-C(5)-C(6)-C(7)	-173(100)
C(11)-C(6)-C(7)-F(7)	-179.43(13)
C(5)-C(6)-C(7)-F(7)	0.7(2)
C(11)-C(6)-C(7)-C(8)	0.4(2)
C(5)-C(6)-C(7)-C(8)	-179.40(15)
F(7)-C(7)-C(8)-F(8)	0.3(2)
C(6)-C(7)-C(8)-F(8)	-179.52(14)
F(7)-C(7)-C(8)-C(9)	-179.29(14)
C(6)-C(7)-C(8)-C(9)	0.8(2)
F(8)-C(8)-C(9)-C(10)	178.85(14)
C(7)-C(8)-C(9)-C(10)	-1.5(2)
F(8)-C(8)-C(9)-C(12)	-3.1(2)
C(7)-C(8)-C(9)-C(12)	176.54(15)
C(8)-C(9)-C(10)-F(10)	179.57(13)
C(12)-C(9)-C(10)-F(10)	1.5(2)
C(8)-C(9)-C(10)-C(11)	1.0(2)
C(12)-C(9)-C(10)-C(11)	-177.10(14)
F(10)-C(10)-C(11)-F(11)	0.6(2)
C(9)-C(10)-C(11)-F(11)	179.27(14)
F(10)-C(10)-C(11)-C(6)	-178.32(13)
C(9)-C(10)-C(11)-C(6)	0.3(2)
C(7)-C(6)-C(11)-F(11)	-179.96(13)
C(5)-C(6)-C(11)-F(11)	-0.1(2)
C(7)-C(6)-C(11)-C(10)	-1.0(2)
C(5)-C(6)-C(11)-C(10)	178.83(14)
C(10)-C(9)-C(12)-C(13)	25(6)
C(8)-C(9)-C(12)-C(13)	-153(6)
C(9)-C(12)-C(13)-C(14)	-70(10)
C(12)-C(13)-C(14)-C(15)	-131(6)
C(12)-C(13)-C(14)-C(19)	48(6)
C(19)-C(14)-C(15)-C(16)	-0.4(3)
C(13)-C(14)-C(15)-C(16)	178.61(16)
C(14)-C(15)-C(16)-C(17)	-0.2(3)

C(15)-C(16)-C(17)-C(18)	0.6(3)
C(16)-C(17)-C(18)-C(19)	-0.5(3)
C(17)-C(18)-C(19)-C(14)	0.0(3)
C(15)-C(14)-C(19)-C(18)	0.5(3)
C(13)-C(14)-C(19)-C(18)	-178.51(16)

Symmetry transformations used to generate equivalent atoms:

Appendix B: Seminars, Courses and Conferences Attended.

Seminars

Date	Title	Speaker
9th October 1998	*Carboranes: Exploitation of their unusual geometries and reactivates.*	Prof. M. F. Hawthorne
26th October 1998	*Reactions of the highly electrophilic boranes $HB(C_6F_5)_2$ and $B(C_6F_5)_3$ with Zr and Ta based metallocenes*	Dr. W. Piers
28th October 1998	*Tailoring Solid Surfaces*	Prof. J. P. S. Badyal
4th November 1998	*Computational Adventures in d and f element chemistry*	Dr. N. Kaltscoyannis
11th November 1998	*New Methodology for the Asymmetric Transfer Hydrogenation of Ketones*	Dr. M. Wills
12th November 1998	*From Macrocycles to Metallo-Supramolecular Chemistry*	Prof. S. Loeb
18th Novermber 1998	*Biodegradable Polymers*	Dr. R. Cameron
20th January 1999	*Luminescence of Large Molecules: from conducting polymers to coral reefs*	Dr. A. Jones
28th April 1999	*Ion-selective chemical sensors*	Prof. Klara Toth
12th May 1999	*Transition Metal Containing Liquid Crystals*	Prof. D. Bruce
12th October 1999	*Chocolate for the next millennium*	Dr. S. Beckett
13th October 1999	*Towards a pictorial glossary of intermolecular interactions*	Dr. M. Spackman
12th January 2000	*Atom transfer polymerisation – what is the hype all about?*	Prof. D. M. Haddleton
3rd May 2000	*High throughput screening – a route to customised catalysis*	Dr. C. Barnard and Dr L. Slade

5th June 2000	*Axially chiral cyclopentadienyl ligands*	Dr. R. Baker
9th June 2000	*Can homogenous catalysts be designed?*	Dr. P. Pringle
5th July 2000	*The electron rich three-centre bonding across the Periodic Table*	Prof. R. Hoffmann
18th October 2000	*The hydration of phospha-alkynes*	Prof. T. Hill
8th November 2000	*COSMIC: a universal, DNA-based language for communicating with life-forms and other intelligent life-forms*	Dr. J. P. L. Cox
6th December 2000	*Dual activation approaches to electroanalysis: ultrasound, microwave and laser activation.* *[Physics department]*	Prof. R. Compton
7th December 2000	*A Cambridge Database study of CH_3 and CF_3 exchange*	Dr. A. Nangia
21st February 2001	*Liquid crystal polymers of all shapes and sizes*	Prof. R. Richardson
7th March 2001	*Diborane(4) compounds: synthesis, structure and reactivity*	Prof. N. Norman
14th March 2001	*Probing structural disorder with diffuse neutron scattering*	Dr. Dave Keen
2nd May 2001	*Escapades with arenas and transition metals: from laser spectroscopy to synthetic applications*	Prof. R. Perutz
4th May 2001	*Olefin polymerisations using Ni(II) and Pd(II) diimine catalysts*	Prof. M. Brookhart
15th May 2001	*Silk and slime: successful supramolecular science* *[University of Newcastle-upon-Tyne]*	Prof. C. Viney
6th June 2001	*The melting point alternation of n-alkanes and derivatives*	Prof. R. Boese
19th June 2001	*Phase stability and structural chemistry at high pressure*	Dr. R. Rousseau

Conferences

Date	Title/Details
9th April 1998	RSC Meeting in honour of Prof. K. Wade, University of Durham.
25th May 1999	CatMeet 99- Selectivity in Catalytic Reactions, University of Hull.
29th – 30th March 1999	3rd Anglo-Dutch Symposium - Organometallic Chemistry and Applied Catalysis, University of Sheffield.
7th – 8th July 1999	RSC Coordination Chemistry Discussion Group, University of Bristol.
11th – 15th July 1999	IMEBORON X: The 10th International Conference on Boron Chemistry, University of Durham.
16th - 21st July 2000	16th International Symposium - Fluorine Chemistry, University of Durham. **Poster presentation**: *The structure and electronic properties of an unusual $B_4F_{10}O_2$ dianion containing trigonal planar oxygen atoms*
July 2000	50th Meeting of Nobel Prizewinners, Lindau, Germany: Chemistry, Physics and Medicine combined meeting. **Selected to attend as one of only 10 UK RSC delegates**.

Courses

Date	Title/Details
Michaelmas Term 1998	Postgraduate lecture course *Organometallics in Synthesis* End-of-course exam result: **96%**
Michaelmas Term 1998	Postgraduate lecture course *Practical Spectroscopy* End-of-course exam result: **77%**
Epiphany Term 1999	Postgraduate lecture course *Diffraction and Scattering Methods* End-of-course exam result: **70%**
7th-14th April 1999	BCA School, Trevelyan College, University of Durham. *Seventh Intensive Course in X-ray Structural Analysis*
2nd – 7th April 2001	Research Councils' Graduate Schools Programme, Hatfield College, University of Durham.

Appendix C: Publications

Publications:

Why are B_2O_2 rings rare?

Jacquelyn M. Burke, Mark A. Fox, Andrès E. Goeta, Andrew K. Hughes and Todd B.

Marder, *Chem. Commun.*, 2000, 2217.

Tris(2-methylphenyl)phosphonium tetrachloroborate.

Jacquelyn M. Burke, Judith A. K. Howard, Todd B. Marder and Claire Wilson, *Acta*

Crystallogr., 2000, **C56**, 1354.

Synthesis, characterisation and molecular structure of [Rh(COE)₂(acac)] (COE = cyclooctene, η^2-C₈H₁₄), an important starting material for the preparation of rhodium catalyst precursors.

Jacquelyn M. Burke, R. Benjamin Coapes, Andrès E. Goeta, Judith A. K. Howard,

Todd B. Marder, Edward G. Robins, Stephen A. Westcott, *J. Organomet. Chem.*, 2002,

649, 199.

Rhodium(I) catalysed diboration of (E)-styrylboronate esters: molecular structures of (E)-p-MeO-C₆H₄-CH=CH-B(1,2-O₂C₆H₄) and p-MeO-C₆H₄-CH₂C{B(1,2-O₂C₆H₄)}₃.

Paul Nguyen, R. Benjamin Coapes, Andrew D. Woodward, Nick J. Taylor, Jacquelyn

M. Burke, Judith A. K. Howard, Todd B. Marder, *J. Organomet Chem.*, 2002, **652**, 77.

Manuscripts in preparation:

Synthesis and characterisation of some prototypical Lewis acid-Lewis base adducts of boron trihalides with tertiary phosphines.

Jacquelyn M. Burke, Fabio E. S. Souza, Andrei S. Batsanov, Claire Wilson, Dimitrii S. Yufit, Judith A. K. Howard and Todd B. Marder, *J. Chem. Soc., Dalton Trans.*, in preparation.

The structure of a novel 2:1 adduct between arene and fluoroarene-based conjugated rigid rods.

Stephen W. Watt, Chaoyang Dai, Andrew J. Scott, Jacquelyn M. Burke, Rhodri Ll. Thomas, Jonathan C. Collings, Christopher Viney, William Clegg and Todd B. Marder, *Angew Chem., Int. Ed. Engl.*, in preparation.